PROCEEDINGS

Solar Extreme Events 2007 International Symposium:

Fundamental Science & Applied Aspects

24 – 27 September 2007

Titania Hotel
Athens, Greece

Edited by:

Helen Mavromichalaki (NKUA)
Athanasios Papaioannou (NKUA)

Solar **E**xtreme **E**vents **2007**

Proceedings of the
3rd SEE 2007 International Symposium-
COSPAR Colloquium

Athens, Greece
24 – 27 September 2007

Editors: Helen Mavromichalaki (NKUA)
Athanasios Papaioannou (NKUA)

ISBN: 978-960-466-049-0

Published by:
National and Kapodistrian University of Athens (NKUA)

These Proceedings have been published thanks to the funding of the Greek Ministry of National Education and Religious Affairs.

CONTENTS


Solar Extreme Events 2007: Fundamental Science and Applied Aspects
SEE 2007: International Symposium
Athens, Greece
Monday 24 September– Thursday 27 September
2007
COSPAR
COSPAR Colloquia

Preface

From September 24 to 27, 2007, the third conference on Solar Extreme Events (SEE 2007) was held at TITANIA Hotel in Athens, Greece. A total of 108 scientists and students from 17 countries attended this conference. Previous conferences were held at Moscow, Russia (July 12 to 14, 2004) and Nor Amberd, Armenia (September 26 to 30, 2005).

Solar Extreme Events are important for a number of reasons:

- Those provide unique information on violent processes in the solar corona, including mechanisms of particle acceleration and coronal mass ejections
- Shed light at the interactions occurring at Interplanetary space, of huge amounts of solar plasma with the Interplanetary Magnetic Field and the ambient population of Galactic Cosmic Rays (GCRs).
- Interplanetary shocks and coronal mass ejections, together with solar particle and electromagnetic emissions, trigger dynamic processes at the Earth's magnetosphere, causing global geo-effective events, including geomagnetic storms, heating of the upper atmosphere, changes in the electrodynamic properties of ionosphere, and creation of geomagnetically induced surface currents. All these constitute Space Weather conditions that change dramatically with SEE development.

SEE 2007 Symposium focused on a series of comprehensive discussions on solar, heliospheric and magnetospheric aspects related to the solar extreme events of 2005 and 2006. Highlighted cases as the events of July 2005, August-September 2005 and December 2006, provided us with valuable information, crucial for the understanding of space environment. It seems that the 23rd solar cycle reserved severe, peculiar and fascinating events for its descending phase.

The scientific program was divided into five major areas, including:

A: Solar extreme events of December 2006

B: Energetic processes of the Sun during solar extreme events at both solar minimum and maximum,

C: The chain of physical processes in the solar terrestrial system (Sun-Heliosphere-Magnetosphere-Ionosphere-Atmosphere-Ground)

D: Worldwide particle networks for Space Weather research

E: Integrated systems of forecasting and alerting on the dangerous consequences of violent solar storm

A special session on the International Heliospheric Year (IHY) was also organized, with the occasion of the completion of 50 years of space exploration. On top of which, a Workshop on Neutron Monitors (NMs), entitled: 'The present and the future of NMs', was also held. Principal investigators of more than twenty (20) neutron monitor stations from the Worldwide Network of NMs presented their activities and their future plans.

The SEE 2007 sessions consisted of invited and contributed talks as well as poster presentations. A total of 45 oral (available online at: http://cosray.phys.uoa.gr/SEE2007/Presentations.htm) and 53 poster presentations contributed to its success. High quality invited talks were given by: Galina Bazilevskaya, Anna Belehaki, Anatoly Belov, Ashot Chilingarian, Norma Crosby, Iannis Dandouras, Lev Dorman, Erwin Flueckiger, Nat Gopalswamy, Karel Kudela, Victoria Kurt, Mauro Messerotti, Leonty Miroshnichenko, Michail Panasyuk, Vasilis Tritakis, Ilya Usoskin, Jose Valdes-Galicia, Athina Varotsou and Igor Veselovsky

Within SEE 2007, a number of special events took place. The initiation of the conference was incidental to the celebration of 80 Years Birthday Jubilee of Prof. Ya. I. Feldstein and the participants of SEE 2007 sent a letter honouring his valuable contribution to solar-terrestrial relations. One of the most experienced and yet activated Greek scientists, on the field of Heliospheric researches: Emeritus Professor Constntinos Caroubalos, was awarded by the representative of the IHY (Nat Gopalswamy) for the sum of his research. Finally, SEE 2007 participants put together a letter of support for the United States Neutron Monitors, focusing on their significance and their continuation of operation.

The conference was recognized as a COSPAR colloquium and was supported by the National & Kapodistrian University of Athens, the Hellenic Ministry of Education, the Committee on Space Research (COSPAR), the European Office of Aerospace Research & Development (EOARD), the European Space Agency (ESA) and the Hellenic Physicists Association.

The contribution and the significant help of the Athens Cosmic ray team to the success of this Symposium are highly appreciated. We would especially like to thank Maria-Christina Papailiou for her valuable help in preparing the volume of SEE 2007 proceedings.

Helen Mavromichalaki
Chair

Xenophon Moussas
Co-Chair

Panagiota Preka – Papadema
Vice-Chair

SEE2007 Organizers

National & Kapodistrian University of Athens

Democritus University of Thrace

University of Ioannina

National Observatory of Athens

SEE2007 Sponsors

National & Kapodistrian University of Athens

Hellenic Ministry of Education

Committee on Space Research (COSPAR)

European Office of Aerospace Research & Development

European Space Agency (ESA)

Hellenic Physicists Association

SEE2007 COMMITTEES

Local Organising Committee

Helen Mavromichalaki Chair	National & Kapodistrian University of Athens, Greece
Xenophon Moussas Co-chair	National & Kapodistrian University of Athens, Greece
Panagiota Preka-Papadema Vice chair	National & Kapodistrian University of Athens, Greece
Fr. George Anagnostopoulos	University of Thrace, Greece
Eugenia Eroshenko	IZMIRAN Russian Academy of Science, Russia
Anna Belehaki	National Observatory of Athens, Greece
Panagiotis Fildisis	Hellenic Physicists Association, Greece
Christina Plainaki	National & Kapodistrian University of Athens, Greece
Athanasios Papaioannou	National & Kapodistrian University of Athens, Greece
Maria – Christina Papailiou	National & Kapodistrian University of Athens, Greece
Maria Gerontidou	National & Kapodistrian University of Athens, Greece
Christos Sarlanis	National & Kapodistrian University of Athens, Greece
George Souvatzoglou	National & Kapodistrian University of Athens, Greece
George Mariatos	National & Kapodistrian University of Athens, Greece

International Advisory Committee

Costas Alissandrakis	University of Ioannina, Greece
Dimosthenis Assimakopoulos	National & Kapodistrian University of Athens, Greece
Anatoly Belov	IZMIRAN Russian Academy of Science, Russia
John Bieber	BARTOL University, USA
Costantinos Caroubalos	National & Kapodistrian University of Athens, Greece
Ashot Chilingarian	Alikhanyan Physics Institute, Armenia
Norma Crosby	Belgian Institute for Space Aeronomy, Belgium
Lev Dorman	Cosmic Ray Center & Emilio Segre Observatory, Israel
Erwin Flueckiger	University of Bern, Switzerland
Karel Kudela	Institute of Experimental Physics, Slovakia
Helen Mavromichalaki	National & Kapodistrian University of Athens, Greece
Xenophon Mousas	National & Kapodistrian University of Athens, Greece
Michail Panasyuk	Moscow State University, Russia
Panagiota Preka-Papadema	National & Kapodistrian University of Athens, Greece
Manolis Sarris	University of Thrace, Greece
Epaminondas Stassinopoulos	NASA/GSFC, USA
Marisa Storini	National Institute for Astrophysics (INAF), IFSI-Rome, Italy
Kanaris Tsinganos	National & Kapodistrian University of Athens, Greece
Igor Veselovsky	Moscow State University, Russia
Victor Yanke	IZMIRAN Russian Academy of Science, Russia
Christos Zerefos	National Observatory of Athens, Greece

Chair Welcoming Address

Good morning,

Mr. Vice-Rector of the Athens University Prof. Ioannis Karakostas
Mr. Academician and Prof. of Astronomy George Kontopoulos
Mr. President of the Hellenic Physicists Association Prof. A. Angelopoulos

Dear Colleagues,

On behalf of the Organizing Committee of the Solar Extreme Events 2007 International Symposium organized by the Physics Department of the University of Athens I welcome you in Athens of the Olympic Games. It is a great honor and pleasure to us your participation to this Symposium.

SEE 2007 will focus on a series of comprehensive discussions on solar, heliospheric and magnetospheric aspects, related to the solar extreme events of the two last years 2005 and 2006, as well as their effects to technological and biological systems. Leader scientists from all over the world and from different fields covering all aspects of the Sun, Earth and Heliospheric Sciences as well as Cosmic Rays and Space Weather, will present their works and prosperous discussions will follow.

Moreover, by the occasion of the completion of 50 years of space exploration, a special session on the International Heliospheric Year (IHY) will be held this afternoon, where the oldest and yet activated Greek Professor C. Caroubalos in Heliospheric researches, will be awarded by the representative of the IHY.

Additionally, for first time, a special workshop on Neutron Monitors concerning the present and the future plans of NMs is organised on Thursday. Principal investigators of more than 25 old and new NMs distributed around the world will have the opportunity to present their activities.

Finally the SEE 2007 Symposium aims to create opportunities for new scientific contacts and collaborations.

This Symposium is supported by the National and Kapodistrian University of Athens, the Hellenic Physicists Association, the European Office of Aerospace Research and development, the United States Air Force Research Laboratory, the European Space Agency and the Committee on Space Research recognized this as COSPAR Colloquium. We thank all these sponsors providing the possibility to realize this Symposium.

Athens has the responsibility and the privilege to organize the third of the series of Solar Extreme Events (SEE) symposia, with the previous ones held in Moscow and Yerevan. We express our thanks to the Director of Lomonosov University of Moscow Prof. M. Panasyuk and Prof. I. Veselovsky of the same University that kindly encouraged us to organize this Symposium in our country.

We would also like to take this moment and remember our lovely collaborators: B. Petropoulos of the Research Center of Astronomy and Applied Mathematics of the Academy of Athens, S. Tatsis of the Athens Cosmic Ray Group, Prof. S. Kuznetsov of Russian Academy of Sciences and Dr. P. Lantos of the Meudon Observatory of Paris that recently passed away.

I wish good success to the conference and I hope that you will enjoy your stay in Greece.

Helen Mavromichalaki

SEE2007 LOC Chair

Prof. H. Mavromichalaki

Assoc. Prof. H. Mavromichalaki received her B.Sc.in Physics, M.Sc. in Meteorology and Ph.D. in Cosmic ray Physics by the Physics Department of the National and Kapodistrian University of Athens. She has been an assistant at the Nuclear Physics Laboratory and Lecturer and Assistant Professor at the Nuclear and Particle Physics section. . Scientific collaborator of the Research Center of Astronomy and Applied Mathematics of the Academy of Athens since 1979 and Leader of the Cosmic ray group of Athens University since 1982. Principal Investigator of the Installation and Operation of the Athens Neutron Monitor Station in real-time from 2000 up today and Head of the Athens Neutron Monitor Data Processing Center - ANMODAP Center (2003-today). Her scientific interests include Galactic and Solar Cosmic ray Physics, Magnetospheric Physics, Space Physics, Space Weather monitoring by cosmic rays, Neutron Monitors and Satellite data analysis.

She is the scientific responsible for a number of Greek and European funded projects such as NMDB under FP7 and SREM under ESA. Evaluator of Greek and European Projects on Space Physics. She has been favored with the editing of four monographs on Cosmic rays, Atomic Physics and Nuclear Physics as well as with four Proceedings volume. Has served as a referee for many international journals and as a Professor by supervising Ph.D thesis, M. Sc thesis and diploma (B. Sc.) thesis.

Welcoming by I. Karakostas

On behalf of the University of Athens I would like to welcome you in Greece and participate to the International Symposium 'Solar Extreme Events 2007'. I know that excellent scientists from the entire world have gathered here to present and discuss different fields covering disciplines of the Sun, Earth, Cosmic rays and Space weather.

Humans have been studying the Cosmos since the birth of humanity. In fact the word "anthropos", human in Greek, means *the one that observes the sky*, and it is correct that this differentiates humans from the other living creatures.

The Sun is the only star that affects our lives. Since now it was known that the Sun was affected on our climate, while it is obvious that there is an additional influence to the space and ground based technological systems Today humanity strongly depends on advanced technology and satellites and the solar activity frequently affects several aspects of human activities.

I hope that the results of this conference will try to give solutions to different open topics of the Solar-Terrestrial Physics.

We wish you a very successful and fruitful meeting and a pleasant stay in Athens and Greece.

Prof. I. Karakostas

Prof. I. Karacostas (Vice rector of the National & Kapodistrian University of Athens), obtained his B. Sc. in Law by the National & Kapodistrian University of Athens, and his Ph. D by the University of Regensburg of Germany. He speaks German, English and Italics. He has served as a lawyer since 1968. He has been assigned as a Professor of Urban Law, since 1983. He is a member of the European Law Association, of the Association for Political Rights and of the Judicial Studies Company. He has served as a Dean of the School of Law, Economics and Political Sciences of the National and Kapodistrian University of Athens (2000-2003), and as a President of the School of Law of the same institute. Since 2006, he has been serving as the Vice-rector of the National & Kapodistrian University of Athens.

Welcoming by G. Kontopoulos

I am happy to welcome you to this International Symposium on Solar Extreme Events.

The solar events have become a subject of extreme interest for many reasons. Firstly they provide data about the physical processes that occur in the Sun and the stars, as well as in the solar environment and in the whole planetary system. These data provide the tests of our theories and give information about the most basic physics that should be applied to the stars and their surroundings.

Another important aspect is the possibility to make predictions about the space weather and the general conditions of the interplanetary plasma. This field, which has been developed rigorously in our country by Mrs. Mavromichalaki and her team, has important consequences not only for space navigation but also for several phenomena on the earth.

I am happy that many people have come to this Symposium from many countries and I want to congratulate the organizers for their efforts.

I hope that you will enjoy not only the scientific contents of this meeting, but also your stay in Athens during this nice autumn weather.

Thus, I wish you a very fruitful Symposium and an enjoyable stay in Athens.

Prof. G. Kontopoulos

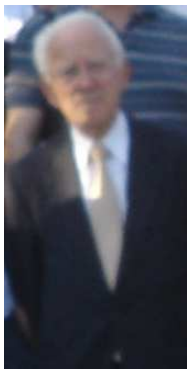

Prof. G. Kontopoulos, Academician, Emeritus Professor of the University of Athens and of the Aristotle University of Thessaloniki, Greece. He received his B.Sc. in Mathematics from the University of Athens, Greece (1950) and his Ph.D. from the same University in 1953. He was elected Professor of Astronomy at the Aristotle University of Thessaloniki (1957) where he has been Chairman of the Faculty of the School of Physics and Mathematics (1961-62). In 1975 he was elected Professor of Astronomy at the University of Athens. He has served as Director of the Astronomical Institute of the National Observatory of Athens (1975-1982), Director of the National Research Foundation (1978-79), vice- Chairman of the Greek National Astronomical Committee (1957-1983), National Representative at the NATO Scientific Committee and member of the research grant committee of NATO (1976-1983), member of the Astronomy Committee of the European Science Foundation (1976-83), member of the organizing Committee of the Astronomy Division of the European Physical Society (1976-1982) and member of the organizing committees of more than 30 international meetings. He has served as Visiting Professor at the Universities Yale (1962), Harvard (1968), MIT (1969), Cornell (1982), Chicago (1969, 1981), Maryland (1971, 1974, 1978) and Florida (1985-1991). He has been scientific associate at the Yerkes Observatory (1963), at the Institute for Advanced Study (1963), at the NASA (1963-67, 1971), at the Columbia University (1968) and at the ESO (1976-88). His scientific interests are mainly centered to the Dynamical Astronomy, the Chaos and the Relativity and he has published hundreds of scientific papers on these subjects. He has also published 8 scientific books and 4 textbooks. He has been elected Member of the Academy of Athens (1996) and currently he supervises its Research Center for Astronomy and Applied Mathematics.

Welcoming by A. Angelopoulos

Dear colleagues

As a member of the Faculty of Physics of University of Athens but also as the president of the Hellenic Physical Society I like to welcome all of you in Athens.

I also like to thank the organizers, especially Helen Mavromichalaki, for giving me the opportunity to address you and to congratulate them for the organization of the Solar Extreme Events conference which starts today.

The Hellenic Physical Society is a member of the European Physical Society and of the Balkan Physical Union and its members include Physics Teachers, Researchers, Physicists working in industry and of course all of us who are working in the Greek universities.

We are a scientific organization and what we are doing is to organize conferences and other events, mainly addressed to high school physics teachers, who are the majority of our members, and to the public trying to keep them up to date with the current physics knowledge and with the topics which very often attract the interest of the people. In collaborations with our colleagues from the rest of the Balkan countries we co-organize scientific events, helping in this way to improve the friendship of our people for the benefit of peace in our region. We also offer our help and experience, when it is asked, to colleagues who want to organize a conference, as happens with the current conference.

We also give our advice to the state about several educational matters which affect physics teaching in Greek schools.

It is not the proper time now to make a more extensive reference to our activities and I will stop now with my best wishes for a productive conference and also a nice stay in Athens.

Thank you.

Prof. A. Angelopoulos

Assoc. Prof. A. Angelopoulos (President of the Hellenic Physicist Association), received his B. Sc. and Ph. D. in Physics by the National & Kapodistrian University of Athens. Has served as a researcher fellow at CERN (1968-1970) and as a research fellow of the Greek National Research Foundation (1975-1977). Has been assigned as an Associate Professor of the National & Kapodistrian University of Athens (2001). Has been serving as the Director of the Physics Faculty Computer Center (2001 -) and as the President of the Hellenic Physicists Association (2006 -). He is also the Greek representative to W.H.O. EMF project (2005 -). His research interests include: Elementary Particle Physics, Nuclear Physics and Medical Physics and he has produced more than 100 publications at international scientific journals. He has served as a Professor of the National & Kapodistrian University of Athens at the topics of Elementary Particle Physics, Special Relativity, Particle Physics, Statistics and Computer Programming. He has participated at a number of experiments and projects as: PS183, PS195, TARC, nTOF, ACE/AD4 and FORFIRE.

Photos from SEE 2007

Inside Titania Hotel, at Athens

From the visit to Acropolis Archaeological Site

Special Events

As mentioned above, during the SEE 2007 International Symposium, three special events highlighted by democratic scientific spirit took place:

I. Professor Constantinos Caroubalos (Emeritus Professor of the Athens University) was honoured for his contribution to heliospheric studies and received a special diploma by Nat Gopalswamy (IHY).

II. The initiation of the symposium was incidental to the celebration of 80 Years Jubilee of Prof. Ya. I. Feldstein. Thus, the participants of SEE 2007 put together a letter in the Professor's honour, signed by N. Gopalswamy (IHY) and H. Mavromichalaki (SEE2007 LOC Chair). This was sent to Prof. Y. I. Feldstein and to IZMIRAN Director Prof. V. D. Kuznetsov.

III. A letter in support of the United States (US) Neutron Monitor Stations was composed, stressing their significance and revealing the arguments for their continuation of operation. This was addressed to anyone concerned on their situation.

I. Honoring the Emeritus Professor of the National & Kapodistrian University of Athens: Constantinos Caroubalos

Prof. **C. Caroubalos** received his B. Sc. in Physics, his M. Sc. on radioelectrology and his Ph. D. from the National & Kapodistrian University of Athens. As well as the Certf. Electr. Orsay and the Doctorat d' Etat from the University of Paris. He has served as Maitre de Research at the CNRS (France), Chief Assistant at the Laboratory of Electronics of the Physics Department of the University of Athens, Greece, Professor of Electronics at the Department of Physics, University of Athens (till 1989), Chairman of this Department for seven years (1982-1989), Director of the Section of Applied Physics and Director of the Electronics Laboratory of the same Department, Director of the Section of Telecommunications and Signal Processing of the Department of Informatics and Telecommunications, Director of the Ionospheric Institute (now Institute for Space Applications and Remote Sensing) of the National Observatory of Athens, Greece and President of the Advisory Committee for Research and Technology of the Government of Greece (1983). His scientific interests include the Solar Radioastronomy, Heliospheric processes, the Ionosphere and the Antennas, the digital signal processing, digital telecommunications e.t.c. He has published many papers on these subjects as well as 7 textbooks.

Prof. Constantinos Caroubalos was awarded by the representative of IHY **Nat Gopalswamy (NASA)**, for his contribution at Heliospheric studies**.**

II. The letter in the Professor's Ya. I. Feldstein honour

To: IZMIRAN Director Prof. V. D. Kuznetsov
Ref: Prof. Ya. I. Feldstein 80 Years Jubilee

Dear Prof. Feldstein,

On behalf of the participants of the International Symposium "Solar Extreme Events 2007: Fundamental science and Applied Aspects" (Athens-Greece, 24-27 September 2007) we cordially congratulate you on the occasion of your 80th Birthday Jubilee.

Your contribution to the modern formulation of the polar oval concept, which was done jointly with Dr. O. Khorosheva about 50 years ago during the International Geophysical Year studies, belongs to one of the most important achievements in this field of solar-terrestrial relations.

We wish you many new discoveries in your scientific work especially associated to the international Heliophysical Year 2007-2009.

Helen Mavromichalaki
SEE2007 LOC Chair

Nat Gopalswamy
IHY

III. Continuation of operation of US neutron monitor stations

Dear Sirs,

The third in the series of Solar Extreme Events International Symposiums recognized also as a COSPAR Colloquium was held in Athens, Greece on 24-27 September, 2007 (SEE 2007: http://cosray.phys.uoa.gr/SEE2007). More than 100 scientists from various countries (Europe, United States of America, South Africa, Israel, Russia, Kazakhstan, Armenia, Mexico, etc.) participated in the SEE 2007. Many scientific and application results presented at the Symposium based on data from the Neutron Monitor Network, implied the importance of Neutron Monitors for the modern Solar-Terrestrial, Heliospheric and Geo- Physics. In the framework of the SEE 2007 International Symposium a special Workshop has been organized, devoted to the present and the future of Neutron Monitors, including new plans of a unified database of neutron monitors, supported by the European Science Foundation, where the 'real-time' technology provides vast possibilities for the use of NM data.

With great surprise and grief we were informed of the situation and the possible closing of a number of ground level cosmic ray USA stations operated by the University of Delaware Bartol Research Institute. These stations (Nain, Peawanuck, Forth Smith, Goose Bay, South Pole, McMurdo, Thule) mostly located in Canada and Antarctic are extremely important for the world scientific community and for the USA in particular. The South Pole Neutron Monitor Station that has been closed from November 2005, recorded the largest CR variations among all other ground level detectors, and sometimes it was the only station capable of recording dangerous solar energetic particles (SEP), which greatly affect several aspects of human activity (satellites, space flights, etc). Moreover, it is well known that these NMs were created due to the project "Spaceship Earth" supported by the United States National Science Foundation under grant ATM-0527878 and by the NSF's Major Research Infrastructure program (grant OPP-9724293). Due to this project these exact NMs were utilized as a united instrument, useful for cosmic ray and space weather studies, monitoring in real time the conditions in the interplanetary space near Earth space, as well as those at the distance of 10 millions km away. Today, the alternative of such an instrument does not exist. Moreover, the cost of cosmic ray stations maintenance is not comparable to their real price.

Cosmic ray Stations at Thule and McMurdo are the only neutron monitors recording particles from sub polar directions. Stations based in Canada (Nain, Peawanuk, Forth Smith) accept particles from a wide latitudinal range that cannot be scanned by any other existing station.

Closure of these stations will lead to a dramatic decrease of the worldwide Neutron Monitor network efficiency, which is crucial for the forecasting of Space Weather in real time. Especially nowadays, where NM stations reveal their true significance, providing the world community with high accuracy data, capable of producing prognosis of dangerous particle fluxes.

For all the above reasons, the Scientific Community, which was represented by many world wide countries in the SEE 2007, hopes that US authorities will do their best in order to continue the operation of these Neutron Monitor stations under USA jurisdiction. It will be an irretrievable mistake and a great loss for science to lose these facilities. It would be extremely difficult and expensive if not impossible to recover these stations after termination of their operation.

Helen Mavromichalaki
Chair of the SEE2007

Participants of the SEE2007

Table of Papers

Session A: Solar Extreme Events of December 2006

Poster Session A

Session B: Energetic Processes on the Sun during extreme events / solar events at solar minimum

Poster Session B

Session C: The chain of physical processes in the solar-terrestrial system (Sun-Heliosphere-Magnetosphere-Ionosphere-Upper Atmosphere-Ground)

Poster Session C

Session D: World-wide particle detector networks for space weather research

Poster Session D

Session E: Integrated systems of forecasting and alerting on the dangerous consequences of violent solar storms

Poster Session E

Session F: International Heliospheric Year 2007

Workshop on Neutron Monitors
'The present and the future of NMs'

Session A

Solar Extreme Events of December 2006

Chair: M. I. Panasyuk, K. Kudela
E. V. Vashenyuk, R. Buetikofer

Solar **E**xtreme **E**vents **2007**

Characteristics of the cosmic ray ground level enhancement on January 20, 2005 and December 13, 2006 as obtained from world-wide neutron monitor data

E. O. Flueckiger

Physikalisches Institut, University of Bern, Bern, Switzerland
(erwin.flueckiger@space.unibe.ch)

Abstract – **The Ground Level Enhancements (GLEs) observed on January 20, 2005, and December 13, 2006, are both large events by historical standards. The January 20, 2005 event is ranked the second largest in fifty years with a peak count rate increase at the south polar NM stations exceeding several thousand percent (McMurdo: ~3000%, Terre Adelie: 4500%), and South Pole: >5000%). The December 13, 2006, GLE had a maximum increase of the order of 100% at Oulu and 80% at Apatity. The paper first summarizes the main characteristics of the two events as derived by various authors from the data of the worldwide network of neutron monitors. Secondly, the unusual time of occurrence near solar minimum is addressed. Finally, the relevance of the January 20, 2005, and December 13, 2006, GLEs is discussed in the context of Solar Extreme Events.**

Two Acceleration Mechanisms for Ground Level Enhancements

H. Moraal[1], K.G. McCracken[2]

[1]*School of Physics, North-West University, South Africa*
(harm.moraal@nwu.ac.za)
[2]*Institute for Physical Science and Technology, University of Maryland, USA*

Abstract – **The SANAE NM observed three distinct intensity peaks during the cosmic-ray ground level enhancement (GLE) of 20 January 2005. Using these observations, together with those of 10 other NMs, it is shown in this contribution that there were two distinctly different cosmic ray populations in this GLE, and that these were accelerated in two different regions of the solar corona, namely the flare associated with the sunpot group and the CME associated with this event.**

Characteristics of relativistic solar cosmic rays in large ground level events

E.V.Vashenyuk, Y.V.Balabin, B.B.Gvozdevsky

Polar Geophysical Institute, Murmansk region, Russia
(vashenyuk@pgi.kolasc.net.ru)

Abstract **–The modelling analysis of 14 large GLEs occurred in the period 1956-2006 on the data of the worldwide neutron monitors has been performed. The special attention is given to SEE on decline phase of the current, 23 solar cycles. The modelling consists of the next steps: 1. Definition of asymptotic viewing cones of the NM stations under study by the particle trajectory computations in a model magnetosphere. 2. Calculation of the NM responses at variable primary solar proton flux parameters. 3. Application of a least square procedure for determining primary solar proton parameters: rigidity spectrum, anisotropy axis direction, pitch-angle distribution outside the magnetosphere by comparison of computed ground based detector responses with observations. In all studied cases two distinct RSP populations (components) were revealed: the early impulse-like intensity increase with exponential energy spectrum (prompt component), and the late gradual increase with a softer energy spectrum of the power law form (delayed component). The possible physical reasons of formation of two populations of relativistic SCR with various spectra are discussed.**

Solar extreme events in the past: What do we know about them?

Ilya G. Usoskin

Sodankyla Geophysical Observatory (Oulu unit), University of Oulu, Finland
(Ilya.Usoskin@oulu.fi)

Abstract – **Solar extreme events accompanied by enhanced irradiation of Earth by solar energetic particles are known since mid-20th century by means of direct measurements of cosmic radiation by ground-based and space-borne detectors. However, the period since 1940's is characterized by the high level solar activity, which is unprecedented for the last few millennia. Therefore, it is of great interest to study such extreme solar event in the past when the Sun was quieter than nowadays. Here a brief review is presented of indirect methods to study solar extreme events in the past, before the instrumental era. The primary method is based on measurements of nitrates/nitrites in polar ice that is sensitive to enhanced flux of solar energetic particles (> 30 MeV). Cosmogenic isotopes 10Be and 14C are less sensitive to solar particles but also can provide additional information on solar extreme events. The results for cosmogenic isotopes are consistent with the nitrate method. The results show that indeed extreme solar events did occur in the past. Moreover, the results suggest that extreme events are more probable during periods when the solar activity is moderate, while very high activity produces a large number of medium-to-strong events but only seldom leads to occurrence of an extreme solar event. Constraints on the rate of extreme events are discussed and some speculations on the possible mechanism are presented.**

Properties of Solar X-Ray Flares and Proton Event Forecasting

A. Belov

Pushkov Institute of Terrestrial Magnetism, Ionosphere and Radio Wave Propagation, Russian Academy of Sciences

Abstract - **X-ray flares and acceleration processes are in the one complex of sporadic solar events (together with CMEs, radio bursts, magnetic field dissipation and reconnection). This supposes the connection (if not physical, but at least statistical) between characteristics of the solar energetic proton events and flares. The statistical analysis indicates that probability and magnitude of the near-Earth proton enhancement depends heavily on the flare's importance and its heliolongitude. These relations may be used for elaboration of the forecasting models, which allow us to calculate a probability of the solar proton event from the X-ray observations. The models of probability for different kinds of solar proton events are obtained on the basis of all accumulated data on X-ray flares on the Sun and solar proton enhancements near the Earth. These models describe well enough the available data, are suitable for practical use and, really, are already utilized in the IZMIRAN prognostic practice. However, we should remember on the limitation of accumulated statistics. X-ray flares and proton enhancements are observed yet so short time that any new burst of solar activity is able to add something to our understanding of a relation "solar flares - proton enhancements".**

Keywords- **solar flares, solar cosmic rays, solar energetic particles, proton enhancements, x-rays, probability model.**

I. INTRODUCTION

A relation between characteristics of solar proton enhancements (SPE) and X-ray flares is a consequence of the simple fact: solar flares and accelerating processes are the parts of one complex of the sporadic solar phenomena (eg. [1]). It assumes, that between characteristics of solar proton events and flares exists, if not a direct physical relation, then, at least, statistical. Other phenomena, such as CMEs and shock waves, bursts in a radio emission, dissipation and reconnection of magnetic fields and so on, enter into the same complex. It seems plausible, that some of these phenomena are connected with energetic particle acceleration processes more obviously, than X-ray emission. However as a possible basis for the solar proton event modeling the X-ray flare observations have some advantages before the other relevant measurements. Thus, in comparison with CME, the observations of X-ray flares are longer, more systematic and more detailed.

For our group the additional benefit was a database which contains data of long term observations on the X-ray flares and solar proton enhancements [2]. Studying of the extensive experimental material collected in this database has shown, that the basic properties of the SEPs observable at the Earth, are closely connected with parameters of the associated X-ray flares on the Sun (first of all, with flare peak flux and heliolongitude).

The models, allowing to predict probability and properties of proton increases at the Earth by the data on solar flares and radio burst observations were actively elaborated in the 70-80-th of the last century [3]-[10] and are used at present (for example, [11]-[14]. Already the first versions of such models have proved the practical utility. From time of their creation a lot of new data about flares is collected and more than 1000 new proton enhancements observable at Earth [2] is selected, that enables to specify parameters of models and to expand an area of their application [15].

In the given work models of probability for various sorts of solar proton events in MeV and GeV energies are considered, which can be used, in particular, for short-term forecasting of energetic solar proton enhancement in a real time mode. For the model elaboration data about solar flares and the near Earth and ground level SPEs, collected over the whole period of regular solar X-ray observations by satellites of series GOES are used.

II. METHODS AND DATA

This work is performed with use the X-ray flare and proton enhancement database (see [2], where the technique of the event selection and identification with flares is described). Data on soft X-ray radiation are received on satellites of series GOES (ftp://ftp.ngdc.noaa.gov/STP/SOLAR_DATA).
Enhancements of solar cosmic rays are selected on the basis of measurements of protons with energy > 10 MeV and > 100 MeV by satellites IMP-8 and GOES. For a given study the database is expanded and now it includes all X-ray flares (within a range 1-8 Å), observed from the end of 1975 till July, 2007. During this period 1274 enhancements of various size for solar protons with energy> 10 MeV are selected, 679 of which have been associated reliably enough with solar flares. We will name further such flares as the proton flares. First of them occurred in November 1975, the last one – in December 2006. Thus, our statistics spans practically three complete solar cycles (21-23) and several events at the end of cycle 20 that is well seen in Fig. 1. For a model creation the 53159 flares of ≥B5 importance have been used, but Fig. 1 demonstrates only part of this amount with ≥C1 importance.

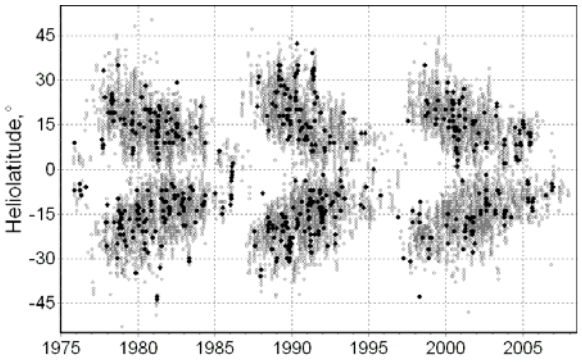

Fig. 1. Butterfly diagram for all X-ray flares with ≥C1 importance (open circles), and for the flares associated with the proton events (filled circles) in 1975-2007.

A portion of identified enhancements essentially grows with the increasing of proton flux. Enhancements identified with the solar sources give a chance to study correlations and to search for the quantitative relations between characteristics of solar flares and energetic proton enhancements near the Earth. Such relations allow us, in particular, to elaborate the models of proton event probability.
Of many characteristics of X-ray flares which statistically are related to SPEs [2] only two have been used in this work: flare X-ray peak flux and flare heliolongitude. Some other characteristics (for example, heliolatitude) have a relatively weak influence on the radiation conditions in the Earth vicinity. Some others are difficulty measurable in the real time mode.

III. DATABASES AND EXTREME EVENTS

In the given work statistical relations between different phenomena are searched for and their practical utilization is discussed. It may be asked why statistical analysis of data during many years accumulated is presented to Solar Extreme Event meeting, where recent, most outstanding events in solar-terrestrial physics are usually discussed? Of course, statistics of the large proton events is in fact the statistics of outstanding (and often extreme) events. But this statistics has been formed for a long time and probably is independent on several recent events. Is it so? To answer this question we can consider the events in 2005-2006, i.e. exactly those to topic of this symposium belonged.
From statistical analysis of data before 2005 obtained, it was followed that proton events associated with far eastern sources are sufficiently rare and never being very large. It is especially true for high energy particles. If to study the events where proton flux with energy >100 MeV exceeded 5 pfu (pfu = p $cm^{-2}sr^{-1}s^{-1}$), the most eastern flare associated with such a kind of events had a longitude of E43. However, flare X17/3B on 7 September 2005, after which proton flux of >100 MeV protons reached 7.4 pfu, occurred at longitude E77. Thus, heliolongitudinal range of sources for the enhancements under consideration widened abruptly by 34º (Fig. 2) and became more than 180º. The longitude E77 is taken from X-ray GOES observations; by the optical observations (ftp://ftp.ngdc.noaa.gov/STP/SOLAR_DATA) this flare was located more close to limb, on the longitude E89. If to accept this longitude, which better corresponds to the location of parent active region 10808 at this time, then longitudinal range widening will be not 34º but 46º.

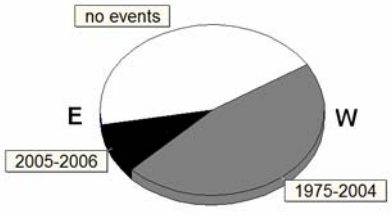

Fig. 2. Heliolongitude range of X-ray flares, associated with >5 pfu flux for >100 MeV protons. Boundaries of sectors are E77, E44 and W125.

Let us consider all proton events associated with flares located to the east from E60. The maximum >10 MeV proton flux throughout 1975-2004 was observed after X12/3B flare with longitude E70, which occurred on 4 June 1991, and it reached 43 pfu. On the 7 December 2006 after flare X6.5/3B with longitude E64 this flux was 1980 pfu, i.e. it turned out to be in five larger. Analogously, maximum flux of >100 MeV protons measured in the same event in 1991 was found about 3.5 pfu, and this flux on 7 December 2006 reached 19 pfu (GOES-11 data), i.e. increased more than in five.

In 2005-2006 some other events have occurred, which may be defined as "record", "anomalous", "outstanding". Flare X9/2N on 5 December 2006 turned out to be the most powerful X-ray flare among all the others related to phase of the solar activity minimum (we should remind that in December 2006 smoothed sunspot number was 12.1 only, and monthly not smoothed - 13.6). It is never before more than one ground level event (GLE) was recorded through two subsequent years with so low solar activity (if to estimate it traditionally by sunspot number). During these 2 years we obtained 3 GLEs: 17 and 20 January 2005 and 13 December 2006. With this, in the event on 20 January the biggest count rate increase whenever registered by standard neutron monitors (NM) was recorded. Not only GLEs, but SEP events were frequent enough during these years. Hudson [16] paid attention to a big (for this phase of the solar cycle) number of SEPs in 2004-2006. In accordance to our data base during these three years 33 solar proton enhancements were occurred, with maximum flux >10 pfu, 22 of which fall on 2005-2006. For a comparison, there were 8 such events in 1984-1985, and during 1994-1995 – only three events.

Thus, we see that events in 2005-2006 essentially changed statistics of X-ray flares, of proton enhancements and relationship between these events as well. Herewith, these changes concerned also our understanding of extreme events in this field. Does it mean some real long term shifts in solar activity? Hopefully we have not a reason for such assumptions. In a whole, 2005-2006 is a relatively quiet period in solar life (by the number of sun spots, by solar radio flux and X-ray background), and in consequence, quite quiescent 2007 came after. Abundance of the news may be explained by the short history of the proton event observation, and especially, X-ray observation. In fact our database is small. It is small random sample from the long solar history which doesn't allow us to make final conclusions about general distribution. Indeed, all events have been collected for 3 solar cycles. But this is only 3 cycles of 24 numbered. And even 24 solar cycles, as the whole period of solar scientific observations, is a negligible small part of the solar history accounting billions years. It means, in particular, that those events which we name now as "extreme" in fact are placed deeply enough in a distribution of all events, and real extreme events are absent not only in our data base but unknown, possibly, for the science at all. Indeed, proton events during the last years give a way by the magnitude to proton enhancement on 23 February 1956 [17],[18]. This is true at least for high energy solar particles. As Smart and Shea [19] showed, the high energy proton events of even bigger power were observed in the 18 cycle by means of ionization chambers. The events with biggest proton fluence for energy >30 MeV were discriminated by Shea et al. [20] using indirect nitrate data over the last 450 years. In recent cycles the biggest fluence of such particles was observed in August 1972 – and, already this period is beyond of the time boundary of our study. But in more far history 19 events were found with bigger fluence than that in August 1972. The largest proton enhancement was likely associated with Carrington flare [20]-[22] in 1859. Extending of time interval increases a number of large proton events and confirms that extreme events included in our statistics are conventionally extreme events.

IV. SOME PROPERTIES OF THE PROTON FLARES

If our sample would be compatible with general distribution of SEP events, it would be possible to get reliable models, having used only a part of the accumulated data. But our sample includes only small part of events, and we have to study and use all available data.

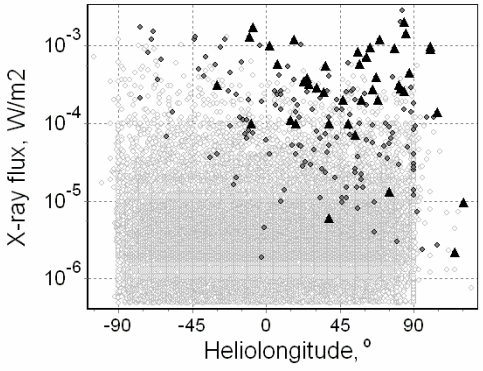

Fig. 3. Distributions by importance and by heliolongitude of all X-ray flares (open circles), flares associated with >10 MeV proton flux >10 pfu (diamonds), and flares associated with GLE (triangles) over the period 1975 September – 2007 July.

Belov et al., [2] showed that probability of proton events correlates with peak flux and heliolongitude of X-ray flare. Let us check this conclusion on the extended data base. The Fig. 3 shows, that proton flares are being met among powerful X-ray flares very often, and there are no flares among the most powerful (>X10, i.e. with maximal flux >0.001 Wt/m^2) which have not been associated with proton enhancements. With approach to east solar limb the quantity of proton flares quickly decreases, whereas at western limb a lot of such flares is observed (see also e.g. [23],[24]).

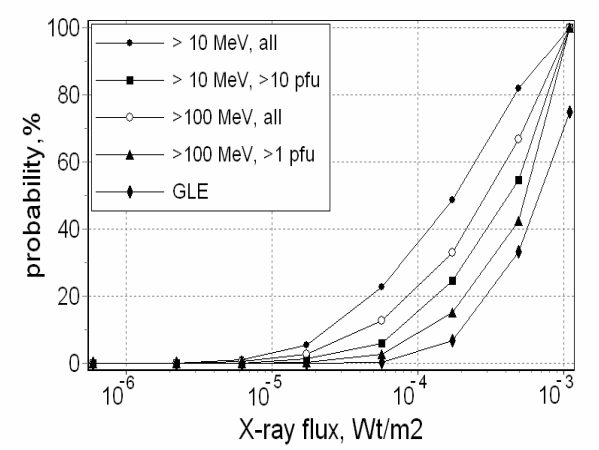

Fig. 4. SEP probability versus X-ray flare peak fluxes for western flares (W15-W75). Flux 10^{-4} Wt/m^2 = X1 importance.

Let us remind that hereinafter we name as "proton" only the flares associated with the protons registered at Earth. If to discuss all flares connected with accelerating processes, it would be necessary to assume, that their distribution on heliolongitude is close to uniform. Proton flares are mainly powerful flares, located in a definite longitudinal sector centered in the western part of a visible solar disk. The analysis shows, that there is a wide enough area of western longitudes inside of which the probability of proton event depends poorly on a longitude, but outside this strip with removal from it the probability falls quickly. Therefore far eastern flares and the majority of flares on the invisible part of the Sun have practically no chance to become proton flares.

A dependence on the X-ray peak flux is more clearly seen in Fig. 4. In order to plot it the flares of western longitudes within W0-W80 have been selected. These flares were divided by groups with the following X-ray
importance: <C1, C1-C2.9, C3-C9.9, M1-M2.9, M3-M9.9, X1-X2.9, X3-X9.9, ≥X10, and for each group the portion of proton events of different type was calculated. It is possible to see, that with increase of flare power the probability of its association with high energy protons grows quickly and at certain, big enough X-ray power reaches 100 % limit. It is clear, that the further increase of a peak flux cannot make the probability higher.

Fig.5 shows a dependence of the mean power of all flares, number of proton flares and flares associated with GLE on heliolongitude. Some increase of averaged power to limbs at all flares appear due to the problem that limb flares are hard to identify optically, so only the brighter X-ray flares will have reported Ha flares to determine their locations. Mean power of proton and essentially GLE flares depends more strongly on the longitude than power of all X-ray flares. Relatively weak flare on suitable western longitudes has more chances to be the proton one than more powerful eastern flare.

If to consider a quantity of flares registered on various longitudes it turns out to be a gradual falls with approach to limbs. However, directly at limbs, on the E90 and W90 this number is significantly higher than near limb and even in central regions. To the limbs, apparently, not only behind of limb flares are attributed, but also the part of near limb ones.

This fact should be considered in a definition of longitudinal dependence of models. Model calculations are performed for various types of proton enhancements and some properties of flares associated with various enhancements are given in the first columns of Table I.

Table I. Characteristics of proton enhancements and associated solar flares.

Ep MeV	I_{PC}, pfu	N	N_I	I_{XM}	φ_m, °	γ	I_0	φ_0	σ_φ, °	p_s> 50	p_s< 1	P_1, X1 45°W
>10	0.05	1274	679	M4.9	36	0.91±0.10	2.4±0.7	35±12	82±12	72	0.24	45.9
>10	1	595	430	M7.5	37	0.93±0.10	5.3±1.0	30±12	97±13	72	0.11	21.2
>10	10	275	215	X1.3	42	1.06±0.12	8.0±1.3	34±12	101±13	76	0.05	11.0
>10	100	100	94	X2.6	46	1.41±0.18	7.8±0.9	42±8	87±8	72	0.04	5.5
>100	0.01	637	399	M7.5	43	0.88±0.10	6.4±1.3	35±14	103±14	72	0.15	19.5
>100	1	120	107	X2.4	52	1.30±0.16	9.3±1.3	43±14	99±12	79	0.03	5.5
>100	10	46	45	X3.3	51	2.00±0.33	8.8±0.7	54±5	63±5	72	0.02	1.3
GLE	-	44	44	X3.2	55	2.02±0.30	8.8±0.6	54±5	63±5	72	0.02	1.2

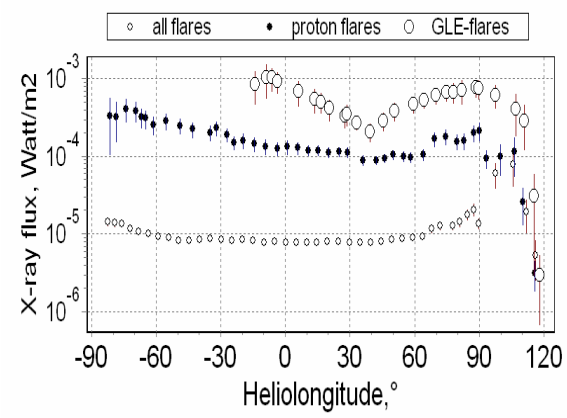

Fig. 5. Heliolongitudinal dependence of the mean importance of all X-ray flares, flares associated with > 10 MeV proton enhancements and flares associated with GLEs.

V. MODEL OF SEP PROBABILITY

The model of proton enhancement probability p_s has been searched as $p_S(I_x,\varphi) = f_x(I_x)\, f_\varphi(\varphi)$, (1) where $f_x(I_x)$ и $f_\varphi(\varphi)$ are the functions of importance and longitude of flare. For function $f_x(I_x)$ the forms $(I_x/I_0)^\gamma$ and $1-\beta\exp(-\alpha I_X)$ have been checked, the results for first of them turned out to be definitely superior. For longitude dependence $f_\varphi(\varphi)$ the next functions were checked: $\cos^n((\varphi-\varphi_0)/(2\pi\sigma_\varphi))$ and $\exp\left[-\left(\frac{(\varphi-\varphi_0)}{\sigma_\varphi}\right)^k\right]$, where parameter k was equal 2 or 4. Exponential form was found surely more preferable, the models with k=2 and k=4 demonstrated almost the same quality with small advantage for k=4. The following description of probability was finally chosen:

$$p_S(I_x,\varphi) = \begin{cases} \left(\frac{I_x}{I_0}\right)^\gamma \exp\left[-\left(\frac{(\varphi-\varphi_0)}{\sigma_\varphi}\right)^4\right] & (I_x < I_0) \\ \exp\left[-\left(\frac{(\varphi-\varphi_0)}{\sigma_\varphi}\right)^4\right] & (I_x >= I_0) \end{cases} \quad (2)$$

Parameter I_0 in $f_x(I_x)$ is the threshold peak flux. On the suitable longitudes the probability p_s reaches 100% limit at $I_x=I_0$ and increase of X-ray power above I_0 has no influence on p_s. It means, in particular, that in real time mode we could obtain the final evaluations for efficiency of the solar event before X-ray maximum if the X-ray flare reached sufficient power.

Parameters I_0, γ, φ_0, σ_φ were derived by the least square method using all flares with importance >B5. The observed probability was taken as 1 if flare was associated with observed proton event, and it was attributed to 0 for all other cases. As has been demonstrated by the tests it is insufficient to use the visible flares only. In this case the solution is not stable and strongly dependent on the longitudinal distribution. It is necessary to use the fact: for majority of invisible longitudes the proton flares are absent. We assumed that on such longitudes only nonproton flares occur and these flares are distributed by importance as all visible flares. The contribution from majority of invisible flares is 0 independently on longitude. The exclusion is the western behind limb sector (conditionally, W90-W150) where proton flares occur sometimes. Their longitudinal distribution is obviously not homogeneous, but we do not know this distribution. Therefore we were forced to exclude the western behind limb sector from calculations. It was possible to use the nearest western behind limb sector only for two high energy kinds of proton events (GLEs and >100 MeV, >10 pfu), where we know the longitudes of associated flares. For these two kinds of proton enhancements the calculations were accomplished within E103-W103 longitude range. For all other kinds the calculations were performed in the range E210-W90. Parameters I_0, γ, φ_0, σ_φ calculated for a model presented by equation (2) are given in Table 1.

Usual criteria of the model quality, such as residual dispersion or correlation coefficient, are not very informative in the case of the probability model. One of the criteria very often applying to an estimation of such models quality is a climatological skill score (e.g. [25]):

$$SS = 1 - \frac{\sum (p_s - p)^2}{\sum (< p > - p)^2} \quad (3)$$

where <p> - is average occurrence rate (number of proton events/number of flares). The magnitude of SS criteria was calculated for all flares observable within longitude range E85 - W85 and for different types of proton events it turned out to be ranged from 0.206 (all proton enhancements with energy >100 MeV) up to 0.283 (proton enhancements with energy >100 MeV and maximum flux >1 pfu). For the SPEs with energy >10 MeV and maximum flux >10 pfu it was obtained SS=0.246. This value is close to SS=0.230, estimated by Balch [12] for the same sort of enhancements. Balch implemented the model SWPC/NOAA to the 3783 X-ray flares, recorded over the 1986-2004, 127 of which were associated with significant proton enhancements.

To estimate a model quality under extremes of probability p_s we calculated mean observed probabilities of the solar proton events for the cases when p_s>50% and p_s<1%. These values are present in Table 1 (in percentages), and they testify sufficiently successful work of the models for all types of the

enhancements. For example, in 13 of 18 events where calculated model probability gave for GLE >50%, the ground proton enhancements were really observed. And of 31231 events with p_s<1% the GLEs were recorded only in 5 cases.

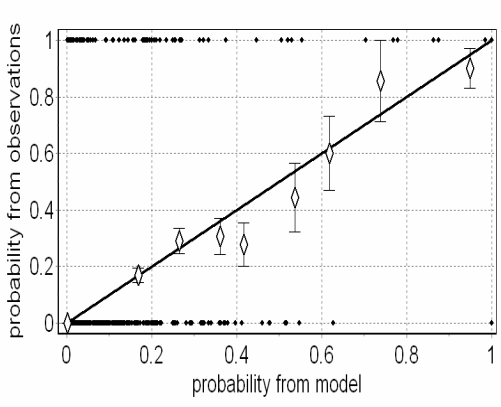

Fig. 6. Correlation between simulated p_s and observed probabilities of the > 100 MeV proton enhancements with flux >1 pfu. Points mark flares associated (upper line) and not associated (lower line) with this kind of proton events. Diamonds are averaged experimental probabilities corresponded to different ranges of p_s.

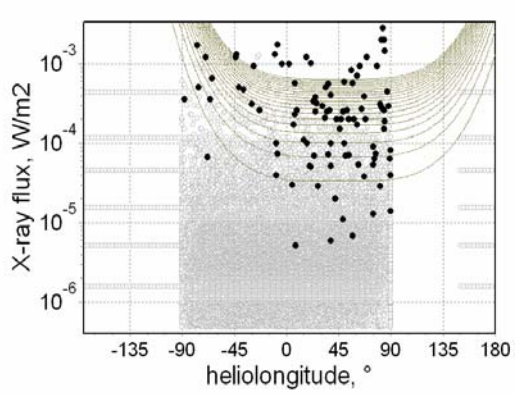

Fig. 7. X-ray flare distribution (light points) by flare importance and heliolongitude. Dark points of larger size represent the flares, associated with the > 100 MeV proton enhancements with flux >1 pfu. Contour curves are depicted for equal simulated probability p_s; inside contour corresponds to probability of 50%, outer one – to 1%.

We can judge about accordance of simulated and experimental probabilities of proton events by Figures 6 and 7. The treated models are approximately equally effective to all types of enhancements. However, the parameters of these models strongly differ. One can see that probability dependence on the SXR flare importance is stronger for the large SEP enhancements than for the small ones. Index γ for the smallest enhancements is ≈0.9, and it is about 2 for the largest events. By the similar way (from X2.4 to ≈X9) changes critical peak flux I_0 of the SXR flare, which is sufficient to provide the 100% probability of the small and large proton enhancements after ideally located flares. In a whole, the weaker proton enhancements the wider longitudinal range of associated flares (parameter σ_φ varies from 63º for large (>100 MeV, >10 pfu) proton events and GLEs up to ≈100º for a greater part of the remained enhancements).

Sector of the effective heliolongitudes is located most to the west (φ_0=54º) for large and ground level enhancements. For relatively small enhancements this region is shifted more close to the central meridian and φ_0=30-35º. To make a dependence of calculated probability on energy threshold and magnitude of the proton enhancement more presentable, we added in Table1 a probability p_1, calculated for definite flare of importance X1 and longitude W45. For such flares model forecasts weak proton enhancements (above the background for >10 MeV) almost in a half of events. At the same time for such flares the most outstanding enhancements (>100 MeV, >10 pfu and GLE) are expected only in one case from 80.

VI. CONCLUSION

The models of probability for different kinds of solar proton events are obtained on the basis of all accumulated data on X-ray flares on the Sun and solar proton enhancements near the Earth. These models describe well enough the available data, are suitable for practical use and, really, are already applied in the IZMIRAN prognostic practice. It is important to note that the model doesn't use an assumption about flare generation of all or majority of solar cosmic rays, and resulted statistical relations is not fruitful to use as an argument for such an assumption. However, the received results can speak well for two others, less strong, statements. The first one is that greater part of high energy protons near Earth observed arrives from area of intermediate size and with centre located close enough to the associated flare. The angle size of this area is less than minimal value of σ_φ in probability models, but at the same time it can be much more than size of flare. Example of such area could be a zone above whole parent active region or its significant part. The second statement is that inside of complexes of the solar sporadic phenomena there is steady enough proportionality between energies released in the soft X-ray radiation and in the high energy protons.

In any case it is possible to use this model as directly for short time forecast based on X-ray observations, and for the long term forecasting in a combination with the forecast of X-ray flares. At the same time, the given model is far from perfect; it is possible and necessary to be improved. Only several of possible dependencies of probability on flare peak flux and its

longitude have been checked. The longitudinal dependence may be very likely improved. Apparently, the model can be improved, having added to used parameters the information on initial phase of X-ray flare and flare latitude. We may hope also to make better a model quality if to replace or add to X-ray power the characteristics of high frequency solar radio bursts, which are more directly connected to accelerating processes than soft X-rays. Obviously the spectral radio bursts are useful as additional input to the models (type II burst, in the first turn), and NOAA model [12] incorporates it successfully. Unfortunately, this information is not always accessible in real time and is often delayed relatively to X-ray measurements.

We should not forget about limitation of our statistics. Our data set is still so short that already some next years are able to change it. We were able to obtain sufficient amount of data on the solar-terrestrial relations to create working and useful model. However, it doesn't mean that we know the exact law

combining X-ray flares and solar proton enhancements. We studied too small part of solar life, and have rather poor information to get accurate quantitative relations between solar and near Earth events. We can apply our models with high efficiency but not because of we know well the "eternal" dependencies. The performance of such kind of models is based mainly on the inertness of described system – this allows us to hope that, for example, the models calculated by the data over 32 years will be only slowly changing during the next several years. However, they may be noticeable varied for the next solar cycle. The models of such a kind need to be often reconsidered and refined, and it should be possibly done after each new proton event.

It is clear that model of probability should be added with the estimations of maximum proton flux near the Earth (or in some other points) and its time delay relatively to solar event. It may be realized using the same data and similar approach to their processing. In result the chance of more detailed prognosis of proton enhancements (in particular, an estimation of their full fluence and prognosis of their whole time profile) may be obtained.

ACKNOWLEDGEMENTS

This work was partly supported by the Russian Foundation for Basic Research (RFBR grants 07-02-00915, 07-02-13525).

I would like to thank all collaborators providing ground level monitoring of cosmic rays and teams of GOES and IMP, provided satellite data via Internet. I am grateful to my coauthors H. Garcia, M. Gerontidou, E. Eroshenko, O. Kryakunova, V. Kurt, H. Mavromichalaki and V. Yanke, at which participation a significant part of results have been obtained. Special gratitude are to Ilya Chertok for valuable help and to reviewers of this paper for numerous useful advices and suggestions.

REFERENCES

[1] Kahler, S.W., The role of the big flare syndrome in correlations of solar energetic proton fluxes and associated microwave burst parameters, J. Geophys. Res., 87, 3439-3448, 1982.

[2] Belov, A., Garcia, H., Kurt, V., Mavromichalaki, H., Proton enhancements and their relation to the x-ray flares during the three last solar cycles, Solar Physics, 229 (1), 135-159, 2005.

[3] Belovsky, M.N., Ochelkov, Yu.P., On some peculiarities of generation of electromagnetic and corpuscular radiation in solar flares, Izvestiya AN SSSR, Phys. Ser., 43, 4, 749-752, 1979 (in Russian).

[4] Smart, D.F., Shea, M.A. PPS76 - A computerized "event mode" solar proton forecasting technique, In: Solar-Terrestrial Prediction Proceedings, Ed.: R.F. Donnelly, Washington, D.C., USA, 1, 406-427, 1979.

[5] Akinyan, S.T., Chertok, I.M., Fomichev V.V., Quantitative forecasts of solar protons based on solar flare radio data, Solar-Terrestrial Prediction Proc., Ed.: R.F. Donnelly, Washington, D.C., v. 3, D14-D26, 1980

[6] Chertok I.M., Estimates of the proton energy spectrum exponent on the basis of solar microwave radio-burst data, Geomagneizm and Aeronomy, 22(2), 182-186, 1982.

[7] Heckman, G., Hirman, J., Kunches J., Balch C., The monitoring and prediction of solar particle events - an experience report, Adv. in Space Res. 4, 10, 165-172, 1984.

[8] Miroshnichenko, L.I. The development of diagnostics and prediction methods of solar proton events, in Solar-Terrestrial Predictions: Proc. of Workshop at Meudon, France, June 18-22, 1984, p.244-262, 1986

[9] Smart, D.F., Shea, M.A. A new event oriented solar proton prediction model, Adv. Space Res., 9(10), (10)281-(10)284, 1989.

[10] Smart, D.F. and Shea, M.A.: Predicting and modeling solar flare generated proton fluxes in the inner heliosphere, In: Biological effects and physics of solar and galactic cosmic radiation, Part B; Proceedings of a NATO Advanced Study Institute on Biological Effects and Physics of Solar and Galactic Cosmic Radiation, A95-81431, p. 101-117, 1993.

[11] Balch, C.C., SEC proton prediction model: verification and analysis. Radiation Measurements 30, 231–250, 1999.

[12] Balch, C. C., Updated verification of the Space Weather Prediction Center's solar energetic particle prediction model, Space Weather, 6, S01001, doi:10.1029/2007SW000337, 2008.

[13] Del Pozo, Proton Flux Prediction Model at Earth Environment to E > 10MeV, ESA Space Weather Workshop,http://www.estec.esa.nl/wmwww/wma/spweather/workshops/spw_w5, 2003.

[14] Kahler, S.W., Cliver, E.W., Ling, A.G., Validating the proton prediction system (PPS), JASTP, 69, 43–49, 2007.

[15] Belov, A.V., Eroshenko E.A., Kryakunova O.N., Kurt V.G., Yanke V.G., X-ray flare characteristics and probability of solar proton events, Proc. 30th ICRC, Merida, SH1.6-0907, 2007

[16] Hudson, H., The unpredictability of the most energetic solar events, Astrophys. J., 663, L45-L48, 2007

[17] Smart, D.F. and Shea, M.A.: Probable pitch angle distribution and spectra of the 23 February 1956 solar cosmic ray event, Proc. 21st Int. Cosmic Ray Conf., Adelaide, Australia, 5, 257-260. 1990

[18] Belov, A., Eroshenko, E., Mavromichalaki, H., Plainaki, C., Yanke, V., A study of the ground level enhancement of 23 February 1956 Adv. in Space Res., 35, 697-701, 2005.

[19] Smart, D.F. and Shea, M.A., A comparison of the magnitude of the 29 September 1989 high energy event with solar cycle 17, 18 and 19 events, Proc. of 22nd Int. Cosmic Ray Conf., 3, 101-104, 1991.

[20] Shea, M.A., Smart, D.F., McCracken, K.G., Dreschhoff, G.A.M., Spence, H.E. Solar proton events for 450 years: The Carrington event in perspective, Adv. in Space Res., 38, 232-238, 2006

[21] Carrington, R.C., Description of a singular appearance seen on the Sun on September 1,1859, Mon. Not. R. Astron. Soc., 20, 13-15, 1860.

[22] Cliver, E. W. The 1859 space weather event: Then and now. Adv. Space Res. 38, 119-129, 2006.

[23] Bazilevskaya, G.A. and Sladkova, A.I., Azimuthal distribution and release of accelerated particles from the solar corona, Geomagnetism and Aeronomy, 26, 187-190, 1986.

[24] Shea, M.A., Smart, D.F., The heliolongitudinal distribution of solar flares associated with solar proton events, Adv. Space Res., 17, (2)113-(2)116, 1996

[25] Murphy, A.H. and E.S. Epstein, Skill scores and correlation coefficients in model verification, Monthly Weather Review, 117, 572-581, 1989

Dynamics of relativistic solar cosmic rays during December 13, 2006 GLE

B. B. Gvozdevsky, E. V. Vashenyuk, Y. V. Balabin

Polar Geophysical Institute, Murmansk region, Russia
(gvozdevsky@pgi.kolasc.net.ru)

Abstract— **The dynamics of relativistic solar cosmic rays on data of ground level observations during the GLE of 13.12.2006 have been studied. The data of 32 neutron monitors of the worldwide network were used in the analysis. By least square (optimization) methods parameters of relativistic solar protons: rigidity (energetic) spectra, anisotropy directions and pitch-angular distributions were obtained and their dynamical changes studied during the event. It is shown, that in the beginning of the event solar protons arrived at the Earth along the IMF as a narrow collimated beam. These particles caused short-lived peak increase on a number of neutron monitor stations. On later phase a reverse flux (to the Sun) has appeared and the spectrum became appreciably softer. The rigidity spectral exponent changed from 4 to 6 in course of the event.**

Modeling of the GLE70 event

C. Plainaki[1, 2], H. Mavromichalaki[1], A. Belov[3], E. Eroshenko[3] and V. Yanke[3]

[1]*Nuclear and Particle Physics Section, Physics Department, Athens University, Zografos 15771 Athens, Greece,*
[2] *Istituto di Fisica dello Spazio Interplanetario, Via del Fosso del Cavaliere, 00133 Roma, ITALY,*
[3] *Institute of Terrestrial Magnetism, Ionosphere and Radio Wave Propagation (IZMIRAN), 42092, Troitsk, Moscow Region, Russia*

Abstract—**Solar cosmic ray models contribute to the understanding of physics taking place under extreme solar conditions. The NM-BANGLE model is a new cosmic ray model which couples primary solar cosmic rays at the top of the Earth's atmosphere with the secondary ones detected at ground level by neutron monitors during Ground Level Enhancements (GLEs). The evolution of several GLE parameters such as the solar cosmic ray spectrum and anisotropy as well as the particle flux distribution, are calculated. As a results, crucial information on the energetic particle propagation and distribution is revealed. The total output of the NM-BANGLE model is a multi-dimensional GLE picture of the characteristics of solar energetic particle events being recorded at ground level. In this work, the results of the NM-BANGLE model application to the recent GLE of 13 December 2006 are presented and discussed. Moreover, a comparison with the extreme event of 20 January 2005 (GLE69) is realized.**

Key Words— Solar cosmic rays, ground level enhancement, neutron monitor, solar energetic particles, modeling

I. INTRODUCTION

Ground Level Enhancements (GLEs) characterize only the relativistic part of the entire solar cosmic ray spectrum corresponding to energies bigger than 500 MeV/nucleon. The historical beginning of solar cosmic rays (SCR) observations was set by the occurrence of the GLE on 28 February 1942 whereas the greatest ground level enhancement of solar cosmic rays ever recorded until January 2005 was observed on 23 February 1956 ([1] and references therein). Since that time hundreds of proton events and tens of GLEs were registered, but all of them rank below this one by one order of magnitude or more. On 20 January 2005, one of the largest ground level enhancements ever recorded, also known as GLE69, was registered in the neutron monitors of the worldwide network ([2], [3]). Recently, on 13 December 2006, another big GLE was recorded by the ground cosmic ray detectors ([4], [5]).

Several techniques for modeling the dynamical behavior of GLEs throughout their evolving are presently available ([1], [2], [3], [6], [7], [8], [9], [10]). Realistic geomagnetic field models which take into account possible geomagnetic disturbances ([11], [12]) enabling the accurate determination of viewing directions for ground level instruments, are usually incorporated. On the basis of the Coupling Coefficient Method ([13]), a new improved and extended GLE-Model which couples primary solar cosmic rays at the top of the Earth's atmosphere with the secondary ones detected at ground level by neutron monitors (NMs) during GLEs, was recently proposed ([3]). The results of the application of the so called NM-BANGLE Model to GLE69 were analytically presented in Plainaki et al. (2007a) whereas some preliminary analysis of GLE70, based on the same model, has been also presented ([4]).

In this work an extensive and analytical study of the GLE of 13 December 2006 has been realized. Moreover the evolution of several important GLE parameters, during the period that GLE70 took place, calculated on the basis of the NM-BANGLE Model, is presented and discussed.

II. OBSERVATIONAL ANALYSIS ON GLE70

In December 2006, on the minimum of the 23rd cycle of solar activity, several events occurred on the Sun as well as in the interplanetary space between the Sun and the Earth. On 7 December, a Forbush Decrease (FD) was registered at the neutron monitors of the worldwide network ([4]). The big X3.4/4 B solar flare, originating from sunspot 930 at S06W26, was accompanied by a powerful proton event that produced a sharp growth of cosmic ray flux in the near-Earth space and at ground level.

This flare was also associated with Type II (shock velocity 1534 km/sec) and Type IV radio bursts as well as a fast full-halo CME with velocity ~ 1500 km/sec (http://sgd.ngdc.noaa.gov/sgd/jsp/solarindex.jsp).

Energetic solar cosmic rays on 13 December were guided toward the Earth by the interplanetary magnetic field and caused increase in the count rates of the ground based cosmic ray detectors. As a result, on 13 December, 2006 the worldwide network of NMs recorded the third biggest GLE of the 23rd cycle of solar activity, leaving behind only the enhancements of 15 April, 2001 and 20 January, 2005, classified as GLE70, starting at ~ 2:50 UT (Fig. 1). Anisotropy and cutoff rigidity effects in the intensities recorded by various NM stations can be clearly seen. The maximum cosmic ray variation on 5-min data (~92%) was recorded in Oulu NM at ~3:05 UT. The fact that the maximum enhancement was not registered at sub-polar stations as usual, but at lower latitudes (mid cut-off rigidity stations) leads to the conclusion that the source of anisotropy must have been located near the ecliptic plane. Mid and high latitude stations registered the GLE70 with different amplitudes, giving evidence of strong anisotropy, especially during the initial phase of the event. Nevertheless the north-south anisotropy was small.

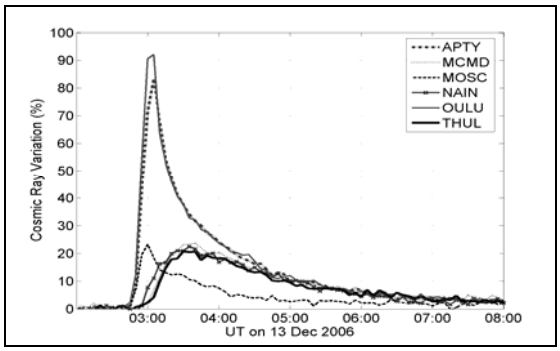

Fig. 1. GLE70 recorded by neutron monitors

III. APPLICATION OF THE NM-BANGLE MODEL – RESULTS

The NM-BANGLE Model, based on the Coupling Coefficient Method ([13]) calculates the evolution of several GLE parameters such as the SCR spectrum and anisotropy as well as the particle flux distribution, revealing crucial information on the SCR particle propagation and distribution ([3], [4]). As an input the NM-BANGLE model uses cosmic ray GLE data from NM stations widely distributed around the world. A detailed presentation of the model can be found in Plainaki et al. 2007a; b.

Five-minute GLE data from 37 NM stations, widely distributed around the Earth, were incorporated to apply the NM-BANGLE Model on the event of 13 December 2006. For the evaluation of the asymptotic directions and the cut-off rigidities for each NM location the Tsyganenko89 model has been used ([12]). The beginning of the event was very difficult to model due to the extremely anisotropic direction of propagation of the solar particles and due to the big differences (1-2 orders of magnitude) in the counting rates recorded between different NMs. The application of the NM-BANGLE model on GLE70 provided us with special quantitative information on the GLE particle spectrum evolution, solar cosmic ray fluxes and anisotropy. The interpretation of our results regards the following areas:

1) Rigidity spectrum - Solar cosmic ray fluxes

In the beginning phase of the event (~2:45 - 2:55 UT) the solar cosmic ray rigidity spectrum outside the atmosphere appears hard enough, with a spectral index varying between 0 and -1.9, whereas in the next 5-min time interval it softens significantly (γ = -4.3). This fact implies that on 13 December 2006 the contribution of high energy particles took place in the early phase of the event. However it should be stated that the spectral index has in general a limited range of applicability. Almost all GLE spectra have a variable slope with rigidity and this variation changes with time. Especially at the initial onset, exists a severe limit on the range of applicability of a specific spectral slope. This is evident in Fig. 3 where the uncertainty in the spectral index is quite large until 03:15 UT when it stabilizes. Therefore the range of applicability of the derived spectral slope is rather placed at the time period after 03:15.

The behavior of the mean integral fluxes of the lower energy solar cosmic ray particles on 13 December 2006, on the basis of the NM-BANGLE Model is presented in Fig. 2. The results displayed for energies greater than 100 MeV and 300 MeV are of course obtained by extrapolation, assuming that the spectral index is independent on energy. It is clearly seen that during the first time intervals, while the anisotropy is big, the mean integral flux is also very big. One should note however that during the first half hour of the event the values of parameters are changing rather rapidly and the corresponding errors are big. The mean integral flux $F_{mean}(>100\ MeV)$ is in good agreement with the satellite observations (http://www.sel.noaa.gov/today.html). The estimated flux for particles with energy >100 MeV takes similar values to those obtained in the case of GLE69, exceeding only by a factor of ~2 the fluxes recorded

on 29 September 1989 (~600 pfu) and on 14 July 2000.

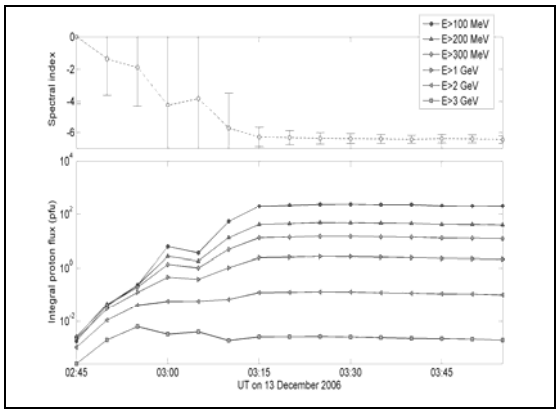

Fig. 2. SCR integral proton fluxes times together with spectral index evolution, on 13 December 2006.

Moreover, we found that all three fluxes of lower energy particles, remain at a high level during the first hour of the event. This result derived from the application of our model to the GLE on 13 December 2006 is also verified by the satellite observations of particles in the lower energy range (>50 MeV and >100MeV). The main part of SCR fluxes of different energies reached maximum at about 3:15 UT. After that moment the SCR flux slowly decreased keeping a soft spectrum with an index varying between -6.4 and -6.0. According to the results of the application of the NM-BANGLE Model the behavior of the most energetic particles (>3 GeV) differs from that corresponding to particles of less energy, reaching the point of maximum flux significantly earlier (at ~ 3:00 UT). Probably, it is not worth to give more emphasis to peculiarities of the profiles for the time period 3:00 – 3:10 UT, due to the fact that they are more or less related to statistical errors since the form of the rigidity spectrum was defined with the less accuracy at that period.

2) Anisotropy

The exact location of the apparent source of solar particles direction is generally difficult to determine. In our analysis we assumed that the relativistic particles arrived in the vicinity of the Earth forming a narrow beam. Such an approach for the anisotropic arrival of particles is quite reasonable, if one takes into account the large differences in the cosmic ray variations between neutron monitors of the same cut-off rigidity and altitude, located at different longitudes ([1], [3], [4]). The time dependent variation of the position of the anisotropy source near Earth, in GSE coordinates, is demonstrated in Fig. 3. It is clearly seen that the source of solar particles was mostly located close to the ecliptic plane. This result is indeed obtained in [5]. In Fig. 3 the mean latitude values are about -50 degrees. According to Fig. 3, during the first half hour the errors of the parameter definition are large and therefore the model does not fit well at that time. This may be due to two main reasons: a) at the very first moments the increases at cosmic ray intensities were not big yet or b) the physical model is not sufficiently adequate for the beginning phase of the event. In other words, it is possible that the form and the angular dependence of the anisotropy and the shape of the energy spectrum differ sufficiently from the real ones. Starting approximately from 3:15 UT the model works much better and the parameter variations become sufficiently small. The source of anisotropy is initially located westwards (longitude=-50^0), close to the ecliptic plane, whereas it moved eastwards with time (longitude=~0^0 after 3:00 UT). It's worth noticing that, according to the ACE spacecraft data taken from OMNIWEB, the IMF vector during these hours has a location in the right sector (longitudes -26° and -14° during the 3-rd and 4-th hours) and it is located close to the ecliptic plane (latitudes -10°and -4°).

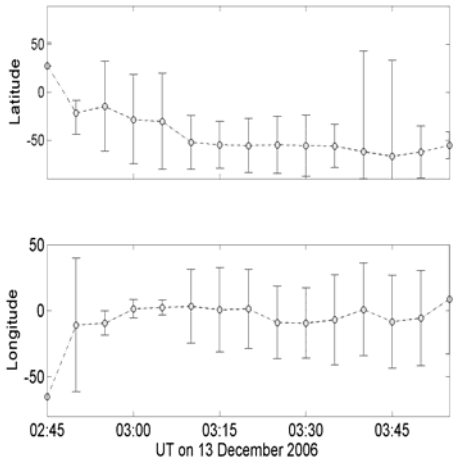

Fig. 3. Location of the anisotropy source in GSE coordinates.

According to the NM-BANGLE Model, the anisotropy source moved southwards with time. The longitude parameter as extracted from our model does not vary significantly after the time of maximum of the event, leading to the possible conclusion that after 3:00-3:10 UT the anisotropy decreased significantly. Moreover, the angular distribution is narrow during the initial period of the event (Fig. 4). Unfortunately, the errors at the beginning are large and therefore the respective peculiarities extracted by the NM-BANGLE model are not much reliable. As a result the concept of the narrow beam particle distribution

continues to comprise a subject of continuous analysis.
However, if these peculiarities really exist one can be drawn to the conclusion that there is evidence of either a long lasting particle acceleration on the Sun, with variable efficiency, or changing in particle propagation conditions in the Sun-Earth interplanetary space. Later the beam widened suggesting a wider particle distribution.

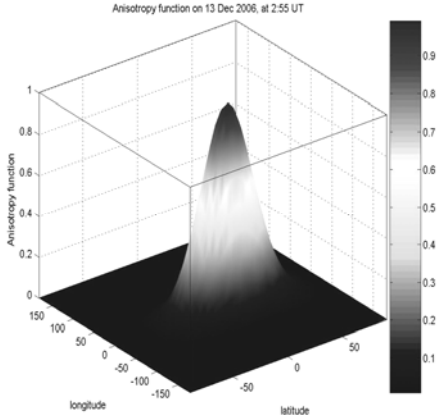

Fig. 4. Anisotropy function versus geographical latitude and geographical longitude of the anisotropy source, according to the NM-BANGLE model, on 13 December 2006 - 2:55 UT.

IV. GLE69 AND GLE70 COMPARISON – DISCUSSION

Comparing the above results with those calculated after applying the same NM-BANGLE Model to GLE69 the following conclusions emerge:

a) In both cases solar particles seem to have started propagating forming a narrow beam, sensed initially by those NMs owning the most favorable positions. A more wide angular distribution occurred with time, in both cases.
b) The narrow beam effect, however, was more intense in case of GLE69 than in case of GLE70 (the angular parameter took bigger values in the former case).
c) In both cases the SCR spectrum appears hard in the beginning but it softens during later phases. However the unusual behavior of the spectral index revealed for GLE69 ([3]) was not noticed in GLE70.
d) Integral proton fluxes for low energy particles calculated on the basis of the NM-BANGLE Model lead to reliable results, testified by the satellite data, in both cases.

As a conclusion, one can say that the application of the NM-BANGLE Model to GLE70 gave satisfactory results concerning the evolution of several important GLE parameters such as the integral solar proton fluxes as well as the position of the anisotropy source, especially in the time period after 3:10 UT. Future improvements of the model regarding the form of the anisotropy and/or the spectrum, as well as model application to more GLEs, may give results that will enrich our current knowledge on solar extreme events.

ACKNOWLEDGMENT

Thanks are due to all our colleagues from the neutron monitor stations, who kindly provided us with the data used in this analysis: Alma Ata, Apatity, Athens, Baksan, Barentsburg, Cape Schmidt, Fort Smith, Hermanus, Inuvik, Irkutsk-1, 2,3, Jungfraujoch, Jungfraujoch-1, Kerguelen, Kingston, Kiel, Larc, Lomnicky Stit, Magadan, Mawson, McMurdo, Moscow, Nain, Norilsk, Novosibirsk, Oulu, Potchefstroom, Peawanuck, Rome, Sanae, San Tiago, Terre Adelie , Thule, Tsumeb, Tixie Bay and Yakutsk.

REFERENCES

[1] Belov, A., E. Eroshenko, H. Mavromichalaki, C. Plainaki and V. Yanke, Solar cosmic rays during the extremely high ground level enhancement of February 23, 1956, *Anal. Geophys. 23*, 1, 2005
[2] Belov, A., E. Eroshenko, H. Mavromichalaki, C. Plainaki and V. Yanke, Ground level enhancement of the solar cosmic rays on January 20, 2005, *Proc. Int. Conf. Cosmic Rays 29th, 1,* 189, 2005b.
[3] Plainaki, C., A. Belov , E. Eroshenko, H. Mavromichalaki, V. Yanke: 'Modeling ground level enhancements: the event of 20 January 2005', Journal of Geophysical Research-Space Physics, 112, A04102, doi:10.1029/2006JA011926, 2007a.
[4] Plainaki, C., Mavromichalaki, H., Belov, A., Eroshenko, E., Yanke, V.: "Application of the NM-BANGLE model to GLE70", Proc. 30th Intern. Cosmic Ray Conf., Merida, 2007b.
[5] Vashenyuk, E.V., Bazilevskaya, G.A., Balabin, Y.V., Gvozdevsky, B.B., Makhmutov, V.S., Stozhkov, Y.I., Svirzhevsky, N.S., Svirzhevskaya, A.K., Schur, L.I.: The GLE of December 13, 2006 according to the ground level and balloon observations, 30th Intern. Cosmic Ray Conf., Merida, 2007.
[6] Humble, J.E., M.L. Duldig, D.F. Smart and M.A. Shea, Detection of 0.5-15 GeV solar protons on 29 September 1989 at Australian stations, *Geophys., Res., Let., 18,* 737, 1991.
[7] Shea, M.A. and D.F. Smart. Possible evidence for a rigidity-dependent release of relativistic protons from the solar corona, *Space Sci.Rev, 32,* 251-271, 1982.
[8] Duldig, M.L., J.L. Cramp, J.E. Humble, D.F. Smart, M.A. Shea, J. W. Bieber, P. Evenson, K.B. Fenton, A.G. Fenton and M.B.M Bendoricchio (1993), The Ground-level enhancement of 1989 September 29 and October 22, *Proc. NASA 10,* 3.
[9] Cramp, J.L., M.L. Duldig, E.O. Flückiger, J.E. Humble, M.A. Shea and D.F. Smart (1997), The October 22, 1989, solar cosmic ray enhancement: An analysis of the anisotropy and

spectral characteristics, *J. Geoph. Res., 102, A11,* 24237, 1997

[10] Bieber, J.W., J. Clem, P. Evenson, R. Pyle, D. Ruffolo and A. Saiz (2005), Relativistic solar neutrons and protons on 28 October 2003, *Geophys. Res. Letters*, 32, 3, CiteID L03S02.

[11] Tsyganenko, N.A.: Global quantitative models of the geomagnetic field in the cislunar magnetosphere for different disturbance levels, *Planet. Space Sci., 35,* 1347, 1987.

[12] Tsyganenko, N.A.: A magnetospheric magnetic field model with the warped tail current sheet, *Planet. Space Sci., 37,* 5, 1989.

[13] Dorman, L.I. (2004), Cosmic Rays in the Earth's atmosphere and underground, Kluwer Academic Publishers, The Netherlands

Spectral-temporal Features of Solar Radio Emission at the Stage of Halo Type CMEs: Formation and Initial Propagation during Solar Extreme Events of December 2006

O. Sheiner, V. Fridman, Y. Tikhomirov

Radiophysical Research Institute, Nizhny Novgorod, Russia
(rfj@nirfi.sci-nnov.ru; oasheyner@gmail.com)

Abstract— **It was established earlier that the majority of the large CMEs events are preceded by phenomena in solar radio emission within a time interval of about 60 min. These phenomena are developed in the form of the sporadic component of radio emission over a wide range of frequencies. This work presents the spectral-temporal special features of radio-events in the centimeter (cm) and decimeter (dm) ranges of the radio waves, preceded Halo CMEs in the two-hour interval of their registration. For studying of these precursors of CMEs the data of the worldwide network of solar observatories in the radio-frequency band are used. Information about the phenomena and the characteristics of CMEs were undertaken from http://sdaw.jsfc.nasa.gov./CME_list. Examined set of the Halo type CMEs consists of "isolated" CMEs events, i.e., when the preceding CMEs event is recorded not less than for 8 hours, and following not less than 6 hours, prior to the event in question. Basic observed CMEs parameters are used for studying: angular width, the initial velocity of propagation, and also the phenomenological type of phenomenon. Such characteristics of the sporadic component of radio emission, as intensity and the duration of sporadic component at different frequencies of cm and dm wavelength range are analyzed taking into account observed type of bursts. It is established the stability of the spectral-temporal structure of CMEs precursors in the radio-frequency band and its dependence on CMEs parameters.**

Observations of Energetic Solar Particles: 13-16 December 2006

J. B. Blake, T. Mulligan, J. E. Mazur

Space Sciences Department, Space Sciences Applications Laboratory,
The Aerospace Corporation, Los Angeles, USA

Abstract – **We observed the extraordinary energetic solar particle events of 13-16 December with several spacecraft including Polar, two HEO satellites, and SAMPEX. Our observations were supported by observations by ACE, STEREO and GOES satellites as well as neutron monitors. A large, prompt ESP event began around 02:50 UT on 13th December 2006. The event included a GLE, unusual for this time in the solar cycle. Prior to the onset the two HEO satellites showed an electron precursor several minutes before the onset of the energetic protons. The electron spectrum was relatively soft with detectable electrons only of a few hundred keV and less, suggestive of electrons resulting from solar neutron decay. The energetic proton fluxes decayed away smoothly until midday on 14th December around the time of shock arrival at 13:55 UT. The temporal profile of the energetic protons differed substantially at GOES in geostationary orbit from the profiles observed upstream of the Earth at L1, and at Polar, near the Earth at 9RE, but on open field lines over the southern polar cap. We will show these detailed comparisons and comment on their significance in such a late solar-cycle event.**

Solar events seen in the 10 − 20 GeV energy range by the Karlsruhe Muon Telescope

I. Braun[1], J. Engler[2], J.R.Horandel[1], and J. Milke[2]

[1] *Institut fur Experimentelle Kernphysik, Universitat Karlsruhe, D-76021 Karlsruhe, Germany*
[2] *Institut fur Kernphysik, Forschungszentrum Karlsruhe, D-76021 Karlsruhe, Germany*

Abstract— **Since 1993, a muon telescope located at Forschungszentrum Karlsruhe (Karlsruhe Muon Telescope) has been recording the flux of single muons mostly originating from primary cosmic-ray protons with dominant energies in the 10 −20 GeV range. The data are used to investigate the influence of solar effects on the flux of cosmic-rays measured at Earth. Non-periodic events like Forbush decreases and Ground Level Enhancements are detected in the registered muon flux. A selection of recent events will be presented and compared to data from the Jungfraujoch neutron monitor. The data of the Karlsruhe Muon Telescope help to extend the knowledge about Forbush decreases and Ground Level Enhancements to energies beyond the neutron monitor regime.**

Key Words— **cosmic rays, muon telescope, heliosphere, Forbush decrease, solar energetic event, ground level enhancement PACS: 94.20.wq, 96.50.S-, 96.50.Xy, 96.60.Q-, 98.70.Sa**

I. INTRODUCTION

The association of solar activity with the cosmic-ray intensity has been studied for various observed effects including Forbush decreases [1], i.e. a rapid decrease in the observed galactic cosmic-ray intensity, and Ground Level Enhancements, which are connected to large solar flares. They can be related to magnetic disturbances in the heliosphere that create transient cosmic-ray intensity variations [2]. From the observation of such events with different experiments, an energy dependent description can be obtained. The heliospheric influence is mostly pronounced for primary particles with low rigidity and has been studied mainly using data of the worldwide neutron monitor network [3]. With its unique median primary energy of 40 GeV for protons, the Karl-sruhe Muon Telescope fills the energy gap between neutron monitors (less than ≈ 33 GeV) and other muon telescopes (≈ 53 − 119 GV rigidity). In the following, we report on the detection of Forbush decreases and the investigation of Ground Level Enhancements with the Karlsruhe Muon Telescope.

II. EXPERIMENTALSET-UP

The flux of single muons from the zenith region has been recorded continuously since 1993 with the Karlsruhe Muon Telescope located at Forschungszentrum Karlsruhe, Germany (49.094◦N, 8.431◦E, 120 m a.s.l). The set-up is sketched in Fig. 1, details are given by [4]. Two double layers of scintillation counters are arranged on top of each other, separated by a 16 cm lead absorber, forming a ”tower”. Each scintillation counter comprises a scintillator (NE 102) with the dimensions 0.6m×0.25m×0.02 m, read out by a photomultiplier via an adiabatic light guide. A double layer is formed by two scintillation counters arranged parallel to each other and two counters oriented perpendicular to them, forming a 2 × 2 detector matrix. The lead absorber selects muons with energies larger than 0.8 GeV. Two such towers with a separation of 1.8 m are operated with a veto trigger logic selecting vertical particles and rejecting showers in which more than one particle hits the detector, thus suppressing the hadronic background to about 0.8% of the events [5]. The muon detector is operated in a climatized room at a stable temperature. The towers of the instrument can be used to calibrate up to 32 liquid ionization chambers for the KASCADE hadron calorimeter, their data are not included in the present analysis.

This analysis includes 80 017 h of data between October 1993 and November 2006.

From simulations with CORSIKA [6] and GEANT 3.21 [7], properties of the primary particles were investigated. The simulations include the physics processes in the atmosphere and the propagation through the building surrounding the

detector, as well as the trigger conditions of the muon telescope.

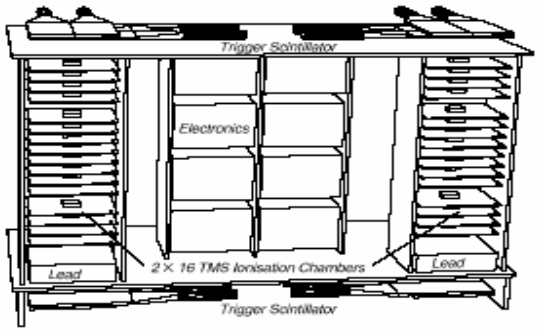

Fig. 1. Sketch of the muon telescope. It consists of two ”towers”,each comprising two double layers of scintillation counters (arranged in a 2 × 2 matrix), separated by a 16 cm lead absorber.

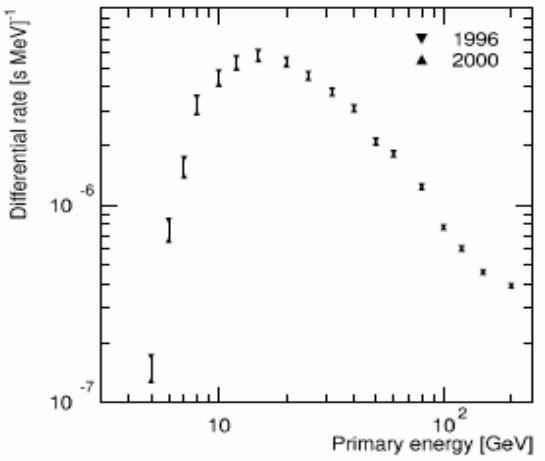

Fig. 2. Simulated differential trigger rate of the Karlsruhe Muon Telescope as a function of primary energy for solar minimum (1996) and maximum (2000)

It turns out that the muons originate mostly from cosmic-ray protons, of which 95% have zenith angles smaller than 18◦.

The differential energy spectrum of primary protons, triggering the telescope was derived for parameterized primary spectra in different solar activity states [8], taking into account modulation parameters according to [9]. The differential trigger rate obtained is presented in Fig. 2. The maximum occurs at primary energies of about 15 GeV. The expected counting rate difference between the two activity states is 2.5%. The median energy EMof a detector is defined so that one half of the detected events originate from primary particles below (or above) EM.The median energy of the Karlsruhe Muon Telescope for both simulated spectra is 40 GeV.

III. Atmospheric Corrections

Muons loose energy and decay on the way from their production site in the atmosphere to the detector, yielding a dependence of the detected rate on the height of the production layer and the amount of material traversed above the detector. Corrections were applied to the recorded muon rate using the atmospheric pressure measured at the Forschungszentrum Karlsruhe. In addition, balloon ascends at noon and midnight conducted by the German weather service (DWD) in Stuttgart provide the heights of specific pressure layers including the 150 g/cm^2 layer (≈ 13.6 km) which is close to the typical production layer of muons triggering the telescope at 130 g/cm2,as determined from simulations. For each year, the muon rate was iteratively corrected for a pressure of 1013 hPa and a nominal height of the 150 g/cm^2 layer of 13.6 km, yielding correction parameters of d(Rate)/dp=(−0.12 ± 0.04) %/hPa and d(Rate)/dh= (−3.8 ± 1.2) %/km. This correction eliminates rate variations from the data-set, which are caused by (periodically) changing atmospheric conditions. For a consistency check, a rough estimate of the muon lifetime can be deduced from these values, assuming that all muons are produced with the same energy at the same atmospheric depth. The obtained lifetime of 2 ± 0.5 μs is consistent with the literature value.

Table 1

Very significant Forbush decreases detected since 1998. A sequential number and the dates are listed. Significances are pre-trials, the amplitudes of the Karlsruhe Muon Telescope refer to the hourly data (not smoothed). The fifth column gives the amplitudes detected by the Jungfraujoch neutron monitor. The last column gives an estimate for the energy dependence of the detected amplitudes, expressed in

#	date	significance(μ)	amplitude(μ) [%]	amplitude(n) [%]	amplitude change [% / energy decade]
1	1998/08/26	6.1σ	3.6	7.1	5.7
2	1998/09/25	6.2σ	3.7	5.7	11.5
3	1999/01/23	4.7σ	3.3	7.0	2.1
4	2000/07/15	8.3σ	4.8	10.5	3.5
5	2000/11/10	6.1σ	3.5	1.5	10.2
6	2001/08/03	8.7σ	4.9	1.7	14.8
7	2003/10/30	8.4σ	5.2	17.0	-10.9
8	2004/11/10	5.0σ	2.9	6.6	7.6
9	2005/01/19	10.6σ	6.1	13.2	0.02
10	2005/09/11	5.5σ	3.2	10.4	-3.9

IV. FORBUSH DECREASES

The muon data were searched for days where the average rate was significantly lower than that of a background region. The background level was determined from hourly count rates within two times two weeks (14 d before the test region and 14 d afterwards), separated by three days from the tested day.

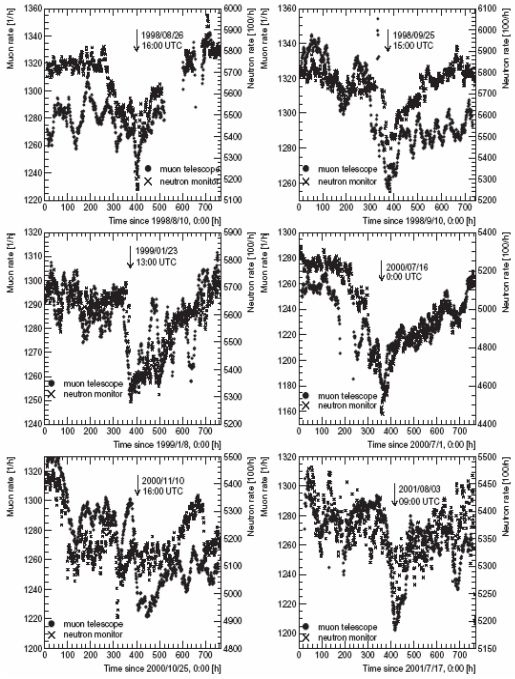

Fig. 3. Count rates of the Karlsruhe Muon Telescope and the Jungfraujoch neutron monitor for several Forbush decreases. The corresponding dates and times are indicated in the figure. Jungfraujoch data scaled by a factor 100, muon counting rate smoothed over a period of 24 hours.

The significances for each day were computed according to [10]. Trial factors were not taken into account. The Karlsruhe Muon Telescope has detected several significant structures. The strongest Forbush decreases in the years from 1998 to 2006 are compiled in Table 1. Shown are a sequential number, the date, the significance and the amplitude at the minimum rate for the muon telescope (based on hourly rates) as well as the amplitude detected by the Jungfraujoch neutron monitor.

The latter has an effective vertical cutoff rigidity of 4.49 GV [11]. It was chosen for this comparison because of its geographic proximity to Karlsruhe.

The detected events compared to the neutron monitor counting rate are depicted in Figs. 3 and 4. To display their development, the muon telescope rates are smoothed by a running mean over 24 hours. Attention should be paid to the different scales for the muon rate (lefthand scale) and for the neutron monitor rate (right-hand scale).

It is worth to point out that the rate development observed at 4.5 GV (Jungfraujoch) and for the muon telescope (15 GeV) are quite similar, despite of their different energy thresholds. This illustrates that Forbush decreases are clearly detectable with a muon detector with 15 GeV peak energy. Forbush decreases were detected already with the GRAND muon detector [12] at 10 GeV peak energy. With the Karlsruhe Muon Telescope we push the detection towards higher energies.

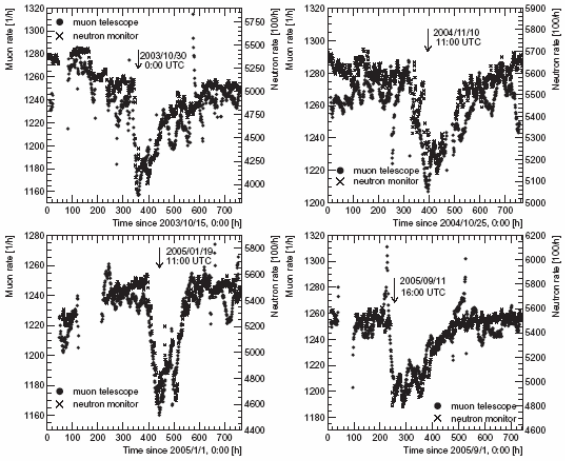

Fig. 4. Count rates of the Karlsruhe Muon Telescope and the Jungfraujoch neutron monitor for several Forbush decreases. The corresponding dates and times are indicated in the figure. Jungfraujoch data scaled by a factor 100, muon counting rate smoothed over a period of 24 hours.

Many structures in these Forbush decreases are visible at both energies. A closer look reveals that for events 7, 8, 9, and 10 (close to the solar minimum) the rates of both detectors follow each other extremely closely. On the other hand, for events 1, 2, 4, and 6 there are systematic differences between the two energies in the behavior before or after the Forbush decrease. For the Forbush decrease in the year of the solar maximum (# 5) the strongest differences between the two rates are observed. It appears as during solar maximum there are significant differences between the fluxes observed at 4.5 GV and 15 GeV, while the fluxes are correlated well during periods of low solar activity.

To study the energy dependence of the amplitudes of a Forbush decrease, the amplitudes of the muon telescope and change per decade in energy has been calculated. The latter is listed in the last column of Table 1. To investigate a possible dependence on the solar activity, the amplitude change per energy decade is depicted as function of the international sunspot number (taken from [13]) in Fig. 5. No

clear correlation between the two quantities can be inferred from the figure. Thus, earlier claims by [14] cannot be confirmed. A study of the energy dependence of the recovery time of the Forbush decreases is published elsewhere [15].

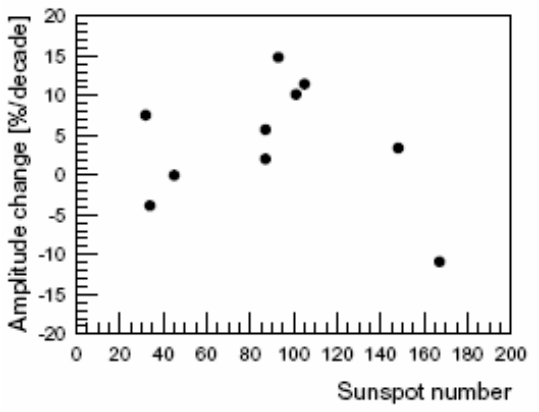

Fig. 5. Energy dependence of the amplitude of the Forbush decreases registered by the Karlsruhe Muon Telescope and the Jungfraujoch neutron monitor (expressed as change in amplitude per energy decade) as function of the sunspot number.

V. GROUND LEVEL ENHANCEMENTS

Due to their relatively short duration, Ground Level Enhancements (GLEs) are difficult to detect with the Karlsruhe Muon Telescope. Therefore, the data were scanned for correlations with all events marked in the GLE database, as provided by the Bartol group [16] and listed in Table 2. The muon flux was recorded for events marked with an ”a”. During events marked with ”i” the muon telescope was not active. The hourly rates for GLEs 56 to 67 as registered by the Karlsruhe Muon Telescope and the Jungfraujoch neutron monitor are depicted in Fig. 6. Jungfraujoch data are scaled by a factor 100 and the muon counting rates are smoothed over a period of three hours.

For GLE 57, no significant excess was observed in the muon counting rate. However, about seven hours before the Ground Level Enhancement a small peak is visible in the registered muon flux. For GLE 58, no significant muon excess has been observed.

GLE 59, the ”Bastille day event” on July 14, 2000 has been registered by many detectors, including neutron monitors and space crafts [16].

In particular, the event could be measured for primary cosmic rays with GeV energies [17]. It has been detected by the GRAND muon detector (10 GeV most probable energy) [18], by the L3+C

detector at CERN (≈ 40 GeV primary energy) [19], and also by the Karlsruhe Muon Telescope. An excess in the muon counting rate can be recognized a few hours before the event.

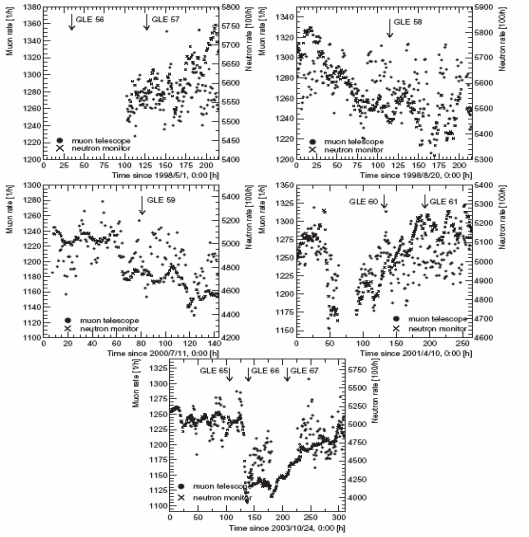

Fig. 6. Hourly count rates registered by the Karlsruhe Muon Telescope and the Jungfraujoch neutron monitor for several Ground Level Enhancements, as marked in the figures, see also Table 2. Jungfraujoch data are scaled by factor 100, muon counting rates smoothed over a period of three hours.

Table 2

Solar Ground Level Enhancements according to the Bartol group database [16]. The last column denotes the status of the Karlsruhe Muon Telescope: a: active, i: inactive, +: GLE detected.

GLE number	event date	status
55	1997/11/06	i
56	1998/05/02	i
57	1998/05/06	a (+)
58	1998/08/24	a
59	2000/07/14	a +
60	2001/04/15	a +
61	2001/04/18	a
62	2001/11/04	i
63	2001/12/26	i
64	2002/08/24	i
65	2003/10/28	i
66	2003/10/29	a
67	2003/11/02	i
68	2005/01/17	a
69	2005/01/20	a

A muon count excess can be recognized at the time of GLE 60, while no signal is observed from GLE

61. It should also be noted that the Jungfraujoch neutron monitor detects GLE 60 with a large signal. On the other hand, the muon flux is only slightly increased at the time of the event.

Some of the greatest bursts in the 23rd solar cycle occurred on 28/29 October and 2 November 2003 (GLE 65 − 67). They are extensively discussed in the literature, [20], [21], [22], [23]. Unfortunately, the muon telescope was not active

during GLEs 65 and 67. At the time of GLE 66, no significant signal is seen in the muon count rate. However, about one day before GLEs 65 and 66 a peak can be recognized in the registered muon flux. It is not clear if these increases are statistically significant, since there are gaps in the observing time. Thus, it is not obvious if the detected rate variations are correlated with the Ground Level Enhancements. Unsmoothed hourly count rates of the Karlsruhe Muon Telescope compared to the Jungfraujoch neutron monitor data during the Forbush Decrease in January 2005 are depicted in Fig. 7.

For comparison the reader may refer to Fig. 4 for the smoothed counting rate of the same event. In the interval shown, two Ground Level Enhancements (GLE 68 and 69) have been observed, the corresponding times are marked in the figure. For GLE 69 it is assumed that protons were accelerated in a process or processes directly related to a solar flare [24]. The right-hand panel of Fig. 7 shows the region around GLE 69. No indication for a significant increase in the muon rate associated with GLE 69 can be seen in the figure.

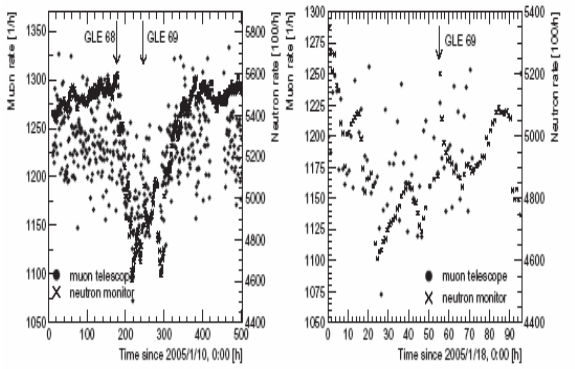

Fig. 7. Count rates of the Karlsruhe Muon Telescope and the Jungfraujoch neutron monitor for the Forbush Decrease on January 19th, 2005. Jungfraujoch data scaled by a factor 100, hourly (unsmoothed) muon counting rate. The arrows indicate the positions of GLEs 68 and 69. Right:zoom into the region around GLE 69.

VI. CONCLUSIONS

The Karlsruhe Muon Telescope provides information about e□ects of solar activity on the cosmic-ray flux observed at Earth since 1993. The recorded muon flux corresponds to 15 GeV peak energy (40 GeV median energy) for primary protons. Several strong Forbush decreases, i.e. a rapid decrease in the observed galactic cosmic-ray intensity, could be measured with the muon telescope, indicating that these effects can be seen at energies exceeding the typical energies of neutron monitors. Comparing the observed amplitudes to the Jungfraujoch neutron monitor data, the spectral in dex of the events has been estimated. No dependence of the spectral index on the sunspot number has been found. However, there are significant differences in the timely development of the rates observed at 4.5 GV and 15 GeV for different states of solar activity. For Forbush decreases during solar maximum, the rates of the muon telescope and the neutron monitor behave quite different, while they are well correlated for periods of low solar activity. It has been investigated whether Ground Level Enhancements, which are connected to large solar flares, observed between 1997 and 2005 can be detected in the registered muon flux. For the strong Ground Level Enhancements 59 and 60 a clear signal can be seen in the muon count rate at the times of the events. This provides direct evidence for particles being accelerated to energies as high as 15 GeV during solar flares. Indirect evidence has been obtained previously by observations of lines in the gamma ray spectrum measured during solar flares [25], [26]. On the other hand, no signal has been detected for the GLEs 58, 61, 66, 68, and 69. If the underlying physics processes of all Ground Level Enhancements are the same, this means that the energy spectra of 7 GLEs 59 and 60 difer from the spectra of the other GLEs. Taking the peak energy of the Karlsruhe Muon Telescope as characteristic energy, we can set an upper limit of ≈ 15 GeV to the maximum energy achieved during events 58, 61, 66, 68, and 69.

ACKNOWLEDGMENT

We are grateful to Mrs. Heike Bolz for her enthusiastic efforts in continuously operating the Karlsruhe Muon Telescope and to J¨urgen Wochele for his help during the construction of the detector. We thank the team operating the Jungfraujoch neutron monitor for making their data publicly available. We acknowledge the help of the Deutscher Wetter-Dienst (DWD) and the Institut f¨ur Meteorologie und Klimaforschung of Forschungszentrum Karlsruhe providing atmospheric data. We thank Jan Kuijpers for critically reading the manuscript.

REFERENCES

[1] S. E. Forbush, Worldwide cosmic ray variations, J. Geophys. Res., 59, 525 -542, 1954

[2] M-B. Kallenrode, Current views on impulsive and gradual solar energetic particle events, J. Phys. G: Nucl. Part. Phys., 29, 956 -981, 2003

[3] J.A. Simpson, The cosmic ray nucleonic component: the invention and uses of the neutron monitor, Space Sci. Rev. 93, 11 -32, 2000 J.

[4] Engler, F. Fessler, J.R. H¨orandel et al., A warm-liquid calorimeter for cosmic-ray hadrons, Nuclear Instruments and Methods A 427, 528 -542, 1999

[5] J.R. Horandel, Kalibration von TMS-Ionisationskammern mit Myonen der H¨ohenstrahlung und Messung des Myonflusses, Report KfK 5320, Kernforschungszentrum Karlsruhe (1994) ISSN 0303-4003

[6] Heck, D., Knapp, J., Capdevielle, J., et al., 1998. CORSIKA: a Monte Carlo code to simulate extensive air showers. Report FZKA 6019, Forschungszentrum Karlsruhe.

[7] GEANT 3.15, Detector Description and Simulation Tool, CERN Program Library Long Writeup W5013, CERN, 1993

[8] I.H. Urch and L.J. Gleason, Galactic cosmic ray modulation from 1965-1970, Astronom. Space Sci., 17(2), 426 -446, 1972

[9] I.G.Usoskin, G. A. Kovaltsov, K. Mursula, et al., Long-term cosmic ray modulation by heliospheric parameters: nonlinear relations, Proceedings 28th International Cosmic Ray Conference 3803 -3806, 2003

[10] T.-P. Li and Y.-Q. Ma, Analysis methods for results in gamma-ray astronomy, Astrophysical Journal, 272, 317 -324, 1983

[11] Bern Cosmic Ray Group, Physikalisches Institut, University of Bern http://cosray.unibe.ch.

[12] J. Poirier, M. Herrera, P.Hemphill, et al., A study of the Forbush decrease event of September 11, 2005 with GRAND Proceedings 30th International Cosmic Ray Conference, Merida, 2007

[13] SIDC: Sunspot Index Data Center, Royal Observatory of Belgium, http://sidc.oma.be

[14] S.O. Ifedili, Spacecraft measurement of forbush decreases in the cosmic radiation, Solar Physics 168, 195 -203, 1996

[15] I.G.Usoskin, I. Braun, O.G. Gladysheva, et al., Forbush decreases of cosmic rays: Energy dependence of the recovery phase, submitted to Journal of Geophysical Research, 2007

[16] J.W. Bieber, W. Dr¨oge, P.A. Evenson et al., Energetic Particle Observations during the 2000 July 14 solar event, Astrophysical Journal 567, 622 -634, 2006
Bartol Research Institute neutron monitor program, http://neutronm.bartol.udel.edu.

[17] R. Wang and J. Wang, Spectra and solar energetic protons over 20 GeV in Bastille Day event, Astroparticle Physics 25, 41 -46, 2006

[18] J. Poirier, C. D'Andrea, M. Dunford, A project GRAND study of the GLE of July 14, 2000, Proceedings 27th International Cosmic Ray Conference, Hamburg, 2001

[19] L3 Collaboration, The solar flare of the 14th of July 2000 (L3+C detector results), Astronomy and Astrophysics 456, 351 -357, 2006

[20] K. Watanabe, M. Gros, P.H. Stoker et al., Solar Neutron Events of 2003 OctoberNovember, Astrophysical Journal 636, 1135 -1144, 2006

[21] Y. Liu and K. Hayashi, The 2003 October-November fast halo coronal mass ejections and the large-scale magnetic field structures, Astrophysical Journal 640, 1135 -1141, 2006

[22] G.J. Hurford, S. Krucker, R.P. Lin et al., Gamma-ray imaging of the 2003 October/November solar flares, Astrophysical Journal 644, L93-96, 2006

[23] E. Eroshenko, A. Belov, H. Mavromichalaki et al., Cosmic-ray variations during the two greatest bursts of solar activity in the 23rd solar circle, Solar Physics 224, 345 358, 2004

[24] G.M. Simnett, The timing of relativistic proton acceleration in the 20 January 2005 flare, Astronomy and Astrophysics 445, 715 -724, 2006

[25] E. Rieger, Solar flares: high-energy radiation and particles, Solar Physics 121, 323 -345, 1989.

[26] L. Fletcher, Energetic particles in the solar atmosphere, Proc. 10th European Solar Physics Meeting, Prague, Czech Republic, ESA SP-506, 223 -232, 2002

The influence of Solar Extreme Events of December 2006 on near-Earth space environment at low altitudes

Myagkova I.N., Panasyuk M.I, Lazutin L.L., Muravieva E.A., Starostin L.I., Ivanova T.A., Pavlov N. N., Rubinshtein I.A., Vedenkin N. N., Vlasova N.A.

Lomonosov Moscow State University Skobeltsyn Institute of Nuclear Physics, 1- 2, Leninskie Gory, Moscow, 119992[E-mail: irina@srd.sinp.msu.ru]

***Abstract*— Two main aims of russian scientific and education project "MSU-250" were declared: monitoring of the energetic particles dynamics in the near-Earth's space after the solar events and during quiet time and educational activity on the basis of experimental data obtained from the small spacecrafts. In the frames of this project the microsatellite "Universitetskiy-Tatiana" was launched on January 20, 2005. This satellite has operated during time period of Solar Extreme Events 2006 - from December, 5 to December, 16, and we have the opportunity to analyze them. The "Universitetskiy-Tatiana" microsatellite orbit permits one to measure both solar energetic particle dynamics and variations of the boundary of solar particle penetration as well as relativistic and sub-relativistic electrons of ERB during and after magnetic storms. Both relativistic electrons of the Earth's outer radiation and solar energetic particles form an important source of radiation damage in near-Earth space. Therefore, the presented experimental results demonstrate the possibilities of successful application of small educational spacecrafts both in the scientific and educational programs.**

***Key Words*— flares, solar cosmic rays, radiation belts of the Earth.**

I. INTRODUCTION

Now it is well known that different space weather effects can range from damage of space missions to the disruption of power grids on the Earth. The most important part of the radiation damage is caused by solar energetic particles (SEPs) - protons and electrons. These energetic charged particles, produced in the solar flares, reached the orbit of the Earth after the interaction with the interplanetary medium and coronal mass ejection (CME). Direct measurements of SEP penetration boundary variations at low altitudes are very important for estimations of the local space weather conditions, e.g. [1].

It is clear that near-Earth's space environment monitoring al low altitudes should be continued even during the minimum of Solar Activity (SA) cycle because solar extreme events sometimes take part in the minima of SA. The variations of the relativistic electrons in the Earth's radiation belts (ERB) also can play the important role in the near-Earth's environment, especially during and after the geomagnetic storms (e.g. [2], [3]). Relativistic electrons of ERB (REB) cause volumetric ionization in the microcircuits of spacecraft, so the monitoring of relativistic electron flux dynamics at low altitudes is important also. So low-altitude polar satellites (in particular, small educational satellites) can be useful for such measurements.

II. EXPERIMENT

Microsatellite "Universitetskiy-Tatiana" was launched into a circular polar orbit with an inclination of ~83^o and with an initial altitude of about 1000 km on 2005, January, 20 (during one of the most powerful solar flare of 2005). It operated until 2007, March 08. During 2006, December its altitude varied in the range 910-980 km. It was made in the frames of Space Scientific and Education project of Lomonosov Moscow State University "MSU-250".

This project was timed to its 250-th anniversary (Internet site of this project - http://cosmos.msu.ru/eng/). The main educational task of this project is the development of scientific potential of young scientists in Russia and other countries. The main scientific tasks of this experiment was monitoring of the radiation

enviroment in the near Earth space [4]. In this work we have used the data on protons with energies 2-14, 7-16, 15-40 and 40-100 MeV and electrons with energies >70 keV, 300-600 keV, 700-900 keV and >3.5 MeV, measured by two semiconductor detectors and scintillation detector [4]. Due to the low polar orbit of the satellite SEP fluxes were measured on board "Universitetskiy-Tatiana" microsatellite only in the areas of open magnetic field lines (in the north and south polar caps) during 15-20 minute intervals every ~ 50-55 minutes. The location of the solar particle boundary penetration can be measured during each of four crossing of polar caps boundaries – as well as relativistic and sub-relativistic electrons of the Earth's outer radiation belt.

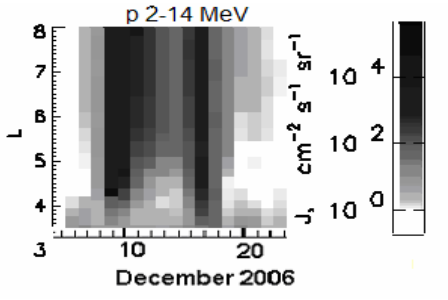

Fig. 1. Proton (2-14 MeV) flux variation at altitude 950 km in December 2006 according to "Universitetskiy-Tatiana" data.

III. Solar Extreme Events in 2006, December

Flare activity observing in the beginning of the winter of 2006 was rather unusual for SA minimum period. In spite of relatively low value of sunspot number (59 and less, http://www.swpc.noaa.gov/ftpdir/indices/old_indices/2006_DSD.txt) four solar flares of X-class in Soft X-Ray (SXR) emission were observed during the first half of December 2006. Three of them were accompanied by the Coronal Mass Ejection (CME). Parameters of these flares (data, times of start, maximum and finish, coordinates, class in SXR, optical ball) and accompanying CMEs (linear speed and Position Angle (PA) measured from Solar North in degrees) are presented in the Table 1 according with the data of sec.noaa.gov and on http://cdaw.gsfc.nasa.gov/CME_list.

Table 1

Flare of X-class observed in AR NOAA0930 in December 2006

Date	Flare time, UT (start-maximum-finish)	Flare coord.	SXR Class/ Ball	CME start time, UT	V_CME, km/s	PA, deg
Dec. 05	10:18-10:35-10:45	S07E68	X9.0/2N	-	-	-
Dec. 06	18:29-18:47-19:00	S05E64	X6.5/3B	20:12:05	-	360 (Halo)
Dec. 13	02:14-02:40-02:57	S06W23	X3.4/4B	02:54:04	1774	360 (Halo)
Dec. 14	21:07-22:15-22:26	S06W46	X1.5/ -	22:30:04	1042	360 (Halo)

Produced in these flares solar particles after their interaction with the interplanetary medium were observed in near-Earth space by different scientific missions. The recent experimental results and theoretical studies show that interplanetary shocks driven by CMEs play a major role in accelerating SEPs (e.g. [5], [6]).

IV. Solar Particles Dynamics - Observations and Data Analysis

It is clear that solar energetic particles (both protons and electrons) are very important source of radiation damage in the near-Earth space. As an example of obtained experimental data the proton flux (2-14 MeV) variation at altitude about 950 km during December 2006 for different L-shells (from

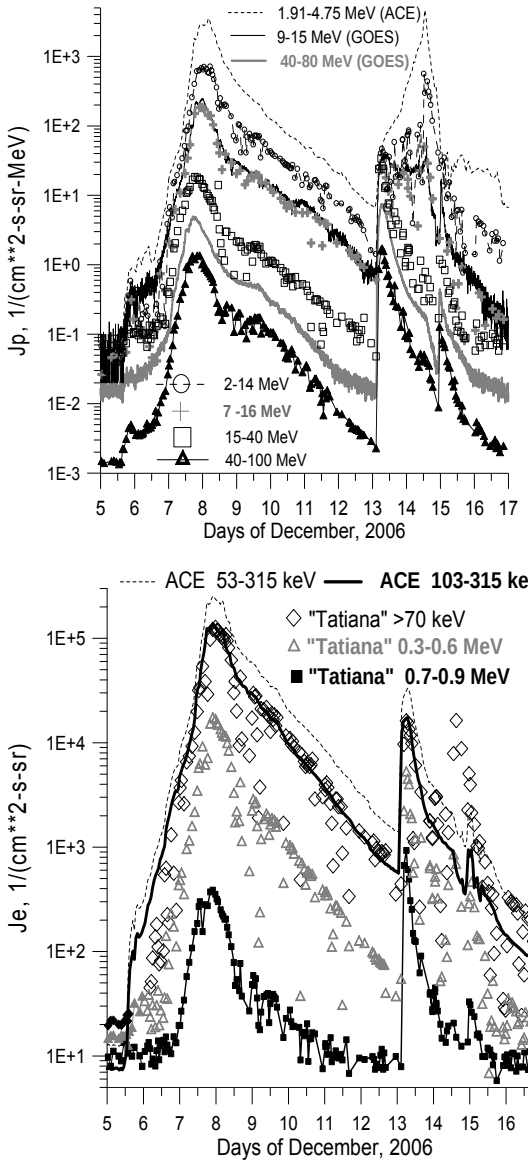

Fig. 2. SEP (1- protons, 2 – electrons) variations from 05 to 16 December 2006 in different experiments.

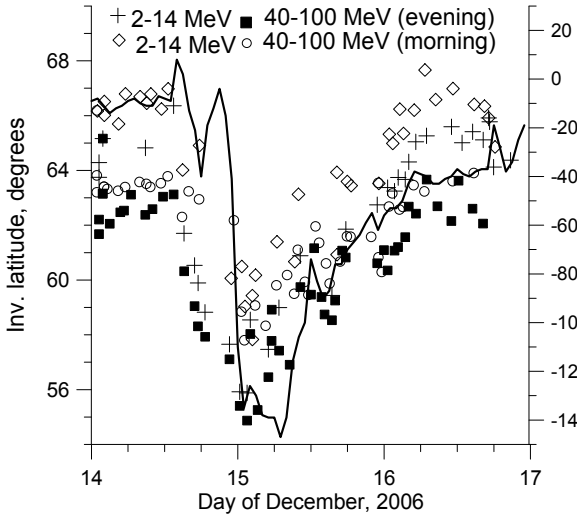

Fig. 3. SEP penetration boundary variations during the geomagnetic storm 2006, December 14-15. Dst-variation is shown by solid line.

3 to 8) measured on board "Universitetskiy-Tatiana" satellite are shown in Figure 1. We can see that powerful enhancements were observed not only at high latitudes but al L=3.5-4 also.

Figure 2 presents the time profiles of solar proton and electron flux measured on board four different satellites during the time period December, 5-16 – "Universitetskiy-Tatiana", ACE and GOES. We have compared solar particle fluxes measured in similar energy ranges and obtained their good agreement.

Four X-class flares occurring during the first half of December 2006 have led to only three powerful SEP events.

The spectra of the solar particles (both protons and electrons) observed after the flare 13.12.2006 and 14.12.2006 were significantly harder than after 06.12.2006 one, especially before the CME's arriving. In fact, the significant proton enhancement after the last flare was clearly seen only for particles with the energy >15 MeV. The fast arriving of more energetic particles can be explained due to central and west position (W23 and W46) of AR 0930 in the moments of these flares.

V. SOLAR PROTON PENETRATION BOUNDARY VARIATIONS

The low polar orbit of the satellite permits us to measure not only the variations of the solar particle flux in the south and north polar caps every ~50-55 minutes but the location of SCR penetration boundary into the Earth's magnetosphere during the geomagnetic storms.

The experiment on board "Universitetskiy-Tatiana" microsatellite (due to its low Earth polar orbit) has demonstrated that for the estimation of possible SEP damage both the intensity of energetic solar particles and the data about the boundaries of solar particle penetration in the Earth's magnetosphere are very important. High energy solar particle penetration in the polar caps during the main phase of magnetic storms is one of the

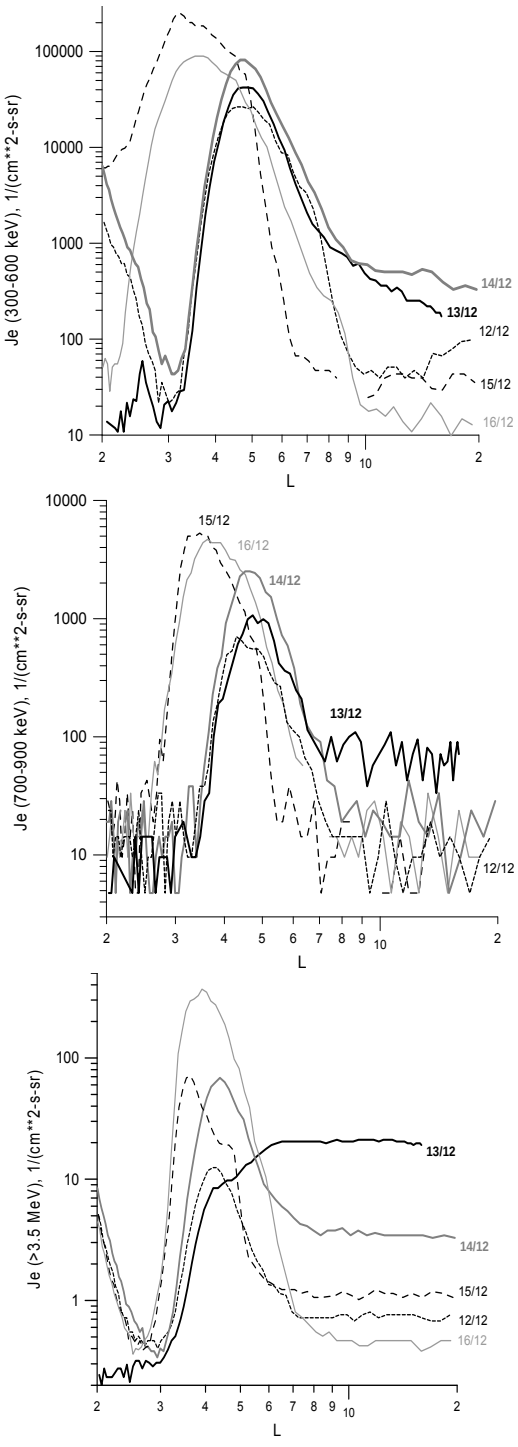

Fig. 5. Comparison of the profiles of the radiation belt particle fluxes: electrons with energies of 300-600 keV, 700-900 keV and >3.5 MeV during 12-16 December 2006.

important sources of radiation danger in the near-Earth space, especially for low-altitude satellites. The size of the solar particle penetration area depends on proton energy and on geomagnetic conditions.

After flares 5 and 6 December there were no observed significant magnetic storms (the maximal measured Dst was –34 nT near noon of 06.12.2006) and we could not measure SEP penetration boundaries in the Earth magnetosphere. The influence of the flares 13 and 14 December on the Earth's magnetosphere was more impressive due to two CME (Halo). In Figure 3 we present the variations observed in the SEP penetration boundary measured by "Universitetskiy-Tatiana" (protons with energies 2-14 and 40-100 MeV) during magnetic storms occurring in the time period 2006, December, 14 -15. Different criteria for the analysis of the penetration boundary position exist.

As was done in [7], in this work we use the next criterion for the SEP penetration boundary: the boundary of proton penetration was determined for each polar cap region crossing when the intensity of the SEP flux was two times smaller than the maximal flux of SEP in this polar cap. The values of penetration boundary obtained during the late morning (MLT ~ 7-10 h) magnetic local time (MLT) are marked as open diamonds and circles, during the late evening MLT (MLT ~ 19-22 h) as plusses and squares in Figure 3. For comparison, the time variation of the Dst-index is also shown in Figure 3. We can see that the location of SEP penetration boundary in the Earth's magnetosphere during the main phase of the magnetic storm was about 55 degrees in the late evening MLT sector and about 57 degrees in the late morning one, and the penetration of 40-100 MeV protons deeper than of 2-14 MeV ones due to their highest rigidity. The evening sector the SEP penetration was deeper, like for November 2001, October-November 2003 and November 2004 solar events, as have been published in earlier our papers, e.g. [7], [8]. Variations of SEP penetration boundaries are connected with the growing of the polar cap size during the main phase of geomagnetic storms. The deeper penetration of solar energetic particles in the evening sector could be connected with the fact that magnetic field of the Earth has the minimal value for late evening MLT - ~22 h. It is possible that it allows to solar particles to penetrate deeper in the Earth's magnetosphere.

VI. OUTER ELECTRON RADIATION BELT VARIATIONS

Dynamics of the outer radiation of the Earth, especially of the relativistic electrons is one of the most important physical processes which influence on the near-Earth's environment. The most dramatic
variations of electron ERB take place during magnetic storms.

The figures 4 and 5 show the relativistic and sub-relativistic electron dynamics in the outer radiation belt during December 2006 observed by board "Universitetskiy-Tatiana" microsatellite. At the parameters of the orbit, the instruments on board "Universitetskiy-Tatiana" microsatellite could detect trapped radiation in the region of the South Atlantic magnetic anomaly. We analyzed the variations of the trapped electrons with the energies 300-600, 700-900 keV and >3.5 MeV. We have analyzed the radiation belt variations during two time periods – 5-10.12.2006, near the weak magnetic disturbance near the noon 06.12.2006 (Dst=-34 nT) caused by the first CME (see Table 1) and 12-16/12/06, during and after the magnetic storm with Dst=-144 nT which had the main phase in midnight from 14 to 15 December, 2006. We should noticed, that used electron channel besides electrons >3.5 MeV detected the protons with the energies some tens MeV. This fact explained its high counting rate in polar caps, but in the areas of outer ERB, where the protons of such energies are absent, the measurements of these channels can be taken into account.Two panels of figure 6 show the relativistic electron (300-600 keV and >3.5 MeV) flux dynamics in the outer radiation belt during December 2006 and January 2007. The electron flux is shown by grey-scale color. The X and Y axes show the day and the L-shell value respectively. We can see that the significant enhancements of relativistic electrons (> 3.5 MeV) in the outer ERB, which was caused by solar extreme events in December 2006, were observed during this long time period.

The presented data indicate that the radiation belt dynamics during the December 2006 storms was rather similar to such a dynamics during the earlier strong storms, e.g. [1], [8]-[11] namely:

(1) the intensity of the flux of relativistic electrons decreased during the magnetic storm main phase, even for weak geomagnetic disturbances like 06.12.2006;

(2) during the recovery phase the intensity of the electron fluxes from the Earth's outer radiation belt sharply increased, the electron belt significantly widened, and the belt maximum shifted to smaller L.

In fact, we observed the strong long-time variations of the relativistic and sub-relativistic electrons in the outer ERB after the geomagnetic storm 15 December at low (950 km) altitudes

measured by “Universitetskiy-Tatiana”. Instead of the weak belt with the boundaries 4-5 L, since 16 December and up to the end of the year 2006 we could detected the strong belt of relativistic electrons from L=3 to L-5.5-6 with the maximum near L=4.

The most impressive variations of 300-600 and 700-900 keV electron belts was observed 15.12.2006, when its intensity increased in the half of order and the maximum shifted from L=5 to L=3.2.-3.5. The strong variations of IMF parameters (B, Bz, solar wind speed and plasma density) took place in the midnight 14-15 December.

We have proposed that in some similar cases observed relativistic electron flux variations can be explained by particle acceleration due to the radial diffusion and their scattering in the loss cone due to interactions with the whistler mode of electromagnetic waves [10].

It is possible, that electron flux increases can be caused by diffusion on the cyclotron emission of the enhanced flux of some tens keV proton (electrons can be in a parasitic resonance with the protons of much smaller energy).

Some experiments permit to suggest that the relativistic electrons are scattered into the loss cone by EMIC waves. In the anisotropic zone the RC protons are unstable and can generate EMIC waves [12]. It is in the agreement with the theory that suggested that ion cyclotron waves generated by the unstable proton population can precipitate relativistic electrons in the > 1 MeV range [13]. The important results of outer ERB studies were published in [2]. They found that above a half of magnetic storms led to increase of REB flux increase, however, for the other cases both decreases and absence of significant variations were still observed.

In the paper [14] have been shown that the solar wind speed is the leading controlling parameter on the variations of daily averaged energetic electron fluxes at geosynchronous orbit over a wide energy range: 50 keV to 6.0 MeV. Electrons with energy >1 MeV respond more to the solar wind speed but all the electrons in this energy range are well correlated with solar wind speed. Two possible interpretations for the enhancements of higher energy (>1 MeV) can be used: inward radial diffusion or in situ heating by ULF and VLF waves. However, the relative importance of these two mechanisms is still unknown.

Such electrons are sometimes named "killer electrons" as they are very dangerous to electronic devices, in particular the microcircuits that are used in spacecraft. Relativistic electrons of the outer ERB produce volumetric ionization in microcircuits of spacecrafts and breakdown their normal operation.

Therefore, the measurement of relativistic electron dynamics has both practical and scientific interest (e.g. [2], [10], [11] and references therein). We suggest that the high enhancements of relativistic electrons in the outer ERB observed by “Universitetskiy-Tatiana” microsatellite are useful for space weather studies.

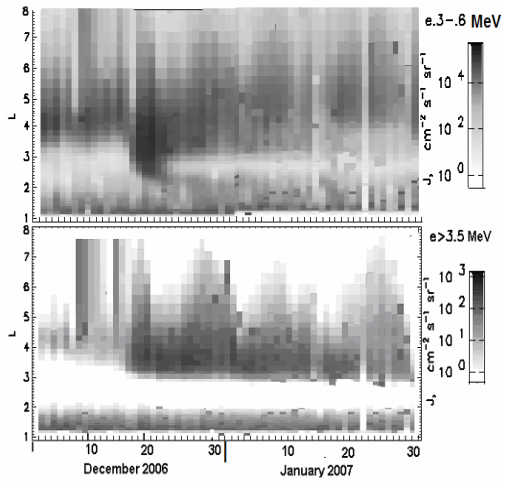

Fig. 6. Relativistic and sub-relativistic electron flux variation in the outer ERB in December 2006 - January 2007, according to “Universitetskiy-Tatiana” data.

VII. CONCLUSION

In this paper we have presented observational results obtained by the “Universitetskiy-Tatiana” spacecraft. The main results are listed here:

1. “Universitetskiy-Tatiana” microsatellite observations during December 2006 demonstrate that near-Earth space environment monitoring at low-altitude orbits is important during all SA cycle.

2. Monitoring of SEP penetration boundaries in the Earth’s magnetosphere is also useful during magnetic storms, since solar energetic particles can penetrate deep into the Earth’s magnetosphere during the main phase of moderate and even weak magnetic storms. In particular due to measurements of the SEP penetration boundaries one has the opportunity to estimate the radiation damage for space missions.

3. One can see that the joint influence of the magnetic storm+SEP on near-Earth’s environment is more significant due to SEP penetration into the Earth’s magnetosphere.

4. The presented experimental results demonstrate the real opportunity of small educational spacecrafts successful application in the important scientific programs like Space Weather one.

ACKNOWLEDGMENT

This work was partly supported by the Russian Foundation for Basic Research (grant 06-02-08263-офи).

REFERENCES

[1] I. N. Myagkova, S.N. Kuznetsov, V.G., Kurt et al. "X-ray, gamma-emission and energetic particles in near-Earth space as measured by CORONAS-F satellite: from maximum to minimum of the last solar cycle", *Adv. Space Res.*, vol. 40(2), pp 1929-1934, 2007.

[2] G.D. Reeves, K. L. McAdams, R. H. W. Friedel, et al. "Acceleration and loss of relativistic electrons during geomagnetic storms" , *Geophys. Res. Lett*., vol. 30(10), p. 1529 doi:10.1029/2002GL016513, 2003.

[3] T.P. O'Brien, M.D. Looper J.B. Blake "Quantification of relativistic electron microburst losses during the GEM storm", *Geophs. Res. Letters*, vol. 31, L04802/1-L04802/4, 2004.

[4] V.A. Sadovnichy, M.I. Panasyuk., S.Yu. Bobrovnikov et al. "First Results of Investigating the Space Environment onboard the Universitetskii-Tatyana Satellite" , *Cosmic Research*, vol.45 (4), pp. 273–286, 2007

[5] E.G. Berezhko, S.I. Petukhov, S.N., Taneev "Acceleration of solar cosmic rays by shock waves in the solar corona" , *Izvestiya RAN. Phys. Ser*., vol. 64 (3), pp. 339-342, 2001.

[6] D.F. Webb, N.U. Crooker, S.P. Plunkett, et al. "The solar sources of geoeffective structures". in: Song, P., Siscoe, G., Singer, H. J. (Eds.), Space Weather: Progress and Challenges in Research and Applications. Geophys. Monograph 125, AGU, Washington, D.C., 2001, p. 123.

[7] S.N. Kuznetsov, B.Yu. Yushkov, Yu.I., Denisov , Yu. I., et al. "Dynamics of the Boundary of the Penetration of Solar Energetic Particles to Earth's Magnetosphere According to CORONAS-F Data", *Solar System Research*, vol. 41(4), pp.348–353, 2007

[8] Yu. I.Yermolaev, L. M. Zelenyi, G. N. Zastenker et al. "A Year Later: Solar, Heliospheric, and Magnetospheric Disturbances in November 2004" in *Geomagnetism and Aeronomy*, vol. 45(6), pp.681-719, 2005

[9] M.I. Panasyuk, S. I., Kuznetsov, L. L., Lazutin et al. "Magnetic Storms in October 2003" in *Cosmic Research*, vol. 42 (5), 2004, pp. 489-534, 2004

[10] I.N. Myagkova, S.N, Kuznetsov, B.Yu., Yushkov et al. "Dynamics of the Earth's Radiation Belts during time period April 14-24, 2002 - experimental data" in: Pulkkinen, T.I., Tsyganenko, N.A., Friedel, R.H.W. (Eds.), The Inner Magnetosphere: Physics and Modeling,. Geophysical Monograf 155, AGU, Washington, 2005, pp. 127-134.

[11] S.N. Kuznetsov, K. Kudela, I.N. Myagkova et al. "Dynamics of the Earth's radiation belts during the magnetic storm of November 6 2001. *Adv. Space Res.,* vol. 36(10), pp. 997-2002, 2005.

[12] F. Soraas, K. Oksavik, M.I.Sandanger et al. "Relativistic electron losses in regions of anisotropic proton precipitation". *Geophysical Research Abstracts*, vol. 6, p. 04226, 2004.

[13] R.M. Thorne and C.F. Kennel "Relativistic electron precipitation during magnetic storm main phase", J. Geophys. Res., vol. 76, pp 4456-4468, 1971.

[14] X. Li, D. N. Baker, M. Temerin, et al. "Are energetic electrons in the solar wind the source of the outer addition belt?", *Geophys. Res. Lett*., vol. 24 (8), pp. 923–926, 1997

Poster Session A

Solar Extreme Events of December 2006

Chair: E. Eroshenko

Solar **E**xtreme **E**vents **2007**

Study of the 13 December 2006 Halo CME and its interplanetary signature

E. Mitsakou, G. Babasidis, X. Moussas

University of Athens, Section of Astrophysics, Astronomy and Mechanics, Faculty of Physics, Panepistimioupoli, GR 15783, Zografou, Athens, Greece
emitsaku@phys.uoa.gr, gbabasid@phys.uoa.gr, xmoussas@phys.uoa.gr

***Abstract*—We have used Omniweb data in order to identify the sheath and the ejecta boundaries of the 13 December 2006 halo Coronal Mass Ejection and compare its characteristics with a population of 67 shock-driving Interplanetary Coronal Mass Ejections during the time period 2003-2006. We identify the interplanetary shock of every ICME and determine the boundaries of the sheath and the ejecta. The frequency distribution of the average ICMEs physical characteristics has been studied and their temporal evolution observed. We examine and compare their statistical properties (speed, magnetic field strength, proton density and temperature, proton plasma beta), with those of the typical solar wind. Their passage time and radial width is also calculated. We study the correlation between the ejecta and sheath characteristics and indicate the significance of the 13 December 2006 event.**

***Key Words*—ICME, ejecta, sheath, statistical properties**

I. Introduction

Coronal mass ejections (CMEs) are dramatic explosions on the solar atmosphere which lead to massive releases of mass and energy into the interplanetary space, that can range from 10^{13} g to 10^{16} g and from 10^{27} erg to 10^{33} erg respectively [21], [9]. The occurrence CME rate depends on the phase of the solar cycle and can differ from 3.5 per day during solar maximum, to 0.2 per day during solar minimum [11]. The CMEs speed can be higher or lower than the ambient solar wind speed and can range from a few km/s to 3000 k/s [13], [5], [9].

CMEs which occur close to the sun center and appear to surround the solar disk like a bright halo are called halo CMEs [12]. Halo CMEs can be Earth directed (frontsided) or back-sided. Earth directed halo CMEs often have great consequences on the Earth's geomagnetism [20], [8], [14].

The manifestations of the CMEs in the interplanetary medium are called interplanetary coronal mass ejections (ICMEs), ejecta, clouds or plasma clouds. In this study they will be referred to as ejecta or ICMEs. They are recognized by in situ spacecraft observations of plasma and magnetic field data and most of them can be clearly associated with a CME on the sun [17]. The signatures of ICMEs can include low plasma temperature [11], strong and smooth magnetic field [3], enhanced helium abundance [1], [6] and low plasma beta and density [3], when compared to the ambient solar wind. CMEs with superalfvenic speeds can drive shocks into the interplanetary medium, which accelerate particles. The shock can usually be identified by a sudden rise of the plasma speed, magnetic field strength, density and temperature. The area between the shock and the ICME is called sheath.

II. The 13 December 2006 Coronal mass ejection

On 13 December 2006, while at the descending phase of solar cycle 23, a HALO CME was observed by the SOHO/LASCO coronographs, which caused a Forbush decrease a few days later. In this study we determine the physical properties of this particular Earth-directed halo CME by its interplanetary signature and compare them with the properties of similar events, which occurred during the time period 2003-2006. In order to accomplish that, we perform statistical analysis to the characteristics of 67 Earth-directed HALO CMEs observed during the descending phase of solar cycle 23, which we have recognized by their interplanetary signatures using OMNI data and then compare them with the December 13 event.

III. METHOD

We have identified 67 shock driving ICMEs, through their interplanetary signatures using Omniweb data for the time period 2003-2006. The data include magnetic field strength, solar wind speed, proton density and temperature. All of our events had a halo CME as a solar source possible candidate. Our population includes the December 13 event.

For each ICME the boundaries of the shock, the sheath and the ejecta have been identified, although that remains a subjective matter, since no unambiguous and universal signature has been found yet [19], [7], [22]. Of course, the shock arrival is very clear, but the identification of the ejecta is often pretty difficult. The front boundary of the ejecta is determined through the interplanetary signatures mentioned above, while the rear boundary can be placed at the time of an increase in temperature, plasma or magnetic field strength, after the ICME passage. An important subsection of ICMEs (almost one third of them) are magnetic clouds [3], which are easier to identify. They exhibit a smooth rotation of the magnetic field vector, in addition to low plasma beta. However, we have included all types of ICMEs in our study, not just the magnetic clouds.

IV. SHEATH AND EJECTA PROPERTIES

For each of the 67 identified ICMEs we calculate its mean characteristic quantities, such as magnetic field strength, speed, density, temperature and plasma beta both of the sheath and the ejecta. We also estimate the mean passage time t and radial width, also known as length scale (ICME size in the radial direction). Fig. 1 shows the interplanetary signature of the December 13 CME.

Throughout the mentioned characteristic quantities, such as magnetic field strength, speed, density, temperature, plasma beta, passage time and radial width, are symbolized as *j=B*, *V*, *d*, *T*, *beta*, *t*, *w*, respectively.

We plot the statistical distributions of each j and deal further with its mean value in the sheath and the ejecta, in order to have an idea of ICMEs properties in general. The results of our analysis on the 67 events show that ICMEs properties differ from the properties of the typical SW (solar wind).

We find that B_{sheath} (11.2nT±0.7nT) and B_{ejecta} (9.2nT±0.7nT) are much higher than the typical SW values (6nT), as it was expected [10], [4]. The December 13 event has a magnetic strength value B_{ejecta} (15.1nT±0.1nT), and B_{sheath} (13.5nT±0.1nT).

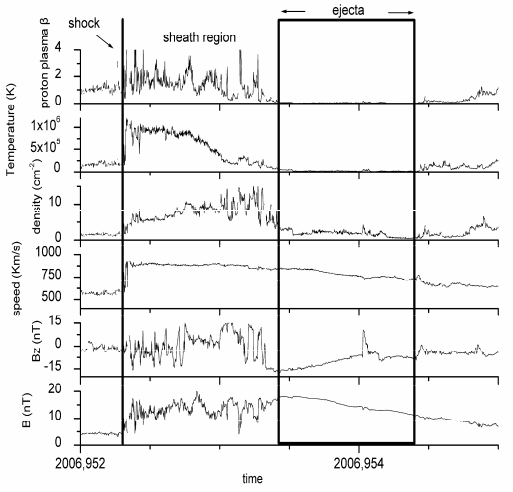

Fig. 1. The interplanetary signature of the 13 December 2006 HALO CME. The shock that was formed as well as the ejecta of the ICME are indicated. The figure shows the solar wind parameters, proton plasma beta, temperature, density, speed, magnetic field Bz, and magnetic field strength B.

Fig. 2 shows the temporal evolution of the average B_{ejecta} values of the 67 ICMEs during the period 2003-2006.

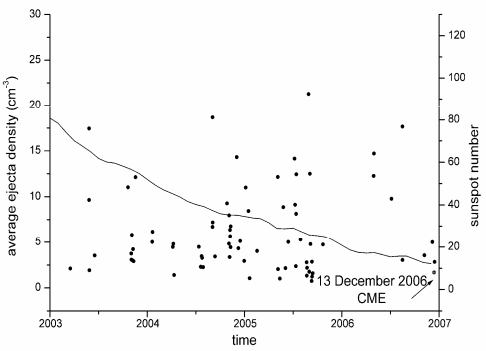

Fig. 2. The temporal evolution of the average ejecta magnetic field strength B values, during the time period 2003-2006. The straight line shows the sunspot number.

N_{sheath} (11.5cm^{-3}±0.9cm^{-3}) is much higher than N_{SW} (7 cm^{-3}). However, N_{ejecta} (6.5 cm^{-3}±0.5 cm^{-3}) is comparable with the typical SW values (7 cm^{-3}) in agreement with [18]. Our event has a much lower N_{ejecta} value (1.82 cm^{-3}±0.03 cm^{-3}) and N_{sheath} (7.81 cm^{-3}±0.11 cm^{-3}). In Fig 3 the temporal evolution of the ICMEs ejecta density is shown.

T_{sheath} (2.3 10^5 K±0.3 10^5 K) is much higher than T_{SW} (1.5 10^5 K), while T_{ejecta} (1.28 10^5 K±0.11 10^5 K) lies in lower and comparable to typical T_{SW} values.

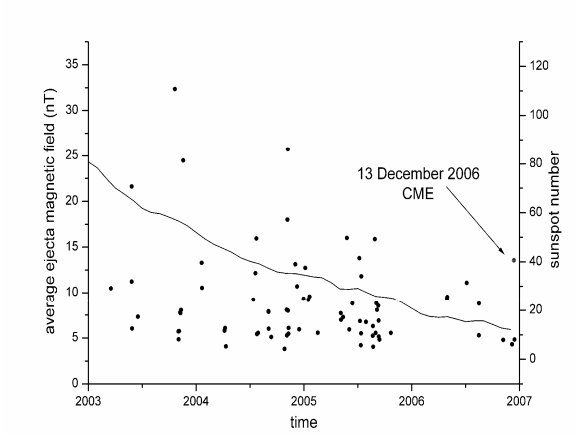

Fig. 3. The temporal evolution of the average ejecta proton density N, during the time period 2003-2006. The straight line shows the sunspot number.

The December 13 event exhibits higher sheath temperature (5.81 10^5 K±0.14 10^5 K), but much lower ejecta temperature (0.239 10^5 K±0.005 10^5 K). Fig 4 shows the temporal evolution of the average T_{ejecta} values.

ICMEs travel faster than the typical V_{SW} (440km/s), with V_{ejecta} (525 km/s ±15 km/s) and V_{sheath} (529 km/s ±17 km/s). The event which we study however travels faster, with V_{ejecta} (785 km/s ±1 km/s). and V_{sheath} (878 km/s ±1 km/s). The difference between the sheath and ejecta speed, as well as the fact that the sheath travels faster than the ejecta indicates that our investigated ICME expands.

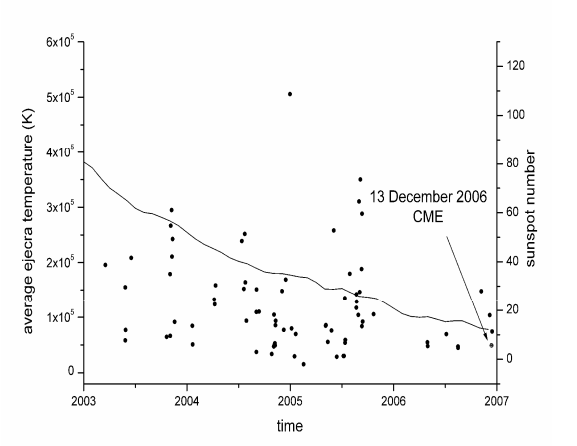

Fig. 4. The temporal evolution of the average ejecta temperature T, during the time period 2003-2006. The straight line shows the sunspot number.

Fig 5 shows the temporal evolution of the average V_{ejecta} values. Plasma $beta_{ejecta}$ (0.41±0.04) is lower than $beta_{sheath}$ (0.65±0.06), which indicates the dominance of the magnetic pressure. These values are higher than the average of fast ejecta delivered by [4]. The December 13 event has very low plasma $beta_{ejecta}$ (0.049±0.001), and higher $beta_{sheath}$ (1.46±0.06). The temporal evolution of the $beta_{ejecta}$ is shown in Fig 6.

The passage time t of the ICMEs is estimated, from the derived ejecta and sheath boundaries. t_{sheath} is (0.48 days±0.04 days) and t_{ejecta} is (0.95 days±0.08 days), while the whole disturbance lasts on average 1.43 days. It should be noted that t_{sheath} is also the time delay between the appearance of the ejecta and the shock and agrees with the 11 hour average of [2]. In our event, t_{ejecta} and t_{sheath} are 0.363 days and 0.403 days respectively, which are lower than the corresponding values mentioned above.

Since the ICME V and t are known, the radial width w can be easily delivered. Our results show that w_{ejecta} is (0.29 AU±0.03 AU), quite typical for 1 AU clouds [15], [2], [18], [16], while w_{sheath} is (0.148 AU±0.012 AU).

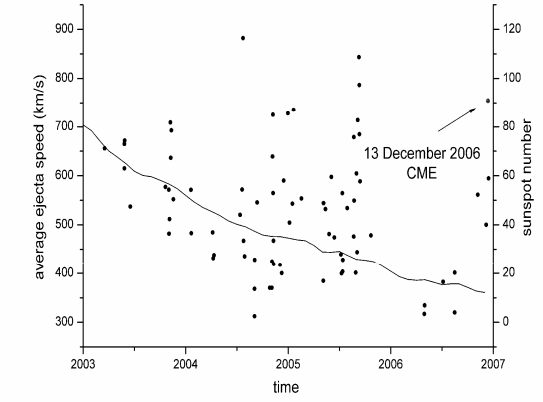

Fig. 5. The temporal evolution of the average ejecta speed V, during the time period 2003-2006. The straight line shows the sunspot number.

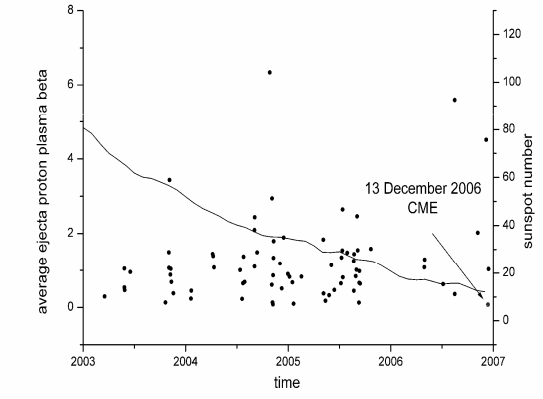

Fig. 6. The temporal evolution of the average proton plasma beta, during the time period 2003-2006. The straight line shows the sunspot number.

It should be noted that in the particular ICME under study, the sheath is wider than the ejecta with w_{sheath} (0.2043 AU±0.0003 AU) and w_{ejecta} (0.1647 AU±0.004 AU).

V. Summary and Conclusions

We have identified 67 shock-driving ICMEs during the time period 2003-2006 and examined their mean ejecta and sheath properties.

In the ejecta, the magnetic field strength is higher than the typical SW. The proton density is slightly lower than the typical SW values. The ejecta speed is higher than the typical SW and has low plasma beta. The mean ejecta passage time is 0.95 days, while the shock appears 0.45 days earlier. The radial width is 0.29 AU, which is a typical characteristic of the 1 AU ICMEs. The ejecta are the shock drivers even at 1 AU, which has also been indicated in other studies.

In the region between the ejecta and the shock, which is called the shock sheath, we find that the magnetic field strength, proton density, temperature and speed are much higher than the typical SW values. In addition, the sheath has higher magnetic field, proton density, temperature and plasma beta than the ejecta, while its radial width is smaller.

As far as our investigated ICME is concerned, it seems to have properties which differ from the average. It has high magnetic field strength values and travels fast in the interplanetary medium. The ejecta has low density and plasma beta. In addition there is an indication of expansion of the specific ICME. All of the above come to conclude that the interplanetary signature of the December 13 2006 CME, was a magnetic cloud and appears to be a significant event.

Acknowledgment

E. M. Author is grateful for the support given by the greek SSF during her PHD studies. The authors want to thank the Special Account for Research Grants of the Athens University.

References

[1] Borrini, G., Gosling, J. T., Bame, S. J., Feldman, W. C., Helium abundance enhancements in the solar wind, Journal of Geophysical Research, vol. 87, p. 7370-7378, 1982.

[2] Bothmer, V., Schwenn, R., The structure and origin of magnetic clouds in the solar wind, Annales Geophysicae, vol. 16, Issue 1, pp.1-24, 1998.

[3] Burlaga, L., Sittler, E., Mariani, F., Schwenn, R., Magnetic loop behind an interplanetary shock: Voyager, HELIOS and IMP-8 observations, Journal of Geophysical Research, vol. 86, p. 6673, 1981.

[4] Burlaga, L. F., Skoug, R. M., Smith, C. W., Webb, D. F., Zurbuchen, T. H., Reinard, Alysha, Fast ejecta during the ascending phase of solar cycle 23: ACE observations, 1998-1999, Journal of Geophysical Research, Volume 106, Issue A10, p. 20957-20978, 2001.

[5] St. Cyr, O. C., Plunkett, S. P., Michels, D. J., Paswaters, S. E., Koomen, M. J., Simnett, G. M., Thompson, B. J., Gurman, J. B., Schwenn, R., Webb, D. F., Hildner, E., Lamy, P. L., Properties of coronal mass ejections: SOHO LASCO observations from January 1996 to June 1998, Journal of Geophysical Research, Volume 105, Issue A8, p. 18169-18186, 2000.

[6] Galvin, A. B., Ipavich, F. M., Gloeckler, G., Hovestadt, D., Tsurutani, B. T., Solar wind iron charge states preceding a driver plasma, Journal of Geophysical Research, vol. 92, p. 12069-12081, 1987.

[7] Goldstein, R., Neugebauer, M., Clay, D., A statistical study of coronal mass ejection plasma flows, Journal of Geophysical Research, vol. 103, p. 4761, 1998

[8] Gonzalez, Walter D., Tsurutani, Bruce T., Clúa de Gonzalez, Alicia L., Interplanetary origin of geomagnetic storms, Space Science Reviews, v. 88, Issue 3/4, p. 529-562, 1999.

[9] Gopalswamy, N., A Global Picture of CMEs in the Inner Heliosphere, ASTROPHYSICS AND SPACE SCIENCE LIBRARY, Volume 317, Kluwer Academic Publishers, p.201, 2004.

[10] Gopalswamy, N., Properties of Interplanetary Coronal Mass Ejections, Space Science Reviews. Volume 124, p 145-168, Springer Netherlands, 2006.

[11] Gosling, J. T., Coronal mass ejections and magnetic flux ropes in interplanetary space, in Physics of magnetic flux ropes, American Geophysical Union, p. 343-364, 1990.

[12] Howard, R. A., Michels, D. J., Sheeley, N. R., Jr., Koomen, M. J., The observation of a coronal transient directed at earth, Astrophysical Journal, Part 2 - Letters to the Editor, vol. 263, p. L101-L104, 1982.

[13] Howard, R. A., Sheeley, N. R., Jr., Michels, D. J., Koomen, M. J., Coronal mass ejections - 1979-1981, Journal of Geophysical Research, vol. 90, p. 8173-8191, 1985.

[14] Huttunen, K. E. J., Schwenn, R., Bothmer, V., Koskinen, H. E. J., Properties and geoeffectiveness of magnetic clouds in the rising, maximum and early declining phases of solar cycle 23, Annales Geophysicae, vol. 23, Issue 2, p.625-641, 2005.

[15] Klein, L. W., Burlaga, L. F., Interplanetary magnetic clouds at 1 AU, Journal of Geophysical Research, vol. 87, p. 613-624, 1982.

[16] Lepping, R. P., Burlaga, L. F., Jones, J. A., Magnetic field structure of interplanetary magnetic clouds at 1 AU, Journal of Geophysical Research, vol. 95, p. 11957-11965, 1990.

[17] Lindsay, G. M., Luhmann, J. G., Russell, C. T., Gosling, J. T., Relationships between coronal mass ejection speeds from coronagraph images and interplanetary characteristics of associated interplanetary coronal mass ejections, Journal of Geophysical Research, Volume 104, Issue A6, p. 12515-12524, 1999.

[18] Liu, Y., Richardson, J. D., Belcher, J. W., A statistical study of the properties of interplanetary coronal mass ejections from 0.3 to 5.4 AU, Planetary and Space Science, Volume 53, Issue 1-3, p. 3-17, 2005.

[19] Richardson, I. G., Cane, H. V., Signatures of shock drivers in the solar wind and their dependence on the solar source location, Journal of Geophysical Research, vol. 98, p. 15295-15304, 1993.

[20] Tsurutani, Bruce T., Smith, Edward J., Gonzalez, Walter D., Tang, Frances, Akasofu, Syun I., Origin of interplanetary southward magnetic fields responsible for major magnetic storms near solar maximum (1978-1979), Journal of Geophysical Research, vol. 93, p. 8519-8531, 1988.

[21] Vourlidas, A., Buzasi, D., Howard, R. A., Esfandiari, E., Mass and energy properties of LASCO CMEs, Proc 10th European Solar Physics Meeting, 9-14 Sept 2002 (ESA SP-506), 2002.

[22] Wei, Fengsi, Liu, Rui, Fan, Quanlin, Feng, Xueshang, Identification of the magnetic cloud boundary layers, Journal of Geophysical Research Space Physics, Volume 108, Issue A6, p. H10-1, 2003.

Prehistory and history of the December 2006 GLE

M. Storini, P. Diego, M. Laurenza

National Institute for Astrophysics (INAF) - IFSI, Rome, Italy
(piero.diego@ifsi-roma.inaf.it; diego@fis.uniroma3.it)

National Institute for Astrophysics (INAF) - IFSI, Rome, Italy
(piero.diego@ifsi-roma.inaf.it; diego@fis.uniroma3.it)

Abstract – **GLEs (Ground Level Enhancements) constitute an important subset of Solar Energetic Particle (SEP) events registered in the terrestrial environment. Being the GLE particles of relativistic energy, they are able to affect ground-based records of cosmic ray detectors. From 1942 to present seventy GLEs were identified by the world-wide cosmic-ray community. They often occur during active periods of solar activity, but there exist several exceptions during low solar activity levels. The 13 December 2006 GLE is one of them. Several papers on the topic were presented at the 30th ICRC 2007. This paper mainly focuses on the possible solar-terrestrial phenomena tied to the event occurrence, by analyzing the solar/interplanetary prehistory and history. We describe various features collected for December 2006 and discuss the identified peculiar signatures useful for the comprehension of the particle generation, acceleration, and propagation of the December 13 event. The individuation of key solar conditions, producing such kind of energetic events, is a relevant topic to build up a scenario for a GLE forecast code, which is still missing.**

The solar cosmic ray ground level enhancements on 20 January 2005 and 13 December 2006

R. Buetikofer, E. O. Flueckiger, L. Desorgher, M. R. Moser and B. Pirard

Physikalisches Institut, Universit¨at Bern, Sidlerstrasse 5, CH3012 Bern, Switzerland

Abstract— **Close to the current solar activity minimum, two large solar cosmic ray ground level enhancements (GLE) were recorded by the worldwide network of neutron monitors (NM). The enormous GLE on 20 January 2005 is the largest increase observed since the famous GLE in 1956, and the solar cosmic ray event recorded on 13 December 2006 is among the largest in solar cycle 23. From the recordings of the NMs during the two GLEs, we determined the characteristics of the solar particle flux near Earth.**

Key Words— **Solar cosmic rays, ground level enhancements, neutron monitor**

I. INTRODUCTION

Although the solar activity in the years 2005/2006 was close to its minimum, the Sun showed phases of high activity in January 2005 and December 2006. During each of these intervals a large solar cosmic ray (SCR) ground level enhancement (GLE) was recorded by the worldwide network of neutron monitors (NM). The GLE on 20 January 2005 is ranked among the largest in years with gigantic count rate increases at the south polar NM stations of some thousands of percent. The GLE recorded on 13 December 2006 is among the largest in solar cycle 23, with count rate increases up to almost 100% at the NM stations Oulu and Apatity. For both GLEs the associated solar flares were favorably located in the western region on the Sun so that SCR particles could reach the Earth. The main features of the two solar flares are summarized in Table 1.

	20 January 2005	13 December 2006
Flare class	X7.1 (NOAA AR 10720)	X3.4 (NOAA AR 10930)
Flare position	12◦N, 58◦W	06◦S, 24◦W

Table1 1. Characteristics of the solar flares on 20 January 2005 and 13 December 2006 (Solar Geophysical Data).

In this paper the characteristics of the SCR particle flux near Earth were determined from the recordings of the NMs for the two events.

II. NEUTRON MONITOR MEASUREMENTS DURING THE GLES ON 20 JANUARY 2005 AND 13 DECEMBER 2006

Figure 1 shows the relative count rates of selected NMs during the GLEs on 20 January 2005 and 13 December 2006. Both events were characterized by a very anisotropic SCR flux during the initial phase and a rapid increase for the NM stations looking into the direction of the apparent source direction (GLE 20 January 2005: 6 minutes and GLE 13 December 2006: 15 minutes from onset to maximum count rate increase). These features suggest scatterfree propagation in the interplanetary space between the Sun and the Earth. The maximum count rate increase of more than 5000% at the NM South Pole during the GLE on 20 January 2005 was larger by more than one magnitude compared to the GLE on 13 December 2006 where the maximum increase was ~90% (NMs Oulu and Apatity). The duration of the events at NM energies was ~19 hours (20 January 2005) and ~5 hours (13 December 2006). As for many previous major GLEs, both GLEs reported here occurred during the recovery phase of a Forbush decrease.

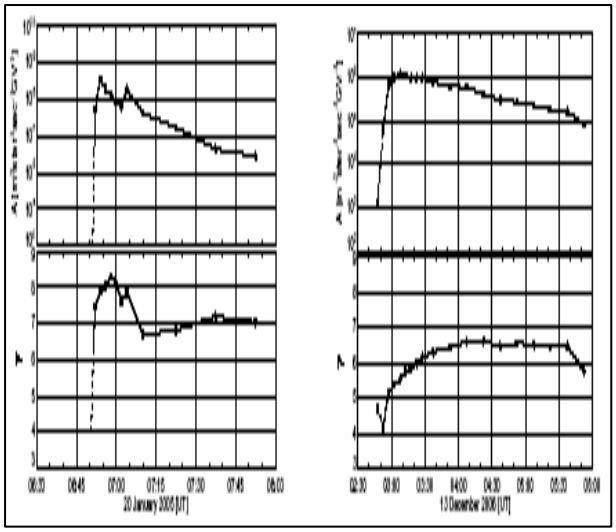

Fig. 1. GLE70 recorded by neutron monitors

III. ANALYSIS

From the recordings of the worldwide network of NMs (40 NM stations), we determined the characteristics of the solar proton flux near Earth during both GLEs by using the method of Smart et al. (1971) and Debrunner and Lockwood (1980). By a trial and error procedure, the solar proton flux in the rigidity range ~1 GV to ~15 GV, the pitch angle distribution, and the apparent source direction are determined by minimizing the difference between the calculated and the observed NM increases for the set of selected NM data. For the solar proton spectrum near Earth, I, a power law dependence on rigidity, R, was adopted: $I(R, t) = A(t) \cdot R[GV]^{-\gamma(t)}$. The Geant4 code PLANETOCOSMICS (Desorgher) was used to simulate the transport of charged particles through the Earth's magnetic field and to determine the cutoff rigidities and the asymptotic directions of cosmic ray particles for the time of the events. The solar proton flux in interplanetary space is usually assumed to be approximately symmetrical with respect to the interplanetary magnetic field (IMF) direction. Figure 2 shows the directions of the IMF near Earth, the deduced apparent source directions, and the asymptotic directions of selected NM stations during the main phase of the GLEs.

IV. RESULTS

Forboth GLEs the evolution of the SCR spectrum near Earth can be seen in Fig. 3. In both events the spectrum appears to have been hard shortly after the onset and to have softened significantly thereafter. The spectrum seemed to be somewhat harder again during the event in January 2005 after 0700 UT and was constant after about 0710 UT with $\gamma \sim 7$ during the time interval investigated in this analysis. From the plot of the amplitude, A, it seems that there was a second peak at around 0705 UT in the January 2005 GLE. In the December 2006 GLE the spectral parameter increased steadily after 0300 UT during about one hour and afterwards remained constant at ~6.5 during »1.5 hours. The maximum solar particle intensity near Earth at 1 GV, $I(1\ GV, t_{max})$ of ~20 cm^{-2} $ster^{-1}$ sec^{-1} MV^{-1} during the January 2005 GLE was a factor of ~200 larger than during the event in December 2006. The deduced SCR spectra near Earth, I, from this analysis are plotted in Fig. 4 for the main phase

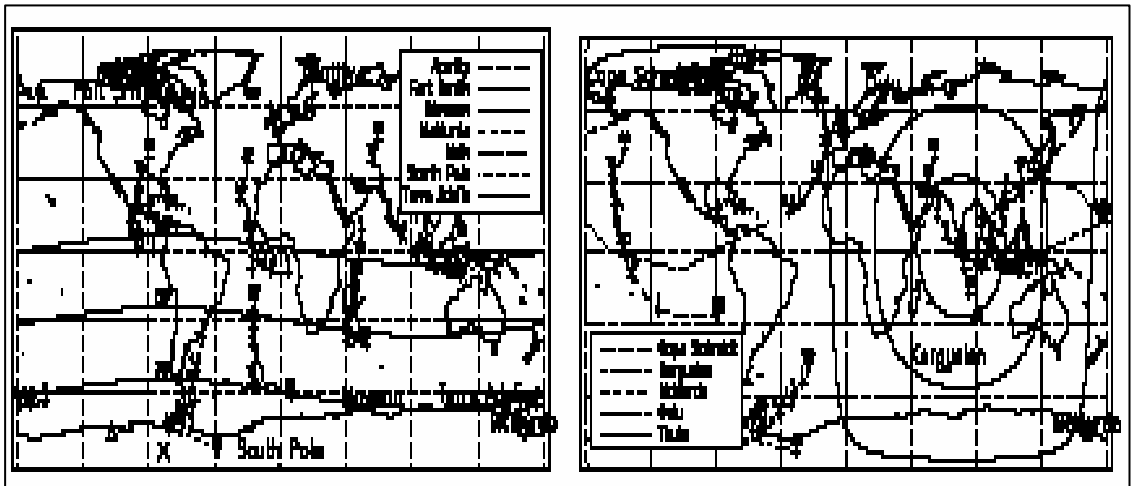

Fig. 2. World map with asymptotic directions of cosmic ray particles of vertical incidence at selected NM stations during the main phase of the GLEs on 20 January 2005 (left) and on 13 December 2006 (right). x: Indicates the apparent source direction. Δ: Indicates the direction of the IMF near Earth as measured by ACE spacecraft (ACE). The contours for equal angular distances from the apparent source direction are plotted for 30±, 60±, and 90±.

of both GLEs in the rigidity range 1–20 GV.

The pitch angle distributions during the two GLEs are plotted in Fig. 5. Both GLEs were characterized by very narrow pitch angle distributions during the first minutes, but already some minutes later the anisotropy decreased clearly. During the event in December 2006 the pitch angle distribution broadened in the course of the GLE, as one would expect. In contrast, it seems that in the January 2005 GLE the SCR flux became more anisotropic again after the main phase.

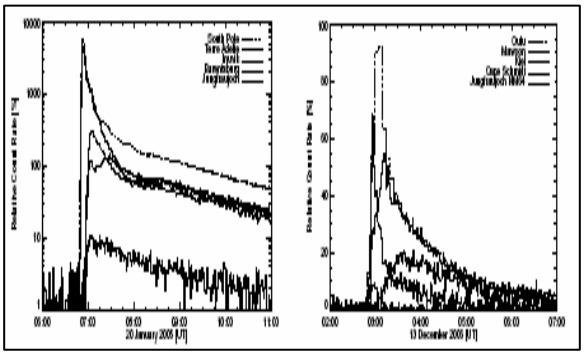

Fig. 3. Parameters of the solar particle rigidity spectrum. Amplitude A (top) and spectral index γ (bottom) for the assumed power law in rigidity vs. time for the GLEs on 20 January 2005 (left) and on 13 December 2006 (right).

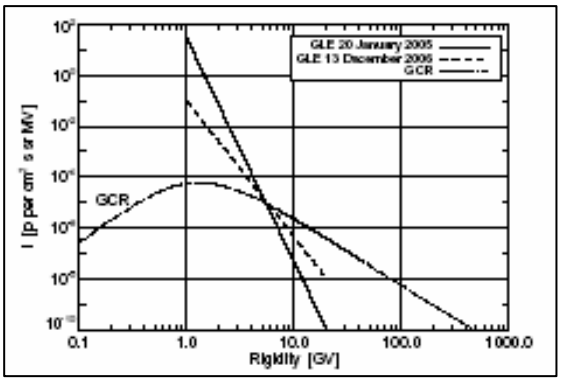

Fig. 4. Solar cosmic ray spectra near Earth, I(R), during the main phase of the GLE on 20 January 2005 (solid line) and of the GLE on 13 December 2006 (dashed line) from GLE analysis of NM data. For comparison the galactic cosmic ray flux near Earth for the time 2005/2006 is also shown (dashed-dotted line).

This fact, together with the hardening of the SCR spectrum and the second peak after 7 UT, could be due to a second population of SCRs during the 2005 event [4], [5], [7], [8].

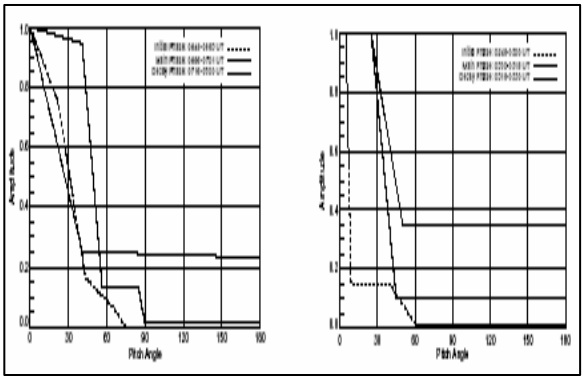

Fig. 5. Pitch angle distribution F(±(P), t) for selected time intervals for the GLEs on 20 January 2005 (left) and on 13 December 2006 (right).

V. Summary and Conclusions

Although the Sun was close to its sunspot minimum in the years 2005/2006, it had two periods of high activity during which two extreme GLEs on 20 January 2005 and on 13 December 2006 were observed. During both GLE onsets, the rigidity spectrum of the SCRs near Earth was very hard and softened immediately afterwards. During the main phase, the spectrum of the GLE on 20 January 2005 was significantly softer (γ~ 8) than in the GLE on 13 December 2006 (γ~ 5–6). In the decay phase, the spectral parameter of the two GLEs was almost the same (20 January 2005: γ~ 7, 13 December 2006: γ~ 6.5). The evolution in time of the spectrum and of the pitch angle distribution during the GLE on 20 January 2005 indicates that this event has two separate episodes. Both GLEs were very anisotropic during the initial and main phase. This suggests that at least during the first minutes of the events, the propagation from Sun to Earth occurred with almost no pitch angle scattering.

To learn more about the acceleration mechanisms at or near the Sun, the spectrum information deduced here from the NMs should be compared with the particle measurements made by space based detectors at lower energies and by muon detectors at higher energies as well as with observations of electromagnetic radiations from the Sun at different wavelengths. In addition, the transport of the SCR particles along the IMF from the Sun to the Earth has to be investigated to deduce the particle spectrum at or near the Sun as a function of time.

Acknowledgment

This research was supported by the Swiss National Science Foundation, grants 200020105435/1 and 200020113704/1, by the Swiss State Secretariat for Education and Research, grant C05.0034, and by

the High Altitude Research Stations Jungfraujoch and Gornergrat. We thank the investigators of the following NM stations for the data that we used for this analysis: Alma Ata, Apatity, Athens, Barentsburg, Cape Schmidt, Durham, Fort Smith, Hermanus, Inuvik, Irkutsk, Kerguelen, Kiel, Kingston, Larc, Lomnick´y St´ıt, Los Cerrillos Observatory, McMurdo, Magadan, Mawson, Moscow, Mt. Aragats, Nain, NorAmberd, Norilsk, Novosibirsk, Oulu, Peawanuck, Potchefstroom, Rome, Sanae, Terre Adelie, Thule, Tixie Bay, Tsumeb, Yakutsk

REFERENCES

[1] ACE, http://www.srl.caltech.edu/ACE/ASC/

[2] Debrunner, H., & Lockwood, J.A., The spatial anisotropy, rigidity spectrum, and propagation characteristics of the relativistic solar particles during the event on May 7, 1978, J. Geophys. Res., 85, A11, 6853-6860, 1980.

[3] Desorgher, L., http://cosray.unibe.ch/~laurent/planetocosmics. Solar Geophysical Data, http://sgd.ngdc.noaa.gov/sgd/jsp/solarindex.jsp.

[4] Moraal, H., McCracken, K.G., & Stoker, P.H., Analysis of the 20 January 2005 cosmic ray ground level enhancement, Proc. 30th International Cosmic Ray Conference, 2007.

[5] S´aiz, A., Ruffolo, D., Rujiwarodom, M. et al., Relativistic particle injection and interplanetary transport during the January 20, 2005 ground level enhancement, Proc. 29th International Cosmic Ray Conference, 1, 229-232, 2005.

[6] Smart, D.F., Shea, M.A., & Tanskanen, P.J., A determination of the spectra, spatial anisotropy, and propagation characteristics of the relativistic solar cosmicray flux on November 18, 1968, Proc. 12th International Cosmic Ray Conference, 2, 483-488, 1971.

[7] Struminsky, A.B., Multiple acceleration of protons on the Sun and their free propagation to the Earth on January 20, 2005, Astron. Lett., 32, 688-697, 2006.

[8] Vashenyuk, E.V., Miroshnichenko, L.I., Balabin, Y.V. et al., Twocomponent features of the two largest GLEs: February 23, 1956 and January 20, 2005, Proc. 30th International Cosmic Ray Conference, 2007.

The Forbush decrease after the GLE on 13 December 2006 detected by the muon telescope at BEO - Moussala

I. Angelov [1,2], E. Malamova [1], J. Stamenov [1]

[1] *Institute for Nuclear Research and Nuclear Energy, Bulgarian Academy of Science, 72 Tzarigradsko chaussee Blvd, 1784 Sofia, Bulgaria,*
[2] *South West University "N. Rilski", 66 Ivan Mihailov str. , 2700 Blagoevgrad, Bulgaria*

Abstract— **The Basic Environmental Observatory - Moussala is located at peak Moussala, 2925 m a.s.l. (25 deg 35' E , 42 deg 11' N) , Rila Mountain, Bulgaria. A muon telescope with effective area 1 square meter, using 8 water cherenkov detectors, is in operation at the observatory since August 2006. A Forbush decrease with amplitude approximately 4% in the intensity of the muon component of cosmic rays was detected after the GLE on 13 December 2006. Brief description of the instrument and the experimental results are presented.**

***Key Words* — Forbush decrease, muon telescope, cherenkov detectors**

I. INTRODUCTION

FORBUSH decreases (FD) are fast decreases in the galactic cosmic rays intensity with amplitude from several per sent to 20% or more, onset time about several hours to a day and relatively slow, about several days to weeks, exponential return to the normal values. The FD is a result of magnetic field perturbations in the near Earth space, caused by plasma cloud emitted from the Sun during solar flare and coronal mass ejections. Ground level enhancements (GLE) are short increases of the intensity of the secondary cosmic rays caused by nuclear cascades initiated in the Earth's atmosphere by solar particles. GLE and FD are studied by worldwide neutron monitors network and muon telescopes, the last providing more detailed data about the direction of the events, but working in higher energy range than the neutron monitors.

The Basic Environmental Observatory - Moussala is a site for complex monitoring of the environmental parameters. It is located at peak Moussala, 2925 m. a. s. l. in Rila Mountain, Bulgaria and has geographical coordinates 25 deg 35' E , 42 deg 11' N. The observatory is operated by the Institute for Nuclear Research and Nuclear Energy, Bulgarian Academy of Science. A muon telescope of cubic design with effective area 1 m2 has been constructed at the observatory for exploring the cosmic rays variations. We use water cherenkov detectors of original design, which is the main difference from all muon telescopes, based on scintillator detectors or proportional counters. The telescope is in continuous operation since August 2006.

II. DESCRIPTION OF THE INSTRUMENT

a. The detectors setup.

All The detectors of the telescope are of the same type as the detectors used in the muon telescope at the South West University "N. Rilski". The construction of the detectors in their present version is a result of series of methodical experiments and studies with different reflective coatings of the tank, different levels of the water radiator and different gains of the preamplifier [1].

The detectors are made of glass mirror tank with dimensions 50x50x12.5 cm. The thickness of the distilled water radiator layer is 10 cm. A transparent circle with diameter 67 mm is made by etching the reflective coating at the base of each mirror tank and a 2.5" photomultiplier tube (PMT) is attached to it. When a muon with Ekin > 54.12 MeV (the energy threshold for generation of cherenkov light for muons in water) passes through the radiator, part of the emitted cherenkov photons reach the cathode of the PMT after multiple reflections from

the mirror walls of the tank.

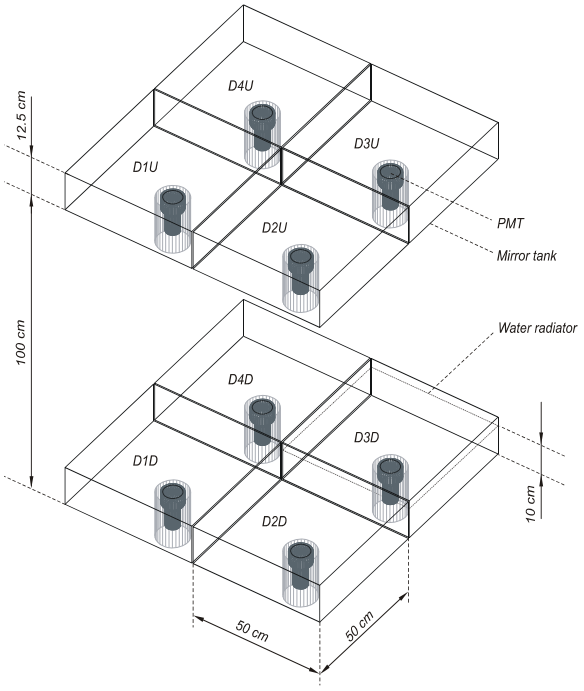

Fig. 1. Schematic view of the telescope.

We use photomultiplier tubes FEU-110 and FEU-139, powered with grounded cathode. The anode load resistor is 300 Ohm, the anode pulses are connected to amplifier with gain 50 and 90 MHz bandwidth mounted in the housing of the PMT and lead through coaxial cables to the discriminators-coincidence board.

The detectors of the telescope are placed in two separated by 1 m planes, 2x2 configuration (see Fig.1).

Five different directions are determined using combinations of pairs of detectors connected to coincidence circuits – vertical, north-south, south-north, east-west, west-east [2].

The telescope is placed at the basement of the observatory building and there is a 40 cm concrete layer above it, rejecting the soft component of the secondary cosmic rays. A 5 cm lead layer is mounted between the two detector planes for additional filtering.

b. The data acquisition system

The discriminators consist of fast comparators and one-shot multivibrators and form 60 nanoseconds digital pulses if the incoming pulse exceeds the given for the discriminator threshold. The threshold can be regulated in the range 15-50 mV. (The actual threshold adjusted is 28 mV.) The formed pulses are led to the inputs of the coincidence circuits.

The coincidence circuits consist of 12 fast AND logical elements. The counters circuit has 12 binary 8-bit counters and one 24 bit counter. The 8 bit counters count the pulses from the coincidence circuits for 15 s time intervals. The time intervals are determined by quartz stabilized timer. The value from each counters register is written in a file on a hard disc drive of the data acquisition personal computer after the time interval is finished, and counting for the next interval is started.

The 24 bit counter counts every time interval the count rate of one of the detectors, and these data are used to control the proper operation of the detectors.

The high voltage power supply provides stabilized voltage with low ripple amplitude to power the photomultiplier tubes. The main high voltage is regulated in the range 1500 – 1950 V. A separate regulated in 15 steps of 25 volts output is present for each of the photomultipliers.

The data acquisition personal computer is a 586 family. The parallel port is used as an interface to the counters circuits. The software is working in any Windows operational system and visualizes on the monitor screen each counter state and writes the data in formatted ASCII files on the hard disk drive.

The data are recorded on the hard disk of the data acquisition PC in three types of files. The raw data are the coincidence count rates for 15 seconds time intervals. The averaged data present the average count rate for each direction for 5 minute intervals, and its relative variations. The third type of data recorded is the individual dark count rate of each

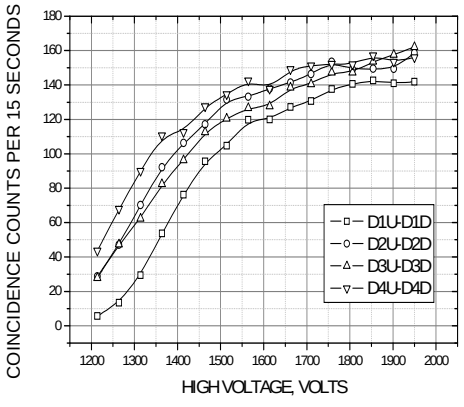

Fig. 2. Counting characteristics.

PMT for 15 second interval, once in 2 minutes.

The telescope was upgraded with a microcontroller based unit with USB interface, measuring continuously the main high voltage, the room temperature, and the atmospheric pressure, in October 2007.

c. Setting up the high voltage of the PMTs. Plateau characteristics.

To tune the detectors for maximum efficiency keeping at the same time the number of random coincidences minimal, we used the known in photon counting method of plateau characteristics. [3]

The dependencies of the single counting rates for each pair of detectors (one with the one above it) and the number of vertical coincidences per minute on the high voltage and on the discriminator threshold over the ranges 1500-1950 V, 15mV–50mV had to be taken and the

values for the operation of the given detector to be selected, looking for highest detectors efficiency and lowest random coincidences.

The dependence of the count rate for the detector pairs counting the muon flux in vertical direction on the high voltage power supply of the photomultiplier tubes at the selected discriminator level 28 mV is presented on Fig. 2.

III. MAIN CHARACTERISTICS OF THE TELESCOPE

d. Energy threshold and count rate.

To calculate the energy threshold of the telescope we used the MMC software[4], [5]. The energy loss for vertical incident muons passing the concrete layer above the telescope and the 5 cm lead layer were calculated and the threshold energy for the water cherenkov detector (Ekin > 54.12 MeV) was taken into account. The calculated energy threshold is ~ 0.45 (~345 GeV kinetic energy) GeV for vertical muons.

The count rate of the telescope for vertical direction is ≈ 580 min^{-1} for a detector pair. This corresponds to intensity of the muon flux I_0 ≈ 0.0188 $cm^{-1}s^{-1}ster^{-1}$, without any corrections for the efficiency of the detectors.

For comparison we calculated the intensity from the measurements of the muon spectrum with the BESS spectrometer at mount Norikura - 2770m a.s.l. , Rc=11.2GV. [6] The differential muon spectrum was integrated over the whole momentum range of the BESS spectrometer (corresponding to kinetic energies ~ 0.48 – 106 GeV) and the obtained intensity is I0 ≈ 0.0105 $cm^{-1}s^{-1}ster^{-1}$. The difference can be explained taking in mind the lower rigidity cut-off at the observation site and the geometry uncertainties since the thickness of the detectors (0.1m) is not negligible compared to the distance between the detector planes. The main aim of the instrument is the measurement of the relative variations of the muon flux, and the long time stability of the detectors, not the measurement of the absolute intensities.

e. Sensitivity to the primary spectrum.

Simulations with the Planetocosmics software code [7] were carried out to estimate the response of the telescope to the primary cosmic rays spectrum. The primary protons spectrum was divided into several sub ranges and the integral energy spectrum for muons at 2925 m a.s.l. was calculated for each sub range. Taking the intensities for muons with energies above 0.45 GeV we calculated the fraction of the total muons intensity, for vertical direction, corresponding to each sub range. The results are presented on fig. 3. About 80% of the generated by primary protons muons are

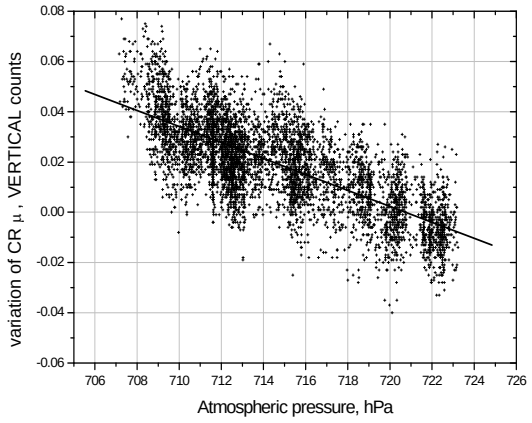

Fig. 4. The barometric effect for cosmic rays muons, vertical direction.

from protons in the energy range 7 - 160 GeV, with main contribution – 60% - of the energy range 10 – 80 GeV.

f. Rigidity cut off.

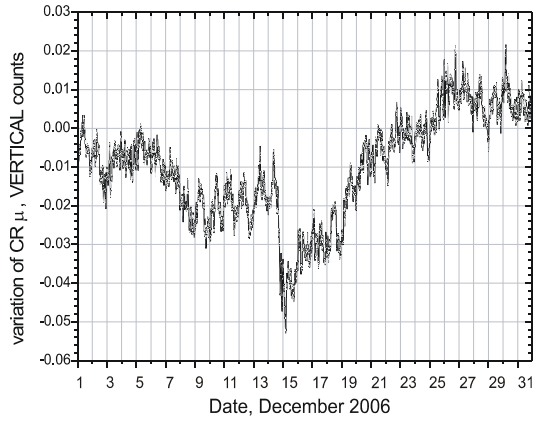

Fig. 5. The December 2006 Forbush decrease, vertical direction – BEO muon telescope.

The rigidity cut off for the observation site was calculated using Planetocosmics code and the obtained value is Rc = 6.3 GV.

g. Meteorological corrections.

The data for the atmospheric pressure were taken from the automatic weather station at the observatory, with pressure sensor type Vaisala PTB100B (After an upgrade, a dedicated barometer based on Freescale MPX4115A sensor is used now).

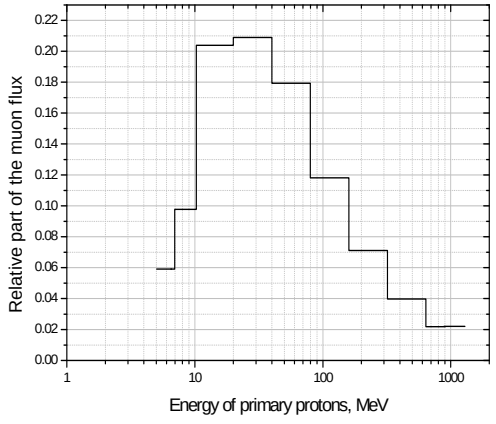

Fig. 3. Response to the primary protons spectrum (simulation results).

The anti-correlation of the measured muon flux intensity with the atmospheric pressure is clearly visible in the telescope data and the found barometric coefficient is β=0.318% / hPa for vertical direction. (See Fig. 4) No data for the temperature profile of the atmosphere above the observation site are available and no temperature corrections are performed at this moment.

IV. The Detected Forbush Decrease - Experimental Results and Discussions

The measured relative intensity of the cosmic rays muons - vertical direction - for December 2006 is presented on Fig. 5. The data are pressure corrected 5 minute arbitrary count rates, smoothed by 16 points moving average. The calculated standard deviation is 0.25%

As registered by our instrument, a decrease of the galactic cosmic rays intensity begins on 6 Dec., about 11:00-12:00 UT. A sharp decrease follows beginning on 14 Dec. , 15:30-16:30 UT. The Forbush decrease reaches its maximum of ~4% on 15 Dec., 05:00 UT.

For comparison the Forbush decrease registered by the Nagoya Muon telescope is shown on Fig. 6

A GLE in CR muons was detected by MEPHI group with the muon hodoscope URAGAN (2.4 GV cut-off rigidity, ~0,2 GeV energy threshold) , but was not observed in the data of the muon hodoscope TEMP (~0.5 GeV threshold). [8] We analyzed our 15 seconds records with different averaging to search for GLE. As expected GLE in cosmic rays muons was not found - our telescope has higher cut-off rigidity than the Moscow muon hodoscopes and ~ 0.5 Gev energy threshold.

V. Summary and Conclusions

A Forbush decrease with amplitude ~4% was

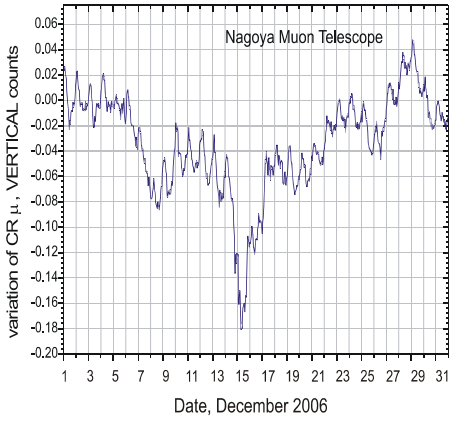

Fig. 6. The December 2006 Forbush decrease, vertical direction – Nagoya muon telescope.

registered on 14th December 2006 at coordinates 25° 35' E, 42° 11' N, 2925 m a.s.l. , with a new muon telescope, using water cherenkov detectors. The characteristics of the instrument are:

- observation level : 730 g/cm2
- cut-off rigidity : ~ 6.3 GV (Vertical direction)
- energy threshold : 0.45 GeV (Vertical direction)
- count rate : 2300 min^{-1} (Vertical direction)
- statistical error : 0.27% for 1 hour intervals (Vertical direction)

In spite of the small area - 1m^2 - the statistical errors are acceptable, because of the higher counting rates at high altitudes.

The instrument performs steady operation and the used detectors are cost effective alternative to scintillator detectors, suitable for construction of larger muon telescopes.

ACKNOWLEDGMENT

The telescope was constructed and funded as a part of the FP6 BEOBAL project - BEO Centre of Excellence Research Capacity Improvement for Sustainable Environment and Advanced Integration into ERA.

The data from the Nagoya Multidirectional Muon Telescope were kindly provided by the Cosmic Ray Section, Solar-Terrestrial Environment Laboratory, Nagoya University.

REFERENCES

[1] E. Malamova, I. Angelov, I. Kalapov, K. Davidkov, J. Stamenov, Muon cherenkov telescope, Proceedings of the 27th ICRC, Hamburg, 2001, Available : http://www.copernicus.org/icrc/papers/ici6585_p.pdf

[2] I. Angelov, E. Malamova, J. Stamenov, Muon Telescope at BEO - Moussala, 2007, Available : http://arxiv.org/ftp/physics/papers/0702/0702242.pdf

[3] Hamamatsu Photonics K. K. Photon counting using photomultiplier tubes, 2005, Available : http://sales.hamamatsu.com/assets/applications/ETD/PhotonCounting_TPHO9001E04.pdf

[4] D. Chirkin, W. Rhode, All Lepton Propagation Monte Carlo, Proceedings of the 29th ICRC, Pune, 2005, Available : http://icrc2005.tifr.res.in/htm/Vol-Web/Vol-19/19093-usa-chirkin-D-abs2-he21-poster.pdf

[5] D. Chirkin, W. Rhode, Muon Monte Carlo: a high-precision tool for muon propagation through matter, 2004, Available : http://arxiv.org/PS_cache/hep-ph/pdf/0407/0407075v1.pdf

[6] T. Sanuki, M. Fujikawa, K. Abe et al, Measurements of atmospheric muon spectra at mountain altitude, 2003, Available : http://arxiv.org/PS_cache/astro-ph/pdf/0205/0205427v3.pdf

[7] L. Desorgher, PLANETOCOSMICS Software User Manual, 2005, Available : http://cosray.unibe.ch/~laurent/planetocosmics/doc/planetocosmics_sum.pdf

[8] D. Timashkov, Y. Balabin, V. Borog et al, GLE event of December 13, 2006 in muon hodoscopes TEMP and URAGAN, to be published in the Proceedings of the 30th ICRC, Merida, Mexico, 2007

Rigidity spectrum variations and cosmic ray anisotropy in December 2006

V. M. Dvornikov, V. E. Sdobnov

Institute of Solar-Terrestrial Physics SB RAS, Irkutsk, Russia, 664033, Irkutsk, p/o box 291; Lermontov st., 126a, sdobnov@iszf.irk.ru

Abstract — **According to ground-based measurements of cosmic ray (CR) intensity on a worldwide network of stations variations are investigated of the rigidity spectrum and CR anisotropy during December 2006 using the method of spectrographic global survey. It is shown that for the CR flare of December, 13 the highest degree of anisotropy (up to ~150 %) with a maximal intensity of particles with rigidity of 4 GV in antisolar direction (asymptotic direction ~ –25°, ~160°) was observed at 04:00 UT. Through the complex analysis of ground and satellite measurements of protons in the energy range from units of MeV to tens of GeV the parameters of CR rigidity spectrum, which reflect electromagnetic characteristics of heliospheric fields for the period under investigation are determined. On the basis of analysis the explanation of the observable anisotropy and CR variations in a wide energy range is given.**

Key Words — **cosmic rays, GLE**

I. Introduction

December 2006 was characterized by a number of solar events related with the active region (AR) 0930. In particular, the increase of 0.8–4 MeV proton fluxes generated by the X9 solar flare of 05.12.06 with S07, E68 coordinates (10:21, 10:35, 10:45 UT – beginning, maximum and ending, respectively) was registered by GOES-11 on December 5 at 11:40 UT. The increase of fluxes of higher-energy particles commenced later (at about 16–17 UT).

The X3 solar flare of December 3 begun at 02:17 UT in the AR S05, W23 was accompanied by coronal mass ejection (CME) and solar proton event (SPE). The increase of intensity of low-energy cosmic rays (CR) registered by GOES-11 commenced at 03:25–03:30 UT. For high-energy CRs (ground level event – GLE) such increase was registered on December 13 2006 by the network of neutron monitors at 02:50 UT. Those events generated disturbances in the interplanetary medium as well as in the Earth's ionosphere and magnetosphere the strongest of which occurred on December 6 and 15. In particular, the strong geomagnetic storm was observed on December 15 (D_{st} ~ –150 nT).

The purpose of this study is the investigation of manifestations of a whole complex of phenomena in the interplanetary space through variations of a CR rigidity spectrum the parameters of which characterizes electromagnetic properties of the interplanetary medium in accordance with a model of CR modulation by regular heliospheric electromagnetic fields [1].

II. Data and method

Proton intensity data averaged over hour intervals and corrected for the geometric factor were used in analysis. The data were registered by GOES-11 satellite in the energy ranges of 4–9, 9–15, 15–40, 40–80, 80–165 и 165–500 MeV [2]. The data on variations of higher-energy CR intensity were obtained with the method of spectrographic global survey (SGS) [3] using ground-based measurements at world-wide network of neutron monitors included 32 stations. The SGS method makes it possible to have information on variations of angular and energy distributions of primary CRs outside the Earth's magnetosphere as well as on variations in the planetary system of geomagnetic cutoff rigidities for each hour of observation. The variations of the rigidity spectrum and anisotropy as well as those of threshold geomagnetic cutoff rigidities were analyzed for the period from December 1 to 31 relative to the base level of June 10, 2004.

In order to describe the CR rigidity spectrum in a wide energy range the expression obtained in [1] was used.

$$J(R)=A\left[\frac{(\varepsilon^2-\varepsilon_0^2)}{(\varepsilon+\Delta\varepsilon)^2-\varepsilon_0^2}\right]^{3/2}\frac{\varepsilon+\Delta\varepsilon}{\varepsilon}\left[\frac{2\sqrt{(\varepsilon+\Delta\varepsilon)^2-\varepsilon_0^2}-\sqrt{(\varepsilon^2-\varepsilon_0^2)}}{\sqrt{(\varepsilon^2-\varepsilon_0^2)}}\right]^{-\gamma}, \quad (1)$$

where ε is the total energy of particles; ε_0 is the rest energy; A and γ are spectral indices of the galactic spectrum; $\Delta\varepsilon$ is variation of particle energies in heliospheric electromagnetic fields. The $\Delta\varepsilon$ is defined by the following expression:

$$\Delta\varepsilon(R)=\Delta\varepsilon_0+\Delta\varepsilon_1\left[1-f(R,\,b+R_0)\right]+\Delta\varepsilon_2\left[1-f(R,\,b+R_0)\right]f(R,\,R_0)+ \quad (2)$$
$$+\left[\varepsilon(1-e^{\alpha/2})+\varepsilon-\sqrt{\beta(\varepsilon^2-\varepsilon_0^2)+\varepsilon_0^2}\right]f(R,\,R_0),$$

The Eq (1) has been obtained on the base of the Liouville theorem on the assumption that there are no sources of solar cosmic rays (SCR) in the energy range under consideration. If the assumption is not fulfilled then the expression (1) does not describe the observed particle spectrum. In this case the SCR incoming can be identified through these discrepancies. The expression (2) was obtained from the solution of particle motion equation in a general form in the drift approximation [4] and on the assumption that polarization and vortical electric fields can be generated in the heliosphere along with an induced electric field. There is some evidence obtained in Lindberg's laboratory experiments for generation of such fields [5 including references].

The spectrum parameters $\Delta\varepsilon_1$, $\Delta\varepsilon_2$, α, β, and R_0 determine the following characteristics of the heliosphere: R_0 is the parameter which characterizes the scale of structural formations in the heliosphere with nonstationary electromagnetic fields; $\Delta\varepsilon_1$ determines the CR energy variations due to the gradient and centrifugal drifts of particles in the spiral interplanetary magnetic field (IMF) in the direction opposite to the induced electric filed and is proportional to the IMF intensity; $\Delta\varepsilon_2$ determines such variations in the fields of coronal mass ejections (CME) and is proportional to the magnetic field intensity in CME and to the solar wind (SW) velocity [6]; the parameter $\beta=B/B_0$ where B_0 is the intensity of the background field and B is the intensity of time-variable IMF characterizes the influence of nonstationary magnetic fields on a CR spectrum (with magnetic rigidity of particles $R \le R_0$); the parameter $\alpha=E_{pl}^2/B^2$ characterizes the influence of electric fields E_{pl}. The quasi-step functions $f(R,\ R_0)$, $f(R,\ b+R_0)$ are introduced for estimating the contribution of one or other mechanism of particle energy variations in the ranges [0.108, R_0], [R_0, R_0+b] и [R_0+b, ∞] GV where b=5 GV. These functions tend to 1 at $R < R_0$ or $R < b+R_0$ and to 0 at $R > R_0$ or $R > b+R_0$ respectively. The expression for the quasi-step function as well as its parameters and the constant $\Delta\varepsilon_0$ which includes the residual modulation for low-energy particles were found empirically in [7].

The parameters of the CR rigidity spectrum and anisotropy were determined for each hour of observation over the whole period under consideration.

III. Analysis Results

In Fig. 1 the proton intensities in the energy ranges of 4–9 MeV (0.108 GV), 9–15 MeV (0.149 GV), and 5 GV are shown on three upper panels (triangles). The full curves illustrate the results of calculations with the use of the model spectrum and the values of its parameters. The fourth panel gives hourly averages of amplitude of the first spherical harmonic, and the fifth panel shows those of the second harmonic in the angular distribution of 4 GV particles. Next four panels illustrate the rigidity spectrum parameters $\Delta\varepsilon_1$, $\Delta\varepsilon_2$, α, β и R_0 determined for the period under consideration. Then, four panels show the IMF module, the angles ψ and λ which characterize the IMF vector orientation in the interplanetary space, and the SW velocity respectively. On the lower panel the values of GCR variations at R_c = 4 GV are given along with the

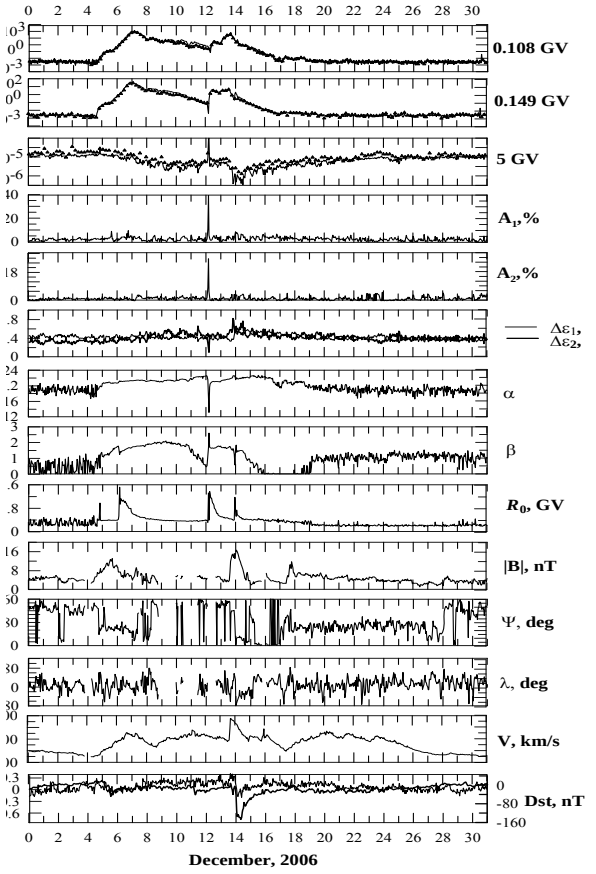

Fig. 1. Time profiles of different cosmic ray parameters.

D_{st}-index.

Figure 2 gives differential CR rigidity spectra at definite moments of the period under study along with the background CR spectrum. The results of calculating the model spectrum at the moments given in diagrams are shown by curve 2, and triangles depict the observation data. The calculated background spectrum (curves 1) is illustrated by the dashed curve and the observation data are shown by dots. Figure 3 illustrates the relative variations of the CR intensity with R = 4 GV depending on asymptotic directions in the solar-ecliptic geocentric coordinates for different moments of December 13, 2006 when observing GLE.

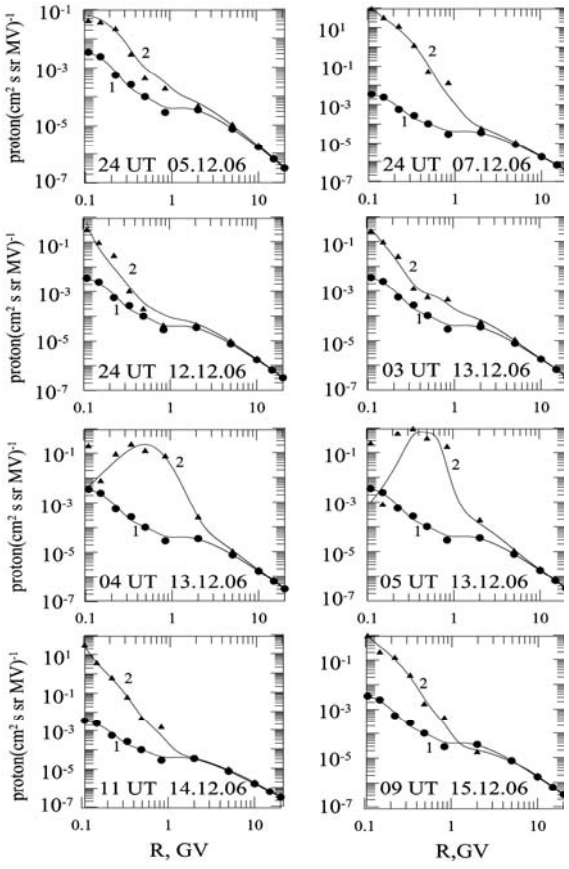

Fig. 2. Differential CR rigidity spectra at definite moments of the period under study along with the background CR spectrum.

IV. Discussion and Conclusion

When comparing time variations of the rigidity CR spectrum parameters with time profiles of low-energy proton intensity (two upper panels in Fig. 1) it may be concluded that an intensity increase of low-energy CRs is caused by acceleration of interplanetary medium particles by polarization and vortical electric fields (increase of α and β parameters). The acceleration began on December 5 when crossing the current sheet by the Earth.

From the analysis of Fig. 2 it follows that spectrum form in use describes well the observed dependence of CR intensity on their rigidity over all time interval under study except for the moments 04:00 and 05:00 UT on December 13 that is at the GLE beginning phase. As follows from the given condition, in the energy range under consideration variations of intensity of energetic particles are caused by energy variations of galactic cosmic rays (GCR) under the action of electromagnetic fields generated in the heliosphere as a result of SCR propagation. Such SCRs in turn because of an energy interchange with GCRs and SW plasma particles propagate into the region of lower energies and are registered only at definite moments (for example, at 04:00 and 05:00 UT on December 13, 2006; see Fig. 2) as evidenced by differences between model and observed spectra in the range of low energies.

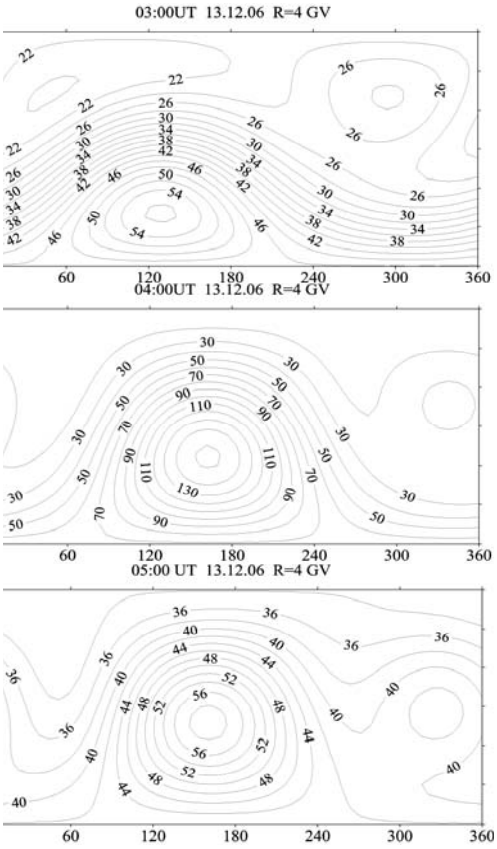

Fig. 3. The relative variations of the CR intensity with R = 4 GV depending on asymptotic directions

As follows from the R_0 parameter dynamics acceleration processes are accompanied by extension of regions of nonstationary

electromagnetic fields. With increasing R_0 to values exceeding 1–2 GV (at corresponding values of α and β parameters) GLEs are observed.

It is evident from the behavior of A_1 and A_2 parameters (see panels 4 and 5 in Fig. 1) that the significant anisotropy is observed at the moment of GLE registration. The analysis of distribution of 4 GV particles according to incoming direction shows that CR maximal fluxes are observed at 04:00 UT from the direction of 170°, –20° (~150 %) that is practically from antisolar direction.

On the base of the results and taking into account those obtained in studies of variations of CR rigidity spectrum parameters the day before a solar proton event (SPE) [7] the following scenario has been suggested for CR acceleration in solar corona and heliosphere. As assumed magnetic fields above solar active regions have a fiberlike structure. If intensities of magnetic fields in such structures increase with time then a drift of particles into fibers occurs (the Larmor radius is less than the size across such structure) as well as an acceleration of particles due to betatron mechanism. Increase of currents forming these structures results in increase of electrodynamic force caused by magnetic field of these currents. This force tends to extend the current circuit and is usually balanced by electrodynamic forces of adjacent current circuits, gas pressure and gravity forces. However, if the current exceeds the definite critical value the force

balance can be disturb. In this case, two adjacent current circuits may combine or it may be a circuit break accompanied by explosive process and precipitation of accelerated particles. This may result in enlargement of size across a fiberlike structure and decay of small-scale magnetic fields. When propagating in inhomogeneous fields of solar corona and heliosphere the beams of precipitating accelerated particles become polarized because of the drift of protons and electrons in the opposite direction. Under the spatial inhomogeneity of particle density this results in charge separation and potential difference between the beam borders along magnetic drift trajectories. This fact results in generation of increasing polarized electric field and, as a consequence, in polarization drift of background particles of SW plasma, solar corona and GCR along the field. In this case, acceleration of particles (the Larmor radius is less than the size across the beam) of solar corona and interplanetary medium takes place.

Depolarization longitudinal currents causes the formation of a current system and generation of magnetic field and consequently vortical field which accelerates particles due to betatron mechanism and so on. Thus, there is an energy interchange between accelerated particles and background ones of solar corona, SW, and GCR as well as forming of heliospheric current structures and generation of IMF structures. Therefore, we have a self-consistent process of acceleration and propagation of particles in electromagnetic fields of the heliosphere.

ACKNOWLEDGMENT

The study was partly supported by the Complex Integration Project of RAS SB 2006 N 3.10 and the RAS Presidium Program “Neutrino Physics” within the limit of the Project “Research into modulation effects of cosmic rays with ground-based and stratospheric monitoring”.

REFERENCES

[1] V.M, Dvornikov, M.V. Kravtsova, V.E. Sdobnov, “Correlations between variations of cosmic rays spectrum and interplanetary medium parameters”, in 2006. Proc. of 2nd International Symposium SEE-2005, Nor-Amberd, Armenia, pp. 172–175.

[2] http://spidr.ngdc.gov/spidr/index.html.

[3] V.M. Dvornikov, V.E. Sdodnov, “Time variations of the cosmic ray distribution function during a solar event of September 29, 1989”, *J. Geophys. Res*. vol. 102, A11, 1997, pp. 24209–24

[4] A.I. Morozov, L.S. Soloviev, “The motion of charged particles in electromagnetic fields”, *Voprosy Teorii Plazmy. 2.* Gosatomizdat, Moscow, 1963, p. 177 (in Russian)

[5] H. Alfven, *Cosmic plasma*. Dordrecht, Holland, 1981, p. 213.

[6] V.M. Dvornikov, V.E. Sdobnov, “Variations in the rigidity spectrum and anisotropy of cosmic rays at the period of Forbush effect on 12–15 July”, *International Journal of Geomagnetism and Aeronomy*. vol. 3, N 3, 2002. pp. 217.

[7] V.M. Dvornikov, M.V. Kravtsova, A.A. Lukovnikova, V.E. Sdobnov, “Possibility of prediction of solar proton events”, *Bulletin of the Russian Academy of Science: Physics.* vol. 71, N 7, 2007. pp. 945–947.

Solar Extreme Events at the Middle Latitudes: Identification of Ground Level Enhancements

U. Beisembaev[1], V.I. Drobzhev[2], E. A. Dryn[2], O. N. Kryakunova[2], N.F.Nikolaevskiy[2]

[1]*Lebedev Physical Institute, Russian Academy of Sciences, Russia*
(krolganik@yandex.ru)
[2]*Institute of Ionosphere, Ministry of Education and Science of Republic of Kazakhstan*

Abstract – **This work is directed toward the experimental and theoretical investigation of the ground level solar cosmic ray enhancements (GLE). Relativistic protons (>1 GeV) are generated in powerful flares more often than they are observed at the Earth. Especially it concerns to observation at the middle latitudes. Although recorded magnitudes of ground level enhancements are usually very small at these geomagnetic latitudes the high statistical accuracy of the 18-tube NM-64 Alma-Ata neutron monitor, located at 3340 m altitude, make possible detection of these events. The possible solar proton contribution into general flux of galactic cosmic rays registered by means of Alma-Ata high altitude neutron monitor has been investigated in those events when it is difficult to notice visually GLE events. GLE were investigated using Student's criterion. Some last GLE on November 1997, on August 1998 and on December 2006 were analyzed. It is shown that using of Student's criterion allows to reveal effectively GLE at the middle latitudes and to defined upper limit energy spectra of particles.**

I. INTRODUCTION

Relativistic protons with energy > 1 GeV can be generated during powerful solar flares. They are registered at ground based detectors - neutron monitors and muon telescopes. These events have been named ground level enhancements (GLE) of solar cosmic rays [1], [2].

The GLE is rare event: during 65 years (from the first event on 28 February 1942 up to now) only 70 events have been registered [3]. There is a problem of detection of solar cosmic rays flux on a background of galactic particles. For unification of the approach to GLE detection the uniform base hour is entered for each event.

The effects are observed in high-latitudes. Only powerful GLE can be found out by sight in mid-latitudes. For all period of the investigation of such events by means of high mountain Alma-Ata B neutron monitor (3340 m above sea level, geomagnetic rigidity R_c=6.7 GV) the maximal amplitude of effect was observed during event on 29 September 1989 (151 %) [4], [5], [6]. The amplitudes of the majority of events are about 1-5% for middle latitude Alma-Ata B neutron monitor [7], [4]. The main goal of this work is to use one of the statistical criterion to reveal small GLE by mid-latitude neutron monitors.

II. DESCRIPTION OF STATISTICAL CRITERION

With the purpose of detection GLE by means of the high mountain neutron monitor Alma-Ata B, we had been carried out the statistical analysis of cosmic ray intensity. For every GLE, found out at any station of the worldwide network of neutron monitors, we investigated ten-hour time interval, registered by means of Alma-Ata B neutron monitor. The beginning of the base hour of the examined GLE data, was accepted as the beginning of a time interval.

For everyone GLE average value of intensity of the particles registered by means of the monitor within base hour was defined

$$\mathcal{J}(t_{base}) = \frac{1}{n} \cdot \sum_{k-1}^{n} J_k(t_{base}) \quad (1a)$$

Also average values of intensity of particles for each hourly interval of time outside of base hour were defined

$$\mathcal{J}(t) = \frac{1}{n} \cdot \sum_{k-1}^{n} J_k(t) \quad (1b)$$

In (1a) and (1b) n is the number of steps of registration during an hourly interval of GLE and it is defined by an interval of registration of this GLE (n=12 if the interval of registration is equal to 5 min, n=60 if the interval of registration is equal to 1-min);

$J_k(t_{base})$ is the quantity of particles registered by means of neutron monitor on that step of registration inside of base hour; $J_k(t)$ is the quantity of particles registered by means of neutron monitor on that *k*-th step of registration inside of an interval of time (t; $t+\Delta t$), where Δt=1 hour.

At each value t the average value of intensity $\mathcal{J}(t)$ was compared to average value of intensity $\mathcal{J}(t_{base})$ by means of Student's criterion

$$K_S(t) = \frac{\mathcal{J}(t) - \mathcal{J}(t_{base})}{\sqrt{\widetilde{D}(t) + \widetilde{D}(t_{base})}} \quad (2)$$

Estimations of dispersions for averages intensities $\mathcal{J}(t)$ and $\mathcal{J}(t_{base})$ were defined, accordingly, under formulas

$$\widetilde{D}(t) = \frac{1}{(n-1)\cdot n} \cdot \sum_{k=1}^{n} (J_k(t) - \mathcal{J}(t))^2 \text{ , (3a)}$$

$$\widetilde{D}(t_{base}) = \frac{1}{(n-1)\cdot n} \cdot \sum_{k=1}^{n} (J_k(t_{base}) - \mathcal{J}(t_{base}))^2 \text{ (3b)}$$

Student's criterion is a random variable which submits to Student's law with N=2·n-2 degrees of freedom and is described by density of distribution

$$f(K_s) = B_N \cdot \left(1 + \frac{K_S^2}{N}\right)^{-\frac{N+1}{2}} \quad (4)$$

where B_N - normalizing multiplier which depends only on number of degrees of freedom N.

Cosmic ray intensity was registered during 1978-1990 by means of neutron monitor Alma-Ata B with five-minute time interval, and during 1991-2005 - with one-minute interval (http://213.211.74.116/CosRay/prod05.htm). On a hourly interval of time (t; $t+\Delta t$) it is necessary n=12 five-minute and n=60 one-minute interval of registration. Therefore at use of data with five-minute interval of registration it is necessary to take Student's distribution with N=22 degrees of freedom, and for data with one-minute step of registration to take Student distribution with N=118 degrees of freedom.

Let's assume: 1) within base hour only galactic cosmic rays are registered; 2) in any interval of time considered after base hour (t; $t+\Delta t$) intensity of galactic particles which are registered by means of the monitor, remains the same, as well as at base time interval. Then size $K_S(t)$ serves as confidential border, which allows to calculate probability $P(t)$ that in an interval of time (t; $t+\Delta t$) the intensity of particles of solar cosmic rays, in the form of surplus above a background of galactic particles is found out under the formula

$$P(t) = \int_{-\infty}^{K_S(t)} f(x)dx \quad (5)$$

III. PROCESSING OF EXPERIMENTAL DATA OF NEUTRON MONITORS BY MEANS OF STATISTICAL CRITERION

3.1. Event of 6 November 1997 (GLE55)

In Figure 1 cosmic ray intensity registered on 6th November 1997 by means of neutron monitors Alma-Ata B (latitude 43.1°), Moscow (latitude 55.5°) and Apatity (latitude 67.5°) are shown. In the same figure the behavior of Student's criterion $K_S(t)$, showing excess of average intensity of particles on hourly intervals after base hour above average intensity within base hour is shown.

In Figure 1 we can see that on the time interval reaching after base hour registered on the neutron monitor Alma-Ata B, "visually" GLE it is not found out. Student criterion $K_S(t)$ finds out on seven intervals surplus of an intensity of particles above an intensity at base hour. Statistical validity of this surplus exceeds a level 0.9995. It means that the probability of random occurrence of surplus on each of these intervals is less than 0.05 %. Probability of random occurrence of surplus on seven intervals simultaneously it will be essential less.

Cosmic ray intensity on 6 November 1997 during GLE55 is well visible by means of neutron monitor Moscow. Student's criterion $K_S(t)$ reaches great values equal to 10 and above. It is visible, that dependence $K_S(t)$ from time approximately reflects the form of a curve of a trend time of some and shows, that duration GLE was not less than 6 hours.

Cosmic ray intensity during GLE55 by means of Apatity neutron monitor has proved essentially more strongly, than by means of Moscow neutron monitor. Student's criterion $K_S(t)$ reaches values exceeding 20, i.e. Moscow reveals GLE on a time series of this monitor with security of much greater, than on the monitor. Dependence $K_S(t)$, from time reflects the form of a trend time of some and shows, that duration GLE was not less than 8 hours.

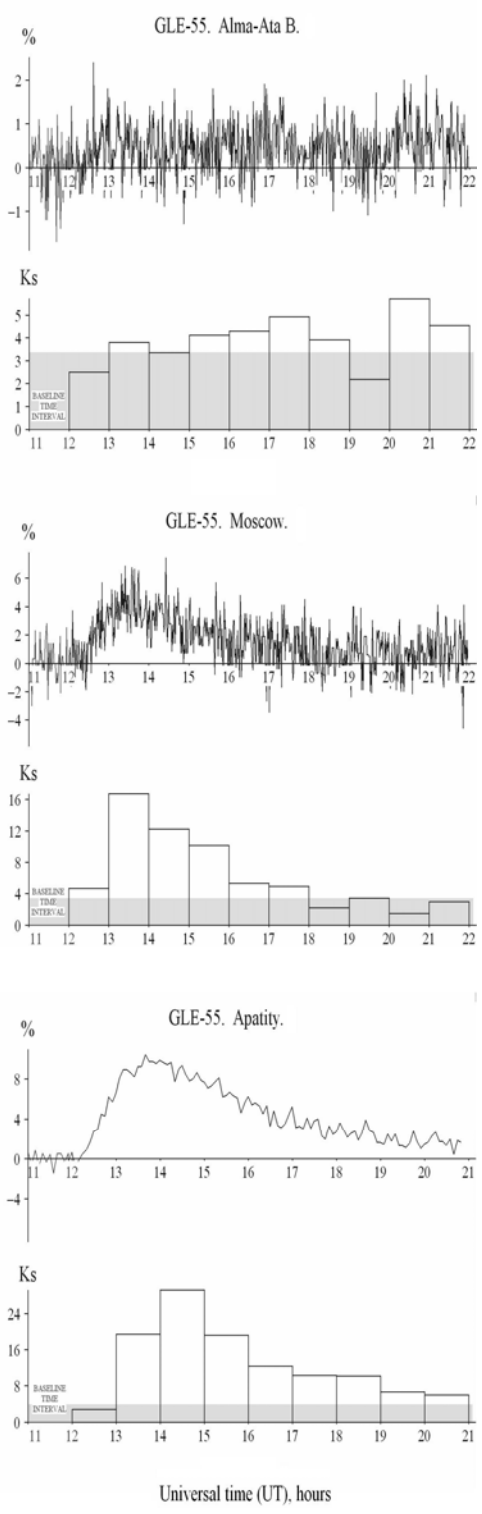

Fig. 1. Variations of the cosmic ray intensity registered by means of neutron monitors Alma-Ata B, Moscow and Apatity (%) and results of data processing by means of Student's criterion (K_S) for the event of 6 November 1997 (GLE55).

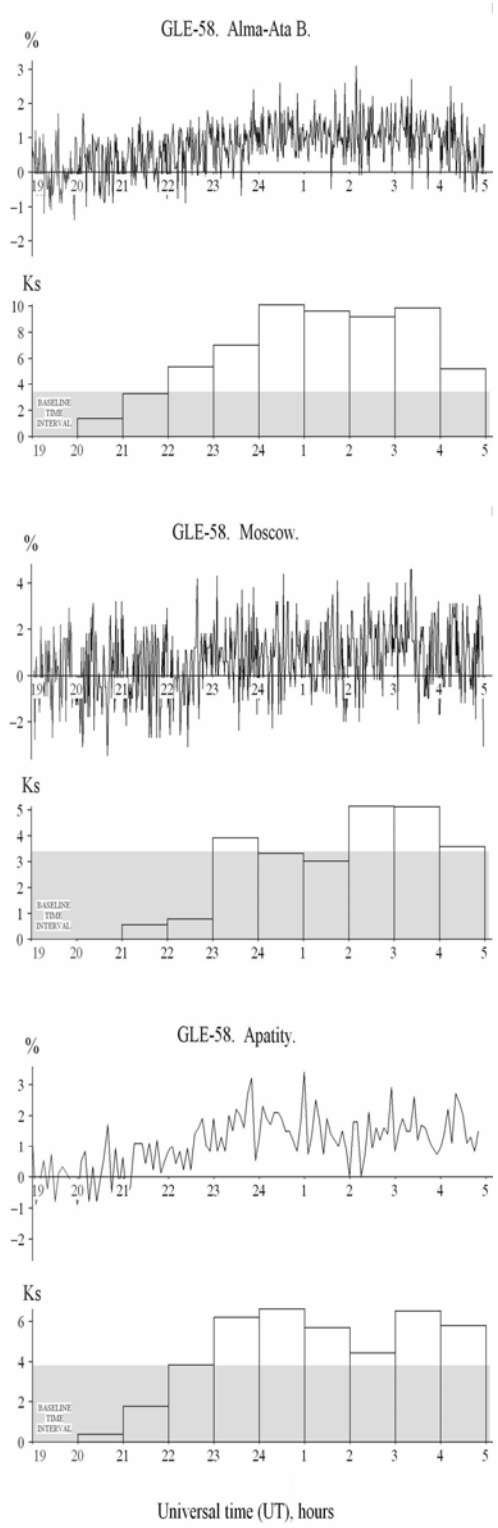

Fig. 2. Variations of the cosmic ray intensity registered by means of neutron monitors Alma-Ata B, Moscow and Apatity (%) and results of data processing by means of Student's criterion (K_S) for the event of 24 August 1998 (GLE58).

3.2. Event of 24 August 1998 (GLE58)

In Figure 2 the cosmic ray intensity registered by means of Alma-Ata B, Moscow and Apatity monitors during time since the base hour chosen for GLE58 on 24 August 1998 are shown. These intensity are interesting to that GLE58 has visually proved by means of Alma-Ata neutron monitor stronger, than by mans of Moscow and Apatity monitors. The same has shown Student's criterion. Student's criterion for Alma-Ata monitor data is equal to 10, for Moscow monitor data the value of criterion is equal to 5 and for Apatity monitor is equal to 6. Thus, the strongest GLE58 has been registered by means Alma-Ata neutron monitor. GLE58 has proved essentially more weakly on Moscow and Apatity neutron monitor data.

3.3. Event of 13 December 2006 (GLE70)

On 13 December 2006 the Sun produced a X3.4/4B class solar burst at S06W23 with onset time at 02:14 UT and maximum at 02:40 UT. This event was sufficiently energetic to be detected by worldwide network of neutron monitor stations and has been registered as a Ground Level Enhancement (GLE70) [8].

In figure 3 variations of the time series registered on 13 December 2006 on monitors Alma-Ata B, Moscow and Apatity are shown during time since the base hour chosen for GLE70. As can be seen from the figure 3, on the reaching after base hour time series registered on the neutron monitor Alma-Ata, GLE is not clearly seen. Student's criterion $K_S(t)$ finds out on five intervals surplus of an intensity of particles above an intensity at base hour. Statistical validity of this surplus exceeds a level 0.9995.

IV. CONCLUSIONS

From the above analysis it is resulted that the use of the Student's criterion allows to find out more effectively the Ground Level Enhancements of cosmic ray intensity at the middle latitude stations.. It means that it may be useful to determine the upper energy limit of particles generated at the Sun.

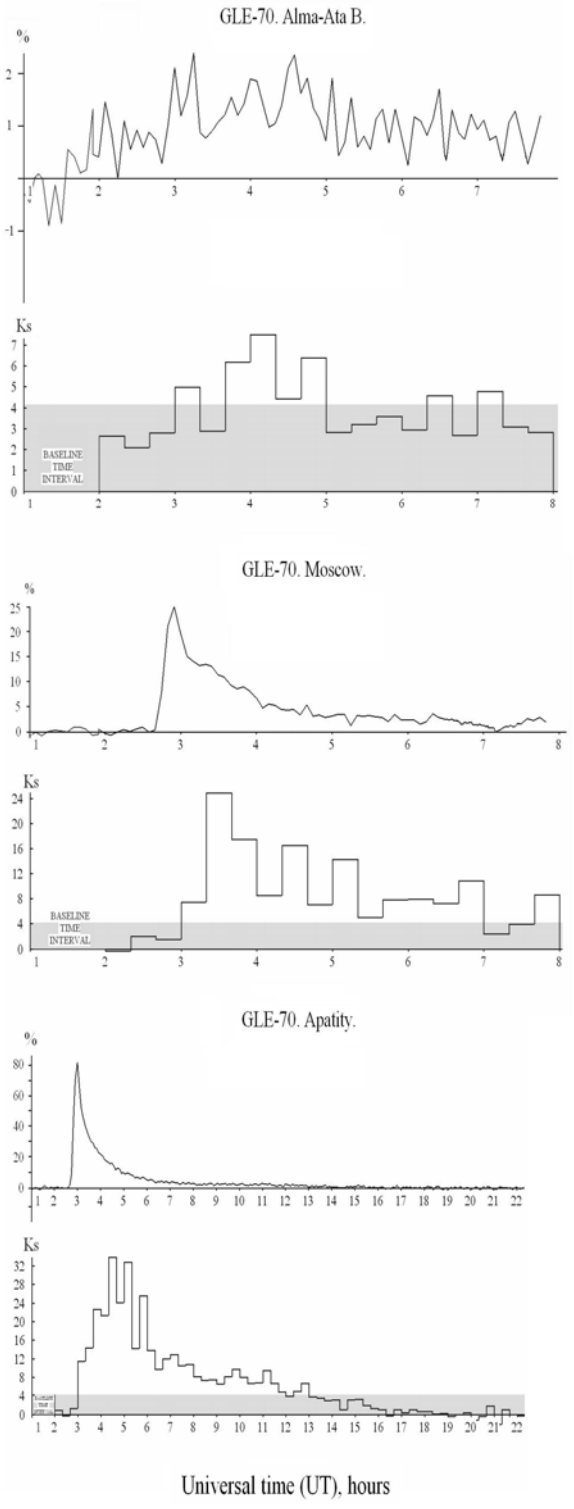

Fig. 3. Variations of the cosmic ray intensity registered by means of neutron monitors Alma-Ata B, Moscow and Apatity (%) and results of data processing by means of Student's criterion (K_S) for the event of 13 December 2006 (GLE70).

REFERENCES

[1] Smart, D and Shea, M. Solar proton events during the past three solar cycles. J. Spacecraft and Rockets, 26, 403, 1989.

[2] Shea, M. and Smart, D. A summary of major solar proton events. Solar Phys, 127, 297, 1990.

[3] Belov, A., Eroshenko, E., Mavromichalaki, H. et al. Solar cosmic rays during the extremely high ground level enhancement of February 23, 1956. Annal. Geophys., 23, 1-8, 2005

[4] Kryakunova, O. N., Aushev, V. M., Dryn, E. A., Nikolaevskyi, N. F. Investigation of ground level solar cosmic ray enhancements by means of Alma-Ata high-altitude neutron monitor. Proc. 27th ICRC, 3276-3279, 2001

[5] Duldig, M. L., Cramp, J. L., Humble, J. E., Smart, D. F. et al. The Ground-level enhancement of 1989 September 29 and October 22. Proc. NASA 10, 1993.

[6] Smart, D. F., Shea M. A., Wilson M. D., Gentile, L. C. Solar cosmic rays on 29 September 1989: An analysis using the worldwide network of cosmic ray stations. Proc. 22nd ICRC, 97-100, 1991.

[7] Aushev, V., Dorman, L.I., Kryakunova, O. N. et al. The ground level solar cosmic ray enhancements in 1989-1990. Proc. 23rd ICRC, 75-78, 1993.

[8] Plainaki, C., Mavromichalaki, H., Belov, A. et al. Application of the NM-BANGLE model to GLE70. Proc. 30th ICRC, 2008 in press.

Estimation of the Solar Proton Spectrum in the GLE70 Event

V.G. Grigoryev[1], S.A. Starodubtsev[1], V.M. Dvornikov[2], V.E. Sdobnov[2]

[1]*Yu.G. Shafer Institute of Cosmophysical Research and Aeronomy SB RAS, Yakutsk, Russia*
[2]*Institute of Solar-Terrestrial Physics SB RAS, Irkutsk,*
Russia, 677980, Yakutsk, Lenin avenue, 31, grig@ikfia.ysn.ru

Abstract — **The GLE event on December 13, 2006 as observed by network station neutron monitor data is investigated (is considered). The GLE energetic spectrum suggested for this event is estimated taking into account the primary differential spectrum of galactic cosmic rays, coupling coefficients and integral multiplicities of concrete detectors at different latitudes and observation levels. It is noted that the additional increase of solar protons is also manifested in the ionization chamber ASK-1 data at the Yakutsk station.**

Key Words — **cosmic rays, GLE**

I. Introduction

In spite of the fact that amplitude of the current 23-rd solar activity cycle is below than for the two previous cycles, nevertheless there is one remarkable peculiarity. Of 92 solar energetic particle (SEP) events (with peak flux exceeding 10 $cm^{-2}s^{-1}sr^{-1}$ for more than 10 MeV solar protons), 16 ground level enhancements (GLE) (~ 15 %) have been registered. It is interest to study the last ground increase (GLE70) of cosmic ray (CR) flux on December 13, 2006 which occurred near solar minimum.

II. Results and Discussion

The flare (importance X3/4B; at 02:40 UT) and the accompanying halo–CME (at 02:54 UT) originated from the active region NOAA 10930 with coordinates S05W23 (*http://umbra.nascom.nasa.gov/SEP/seps.html*). It has been detected with network station monitors

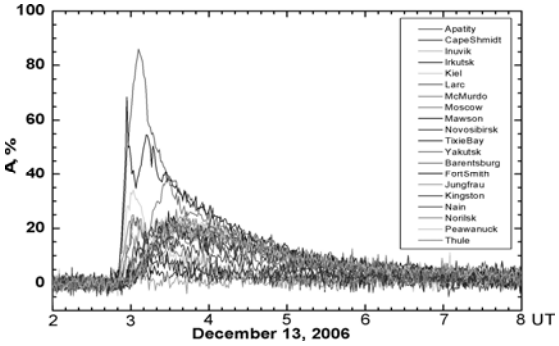

Fig. 1. Temporal profiles of GLE70 by 1-min data of 20 neutron monitors

(see Fig. 1). To determine the spectrum for the GLE70 event on December 13, 2006, we used 1-min data of 20 neutron monitors of network CR stations (*ftp://cr0.izmiran.rssi.ru/Cosray/FTP GLE*). The stations were selected in such a way that their asymptotic receiving cones of solar particles were rather uniformly distributed in direction. As is seen from Fig. 1, the essential difference in onset and maximum time of the event is observed. Besides, the noticeable difference in the intensity profile is also observed. This points out the presence of strong anisotropic effects which are not considered in this paper.

Table 1 presents a list of stations, data of which are used in the analysis, count rate for each station, threshold rigidity, amplitude of CR intensity at a maximum and time moment 15, 30 and 60 min from the beginning of particle flux increase at the station.

The estimation of CR flux spectrum (without anisotropy) by using neutron monitor data was carried out by the method suggested in [1], [2]. The integral intensity of secondary particles observed on the Earth is given in the form:

$$N(p) = \int_{p_{\min}}^{\infty} p^{-\gamma} m(p) dp, \quad (1)$$

where $m(p)$ is an integral multiplicity of the secondary particle generation from a primary particle with the impulse p at the atmosphere boundary, $p^{-\gamma}$ is a galactic CR spectrum. Calculations of the $N(p)$ will be carried out, if integral multiplicities are known. Conditions of CR registration at different stations essentially differ

from each other, therefore, $m^i(p)$ is separately calculated for each *i*-station. To determine the integral multiplicity for *i*-detector, we use the expression [2]:

$$m(p) = \frac{W^i_{\min}(p) N^i(p)}{p^{-\gamma}} \quad (2)$$

where $W^i_{\min}(p)$ are coupling coefficients of neutron monitors at solar activity minimum known from latitudinal observations [3], $N^i(p)$ is a flux observed of galactic CRs at the same period.

As an example, Fig. 2 and Fig. 3 present calculation results of coupling coefficients and integral multiplicities for Apatity, Mawson, Novosibirsk, Tixie Bay, Fort Smith and Thule stations for the different γ.

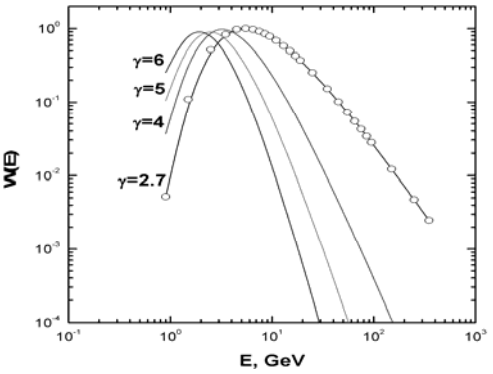

Fig. 2. The normalized coupling coefficients for different γ. Observational results are shown by the open circles.

For the case of solar particle rise, the Eq. 1 can be written in the form: $N(p) = \int_{p_{\min}}^{\infty} p^{-\gamma} m(p) dp$, where $m^i(p; \gamma)$ is the integral multiplicity depending on index γ.

If $N^i(p)$ is the galactic CR intensity registered at *i*-station before the arrival of solar particles, N^i_{obs} is the additional flux at *i*-station, then the coefficient $k = N^i_{obs} / N^i$ will reflect the relative density of this flux at the observation moment. In this case, to determine $m^i(p; \gamma)$ there is a need to know the coupling coefficients $W^i(p; \gamma)$ for the solar particles. To calculate $W^i(p; \gamma)$ for different γ (see Fig. 2), we used the expression: $m(p) = \frac{W^i_{\min}(p) N^i(p)}{p^{-\gamma}}$.

Thus, taking into account results obtained and according to Eq. 2, we determine integral multiplicities of solar protons $m^i(p; \gamma)$ depending on the spectrum index γ (see Fig. 3).

The solar proton fluxes $N^i_{\exp}$ expected are calculated for the GLE70 event at *t* = 15, 30 and 60 min from the beginning of intensity rise. To find the spectrum index γ, we determined, according to [2], a ratio $a_i(\gamma)$ of theoretical expected values $N^i_{\exp}$ to observational values N^i_{obs}. In this case, the value A(γ) is a characteristic of constancy of this ratio: $A(\gamma) = \frac{1}{20}\sum_1^{20} \left| \lg a_i(\gamma) - \overline{\lg a(\gamma)} \right|$, where $\overline{\lg a(\gamma)} = \frac{1}{20}\sum_1^{20} \lg a_i(\gamma)$. Here, the value γ is considered to be the most real, when $A(\gamma)$ is minimum.

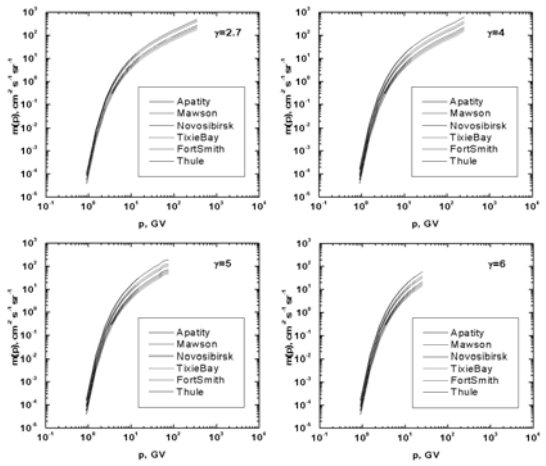

Fig. 3. Integral generation multiplicities for six CR station selected.

The estimation of the spectrum index for the solar protons in the event GLE70 shows that during the first hour after the beginning of the event, the effective index is enough hard: γ_{eff} ~ 5. This is consistent with data of the ionization chamber ASK-1 (R_c ~ 6.6 GV) at the Yakutsk station, which is registered a small (~ 0.6 %) increase of CR intensity, although the ground-based muon telescope (R_c ~ 3 GV) no increase is registered. Note that the ionization chamber registers, on the whole, the CR muon component, but the secondary neutrons also make the small contribution. The small GLE (~ 1 %) was observed at the Alma-Ata neutron monitor station (R_c ~ 6.6 GV).

TABLE I
SOME CHARACTERISTICS OF CR STATIONS AND EFFECTS OF GLE OBSERVABLE ON THEM

NN	Station	Count Rate (mp/s)	R_c (GV)	A_{max} (%)	A_{15min} (%)	A_{30min} (%)	A_{60min} (%)
1	Apaptity	160	0.6	86	86	48	28
2	Cape Shmidt	100	0.5	20	13	30	16
3	Inuvik	215	0.16	21	14	20	17
4	Irkutsk	220	3.6	6	6	4	3
5	Kiel	175	2.3	33	30	13	7
6	Larc	77	3	23.5	23.5	9	5
7	McMurdo	250	0.5	26	14	23	20
8	Moscow	162	2.4	25	23	13	9
9	Mawson	240	0.5	68	35	45	28
10	Novosibirsk	175	2.8	10	4	10	5
11	Tixie Bay	110	0.5	26	16	26	15
12	Yakutsk	210	1.6	16	8	16	14
13	Barentsburg	145	0.5	39	20	39	22
14	Fort Smith	290	0.5	24	15	24	17
15	Jungfraujoch	155	4.5	9.5	5	0	0
16	Kingston	205	1.8	16.5	11	16.5	12
17	Nain	205	0.9	24	16	22	19.5
18	Norilsk	108	0.64	23	23	23	20
19	Peawanuck	225	0.9	23	18	23	19
20	Thule	220	0.5	22	12	22	18

III. CONCLUSION

The above analysis shows that the event GLE70 considered is characterized by the enough hard energy spectrum with $\gamma \sim 5$.

ACKNOWLEDGMENT

This work was supported by the RFBR grants 06-02-96008-r-East, 05-02-16954, 07-02-01405 and 07-02-00972; the Program of the RAS Presidium N16, part 3, the project 14.2; the Complex Integration Project of SB RAS No.3.10; the program of Presidium of RAS "*Neutrino* Physics" in the framework of the project "*Investigation of modulation effects of cosmic rays with the use of the method of ground-based and stratosphere monitoring"*. We thank all Cosmic Ray Station teams for providing the data online.

REFERENCES

[1] N.S. Kaminer, Ya.L. Blokh, L.I. Dorman, "Cosmic-Ray Burst of 4 May 1960"*, Izdatel'stvo Akademii Nauk SSSR*, 4: 1961, pp. 146–167.

[2] L.I. Miroshnichenko, *Solar Cosmic Rays*, Kluwer Academic Publishers, Dordrecht /Boston/ London, 2001.

L.I. Dorman, *Cosmic Ray Variations*, Transl. Techn. Doc. Liaison Office, Wright-Patterson Airforce Base, USA, 195

Asymptotic directions of viewing during the GLE70 event

C. Plainaki[1,2], H. Mavromichalaki[1], A. Belov[3] , E. Eroshenko[3] and V. Yanke[3]

[1] *Nuclear and Particle Physics Section, Physics Department, Athens University Pan/polis-Zografos 15771 Athens, Greece*
[2]*Istituto di Fisica dello Spazio Interplanetario, Via del Fosso del Cavaliere, 00133 Roma, ITALY,*
[3] *Institute of Terrestrial Magnetism, Ionosphere and Radio Wave Propagation (IZMIRAN), 42092, Troitsk, Moscow Region, Russia*

Abstract **— During the recent ground level enhancement of 13 December 2006, also known as GLE70, solar cosmic ray particles of energy bigger that ~500 MeV/nucleon propagated inside the Earth's magnetosphere and finally accessed low-altitude satellites and ground level neutron monitors. The magnitude and the characteristics of this event registered at different neutron monitor stations of the worldwide network can be interpreted adequately on the basis of an estimation of the solar particle trajectories in the near Earth interplanetary space. In this work, an extended representation of the Earth's magnetic field was realized applying the Tsyganenko 1989 model. Using a numerical back-tracing technique the solar proton trajectories inside the magnetospheric field of the Earth were calculated for a variety of particles, initializing their travel at different locations, covering a wide range of energies. In this way, the asymptotic directions of viewing were calculated for a significant number of neutron monitor stations, providing crucial information on the Earth's "magnetospheric optics" for primary solar cosmic rays, on the top of the atmosphere, during the big solar event of December 2006. The neutron monitor network has been treated, therefore, as a multidimensional tool that gives insights into the arrival directions of solar cosmic ray particles as well as their spatial and energy distributions during extreme solar events.**

***Key Words*—Magnetospheric field, asymptotic directions of viewing, cosmic rays, neutron monitor, modeling**

I. INTRODUCTION

eutron monitors located at different places on the Earth's surface record secondary particles originating from primaries that come in general from different directions in space. Charged galactic and solar cosmic ray particles approaching the Earth encounter its geomagnetic field. If they are sufficiently energetic they can propagate inside the magnetosphere and enter the Earth's atmosphere. Products of the interaction of these particles with the molecules of the atmosphere, access ground level neutron monitors located at different sites around the globe. Due to the geometry of the geomagnetic field the rigidities of primary cosmic ray particles responsible for the counting rates registered at ground level have values bigger than the so called cut-off rigidity of the specific site. Moreover, due to the particle motion inside the geomagnetic field, each ground level detector is capable of recording particles produced by primaries originating from a limited set of directions in space, which is called asymptotic cone of viewing. The problem of defining these asymptotic directions of viewing for a specific neutron monitor has been always of great interest and therefore several efforts for calculating the cut-off rigidities as well as the particle trajectories and the asymptotic cones of viewing have been made over the years ([1], [2], [3] and [4]). However, due to the complexity of the real magnetospheric field of the Earth, the problem of defining the particle

trajectories inside the magnetosphere has no solution in closed form yet.

Due to the fact that each neutron monitor records secondary particles produced by primaries originating from different parts of the sky, it is proved to be a magnetospheric window in the near Earth interplanetary space providing crucial information on the Earth's "magnetospheric optics" for primary cosmic rays ([5]). Getting this information at ground level is very important and can be utilized in means of space weather monitoring and forecasting. The neutron monitor network, as a whole, can be consequently treated as a multidimensional tool that gives insights into the arrival directions of solar cosmic ray particles as well as their spatial and energy distributions during several cosmic ray events ([5], [6]). A significant number of solar extreme events resulting in count rate increase of the cosmic ray intensity registered at ground level neutron monitors took place during the descending phase of the 23rd solar cycle. Several studies on the ground level enhancements (GLEs) of October– November 2003 ([7]; [8], [9]) and January 2005 ([5]) have been realized. Recently, on 13 December 2006, a new GLE was recorded by the worldwide network of neutron monitors. This GLE was the third biggest GLE of the current cycle of solar activity, leaving behind only the enhancements of 15 April, 2001 and 20 January, 2005 having a magnitude of ~92% recorded at Oulu Neutron Monitor.

The peculiarities and differences between the intensities of secondary solar particles occurring between different neutron monitor stations during the ground level enhancement of 13 December 2006 can be interpreted on the basis of their asymptotic directions of viewing during that exact period. In this work an effort for calculating the asymptotic directions of viewing for a significant number of neutron monitors stations widely distributed around the globe covering a wide range of latitudes, longitudes and rigidities has been made using the Tsyganenko 1989 magnetospheric field model for the time period of the big solar cosmic ray event of December 2006 (GLE70).

II. CALCULATION METHOD

Incoming charged particle trajectories to various locations on the surface of the Earth can be traced if the Earth's magnetospheric field is well defined. The equation of motion is expressed as:

$$\ddot{\vec{r}} = e/mc \cdot \dot{\vec{r}} \times \vec{B} \qquad (1)$$

where $\ddot{\vec{r}}$ is the particle acceleration, $\dot{\vec{r}}$ is the particle velocity, and $\vec{B}$ is the magnetic field vector. The electronic charge is denoted by e, m is the particle's relativistic mass, and c is the speed of light.

In the current analysis, in order to describe the Earth's magnetospheric field, we have used Tsyganenko 1989 model, which is a semi-empirical best-fit representation, based on a large number of satellite observations (IMP, HEOS, ISEE, POLAR, Geotail, etc), providing quite a realistic description of the field configuration in the magnetosphere ([10]). The model includes the contributions from external magnetospheric sources: ring current, magnetotail current system, magnetopause currents and large-scale system of field-aligned currents. It also takes into consideration the seasonal and diurnal changes of the magnetospheric field as well as the geomagnetic activity level Kp. In contrast with the majority of previous geomagnetic field models (e.g. [11]), the Tsyganenko 1989 model takes into account the effect of the current sheet warping. This means that it is built in such a way as to account that for non-zero tilt angle ψ between the z-GSM axis and that of the Earth's dipole the average shape and position of the tail neutral sheet undergoes a two-dimensional warping ([12], [13] and [14]). Near the midnight meridian plane the warping results in a gradual departure of the current sheet from the dipole equatorial plane towards that parallel to the solar wind stream. This is accompanied by a bending of the sheet in the YZ projection in such a way that, for $\psi > 0$, the current surface is raised above the GSM equatorial plane in the central tail region, whereas it is depressed below this plane near the tail flanks (and vice versa for $\psi < 0$). The geometry of the current sheet according to the Tsyganenko 1989 magnetospheric field model, for the time period of GLE70 (tilt angle ~31.88 degrees) is demonstrated in Fig. 1. The current sheet geometry of the geomagnetic filed is very important for the calculation of the particle trajectories, since it reflects the distribution of the magnetic field lines. Therefore, taking it into account results in a more accurate and reliable representation of the field and consequently in a more detailed calculation of the neutron monitor asymptotic directions of viewing. Nevertheless, one should notice that apart from the Tsyganenko 1989 model there is a variety of other magnetic field models, suitable also for geomagnetically disturbed periods ([15]). However, because of the fact that this event took place during a moderate geomagnetic disturbance, their use would not affect significantly the present results.

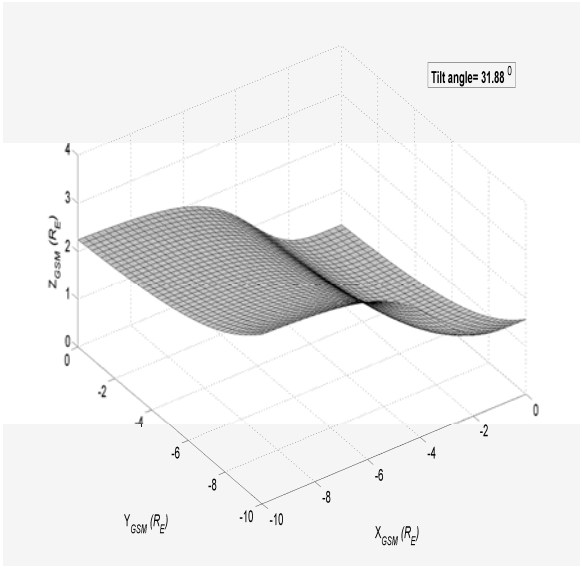

Fig.1: Geometry of the Current Sheet on 13 December 2006 during the time period of GLE70. The unit along *X, Y, Z* axes is the Earth's radius (R_E).

In order to calculate the particle trajectory inside the magnetic field a numerical back-tracing trajectory technique has been used Charged particles are assumed at the site of each ground level detector and their path as they are moving away from the detector is being traced. The trajectory starts from the observational site and is traced back by reversing the particle's velocity vector and the sign of charge. Particles of the same rigidity (momentum per unit charge) but opposite charge will follow the same path through the field as particles arriving from the sun. The computed trajectory is defined as allowed if it crosses the magnetospheric boundaries whereas it is defined as forbidden if it rests on the Earth's surface or it remains trapped within the magnetosphere. Thus rigidity dependent viewing directions can be determined for each observational site and therefore independently for each neutron monitor. One should note that in many cases (as in this analysis) it is sufficient to consider only those particles arriving with vertical incidence at the detector. Since the system expressed by equation (1) consists of three simultaneous differential equations with six unknowns (three accelerations and three velocities expressed in spherical coordinates) the problem of defining the particle trajectory and motion can be solved numerically on the basis of Runge Kutta Method ([16]).

III. RESULTS-DISCUSSION

For the time period of 13 December 2006 the asymptotic directions of viewing calculated for a big number of neutron monitor stations widely distributed around the globe covering a wide range of vertical cut-off rigidities are shown in Fig. 2. Assigning the term "neutron monitor asymptotic cone" to the set of allowed trajectories traces at the altitude of ~ 80 km above the Earth surface for this specific station, the magnetospheric windows for all the existing worldwide neutron monitor network were defined (Fig.2). Commenting Fig. 2, one should point out that each point refers to a particular rigidity. For example, particles that reached the NM of Oulu, in the time period of GLE70, produced from primaries of rigidity of ~1 GV originated from (long = 22.68^0, lat = 2.99^0),

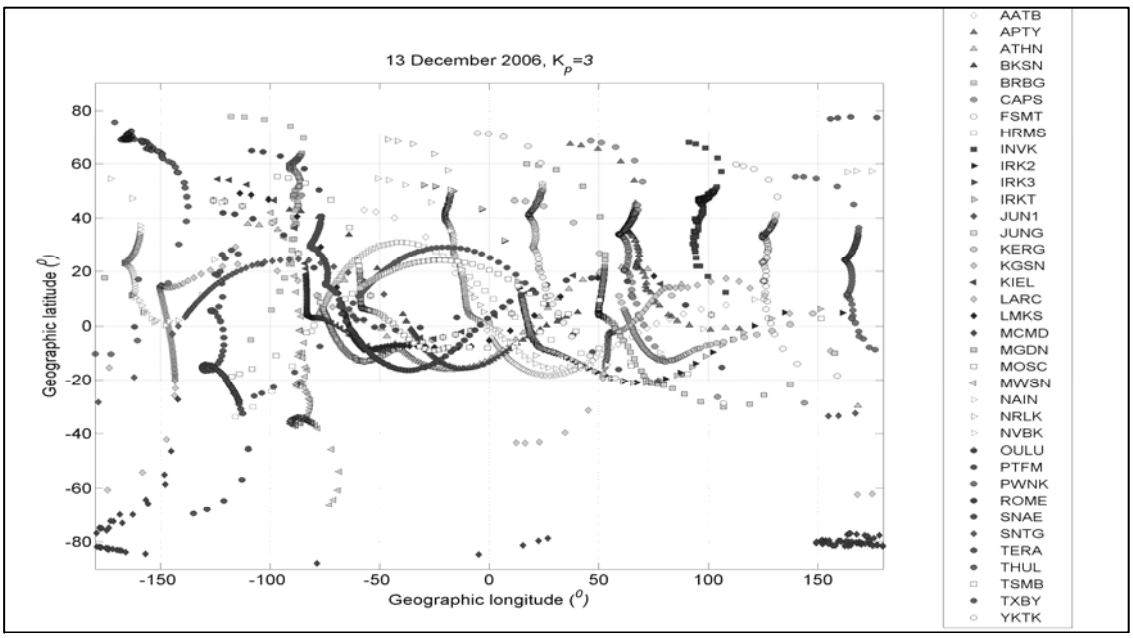

Fig. 2. Asymptotic directions of viewing for the neutron monitors of the worldwide network. The calculation step in rigidity scale was taken as 0.1 GV.

whereas those produced from primaries of rigidity of ~ 2 GV came from (long = 80.24^0, lat = 2.08^0), at the altitude of 80 km. For a mid latitude station the situation changes. For example for Moscow NM station the primaries of rigidity of 2.6 GV, producing the respective NM fluxes, originated from (long = -172.05^0, lat = 9.37^0).

It is clearly revealed that the counting rates registered at different observational sites correspond to primary particle fluxes originating from different points of the sky. This fact can give explanation to various questions arising from the observations. For example, during the ground level event of Deecember 2006, some low cut-off rigidity neutron monitor stations (e.g. McMurdo) recorded enhancements of significantly smaller magnitude in comparison with those registered at other stations of the same cut-off rigidity (e.g. Apatity, Oulu). Moreover, these differences were even bigger during the initial phase of the event. At this point it should be stated that in the general case of an anisotropic GLE, the source of anisotropy above the Earth's atmosphere is located at some specific position, which may or may not change with time. Therefore, any differences in the counting rates of the ground level neutron monitors of the same cut off rigidity can be possibly attributed to different asymptotic directions of viewing between these stations in relation to the location of the source of the anisotropic solar particle flux. In other words, stations with asymptotic cones at the most favourable positions are those that record the maximum effect, whereas other record smaller increases or not enhancements at all. Results of the calculation of the position of the anisotropy source during the time period of GLE70 on the basis of the NM-BANGLE model, showed that the solar particle anisotropic source must have been located close enough to the ecliptic plane ([17]). This seems to be also the reason why this event was recorded bigger at sub-polar stations and not at polar ones, as it happens usually during GLEs.

According to the results of the application of theNM
BANGLE model, the solar energetic particles seemed
to have arrived forming a narrow beam that could be
sensed better by those neutron monitors with asymptotic cones in the most favourable positions in relation to the beam (e.g. Apatity, Oulu, Mawson). Other stations with asymptotic viewing directions far from the anisotropic source (e.g. Tixie Bay) recorded smaller increases at that moment. It should be pointed out, however, that during later phases of the event, the results of the NM-BANGLE model application, showed that the narrow particle beam was getting wider with time and consequently more and more NM stations could sense the solar particle event ([17]).

IV. CONCLUSIONS

The neutron monitors asymptotic directions of viewing were calculated applying the Tsyganenko 1989 magnetospheric field model for the time period of the solar extreme event of 13 December 2006 (GLE70). From the current analysis, the following main points are revealed:

- On 13 December 2006, neutron monitors around the world had different asymptotic cones recording cosmic rays which came in general from different parts of the sky
- Due to their different cut-off rigidity as well as to their different asymptotic cones, the neutron monitors of the worldwide network recorded the GLE with different intensity. The enhancement was recorded bigger at sub-polar stations.
- The neutron monitors asymptotic directions of viewing obtained on the basis of Tsyganenko 1989 in combination with the NM-BANGLE Model ([17]) give possible analytical explanations to differences between neutron monitors recordings during GLE70.

Concluding, one should emphasize the importance of the existence of a worldwide network of neutron monitors in studying solar proton events recorded at ground level. Moreover real-time technology provides such a network with the capability of continuous cosmic ray recordings as well as real-time calculation and on line distribution of the values of several primary proton flux parameters by applying suitable models.

ACKNOWLEDGMENT

Thanks are due to all our colleagues from the neutron monitor stations, who kindly provided us with the data used in this analysis: Alma Ata, Apatity, Athens, Baksan, Barentsburg, Cape Schmidt, Fort Smith, Hermanus, Inuvik, Irkutsk-1, 2,3, Jungfraujoch, Jungfraujoch-1, Kerguelen, Kingston, Kiel, Larc, Lomnicky Stit, Magadan, Mawson, McMurdo, Moscow, Nain, Norilsk, Novosibirsk, Oulu, Potchefstroom, Peawanuck, Rome, Sanae, San Tiago, Terre Adelie , Thule, Tsumeb, Tixie Bay and Yakutsk.

REFERENCES

[1] McCracken, K.G., Rao, V.R. and Shea, M.A.: The trajectories of cosmic rays in a high degree simulation of the geomagnetic field, *Technical report*, 77, Massachusetts Institute of technology, USA, 1962.

[2] McCracken, K. G., Rao, U. R., Fowler, B. C., Shea, M. A., and Smart, D. F.: Cosmic Ray Tables (Asymptotic Directions, etc.)', *Annals of the IQSY* 1, 14, 198–214, MIT Press, Cambridge MA, U.S.A, 1968.

[3] Shea, M. A., Smart, D. F., and McCracken, K. G.: A Study of Vertical Cutoff Rigidities Using Sixth Degree Simulations of the Geomagnetic Field, *J. Geophys. Res.* 70, 4117–4130, 1965.

[4] Smart, D.F., Shea, M.A. and Flückiger, E.O.: Magnetospheric models and trajectory computations, *Space Sci. Rev*., 93, 281-308, 2000.

[5] Plainaki, C., A. Belov, E. Eroshenko, H. Mavromichalaki, V. Yanke: 'Modeling ground level enhancements: the event of 20 January 2005', J. Geophys. Res.-Space Physics, 112, A04102, doi:10.1029/2006JA011926, 2007a.

[6] Mavromichalaki, H., Plainaki, C., Gerontidou, M., Sarlanis, C., Souvatzoglou, G. Mariatos, G., Belov, A., Eroshenko, E., Klepach, E. and Yanke, V.: 'GLEs as a warning tool for radiation effects on electronics and systems: A new Alert System based on real-time Neutron Monitors', IEEE TRANSACTIONS for Nuclear Science, 54, 4, 1082, 2007.

[7] Plainaki, C., A. Belov, E. Eroshenko, V. Kurt, H. Mavromichalaki and V. Yanke: Unexpected burst of solar activity recorded by neutron monitors during October-November 2003, *Adv. Space Res., 35,* 691, 2005.

[8] Eroshenko, E., Belov, A., Mavromichalaki, H., Mariatos G., Oleneva, V., Plainaki, C., Yanke, V.: 'Cosmic ray variations during the two great bursts of solar activity in the 23rd solar cycle', *Solar Phys*. 224, 345-358, 2004.

[9] Bieber, J.W., J. Clem, P. Evenson, R. Pyle, D. Ruffolo and A. Saiz: Relativistic solar neutrons and protons on 28 October 2003, *Geophys. Res. Letters*, 32, 3, CiteID L03S02, 2005.

[10] Tsyganenko, N.A.: A magnetospheric magnetic field model with the warped tail current sheet, *Planet. Space Sci., 37,* 5, 1989.

[11] Tsyganenko, N.A.: Global quantitative models of the geomagnetic field in the cislunar magnetosphere for different disturbance levels, *Planet. Space Sci., 35,* 1347, 1987.

[12] Russell, C.T. and Brody, K.I.: Some remarks on the position and shape of neutral sheet, *J. Gephys. Res.*, 72, 6104, 1967.

[13] Fairfield, D.H.: A statistical determination of the shape and position of the geomagnetic neutral sheet., *J. Geophys. Res*., 85, 775, 1980.

[14] Gosling, J. T., McComas, D.J., Thomsen, M.F., Bame, S.J. and Russell, C.T.: The warped neutral sheet and plasma sheet in the near-Earth geomagnetic tail., J. Geophys. Res., 91, 7093, 1986.

[15] Kudela, K., Bučík, R. and P. Bobík: On transmissivity of low energy cosmic rays in disturbed magnetosphere, J. Adv. Space Res., doi:10.1016/j.asr.2007.09.033, 2007.

[16] Ralston, A. and Wilf, S. H.: Mathematical Methods for Digital Computers, John Wiley and Sons, New York NY, USA, 1960.

[17] Plainaki, C., Mavromichalaki, H., Belov, A., Eroshenko, E., Yanke, V.: "Application of the NM-BANGLE model to GLE70", Proc. 30th Intern. Cosmic Ray Conf., Merida, 2007b.

Cosmic ray variations in relation to human physiological state during December 2006

M. Papailiou[1], H. Mavromichalaki[1], A. Vassilaki[1], K. M. Kelesidis[2], G. A. Merztanos[2] and B. Petropoulos[3]

[1] *Nuclear and Particle Physics Section, Physics Department, University of Athens, Athens, Greece*
[2] *Cardiological clinic of the KAT Hospital, Athens, Greece*
[3] *Research Center of Astronomy and Applied Mathematics, Academy of Athens, Athens, Greece*

Abstract— **There is an increasing amount of evidence linking biological effects to solar and geomagnetic disturbances. A series of studies is published referring to the changes in human physiological responses at different levels of geomagnetic activity. In this study the possible relation between the daily variations of cosmic ray intensity, measured by the Neutron Monitor at the Cosmic Ray Station of the University of Athens (http://cosray.phys.uoa.gr) and the average daily and hourly heart rate variations of persons, with no symptoms or hospital admission, monitored by Holter electrocardiogram, is considered. This work refers to a group of persons admitted to the cardiological clinic of the KAT Hospital in Athens during the time period from 4th to 24th December 2006 that is characterized by extreme solar and geomagnetic activity. A series of Forbush decreases started on 6th December and lasted until the end of the month and a great solar proton event causing a Ground Level Enhancement (GLE) of the cosmic ray intensity on 13th December occurred. A sudden decrease of the cosmic ray intensity on 15th December, when a geomagnetic storm was registered, was also recorded in Athens Neutron Monitor station (cut-off rigidity 8.53 GV) with amplitude of 4%. It is noticed that during geomagnetically quiet days the heart rate and the cosmic ray intensity variations are positively correlated. When intense cosmic ray variations, like Forbush decreases and relativistic proton events produced by strong solar phenomena occur, cosmic ray intensity and heart rate get minimum values and their variations, also, coincide. During these events the correlation coefficient of these two parameters changes and follows the behavior of the cosmic ray intensity variations. This is only a small part of an extended investigation, which has begun using data from the year 2002 and is still in progress.**

Key Words—**Cosmic ray intensity, Forbush decreases, heart rate variations, human physiological state**

I. INTRODUCTION

Over the last years many studies have been carried out concerning the possible effect that solar and geomagnetic activity might have on human physiological state [2], [4], [6], [20]. Even though there is skepticism in the scientific community regarding the possibility that heliogeophysical changes can influence human health, the results are irrefutable. Human physiological status is influenced by environmental factor changes requiring from the organism and its nervous system a large range of adaptation reactions, which are decreased in case of different diseases [4].

It is obvious that solar or geomagnetic variations could not be solely responsible for all the changes or fluctuations of physiological parameters measured in a human organism. The physiological status of a human being and the abnormalities such as myocardial infractions, brain strokes, cardiac arrhythmias etc. that an organism might exhibit are influenced by many factors such as environmental physical activity and social parameters, smoking, age, etc. Nevertheless it is shown that geomagnetic variations of solar origin can influence at some level the human health and cause a chain of serious problems [24], [28]. It has been shown that, apart from cardiovascular diseases, like
myocardial infraction and brain strokes, also train malfunctions of man – related origin can be influenced by space weather parameters, both in short (during Forbush decreases events) and long – term scale (solar activity cycle). These results on man – related train accidents give additional support to the idea that the capability of operators to

react correctly to the environmental circumstances can be influenced by space weather parameters. In short – term scale the cosmic ray intensity seems to be the best indicator of such correlation [6].

In the last decades many scientists have worked on the impact of space weather parameters, through the geomagnetic field, on different diseases [3], [6], [8], [9], [21]. It has been revealed that cardiovascular circulatory, nervous and other functional systems react under changes of geophysical factors [2], [10], [12], [16], [29], [30]. It has long been claimed that geomagnetic storms and other electromagnetic variations are associated with changes in the incidence of various diseases, myocardial infractions and strokes [11]. Some evidence has also been accumulated on the association between geomagnetic disturbances and increases in work and traffic accidents [7], [18], [19].

Recent studies consider the links between life threatening cardiac arrhythmias, sudden cardiac deaths and the level of environmental physical activity factors like geomagnetic activity and cosmic ray and high energy proton flux [23]. Moreover a new field, called 'Clinical Cosmobiology', is slowly developing. This field studies the relationship between the frequency of total deaths, cardiac arrhythmias, occurrence of acute myocardial infraction, risk related cardiovascular parameters, deaths from cardiovascular diseases, temporal distribution of sudden cardiac death, stroke, life threatening cardiac arrhythmias, homicide and suicide and the level of major environmental physical activity factors [23].

In this work the problem of the possible synchronization of the sudden changes in cosmic ray intensity with the ones of heart rate variations on a daily basis is considered. Cosmic ray intensity data from the Athens Neutron Monitor for December 2006 are used. A comparison of these with those involving the heart rate variations of thirty persons with no symptoms and hospital admission, which have been obtained by the method of Holter electrocardiogram, also in Athens region, is performed.

II. DATA SELECTION AND METHODS

The time period from 4th to 24th December 2006, being very close to the end of the 23rd solar cycle was characterized by extreme solar and geomagnetic activity. In this study hourly, pressure corrected, data of the hadronic component of the cosmic ray intensity obtained from the Cosmic Ray Station of the University of Athens (Super 6NM-64) have been used. This station is located 260m above sea level and detects particles with a cut – off rigidity of 8.53 GV. It is operational since November 2000 providing high quality real-time data through Internet (http://cosray.phys.uoa.gr). These data have a time resolution of 1 hour, 1 min and 1 sec as well, unique in the world [13], [14]. The statistical error is smaller than 0.30% on hourly data.

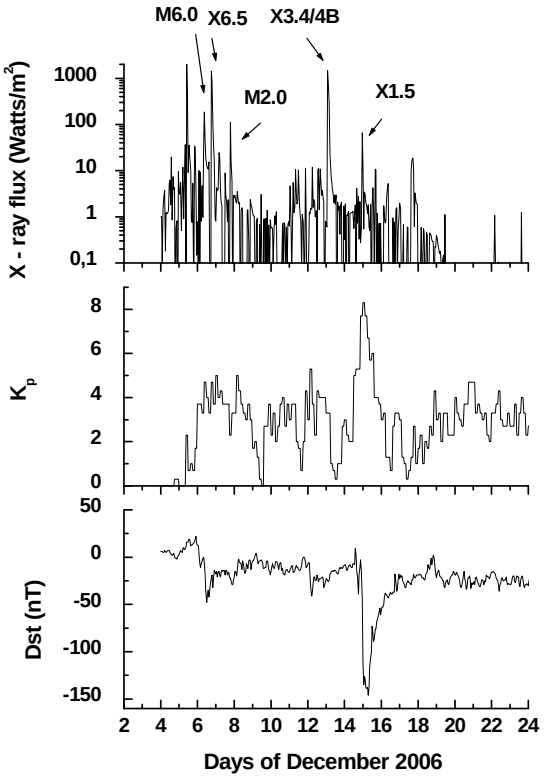

Fig. 1. The X – ray flux as measured by GOES – 12 satellite (top panel), the K_p index (middle panel) and the variation of the Dst index (bottom panel) during December 2006 are illustrated.

Data are also used concerning solar flares registered by GOES satellites. Moreover data for the X-ray flux and the geomagnetic index K_p (http://spidr.ngdc.noaa.gov/spidr/index.jsp) have been used for the time period under study. The geomagnetic index Dst from the World Data Centre for Geomagnetism, Kyoto (http://swdcwww.kugi.kyoto-u.ac.jp/) is also used for December 2006 (Fig. 1, bottom panel).

A series of solar flares of classes M and X was registered starting from 6th December until 14th December. The hourly X – ray flux data from GOES – 12 satellite concerning this period were plotted and the most important solar flares are shown in Figure 1 (top panel). We are mostly interested in the two big solar flares on 13th and 14th December 2006. The first flare was of class X3.4/4 B with maximum at 2:40 UT and the second one

was a solar flare of class X1.5 and maximum at 22:15 UT. These flares produced energetic solar cosmic rays that were guided towards the Earth and resulted in an increase in the count rates of the ground based cosmic ray detectors. The middle panel in the same figure shows the variations of the geomagnetic K_p index. On 15th December K_p had a value of 8^+ that means that a geomagnetic storm occurred.

The data concerning the heart rate variations

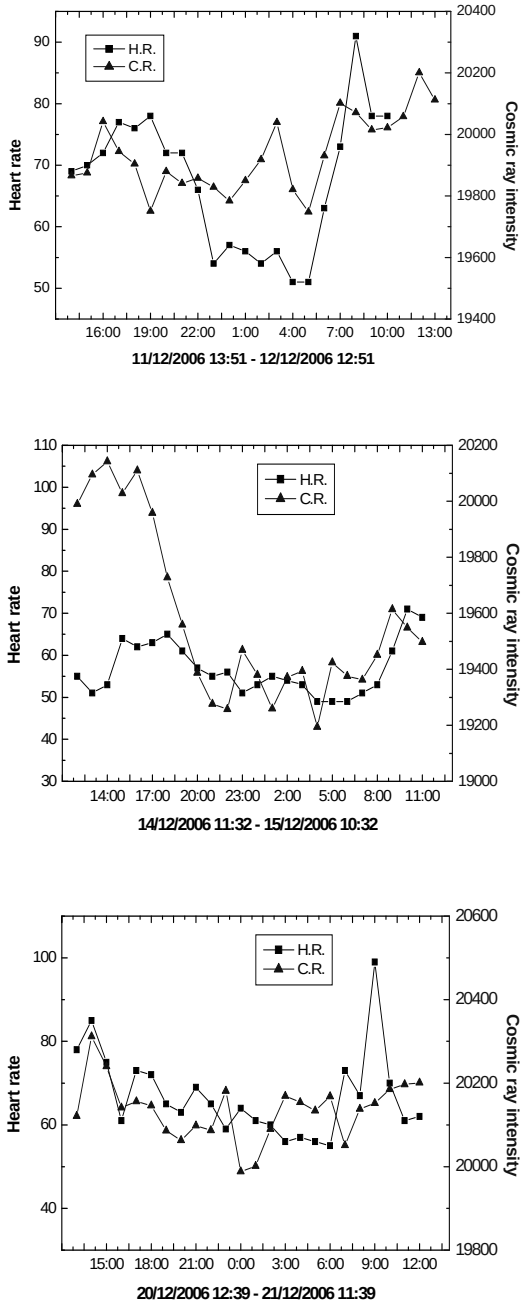

Fig. 3. Time profiles of the hourly values of cosmic ray intensity (triangle) and heart rate (square) of different persons for the days 11, 14 and 20 of December 2006.

came from a group of patients, who were not admitted to the hospital and had no symptoms, but had some cardiovascular problems and that is why they were monitored by the hospital using the method of Holter electrocardiogram. This method records, on

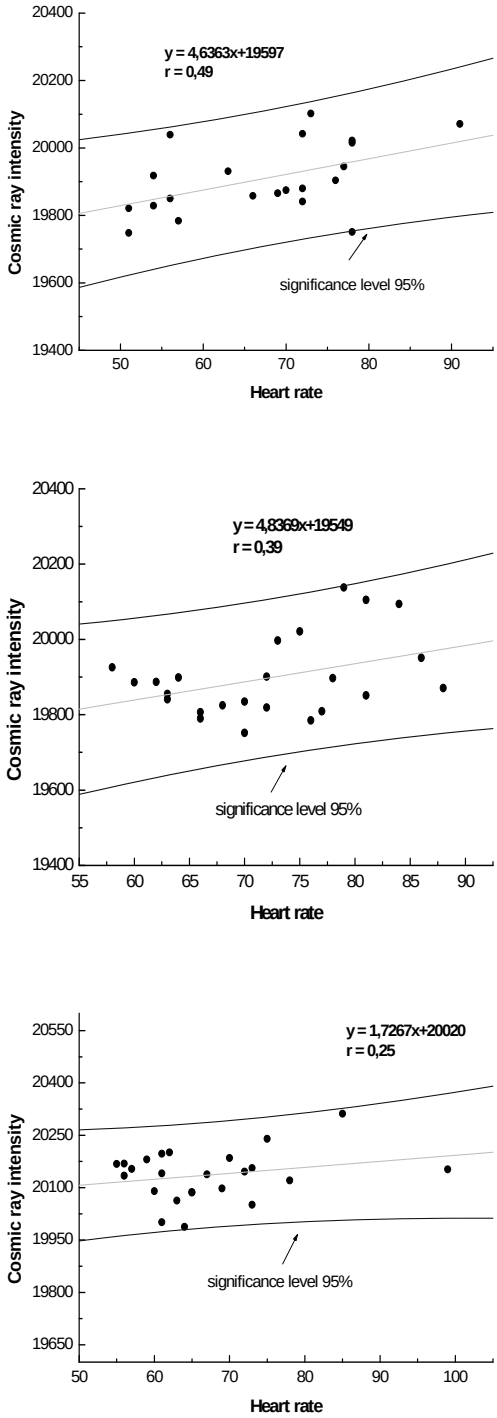

Fig. 4. The equivalent correlation diagrams of the cases given in Fig. 3 with a significance level of 95%.

a 24hour base, the heart rate variations while the patient carries out his/her routine activities. The results, then, are gathered and analyzed by computer.

The Holter electrocardiogram can detect many cardiovascular irregularities, such as arrhythmias and ischemic strokes. Our group consisted of thirty people (ranged from 35 to 88 years old) and our measurements refer to the period of December 2006.

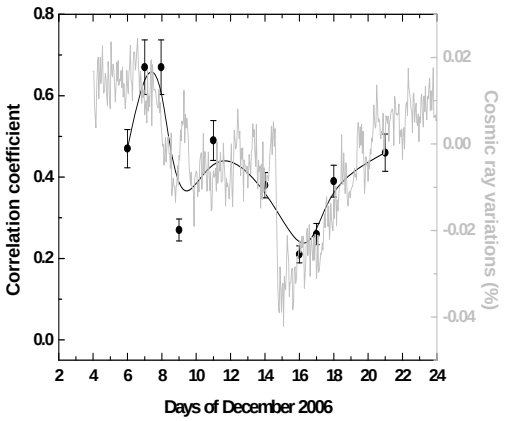

Fig. 2. The percentage variation of the cosmic ray intensity as measured by the Athens Neutron Monitor from 4th to 24th of December 2006 (grey line) and the correlation coefficient of cosmic ray intensity and heart rate variations (black line) are presented.

III. RESULTS AND DISCUSSION

One of the biggest problems of biogeomagnetics is to determine those characteristics of solar and geomagnetic activity with the greatest effect on human health. Indices of interplanetary disturbances, which are connected to geomagnetic activity and short-term cosmic ray intensity variations, are used for the research on biological rhythms variations. In [5], [18], [26], [27], [28] it is shown that Forbush decreases are the most sensitive indicators of the connection between geomagnetic field disturbances and health parameters, as incidence of ischemic strokes, myocardial infractions and vehicular traffic accidents. The most remarkable and statistically significant effects have been observed during days of geomagnetic perturbations defined by the days of the declining phase of Forbush decreases in cosmic ray intensity.

Using the hourly data of the cosmic ray intensity recorded at the Cosmic Ray Station of the University of Athens, the normalized cosmic ray intensity variations were calculated using the relation $\Delta I = \frac{I - \bar{I}}{\bar{I}}$, where I is the hourly cosmic ray intensity and $\bar{I}$ is the average cosmic ray intensity. These results are plotted for 4th – 24th December 2006 and are shown in Figure 2 (continuous grey line). Intense cosmic ray events were recorded during this period, such as a series of Forbush decreases started on 6th December and lasted until the end of the month and a solar proton event causing a Ground Level Enhancement (GLE) of the cosmic ray intensity on 13th December. A sudden decrease of the cosmic ray intensity on 7th December was recorded in Athens Neutron Monitor station with amplitude of 3%. Cosmic ray intensity started decreasing on 7th December at 09:00 U.T. (0.02%), took its minimum value (-0.01%) on 8th December, at 17:00 U.T. and then the recovery phase started. Then another Forbush decrease was recorded with amplitude of 4% starting from 14th December at 12:00 U.T. and taking its minimum value on 15th December, at 02:00 U.T. The cosmic ray intensity reached the pre – decrease level on 23rd – 24th December.

During the examined here time interval the index K_p reached the value of 8^+ on 15th December (Figure 1, middle panel) and also the index Dst reached its minimum value (-146 nT) on the same day, which means that a geomagnetic storm was recorded. It is known that a geomagnetic storm occurs when $K_p > 5$ and Dst < - 100nT. The variations of the Dst index for December 2006 are presented in Figure 1 (bottom panel).

Studying in detail the solar, interplanetary and geomagnetic activity of periods connected with Forbush decreases recorded by neutron monitor, during the examined here time interval, very interesting results have been obtained. The hourly variations of the cosmic ray intensity on a daily basis compared to the average heart rate variations of patients are given in Figure 3 for the cases of the above mentioned Forbush decreases. Generally it seems that the heart rate variations coincide with the cosmic ray intensity ones [17]. The correlation diagrams along with the regression line between these two parameters, with a significance level of 95%, are shown in Figure 4. The correlation coefficients for some of the cases under study during December 2006 are presented in Table I.

The two parameters, heart rate variations and cosmic ray intensity, under study coincide during Forbush decreases and the restoration phase of Forbush events. But for time periods when a strong event is detected we are not only interested in the correlation coefficient's absolute value but also its variation during the days of the cosmic ray event. It is noticed that the correlation coefficient decreases

TABLE I

The date, the time interval, the gender, the age and the correlation coefficient between cosmic ray intensity and heart rate variations for a group of patients under study.

	Start of measurement		End of measurement		Gender	Age	Correlation coefficient
	Date	Time	Date	Time			
1	6/12/06	11:58	7/12/06	10:58	M	70	0.47
2	6/12/06	6:12	7/12/06	5:12	F	77	0.47
3	7/12/06	21:43	8/12/06	22:43	M	53	0.67
4	9/12/06	20:36	10/12/06	19:36	F	88	0.27
5	11/12/06	13:51	12/12/06	12:51	F	58	0.49
6	11/12/06	15:22	12/12/06	14:22	F	80	0.32
7	14/12/06	11:32	15/12/06	10:32	M	70	0.31
8	17/12/06	11:12	18/12/06	10:12	F	50	0.26
9	18/12/06	14:53	19/12/06	13:53	F	51	0.39
10	21/12/06	18:47	22/12/06	17:47	F	70	0.46

during the descending phase of a Forbush decrease and increases during the restoration phase of a Forbush decrease [17]. Figure 2 shows this behavior of the correlation coefficient variations in comparison to the cosmic ray variations.

The cosmic ray intensity started to decrease on 6th December and had its minimum value on 15th December. The same variations are, also, noticed for the Dst index (Fig. 1, bottom panel). On the other hand the correlation coefficient's decrease started on 7th December and had its minimum value on 16th December (Fig. 2, continuous black line). A time delay is noticed. This delay might be due to the fact that our group of patients is rather small and consists of only thirty people. The correlation coefficient shows the same behaviour, as described here, with no significant time delay in a wider investigation, which uses a sample of 250 people and data from 2002 [17].

Another interesting result is that this correlation is much stronger in women than in men. For the group of people under study the 40% of women and only the 20% of men had a correlation coefficient over 0.25. Gender differences in acute coronary syndromes, atherogenesis, concomitant pathologies, like diastolic heart failure, hypertension, diabetes, heart rupture, outcomes in coronary revascularization are widely discussed [22]. Unfortunately women show higher risk in revascularization procedures, more heart failure and higher mortality in acute coronary syndromes [22]. When geomagnetic and cosmic ray activity is correlated with the irregularities mentioned above it seems that in women those links are much stronger. In [22] it is mentioned that 'like in many other fields, older women are more susceptible to environmental physical activity compared to younger men with the same pathology'.

IV. CONCLUSIONS

In our days there is an increasing amount of evidence linking biological effects to solar and geomagnetic conditions. Reference [20] has published a series of studies of changes in human physiological responses and the natural history of various pathological events at different levels of daily and monthly geomagnetic activity.

Over the last decades many researches have taken place involving biogeomagnetics and the effect of Space weather, through the geomagnetic field, on some diseases [6], [15], [21].

In the last decades many scientists have worked on the impact of space weather parameters, through the geomagnetic field, on different diseases [3]. Changes in the geomagnetic activity level are related to fluctuations in solar activity and are involved in climate regulation and various animals [31], [32] and human behaviour [1]. The living species examined, including man, have adapted to normal variation in geomagnetic activity [20]. Cosmic ray Forbush decreases, which are connected to interplanetary disturbances, can be used as indicators of the relationship between the geomagnetic field fluctuations and health parameters [6]. The most important results are those concerning cardiovascular diseases and diseases of the nervous system, especially strokes, myocardial infarctions and traffic accidents as well [5], [18], [26], [27]. It is proved that the monthly number of acute myocardial infraction is significantly related to solar, geomagnetic and cosmic ray activity [22], [25].

Solar, geomagnetic and cosmic ray activities and their changes have an influence on human health. Comparison of the monthly sudden cardiac death data revealed a significant and inverse correlation with solar activity indices and with geomagnetic

activity indices. A positive correlation was found for cosmic ray activity [24].

In this study we have examined a group of thirty persons for the period 4th – 24th December 2006 and the following conclusions are outlined:

- A significant correlation of cosmic ray activity level with heart rate variations exists. These results are in agreement with those ones noticed also by [22] for the time interval 1983 – 1999.
- The correlation coefficient between cosmic ray intensity and heart rate variations seems to decrease during the declining phase of strong cosmic ray events, such as Forbush decreases and increase during the ascending phase of such events.
- The correlation between cosmic ray intensity and heart rate variations is stronger when women are concerned.

Over the last years many scientists have tried to connect solar and geomagnetic activity to changes of human physiological state. We are mostly concerned about how cosmic ray variations may influence heart rate variations and the effect they may have on different cardiovascular diseases. As there seems to be a connection between these two parameters, it is important to continue this investigation using a larger group of patients during a wider period of time.

ACKNOWLEDGMENT

Thanks are due to our colleagues from the Neutron Monitor stations who have kindly provided us with their cosmic ray data and the cardiological clinic of the KAT Hospital for the heart rate data. We are grateful to the Special Account of Research of Athens University for supporting this study. The authors would like to thank the referees for improving significantly this paper with their comments.

REFERENCES

[1] Babayev, E.S., Allahverdiyeva, A.A.: "Effects of geomagnetic activity variations on the physiological and psychological state of functionally healthy humans: some results of Azerbaijani studies", Advances in Space Research, 40, 1941-1951, 2007

[2] Cornelissen, G., Halberg, F., Breus, T., Syutkina, E., Baevsky, R., Weydahl, A., Watanabe, Y., Otsuka, K., Siegelova, J., Fiser, B., Bakken, E.: "Non-photic solar associations of heart rate variability and myocardial infraction" Journal of Atmospheric and Solar – Terrestrial Physics, 64, 707 - 720, 2002

[3] Dimitrova, S., Stoilova, I., Cholakov, I.: "Influence of local geomagnetic storms on arterial blood pressure", Bioelectromagnetics 25, 408 - 414, 2004

[4] Dimitrova, S.: "Relationship between human physiological parameters and geomagnetic variations of solar origin", Advances in Space Research, 37, 1251 - 1257, 2006

[5] Dorman, L.I., Iucci, N., Ptitsyna, N.G., Villoresi, G.: "Cosmic ray Forbush decreases as indicators of space dangerous phenomena and possible use of cosmic ray data for their prediction", Proc. 26th ICRC (Salt Lake), 6, 476 - 479, 1999

[6] Dorman, L.I., Iucci, N., Ptitsyna, N.G., Villoresi, G.: "Cosmic rays as indicator of space weather influence on frequency of infract myocardial, brain strokes, car and train accidents", Proc. 27th ICRC (Hamburg), 3511 - 3514, 2001

[7] Dorman, L.I.: "Space weather and dangerous phenomena on the Earth: principles of great geomagnetic storms forecasting by online cosmic ray data", Annales Geophysicae, 23, 2997 - 3002, 2005

[8] Gmitrov, J., Ohkubo, C.: "Artificial static and geomagnetic field interrelated impact on cardiovascular regulation", Bioelectromagnetics, 23, 329 - 338, 2002

[9] Gmitrov, J., Gmitrova, A.: "Geomagnetic field effect on cardiovascular regulation", Bioelectromagnetics, 25, 92 - 101, 2004

[10] Gurfinkel, Iu. I., Liubimov, V.V., Oraevskii, V. N., Parfenova, L.M., Iur'ev, A.S.: "The effect of geomagnetic disturbances in capillary blood flow in ischemic heart disease patients", Biofizika, 40, 793 - 799, 1995

[11] Halberg, F., Cornelissen, G., Otsuka, K., Watanabe, Y., Katinas, G.S., Burioka, N., Delyukov, A., Gorgo, Y., Zhao, Z.Y., Weydahl, A., Sothern, R.B., Siegelova, J., Fiser, B., Dusek, J., Syutkina, E.V., Perfetto, F., Tarquini, R., Singh, R.B., Rhees, B., Lofstrom, D., Lofstrom, P., Johnson, P.W.C., Schwartzkopff, O.: "Cross-spectrally coherent ~10.5- and 21-year biological and physical cycles, magnetic storms and myocardial infarctions", Neuroendocrinology Letters 21, 233 - 258, 2000

[12] Kay R.W.: "Geomagnetic storms: association with incidence of depression as measured by hospital admission", Br. J. Psychiat. 164 (3), 403 - 409, 1994

[13] Mavromichalaki, H., Sarlanis, C., Souvatzoglou, G., Tatsis, S., Belov, A., Eroshenko, E., Yanke, V. and Pchelkin, A.: "Athens Neutron Monitor and its aspects in the cosmic-ray variations", Proc. 27th ICRC 2001 (Hamburg), 10, 4099 - 4102, 2001

[14] Mavromichalaki H., Papaioannou, A., Petrides, A., Assimakopoulos, B., Sarlanis, C. and Souvatzoglou, G.: "Cosmic-ray events related to solar activity recorded at the Athens neutron monitor station for the period 2000-2003", International Modern Journal of Physics A, 20, 6714 - 6716, 2005

[15] Palmer, S.J., Rycroft, M.J., Cermack, M.: "Solar and geomagnetic activity, extremely low frequency magnetic and electric fields and human health at the Earth's surface", Surv. Geophys, 27, 557 – 595, 2006

[16] Persinger, M.A., Richards, P.M.: "Vestibular experiences of humans during brief periods of partial sensory deprivation are enhanced when daily geomagnetic activity exceeds 15 – 20nT", Neurosci. Lett. 194 (1-2), 69 - 72, 1995

[17] Petropoulos, B., Mavromichalaki, H., Papailiou, M., Kelesidis, K., Mertzanos, G.: "The effect of the daily anisotropy of the cosmic ray intensity on the heart rate frequency variations", Praktika of Academy of Athens, 81, 51 - 106, 2006

[18] Ptitsyna, N. G., Villoresi, G., Kopytenko, Y.A., Kudrin, V.A., Tyasto, M.I., Kopytenko, E.A., Iucci N., Voronov, P.M. and Zaitsev D.B.: "Coronary heart diseases: an assessment of risk associated with work exposure to ultra low frequency magnetic fields", Bioelectromagnetics 17, 436 - 444, 1996

[19] Reiter, R.: "Bio-meteorologie auf physikalischer Basis", Phys. Blatter, 11, 453 – 464, 1955
[20] Stoupel, E.: "Effect of geomagnetic activity on cardiovascular parameters", J. Clin. Basic Cardiol. 2, 34 - 40, 1999
[21] Stoupel, E.: "The effect of geomagnetic activity on cardiovascular parameters", Biomedicine and
[22] Pharmacotherapy 56, 247 - 256, 2002
[23] Stoupel, E., Domarkiene S., Radishauskas R., Israelevich P., Abramson E., Sulkes J.: "In women myocardial infraction occurrence is much stronger related to environmental physical activity than in men-a gender or an advanced age effect?", J. Clin. Basic Cardiol., 8, 59 - 60, 2005
[24] Stoupel, E.: "Cardiac Arrhythmia and geomagnetic activity", Indian Pacing and Electrophysiology Journal, 6, 49 - 53, 2006
[25] Stoupel, E., Babayev, E. S., Mustafa, F. R., Abramson, E., Israelevich, P., Sulkes, J.: "Clnical Cosmobiology – Sudden Cardiac death and Daily / Monthly Geomagnetic, Cosmic ray and solar activity – the Baku study (2003 – 2005)", Sun and Geosphere, 1, 13 - 16,
[26] 2006
[27] Stoupel, E., Babayev, E.S., Mustafa, F.R., Abramson, E., Israelevich, P., Sulkes, J.: "Acute myocardial infarction (AMI) occurrence – environmental links, Baku 2003-2005 data". Medical Science Monitor, International Medical Journal for Experimental and Clinical Research, New-York., 13, BR175-BR179, 2007
[28] Villoresi, G., Breus, T.K., Iucci, N., Dorman, L.I., Rapoport, S.I.: "The influence of geophysical and social effects on the incidences of clinically important pathologies (Moscow 1979-1981)", Physica Medica 10, 79 - 91, 1994a
[29] Villoresi, G., Kopytenko, Y.A., Ptitsyana, N.G., Tyasto, M.I., Kopytenko, E.A., Lucci, N., Voronov, P.M.: "The influence of geomagnetic storms and man-made magnetic field disturbances on the incidence of myocardial infraction in St. Petersburg (Russia)", Physica Medica 10, 107 - 117, 1994b
[30] Villoresi, G., Ptitsyana, N.G., Tyasto, M.I., Lucci, N.: "Myocardial infarct and geomagnetic disturbances: analyses of data on morbidity and mortality " Biofizika 43, 623 – 631, 1998
[31] Watanabe, Y., Hillman, D.C., Otsukak., Bingham, C., Breus, T.K., Cornelissen, G., Halberg, F.: "Cross – spectral coherence between geomagnetic disturbance and human cardiovascular variables at non-societal frequencies", Chronobiologia, 21 (3-4), 265 - 272, 1994
[32] Zhadin, M.N.: "Review of Russian literature on biological action of DC and low frequency AC magnetic fields", Bioelectromagnetics, 22, 27 - 45, 2001
[33] Wiltschko, R., and Wiltschko, W.: "Magnetic orientation in animals", Zoophysiology, 33, 297, 1995
[34] Wiltschko, W., and Wiltschko, R.: "Magnetic orientation and magnetoreception in birds and other animals", J. Comp. Physiol. A 191, 675 - 693, 2005

Neutron monitor multiplicity measurements during the December 13, 2006 GLE

B. Gvozdevsky, Yu. V. Balabin, E. V. Vashenyuk, L. I. Schur

Polar Geophysical Institute, Murmansk region, Russia
(gvozdevsky@pgi.kolasc.net.ru)

Abstract – **Neutron monitor multiplicity can give the information on a spectrum of primary solar protons and its variations during ground level enhancements (GLE) related to relativistic solar cosmic rays. Recently we designed and installed a new data acquisition system on the neutron monitor (NM) in Barentsburg, Spitsbergen archipelago. It is able to register a multiplicity. The system is based on ordinary PC, equipped with an extension card ADLINK PCI-7233H, which is a high-speed 32-channel digital input card. Via this card the specially written collecting program continuously registers pulses from all 18 channels of the NM and intervals between pulses. Elapsed time between pulses is measured with a precision of 1 microsecond. Each pulse is processed during 6 microseconds, which is a dead time of the registering system. The GLE of December 13, 2006 was recorded by the Barentsburg NM. We have derived multiplicities 2-10 and studied their behaviour during this event and subsequent Forbush decrease. Count rates of multiplicities 2-3 show a significant increase during the GLE, while the Forbush decrease is seen in multiplicities up to 5. The multiplicity spectrum changes are comparable with the solar proton spectrum dynamics during the GLE. The spectra of relativistic solar protons were derived from the worldwide NM network by modelling technique.**

Solar protons and outer radiation belt during solar extreme events of December 2006: Glonass and express data

N.N. Vedenkin, S.V. Balashov, V.V. Ivanov, T. A. Ivanova, D.S. Karpenko, I. A. Maksimov, N.N. Pavlov, I. A. Rubinstein, L.V. Tverskaya, D. A. Trofimchuk, V.I. Tulupov

Skobeltsyn Institute of Nuclear Physics, Moscow, Russia
(cool23@pochtamt.ru)

Abstract **– We study the behavior of the trapped radiation (electrons and protons) and solar protons in the magnetosphere in December 2006, as seen from GLONASS (circle orbit h~20000 km, inclination ~65^{o}) and geostationary Express-A3 satellites. Particles were observed in the energy ranges: 0.04 - 1 MeV electrons and 3 - 70 MeV protons. Prior to a strong (|Dst|max~150 nT) storm of 15 December, outer belt of 0.7 MeV electrons peaked at L~4.5; after the storm, the flux increased as high as one order of magnitude, and its peak shifted to L<4 (GLONASS does not traverse L<4). The flux of 0.8-1 MeV electrons on Express-A3 increased only twice of the pre-storm level. In quiet conditions, solar protons of >3 MeV energy are seen exclusively in the high-latitude parts of the GLONASS orbit. During the storm 15 December, solar protons flooded all parts of the orbit including the equatorial one where previously we saw only a peak of the proton radiation belt. Intensity of the trapped protons decreased during the main phase of the storm and returned back to the pre-storm level at the end of the recovery phase.**

Session B

Energetic Processes on the Sun during extreme events, solar events at solar minimum

Chair: N. Gopalswamy, N. Crosby, J. Valdes-Galicia
A. Chilingarian, M. Messerotti, L. Lazutin

Solar **E**xtreme **E**vents **2007**

Geoeffectivity of solar radio flares near solar minimum: Analysis of metric and decimetric flares detected by the Trieste solar radio system (TSRS) in 2005 and 2006

M. Messerotti[1,2]

[1]*National Institute for Astrophysics (INAF)-Astronomical Observatory of Trieste, Italy,*
[2]*Department of Physics, University of Trieste, Italy*

Abstract **– The Sun is a non-directional, broad-band radio noise source whose background level increases with the emission frequency. Radio outbursts, characterized by gradual and/or impulsive evolution at different time scales, can exhibit a level increase of orders of magnitude with respect to the quiet Sun values, in association with non-thermal plasma processes in perturbed chromospheric and coronal layers. In recent years, various authors considered the potential direct effect of enhanced solar radio noise on mobile radio communications and on Global Positioning Systems (GPSs). In this work, we will review such effects and, in this framework, we will consider a selection of relevant solar radio flares observed by the Trieste Solar System (TSRS) in 2005 and 2006, i.e., in the proximity of the solar activity minimum, expected in 2007.**

Strong perturbations on the Sun and in the heliosphere: similar and individual characteristics

I .S. Veselovsky[1,2], M.I.Panasyuk [1], Yu.I.Yermolaev [2], L.M.Zelenyi [2]

[1] *Skobel'tsyn Institute of Nuclear Physics (SINP), Moscow State University, Moscow, 119992, Russia*
[2]*Institute of Space Research (IKI), Russian Academy of Sciences, Moscow, 117997, Russia*

Abstract— **We briefly present the selected results obtained up to now by the Russian scientific groups regarding powerful solar ejections as main causes of large geomagnetic storms in the near-Earth space. Strongest perturbations on the Sun and in the near-Earth space responsible for large geomagnetic storms were well registered and analyzed during the 23rd solar cycle. Open issues and perspectives are discussed.**

Key Words—**Sun, heliosphere, strong perturbations**

I. INTRODUCTION

Large geomagnetic storms attract attention of researchers and general public because of scientific interests and practical reasons. Progress in their study and understanding during last dozen years is very impressive due to efforts of many groups and individuals. The important contribution to the information about physical conditions on the Sun, in the interplanetary space and in magnetosphere-ionosphere system related to large geomagnetic storms during 23rd solar cycle has been obtained in Russia onboard satellites (4 satellites of INTERBALL project, CORONAS-F, Meteor-3M, Express-A2 and A-3, Universitetskii-Tatyana [1] and in ground based measurements. For the study of this information, the Solar Extreme Event (SEE) initiative collaboration headed in Russia by M.I. Panasyuk was established in 2003 during a series of seminars and discussions in SINP MSU just after the famous October-November storms on the Sun, in the heliosphere, magnetosphere, ionosphere, upper atmosphere and on the ground. The International SEE Symposia were held in 2004 (http://www.magnetosphere.ru/see/) in Moscow (Russia), in 2005 in Nor Amberd (Armenia) and in 2007 (http://cosray.phys.uoa.gr/SEE2007/Previous%20SEE.htm) in Athens (Greece). The papers with the first results presented at the SEE-2004 meeting and submitted for publication as the special issue of the Advances in Space Research are still waiting their turn. Preliminary reports can be found in collaborative compilations [2],[3],[4], [5]) and in original papers published in special issues of Cosmic Research, N 5, 2004 and Geomagnetism and Aeronomy, N 1 and 6, 2005. Proceedings of the SEE-2005 were also published http://crdlx5.yerphi.am/index.php?Page=/Online_News/CRDSEE/Proceedings/&Title=0. Papers in the national journals are not readily available for the broader community. Nevertheless, these studies contributed additional information to the detailed investigations by other authors (see e.g. papers by [6],[7],[8],[9],[10],[11]. We are aimed here to bring brief account in telegraphic style and discuss only several selected results obtained up to now mostly focusing on solar flares and coronal mass ejections (CMEs) as immediate physical causes of the strongest storms in the near space.

II. OBSERVATIONS AND SELECTED RESULTS

INTERBALL mission [12], [13] consisted of four satellites for solar, interplanetary space and magnetospheric studies and operated from 1995 to 2000. One of the first interesting and strong events observed by INTERBAL in the solar cycle 23 was interaction of magnetic clouds with the Earth on 10 January, 1997 [see, for instance, [14] and other papers by INTERBALL team in the same GRL special issue]. In particular, several important consequences of this interaction were: (1) observations of the magnetopause position 6RE nearer to the Earth than on average; (2) a huge increase in the magnetosheath plasma density and temperature; and (3) oscillation of magnetospheric tail structures past the satellite. Correlations of

strong magnetosphere disturbances during 1995-2000 with interplanetary perturbations have been discussed by [15]. Solar sources of magnetospheric disturbances were studied with AKR-2X radiometer and DOK-2 spectrometer of energetic particles on the INTERBAL-1 satellite [16].

CORONAS-F mission [17] operated from July 31, 2001 to December 6, 2005. The most important results obtained with the CORONAS-F satellite in 2001-2004 are published in the Solar System Research special issue [18]. They are related to global oscillations of the Sun, active regions and solar flares, the lower corona, ultraviolet and X-ray solar radiation, and solar cosmic rays. We refer to this review for references to original papers. A part of them was published in the same issue as well as in other journals.

Nearly total polarization of the hard X-ray emission observed during the flare of October 29, 2003 by the spectral polarimeter CORONAS-F/SPR-N was tentatively associated with the horizontal part of the effective electric current loop where acceleration of electrons took place. Absence of strong polarization in other cases could be understood as a consequence of a more complicated and tangled geometry [2]. This interpretation does not contradict telescopic observations onboard RHESSI satellite. Accelerated protons and nuclei in solar cosmic rays were investigated directly in populations arriving to the Earth's orbit and indirectly by their gamma radiation in the source regions on the Sun. Nuclear processes in solar flares leaded to the gamma-line radiation and neutron emissions. Positron annihilation and pi-meson formation processes were documented and investigated with the CORONAS-F/SONG data. The hardest gamma-ray spectra and tooth-like X-ray oscillations were measured in solar flares with CORONAS-F/GELIKON and CORONAS-F/IRIS. Atlas of spectral lines of solar flares in X-ray region was compiled based on CORONAS-F/RESIK. Doppler shifts in X-ray lines were measured during August 25, 2001 solar flare by CORONAS-F/DIOGENNES. Soft EUV emissions during this flare preceded X-ray emissions for several minutes according to CORONAS-F /VUSS-L data. This delay is indicative of the flare development from the chromosphere upwards. New lines found and identified in several experiments during flares. Impacts on the terrestrial atmosphere density, composition and satellite orbits documented and analyzed.

Low noise CORONAS-F/SPIRIT XUV and X-ray telescopic experiment allowed a good quality of images [19]. Hemispheric asymmetry in the solar activity distribution was clearly documented during October 2003 eruptions on the Sun. The activity complex consisting of three active regions with erupting trans-equatorial loops was involved in this case in the multiple interacting CMEs generation and series of repeated flares development on the visible side of the Sun. This resulted in a very strong and complicated long lasting geomagnetic perturbation with all its attributes. Interesting results were obtained regarding localization and fast propagation of strongest perturbations on the Earth at all levels of the magnetosphere, ionosphere, atmosphere, and on the ground [3]. In other cases of extreme events even solitary active region perturbations on the visible side of the Sun not too far from the disk center can produce comparable geomagnetic storms under favorable magnetic field orientation inside and around the propagating ejection. It was not the case, for example, for the powerful solar event of November 4, 2003.

The global asymmetry of the solar activity has important consequences in electromagnetic fields and emissions of the Sun, in the interplanetary magnetic fields and the solar wind flows [2]. Global CMEs were identified in several instances when observing huge dimmings encompassing more than 180 degrees in the low corona on the Sun [20]. These observations substantiate ideas about CME initiation by enhanced convection processes coupled with electromagnetic fields, currents and charges in the solar interior and atmosphere.

Strong CMEs and solar flares never happen just as a spontaneous instability of the stored magnetic energy in the corona apart of driving photospheric causes. We believe that powerful subphotospheric electric currents, potential and inductive fields play important role in these connections. Fast development of sufficiently strong magnetic fluxes measured by photospheric magnetogram patrol can be monitored and practically used for successful warnings [21]. Necessary conditions are clear and quantified in many instances. Sufficient conditions are more delicate and need further studies.

Enhanced horizontal and vertical convective motions with velocities of the order of 1 km/s at the photospheric level precede strongest active region appearance and eruptions on the Sun. We believe that sometimes horizontal motions can dominate (cyclone and tornado type behavior), but in other cases vertical flows (developing like thunderstorm clouds on the Earth) are more readily seen and documented [22]. The formation of cyclone type motion was well documented recently for 'colliding sunspots' in December 2006 by Hinode spacecraft observations. Like in the planetary atmospheres, dynamical vortices on the Sun can have vertical, inclined or horizontal main axes. The aspect ratio of large and small radii is variable from case to case for such toroidal and spiraling motions, which are

ubiquitous in the atmosphere, but sometimes especially strong.

Strongest CMEs and flares accompany each to other. They represent manifestations of two different energy channels in the free energy release, which is shared between the plasma motion and radiation respectively. Any cause-consequence chain between them in this sense does not exist, contrary to flare and anti-flare myths discussed in the literature. The useful quantitative delimitation between flare-like and CME-like behavior can be provided by the dimensionless parameter V_e [23]. It is the ratio between electromagnetic emission and kinetic power, which is larger in first type of events and relatively small in another. The unifying term 'eruption' is often used for solar flares and CMEs.

World-wide neutron monitor network was used jointly with spacecraft data to investigate the galactic (GCR) and solar (SCR) cosmic ray variations during extreme events. Universitetskii - Tatyana small satellite launched in January 2005 registered SCR penetrating in polar caps of the magnetosphere as well as radiation belt transformations during SEE in 2005-2006. Very detailed information was obtained (http://cosmos.msu.ru/). Radiation conditions were also simultaneously monitored onboard ISS, Meteor and GLONAS satellites. Among new findings one can mark detailed information about large transient anisotropy of SCR and GCR, direct propagation of enhanced SCR fluxes, neutrons in SCR. This information can be used for the development of the methods of the now cast and short term forecasts. It is also used in MSU for educational purposes.

III. DIMENSIONLESS SCALING APPROACH TO THE THEORY OF EXTREME EVENTS

The theory of extreme events on the Sun is not well developed. It can be based on statistical or dynamical considerations. Statistics is rather poor. Extreme events are rare by definition. Dynamical approaches based on dissipative MHD or kinetic models assume given boundary and initial conditions as well as other input information about parameters, which are often not known a priori because of lack of needed measurements. The situation resembles a strong turbulence with many degrees of freedom. It is complicated, multi-scale in its nature, not homogeneous, non-stationary, intermittent in space and in time. Any universal geometry scenario does not exist. Because of this, morphological classifications using dimensionless scaling are suggested and appear to be useful for the qualitative and semi-quantitative representation of observed realizations. Dimensionless scaling is useful in this situation to clarify and fix the relative importance of physical processes under consideration.

Let us consider the set of such parameters in Table1. The Knudsen number is the natural measure of the length scale of the problem. It compares this length with the corresponding mean free path lengths. As usually, the Knudsen number delimits microscopic (kinetic) and macroscopic (fluid) regimes. The Faraday number represents the natural measure of importance (or non-importance) of Coulomb potential electric fields due to electric charges versus inductive (Faraday's) electric fields due to time variable magnetic fields. It is easy to see that this number is large for slow time variations and small space scales. The a priori neglect of electric charges in plasmas can lead to serious physical errors. Non-compensated electric charges in plasma exist every time. They could be 'small' and not essential only under special boundary conditions, which need investigations. Plasma quasi-neutrality does not mean total absence of electric charging and potential electric fields in the commoving 'plasma reference frame' or 'frozen coordinate systems'. It is not possible indicate such a global coordinate system in the inhomogeneous plasma in most interesting cases, contrary to opposite statements in papers and some textbooks (see e.g. E.N. Parker, The alternative paradigm for magnetospheric physics, J. Geophys. Res., Vol. 101, pp. 10587-10625, 1996; Priest, E. and Forbes, T., Magnetic Reconnection: Magnetohydrodynamic Theory and Applications, Cambridge Univ. Press, 2000). Hence, electric fields can be not completely reduced to velocity and magnetic field

Table 1. Dimensionless parameters and their physical role [23]

Name	Description	Role
Strouhal	Time / Flight times	Time scales
Knudsen	Mean free path / Length	Length scales
Velocity-emission	Kinetic energy / EM emission	Plasma density
Mach	Bulk speed / Thermal speed	Temperature
Magnetic Mach	Bulk speed / Alfvén speed	Magnetic field
Froude	Bulk speed / Free escape speed	Gravity
Faraday	Potential fields/ Inductive fields	Electric field
Trieste numbers	Inflows (outflows) / Inner flows	Openness degrees

considerations, as assumed by these authors based on extrapolations of the frozenness conception beyond its very restricted validity domain.

A priori neglect of electrostatic fields appeared a very serious limitation for the thermonuclear fusion using magnetic plasma confinement. It is easy to see from estimates of the Faraday parameter, that long-term asymptotic behavior of the plasma in general determined not by inductive, but by Coulomb fields. Quasi-steady confinement is difficult to attain with the 'frozen degree of freedom' (potential electric fields due to charging assumed to be irrelevant). This assumption appears to be misleading in practical laboratory devices. This degree of freedom plays crucial role also in the solar atmosphere especially during flares and CMEs.

Finally, we should comment on Trieste numbers in Table 1. The set of these numbers is defined as ratios of energy, momentum and mass flows inside considered volumes, outside of them and through their boundaries. The set of corresponding numbers defines the openness degree of the considered physical object against energy, momentum and mass flows. The system is adiabatically closed if corresponding Trieste numbers are small, T <<1. Otherwise, it is essentially open in the sense of the exchanges with the surrounding medium. One example: the standard paradigms of quiescent prominences as 'plasma equilibrium in magnetic fields with normal and abnormal configurations' is practically not tenable. It is because of permanent plasma motions through the boundaries of loop systems considered as main structuring elements of prominences. Quiescent prominences during their life time replenish their material many times. In other words, prominences are not isolated systems, but open ones. Inflows and outflows through the legs, red- and blue- shifts are big enough. Eruptive prominences with a loop-like shape are directly driven by non-local electric fields and electric currents supplied from below the photosphere. The main mechanism of motion – plasma drifts in crossed electric and magnetic fields.

IV. Open questions and perspectives

Results obtained up to now allow us to formulate several open physical questions, which remain to be investigated in future, and possible ways of their solution for better understanding of the solar extreme events:

1) We know from available measurements very little about potential electric fields and corresponding electric charges involved in flares and CMEs. This important 'degree of freedom' is usually supposed to be frozen in most theories and interpretations of solar phenomena. Similar neglect led to failure of initial simplistic concepts of 'magnetic confinement' in the controlled thermonuclear fusion problem. Stark effect measurements could be helpful, but they are not easy to interpret.
2) We have not sufficient data about the real quantitative role of the white light emissions in the energy balance of eruptive processes on the Sun. The problem is difficult because of the low contrast of perturbations, which are underestimated. Existing data is too scarce and based on telescopic measurements with a not sufficient sensitivity, resolution and signal/noise ratio. More accurate spectral and telescopically resolved measurements from space are possible similar to, but surpassing the SORCE mission capabilities.
3) Reliable deterministic predictions of extreme solar events are impossible without knowledge and monitoring of subphotospheric processes which govern solar flares and CMEs. Helioseismology methods and signals seen on the surface could be helpful, but there is a principal question if they appear sufficient. Monitoring of photospheric magnetic fluxes and inferred electric currents in the solar atmosphere with a good space-time resolution is very promising as a first step.
4) Possible limits on amplitudes, probabilities and predictability horizons of the uppermost attainable perturbations on the Sun and in the heliosphere are difficult to establish based on first physical principles. Statistics of their observations is scarce. Long term coordinated programs in observations and in theory are needed for the progress in this respect because such extreme events are very rare.
5) Geomagnetic observatories registered global and local perturbations even before the space era. Modeling efforts developed for all solar-terrestrial manifestations allow partial reconstruction of parent solar and heliospheric extreme events in the past based on geomagnetic and other archives.

V. Conclusions

Ongoing space research and ground based measurements shed new light on physical processes involved in large geomagnetic storms and clarified

some important fragments in the complicated dynamical picture of the non-linear solar-terrestrial relations originating in the interiors of the Sun. Principally, one can expect and even predict perturbations on the Sun, in the solar atmosphere, heliosphere and magnetosphere leading to geomagnetic storms within some confidence levels for their parameters, but not schedule them in a manner of any calendars or time tables. We would like to remind the words and opinions expressed long ago by W.N. Hess (1964) regarding solar flares: 1) "Satellites have contributed significantly to our knowledge of flare phenomena." 2) "The visible flare may well be a secondary effect, and the real flare process invisible by our present observational techniques." These words still actual even in a broader context of solar-terrestrial relations and stimulate our further studies.

ACKNOWLEDGMENT

The authors thank all experimental groups providing us various data measured both on spacecraft and ground-based observatories. We are grateful to our colleagues in the Russian and international SEE community for discussions and sharing information before publication. This study was supported by the RFBR grants 07-02-00147, 06-05-64500, INTAS 03-51-6202 and MSU Interdisciplinary Scientific Project. It is also fulfilled as a part of the Programs of the Russian Academy of Sciences: "Origin and evolution of stars and galaxies" (P-04), "Solar activity and physical processes in the Sun-Earth system" (P-16, Part 3) and "Plasma processes in the Solar system (OFN-16).

REFERENCES

[1] Sadovnichy,V.A., Panasyuk, M.I., Bobrovnikov ,S.Yu. et al. First results of investigating the space environment onboard the Universitetskii-Tatyana satellite, Cosmic Res. 45, 273-286, 2007. DOI:10.1134/S0010952507040016.

[2] Veselovsky, I. S., Panasyuk, M. I., Avdyushin, S. I. et al. Solar and heliospheric phenomena in October-November 2003: causes and effects, Cosmic Res. 42, 435-488, 2004.

[3] Panasyuk, M.I., Kuznetsov, S. N.; Lazutin, L. L. et al. Solar Extreme Events in2003 Collaboration (SEE-2003). Magnetic storms in October 2003, Cosmic Res.42, 489-535, 2004.

[4] Yermolaev, Yu. I., Zelenyi, L. M.; Zastenker, G. N.; et al. A year later: solar, heliospheric, and magnetospheric disturbances in November 2004, Geomag. and Aeron.45, 681-719, 2005.

[5] Ermolaev, Yu. I., Zelenyi, L. M., Zastenker, G. N. et al. Solar and heliospheric disturbances that resulted in the strongest magnetic storm of November 20, 2003. Geomag. and Aeron. 45, 23-50, 2005.

[6] Gopalswamy, N.; Yashiro, S.; Liu, Y.; et al. Coronal mass ejections and other extreme characteristics of the 2003 October-November solar eruptions. J.Geophys. Res., 110, Issue A9, 2005. DOI:10.1029/2004JA010958

[7] Kozyra, J. U., Shibata, K., Fox, N. J. et al. Investigating the state of the Sun-Earth system during extreme events: first science results of a worldwide online conference series, American Geophysical Union, Fall Meeting 2006, abstract #SA43A-01.

[8] Bothmer,V. The solar atmosphere and space weather, in Blondel, P. and Mason, J. (Eds.), Solar System Update, Springer, Berlin, IX + 329 pp., 2006, p.1.

[9] Hudson, H.S. The unpredictability of the most energetic solar events, Astrophys. J. 663, L45-L48, 2007. DOI: 10.1086/519923.

[10] Fletcher,L., Hannah, I.G., Hudson, H. S.,& Metcalf,T.R. A TRACE white light and RHESSI hard X-ray study of flare energetics. Astrophys. J. 656, 1187-1196, 2007. DOI:10.1086/510446.

[11] Zhang, J., Richardson, I.G., Webb, D.F. et al. Solar and interplanetary sources of major geomagnetic storms (Dst <= -100 nT) during 1996-2005. J. Geophys. Res. 112, Issue A10, [12] Galeev, A. A., Galperin, Yu. I., & Zelenyi, L. M. The INTERBALL project to study solar-terrestrial physics. Cosmic Res. 34, 313-331, 1996.

[12] Galeev, A. A., Galperin, Yu. I., & Zelenyi, L. M. The INTERBALL project to study solar-terrestrial physics. Cosmic Res. 34, 313-331, 1996.

[13] Zelenyi, L. M., Triska, P., Petrukovich, A. Interball-dual probe and dual mission. Adv. Space Res. 20, 549-557, 1996.

[14] Yermolaev, Y. I., Zastenker G.N., et al. Plasma populations in the magnetosphere during the passage of magnetic cloud on January 10-11, 1997: INTERBALL/Tail probe observations, Geophys. Res.Lett. 25, 2565-2568, 1998

[15] Yermolaev, Yu. I. Strong geomagnetic disturbances and their correlation with interplanetary phenomena during the operation of the INTERBALL project satellites. Cosmic Res. 39, 303-310, 2001.

[16] Kuril'chik, V. N., Prokudina V. S., Kudela, K.,& Slivka, M. Hectometer radio bursts and energetic electrons during solar flares according to observations onboard the Interball-1 satellite. Cosmic Res. 44, 187–196. 2006.

[17] Oraevskii, V. N., Sobel'man, I. I.,. Zhitnik, I. A.,& Kuznetsov, V. D. Complex studies of solar activity on the CORONAS-F satellite: new results. Physics-Uspekhi 45, 886-896, 2002.

[18] Kuznetsov,V.D. The results of study of the Sun and solar-terrestrial relations with the CORONAS-F satellite: a review. Solar System Res.39, 433-441, 2005.DOI: 10.1007/s11208-005-0056-8.

[19] Grechnev, V. V.; Chertok, I. M.; Slemzin, V. A.; et al. CORONAS-F/SPIRIT EUV observations of October-November 2003 solar eruptive events in combination with SOHO/EIT data. J. Geophys. Res.110, Issue A9, 2005. DOI:10.1029/2004JA010931.

[20] Zhukov,A.N., Veselovsky, I.S. Global coronal mass ejections, Astrophys. J. 664, L131-L134, 2007. DOI:10.1086/520928.

[21] Ishkov, V.N. The short term forcecast of solar geoeffective flare events, in: Wilson A. (Ed.). Solar variability as an input to the Earth's environment. International Solar Cycle Studies (ISCS) Symposium, 23 - 28 June 2003, Tatranská Lomnica, Slovak Republic.. ESA SP-535, Noordwijk: ESA Publications Division, 2003, p. 559 – 560.

[22] Grigor'ev, V.M., Ermakova L.V., & Khlystova, A.I. Dynamics of line-of-sight velocities and magnetic field in the solar photosphere during the formation of the large active region NOAA 10488. Astron. Lett. 33, 858-862, 2007.

[23] Veselovsky, I.S. Dimensionless scaling approaches to the solar and heliospheric processes. Adv. Space Res. 40, 1087-1092, 2007. DOI:10.1016/j.asr.2006.12.051.

On the early phase of relativistic solar particle events: Are there signatures of acceleration mechanism?

G. A. Bazilevskaya

Lebedev Physical Institute of Russian Academy of Sciences, 53, Leninsky prospect, Moscow, 119991, Russia, (gbaz@rambler.ru)

***Abstract*— Many physical processes precede and accompany the Solar Energetic Particles (SEP) occurrence on the Earth's orbit. Explosive energy release on the Sun gives rise to a flare and a coronal mass ejection (CME). X-ray and gamma emissions are believed to be connected with flares. Radio emission is signature of disturbances traveling through the corona and interplanetary space. Particles can gain energy both in the flare and the accompanying wave processes. The beginning of the SEP events has the advantage of being the phase most close to the time of acceleration. Influence of interplanetary transport is minimal in the case of first arriving relativistic solar protons recorded by ground based neutron monitors in so called ground-level enhancements (GLE). The early phase of the SEP events attracts attention of many scientists searching for the understanding of particle acceleration. However, they come to the opposite conclusions. While some authors find arguments for coronal mass ejections as a sole accelerator of SEPs others prove a flare to be the SEP origin. Here, the circumstances of SEP generation for several GLEs of the 23rd solar cycle are considered. Timing of X-ray, CME, and radio emissions shows a great variety from event to event. However, the time of particle ejection from the Sun is closer to maximum of X-ray emission than to any other phenomena considered. No correlation is found between the particle fluxes and the CME characteristics.**

***Key Words*— Acceleration, coronal mass ejection, flare, relativistic solar particles, shock, solar radio emission.**

I. Introduction

The relative role of flares and shocks in the SEP acceleration is one of the central problems in the solar-heliospheric aspect of the cosmic ray physics. Up to now, there is no generally accepted opinion about the place and dominant mechanism of acceleration. Since the powerful SEP events always occur after big solar flares the SEP origin seemed to be clear until the early 1990-ies. However, flare identification often met significant difficulties. That led to revision of the existed paradigm, and during some recent decades many researchers hold the opinion that two separate SEP classes exist owing to different source where acceleration took place ([1]-[4]). In the impulsive, rather small, events particles are accelerated in the flare processes, and in the big gradual events acceleration occurs on the shocks driven by a coronal mass ejection (CME) in the corona and in the interplanetary space.

General scenario of the CME driven shock acceleration includes formation of a wide shock in front of a CME where particles are subject to the first order Fermi acceleration. It is important that particles themselves generate the turbulence in vicinity of the shock by amplifying the preexisting Alfvén waves. Evolution of the moving accelerating region leads to the complicated dynamics in the observed SEP characteristics, for example, to peculiar temporal changes in the SEP composition, streaming-limited intensities, flattening of
energy spectra in the low-energy range. These features were confirmed by both modeling and observations and became a crucial argument for the shock origin of SEPs
(Tylka, 2001). However the observations did not relate to the relativistic solar particles (RSP) which are the main signature of the most powerful SEP events recorded by the ground-level neutron monitors, so called Ground Level Enhancements (GLEs).

The GLEs refer to the gradual class, and therefore they are believed to originate from the CME driven shocks. Indeed, the authors of [2], [5]-[7] adhere to such point of view. However, a number of observational facts argue against such a conclusion, for example, the attribution of virtually all GLEs to the flares at the western solar hemisphere ([8]), strong connection with the flare gamma emission ([9], [10]) and with most powerful solar X-ray bursts ([11]). The flare origin of RSPs

is supported by analysis made in [12] and [13]. It seems more properly to admit the contribution to SEP in gradual events of both the flare and the shock sources ([14]-[16]). Still the relative role of a flare and a CME driven shock is of great interest. Concerning the GLEs, fast CMEs and flares always occur together, which makes it difficult to identify the actual source of SEP events detected near Earth orbit.

The observed SEPs are influenced by many processes of multiple and/or prolonged acceleration, and propagation in the corona and interplanetary space. Therefore, it is difficult to distinguish signatures of acceleration mechanisms from particle observations. However, the early phase of the SEP events is most close to the time of acceleration, and the role of interplanetary transport is minimal for the first arriving particles. Extreme events provide the best opportunity for study of the initial phase because of high signal to noise ratio. Relativistic solar protons are the most proper candidates for approach a problem of particle acceleration. In this work, the initial phase of several powerful GLEs of the 23rd solar cycle is studied together with concomitant phenomena on the Sun with the aim to find the closest relations to exist. Recently, similar work was fulfilled by the authors of [17] and the pioneer paper belongs to the authors of [18].

II. Data Selection

All the GLEs of the cycle 23 were examined ([19]), and those with the amplitude of enhancement greater than 10 % at any polar neutron monitor were selected for further analysis. This provided a good signal to noise ratio. Nine GLEs were selected. Concomitant solar parameters were chosen as follows. Powerful solar flares are always preceding the RSP occurrence. Information on the solar flares was taken from [20]. Hard X-ray emission is one of most energetic demonstrations of the flare process. The data of RHESSI on the hard X-rays are available for the events beginning from 2002 ([21]). Radio emission of the type II is believed to be an indicator of shock formation in the corona, and that of the type III means existence of the magnetic field lines connecting the flare area with the interplanetary space ([22]). The data on the solar radio emission was taken from [23]. CMEs are considered to be the main alternative to flares as the sources of RSPs. Information on CMEs is available onn [24]. All the CMEs related to the chosen GLEs were of the halo type.

III. Relative timing of the First RSP ejection and the Concomitant phenomena on the Sun

Because of strong anisotropy in the first arriving RSP fluxes (e.g., [12]) the first RSPs come to different places not simultaneously. For each GLE, the station with the earliest RSP arrival time was found. In order to infer the solar time of RSP ejection it is necessary to know the time of particle flight from the Sun to the Earth

$$t = L/(c\beta \cos\theta),$$

where L is the length of the field line of interplanetary magnetic field, c is the speed of light, $c\beta$ is the particle velocity and θ is the pitch angle. For the first arriving RSPs $\cos\theta = 1$ was suggested. The effective particle velocity depends on the energy spectrum of the first arriving RSPs and could be estimated for 7 GLEs of 9 selected using the spectra of [13] and the yield functions for the neutron monitors of [25]. The mean effective energy of the first arriving RSPs for the chosen GLEs was 1.5 GeV, which corresponds to $\beta = 0.923$. The path length along the field line of interplanetary magnetic field depends on the solar wind velocity, the hourly data being available at [26]. The solar wind velocity for the time of RSP arrival was obtained by interpolation between the neighboring hourly values. The accuracy of the inferred RSP ejection time was estimated in [27] as ±1 min with possible systematic shift by 1.5 min, since RSPs might actually leave the Sun earlier because the mean pitch angle for the first arriving

TABLE 1

GLEs SELECTED FOR ANALYSIS (WITH INTERNATIONAL EVENT NUMBERS), CORRESPONDING FLARES, THE EARLIEST TIME OF PARTICLE ARRIVAL, THE NEUTRON MONITOR RECORDED IT, SOLAR WIND VELOCITY AND TIME OF FLIGHT OF A PROTON WITH ENERGY 1.5 GEV FROM THE SUN TO THE EARTH

GLE number	Date	Flare		Time of the earliest arrival, UT	Neutron monitor	Solar wind velocity, km/s	Time of flight, s
55	6.11.1997	S18 W63	2B/X9.4	12:17	South Pole	349.66	10.94
59	14.07.2000	N22 W07	3B/X5.7	10:32.5	Oulu	593.47	9.76
60	15.04.3001	S20 W87	2B/X14.4	13:57	South Pole	498.85	10.04
61	18.04.2001	S20 W120	.../C2.2	2:33	South Pole	490.15	10.07
65	28.10.2003	S16 E08	4B/X17.2	11:13.5	Moscow	774.26	9.47
66	29.10.2003	S19 W09	2B/X10	20:58	South Pole	No data	11.00
67	02.11.3003	S14 W56	2B/X8.3	17:21	Lomnitsky Stit	525.97	9.95
69	20.01.2005	N12 W58	2B/X7.1	06:48.5	South Pole	855.40	9.39
70	13.12.2006	S06 W23	4B/X3.4	02:47.5	Oulu	641.36	9.66

particles could actually be not zero ([28]). Table 1 summarizes the data on the chosen GLEs, corresponding flares, time of earliest RSP arrival, neutron monitors recorded the earliest RSP arrival, interpolated solar wind velocity, and the time of RSP flight from the Sun to the Earth.

For each GLE, the distance of the leading edge of concomitant CME from the center of the Sun versus solar time was plotted as it is shown in Fig. 1. A parabolic extrapolation of a CME trajectory outside the observation limit was taken from [24]. In the event # 65, there were 2 CMEs in the corona but only the second one starting in around 1.3 hours after the flare was powerful enough. For the event # 69, the CME suggested in [7] is added, but it is not included in the catalogue [24]. It is possible to get roughly the time of the CME start at the trajectory crossing with the height of 1 solar radius, even if such extrapolation is not quite correct. The solar times of RSP ejection, start and maximum of the soft X-ray (SX) burst, maximum of the hard X-ray (HX) burst, and start of type II radio emission are shown in Fig. 1 by vertical bars. Their crossing with a CME trajectory indicates the height of the latter at that time. In addition, the horizontal bars give the duration of the HX emission, SX emission, and radio emission of type III.

The plots in Fig. 1 show a great variety of phenomena sequence and its duration. An order of phenomena accompanying the RSP ejection may be different. In the events # 55, 61, and 69 the extrapolated time of the CME start was earlier than or equal to the moment of the SX flare start, and in event # 65 it was coincident with the RSP ejection. The RSP ejection occurs in the late part of the sequence; it happened slightly earlier than the SX and HX bursts maxima in the event # 67, and

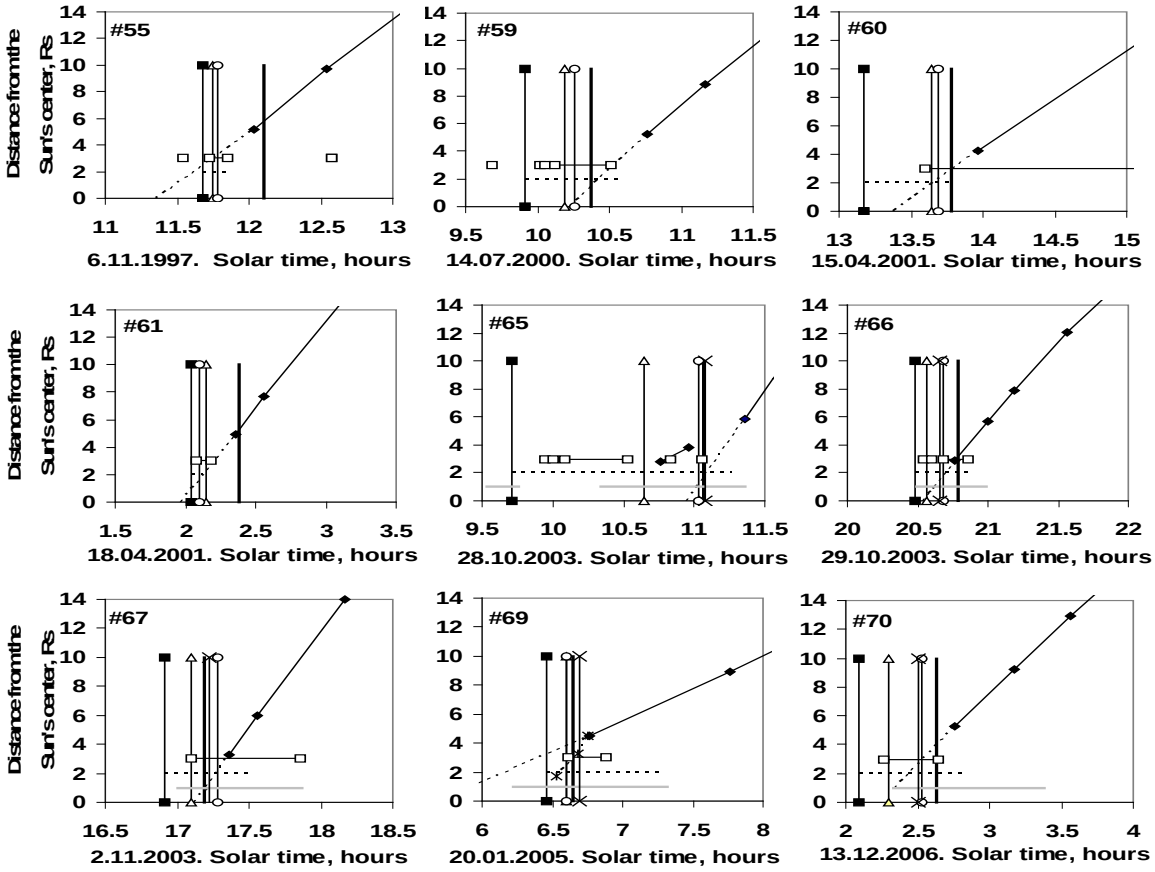

Fig. 1. Timing of the GLE-related phenomena on the Sun. The GLE number is given in the left upper part of each panel. Oblique line shows height of the leading edge of a CME versus time (solid line is the observed height, dashed line is parabolic extrapolation). Vertical bars do not refer to the height but indicate the time of various phenomena on the Sun: RSP injection (thick black bar without symbols), start of the soft X-ray (SX) emission (a bar with black squares), maximum of SX emission (a bar with white circles), maximum of the hard X-ray (HX) emission (a bar with crosses), start of type II radio emission (a bar with white triangles). Horizontal bars denote duration of the HX emission (thick gray), SX emission (dashed), radio emission of type III (a bar with white squares)

before the HX burst maximum in events # 65 and 69. In all events but #55 and 61, the type III radio emission was observed simultaneously with the RSP ejection, although in those events the type III burst were observed earlier.
That means presence of open field lines connecting the flare region with the interplanetary space [22]

Fig. 2 summarizes the timing of selected solar events. Each panel demonstrates distribution of the time shifts of a given parameter relative to the RSP ejection moment taken as a zero time and marked by a vertical dashed line. The mean values of the time shift and the standard deviation are given in each panel. It is clearly seen that the RSP ejection is most closely connected with the representatives of the flare processes. Relation to the HX maximum was available only for 5 events supported by the RHESSI observations but it is remarkable as can be seen in Fig. 2. However the scatter and diversity of the time shifts for all the parameters argue for the conclusion that they have no simple connection to the RSP ejection. It is seen in Fig. 2 that the CME start time relative RSP ejection varies greatly from event to event. The same is correct for the CME heights at the moment of RSP ejection. Fig. 3 presents the CME velocity (in parabolic approximation) versus its height at the moment of RSP ejection. The correlation coefficient is -0.35 indicating independency of these two parameters.

The Alfvén velocity in the corona $V_A = B/(4\pi\rho)^{0.5}$ (here B is magnetic field induction, ρ is the plasma density) was calculated in order to find if a shock was developed. The model of the solar corona from (Mann et al., 1999) was used for getting the plasma concentration

$$n(R) = n_s \exp(A/Rs(Rs/R - 1)),$$

where R is the distance from the Sun's center, Rs is the solar radius, $n_s = n(R = Rs) = 5.14 \cdot 10^9$ cm^{-3}, $A/Rs = 13.83$.

The coronal magnetic field was taken from [30] as

$$B = 1.7(Rs/R)^3 + 1.3(Rs/R)^2.$$

The Alfvén velocity in the corona is also shown in Fig. 3. The Mach number $M = V_{CME}/V_A$ is big enough with exception for one event (# 69). However, it is possible that another faster CME was present during this event [7], see Fig. 1.

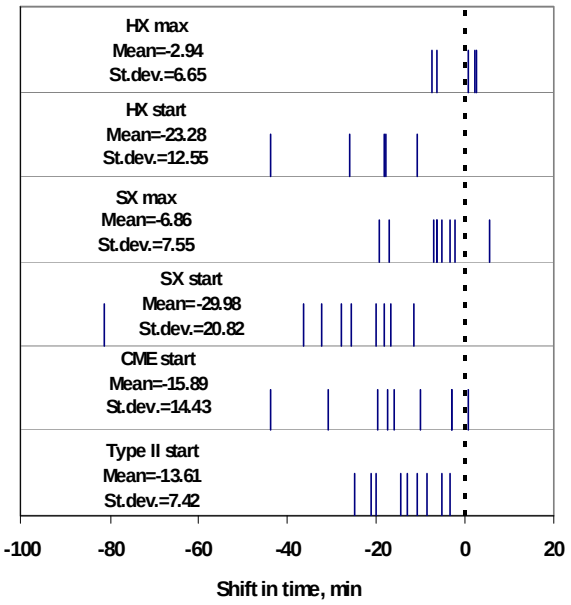

Fig. 2. Time shift between the RSP ejection (zero time and a vertical dashed black line) and various phenomena on the Sun. Each panel presents the timing of one phenomenon as indicated. Vertical bars mark the time of given phenomenon relative to RSP ejection for different GLEs. Negative shift means that a phenomenon occurred before RSP ejection. Mean shift and standard deviation for each phenomenon are

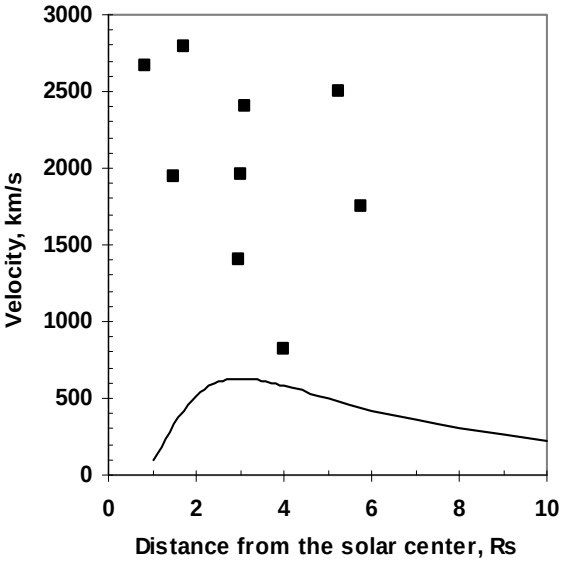

Fig. 3. Velocity versus distance from the Sun's center. Black squares are the CME velocity at the moment of RSP ejection for different GLEs. The curve is Alfvén velocity calculated using models

The speed of the shock connected with the type II radio emission can be derived from the observations and is given as Estimated Shock Speed (ESS) in [23]. No correlation was found between ESS and the CME speed for the events under study [27]. It can be expected bearing in mind rather complicated relation between the CMEs and the metric-decametric-hectometric type II bursts [31].

IV. Relation between the observed RSP characteristics and the parameters of the shocks in the corona

The authors of [12] and [13] found the fluxes J of first arriving (prompt) RSPs for the recent GLEs from the analysis of the neutron monitor network data in the form

$$J(E) = J_0 exp(-E/E_0),$$

where E is the particle energy. The values of J_0 and E_0 can be taken from [12], [13] for all the events under study with exception for # 61 and # 66. In the case of shock acceleration a correlation may exist between the observed RSP fluxes and the shock speed values. Also, it may be supposed that acceleration process started at the moment of coronal shock formation as indicated by the beginning of the type II radio emission and lasted until the RSP ejection. Then the correlation might exist between the observed prompt RSP fluxes and the supposed duration of acceleration. The expected relationships are presented in Fig. 4*a, b*. No significant correlation was found. A slight negative correlation can be seen in Fig. 4*a* between the CME speed and the first arriving RSP fluxes (correlation coefficient is -0.53). However, the expected correlation is positive [32].

In the case the particle acceleration occurs at the shock front certain relationships are expected between energy spectra of particles and wave parameters. For the diffusive shock acceleration, the energy spectrum has a power law form with the spectral index

$$G = (\sigma + 2)/(\sigma - 1),$$

where σ is the compression ratio at the shock front,

$$\sigma = (\gamma + 1)M^2/((\gamma - 1)M^2 + 2),$$

$\gamma = 5/3$ is the adiabatic index for the fully ionized plasma, M is the Mach number [33]. Therefore, given the CME (or ESS) and Alfvén velocities, it is

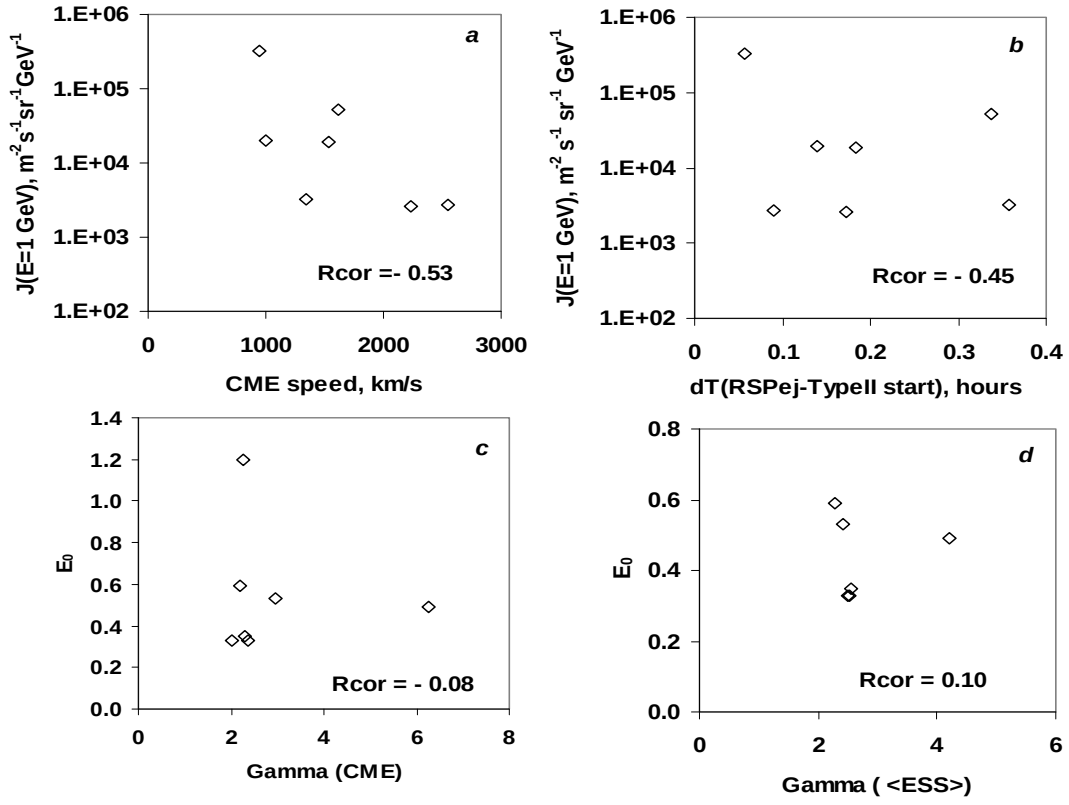

Fig. 4. Correlation between the features of the first arriving RSP as observed in [12], [13] and expected from the shock acceleration: prompt RSP flux at E = 1 GeV and CME speed (*a*), prompt RSP flux at E = 1 GeV and suggested time of acceleration (*b*), characteristic energy E_0 and a power law spectral index calculated for CME driven shocks (*c*) and those connected with the type II radio emission (*d*).

possible to estimate the expected value of the spectral index G. A negative correlation might be expected between values of G and characteristic energy E_0 derived from observations. The expected G values were determined for both the CME-driven shocks and those connected with the type II radio emission (averaged values of ESS as found by different observatories were used). No correlation was found between the parameters of the observed spectra and those expected from the shock acceleration (Fig. 4*c*, *d*). There is also no correlation between the observed RSP intensities and the height of CMEs at the moment of RSP ejection.

V. Conclusion

An attempt to find some relationship between the first arriving RSPs and the concomitant phenomena on the Sun, namely, a flare in SX and HX, CME speed and height at the moment of RSP ejection, and type II radio emission, showed that there is a great variety in the phenomena temporal sequence. Also the time period from the beginning of the flare in SX till the RSP ejection may be from around 20 min to more than 1 hour. To some extent, this can explain the controversial conclusions drawn by different authors analyzing various events. On the other hand, this is an indication that diverse scenarios may happen. Indeed, it is suggested in [34] that the change in the spectrum form during the initial phase of the July 14, 2000 was indicative of the stochastic acceleration of RSPs occurred after the initial acceleration by the CME driven shock, but in the case of 2001 April 15 these authors argue for pure shock acceleration. The statistics should reveal general interrelations between the first RSP and different parameters but now there are few big events with good reporting on accompanying phenomena.

The results of this work favor a powerful flare as the necessary contributor to the first RSP population. The RSP injection time is closer to the maximum in the HX bursts and SX bursts than to any other phenomena considered. No GLEs were till now observed without a powerful flare situated on the western solar hemisphere or close to the central meridian. No correlation were found between the observed first RSP fluxes [12], [13] and the CME-related parameters – speed, height of the leading edge at the moment of the RSP ejection, as well as between expected and observed spectral indices. However, the real speed and height of the halo CMEs are poorly determined from the present observations. It is hoped that the oncoming results of the 3D CME observations will allow a new understanding of CMEs and RSPs relation.

Given complexity of solar conditions concomitant of the RSP generation it is hardly possible to adhere to a single mechanism of particle acceleration, but rather the domination of one or another mechanism or the joint action are possible as it was claimed earlier by many authors. Nevertheless, first-arriving relativistic particles can hardly be generated without a flare. A CME driven shock can contribute to the relativistic particle population later.

Acknowledgment

I thank all the people who make their results accessible via Internet, namely, the neutron monitor community, solar physicists maintaining the flare and radio emission observation, and the RHESSI command. Special gratitude is to E. Vashenyuk and his group whose results are used in this work. This work is partly supported by the Russian Foundation for Basic Research (grants 05-02-16185, 05-02-17346a, 07-02-01019a, 07-02-10018k) and the Program of Presidium RAS Neutrino physics.

References

[1] J. T. Gosling, "The solar flare myth," *J.Geophys. Res.,* 98 (A11), 18937-18949, 1993.

[2] S. W. Kahler, "Characteristic times of gradual solar energetic particle events and their dependence on associated coronal mass ejection properties," *Astrophys. J.*, 628 (2), 1014-1022, 2005.

[3] D. V. Reames, "Particle acceleration at the Sun and in the heliosphere," *Space Sci. Rev*., vol. 90, pp. 413–488, 1999.

[4] A. J. Tylka, "New insights on solar energetic particles from Wind and ACE," *J. Geophys. Res*., 106 (A11), 25333-25352, 2001.

[5] J. W. Bieber, P. Evenson, W. Dröge, R. Pyle, D. Ruffolo, M. Rujiwarodom, P. Tooprakai, T. Khumlumlert, "Spaceship Earth observations of the Easter 2001 solar particle event," *Astrophys. J*., . 601, L103–L106, 2004.

[6] J. W. Bieber, J. Clem, P. Evenson, R. Pyle, D, Ruffolo, A. Sáiz, "Relativistic solar neutrons and protons on 28 October 2003". *Geophys. Res. Lett*., 32, L03S02, doi:10.1029/2004GL02 1492, 2005.

[7] N. Gopalswamy, H. Xie, S. Yashiro, I. Usoskin, "Coronal mass ejections and Ground Level Enhancements," in: Proceedings of the 29th ICRC, Pune, India, 1, 169-172, 2005.

[8] G. A. Bazilevskaya, M. B. Krainev, V. S. Makhmutov, A. K. Svirzhevskaya, N. S. Svirzhevskii, Yu. I. Stozhkov,. E. V. Vashenyuk, "Solar proton events observed in the FIAN stratospheric experiment," *Geomagn. and Aeron*., 43 (4), 412-421, 2003.

[9] S. N. Kuznetsov, V. G. Kurt, B. Yu. Yushkov, I. N. Myagkova, K. Kudela, J. Kaššovicova, M. Slivka, "Proton acceleration during 20 January 2005 solar flare: CORONAS-F observations of high-energy gamma

emission and GLE," in: Proceedings of the 29th ICRC, Pune, India, 1, 49-52,. 2005.
[10] S. N. Kuznetsov, B. Yu. Yushkov, K. Kudela, "Measurement of the spectrum of relativistic protons from solar flares on October 28 and November 2, 2003, onboard the CORONAS-F satellite," *Cosmic Research*, 45 (4), 373-375, 2007.
[11] G. A. Bazilevskaya, A. I. Sladkova, A. K. Svirzhevskaya, "Features of the solar X-ray bursts related to solar energetic particle event," *Adv. Space Res*., 37 (8), 1421-1425, 2006.
[12] E. V. Vashenyuk, Yu. V. Balabin, J. Perez-Peraza, A. Gallegos-Cruz, L. I. Miroshnichenko, "Some features of the sources of relativistic particles at the Sun in the solar cycles 21 2," *Adv. Space Res*., vol. 38 (3), pp. 411-417, 2006.
[13] E. Vashenyuk, Yu. Balabin, L. Miroshnichenko, J. Perez-Peraza, A. Gallegos-Cruz, in: Proceedings of the 30th ICRC, Merida, Mexico, paper 658, 2007.
[14] H. V. Cane, R. A. Mewaldt, C. M. S. Cohen, T. T. von Rosenvinge, "Role of flares and shocks in determining solar energetic particle abundances," *J. Geophys. Res*., 111, A06S90, doi:10.1029/2005/JA011071, 2006.
[15] G. Li, G. P. Zank, "Mixed particle acceleration at CME driven shocks and flares," *Geophys. Res. Lett*., L02101, doi: 10.1029/2004GL021250, 2005.
[16] K. G. McCracken, H. Moraal, "Two acceleration mechanisms for ground level enhancements," in: Proceedings of the 30th ICRC, Merida, Mexico, paper 897, 2007.
[17] S. W. Kahler, G. M. Simnett, M. J. Reiner, "Onsets of solar cycle 23 ground level events as probes of solar energetic particle injections at the Sun," in: Proceedings of the 28th ICRC, Tsukuba, Japan, pp. 3415-3418, 2003.
[18] E. W. Cliver, S. W. Kahler, M. A. Shea, D. F. Smart, "Injection onsets of 2 GeV protons, 1 MeV electrons, and 100 keV electrons in solar cosmic ray flares," *Astrophys. J.,* 260, 362-370, 1982.
[19] http://www.wdcb.ru/stp/data/cosmic.ray
[20] ftp://ftp.ngdc.noaa.gov/STP/SOLAR_DATA/SOLAR_ FLARES/XRAY_FLARES/
[21] http://www.mssl.ucl.ac.uk/www_solar/surfindex.html
[22] H. V. Cane, W. C. Erickson, N. P. Prestage, "Solar flares, type III radio bursts, coronal mass ejections, and energetic particles," *J. Geophys. Res*., 107 (A10), 1315, doi:10.1029/2001JA000320, 2002.
[23] http://www.ngdc.noaa.Gov/stp/SOLAR/ftpsolarradio.html #fixedbursts
[24] http://cdaw.gsfc.nasa.gov/CME_list/
[25] J. A. Lockwood, W. R. Webber, L. Hsieh, "Solar flare proton rigidity spectra deduced from cosmic ray neutron monitor observations," *J. Geophys. Res*. 79. 4149–4155, 1974.
[26] [ftp://nssdcftp.gsfc.nasa.gov/spacecraft_data/omni/
[27] G. A. Bazilevskaya, A. K. Svirzhevskaya, "Arrival of relativistic solar protons and conditions in the solar corona". Accepted by Geomagn. and Aeron., 2008. (In Russian).
[28] K.-L. Klein, A. Posner, "The onset of solar energetic particle events: prompt release of deka-MeV protons and associated coronal activity," *Astron. and Astrophys*. 438, 1029–1042, DOI: 10.1051/0004-6361: 20042607, 2005.
[29] G. Mann, F. Jansen, R. J. MacDovall, M.L. Kaiser, R. G. Stone, "A heliospheric density model and type III radio bursts," *Astron. and Astrophys*. 348, 614–620, 1999.
[30] R. Vainio, J. I. Khan, "Solar energetic particle acceleration in refracting coronal shock waves," *Astrophys. J*. 600 (1), 451–457, 2004.
[31] S. Pohjolainen, N. J. Lehtinen, "Slow halo CMEs with shock signatures," *Astron. and Astrophys*., 449, 359-367, doi: 10.1051/0004-6361:20054118, 2006.
[32] S. Kahler, "Solar fast wind regions as sources of gradual 20 MeV solar energetic particle events," in: Proceedings of the 28th ICRC, Tsukuba, Japan, 3301-3304, 2003.
[33] E. G. Berezhko, V. K. Elshin, G. F. Krymskii, S. I. Petukhov, "Cosmic Ray Generation by Shock Waves. Izdatel'stvo Nauka, Novosibirsk, 1988. (In Russian).
[34] D. J. Bombardieri, K. J. Michael, M. L. Duldig, J. E. Humble, "Relativistic proton production during the 2001 April 15 solar event," *Astrophys. J*., 665, 813-823, 2007.

Solar flares high energy gamma-ray emission and protons and electrons events measured at 1A.U.

V.G. Kurt

Skobeltsyn Institute of Nuclear Physics,
Moscow State University, Moscow, Russia,
(vgk@srd.sinp.msu.ru)

Abstract **– This report is a short overview of our experimental knowledge of high energy gamma-ray emission and solar proton and electron events near the Earth.**
1.Gamma-rays above 50 MeV are mainly due to the decay of pions produced by accelerated ions of energies greater than several hundreds MeV/nucl. Thus, this emission indicates the appearance of high energy nuclei in the corona. The available measurements of temporal behavior of high-energy gamma-ray emission from solar flares are discussed. These very few observations of the gamma-ray emission with the characteristic spectrum of pion-decay process gave us an unique opportunity to compare the acceleration time of protons with Ep>300 - 400 MeV to the release time of high-energy protons measured at ground level by the neutron monitor (NM) network. Proton arrival time to the Earth is consistent with the time of pion decay high-energy gamma-ray emission appearance at the Sun.
2. There is a brief consideration of accelerated electrons characteristics which produce the primary electron bremsstrahlung. Energy spectra of 0.0 4-100 MeV interplanetary electrons originating from solar flare compared with the electron bremsstrahlung.
3. The main result of the comparison of SPEs and Soft X-ray (SXR)flare properties are also discussed. Energetic proton measurements obtained from the GOES and IMP-8 satellites as well as from ground based neutron monitors are compared with the GOES soft X-ray measurements of the associated solar flares for the period 1975-2003. A broad range of phenomenology relating proton events to flares was found. The time frequency and size distributions of the peak intensities of the SPEs have been obtained over the entire mentioned period. The statistical analysis indicates that the probability and magnitude of the near-Earth proton enhancement depends critically on the flare's importance and its heliolongitude. It was also found that the heliolongitude frequently determines the character of the proton event time profile. In addition to intensity, duration and timing proton events were found to be related to the other flare properties such as longer loop lengths.

Thin structure of temporal profiles of solar flares January 15, 17 and 20 2005 by data of AVS-F apparatus onboard CORONAS-F satellite

I.V. Arkhangelskaja, Yu.D. Kotov, A.I. Arkhangelsky, A.S. Glyanenko

Astrophysics Institute of Moscow Engineering Physics Institute (State University), 115409, Kashirskoe shosse, 31, Moscow,Russia
(E-mail: irene.belousova@usa.net)

***Abstract* – The temporal profiles and energy spectra of the solar flares January 15, 17, 20 2005 by data of AVS-F apparatus onboard CORONAS-F satellite are discussed. The energy spectra of these solar flares contain positron line and neutrons capture line. Solar flares January 17 and 20 spectra also contain some nuclear lines. Thin structure with characteristic timescales 33-92 sec is presented on flares temporal profiles in energy bands corresponding observed spectral features, which confirmed by periodogram analysis (confidence level is 99%).**

I. INTRODUCTION

Investigation of large-scale time structure in various energy bands allows to obtain characteristics of particle acceleration in solar flares and properties of surrounding media, for example the energy spectra of solar energetic particles and parameters of its evolution [1], [2], the most probable profile of plasma density in the solar photosphere and adjoining levels during the period of a flare [3] and so on. The presence of thin structure on solar flares temporal profiles can be connected with flare region density fluctuations and acceleration mechanism. Large-scale and thin solar flares temporal profiles structure studying should gives additional information about the acceleration processes during solar flares and the physical conditions in the area in which flare occurs.

II. AVS-F APPARATUS DESCRIPTION

The AVS-F (amplitude-time Sun spectrometry) apparatus [4], [5] was installed onboard CORONAS-F satellite (NORAD catalog number 26873, International Designator 2001-032A), which operated from July 31 2001 up to December 6 2005. The orbit of satellite was approximately circular oriented towards the Sun with inclination ~82.5° and altitude ~500 km.

The AVS-F apparatus use signals produced by the SONG-D detector (energy deposition ranges of 0.1-11.0 MeV and 4.0-94.0 MeV by first time calibration data), anticoincidence signal generated by the plastic scintillation counter of the SONG-D and signal from XXS-1 detector, which is the CdTe based semiconductor detector with energy deposition range 3-30 keV. The SONG-D is CsI(Tl)-based detector ∅20cm and height of 10 cm with electronics unit SONG-E [6], [7]. The system energy resolution is 13.0% for γ-quanta with E_γ=0.662 MeV (^{137}Cs). The energy bands limits are shifted during apparatus operation: the energy threshold and amplification coefficient of low-energy band were changed on 1% and 1.8% per month and on January 2005 the low-energy band boundaries were approximately 0.1-20 MeV [5]).

Because of high inclination of CORONAS-F satellite orbit the approximation of the background temporal profiles was made by polynomials with power 5 or 4 on the equatorial regions of satellite orbit and with linear function or by constant on polar ones. The integration time for all presented temporal profiles on AVS-F data (excluding some ones which

are separately mentioned) is 16 s for 0.1-20 MeV energy band [5], [8].

III. THE CHARACTERISTICS OF SOLAR FLARES OBSERVED DURING JANUARY 2005 BY AVS-F APPARATUS

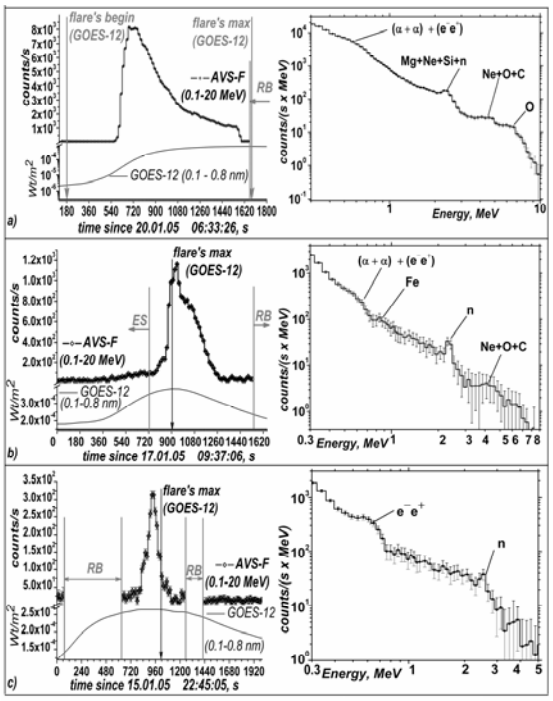

Fig. 1. Temporal profiles and energy spectra in AVS-F low-energy γ-band for solar flares January 20 2005 (a), January 17 2005 (b) and January 15 2005 (c).

Twenty seven solar flares with class M and X were registered on the Sun during January 2005 by detectors onboard satellites GOES, RHESSI, SOHO, TRACE and other instruments. Four active regions 10715, 10718, 10719 and 10720 were sources of these solar flares. Six of them (January 9, January 15, January 17, January 20, and two flares on January 19) were observed in low energy γ-band by AVS-F too [5]. Active region NOAA 10719 was the source of solar flare January 9, the source of other 5 flares was NOAA 10720 one [4]. January 19 flares (M6.7 and X1.3) and solar flare January 9 (M2.4) observed in polar cap regions of CORONAS-F orbit but satellite entered radiation belts during these flares registration.

The flare January 20 (X7.1, 06:36-07:26 UT with maximum in energy band 0.1-8 nm at 07:01 UT by GOES data) was the most powerful of observed ones. It was accompanied by solar particles event (SEP), which was most intensive one for period of the last 29 years [9] and CME. The GLE N°69 related to this flare was the largest one measured by neutron monitors since 1956 [10]. Gamma emission of this flare was observed by AVS-F in both energy bands during X-ray emission rise (before their maximum) by GOES data in equatorial part of CORONAS-F orbit before Radiation belt. This flare temporal profile and energy spectrum in AVS-F low-energy γ-band are shown at Figure 1a, one in high-energy γ-band is discussed in [8], [11]. January 20 flare's temporal profiles shape both in low-energy and in high-energy γ-bands are very simple with one maximum at the same time as in X-ray band on GOES data. Four spectral lines complexes were observed in integral spectra of this flare during whole duration of γ-emission registered by AVS-F in low-energy γ-band corresponding to nuclear, annihilation and neutron capture lines – see Table 1.

The January 17 flare (class X3.8) lasted in time interval 06:59-10:07 UT by GOES data, maximum in energy band 0.1-8 nm was at 9:52 UT. This flare was observed by AVS-F apparatus in equatorial region of satellite orbit too during X-ray emission (by GOES data) maximum and droops. Unfortunately during rise phase of X-ray emission of January 17 flare satellite CORONAS-F was in the Earth shadow and we discuss this flare gamma-emission only since 09:51:13 UT. January 15 class X2.6 solar flare started at 22:35 UT, ended at 23:31 UT and peaked at 23:02 UT by GOES data in energy band 0.1-8 nm. Its gamma-emission registered by AVS-F in the polar cup region of CORONAS-F satellite orbit during X-ray maximum by GOES data. There were not any statistical significant count rate exceeds background level on AVS-F data before and after Radiation belt during this flare.

Table 1. Spectral features of discussed solar flares.

Date	Spectral features and their energy band, MeV
20	αα + e^+e^- (0.4-0.6), $^{24}Mg+^{20}Ne+^{28}Si$ + neutron capture (1.7–2.3), $^{20}Ne+^{16}O+^{12}C$ (3.2-5.0), ^{16}O (5.3-6.9)
17	αα + e^+e^- (0.4-0.6), ^{56}Fe (0.7–0.9), $^{24}Mg+^{20}Ne+^{28}Si$ +neutron capture (1.7–2.3), ^{12}C (3.6-5.0)
15	e^+e^- (0.5-0.6), neutron capture (2.0–2.3)

The temporal profiles and energy spectra of January 17 and 15 flares in AVS-F low-energy γ-band at Figures 1b and 1c correspondingly are presented.

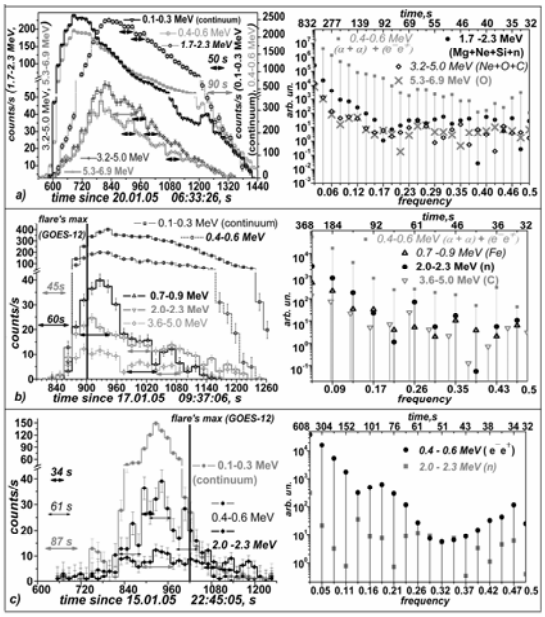

Fig. 2. Periodograms and temporal profiles by AVS-F apparatus data in energy bands corresponding to discussed spectral features for solar flares January 20 2005 (a), January 17 2005 (b) and January 15 2005 (c).

During these flares AVS-F apparatus didn't register any statistical significant count rate exceeds background level in the high-energy γ-band. January 17 and 15 flare's temporal profiles shape in low-energy γ-band and X-ray band are very simple with one maximum too. Four spectral lines complexes were observed in integral spectra of January 17 flare and two in January 15 one. The characteristics of these complexes are presented at Table 1. The January 17 flare's spectral features correspond to nuclear, annihilation and neutron capture lines, but during the January 15 solar flare only annihilation and neutron capture lines were registered. All discussed spectral features were observed during whole duration of γ-emission registered by AVS-F.

IV. JANUARY 2005 20, 17 AND 15 TEMPORAL PROFILES THIN STRUCTURE

As was mentioned above, January 20, 17 and 15 flare's temporal profiles shape in low-energy γ-band on AVS-F data and X-ray band on GOES data are very simple with one maximum. Discussed flares were sufficiently long for studying thin structure at timescales of some tens seconds. We made periodogram analysis of these flares temporal profiles in energy bands corresponding spectral features presented in Table 1. The thin structure is presented at temporal profiles of these three solar flares. Characteristics timescales are in the range 33 – 92 s for January 20 solar flare, 33 – 61 s for January 17 and 34 – 87 s for January 15 ones at 99% significance level – see Table 2. Periodograms and temporal profiles by AVS-F apparatus data in energy bands corresponding discussed spectral features for solar flares January 20 2005, January 17 2005 and January 15 2005 are shown at Figure 2.

There are three main maxima at solar flare January 20 temporal profile in energy band 0.4 – 0.6 MeV at 06:44:36, 06:45:40 and 06:53:46 UT which correspond to maxima in range 0.1 – 0.3 MeV in statistical errors limits. One main maximum at 06:46:36 UT was in energy bands 3.2 – 5.0 MeV and 5.3 – 6.9 MeV and one maximum at 06:47:16 UT was observed in range 1.7 – 2.3 MeV. So, maximum in energy band contained neutron capture line is delayed relatively maxima in ones corresponding to nuclear lines, positron line and continuum.

Following main maxima are separated on January 17 flare temporal profiles: 09:41:26 UT (0.15 – 0.30 MeV), 09:40:36 UT (0.4 – 0.7 MeV), 09:42:31

Table 2. Characteristic timescales of solar flares discussed.

Flare date	Energy band, MeV	Characteristic timescales, s					
20	0.4-0.6	83	64	49	44	38	33
	1.7-2.3	69	52	44	40	35	–
	3.2-5.0	92	46	42	36	–	–
	5.3-6.9	92	59	44	38	–	–
17	0.4-0.6	61	37	–	–	–	–
	0.7-0.9	61	46	33	–	–	–
	1.7-2.3	61	46	33	–	–	–
	3.2-5.0	64	35	–	–	–	–
15	0.4-0.6	87	34	–	–	–	–
	2.0-2.3	125	61	47	42	34	–

UT (0.7–0.9 MeV), 09:42:16 UT (2.0–2.3 MeV) and 09:41:54 UT (3.6–5.0 MeV). Temporal profiles of January 15 solar flare have got one main maximum in each studying energy band: at 23:00:19 UT in corresponding continuum range and at 23:00:45 UT in 0.4–0.6 MeV and 2.0–2.3 MeV ones.

V. CONCLUSIONS

The wide range temporal profiles of January 20, 17 and 15 2005 solar flares time structure by AVS-F data is very simple with one maximum. But temporal profiles structure is more complex in energy bands corresponding nuclear lines, positron line and neutrons capture line observed in these flare energy spectra.

The large-scale time structure mostly contains one maximum in each energy band. But there are three maxima at solar flare January 20 temporal profile in energy band 0.4 – 0.6 MeV, which correspond to maxima in range 0.1 – 0.3 MeV. In other energy bands one main maximum was observed on all discussed solar flares temporal profiles but thin structure with characteristic timescales 33-92 sec is presented on them in energy bands corresponding to observed spectral features exclude 0.1-0.3 MeV range (continuum). Periodogram analysis confirmed existence of such structure (confidence level is 99%).

The character of 2.223 MeV gamma-emission temporal profiles depend mainly on the accelerated particles energy spectrum, density of surrounding atmosphere, content of ^{3}He in the solar atmosphere and angular distribution of accelerated particles. The intensity of nuclear lines depends from the abundance of elements, density, and temperature of the ambient solar atmosphere and parameters of the accelerated ions. So, the presence of thin structure on temporal profiles in corresponding energy bands allows us to make conclusion about fluctuations of mentioned above parameters during solar flares. Of course, determination of concrete fluctuated parameters should require detailed calculations within the frameworks of recent solar flares models. The results of investigation of January 20 2005 temporal profiles in energy bands of 1.7 – 2.3 MeV and 3.2-6.9 MeV presented in this article were used for studying of effect of density enhancement and hardening of particle spectra during solar flare [12], So, the large-scale and thin flares temporal profile structure analysis should gives additional information about the acceleration processes during solar flares and the physical conditions in the area in which flare occurs.

REFERENCES

[1] Ramaty, R., Murphy, R.J. Nuclear processes and accelerated particles in solar flares Space Sci. Rev. 45(3/4), 213-268, 1987.

[2] Gan, W.Q. Spectral Evolution of Energetic Protons in Solar Flares. Astrophys. J. 496, 992-997, 1998

[3] Kuzhevskij, B.M., Miroshnichenko, L.I. and Troitskaia, E.V., Derivation of density profiles in the solar atmosphere by the 2.223 MeV line data for the 6 November 1997 flare, Proc. 27th Int. Cosmic Ray Conf., Invited, Rapporteur and Highlight Papers Special Volume), pp. 285-288, 2001.

[4] Glyanenko, A. S., Kotov Yu. D. Pavlov, A. V. et al. The AVS-F experiment on recording rapidly changing fluxes of cosmic and gamma radiation prepared under the CORONAS-F project. Instrum. Exp. Tech., 42, #5, 596-603, 1999.

[5] Arkhangelskaja, I. V., Arkhangelsky, A. I., Kotov, Yu. D. et al. The solar flare catalog in the low-energy gamma-ray range based on the AVS-F instrument data onboard the CORONAS-F satellite in 2001 2005. Solar System Research, 40, 133-141, 2006.

[6] Kuznetsov, S. N.; Kudela, K.; Ryumin, S. P. et al CORONAS-F satellite: Tasks for study of particle acceleration. Adv. Space Res., 30, 7, 1857-1863, 2002.

[7] Baláž, J.; Dmitriev, A. V.; Kovalevskaya, M. A. et al Solar flare energetic neutral emission measurements in the project CORONAS-I. Proceedings of the IAU Colloquium N°144: Solar coronal structures, held in Tatranska Lomnica; Slovakia; September 20-14; 1993, eds. Rusin, V., Heinzel, P., Vial, J.-C. pp. 635 – 639, 1994.

[8] Arkhangelskaja, I. V., Arkhangelsky, A. I., Glyanenko, A.S., et al. The investigation of January 2005 solar flares gamma-emission by AVS-F apparatus data onboard CORONAS-F satellite in 0.1-20 MeV energy band. Proceedings of the 11th European Solar Physics Meeting "The Dynamic Sun: Challenges for Theory and Observations", (ESA SP-600). 11-16 September 2005, Leuven, Belgium. Eds: D. Danesy, S. Poedts, A. De Groof et al, pp.107.1-107.4, 2005.

[9] Mewaldt, R.A, Looper M.D., Cohen, C.M.S. et al Solar-Particle Energy Spectra during the Large Events of October-November 2003 and January 2005. Proceedings of the 29th International Cosmic Ray Conference. August 3-10, 2005, Pune, India. Eds by Acharya, B. S., Gupta, S, Jagadeesan, P. et al. Mumbai: Tata Institute of Fundamental Research, v. 1, pp.111-114, 2005.

[10] Bieber, J.W., Clem, J., Evenson, P. et al Largest GLE in half a century: Neutron monitor observations of the January 20, 2005 event. Proceedings of the 29th International Cosmic Ray Conference. August 3-10, 2005, Pune, India. Eds by Acharya, B. S., Gupta, S, Jagadeesan, P. et al. Mumbai: Tata Institute of Fundamental Research, v. 1, pp.237-240, 2005.

[11] Arkhangelskaja, I. V., Arkhangelsky, A. I., Kotov, Yu. D. et al. The observation of gamma-ray emission during January 20 2005 solar flare. Proceedings of the International Symposium SEE 2007: Fundamental Science and Applied Aspects, in press, 2007

[12] Troitskaya E. V., Miroshnichenko L. I., Arkhangelskaja, I. V. et al, Study of the 28 October 2003 and 20 January 2005 solar flares by means of 2.223 MeV gamma-emission lines. Proceedings of the International Symposium SEE 2007: Fundamental Science and Applied Aspects, in press, 2007

Study of the 28 October 2003 and 20 January 2005 solar Flares by means of 2.223 MeV gamma-emission line

E. V. Troitskaya[1], I. V. Arkhangelskaja[2], L. I. Miroshnichenko[1,3,4] and A. I. Arkhangelsky[2]

[1] SINP M.V. Lomonosov Moscow State University,
[2] Astrophysics Institute of Moscow Engineering Physics Institute (State University),
[3] N.V. Pushkov Institute IZMIRAN, Troitsk, Moscow Region,
[4]Instituto de Geofisica, UNAM, C.U., Coyoacán, 04510, México, D.F., México

***Abstract*— We have studied some characteristics of solar flares and surrounding medium (solar plasma) by means of 2.223 MeV line time profile of gamma-emission from neutron captures by hydrogen nuclei. It was composed the code with making allowance for the main processes of neutron interactions and deceleration in the solar atmosphere, character of neutron source, losses of neutrons and density model of the solar atmosphere. The comparing of modeled time profiles of 2.223 MeV gamma-line with observed ones allowed us to reveal the density enhancements in the sub-flare regions of the extreme flares of 28 October 2003 and 20 January 2005. We use the data of INTEGRAL and CORONAS-F for analysis. The same analysis let us to detect the values of spectral indexes of charged particles and their evolution with the time during gamma-emission of the flares. The hardening of charged particles spectrum with the time is found. The peculiarities of the 20 January 2005 flare are discussed.**

***Key Words*— Particle acceleration, Solar flares, Solar gamma-emission, Solar plasma density.**

I. Introduction

THE neutron capture line of 2.223 MeV from solar flares has been analyzed directly or by using additional data to obtain the characteristics of particle acceleration in solar flares and properties of surrounding solar atmosphere. In particular, in [1] the fluences of 2.223 MeV line are used for determining the energy spectra of solar energetic particles, in [2] this line is used to study angular distributions of accelerated particles and production of secondary neutrons, and in [3] for investigation of photospheric ^{3}He abundance. Kuzhevskij et al. (e.g. [4],[5]) have developed an approach to determine the most probable profile of plasma density in the solar photosphere and adjoining levels during the period of a flare. By the 2.223 MeV line data on three large flares, 22 March 1991 [7], 6 November 1997 [6] and 16 December 1988 [5] the plausible model of the solar atmosphere density in the period of flare and some evidence of the effect of density enhancement was obtained. Gan [8], [9] was the first who applied the time profiles of calculated partial fluences of neutron capture line and 0.511 MeV annihilation line to deduce the spectral evolution of accelerated charged particles.

In [2] and [10] the energy spectra of solar flare neutrons were calculated in different suppositions on accelerated particle spectra. Founding on these neutron spectra, in the case of the flare 16 December 1988, Kuzhevskij et al. [5] deduced additionally the character of accelerated particles energy spectrum evolution. In the present work we apply the developed approach to the powerful solar events of 28 October 2003 and 20 January 2005.

II. Method

The calculations of neutron propagation in the solar matter and 2.223 MeV line production are carried out using Monte-Carlo simulation, with due account for the models of vertical density profile of the solar plasma. For our SINP code we make allowance for the most important processes, which have impact on neutrons and therefore on the 2.223 MeV time profile. The details of calculations may be found elsewhere (e.g. [5], [11]).

As a basic density model (BDM) (m=1) we have used the standard astrophysical model HSRA

(Harvard-Smithsonian Reference Atmosphere) for the lower chromosphere and quiet photosphere [12] together with a model of convection zone [13] consistent with the first one. To determine possible deviations of the model, realizing in the observable flare from the BDM, we have also composed four additional models (m=2, 3, 4, 5) representing smaller and larger densities at photospheric and adjoining levels as compared with the standard model (m=1) of the quiet Sun (Table 1).

We use the initial neutron spectra calculated in [2] for a case of Bessel spectra of accelerated particles. Initial time profile of neutrons is supposed to be resembled the time history of (4.44 MeV + 6.13 MeV) γ-line fluxes.

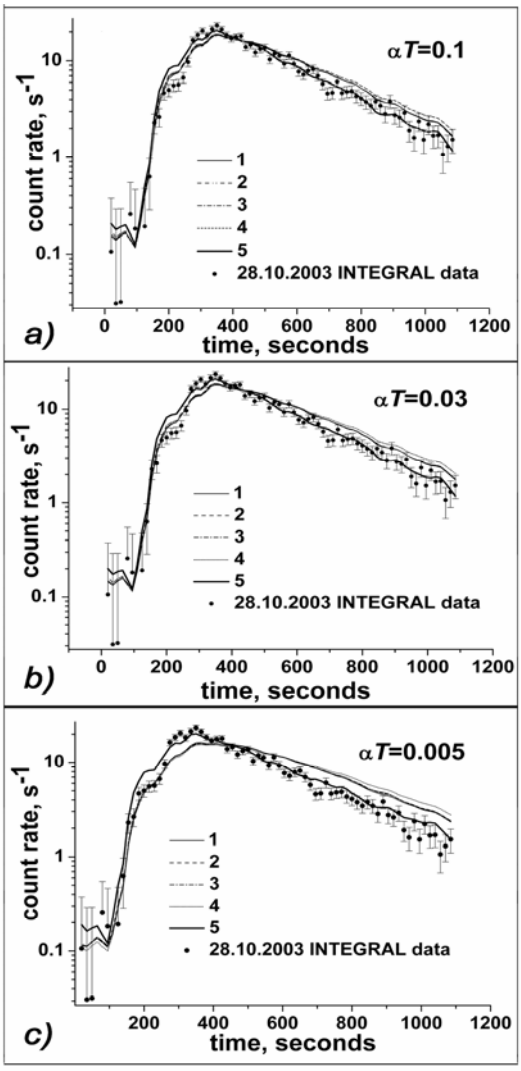

Fig. 1. Observational data of 2.223 MeV gamma-emission and modeling with spectral indexes 0.005, 0.03 and 0.1 for five models for solar flare October 28, 2003.

III. Results

a. October 28 2003

The flare of 28 October 2003 began at 9:41 UT, had its maximum at 11:10 and ended about 11:24 UT. It lasted about 15 min in the gamma-ray band. It appeared in the NOAA active region 10486. We apply our method to investigate the 28 October 2003 solar flare of X17.2/4B importance with coordinates S16E08 and present the results for this powerful and long-duration flare. The data on 2.223 MeV and summarized fluxes of 4.44 and 6.13 MeV gamma emission from INTEGRAL are used [14].

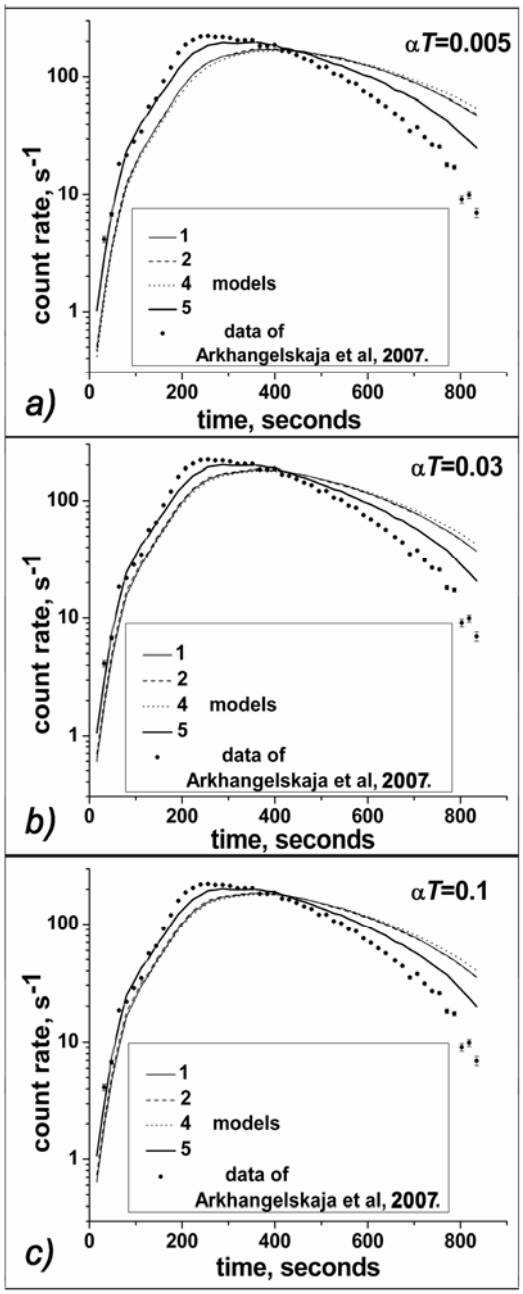

Fig. 2. Observational data of 2.223 MeV gamma-emission and modeling with spectral indexes 0.005, 0.03 and 0.1 for 4 models for solar flare January 20, 2005

The calculations of time profiles of gamma fluxes were made in supposition of Bessel form (stochastic acceleration) of accelerated particles energy spectrum for three meanings of spectral αT parameter: 0.005, 0.03 and 0.1 (Fig.1).

The least square method reveals the best modeling time profile in the case of αT=0.03 and m=5 (Table 1). This means the density enhancement in the whole thickness of photosphere. We can also conclude that m=5 starts to realize at about 400th second. Another conclusion is that the better fitting in the rising phase is αT=0.005 and in the phases of maximum and decay the best fitting is αT=0.1.

b. January 20, 2005

The flare January 20 (X7.1/3B) started at 06:36 UT, had a peak at 07:01 UT and ended at 07:26 UT by GOES data, with maximum in energy band 0.1-8 nm at 07:01 UT. Gamma emission of this flare was registered by instruments on board of CORONAS-F [15] and RHESSI [16]. CORONAS-F satellite with AVS-F electronic apparatus [17], [18] detected this flare gamma-emission in energy band 0.1-140 MeV [19], [20] during X-ray rise (before their maximum) by GOES data.

For this solar flare it is impossible to modeling the time profile using our method with the usually realized meanings of αT parameter, thus we are compelled to recognize the impossibility to understanding this flare in the frame of our suppositions without additional ones.

IV. DISCUSSION

The results for the 28 October 2003 flare on the density enhancement confirm the results for three previously studied flares. The hardening of particle spectra with the time is also confirmed. The hardening of particle spectra is also confirmed. The delay of the beginning of the 5th model realization is also confirmed.

Now we have a question about the origin of the revealed density enhancement. It may be either at the site of primary energy release at the top of magnetic flare loop in the corona or upper chromosphere or it may be connected with the magnetic structures in which the flare is developing. The first process – the response of the atmosphere to the sharp energy release is well studied by some authors. It can be from 1 to several cold condensations, moving downward in the front of shock wave [21].

Estimate the maxima grammage for 5 condensations: 10^6 cm$\cdot 5\cdot 10^{15}$ cm$^{-3}\cdot 1.67\cdot$10-24 g $\cdot 5$ = 0.04 g$\cdot$cm^{-2}. Compare this grammage with those one, required for thermalization of energetic neutron: for neutron energies E_n=1, 5, 10, 20, 30, 50 MeV the grammage of 2.0, 2.6, 3.6, 4.4, 6.2, 10 g/cm^2 correspondingly are necessary for thermalization. The most effective for producing 2.223 MeV gamma-line are neutrons with energies 10-50 MeV. We have to conclude that the reason of density enhancement is not the primary explosive release of energy and the shock waves.

Estimate the maxima grammage for 5 condensations: 10^6 cm$\cdot 5\cdot 10^{15}$ cm$^{-3}\cdot 1.67\cdot$10-24 g $\cdot 5$ = 0.04 g$\cdot$cm^{-2}. Compare this grammage with those one, required for thermalization of energetic

Table 1. Characteristics of the models: m is the number of model, parameter τ is the optical depth for a wavelength of 500 nm and the level τ = 0.005 corresponds to the top of the photosphere.

№, m	Character of density	
	Brief	Detailed
1	The main astrophysical model of the lower chromosphere and photosphere HSRA [11] together with the model of convective zone of Spruit [12]	Grows gradually from $1.5\cdot10^{16}$ cm^{-3} at the top of photosphere up to $2\cdot10^{17}$ cm^{-3} at the 330 km level lower, where τ=1 and sharply grows up to τ=10 in the depth of 60 km.
2	Enhanced into and under the photosphere	Enhanced to $8\cdot10^{17}$ cm^{-3} at the depth ~500 км under the top of photosphere.
3	Enhanced into and under the photosphere	Grows up more slowly under the photosphere and mounts to $6\cdot10^{17}$ cm^{-3} at the same depth.
4	Depressed from the low chromospere down to the lower levels	Reduction of the density from the low chromospere down to the deep layers. The density is $3\cdot10^{15}$ cm^{-3} at the top of photosphere and $2\cdot10^{16}$ cm^{-3}.at the 330 km lower level.
5	Enhanced in the whole thickness of the photosprere.	The density is $2\cdot10^{17}$ cm^{-3} through the complete thickness of the photosphere.

neutron: for neutron energies E_n=1, 5, 10, 20, 30, 50 MeV the grammage of 2.0, 2.6, 3.6, 4.4, 6.2, 10 g/cm^2 correspondingly are necessary for thermalization. The most effective for producing 2.223 MeV gamma-line are neutrons with energies 10-50 MeV. We have to conclude that the reason of density enhancement is not the primary explosive release of energy and the shock waves.

In the case of the 20 January flare we can conclude that too quick decay of gamma-emission, generated by neutrons, requires the loss of a part of protons or neutrons, so that last ones couldn't give the contribution to generation of 2.223 MeV gamma-rays. To satisfy this requirement we may suppose the confinement of a part of accelerated protons in any magnetic structure during the flare. If supposing the small enough quantity of the matter in this structure, we may conclude that these protons may not produce neutrons during the time of this flare. By this way we can explain the sharp decay of 2.223 MeV gamma-line data.

We also ought to consider another possibility of the quick decay of gamma-emission: in this event it is defined with good probability the radiative neutron absorption line 20.58 MeV generated in collisions by neutrons on ^{3}He [22]. One of the factors, leading to appreciable line is the enhanced quantity of ^{3}He in accelerated particles in some flares and losses the neutrons in the reactions with ^{3}He:

$$n + {}^3\mathrm{He} \rightarrow {}^4\mathrm{He} + \gamma(20.58\ \mathrm{MeV}).$$

V. Conclusion

In the present work we confirm for the 28.10.200 flare the previously conclusions about the density enhancements in the deep photospheric or subphotospheric layers that were made earlier for 3 flares. The hardening of particle spectra is also confirmed.

We have analyzed the reasons of the density enhancement in the subflare region and we have to conclude that the reason of density enhancement is not the primary release of energy and the shock waves. The origin may be connected with the magnetic loop in which the flare is developing.

It is shown that the 20.01.2005 flare can't be modeled by usually realized parameters. Two possible explanations of the phenomenon are suggested.

VI. Acknowledgements

The authors are very indebted to Dr. V. Tatischeff for assignment the data on the solar flare of 28 October 2003. This work has been supported partly by the Russian Foundation of Basic Research (RFBR, projects 02-02-39032, 03-02-96026, 05-02-39011), Federal Purpose Scientific and Techncal Program (Section I, Project 4), and President's Grant of Russian Federation (project 1445.2003.2). The work of W. Gan was supported by NNSFC (China) via grants 10221001, 10333040 and by grant 2006CB806302 from the Ministry of Science and Technology of China. The work by L.I. Miroshnichenko was also supported partly by the CONACyT, Mexico (project 45822, PERPJ10332).

References

[1] R. Ramaty and R.J. Murphy, Nuclear processes and accelerated particles in solar flares. *Space Sci. Rev.* vol.45(3/4), pp. 213-268, 1987.

[2] X.-M. Hua and R.E. Lingenfelter, Solar flare neutron production and the angular dependence of the capture gamma-ray emission. *Sol. Phys.*, vol. 107, pp. 351-383. 1987.

[3] M. Yoshimori, A. Shiozawaand, K Suga, Photospheric ^{3}He to H abundance ratio derived from gamma-ray line observations, in *1999 Proc. 26th Int. Cosmic Ray Conf.*, vol. 6, pp. 5-8, 1999.

[4] B.M. Kuzhevskij, S.N. Kuzhetsov and E.V. Troitskaia, Development of the solar flare plasma density investigation method based on the 2.2 MeV gamma-line time profile analysis, *Adv. Space Res.,* vol. 22(7), pp. 1141-1147, 1998.

[5] B.M. Kuzhevskij, L.I. Miroshnichenko and E.V. Troitskaia, Gamma-ray radiation with energy of 2.223 MeV and the density distribution in the solar atmosphere during flares, *Russian Astronomy Reports,* vol. 49, 566-577 (in English), 2005.

[6] B.M. Kuzhevskij, L.I. Miroshnichenko, and E.V. Troitskaia, Derivation of density profiles in the solar atmosphere by the 2.223 MeV line data for the 6 November 1997 flare, in *2001, Proc. 27th Int. Cosmic Ray Conf,* Invited, Rapporteur and Highlight Papers (Special Volume), pp. 285-288.

[7] E.V. Troitskaia and B.M. Kuzhevskij, Absorption of 2.22 MeV solar flare gamma-rays and determining of the solar plasma density altitude profile, in *1999, Proc. 26th Int. Cosmic Ray Conf., Salt Lake City, USA. August 17-25*, vol. 6, pp. 17-20.

[8] W.Q. Gan, Spectral Evolution of Energetic Protons in Solar Flares. *Astrophys. J*., vol. 496, pp. 992-997 1998.

[9] W.Q. Gan, On both the time histories of the 0.511 MeV line and 2.223 MeV line from the X4.8 flare of 23 July 2002 observed with RHESSI., *Solar Phys.*, 2004, vol. 219, pp. 279-287.

[10] X.-M. Hua, B. Kozlovsky, R.E. Lingenfelter, R. Ramaty, A. Stupp, Angular and energy-dependent neutron emission from solar flare magnetic loops, *Astrophys. J. Suppl*., vol.140, pp.563-579, 2002.

[11] E. V. Troitskaia, W. Q. Gan, B. M. Kuzhevskij, L. I. Miroshnichenko, Solar Plasma Density and Spectrum of Accelerated Particles Derived From the 2.223-Mev Line of a Solar Flare, *Solar Phys*, vol. 242, pp. 87-99, 2007.

[12] O. Gingerich, R.W. Noyes, W. Kalkofen, and Y. Cuny, The Harvard-Smithsonian reference atmosphere, *Solar Phys.,* vol.18, pp.347-365, 1971.

[13] H.C. Spruit, A model of the solar convection zone. Solar Phys. 34, 277-290, 1974.

[14] Kiener J., Gros M., Tatischeff V.,and Weidenspointner, *A & A*, vol. 445, pp. 725-733, 2006.

[15] S.N. Kuznetsov, V.G Kurt, B.Yu. Yushkov, et al., Proton acceleration during 20 January 2005 solar flare:

CORONAS-F observations of high-energy gamma emission and GLE, in *2005 Proc. 29th Int. Cosmic Ray Conf., Pune, India, August 3-10,* eds. Acharya, B. S., Gupta, S, Jagadeesan, P. et al. Mumbai: Tata Institute of Fundamental Research, vol. 1, pp.49-52.

[16] G. Share, R.J. Murphy, , D. Smith, et al. RHESSI observations of the 2005 January 20 solar flare, talk on SHINE 2006 Special Session on the 2005 January 20 Event. [Online]. Available: https://creme96.nrl.navy.mil/20jan05/ShareSHINE2006InvitedTalk.pdf, 2006.

[17] A. S. Glyanenko, , Yu. D. Kotov, A. V. Pavlov, et al. The AVS-F experiment on recording rapidly changing fluxes of cosmic and gamma radiation prepared under the CORONAS-F project. *Instrum. Exp. Tech.*, vol.42 (5), pp. 596-603, 1999.

[18] Kuznetsov, S. N.; Kudela, K.; Ryumin, S. P. et al CORONAS-F satellite: Tasks for study of particle acceleration. Adv. Space Res., 30, 7, 1857-1863, 2002.

[19] Arkhangelskaja, I. V., Arkhangelsky, A. I., Glyanenko, A.S., et al. The investigation of January 2005 solar flares gamma-emission by AVS-F apparatus data onboard CORONAS-F satellite in 0.1-20 mev energy band, in *2005 Proceedings of the 11th European Solar Physics Meeting "The Dynamic Sun: Challenges for Theory and Observations", (ESA SP-600). 11-16 September, Leuven, Belgium.* Eds: D. Danesy, S. Poedts, A. De Groof et al, pp.107.1-107.4.

[20] Arkhangelskaja, I. V., Arkhangelsky, A. I., Kotov, Yu. D. et al. Thin structure of temporal profiles of solar flares January 15, 17 and 20 2005 by data of AVS-F apparatus onboard CORONAS-F satellite. *Proceedings of the International Symposium SEE 2007: Fundamental Science and Applied Aspects*, in press, 2007.

[21] Bojko A. Ja., Livshits M.A., *Russian Astronomy Reports,* vol..72(3), pp. 381-392, 1995

[22] Arkhangelskaja I.V., A.I. Arkhangelsky, E.V. Troitskaya, L.I. Miroshnichenko. The role of new gamma-ray observations in investigation of powerful solar flares *Proceedings of the International Symposium SEE 2007: Fundamental Science and Applied Aspects*, in press, 2007.

Solar extreme events: Questions of definition of the phenomena and their forecast

V.N. Ishkov

Institute of Terrestrial Magnetism, Ionosphere and Radio Wave Propagation by Pushkov, Russian Academy of Sciences (IZMIRAN), Russia
(*ishkov@izmiran.ru*)

Abstract **– In the light of sharp splash in interest to solar extreme events (SEE) there is a question on definition of the investigated phenomenon. In opinion one definition SEE completely and entirely depends on those disturbances (significant deviations from background values) in a Earth's environment space or in any point of a heliosphere which make the solar active phenomena. Now influences of the solar active phenomena on environment can be estimated in a five-point scale on three positions:**
-Electromagnetic impact - influence of electromagnetic radiation during development of powerful solar flash basically on an ionosphere (SIDs), breaking a radio communication on a time interval till several o'clock (R1 - 5).
- Solar proton events - arrival to a environment of the solar charged particles, influence basically radiating conditions in a vicinity of the Earth, cause growth of electronic concentration above polar caps absorption, breaking radio communication on polar lines (S1 - 5).
- Disturbances of a geomagnetic field - magnetic storms – consequence of arrival to environment of solar plasma streams with the raised density, speed of particles, temperatures, and with the strengthened magnetic field (G1 - 5). In this case, it would be natural to define solar extreme events as greater powerful the flare phenomena which consequence in a environment is realization of the maximal disturbances in all three positions, i.e. R5, S5, G5. However, the phenomena (S) and (G) essentially depend on localization solar flare events on a visible disk of the Sun and, for example, from the most powerful flares near to western limb the Sun of a geomagnetic field disturbance (phenomenon G) will be minimal, as all energy of coronal mass ejection from this flares will pass by the Earth (flare event 4.11.2003). The most powerful flares on east limb will not be shown, except for phenomenon G, and in high energy particles (S) as also solar protons and coronal mass ejection will be directed aside from the Earth (1.06.1991, 6.03.1989). Other approach in my opinion more natural, conducts to definition SEE as solar flare superevents with a x-ray class not less X15, accompanied powerful coronal mass ejection with V?1500 km/s. Such flares are accompanied by intensive dynamic radio splashes II and IV type, and frequent ejection of solar filaments. Similar events undoubtedly affect all heliosphere, and Earth's environment space is simply a special case only.

The method for utilizing solar observational data to predict of the powerful solar flare events, that a large solar flare and solar filament ejection, is presented. Both phenomena are result of the new emergent flux distinct powerful and rate of emergence. The process of new magnetic flux emergence, its evolution and its interaction with already existing magnetic flux is sufficiently determined that allows us to predict as a period of flare energy release (PFER) so an importance of most solar flare in the flare set of this period. All large solar flares are always accompanied by a series of weaker events.
They formed together the PFER confined within the time intervals about 55±20 hours, when the bulk of the middle and large solar flare are accomplished. The method of the large solar flare event prediction has been put to successful test on Russian scientific satellites such as GRANAT, GAMMA, CORONAS-I. Computer version this forecast techniques has been developed on the base of real-time solar data. The forecasts are accessible via http://www.izmiran.rssi.ru/space/solar/forecast - Russian version and http://titan.wdcb.ru/virbo_rus/viewlast.do?section=RBBulletin – English version.
This research supported by the grant of Russian Foundation for Basic Research 07-02-00246-a and RAS Program No.16 "Solar activity and physical processes in the Solar-Terrestrial system.

Solar particle dynamics during magnetic storms of July 23-27, 2004

S.N. Kuznetsov†, L.L. Lazutin, M.I. Panasyuk, L.I. Starostin, Yu.V. Gotseliuk, (a)
N. Hasebe, K. Sukurai and M. Hareyama (b)

[1]*Moscow State University, Scobeltsyn Institute for Nuclear Physics, Space Physics Division, Vorob'evy Gory, Moscow 119992, Russia*
[2]*Research Institute for Science and Engineering, Waseda University, 3-4-1 Okubo, Shinjuku, Tokyo 169-8555 Japan*

Abstract – **It is a case study of a chain of three magnetic storms with a special attention to the particle dynamics based on CORONAS-F and SERVIS-1 low altitude satellite measurements. Solar proton penetration inside the polar cap and inner magnetosphere and dynamics at different phases of the magnetic storms were studied. We found, that solar protons were captured to the inner radiation belt at the recovery phase of the first and the second magnetic storms and additionally accelerated during the last one. No evidence of SC particle injection was found. Enhanced solar proton belt intensity with small pitch angles decreased slowly during satellite orbits for 30 days until the next magnetic storm. Then in 20-30 hours we registered strong precipitation of these protons followed by the trapped proton flux dropout. Intensity decrease was more pronounced at lower altitudes and higher particle energies.**

I. INTRODUCTION

During magnetic storms usually stable inner proton radiation belt exhibit intensity variations of a short time scale. In [1] observed low-energy (1-15 MeV) proton intensity increases and decreases on L=2-4. [2] supposed that increase of particle flux is associated with solar protons. In [3] found 11 events when new radiation belts appeared during magnetic storms from 2000 to 2002. [4] found additional trapping regions of 2-15 MeV protons during strong magnetic storms of 1998 и 2000. The solar origin of these particles follows from the presence of the helium ions.

After the sudden commencement (SC) of the March 24, 1991 magnetic storm, energetic ions and electrons enhancements were registered by CRRES satellite in the inner magnetosphere [5]. It was explained by the particles resonant acceleration and inward injection by the E-field induced by SC pulse [6], [7], [8]. The SC injection became accepted as a main source of the solar cosmic ray trapping into the inner radiation belt.
Alternative model was suggested by Lazutin et al., (2006)[9], when direct trapping of the 1-5 MeV solar protons was registered by CORONAS-F particle detectors during extreme magnetic storms of October 29-31, 2003. They found that when proton cutoff latitude or penetration boundary (PB) started to retreat during magnetic storm recovery phase, low energy protons remain on the closed drift orbits creating new or changing the old inner radiation belts at L=2-4. PB retreat model was supported by analysis of the measurements during two November 2001 magnetic storms (Lazutin et al., 2007)[10].

During moderate magnetic storms of July 2004 energetic proton and electron trapping was registered by particle detectors of the SERVIS-1 satellites (Kodaira et al., 2005) [11]. Present paper offers analysis of this event based on the measurements of the energetic protons and electrons by the particle spectrometers on board of two polar satellites Coronas-F and Servis-1, which operates on different altitudes. This allows to found new effects of the solar particle dynamics inside the magnetosphere in general and of the trapping process particularly.

II. OBSERVATIONS

Coronas-F (C-F) particle detector MKL has four proton differential channels (1-5, 14-26, 26-50 and 50-90 MeV). At the altitude of 500 km trapped particles may be seen only over the Brazilian Magnetic anomaly (BMA), and adjacent South-Atlantic region, while on the majority of the trajectories only precipitating particles were recorded. Servis-1 (S-1) Light Particle Detectors (LPDs) measured protons and electrons in the energy range from 1.2 to 130 MeV and 0.3 - 10 MeV, respectively. Altitude of 1000 km and inclination of 100 deg on the solar synchronous orbit allows registering trapping particles more often.

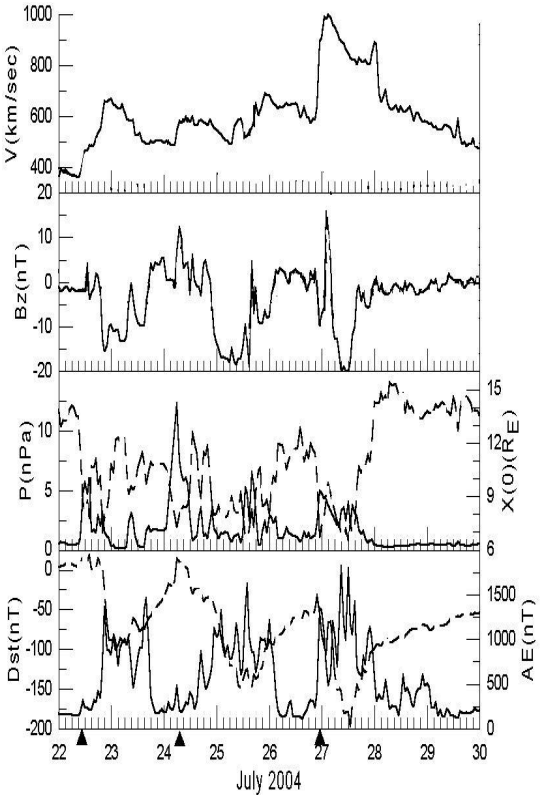

Fig. 1. Solar wind (ACE) and magnetic indexes during July 2004 magnetic storms

2.1 Event description

Solar wind and magnetic activity indexes are shown by Fig. 1. There were three moderate magnetic storms. During all magnetic storms IMF Bz was negative and auroral activity index was at high level. Table 1 presents characteristic time of the magnetic storms development.

Solar wind velocity was at moderate level of 500-600 km/s during first two storms and up to 900 km/s during the third one. Short enhancements of the solar wind pressure were recorded at the main phases of all three storms and associated position of the subsolar magnetosphere boundary approached the Earth to 7-8 Re as calculated by [12] method.

Solar cosmic rays, electrons and protons were registered in IMF by ASE and inside the magnetosphere by both S-1 and C-F satellites.

2.2 Penetration boundary definition and dynamics

There is no exact definition of the PB position. One reason comes from the dependence of the cutoff rigidity from the particle energy. More energetic protons penetrate closer to the Earth as shown by Fig. 2a. Also PB position might be defined eider by the background counting level or by last maximum intensity position, or by 0.5 intensity level position as shown by Fig 2b. Finally, if the PB position overlaps with previously trapped population, then PB boundary can not be found. It was the case for the most of S-1 orbits, the comparison of the S-1 and C-F proton radial profiles shown by Fig. 2b illustrates this statement. Therefore we used C-F to define the PB position and S-1 for the study of the dynamics of trapped radiation.

Figure 3 shows both PBb and PBm dynamics. We use C-F 1-5 MeV proton data, because in other C-F channels intensity was not high enough all that period. During last magnetic storm proton precipitation from the newly trapped belt was high and definition of the PB positions was not accurate. From the Fig 3 one can see that PB approached the Earth to L=3 and therefore trapping of SCR to the inner belt was possible.

2.3. Trapping history of 1-15 MeV protons

Two time intervals every day S-1 orbit enters South Atlantic (or Brazilian) magnetic anomaly (BMA).

We choose one of two namely evening orbit every day from July 22 to 30, 2004 to follow changes of the particle radial profiles. Fig. 4 shows the resulting comparison. First two profiles, July 21 and 22 have a maximum at L=3, such position is typical for the inner belt of 1 MeV protons. The 22.07 profile was measured after the SC but no possible results of the SC injection were seen. July 23 and 24 profiles were measured during the recovery phase of the first magnetic storm. We found there additional enhanced maximum at L=3.8. Penetration boundary at the end of the main phase was as close as L=3.5 and therefore this new belt might be the result of solar proton trapping during the retreat of the PB at the recovery phase.

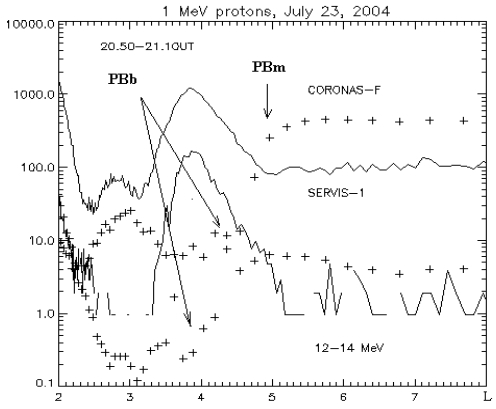

Fig. 2a. Energy dependence of the radial profiles of the solar protons, Coronas-F satellite.

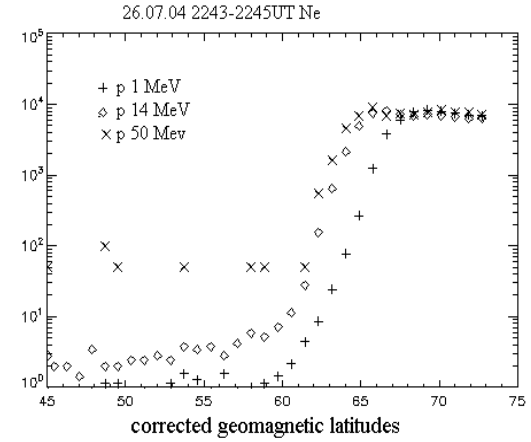

Fig. 2b. Comparison of the radial profiles of solar protons, Servis-1 (solid lines) and Coronas-F (dotted lines). Positions of the penetration boundaries defined at background (PBb) and maximum (PBm) intensity levels are shown by arrows. two energy ranges are shown, ~ 1 MeV and 12-14 MeV.

Next profile transformation was registered on July 25 again during recovery phase. Maximum at L=3.8 disappeared because PB during the main phase of the second magnetic storm approached closer to the Earth and previously trapped particles found themselves at the open drift shells. After PB retreat new maximum arrived located at L=3.

Evening pass of the July 26 was at the end of the recovery phase, maximum position remains at the same place, but intensity increased twofold. Similar intensity increase continued next four days, all profiles measured during recovery phase of the third magnetic storm. Maximum position was shifting gradually earthward, which indicates to the action of the electric (ExB) drift where electric field might be induced by the magnetic field increase during the decay of the ring current. It is possibly also that magnetic field pulsations increase the rate of the inward radiation drift. Radial profiles measured by S-1 12.5 MeV proton channel looks similar to 1 MeV ones.

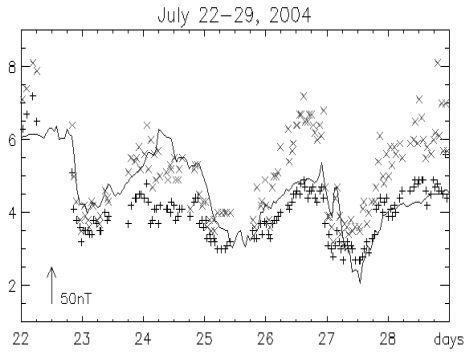

Fig. 3. Dynamics of the 1-5 MeV proton penetration boundary (PBb and PBm) and Dst index (solid line).

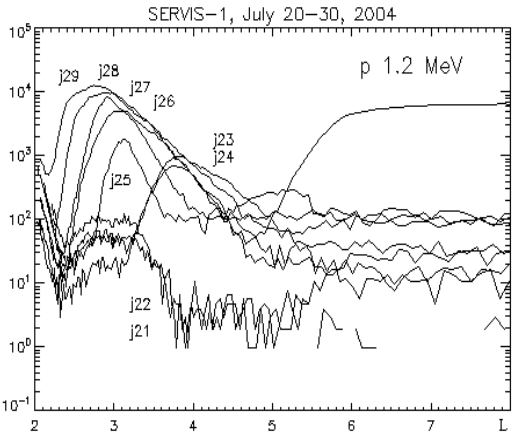

Fig. 4. Latitudinal dependence of the 1 MeV solar proton intensities over BMA, taken one per each day at 20-22 UT from July 21 to 29, 2004, S-1 data.

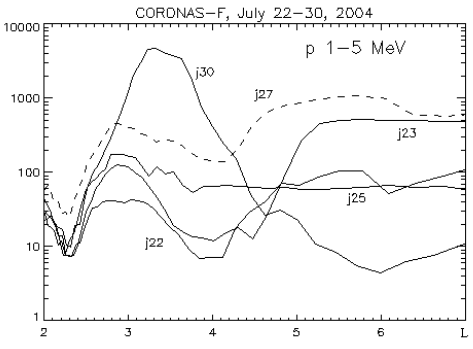

Fig. 5. The same as Fig.4. for C-F measurements.

Radial profiles of 1-5 MeV protons measured by C-F at the 500 km altitude look rather

different (Fig. 5). We do not see trapping protons after the first and the second magnetic storms: loss cone became empty in a short time. After the third storm trapping proton intensity increased significantly and C-F registered trapped particles over BMA, and also precipitating protons in other longitudes.

We will discuss energetic electron dynamics in a separate paper, here will only mention that there is remarkable similarity of proton and relativistic electrons dynamics.

The last magnetic storm has a strongest SC amplitude (40 nT in Honolulu) therefore we inspected particle measurements in nearby orbits is search of possible SC injection effect. Fig 6 presents radial profiles of 1-5 MeV protons measured by C-F 5 minutes before and 25 minutes after the SC. There was large shift of the penetration boundary and measurable increase of the proton intensity which cannot be associated with SC injection. Increase magnitude was the same over all the polar cap and evidently follows the proton increase outside the magnetosphere in the solar wind created by the Fermi acceleration at the front of the CME flux. We also did not found SC injection signatures in other channel of C-F and S-1 as well.

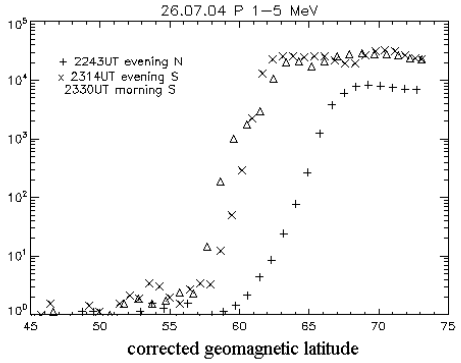

Fig. 6. C-F 1-5 MeV proton radial intensity profiles before and after the SC (26.07 22.49 UT)

2.4. Time history of new trapped belts

New created solar proton radiation belts registered by Coronas-F and investigated in previous studies ([9], [10]) remain observed not for a long time. After two November 2001 magnetic storms particle flux decreased by an order in 15-20 days. After October 29-30, 2003 extreme magnetic storms 1 MeV proton belt exists at the same intensity during 20 days, until the next superstorm and after it disappeared rapidly.

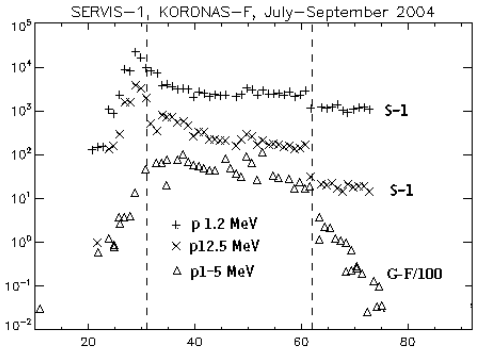

Fig. 7. Temporal behavior of the proton intensity at L=3 after July 22-28 magnetic storms.

In our case during whole August 2004 there were no magnetic storms, and substorm activity was rather low. As a consequence newly trapped particles, both electrons and protons, remain at constant level or decreased much more gradually than after November 2001 storms. Figure 7 shows new radiation belts time history. Trapped 1 MeV proton intensity at S-1 altitude decreased rapidly during several days starting at July 28 until August 3. After that nearly constant intensity level was registered by 1.2 MeV channel and only slow decay by 12.5 MeV channel. At the C-F altitude similar decay rate was registered by 1-5 MeV channel.

Then during whole day of August 30 gradual main phase of the magnetic storm was observed with minimum Dst=130 nT. Also during this whole day magnetospheric substorm activity was registered in auroral zone. As a result, fast decrease of the particle intensity was observed. The rate of the intensity jump was greater at C-F as compared with S-1 and for higher electron or proton energy.

The reason of the intensity dropouts was in strong precipitation observed during more than 12 hours of August 30, 2004. Fig 8 shows example of the proton and electron precipitation measured by

Table 1. Main time-marks of three July 2004 magnetic storms

SC	Main phase	Recovery phase end	Dst max, nT
22 07 1036 UT	22.07 21-23 UT	24.07 06 UT	100
24 07 0614 UT	24.07 12 UT – 25.07 10 UT	26.07 16 UT	150
26 07 2249 UT	26.07 23 UT – 27.07 14 UT	30.07 12 UT	200

C-F detectors. Similar particle behavior was registered by S-1 detectors.

Again we will note that both slow intensity decrease and July 30 dropout were registered also by energetic electron channels of both satellites, but detailed consideration of electron dynamics will be regarded separately.

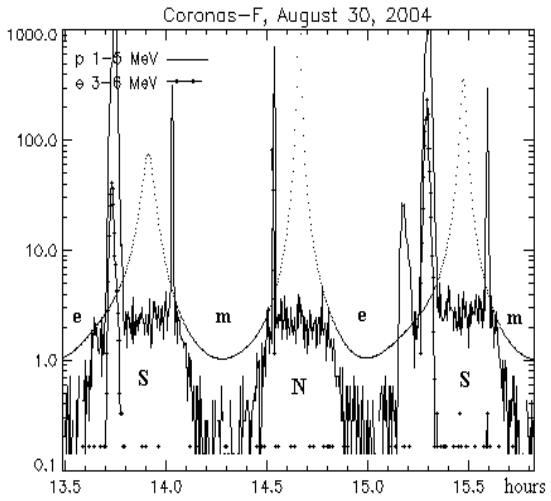

Fig. 8. Several orbits of the C-F with proton and electron measurements, August 30, 2004. Peaks of the precipitation were recorded at L=2.5-4.

III. SUMMARY AND CONCLUSION

Joint analysis of the particle measurements on board of two polar satellites with different altitude not only allows confirming validity of the low energy solar proton trapping mechanism described earlier, but reveals several new features of the solar proton dynamics inside the magnetosphere during magnetic storms.

1. For the first time we have the possibility not only to found the trapping effect, but to record detailed time history of the PB radial motion and associated effects during magnetic storms. Solar protons penetrate directly to low L shells during the main phases of the magnetic storms and during the recovery phase 1-15 MeV protons remain there trapped while more energetic particles were drifting off the magnetosphere.

First solar proton freshly trapped flux was recorded during the first magnetic storm recovery, but in was destroyed when PB went earthward to smaller L during the second storm. Distortion of the magnetosphere during the second storm allows previously trapped protons to escape from this region which transit to the quasi-trapping regime.

At the recovery phase of the second magnetic storm new solar proton trapping occurs with maximum at L=3. During the recovery of the last, third magnetic storm intensity of this belt was gradually increasing and the position of the maximum shifts earthward. Therefore three basic processes are taking place during magnetic storms:

- sweeping away of previously trapped protons beside the penetration boundary caused by the losses of the adiabacity because of the magnetosphere distortion during the main phase of the magnetic storm,
- trapping of the solar protons during the fast magnetosphere recovery during magnetic storm recovery phase,
- acceleration of the newly trapped protons not only due to in situ increase of the magnetic field magnitude, but also due to the earthward shift of the magnetic drift orbits. This shift may be caused by induced electric field or/and fast radial diffusion caused by interaction with electromagnetic emissions.

2. We did not found effects of the solar proton injection and acceleration by SC induced mechanism.

3. After magnetic storm, time history of the trapped solar protons has two regimes. In the absence of the magnetospheric disturbances slow intensity decrease was recorded with the decay factor greater for more energetic protons and for lower altitude of the satellite i.e. lower altitude of the mirror point. Particle interaction with atmosphere may possibly explain these relations. It is therefore appropriate to suppose that 90˚ (trapped) particle intensity will remain constant for a long time.

During magnetic disturbances, storms or substorms, fast intensity decay can took place. One obvious reason is wave-particle interaction leading to pitch-angle diffusion into the loss cone.

Second type of the pitch-angle diffusion might be caused by the loss of the adiabacity, namely when magnetic field line radius of the curvature decreased and became comparable with the trapped particle larmor radius. For more energetic particles this second type diffusion rate is higher which is in accordance with observed relation of the intensity dropouts measured by S-1 and C-F on August 30, 2004.

Solar particle trapping to the inner radiation belt during recovery of the strong magnetic storms therefore might be regarded as a important source of the Earth inner radiation belt.

ACKNOWLEDGMENT

This study was partly supported by the grant № 06-05-64225 of the Russian foundation for Basic Research. One of the authors (LL) is grateful to professor Yu.I. Logachev for helpful discussion.

REFERENCES

[1] Bostrem et al. Time history of the inner radiation zone, October 1965 - December 1968, J. Geophys. Res. 75, 1246-1256, 1970.

[2] Mineev Yu.V., Spirkova E.S., Glukhov G.A., Kratenko Yu.P., Features of solar cosmic ray penetration into the high-latitude regions of the Earth's magnetosphere inferred from Intercosmos-19 data. Proc. of 18th Intern. Cosmic Ray Conf., Bangalore, India, 3 262-265, 1983.

[3] Slocum, P.L., Lorentzen K.R., Blake J.B., Fennell J.F., Hudson M.K., Looper M.D., Masson G.M., and Mazur J.E., Observations of ion injections during large solar particle events, AGU Fall Meeting, SH61A-0501, 2002.

[4] Lorentzen, K.R., Mazur J.E., Loper M.E., Fennell J.F., and Blake J.B., Multisatellite observations of MeV ion injections during storms, J. Geophys. Res. 107, 1231, 2002.

[5] Blake, J.B., Kolasinski W.A., Fillius R.W., and Mullen E.G. Injection of electrons and protons with energies of tens of MeV into L > 4 on 24 March 1991, Geophys. Res. Lett. 19, 821, 1992.

[6] Li, X., Roth I., Temerin M., Wygant J.R.,.Hudson M.K, and Blake J.B., Simulations of the prompt energization and transport of radiation belt particles d uring the March 24, 1991 SSC, Geophys. Res. Lett. 20, 2423, 1993.

[7] Pavlov N.N., Tverskaya L.V., Tverskoy B.A., Chuchkov E.A., Variations of the radiation belt particles during strong magnetic storm of March 24, 1991. Geomagnetism and aeronomie 33, 6, 41-45, 1993 (R).

[8] Hudson, M.K. , Elkington S.R., Lyon J.G. et al. Simulations of proton radiation belt formation during storm sudden commencements, J. Geophys. Res. 102, 14087-14102, 1997.

[9] Lazutin L.L., Kuznetsov S.N. and Podorolsky A.N. Solar proton belts in the inner magnetosphere during magnetic storms. Proc. of the 2nd International Symposium Solar Extreme Events: Fundamental Science and Applied Aspects, Nor-Amberd, Armenia, 26-30 September 2005, Ed. by A. Chilingarian and G. Karapetyan, CRD, Alikhanyan Physics Institute, Erevan, 63-67, 2006.

[10] Lazutin L. L., Kuznetsov S. N., and Podorolsky A.N., Dynamics of the radiation belt created by solar protons during magnetic storms, Geomag. and Aeronomy 47, 2, 187-197, 2007

[11] Kodaira S., Asaeda M., Fujii M., Hareyama M., Hasebe N., Kajiwara N., Sakurai K., Akiyama M., Ichiji K., Hama K. Space and Time Correlations of Particle Fluxes after Giant Flares in Radiation Belts Observed by Two Satellites, USERS and SERVIS-1, Proceedings of 29th International Cosmic Ray Conference, Pune, 101-104, 2005.

[12] Kuznetsov S.N. and Suvorova F.V., Solar wind control of the magnetopause shape and location, in: Rdadiation measurements 26, 413-415, 1996.

Solar Extreme Events 2005-2006: Scientific, Technological and Biological Issues

N. B. Crosby

Belgian Institute for Space Aeronomie, Ringlaan-3-Avenue Circulaire, B_1180 Brussels, Belgium

***Abstract*—"Solar extreme events" have taken on a whole new meaning with the advent of unique solar observatories offering breath-taking images of these phenomena. In parallel the effects that these events can have on technological and biological systems both in space and on ground are becoming more and more evident. Human space travel initiatives have come to include interplanetary space exploration and currently the uncertainties for assuring the crew's safety is being looked at with new eyes. Each solar cycle has its own famous solar extreme events. This paper gives an overview of the space weather induced effects that were encountered during the Jan. 2005 and Dec. 2006 solar extreme events. The implications of these events on interplanetary space travel will be discussed as well. What would have happened if these solar cycle 23 events had occurred during a human mission to Mars? Would an interplanetary spacecraft from Earth have been sufficiently protected against such solar extreme event scenarios?**

***Key Words*—Space weather, solar extreme events, interplanetary travel, technological and biological effects.**

I. INTRODUCTION

Various populations of energetic particles in the energy range from eV to more than 10^{21} eV fill our solar system and are a significant hazard for current space missions as well as for any future interplanetary travel. For a detailed overview about these particle populations see [1]. The most energetic among them are the constant flux of galactic cosmic rays (GCR) and the sporadic solar energetic particle (SEP) events. Earth's magnetic field causes particles (protons and electrons) to become trapped in what is known as Earth's radiation belts. The characteristics of these three particle populations are listed in Table 1 (they all contribute to the "space weather"). Routine human missions to the Moon will doubtlessly be the predecessor for any further human interplanetary mission with the Moon being a possible host for a first solar system "space colony". This will imply crossing the radiation belts numerous times as well as exiting the protective shielding of our magnetosphere making us vulnerable to SEPs and GCRs.

The most energetic particles (energies up to 10^{21} eV) found in our solar system, are those that have origins far outside our solar system, namely GCRs. Their composition is mostly hydrogen nuclei (protons), ~ 7–10 % Helium and ~1 % heavier elements. All GCRs are fully ionized, meaning that they consist of nuclei only. As a first approximation the flux of GCRs in near-Earth space can be considered to be isotropic. It is well-known that the GCR flux in the solar system is modulated by solar activity with the GCR population most intense during solar minimum.

Particle Populations	Energy Range	Temporal Range	Spatial Range
Galactic Cosmic Rays	0.1 – 1000 GeV (the 100 to 1000 MeV fluxes constitute the largest contribution)	Continuous (factor 10 variation with solar cycle)	Entire heliosphere
Solar Energetic Particles	keV-GeV	Sporadic (minutes to days)	Source region properties (flare/CME sites and evolution) and bound to CME driven shock
Trapped Particle Populations	Tens keV - couple of hundreds of MeV (for protons) Tens keV - several MeV (for electrons)	Variations "minutes-years"	Variations "height-width"

Table 1. Characteristics of the most energetic particle populations of the heliosphere.

SEPs are mainly protons, electrons, and α-particles with small admixtures of ^{3}He-nuclei and heavier ions up to iron. Particles constituting a SEP event can be linked to either a solar flare and/or the shock wave driven by a coronal mass ejection (CME). Solar proton events (SPE),

a "sub-group" of SEPs, are very worrisome for interplanetary travel. The proton event threshold for which particles penetrate a space suit is 10 protons /

(cm^2 s sr) at ≥10 MeV and is also the threshold value that forecasters at the Space Environment Center at the National Oceanic and Atmospheric Administration in Boulder, Colorado, U.S.A., monitor to watch for the onset of a SPE.

The "October to November 2003" period ranks as one of the largest outbreaks of solar activity in recent history. Global space weather induced effects of these "Hallowe'en events" were wide-ranging, impacting power grids, airline flights, spacecraft operations, etc.. Especially, on Oct. 28, 2003, a majestic SPE was recorded following the eruption of an intense solar flare and an associated CME. Since the occurrence of the "Hallowe'en events" the term "solar extreme events" has become a term widely used in the space weather community.

SPEs are usually associated with solar maximum and it is rare that such events occur near solar minimum. Interplanetary space travel scenarios, such as a mission to Mars, define solar minimum as the "safe" travel time zone when solar activity (e.g. SPE flux) is low. However recently, two anomalous solar extreme events occurred during the declining phase of solar cycle 23, respectively 1.) Jan. 14-22, 2005, 2.) Dec. 6-15, 2006. It is now evident that the two classical "anomalously large" Aug. 1972 and Oct. 1989 events are not alone anymore.

In Section 2 the Jan. 2005 and Dec. 2006 events will be presented including an overview of the space weather induced effects encountered during these events. The paper ends with a Section considering what these events would have meant for an interplanetary mission such as one to Mars and some concluding words.

I. EXTREME EVENT EXAMPLES

Table 2 lists the solar phenomena comprising the two solar extreme events occurring in mid-Jan. 2005 (Event 1) and mid-Dec. 2006 (Event 2). Both events consisted of halo CMEs, solar flares of X importance and SPEs.

SOLAR EXTREME EVENTS						
	Solar Proton Events			CMEs (halo)	Solar Flares	
Year	Start time (Day/UT)	Max. time (Day/UT)	Proton Flux (pfu @ > 10 MeV)	Occurrence Time (Day/UT)	Day/UT (start-max)	Importance (X-ray)
2005	Jan. 16, 02:10 Jan. 20,	Jan. 17, 17:50 Jan. 20, 08:10	365 (peak 1) 5040 (peak 2) 1860	Jan. 13, 17:54 Jan. 14, 17:06 Jan. 15, 06:30 Jan. 15, 23:06 Jan. 17, 09:30 Jan. 17, 09:54 Jan. 19, 08:29 Jan. 20, 06:54	Jan. 15, 00:22-00:43 Jan. 15, 22:25-23:02 Jan. 17, 06:59-09:52 Jan. 19, 08:03-08:22 Jan. 20, 06:36-07:01	X1.2 X2.6 X3.8 X1.3 X7.1
2006	Dec. 06, 15:55 Dec. 13, 03:10	Dec. 07, 19:30 Dec. 13, 09:25	1980 698	Dec. 06, 20:12 Dec. 13, 02:54 Dec. 14, 22:30	Dec. 06, 18:29-18:47 Dec. 13, 02:14-02:40 Dec. 14, 21:07-22:15	X6.5 X3.4 X1.5

Table 2.
Proton event characteristics (ftp://ftp.ngdc.noaa.gov/STP/SOLAR_DATA/Satellite_ENVIRONMENT/PARTICLES/p_events.lst), Halo coronal mass ejections (CMEs) characteristics (http://cdaw.gsfc.nasa.gov/cme_list/UNIVERSAL/2005_01/univ2005_01.html), Solar flare characteristics (NGDC/NASA, http://www.ngdc.noaa.gov/stp/SOLAR/ftpsolarflares.html#xray)

c. Event 1

Several X-type solar flares and halo CMEs made up the solar extreme event of Jan. 14-22, 2008 (see Table 2). Following the X2.6 flare late on Jan. 15 the >10 MeV proton event began on Jan. 16 at 02:10 UT. The peak proton flux following this flare was 365 pfu (peak 1 in Table 2) on Jan. 16 at 18:40 UTC. The >10 MeV protons decayed to 117 pfu by midday on Jan. 17 when a stronger injection of protons occurred following the X3.8 flare and CME. This new infusion began on Jan. 17 at 12:40 UT and peaked with 5040 pfu (peak 2 in Table 2) on Jan. 17 at 17:50 UT.

The proton event decayed to about 19 pfu early on Jan. 20 when yet another proton flare occurred (see Fig. 1). The X7.1 flare and CME that occurred on Jan. 20 produced the hardest and most energetic proton event of Cycle 23. The >10 MeV protons peaked at 1860 pfu on Jan. 20 at 08:10 UT. The >100 MeV protons peaked at 652 pfu on Jan. 20 at 07:10 UT, which was the highest >100 MeV proton flux level observed since 1989 Oct. (680 pfu). The >10 MeV proton event finally ended on Jan. 22 at 17:55 UT having lasted more than six days.

The left-hand panel of Fig. 1 shows that the onset of the Jan. 20 SEP event was extremely rapid as the intensity of the > 100 MeV protons measured by the GOES11 spacecraft rose to their maximum intensity level within ½ hour. The rapid onset is due in part to the fact that the event originated at W67 degrees, where there is expected to be relatively good magnetic connection with the Earth [2].

This event had very hard energy spectra (see right-panel of Fig. 1). During typical large SEP events the power-law portion of the proton spectra steepen between 10 and 100 MeV. It was found that the Jan. 20 spectrum extends as a power-law to at least 400 MeV [2].

During the Jan. 14-22, 2005 event all types of space weather were observed including radio blackouts, solar radio storms and geomagnetic storms. Specifically, this event has been associated with the following space weather effects:

1. A storm of high energy solar protons on Jan. 20 caused "snow" on the LASCO coronal images of the SOHO satellite by hitting the lens obscuring the Sun as radiation swamped the cameras [3].

2. The JCSAT-1B communications satellite experienced an altitude loss during maneuver anomaly (all channels became unavailable) on 17 Jan. due to an anomaly in one of its thrusters, leading to difficulties with services provided by the satellite; services were recovered the following day [4], [5].

3. The Intelsat IS-804 satellite experienced a sudden and unexpected electrical power system anomaly on Jan. 14, possibly due to the space weather, resulting in the loss of the satellite which left 10 South Pacific nations without telephone contact with the outside world [6], [7].

4. During the Jan. 2005 storms, 26 United Airlines' polar flights operated on less than optimum routes at a cost of approximately $ US 1 million [8].

5. Due to the fortunate orbital phasing of the International pace Station the crew only received around two days of additional radiation dosage in the Jan. 2005 proton event [8].

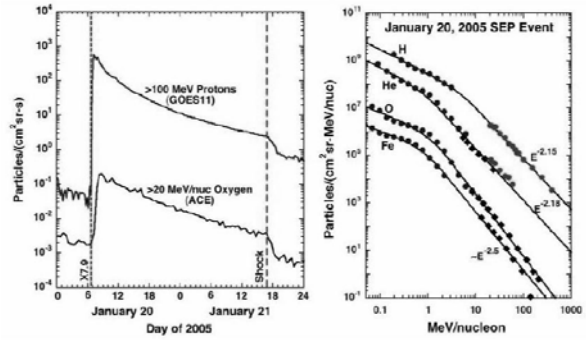

Fig. 1. Space weather aspects of the Jan. 20, 2005 solar energetic particle event (left-side panel: time profiles, right-had panel: energy spectra). Courtesy of [2].

d. Event 2

The space weather event of Dec. 6-15, 2006 has been one of the strongest events occurring during solar cycle 23. On Dec. 6 a X6.5 flare occurred at 18:29 UT followed by a CME.

A large X3.4 solar flare occurred on Dec. 13 at 02:40 UT and a large Earth-directed CME followed. A X1.5 solar flare occurred on Dec. 14 reaching maximum at 22:15 UT also followed by a CME. Strong radio blackouts and an associated moderate solar radiation storm were observed during this event.

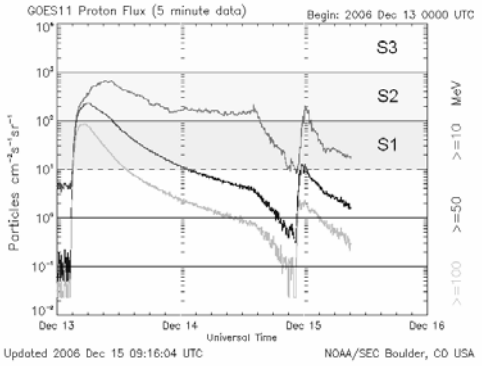

Fig. 2. Proton flux values at different energies during the Dec. 13-16, 2006 event. Courtesy of the National Oceanic and Atmospheric Administration Space Weather Prediction Center

This event has been associated with the following space weather effects:

1. Three anomalies were observed on the CLUSTER spacecraft on Dec. 13. Cluster 1 had a minor instrument anomaly, while Cluster 2 and 4 had on-board systems affected. The Attitude and Orbit Control unit on Cluster 2 lost power and autonomously switched over to its redundant unit. The High-Power Amplifier on Cluster 4 switched itself off. It is not certain that the increased energetic particle flux triggered the anomalies, but their occurrence was strongly correlated with the timing of the peak burst on Dec. 13 [9].

2. Envisat experienced an unexpected anomaly correlated with the particle flux's arrival at Earth. It happened around 19:00 CET, just before the particle peak on Dec.13. The operation of the Envisat Payload Module Computer was autonomously suspended, causing all payload instruments to be switched off [9].

3. The JEM-X and IBIS experiments onboard the Integral spacecraft are sensitive to X-rays and charged particles, respectively. JEM-X automatically switched itself into safe mode twice, and IRIS was manually switched off to avoid over-exposure [9].

4. All three of ESA's deep space missions (Mars Express, Venus Express and Rosetta) happened to be oriented on the side of the Sun opposite to the Earth when the halo CMEs occurred and nothing was observed by these spacecraft [9]. However, radio signals transmitted from these deep space missions must pass by the Sun to reach Earth, and so flight control teams could in fact notice the increased solar activity as higher-than-normal interference in the signals received on the ground [9].

5. On Tuesday 14 Dec., China's People's Daily reported widespread disruption of shortwave radio communications in China on Wednesday morning [9], People's Daily Online [10].

6. Astronauts on board the International Space Station slept in protected areas of the station as a precaution [9].

II. Discussion and Concluding Words

Space environment hazards are a function of location (orbit) of the given spacecraft or planet in question. Health risks for long duration interplanetary explorative missions and those encountered so far in manned space flight differ significantly in two major features, first of all because "emergency returns" are ruled out. Second, the risk for acute early radiation diseases becomes non-negligible due to the loss of geomagnetic shielding available in low Earth orbit.

Only several days away the Moon offers new opportunities for studying the space environment outside the terrestrial magnetosphere. For missions that leave Earth orbit, like the Apollo missions to the Moon, the ability to rapidly traverse the radiation belts and to predict the occurrence of SEP events is essential.

Normally it takes two or more hours for a dangerous solar proton shower to reach maximum intensity at Earth after a solar flare. As mentioned in the previous Section the particles from the Jan. 20, 2005 flare peaked much faster (within 30 min.). This does not give much warning to astronauts or spacecraft that are situated outside Earth's protective magnetosphere. For interplanetary missions onboard space warning capabilities will be essential as well as the ability to predict solar flares in advance. Onboard detectors for monitoring the space environment, especially the Sun, must become standard inventory on any future interplanetary mission.

During the Jan. 2005 proton event occupants in a "shuttle-type" vehicle on the way to the Moon, would have received a dose greater than a ground-based worker is allowed in a year [8]. This is due to the fact that the very energetic particles encountered in this event are difficult to shield against. It has been estimated that during this event an astronaut on the Moon, protected by only his spacesuit, would have received a radiation dose of ~300 rem, sufficient to cause radiation sickness [2].

As was pointed out in Section 2 (point 5), during the Dec. 2006 event higher-than-normal interference in the radio signals sent from ESA deep space missions (Mars Express, Venus Express and Rosetta) to Earth was noticed. Similar to Earth's ionosphere, for planetary missions short-term ionization increases due to solar radiation (ultraviolet and X-ray) in a planet's atmosphere may cause telecommunications problems.

Spacecraft shielding requirements, including space storm shelters, both on the spacecraft as well as radiation protection facilities on a planet (e.g. Mars) need to be taken into consideration with respect to travel time, local target space weather conditions, and the phase of the solar cycle. The ultimate goal is to minimize radiation together with all other health effects and technical hazards by optimizing orbit parameters and shielding. Ofcourse, the faster the trip the better; that is, development of innovative transportation technologies and new propulsion systems as well as orbit optimization are highly important if not the most important challenges for future interplanetary

missions. For more information concerning the scientific, technological and biological challenges in regard to interplanetary space weather see [11].

The Jan. 2005 and Dec. 2006 events were not just "anomalously large" solar extreme events. They were also "anomalies" in another way due to them occurring around the start of solar minimum, when such events are not expected to occur. Engineers and scientists must take such non-standard scenarios into consideration when designing and building spacecraft as well as during the missions themselves. It is also important to note that perhaps we have not yet measured the largest possible SPE event and that statistically such events may be more common than we think they are.

ACKNOWLEDGMENT

The author wants to thank the organizers of the SEE 2007 symposium for organizing a very interesting meeting and inviting her to give this talk.

REFERENCES

[1] Crosby N.B., "Major radiation environments in the heliosphere and their implications for interplanetary travel", in: Bothmer, V., Daglis, I. (Eds.), Space weather: physics and effects, Springer Praxis Books, 438 pp., 2007.

[2] ACE News, #87, "Space Weather Aspects of the January 20, 2005 Solar Energetic Particle Event", Feb 23, 2005, http://www.srl.caltech.edu/ACE/ACENews/ACENews87.html

[3] NASA, "SOHO/LASCO View of January 2005 Solar Events", 2005, http://svs.gsfc.nasa.gov/vis/a000000/a003100/a003159/index.html

[4] JSAT, "JSAT Reports JCSAT-1B Satellite Anomaly", 18 Jan. 2005,2005a, http://www.jsat.net/en/release/2005/index.html

[5] JSAT, "Services Provided by JCSAT-1B Satellite Restored", 19 Jan. 2005, 2005b, http://www.jsat.net/en/release/2005/index.html

[6] Intelsat, "Intelsat Reports Loss of IS-804 Satellite", 16 Jan. 2005, http://www.intelsat.com/press/news-releases/2005/intelsat_2005.asp

[7] NOAA, "Recent solar activity affects satellites", 2005, http://www.ngdc.noaa.gov/nndc/struts/results?eq_0=2005/01&op_3=eq&v_3=N&t=102750&s=3&d=10,6,11

[8] Murtagh W., Onsager T. and Poppe B.: 2005, "Late Solar Cycle Events Featured in Space Weather Week 2005", Space Weather, 3, No. 11, S11001.

[9] ESA, "ESA mission controllers react to solar flare", ht:/www.esa.int/esaCP/SEMB49QJNVE_index_0.htm

[10] People's Daily Online, 2006, http://english.people.com.cn/

[11] Crosby N.B., V. Bothmer, R. Facius, J.-M. Griessmeier, X. Moussas, M. Panasyuk, N. Romanova, and P. Withers: "Interplanetary Space Weather and its Planetary Connection", meeting report, AGU Space Weather Journal Vol. 6, No 1, S01003, 2008

The Solar neutron events as a tool to study particle acceleration at the Sun

F. Valdés-Galicia[1], Y. Muraki[2,3], K. Watanabe[2], Y. Matsubara[2], T. Sako[2], L.X. Gonzalez[1], O. Musalem[1], A. Hurtado[1]

1. Instituto de Geofísica, Universidad Nacional Autónoma de México, 04510 México, D.F., Mexico
2. Solar-Terrestrial Environment Laboratory, Nagoya University, Nagoya 464-8601, Japan.
3. Department of Physics, Konan University, Okamto 8-9-1, Kobe 658-8501, Japan

Abstract – **The Sun provides unique opportunities to study particle acceleration mechanisms using data from detectors placed on the Earth´s surface and on board spacecrafts orbiting our planet. Particles may be accelerated to high energies by several physical mechanisms. Differentiating between these possibilities is a fundamental problem of cosmic ray physics. Energetic neutrons provide us with information that keeps the signatures of the acceleration site. A summary of some representative solar neutron events observed on the Earth´s surface, including X and γ-ray observations from spacecrafts is presented. We discuss evidence of acceleration of particles by the Sun to energies up to several tens of GeV. In addition, a recent solar neutron event that occurred in September 7th 2005 and detected in several observatories at Earth is analyzed in detail.**

I. INTRODUCTION

Crucial information of the acceleration processes in solar flares is contained in solar neutrons as they are the product of intense High energy proton fluxes. As early as 1951 Biermann et al pointed out that neutrons were produced in extreme solar flares and envisaged that they could be detected at Earth [1] However, the detection of solar neutrons was not made until June 21, 1980 when instruments on board the SMM spacecraft recorded a signal that could clearly be ascribed to neutrons [2]. The first detection of solar neutrons by ground level instrumentation was made with neutron monitors operating at European observatories during the solar flare of June 3, 1982 [3],[4]. Protons from neutron decay were also observed as a consequence of this flare.[5]. Only two solar neutron events were observed during solar cycle 21. Therefore, for a long time many scientists believed that the detection of solar neutrons was very difficult, comparable to other rare processes occurring in cosmic ray physics.

Due to interplanetary magnetic effects, charged particles from the Sun usually arrive at the Earth about one to a few hours later than the X-rays or γ-rays that take only around 900 seconds to travel the Sun-Earth distance. Additionally, the solar and interplanetary fields modulate the charged particle fluxes; therefore their characteristics at the source are modified. Observations of neutral particles do not suffer from these disadvantages. The times and locations when and where charged particles are accelerated are in close correlation with X-ray and γ-ray emissions. This is an important motivation to include in our studies of neutral particles γ-rays and X-rays. Neutral pion decay produce γ-rays with energies about 70 MeV, lines from excited nuclei, the 2.223 MeV capture line to form deuterium or Bremsstrahlung from accelerated electrons are also in the γ-ray range. On the other hand, specific information on ion acceleration processes, unclouded by other effects, may be obtained through the neutron channel, because neutrons are produced solely by ions impacting the solar surface.

A scheme of the most popular production mechanism for solar neutrons among solar physicists is depicted in Figure 1 [6]. The origin of particle acceleration is the collision of magnetic loops producing a reconnection that warms up the solar plasma. The warm plasma blows downward constituting a high speed plasma stream. The stream hits the top of a magnetic loop. Particles within an inverse U-shape magnetic loop will be accelerated by collisions with the plasma jet. If we assume the speed of the plasma jet to be around 3,000km/s, every mirroring reflection their energies will change by an amount ΔE where $\Delta E/E=2v/c=0.02$.

After some 400 mirroring collisions, the energy may be boosted from 10 MeV to about 30 GeV ($1.02^{400}=2755$). A realistic assumption for the size of the magnetic loop may be around 10,000 km. With these numbers the time needed for acceleration is of the order of one minute. Of course, this is only a rough estimate; the actual acceleration process is certainly more complex.

Nevertheless this simple calculation shows that particle acceleration may occur passing through the plasma mirror repeatedly back and forth [7].

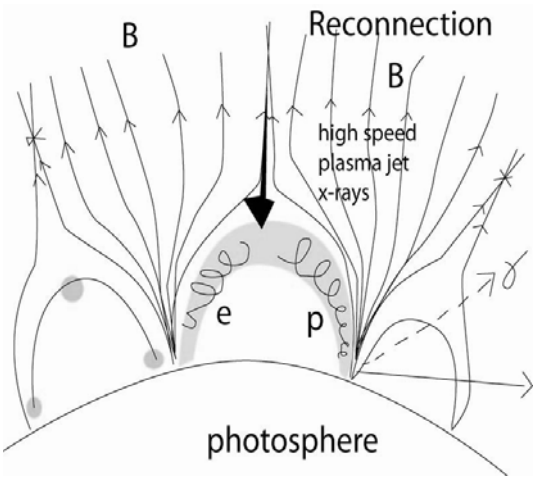

Fig. 1. Particle acceleration model at the solar surface. Collisions and reconnection processes of magnetic loops, warm up the plasma in the loop. The warm plasma then forms a high speed downward stream that hits the top of the lower magnetic loop. Particles are mirrored in the lower magnetic loop. As a consequence of this back and forth processes particles increase their energies with every pass.

Testing this or other plausible scenarios requires extensive observations of the particle and radiation products of the solar flares. In this paper we will discuss observations of solar neutrons at the Earth´s surface and assess its contributions to the knowledge of the solar flare phenomenon.

II. DETECTORS TO OBSERVE SOLAR NEUTRON EVENTS

From the Sun to the Earth, one GeV neutrons are delayed one minute with respect to photons, this lag increases to 11 minutes for neutrons of 100 MeV. Therefore, even in the case of a simultaneous emission at the Sun, their arrival times on Earth differ considerably. As a consequence, in order to establish the neutron emission times at the Sun, both the energies and arrival times at Earth need to be measured. The distinction between continuous and impulsive production of solar neutrons is complicated due to the velocity dispersion.

The neutron monitor in use since the decade of the 1960s detects both neutrons and protons. These interact with a lead target in the detector producing more neutrons. The neutrons undergo successive collisions with protons in paraffin sheets, losing momentum to be gradually thermalized, thus all knowledge of their original energies is lost. The neutron monitor has no directional capabilities either.

To understand the dynamics of acceleration processes occurring at the Sun, Solar Neutron Telescopes (SNT) were developed, they are able to measure both arrival directions and neutron energies. A scheme of the SNT in Sierra Negra, México, is shown in Figure 2. The basic idea is to use a combination of proportional counters (PRCs) and scintillators, in the upper layer and surrounding the scintillators, PRCs working in anticoincidence separate the neutral and charged components of solar energetic particles. To measure the energies of neutrons based on the intensity of the light they produce 30cm thick plastic scintillators in a total area of $4m^2$ are used. The arrays of PRCs underneath the plastic scintillators are used to measure the directions of incoming neutrons.

The detection efficiency of neutrons is about 30%, the arrival directions of neutrons are determined to an accuracy of ±15° approximately. Iron plates of 2cm thickness are located on the four sides of the anti-counter to convert γ-rays to charged particles. At the top of the anti-counter a 5mm thick lead plate is installed for a similar purpose. However the efficiency of the anti-counter is < 100%. It is estimated to be □80% due the conversion rate of photons to charged particles in the lead and iron plates. Thicker plates might be a better shielding at the expense of converting a fraction of incoming neutrons to charged particles and hence being effectively not counted.

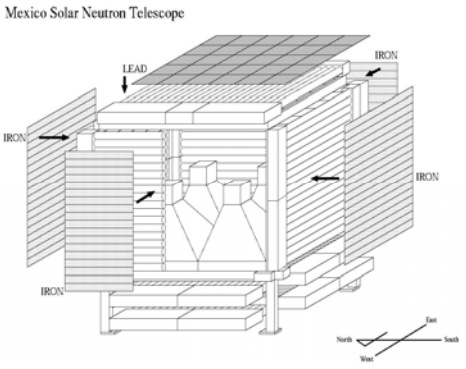

Fig. 2. The Solar Neutron Telescope at the summit of the Sierra Negra volcano, Mexico (97.3W, 19.0N; 4580 m a.s.l.). Five gondolas of PRCs are located at the top and sides of the central scintillators to detect and discriminate charged particles. The lead and iron plates serve the purpose of converting γ-rays into charged particles and prevent being counted as neutrons in the scintillators. The four gondolas underneath the scintillators serve to identify the neutron arrival directions as they detect the protons produced by neutron nuclear interactions inside the scintillator.

The detector records energy deposits by neutrons in 4 ranges, >30, >60, >90 and >120 MeV. This sets the limit for testing production solar models of neutrons. Details of the SNT operating principles may be found elsewhere [7].

III. FIRST SOLAR NEUTRONS DETECTED NEAR AND AT EARTH

The time profile of the gamma ray telescope on board SMM for the event observed on June 21, 1980 is shown in Figure 3 [2]. The first peak is due to gamma-rays, whilst the second broad enhancement corresponds to solar neutrons. Even if the neutrons were impulsively injected from the Sun (within one minute), their arrival times would be spread over a time span of 20 minutes, with high-energy neutrons arriving first and low energy neutrons arriving later. The flux increased in the first 10 minutes, reached a maximum and decreased afterwards due to the decay of low-energy neutrons in transit from the Sun to the Earth. The differential energy spectrum may be expressed by a power index law ($dN/dE \sim E^{-\gamma}$) where $\gamma = 3.5$, assuming impulsive production at the Sun. Observations admit the alternative explanation that neutrons with high energies (say >1 GeV) were emitted for around 20 minutes.

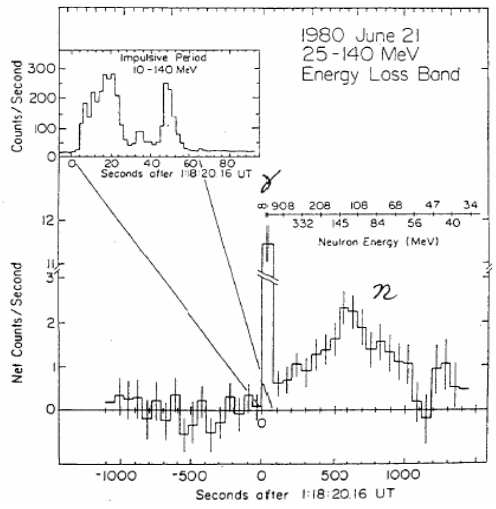

Fig. 3. The first solar neutron event detected onboard the SMM satellite. The initial spike was produced by photons, the broad hump is due to neutrons. The time profile of neutrons may be explained by a simple impulsive production model of neutrons in the MeV range.

Figure 4 shows the data for the event on June 3, 1982, the situation was more complex then [4]. The ground level neutron monitor at Jungfraujoch showed an enhancement that continued for around 12 to 15 minutes. The structure of the gamma ray detector time profile is very similar to that of the 21 June 1980 event. Based on this evidence one could ascribe a similar interpretation to this event; namely the first spike is due to gammas and neutrons cause the broader hump afterwards. However the data of June 3, 1982 shows the arrival of neutrons for an extended time span as indicated by the Jungfraujoch count rates in the bottom panel of Figure 4. Thus, in this event at least some gradual production of high energy neutrons might have occurred since, according to a detailed Monte Carlo simulation [8], neutrons with energy less than 70 MeV cannot reach the ground due to strong attenuation in the atmosphere, because the interaction cross-section of neutrons with the air molecules increases substantially below 100 MeV. The association of high-energy neutrons with the gradual phase establishes that the gradual phase had a significant hadronic component. [9] speculated that the protons responsible for the time-extended phase are not the same as those responsible for the impulsive phase. In any case evidence is ambiguous and, as we have seen, may have several interpretations.

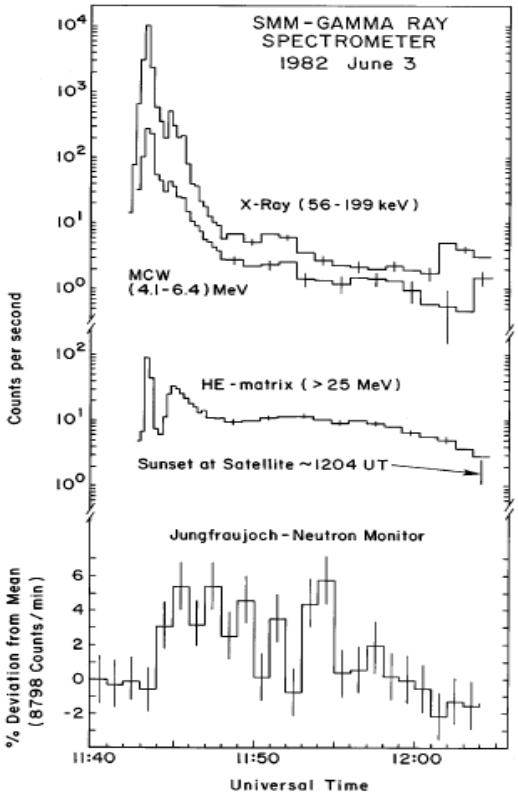

Fig. 4. The first solar neutron event detected by a neutron monitor on june 3, 1982. The first spike is due to photons, the following hump are neutrons (middle panel). This continued for more than 20 minutes. The data of the ground level event on the Jungfraujoch neutron monitor (bottom panel) shows an enhancement lasting some 15 minutes.

Figure 5 shows the event observed on May 24, 1990 by a set of neutron monitors at the Earth´s surface. A spike at 20:40 UT was undoubtedly

caused by neutrons. The significance of the peak is not ordered by the energy cut-off of the stations, rather it decreases with the atmospheric depth of the site. A proton GLE was observed after 21:00 UT. The energy spectrum of solar neutrons follows a power law with differential index γ = -2.9, assuming an impulsive injection. This assumption is justified based on observations of gamma rays by the GRANAT satellite [10].

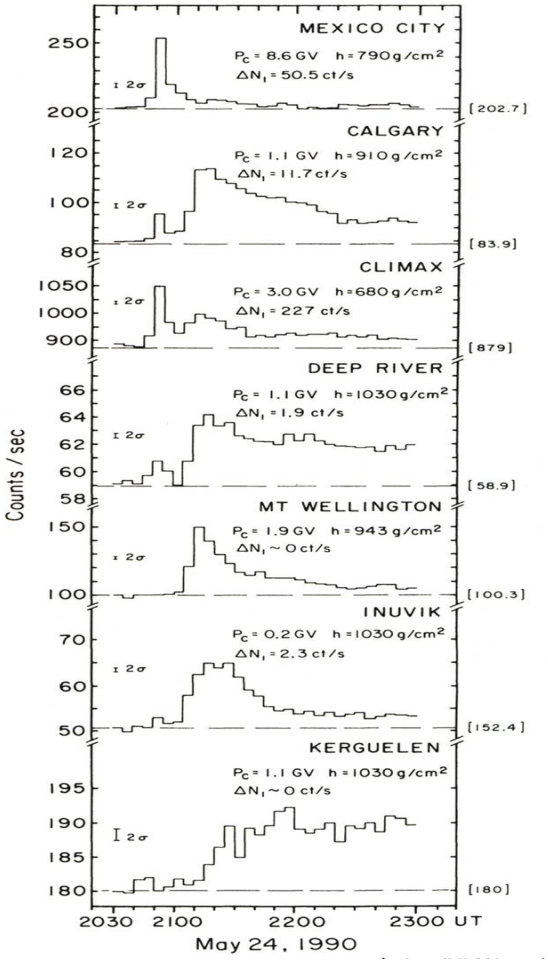

Fig. 5. Solar neutron event observed on May 24, 1990, the first event where solar neutrons induced a GLE. The production spectrum of neutrons can be fit by a power law with a power index γ =-2.9, consistent with an impulsive production at the Sun.

The first solar neutron event to be observed by a SNT was on June 4, 1991. It was detected also by a neutron monitor, and a 36 m^2 muon detector, all operating at Mt. Norikura, Japan. A very soft spectral power index was deduced for this event (γ =-5.4) assuming impulsive injection at the Sun [11]. Because the flare was near the east limb (N30 E70), no prompt protons were expected that could be mixed with neutrons at ground level stations. However, [12] used the neutron monitor data of Mt. Norikura to model a time-extended neutron production. Their model predicts neutron spectra at the Sun that are much harder (around $E^{-3.5}$) than those reported by Muraki et al [10]. This spectrum is in better agreement with the proton spectrum estimate ($E^{-2.8}$) at the Sun by [11], based on the long duration of the γ-ray neutron capture and carbon de-excitation lines (around 160s) .

IV. THE BIG EVENTS OF THE SOLAR CYCLE 23

A gigantic solar flare occurred on "Easter day" 15 April, 2001; the X-ray measurements onboard GOES classified it as an X14 flare, located at S20W85 in the solar surface. The onset was detected by the GOES satellite at 13:19UT, it reached X14 at 13:50UT. This was one of the strongest flares observed during solar cycle 23.

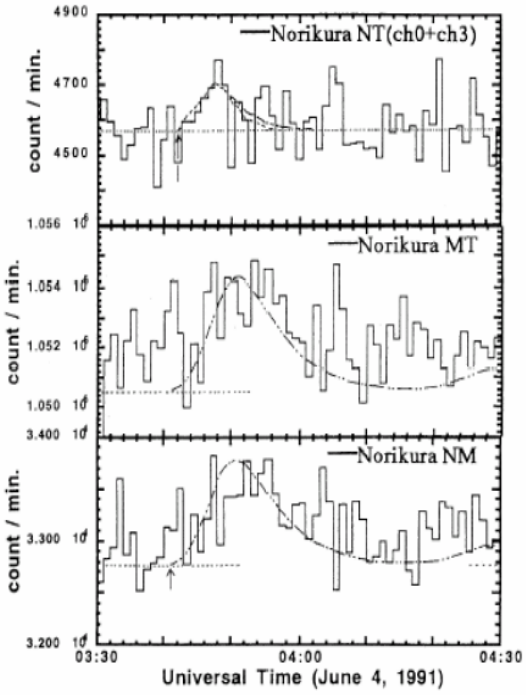

Fig. 6. Solar neutron event observed on June 4, 1991. The first solar neutron event to be detected by a SNT in Mt. Norikura (top panel). The enhancement induced by solar neutrons was also registered in other two detectors at the same site: the 36m^2 muon detector (middle) and the neutron monitor (bottom). The time profile was almost the same at the muon detector and the neutron monitor

The detection of γ-ray lines provides evidence for proton acceleration at the Sun. The Yohkoh satellite recorded γ-ray lines between 13:45UT and 13:51UT. Therefore protons must have been accelerated impulsively to high energies approximately between 13:43 UT and 13:47 UT [10]. A large GLE was observed in many stations as a consequence. The GLE started shortly after 14:00 UT. In some polar stations the counting rates increased over 100% [13].

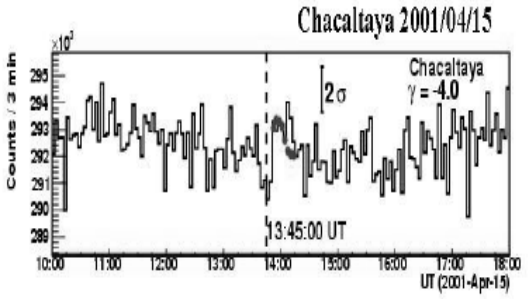

Fig. 7. Three minute values of the Chacaltaya neutron monitor on April 15, 2001. The line at 13:45:00 UT is the estimated time of particle acceleration and the red dots represent the expected curve for the impulsive production of neutrons with γ=-4.0. Around 14:06-14:12UT, there is another enhancement due to the GLE, caused by high energy protons.

The neutron monitor at Chacaltaya (5250m a.s.l.) recorded a significant increase after 13:51 UT continuing until 14:15UT. Muraki et al. (2007) estimated the significance of the hump to be 8.2σ. The 3 minute time profile counting rates are shown in Figure 7, a second peak can be observed between 14:06 and 14:12, coincident with the onset of the GLE. Thus it is very probable that this second peak was produced by GLE protons. The rigidity cut-off of the Chacaltaya observatory is 12.1 GeV, therefore this should be considered as evidence that protons were accelerated to at least 12 GeV. An additional remarkable fact is that the flux may be represented by a simple power law with an index γ= -2.75±0.15, in the energy range between 650 MeV and 12 GeV, the range of the neutron monitors. Fitting the Chacaltaya neutron monitor data excluding second peak, implies a spectral index γ=-4.0 for the neutrons.

The Sun was intensely active during October-November 2003, 11 X-class flares were observed between 19 October and 4 November, from those, two remarkable solar neutron events were observed by ground-based neutron monitors.

On October 28, 2003, in association with an X17.2 large flare, solar neutrons were detected with high statistical significance (6.4σ) by the neutron monitor at Tsumeb, Namibia. γ-ray lines from neutron capture and excited ions of C and O nuclei were clearly observed, these were quite different from the time profile of bremsstrahlung γ-rays. It appears that the time profile of electron acceleration was distinctly different from the time profile of ion acceleration. From the time profile of the neutron capture γ-rays it seems that high energy neutrons were produced with the same time profile as the γ-ray lines of the de-excited ions. The corresponding spectrum for these solar neutrons is somewhat harder than other events (γ= 2.9).

In association with an X28 class flare, relativistic solar neutrons were observed by the neutron monitors at Haleakala in Hawaii and Mexico City, and by the solar neutron telescope at Mauna Kea in Hawaii simultaneously on November 4, 2003. Clear excesses are present in the time profiles of these detectors, with a significance of 7.5 σ for Haleakala, and 5.2 σ for Mexico City. The detector onboard the INTEGRAL satellite observed a high flux of hard X-rays and γ-rays at the same time. Using the time profiles of the γ-ray lines, [14] explained those of the neutron monitors. From the time profile of the 2.2 MeV neutron capture γ-ray line, it appears that the time profile of ion acceleration was approximately the same as that of bremsstrahlung emissions. Assuming that solar neutrons were produced at the time when these γ-rays were emitted, the observed excesses are explained. The data may be fitted with a propagation model with spectral index γ= 3.5.

A summary of spectral indexes determined for solar neutron events observed by neutron monitors was done by [14], it is shown in Figure 7. The power index for the 4 June 1991 event is that of Muraki et al [9] and not the estimate given by Struminsky et al. [12]. If we use this last result, all these solar neutron events spectra may be described by power laws with power indexes -4 ≤γ≤ -3. In the two cases where we have also estimates of the proton spectra, these tend to be harder. This may be a systematic fact that would require further detailed investigations to determine whether the difference is due to the solar source or to proton interplanetary modulation. Nevertheless, the most relevant fact here is that both, proton and neutron spectra tend to adjust to power law fits, as predicted by shock acceleration theory.

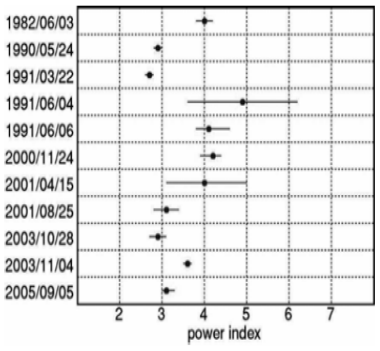

Fig. 7. The estimated spectral indexes of solar neutron events detected by neutron monitors with energy range around En=70-700MeV. Most of the indexes are between 3 to 4.

We have reserved the following section to discuss a remarkable solar neutron event registered on September 7, 2005. The event was detected by the SNTs at Sierra Negra and Chacaltaya, and by neutron monitors at Chacaltaya and Mexico City. This example illustrates the capabilities of these types of detectors.

V. SEPTEMBER 7, 2005 NEUTRON EVENT AT AMERICAN SECTOR SNT AND NM

The SNT world network has detectors located at Gornergrat (Switzerland) [15], Tibet (China) [16], Mt. Norikura (Japan) [17], Mauna Kea (Hawaii) [18] and Sierra Negra (Mexico). Although not identical, all the SNTs are similar; the SNT installed at Sierra Negra is shown in Figure 2.

In September 2007, an extensive active region (NOAA10808) produced 10 X-class solar flares. The first of them (17:17 UT, September 7) was the most energetic; it had a magnitude of X17. This event was at the East solar limb (S06, E89). At that time, the Sun was above the Atlantic side of the American continent. The intensity of solar neutrons was extraordinarily strong, four detectors located at Sierra Negra, Mexico City and Chacaltaya made successful detections. This provided an opportunity to compare the detection efficiency of the SNTs at Chacaltaya and at Sierra Negra [18].

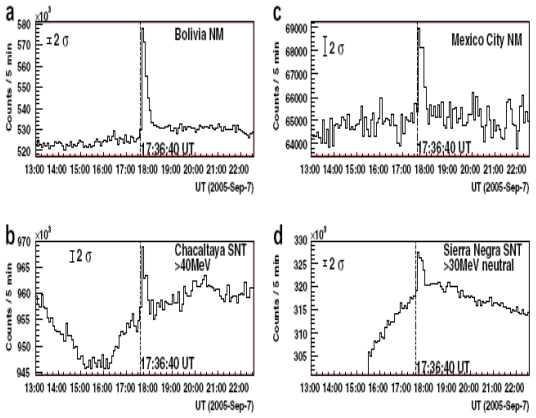

Fig. 8. .It displays the respective responses for this flare. The neutron monitor at the Chacaltaya observatory recorded 95,000 neutrons during 10 minutes, while the neutron telescope at Sierra Negara recorded 21,500 events for En > 30MeV, 11,700 events for En > 60MeV, 3,000 events for En > 90MeV and 820 events for En > 120MeV.

Figure 8 shows data from the neutron monitors and SNTs located in Bolivia and Mexico. Clear excesses were observed by all four detectors after 17:36:40 UT, the peak of the γ-ray event. Solar neutron telescopes have energy resolution [18], [19], [20], although we show here only the > 120 MeV channel, significant excess signals were observed in all channels.

The highest neutron energy channel at Sierra Negra is E>120 MeV. At those energies, neutrons will arrive to the Earth nine minutes later than the electromagnetic radiation produced in the solar flare. Therefore a neutron signal lasting longer than nine minutes is an indication of an extended neutron emission at the Sun. An impulsive emission will produce a signal of less than nine minutes duration. It is therefore not surprising that an attempt to fit the observed solar neutron profiles at Chacaltaya neutron monitor, assuming a simple δ-function injection and a simple power law spectrum at the source was not successful [21]. In contrast, a much better agreement with the observed profile was obtained using the 4.4 MeV γ-ray line emission from Carbon nuclear de-excitation line with counting rates above the background level from 17:36 to 18:00 UT, and a power law spectrum with index of -3.1 [19].

A completely independent study using a comparison of the Sierra Negra SNT data, with Monte Carlo simulations of the detector response, reached the conclusion that the solar neutron spectrum was a power law whose index was most likely around -3, in agreement with the previous determinations based on the Chacaltaya neutron monitor data [22].

There are, however, subtle differences between the last reported investigations of the event as an energy cut-off of 500MeV was assumed by [19], but no cut-off was included in the simulations of [22]. Further analyses are necessary to decide on the solar neutron spectra and time profile of the emission at the Sun. These will undoubtedly shed light as to the acceleration process and the physical scenario of the flare occurrence.

VI. SUMMARY AND CONCLUSIONS

The lessons learnt from solar neutron observations may be summarized as follows:

- Observation of solar neutron events may be an important tool to understand solar particle acceleration mechanisms during strong flares as solar neutrons carry unmodulated information from the solar source.

- Simultaneous observations of X-rays and γ-rays together with ground located neutron detectors are necessary to elucidate the time profiles of the solar particle emissions and the particular conditions of the solar magnetic loops producing the flares. With

the accumulation of more data, we could discriminate between various acceleration models for particles at the Sun.

- Most solar neutron events may be fitted with an impulsive injection model. However the strongest solar flares (rated X>10) present strong evidences of extended injection. Examples are the events on 15 April 2001, 28 October 2003 and 7 September 2005.

- Further analyses of the available data are needed to determine the injection profiles and energy spectra for the flares where there is evidence of extended injection.

- Solar Neutron Telescopes have proved to be a useful tool to study solar neutrons as they separate the neutral and charged particle fluxes and provide spectral and directional information of the solar neutron fluxes. The improvement of the particle identification ability of the present solar neutron telescope world network is an important task for the solar cycle 24.

REFERENCES

[1] Biermann, V.L., et al., Z. Naturforshch, 6a, 47, 1951.
[2] Chupp, E.L. , et al., Ap. J., 263, L95, 1982.
[3] Efimov, Yu. .E., et al., Proc. 18th ICRC, 10, 276, 1983.
[4] Chupp, E.L., et al., ApJ, 318, 913, 1987.
[5] Evenson, P., et al., Ap. J., 274, 875, 1983.
[6] Dennis, B. R. and R. A. Shwartz, Solar Physics, 121, 75, 1989.
[7] Muraki , Y., et al., Proc. 22nd ICRC, 3, 1991.
[8] Shibata, S., JGR, 99, 6651, 1994.
[9] Murphy, R. J., Dermer, C. D. and Ramaty, R.: *Astrophys. J.* 63, 721, 1987.
[10] Muraki, Y., H. Tsuchiya et al., Astropart. Phys. 28, 119, 2007.
[11] Murphy, R. et al.: 1994, in J. M. Ryan and W. T. Vestrand (eds), 'OSSE Observations of the 4 June 1991 Solar Flare', *Proc. of High-Energy Solar Phenomena – A New Era of Spacecraft Measurements, AIP Conference Proceedings* 294, 15.
[12] Struminsky, A., Matsuoka, M. and Takahashi, K.: *Astrophys. J.* 429, 400, 1994.
[13] Bieber, J. et al., Proc. 22nd ICRC 2001
[14] Watanabe, K., Doctoral thesis to Nagoya University, 2005
[15] Buetikofer, R., et al., Proc. 27th ICRC, 8, 3053, 2001.
[16] Katayose Y., et al., Proc. 26th ICRC, 6, 46, 1999.
[17] Tsuchiya, H., et al., Nucl. Instr. Meth., 463, 183, 2001.
[18] Matsubara, Y., et al., Proc. 23rd ICRC, 3, 139, 1993.
[19] Watanabe, K. et al, Proc 30th ICRC, 2008 (in press)
[20] Valdes-Galicia, J.F., et al., NIM, 535, 656, 2004.
[21] Watanabe, K., et al, *Adv Sp Res.*, 39*, no. 9*, 1462, 2007.
[22] Sako, T., Proc 30th ICRC, 2008 (in press)

Astrophysical aspects in the studies of solar cosmic rays

L.I. Miroshnichenko[1, 2], J. Perez-Peraza [2]

[1] *N.V. Pushkov Institute IZMIRAN, Troitsk, Moscow Region,Russia*
[2] *Instituto de Geofisica, UNAM, Mexico, Mexico*
(leonty@geofisica.unam.mx; leonty@izmiran.ru)

Abstract **– This review comprises main concepts, available observational data and recent theoretical results related to astrophysical aspects of particle acceleration at/near the Sun and extreme capacities of the solar accelerator(s). We summarize underground and ground-based observations of solar cosmic rays (SCR) accumulated since 1942, direct spacecraft measurements of solar energetic particles (SEP) near the Earth's orbit, indirect information on the SCR variations in the past, and other relevant astrophysical, solar and geophysical data. The list of the problems under discussion includes: upper limit spectrum (ULS) for solar cosmic rays; maximum energy (rigidity), Em (Rm), of particles accelerated at/near the Sun; production of the flare neutrinos; energetics of SCR and solar flares; production of flare neutrons and gamma rays; charge states and elemental abundances of accelerated solar ions; coronal mass ejections (CMEs) and extended coronal structures in acceleration models; magnetic reconnection in acceleration scenarios; size (frequency) distributions of solar proton events (SPE) and stellar flares; occurrence probability of giant flares; archaeology of solar cosmic rays. The discussion allows outlining a series of interesting conceptual and physical associations of SCR generation with the high-energy processes at other stars. The most reliable estimates of various parameters are given in each of research fields mentioned above; a set of promising lines of future studies is highlighted. It is emphasized a great importance of SCR data for resolving some general astrophysical problems.**

Solar extreme events in minimum of the solar activity

R.A. Nymmik

Skobeltsyn Institute of Nuclear Physics, Moscow State University, Russia
(nymmik@sinp.msu.ru)

Abstract **– The probability of occurrence of extremely large SEP events is determined by both the general properties of the distribution function, and the character of this function in the region of large fluxes (fluences and peak fluxes) of particles. The analysis of experimental data has shown that the distribution function describing a set of events, divided by the sum of Wolf numbers during the measurement of this set, is identical for any period (phase) of solar activity. This means that the probability of occurrence of SEP events for the identical sum of Wolf numbers is the same for any phase (maximum or minimum, ascending or declining) of solar activity.**

Jovian periodicities (10h, 40 min) around CIRs during Ulysses' Distant Jupiter Encounter after the Halloween Events

G. C. Anagnostopoulos, I. Louri, P. Marhavilas, and E.T.Sarris

Research Laboratory, Democritus University of Thrace, Greece

Abstract— **We analyzed data from four different instruments (HI-SCALE, URAP, SWOOPS, VHM/FGM) onboard Ulysses spacecraft (s/c) and we searched for possible evidence of Jovian emissions when the s/c approached Jupiter during the times of Halloween events (closest time approach / position to Jupiter: February 5, 2004 / R = 1683 R_J, θ = ~ 49^0). In particular, we analyzed extensively the low energy ion measurements obtained by the HI-SCALE experiment, in order to examine whether low energy ion / electron emissions show a symmetry, and whether are observed at north high latitudes upstream from the jovian bow shock, as is known to occur in the region upstream from the south bow shock (*Marhavilas et al*., 2001). We studied the period from October 2003 to March 2004, as Ulysses moved at distances 0.8-1.2 AU from the planet at north Jovicentric latitudes <75^0, and we present here an example of characteristic Jovian periodicities in the measurements around a CIR observed by Ulysses on days ~349-350 / 2003 (R = 1894 R_J, θ = 72^0). We show that Ulysses observed low energy ion (~0.055 - ~4.7 MeV) and electron (>~40 keV) flux and / or spectral modulation with the Jupiter rotation period (~ 10 hours), as well as, variations with the same period in solar wind parameters, radio and magnetic field directional data. In addition, characteristic ~ 40 min periodic variations were found superimposed on the ~ 10 hour flux / spectral variations. Both the ~10 hour and ~40 min ion periodicities in HI-SCALE measurements were present in several cases during the whole period examined (October 2003 to March 2004) and were found to be more evident around times of passage of CIRs. We infer that the Jovian magnetosphere was triggered by the impact of the CIRs, after the Halloween events, and it caused the generation of ~10 hour quasi-periodicities in low energy ion / electron, magnetic field, plasma and radio observations at Ulysses.**

I. INTRODUCTION

Previous studies based on Ulysses measurements demonstrated the presence of characteristic ~10 hour and ~40 min periodicities in low energy ion and electron observations within the Jovian magnetosphere and its environment at distances as far as ~1800 R_J from the planet [1], [2], [3]. Alfven waves with a period equal to Jupiter's rotation (~10 hours) have also been reported during Ulysses flyby of Jupiter (year 1992), upstream from the Jovian bow shock (*Anagnostopoulos et al*., 1998)[1]. Furthermore, Jovian relativistic electrons have been confirmed to travel from Jupiter to the Earth's environment [4]. The relativistic electrons have been known for many years to show ~10 hour cycle variation in their spectral index at distances at least of the order of 1 AU from Jupiter [5]. Furthermore, solar wind structures were found to affect the relativistic electron and radio emissions from the Jovian magnetosphere [6], [7].

It was an important coincidence that during the intense solar events strongly affecting the Heliosphere at the end of the year 2003, known as Halloween events, Ulysses approached Jupiter and could explore the Jovian environment at north high latitudes [8] under extreme solar wind conditions. It is the main purpose of this study to examine the possible presence of characteristic Jovian (~10 hours and ~40 min) periodicities in various kind of measurements, and in particular in low energy ion and electron measurements, during that interesting period with an active Sun-highly disturbed heliosphere, when a spacecraft (Ulysses) visiting for the first time the far (0.8-1.2 AU) north (>≅70^0) region upstream from the Jovian bow shock.

II. OBSERVATIONS

Figure 1 (panel a) shows the Ulysses trajectory, in the Jovicenter Coordinate system, for about three years (2002/01/01 to 2004/12/01) around the time of the closest approach. In particular, Fig.1a displays the Ulysses' latitude versus the spaceccraft Jovian Local Time, while the bottom panel of Figure 1 (panel c) shows both the jovicentric and the heliographic latitude as a function of time

(http://urap.gsfc.nasa.gov/jupiter_distant_encounter.html)

The second Ulysses' "Encounter" with Jupiter on February 5 (d. 36), 2004 was a distant one, with the closest approach at ~0.8 AU (R = 1683 R_J, $\theta = \sim 49^0$) from the planet. The time interval studied in this paper is October (d. 289) 2003 to March (d. 90) 2004, while Ulysses travelled over distances ranging from ~0.8 AU to ~1.2 AU from Jupiter. It is noted that during the second Ulysses (Distant) Jupiter Encounter, the spacecraft approached the planet from north Jovicentric / Heliographic latitudes, and made measurements which can complement the picture of the intense Jovian particle emissions originating from the south Jovian magnetosphere which we obtained due to the Ulysses outbound trajectory after the flyby of Jupiter in 1992 [2]. During the time interval studied in this paper, Ulysses reached about 75 degrees North Jovigraphic Latitude in late 2003, and remained at latitudes as high as >~70^0 in the period October – December 2003.

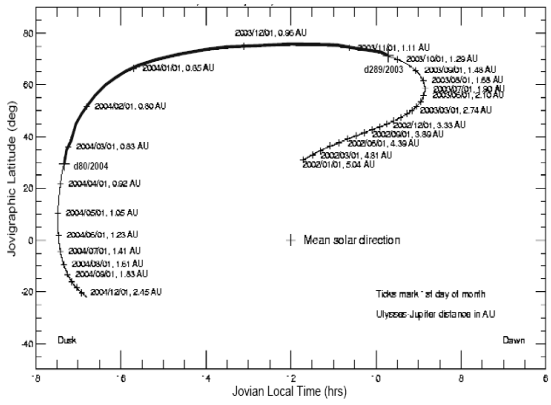

Fig. 1. Ulysses trajectory for a time interval of about two years (2002/01/01 to 2004/12/01) centered on the time of the closest approach to Jupiter on Feb. 5 (d. 36) 2003. Panel a: Ulysses' Jovicentric latitude θ versus the Jovian local time. Panel b and c: the distance R from the planet (in Jovicentric coordinates) and the latitude (both in Jovicentric and heliographic coordinates) as a function of time. Ulysses arrived at a closest approach to Jupiter at a position with R = 1683 R_J, $\theta = \sim 49^0$.

Figure 2 displays energetic ions observations made by Ulysses HI-SCALE instrument between days ~290/2003-80/2004 as long as the spacecraft approached the Jovian magnetosphere from north high latitudes. This time period was separated in six 27-day intervals to facilitate the search for possible periodic solar wind structures. At the beginning of each 27-day long graph the distance (in AU) and the latitude of Ulysses is given in the Jovicentric Coordinate System. During the time interval examined here, two CIR structures had been formed in the heliosphere [9]. Indeed, two Corotating Interaction Regions can be seen in Ulysses / HI-SCALE data in Fig. 2, near the beginning and the end of panels a-f (horizontal black bars on the top of each panel). The CIRs were often accompanied by Forward (FF) and Reverse (FR) shocks (http://ulysses.jpl.nasa.gov/science/observed_data.html; X. Zhou and E. Smith).

In particular, in Figure 2 we show energetic ion fluxes from the lowest and the highest energy channels of the HI-SCALE detectors LEMS30 (P1:56-78 keV, P8: 1802-4752 keV) and LEMS120 (P1′:61-77 keV, P8′:1874-4752 keV), in order to investigate the energetic ion events over a large range of enrgies. From Fig. 2, we see that the ion fluxes are strongly modulated by the presence of CIRs. The ion fluxes increase well above the interplanetary background level around all Forward and Reverse shocks, and evidently suggest local acceleration at the FF and FR shocks. In general, we see that the most intense and long-lived shock associated ion structures were observed around FR shocks, in agreement with previous observations obtained by Pioneer, Voyager and Ulysses [10]. In the following, we elaborate the form of the specific small intensity fluctuation seen in Fig. 2 around FF and FR shocks, and, in general, around the times of arrival of the CIRs.

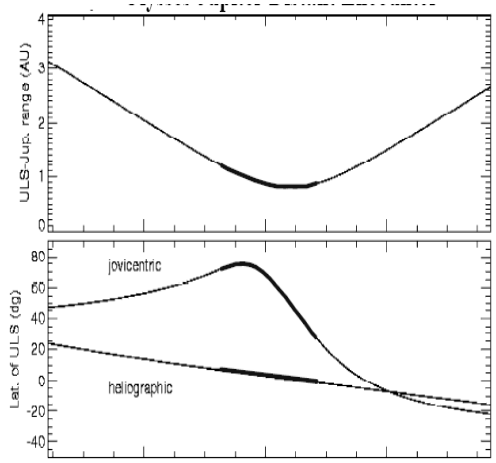

Fig. 2. Energetic ion observations derived by the HI-SCALE instrument onboard Ulysses during the spacecraft Distant "Encounter" with Jupiter. The whole time period shown in this plot (days ~289/2003-80/2004) is divided in 27 days intervals. Corrotating Interaction Regions (CIRs) (horizontal black bars on the top of the panels) often accompanied by Forward (FS) and Reverse (FS) Shocks reach almost periodically the space near Ulysses. Ion intensity structures associated with the passage of CIRs and CMEs are evident in Fig. 2 as have been noted in previous studies on the Halloween events (Lario et al., 2005). More detailed data analysis (see Fig. 3 and 4 and their discussion in the text) of some intensity fluctuations of the CIR - associated ion structures reveals a modulation with the Jupiter rotation period (~10 hours).

Figure 3 contains measurements made by four different Ulysses instruments (HI-SCALE, URAP, SWOOPS, VHM/FGM) for the time interval of days 346-356/2003 that includes a CIR structure; at

that time Ulysses approached Jupiter (~1894 R_J) from north high latitudes (~72^0). The three bottom panels of this figure display measurements made by the solar wind plasma experiment (SWOOP): speed (panel j), density (panel i) and temperature (panel h). The next three panels (forth to sixth from the bottom) show the magnetic field magnitude (g) and the direction of the magnetic field in polar coordinates (angles φ in f and θ in e panels) as measured by the magnetic field experiment VHM/FGM.

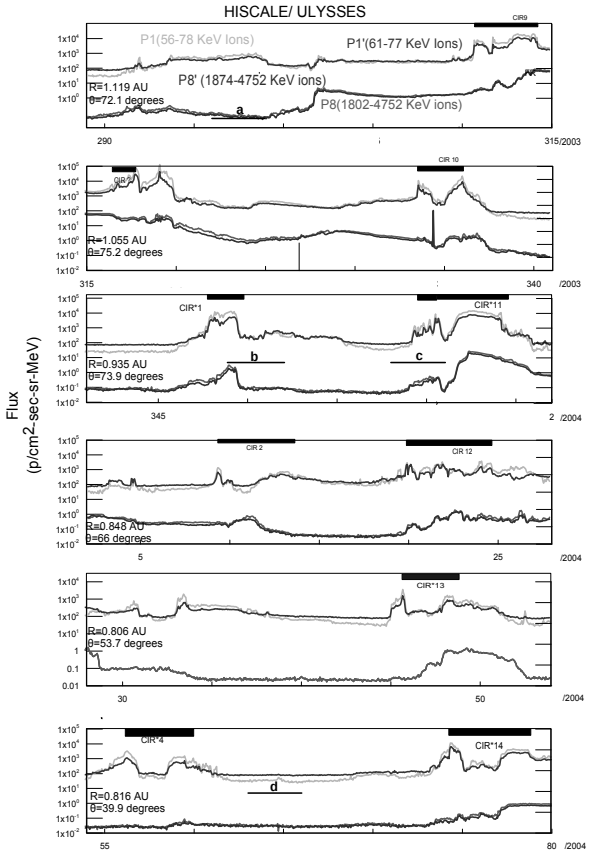

Fig. 3. From the top to the bottom, measurements from four different instruments onboard Ulysses made on days 346 - 356/03, around the passage of a CIR: HI-SCALE (panels a, b, d), URAP (c), VHM/FGM (panels e, f, g) and SWOOPS (panels h, I, j). The vertical pink sheets have been drawn ~10 hours apart from each other. Modulation with the Jupiter rotation period (~10 hours) are seen in low energy electron spectral data (flux ratio DE2/DE1: panel d) and magnetic field direction (angle θ: panel e) even before the CIR arrival, in solar wind density and temperature (panels h and j) during the CIR passage, in Jovian radio (bKOM, nKOM / nonthermal continuous) emissions (panel c), and in ion spectral (a) and flux (b) observations both during and after the CIR passage (see in the text).

Panel d displays the ratio DE2 / DE1 of the flux from the two low energy electron channels DE2 (~55-100 keV) and DE1 (~40-55 keV) from the LEMS30 detector of the HI-SCALE experiment [11]; this flux ratio will be considered in the following as a spectral index. Above the panel with the electron flux ratio DE2/DE1, the dynamic spectrum from the radio receivers of the URAP experiment (panel c), and low energy ion data from the LEMS30 detector of the HI-SCALE experiment are shown: the flux of the P1 channel (panel b) and the flux ratio P1/P2 (panel a) from the channels P1 and P2 correspondingly (P1: 56-78 keV, P2: 78-130 keV). The vertical pink sheets in various panels in Figure 3 have been drawn ~10 hours apart from each other and are used to indicate the characteristic ~10 hour periodicities in the data. From the four bottom panels j-g a CIR (CIR*1) can be seen, which lasts for about two days (from the end of day 347 to the end of day 349/2003) and is marked by a black bar at the bottom of Panel g; we clearly see that the magnitude of the magnetic field was strongly enhanced at that time interval.

During the passage time of CIR*1 by Ulysses, ~10 hour modulations were observed in solar wind parameters; in particular in the values of solar wind temperature T and density ρ, with relative changes as high as $\Delta T/T \approx 1–3$ and $\Delta\rho/\rho \approx 0.5$-4 (panels h and i); it is important to note that this periodic variation with the rotation period of Jupiter (~10 hours) in plasma measurements within a CIR was observed by Ulysses as far as 1894 R_J, and at north high latitudes of ~72^0 and suggests a strong Jovian influence on the outer heliosphere, during the period of Halloween events.

We proceed now to note a Jovian influence on the north heliosphere even before the arrival of the CIR. From panels d and e of Figure 3 we can see that on days 346-347, four distinct (or pair of) increases were observed in the electron flux ratio DE2/DE1 associated with increases in the angle θ of the magnetic field (panel e). This ~10 hour phase modulation of the slope of the low energy electron spectrum in association with the magnetic field direction is clear until the end of day 347, when Ulysses detected two magnetic field discontinuities (the first pair of the vertical dashed lines in panel f), which are related to the arrival of the CIR*1 at Ulysses. These magnetic field low frequency long wavelength waves extend previous wave observations made by Ulysses closer to the Jovian bow shock during Ulysses inbound trajectory to Jupiter in 1992. These observations suggest that Ulysses observed low energy electrons and large scale magnetic field fluctuations with the rotation period (~10 hours) of Jupiter for a long time (~2 days) before the CIR arrival. The quasi-periodic ~10 hour modulation of the low energy electron spectrum and of the magnetic field vector (panel e) is probably present throughout the whole CIR structure and after its passage by Ulysses, but we think is not well seen because of the distortion of the periodic modulation by the large changes in phi angle (time periods marked by the three solid bars bound by three pairs of vertical dashed lines in panel f). Detailed examination of the measurements

during the whole time interval examined for this study (October 2003- March 2004) reveals that such behaviour with ~10 hour modulation of the low energy electron spectrum almost in phase with periodic variation of the magnetic field direction was often observed by Ulysses around times of CIRs.

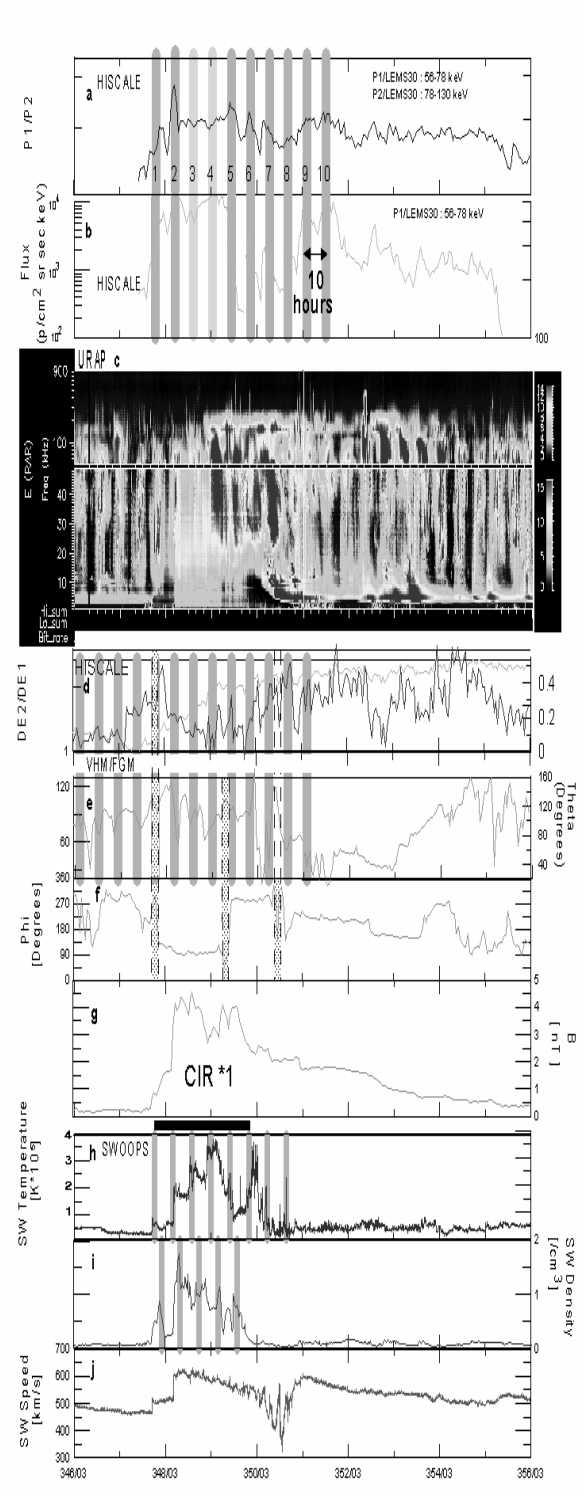

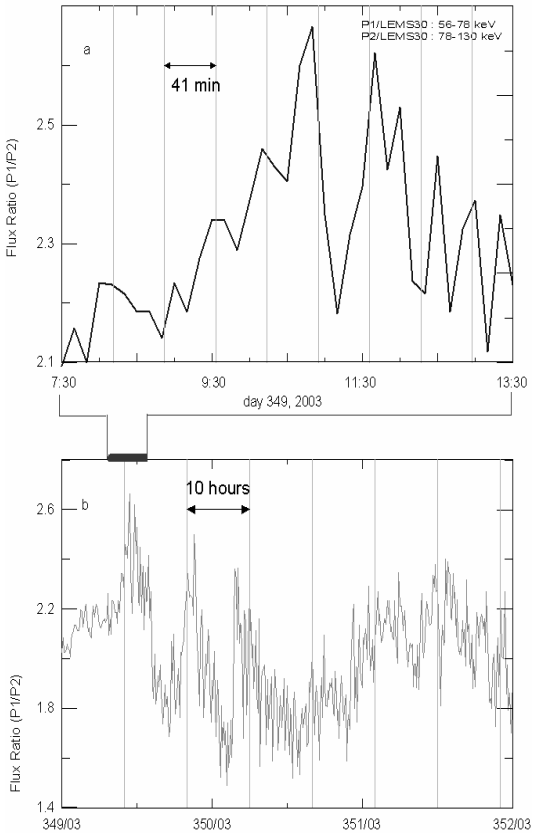

Further examination of Fig. 3 clearly shows that the presence of quasi-periodic ~10 hour bKOM (~10-200 kHz) Jovian radio emissions was observed by URAP in most of the time interval examined in Fig. 3. However, after the middle of the CIR (end of d. 348 to d. 350), the ~10 hour periodic radio emission appears further brightening followed by a cessation of the bKOM and an onset of an nKOM event (d.351). In addition, characteristic Jovian continuous nonthermal (<~15 kHz) emission was observed after the passage of the CIR (~d. 351) that is seen at the bottom of panel c; all these radio emissions are known to be generated in the Jovian magnetosphere, when triggered by solar wind structures [7], [12].

In the following we elaborate the low energy ion and electron flux variations. Important to note for the low energy particle behaviour around the time interval of the CIR passage by Ulysses (d. 347-351) are the following: (a) the low energy flux ratio P1/P2 produces six clear ~10 hour separated peaks (numbered 5-10 in panel a), with the first two peaks (5-6) seen within the CIR structure and the peaks numbered 7-10 after the end of the CIR, (b) the flux ratio Peaks #6-10 are clearly correlated with P1 flux increases and suggest a softening of the spectrum at those times, (c) the two first P1/P2 peaks (#1-2) were observed just with the arrival of the CIR (d 347-348), about ~3 and 4 planetary rotation periods earlier than the onset of the series

of peaks #5-10, (d) the flux ratio Peak #5 was observable despite the abrupt flux depression at the edge of the CIR ion intensity structure (d.349, ~10 UT), (e) the series of the ~10 hour separated flux ratio Peaks # 1-2, 5-10 started some (~8 hours) after the intensification (d. 349, ~00 UT) of the ~10 hour quasi-periodic bKOM Jovian radio emissions.

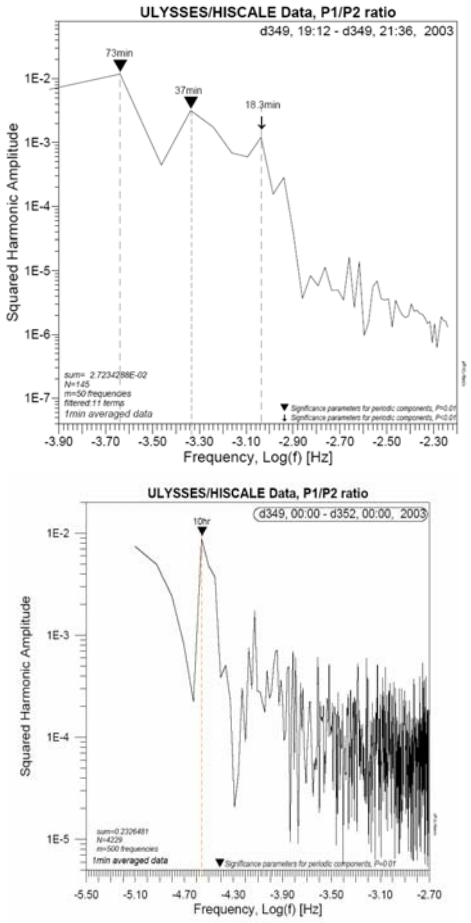

Fig. 4. Data from Ulysses' exploration of the Jovian environment far upstream from the north side of the bow shock (R= 1894 R_J, θ = 72^0) on days 349-351/2003 and for selected intervals within the same period. Panels a and b show the HI-SCALE flux ratio from the low energy ion channels P1/LEMS 30 (56-78 keV) and P2/LEMS30 (78-130 keV) while Panels c and d display results of a power spectrum analysis. Both the flux time-profiles and the results of the power spectral analysis demonstrate significant periodicities (P ≤ 0.01) at ~10 hours and ~40 min, which are a signal of Jovian particle emissions.

In Figure 4 we focus on the quasi-periodic modulation of the low energy ion data and in particular for the time interval of the P1/P2 Peaks # 5-10 of Figure 3, on days 349-351/2003. A quasi-periodic ~10 hour variation periodicity in flux ratio P1/P2 is evident in panel b, in particular in the three first flux increases in the period d. 349 / 00 UT – d.350 / ~12UT). Furthermore, in panel a, we have expanded the data for the first flux ratio P1/P2 increase (day 349/2003, 7:30-13:30 UT; Peak #5), in order to examine the nature of the striking variable fine structure of this particular event. Surprisingly enough, we see that there appears an approximately 40 min modulation (which is superimposed on the 10 hour periodic modulation of data shown in Fig. 4a).

In order to further check the periodicities of low energy ions of Fig. 4a-b we present in the right side of Figure 4 the results of harmonic analysis. In the bottom right panel (panel d) we display results for the time period examined in Fig.4a (d. 349, 00 UT – d. 351, 24 UT), and in the top panel we focus on a shorter time interval that includes the P1/P2 Peak #6. The results of the power spectrum analysis show frequency peaks at 10 hours and at 37 / 73 min (panels d and c, respectively), which are found to be significant at the levels $P = 0.01$ (error probability $P = 0.01$) [13]. The significant peaks are indicated by a solid triangle (Fig. 4c-d).

III. Summary of Observations - Discussion

We have documented measurements made by four different instruments (HI-SCALE, URAP, SWOOPS, VHM/FGM) onboard Ulysses between October 2003 – March 2004, during the spacecraft Distant Encounter of Jupiter (closest approach on February 5 at a distance / latitude R = 1683 R_J, θ = ~ 49^0N from Jupiter), while the outer heliosphere was unusually disturbed due to the Halloween events [8], [9]. In particular, we searched for the possible presence of characteristic Jovian periodicities in low energy ion and electron, magnetic field, radio and solar wind observations in a region far upstream from the north Jovian bow shock. As an example of our results, we present data with characteristic Jovian periodicities around a CIR observed by Ulysses on days ~ 349-350 / 2003, when Ulysses was at a distance of ~1894 R_J, from Jupiter and at high north latitudes of ~72^0 .

The most important findings for this period are the following: (1) Distinct ~10 hour separated increases were observed in phase in solar wind temperature T and density ρ ($\Delta T/T \approx 1–3$ and $\Delta\rho/\rho \approx 0.5–4$) throughout the CIR (Fig. 3h-i), (2) The low energy electron spectrum and the IMF direction were modulated with the period of the Jovian rotation (~10 hours) about two days prior to (d. 346-347/2003) arrival of the CIR at Ulysses, and this phenomenon was rather present during (d. 348-349/2003) and after the CIR passage (d. 350-351/2003) (3a) After the middle of the CIR (days 348 – 351) intensification of the quasi-periodic ~10 hour Jovian bKOM emission was observed, followed by a cessation of the bKOM and an onset of an nKOM event, (3b) After the end of the CIR, Jovian continuous nonthermal emission was detected, (4) Low energy ion flux increases and

softening of the spectrum were observed every ~10 hours within the CIR structure and more clearly after its passage (Fig. 3a-b) by Ulysses, (5) Examination of the fine structure of the low energy (>~50 keV) spectral data demonstrate clear ~40 min periodic variations (~41min and ~37 min in the two cases examined in Fig. 4a-c), which were found superimposed on the quasi-periodic ~10 hour spectral modulation both within and outside the CIR (days 349-351/03).

The above findings allow new important insights into the plasma and energetic particle processes taking place within the Jovian magnetosphere and in the "near" (0.8-1.2 AU from) Jupiter's outer heliosphere due to the observations made by Ulysses during the spacecraft Distant Jupiter Encounter, under extreme solar / heliospheric conditions (Halloween events).

In particular, the appearance of the characteristic jovian periodicities (~10 hours and ~40 min) in ion observations around times of passage of CIRs suggests that the north Jovian magnetosphere was a rich source of low energy ions and electrons at those times; this finding recalls the picture we obtained after Ulysses Jupiter flyby in 1992 for the radio and energetic particle emissions from the south high latitude magnetosphere. Relative studies have shown that the south high latitude magnetosphere was an important source for magnetosheath / upstream ion events ([3] and that the Jovian ~40 min periodic emissions were more frequently observed upstream from the Jovian bow shock, on the out-of ecliptic trajectory, than on the ecliptic trajectory [2]. Therefore, the out-of-ecliptic north (2003-2004)-south (1992) Ulysses observations suggest that there are in process similar acceleration-leakage processes of energetic particles in the south and the hemisphere of the Jovian magnetosphere.

The detection of the ~10 hour quasi-periodic low energy (40-100 keV) electron spectral modulation associated with magnetic field fluctuations (Point #2) extends our knowledge of Jovian electron emissions in the outer heliosphere to low energy electrons [5], and probably suggests that these low energy electrons disturbed the IMF and produced the (observed by Ulysses) ~10 hours period magnetic field waves in the outer heliosphere (A. Vinas; personal communication).

Finally, Points 2, 3, 4 and 5 suggest that the solar wind structures (CIRs) triggered the dynamic of the Jovian magnetosphere and caused, beside the well known radio bKOM, nKOM and continuous nonthermal [6], [7], the quasi-periodic acceleration / leakage of low energy ions and electrons and the striking ~10 hour quasi-periodic modulation of the upstream solar wind (Fig. 3h-i).

The time interval around the CIR on days 348-349, 2003 examined in Fig. 3 and 4 is a representative example of similar quasi-periodic (~10 hours, ~40 min) events found in the data obtained from the HI-SCALE, URAP and VHM/FGM data during Ulysses' Distant Jupiter Encounter. Quasi-periodic ~10 hour periodicities in HI-SCALE data were found for instance during the time intervals marked by the horizontal bars a-d in Fig. 2 (b corresponds to the event examined in Figures 3 and 4)

In the case of energetic ion observations, it seems that further acceleration of Jovian particles occurred at the Forward and the Reverse shocks of the CIRs and produced the enhanced flux of the shock-associated ion events. These observations suggest that Jupiter was an important source of the CIR associated ion structures at those times.

IV. CONCLUSIONS

Low energy ion flux and spectral modulation with Jupiter's rotation period (~10 hours) and the characteristic ~40 min Jovian periodicity were observed by Ulysses around times of passages of CIRs, as long as the spacecraft approached up distances of ~0.8-1.2 AU the Jovian magnetosphere on days 289/2003-90/2004. Quasi periodic ~10 hour modulations were also observed in low energy electrons, magnetic field direction and in solar wind parameters (temperature and density). We suggest that the Jovian magnetosphere was most probably the source of the low energy ion and electron quasi-periodic (~10 hours, ~40 min) modulations measured by Ulysses at distances 0.8 AU -1.2 AU northward of Jupiter, during the Halloween events. Further work is in progress to further confirm, combine and interpret the important solar wind, magnetic field and energetic particle quasi-periodic modulation (with characteristic Jovian periodicities) detected by Ulysses at that unusual time period.

ACKNOWLEDGMENT

We thank Drs R. MacDowall, D. McComas and A. Balogh, the P.I. of the URAP, SWOOPS and VHM/FGM instruments onboard Ulysses, for providing the data used for this study. The leading author (G.A) thanks Drs A. Balogh, A. Vinas, E. Roelof, D. McComas, D. Lario, and P. Preka for their helps during various stages of this study, and in particular Dr S. Krimigis for his hospitality and the helpful discussions at the Academy of Athens as well as for his comments on the manuscript. This study was supported by Program EPEAEK/Pythagoras-2004.

REFERENCES

[1] Anagnostopoulos, G. C., Marhavilas, P. K., Sarris, E. T., Karanikola, I., Balogh, A., Energetic ion populations and periodicities near Jupiter ,Journal of Geophysical Research, Vol. 103, Issue E9, 1998.

[2] Marhavilas, P.K. , Anagnostopoulos, G.C., Sarris, E.T., Periodic signals in Ulysses' energetic particle events upstream and downstream from the Jovian bow shock, *Planet. and Space Sci.*, Volume 49, 10, 2001.

[3] Karanikola, I., Athanasiou M., Anagnostopoulos G. C., Pavlos G. P., Preka-Papadema P., Quasi-Periodic Emissions (15-80 min) from the Poles of Jupiter as a Principal Source of the Large-Scale High-Latitude Magnetopause Boundary Layer of Energetic Particles, *Planet. Space Sci.,* 52, 543, 2004.

[4] Krimigis, S. M., E. T. Sarris, and T. P. Armstrong, Observations of Jovian electron events in the vicinity of Earth, *Geophys. Res. Lett., 2,* 561-564, 1975.

[5] Chenette, D.L., Conlon, T.F. and Simpson, J.A., Bursts of relativistic electrons from Jupiter observed in interplanetary space with the time variation of the planetary rotation period. *J. Geophys. Res*. 79, p. 3551, 1974.

[6] Conlon, T. F. and J. A. Simpson, Modulation of Jovian electron intensity in interplanetary space by corotating interaction regions, Astrophys. Jour., vol. 211, pt. 2, p. L45-L49,1977.

[7] Reiner, M., Kaiser M.L., Desch M.D., Long-term behaviour of Jovian bKOM and nKOM radio emission observed during the Ulysses-Jupiter encounter, *Geophys. Res. Lett.,* 27, 297, 2000.

[8] McKibben, R.B, Anglin, J.D., Connell, J. J., Dalla, S., Heber B., Kunow, H., Lopate, C., Marsden, R. G., Sanderson, T. R., and Zhang, M., Energetic particle observations from the Ulysses COSPIN instruments obtained during the October–November 2003 events, *J. Geophys. Res*., Vol.110, A09S19, 2005.

[9] Lario, D., Decker R. B., Livi S., Krimigis S. M., Roelof E. C., Russell C. T., Fry C. D., Heliospheric Energetic Particle Observations During the October-November 2003 Events, *J. Geophys. Res*., 110, A09S11, 10.1029/2004JA01094, 2005.

[10] Mason, G.M., R. von Steiger, et al., Balogh A., Gosling J.T., Jokipii J.R., Kallenbach R., and Kunow H. (Eds.), Origin, injection, and acceleration of CIR particles: Observations, in Corotating Interaction Regions, *Space Sci. Rev*., 89, 327, 1999.

[11] Lanzerotti et al., Measurements of hot plasmas in the magnetosphere of Jupiter, Planet. Space Sci., 41.893. 1993.

[12] MacDowall, R.J. et al. (2004), Radio (URAP) studies of Jupiter data from the Ulysses "Jupiter Distant Encounter", HI-ACALE Team Meeting Proceedings, APL/JHU, Laurel, MD.

[13] Shimshoni, M., On Fisher's test of significance in harmonic analysis, *Geophys. J. R. Soc*., 23, 373, 1971.

The unusual cosmic ray variations on July 2005 resulted from western and behind the limb solar activity

A.Papaioannou[1], A. Belov[2], H. Mavromichalaki[1], E. Eroshenko[2], V. Oleneva[2]

[1] *Nuclear and Particle Physics Section, Physics Department, Athens University Pan/polis15771 Athens, GR (atpapaio@phys.uoa.gr; emavromi@phys.uoa.gr)*

[2]*Institute of Terrestrial Magnetism, Ionosphere and Radio Wave Propagation by Pushkov, Russian Academy of Sciences IZMIRAN (abelov@izmiran.ru; erosh@izmiran.ru)*

Abstract – **One of the most interesting and unusual periods of the recent solar activity was July 2005. Despite the fact that this month was at the end of the 23rd solar cycle, it was a period of extreme activity. The main events of this occurred at the invisible side of the Sun and did not revealed significantly in the Earth or near the Earth consequences. However, cosmic ray variations testify high power of these events. A rather unusual Forbush effect was observed starting from July 16, 2005. It was characterized by very large cosmic ray anisotropy, the magnitude and direction of which are in accordance with a suggestion on a western powerful source. Usually in such a case when the main interplanetary disturbance is far on the west, the Forbush effect is absent or it is very small and short lasted. In July 2005 a rare exclusion was observed which may testify the giant (quite possible >=30%) decrease of 10 GV cosmic ray density to the west from the Sun-Earth line.**

In this work a description of the July 2005 situation as well as the results of the convection- diffusion treatment with space cosmic ray gradients is presented. Some general remarks concerning extreme western solar events and their impact on cosmic rays are also discussed.

Keywords – **Convection diffusion model, Forbush effects, Coronal Mass Ejections, Solar Flares**

I. INTRODUCTION

At the declining phase of the 23rd solar cycle, a number of extreme events characterized by rather peculiar properties have taken place, such as those of October-November 2003, January 2005, August-September 2005 and the recent ones of December 2006 [1], [2], [3]. Dynamic phenomena related to solar flares (SF) and coronal mass ejections (CMEs) dominated the heliosphere in a most profound way and resulted in large variations in cosmic ray (CR) intensity at least up to tens GeV energies. A number of attempts have been made in order to explore the relation between solar extreme phenomena and their impact on cosmic rays [4], [5], [6], [7], [3], [8]. It is commonly pointed out that solar extreme events influence cosmic rays in a dynamic way and different correlations can possibly be established between the cosmic ray variations and various characteristics of solar wind and interplanetary space [9]). On July 16, 2005 a deep decrease of the cosmic ray density (of about 8% for 10 GV particles) with a complicated shape and an intermediate large increase was recorded by neutron monitors during a non significant disturbance of the solar wind [10]. Right after the main phase of this Forbush effect (FE), a sharp enhancement of cosmic ray intensity starting from July 17, was registered only to be followed by a second decrease within less than 12 hours. The enhancement on July 17 was related neither to a ground level enhancement (GLE) nor to a geomagnetic effect. The analysis of this peculiar event shows that it could be connected with an internal structure of the disturbance similar to the event of March 1991 described by [11], but in our case it is not confirmed by solar wind data. Usually short - term cosmic ray variations are well correlated with solar wind changes near the Earth. During the events of July 2005 unusual CR variations were recorded and the most unusual fact was that these variations are not related with the changes in the solar wind.

In this work an extended analysis of these cosmic ray variations during the extreme events of July 2005 based mainly on the terms of anisotropy and space gradients of cosmic rays, is performed. The possibility to provide explanations on this kind of cosmic ray events is also being discussed.

II. DATA SELECTION

In this analysis the used data taken from the following web sites: http://sec.ts.astro.it/sec_ui.php on the solar and space conditions; http://www.ngdc.noaa.gov for solar flare data from and http://lasco-www.nrl.navy.mil for CME data.

In order to obtain variations in the flux and the first harmonic of anisotropy for 10 GV cosmic rays, data from as many stations as possible from the entire global network of neutron monitors (40 – 45 stations operating at present), with their own properties as coupling coefficients and yield functions, have been used. The calculation of the anisotropy components has been performed using the global survey method (GSM) (e.g. [3]).

III. SOLAR AND GEOMAGNETIC CONDITIONS

Solar activity: In the beginning of July, although several sunspot groups appeared on the face of the Sun, the main active region was the AR 786. It was the return of AR 775, a powerful active region (AR) from the previous rotation that caused long duration solar flares. Solar activity was dominated by AR 786 in the northern hemisphere, until it rotated over the west limb on July 14. In this period, this AR had produced 12 M-class and one X-class flares.

On July 12 there was a long duration M1.5 flare starting at 12:47 UT associated with a bright partial halo CME directed to the NW. In the next day, July 13, two bright CMEs occurred in association with two long-duration flares. The second CME was first seen in LASCO C2 images at 14:30 UT and had an estimated speed of 1420 km/s. The event triggered a gradual increase of the proton and electron fluxes, which reached to the value of 134 pfu on July 14 (http://www.ngdc.noaa.gov). On July 14two flares occurred: an M9.1 flare peaked at 07:25 UT and finally an X1.2 flare with long duration started at 10:16 UT. The high energy proton fluxes rose above the NOAA event threshold and a full halo CME was first visible in LASCO C2 at 10:54 UT and arrived at the Earth on July 17, as it is shown in Fig. 1.

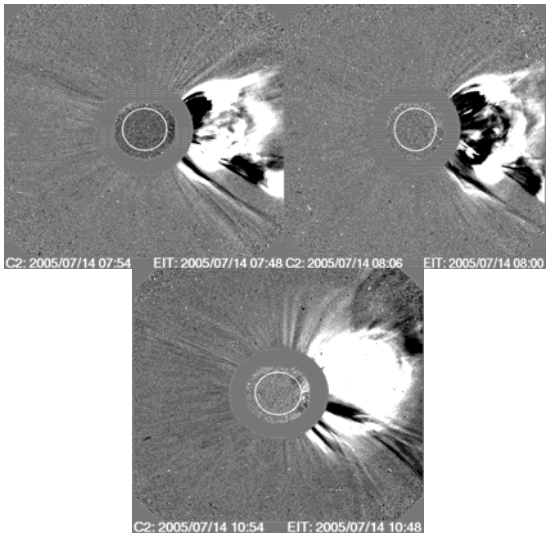

Fig. 1. The most significant CMEs on July 14, 2005 from AR 786 as seen by LASCO C2.

Geomagnetic activity. A minor geomagnetic storm occurred on July 13, probably due to the arrival of the partial halo CME from July 10 (C1.6 flare in AR 783). The solar wind speed was > 600 km/s (shock recorded at 04:24UT) and Bz component of the IMF (Interplanetary Magnetic Field) turned southward for a short period with a value of -5 nT. The geomagnetic activity then returned to the quiet - unsettled level, except of temporary active conditions recorded at some ground-based magnetometers on July 15 and 16. This weak geomagnetic activity may be a consequence of the partial halo CME originated on July 13 (~ M5.0 flare and the CMEs from early July 14, which erupted before the full halo CME related to the X1.2 flare. None of the blast waves were Earth directed, nevertheless, Earth's magnetic field was impacted by a weak shock that arrived at the Earth on July 17 at 1:23 UT. This caused mostly active conditions during July 17 (Dst=-74, Kp=5). Around 19:00 UT on July 17, the interplanetary magnetic field turned southward again to -10 nT. This immediately caused a major geomagnetic storm that persisted from late July 17 to around 12:00 UT of July 18.

IV. COSMIC RAY VARIATIONS

In the second decade of July 2005, heightened solar activity, especially in the western part of the solar disk, created a disturbed situation in the interplanetary space which was reflected in the CR behavior. The density of galactic cosmic rays started decreasing from July 10 after a series of relatively weak Forbush effects and by 16 July it had a decrease of ~2%. Most unusual events occurred on 16-17 July when the FD reached the value of 8% at high latitude neutron monitors within just a few hours. The CR intensity recovered

rapidly up to almost the pre-event level, but in the mid of July 17 a sharp CR decrease started again and reached the same amplitude of 8% at many neutron monitor stations. Finally it followed the classical FE recovery, as it is shown in Fig. 2 (Papaioannou et al., 2005)[10]. A disturbance in near Earth space at that time (V=500 km/s, H~ 10 nT, Bz was nearly -10 nT) could not provide such a magnitude of the FE. Usually a Forbush decrease hardly reaches ~2% under such modest parameters (Belov et al., 2001)[9]. The observed CR density behavior and especially CR anisotropy with an unusually big equatorial sunwards component along the field line at this time may be caused by other reasons (Belov et al., 2003)[12].

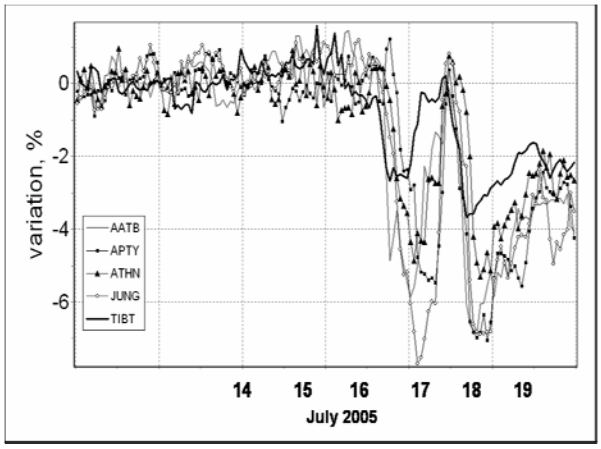

Fig. 2. Time profiles of the cosmic ray varisations observed on the Neutron Monitor stations: Alma-Ata B (aatb), Apatity (apty), Athens (athn), Jungfraugh (jung), Tibet (tibt). The curves are plotted in % relatively to the quiet period on July 14, 2005.

4.1 Cosmic Ray Anisotropy

The singularity of the events recorded on July 16-17, 2005 manifests itself in the size and temporal evolution of the CR density and anisotropy. The calculated equatorial component of the anisotropy A_{xy} is presented by a series of coupled vectors in Fig. 3. Thin lines connect the equal time points corresponding to the vector and CR density diagram. Vertical vectors along the density curve present the magnitude and direction of north-south anisotropy A_z (Chen and Bieber, 1993)[13]. As can be seen in Fig. 3, the north-south anisotropy A_z increases significantly, up to ~4% within the declining phase of the FE on July 16 to 17, and changes its direction from positive to negative in the mid of July 17. The equatorial component of anisotropy was abnormally big, A_{xy} increased up to >5%. All components of anisotropy reveal sharp and big changes on the background of more or less quiescent interplanetary and geomagnetic conditions (IMF~10-15 nT, Dst=-74, Kp=5+). We have analyzed all events in our database which occurred under Kp=5+ (377 events during 45-years of observation). The averaged magnitude of the Forbush effects (FE) over these events was found to be 1.57 %, the mean equatorial and the A_z components were correspondingly 1.44% and 1.55%. On this background the event on July, 16-17 looks outstanding as well as the number of other events (~10-15) recorded under similar geomagnetic conditions (Kp=5+).

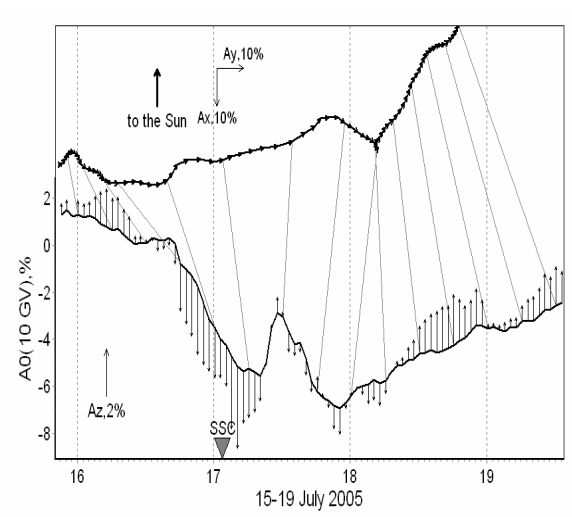

Fig. 3. The CR density (A0) temporal variations on July 15-19, 2005. The vector diagram presents the equatorial component (A_{xy}) of CR anisotropy, while the vertical vectors along the density curve present the north-south component of anisotropy (A_z). Thin lines connect the equal time moments on the density curve and vector diagram. Triangle (SSC) marks the time of Sudden Storm Commencement (the time of shock arrival at Earth).

The anisotropy shows more singularity than the hourly rate of CR decrease (hourly decrement) during the main phase of FE. Such great anisotropy is usually being observed within the largest Forbush effects with high magnitude of decrease where the CR intensity goes down on 15-25% (for example, events in August 1972, February 1978, October 2003). The maximum equatorial anisotropy for about 6000 analyzed FEs plotted versus the maximum rate of CR decrease during those events is illustrated in Fig. 4. This statistical presentation shows that the point corresponding to July 17, 2005, with a relatively low decrease rate (decrement <1%/hour) is located much above the averaged regression curve because of the very high anisotropy in this event. In a vicinity of this point we have a group of events incorporated by attributes similar to the event on July 17, which is a basis for further study. Singularity of the anisotropy in this event is also emphasized by the dependence of the equatorial component on the magnitude of IMF which is presented in Fig. 5. According to the

regression dependence with an IMF intensity of about 15 nT the maximum averaged equatorial anisotropy should be ranged within 0.5-2.6%, whereas, in our case, it was >5%. Again, we see a group of points around July 17 (not numerous) which appear to have the common properties. A great anisotropy was observed even before the arrival of the shock at the Earth.

All aforesaid testifies that it is difficult to explain the properties of the anisotropy and CR variation by local parameters of the interplanetary space near the Earth. Here it is necessary to recollect events which were observed at the western limb.

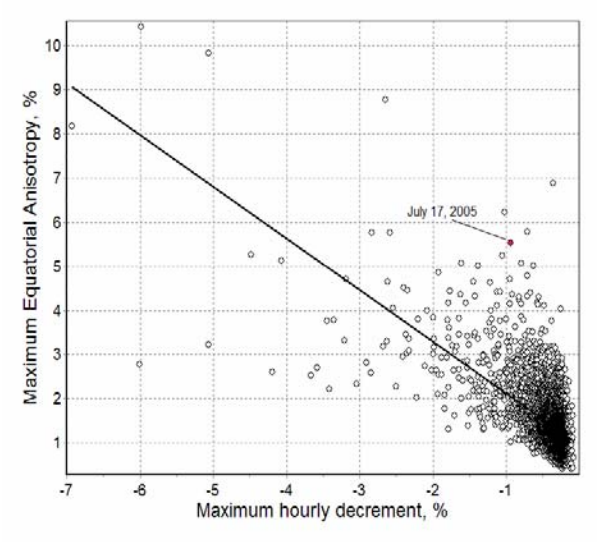

Fig. 4. Maximum equatorial component of CR anisotropy (Axy) versus
maximum hourly decrement for FEs over 45-years of observation
(~6000 events).

As it is known, powerful X-ray western (limb) flares on July 14 (M9.1 and X1.2) in the AR 10786 were followed by CMEs with a full asymmetric halo, and CME from X1.2 flare is profoundly affected by the CME event associated to the M9.1 X-ray flare. The shock which has arrived at Earth on July 17 at 1:34UT is apparently connected with these ejections. This assumption leads to the mean transit velocity of 1430 km/s that corresponds to the initial speed of CME (~2280 km/s), as by it was observed LASCO/EIT.

It is not improbable that such a disturbance might have caused a gigantic Forbush effect in the western part of the inner heliosphere, and Earth crossed its periphery area on the beginning of July 17. The big equatorial component of CR anisotropy at this time is an evidence of intensive inflow of particle flux from the eastern direction that provided fast recovery of the FD. On the other hand, LASCO/EIT observed also this day an asymmetric Full Halo Event started at 11:30 UT as a very strong brightening above the NW limb associated to a flare behind the limb from the same AR 786. By 11:54 UT, faint loop-like extensions can be seen all above the Sun's South Pole. The velocity of this "backside" event was 1300 km/s. Directly from this moment the new sharp decrease of CR intensity started on the background of very high anisotropy, and this coincidence in time seems to be not occasional but caused by a change in the conditions for particle propagation.

4.2 Cosmic Ray Gradients

It is clear that CR anisotropy is responsible for the space gradient. A treatment of CR with the convection-diffusion model (CDM) to the events on July 2005 has been performed in order to obtain CR gradient and its components. The model proposed by Krymsky (1964)[14] was developed at several works [15], [16], [13]. Despite the fact that a lot of other models concerning cosmic rays appeared through the years, the convection-diffusion model still remains the most basic one and is valid to a degree sufficient for this analysis.

Using a simple approach by solving an inverse problem in Belov et al. (1987), the three components of the CR space gradient, g_x, g_y, g_z are given by the following equations:

$$g_x = \frac{1}{\rho}[-\sqrt{\kappa}(A_x - A_c) - \sin\psi\sqrt{1-\kappa}] \quad \text{(1a)}$$

$$g_y = \frac{1}{\rho}[-\sqrt{\kappa}A_y + \cos\psi\sqrt{1-\kappa}A_z] \quad \text{(1b)}$$

$$g_z = \frac{1}{\rho}[\sin\psi\sqrt{1-\kappa}(A_x - A_c) - \cos\psi\sqrt{1-\kappa}A_y - \sqrt{\kappa}A_z] \quad \text{(1c)}$$

Where Ax, Ay and Az are the three components of anisotropy in the coordinate system related to the IMF field line (OX and OY are in the ecliptic plane, herewith OX is directed along the IMF force line); ψ is the angle between IMF direction $\vec{H}$ and solar wind velocity $\vec{u}$; ρ is the particle's hyroradius in the total IMF; k is a degree of the IMF irregularity.

The calculated g_x, g_y have been used to obtain ecliptic component (G_E) of CR space gradient which is plotted in Fig.6 together with the IMF intensity (upper panel). Periods of strong IMF and large values of CR gradient are seen on the days 1-2, 9-12, 19-21 and 27-29 of July (on July 16-17 we see very large gradient, but not strong IMF). Usually the biggest CR gradient is observed together with the increasing of IMF intensity because of additional CR modulation produced

within the regions with strengthened IMF (Forbush effect). Besides, the strengthened field is able to separate regions of different CR density. In July the strongest IMF intensity (up to 25 nT) was on July 10 and the magnitude of G_E in this day exceeded the value of 50%/AU.

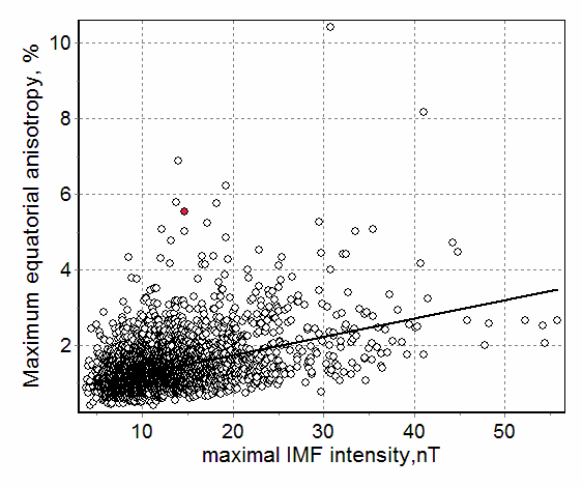

Fig. 5. Maximum equatorial anisotropy versus maximum IMF intensity
(hourly values) by events over ~45 years observation. The red point
references to July, 17, 2005.

However, the biggest gradient was not observed during this day, but on July 16-17. It exceeded 150%, when the IMF intensity was nearly 10 nT. There are many days in July with approximately the same or even higher IMF intensity, but the magnitude of G_E those days was many times less than that on 16-17 July. In the lower panel of this figure a relation between the IMF intensity (B) and the magnitude of G_E is presented. In general a good correlation between these two parameters is observed, but there are also some evidently outstanding points, all of them being related to 16-17 July. This is one more evidence of the unusual situation on July 16-17, when an anomalously large gradient of cosmic rays was produced not by disturbances of interplanetary space near Earth but by other, remote from the Earth, solar wind disturbances.

V. CONCLUSIONS

The solar activity burst in July 2005 was distinguished by the main events occurred near the western limb and at the invisible side of the Sun. Great disturbances of the solar wind comparable with those observed earlier in the last solar cycle – in 2000, 2001 and 2003 have not arrived to the Earth and there was no severe magnetic storm recorded at the Earth. On this background the CR variations look more interesting and unusual, especially on 16-17 July. A set of peculiarities in the behavior of CR density and anisotropy contradicts an explanation of this behavior by variations in parameters of near Earth interplanetary medium. The main reason of the large and unusual Forbush effect on July 16-17 has apparently to be searched near the western limb of the Sun where, starting from July 14, under interferential influence of several CMEs a giant and complicated decrease of galactic CR was created.

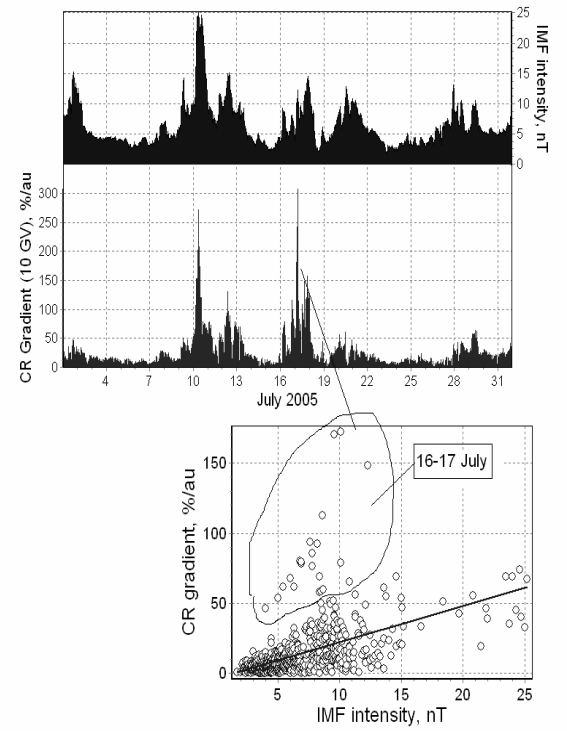

Fig.6. Hourly means of the IMF intensity (upper panel) and of the ecliptic component G_E of the CR gradient for 10 GV particles derived from data on CR anisotropy by means of the convective-diffusive model (middle panel) in July 2005. The CR gradient versus IMF intensity by events in July 2005 is given in the lower panel.

A discrepancy between the Forbush decrease magnitude and the parameters of near Earth disturbance of solar wind is being observed from time to time and such events have been studied earlier [17], [18], [12]. Usually such events are caused by remote ea stern solar sources. But in July 2005 we encountered with another type of inconsistency related to remote but western source. Such events differ from the events of eastern origin by greater anisotropy. They occur significantly rarer, however, as a retrospective analysis shows, they consist a definite sub-class of Forbush effects. Analysis of such events testifies that the CR variations are able to give us the information on sufficiently remote heliospheric phenomena. Such events are worthy the special attention and individual studying

ACKNOWLEDGMENT

The authors thank all collaborators providing continuous ground level monitoring of cosmic rays and researchers providing satellite data via internet. Thanks are due to all our colleagues from the neutron monitor stations, who kindly provided us with the data used in this analysis: Alma Ata, Apatity, Athens, Baksan, Barentsburg, Cape Schmidt, Fort Smith, Hermanus, Inuvik, Irkutsk-1,2,3, Jungfraujoch, Jungfraujoch-1, Kerguelen, Kingston, Kiel, Larc, Lomnicky Stit, Magadan, Mawson, McMurdo, Moscow, Nain, Norilsk, Novosibirsk, Oulu, Potchefstroom, Peawanuck, Rome, Sanae, San Tiago, Terre Adelie , Thule, Tsumeb, Tixie Bay and Yakutsk. This work was supported partly by Greek grant PYTHAGORAS II which is funded by European Social funds and National recourses and Russian Foundation for Basic Research (RFBR grants 07-02-00915, 07-02-13525, 06-02-39028 and Program BR of the Presidium RAS "Neutrino Physics". Thanks for stations see also in http://cr0.izmiran.rssi.ru/ThankYou/main.htm.

REFERENCES

[1] Eroshenko, E., Belov, A., Mavromichalaki, H., Mariatos G., Oleneva, V., Plainaki, C., Yanke, V. Cosmic ray variations during the two great bursts of solar activity in the 23rd solar cycle. Solar Physics, 224, 345-358, 2004

[2] Plainaki C, Belov A., Eroshenko E., Mavromichalaki H., Yanke V. Modeling ground level enhancements: The event of 20 January 2005, J. Geophys. Res, 112, A04102, doi:10.1029/2006JA011926, 2007

[3] Belov A., Baisultanova L., Eroshenko E., Mavromichalaki H., Yanke V. Pchelkin V, Plainaki C., Mariatos G. Magnetospheric effects in cosmic rays during the unique magnetic storm on November 2003, J. Geophys. Res. 110, A09S20, doi:10.1029/2005JA011067, 2005

[4] Harrison, R.A The nature of solar-flares associated with coronal mass ejection, Astron. and Astrophys. 304, 585 - 594, 1995

[5] Hundhausen, A.J. Coronal mass Ejections, in K.T. Strong, J.L. Saba, B. H. Haisch and J.T. Schmelz, (eds.), The many faces of the Sun: A Summary of the results from NASA's Solar Maximum Mission, Springer, New York, 143, 1999

[6] Cane, H. V.: Coronal Mass Ejections and Forbush Decreases, Space Science Rev. 93, 55-77, 2000

[7] Kudela, K. and Brenkus R. Cosmic ray decreases and geomagnetic activity: List of events 1982-2002, J. Atm. and Solar-Terrestrial Physics, 66, 1121-1126, 2004

[8] Mavromichalaki H., Papaioannou A., Mariatos G., Papahliou M., Belov A., Eroshenko E., Yanke V. and Stassinopoulos E.G. Cosmic ray radiation effects on space environment associated to intense solar and geomagnetic activity, IEEE TNS, 54, 1089, 2007

[9] Belov A.V., E. A. Eroshenko, V.A. Oleneva, A.B., A.B. Struminsky, and V.G. Yanke: What determines the magnitude of Forbush decreases? JASR, 27, 625-630, 2001.

[10] Papaioannou A., Gerontidou M., Mariatos G., Mavromichalaki H., Plainaki C. Unusually extreme cosmic ray events in July 2005, 2-nd ESA SWW (14-18 November 2005) Holland http://esa-spaceweather.net/spweather/workshops/eswwII/

[11] Hofer M. and Flueckiger E. O. Cosmic Ray Spectral variations and anisotropy near Earth during the March 24, 1991 Forbush decrease, J. Geophys. Res., 105, 23085-23097, 2000

[12] Belov A. V., Butikofer R., Eroshenko E. A., Fluekiger E. O., Oleneva V. A., Yanke V.G. Interplanetary magnetic field disturbances with particularly large cosmic ray modulation efficiency, *Proc. 28-th ICRC*, 6, 3581-3585, 2003.

[13] Chen J. & Bieber W. J. Cosmic ray anisotropies and gradients in three dimensions, The Astrophys. Journal 405, 375-389, 1993

[14] Krymsky G.F. Diffusion mechanism of the diurnal cosmic ray variation, Geomagn. and Aeronomy, 4, 977-986, 1964 (in Russian)

[15] Forman, M. A. and Gleeson, L. J. : Cosmic Ray streaming and Anisotropies, Astrophys. and Space Sci., 32, 77-94, 1975

[16] Belov A. V. The First Harmonic of Cosmic Ray Anisotropy in the Convection-Diffusion Model, Proc. 20th ICRC, 4, 119-123, 1987

[17] Iucci, N., Parisi, M., Storini, M., Villoresi, G., Pinter, S. Longitudinal dependence of the interplanetary perturbation produced by energetic type 4 solar flares and of the associated cosmic ray modulation. 19th ICRC, 5, 234-237, 1985.

[18] Iucci, N., Pinter, S., Parisi, M., Storini, M. Villoresi, G. The longitudinal Asymmetry on the interplanetary perturbation producing Forbush decreases. Nuovo Cimento, 9C, 39-50, 1986.

Poster Session B

Energetic Processes on the Sun during extreme events, solar events at solar minimum

Chair: G. Maris

Solar **E**xtreme **E**vents **2007**

Interplanetary and solar aspects of two – component concept for ground level enhancements of solar cosmic rays

L.I. Miroshnichenko[1, 2], E.V. Vashenyuk[3], J. Perez-Peraza[1], Yu.V. Balabin[3], A. Gallegos-Cruz[4]

[1]*Instituto de Geofisica, Universidad Nacional Autonoma de Mexico, D.F., Mexico (leonty@geofisica.unam.mx; leonty@izmiran.ru)*
[2]*N.V. Pushkov Institute IZMIRAN, RAS, Moscow Region, Troitsk, Russia*
[3]*Polar Geophysical Institute, Murmansk region, Russia*
[4] *UPIICSA, I.P.N., Depto. de Ciencias Basicas, Mexico, D.F., Mexico*

Abstract – **We summarize our results obtained earlier for a number of Ground Level Enhancements (GLEs) of solar cosmic rays (SCR) that have demonstrated distinctly two-component structure of relativistic solar proton (RSP) populations, namely, Prompt and Delayed ones (PC and DC). Observationally, PC and DC differ from each other by the form of time profiles (pulse-like and gradual ones), pitch-angle distributions (PAD) (anisotropic and isotropic ones) and spectrum rigidity, namely, by hard (flat) and soft (steep) spectra, respectively. In particular, at the GLE onset the PC is extremely anisotropic. The particles of PC are presumably accelerated in the processes of magnetic reconnection in the low corona, in close association with H-alpha eruption, onset of CME and type II radio emission. Theoretically, in terms of the SCR propagation theory, the DC may be treated as a result of transformation of the PC in the process of interplanetary propagation (SCR scattering at the irregularities of IMF). On the other hand, particles of DC may be accelerated in the low corona and then carried out to the outer corona by an expanding CME. In general, the underlying physical circumstances leading to the initial spikes and two-peak structures in some GLEs are not presently well understood. Taking into account our modeling results, we do not believe, however, that above hypothesis of "an interplanetary origin" of the features mentioned can resolve alone the problem of relativistic proton events. There are some grounds to accept a two-source model of SCR generation itself at/near the Sun, in the frame of the concept of multiple acceleration processes in the solar atmosphere.**

Two-component features of the two largest GLEs: 23 February 1956 and 20 January 2005

E.V. Vashenyuk [1], L.I. Miroshnichenko [2, 3], J. Perez-Peraza [3],
Yu.V. Balabin [1], A. Gallegos-Cruz [4]

[1] *Instituto de Geofusica, Universidad Nacional Autonoma de Mexico, D.F., Mexico*
[2] *N.V. Pushkov Institute IZMIRAN, RAS, Moscow Region, Troitsk, Russia*
(leonty@geofisica.unam.mx; leonty@izmiran.ru)
[3] *Polar Geophysical Institute, RAS, Apatity, Murmansk Region, Russia*
[4] *UPIICSA, I.P.N., Depto. de Ciencias Basicas,, Mexico D.F., Mexico*

Abstract – **The comparative analysis of the characteristics of relativistic solar cosmic rays (SCR) in the two largest Ground Level Enhancements (GLEs), of 23rd February 1956 and 20th January 2005, has been performed. The parameters of relativistic solar protons (RSP) were obtained from ground-based observations on neutron monitors and muon detectors by a modeling technique. It included: a) calculation of asymptotic cones of ground-based detectors; b) modeling of cosmic ray detector responses at variable parameters of solar proton flux; c) determination by a least square procedure of primary solar proton parameters by comparison of computed responses with the observations. The two particle populations (components), the prompt (PC) with high anisotropy and exponential energetic spectrum and delayed one (DC) with moderate anisotropy and power law energetic spectrum, were shown to exist in both cases. The prompt component was a cause of a giant impulse increase at a limited number of NM stations; the DC formed a gradual increase with moderate amplitude at the most NM stations over the globe. It is argued that only exponential energetic spectrum (not power-law) in aggregate with specific yield function energetic dependence could cause such great increase effect (~5000%) in both cases. Selected two GLEs provide a bright demonstration of existence of two separate RSP sources at/near the Sun. The interplanetary propagation, in itself, is not capable to create such different properties of two populations of relativistic solar particles.**

The largest in history GLEs January 20, 2005 and February 23, 1956. Comparative modeling study

E.V. Vashenyuk[1], Y.V. Balabin[1], B.B. Gvozdevsky[1], L.I. Miroshnichenko[2, 3]

[1]Polar Geophysical Institute, Murmansk region, Russia
(vashenyuk@pgi.kolasc.net.ru)
[2] N.V. Pushkov Institute IZMIRAN, RAS, Moscow Region, Troitsk, Russia
[3] Polar Geophysical Institute, RAS, Apatity, Murmansk Region, Russia

Abstract – **Comparative analysis of the characteristics of relativistic solar cosmic rays (SCR) in the two largest GLEs of February, 23 1956 and January 20, 2005 has been performed. Both events have taken place near to a solar minimum: GLE 23.02.1956 on a rise and the GLE 20.01.2006 on a decay phases of solar cycle respectively. Using a modeling technique, the parameters of relativistic solar protons (RSP) were obtained from ground-based observations by neutron monitors (NM) and muon detectors. The two particle populations (components), prompt (PC) with high anisotropy and exponential energy spectrum and delayed one (DC) with moderate anisotropy and power-law spectrum, were shown to exist in both cases. The prompt component was a cause of a giant pulse-like increase at a limited number of NM stations, and the DC caused a gradual increase with moderate amplitude at the most NM stations over the globe. It is argued that only exponential energy spectrum (but not power-law one), in combination with energy dependence of the NM specific yield functions, could cause such great increase effect (~5000%) in both events.**

Special type of the magnetic and auroral activity produced by sudden commencement of the extreme magnetic storms

L.L. Lazutin, S.N. Kuznetsov

Space Physics Division Moscow State University,
Scobeltsyn Institute for Nuclear Physics, Moscow, Russia
(lll@srd.sinp.msu.ru)

Abstract – **Sudden Commencements of several strong magnetic storms were accompanied by unusual magnetic and auroral activity. Magnetic bays grow in several minutes to 400-2000nT simultaneously in a wide longitudinal sector from midnight to early morning. Although such events were usually identified as a special type of the magnetosperic substorm, a supersubstorm, there are strong reasons to state that it is not a substorm at all. Isolated substorms or complicated substorm activity include two basical processes: gradual accumulation of the energy inside the magnetosphere (growth phase) and explosive instabilities releasing the energy during localized auroral breakup and following activations during expansion phase. During analyzed events which we named as a sudden auroral activations (SA), growth phase was absent, energy are not accumulated but supplied by solar wind SC pulse instantly. Also there are simultaneous activation in a wide area instead of the localized activation. We analyzed 5 SA events and come to the conclusion that the main process which accelerates auroral particles with following precipitation into the ionosphere was a ExB radial injection, the process which is rather common in the magnetosphere but usually more gradual and less powerful.**

Solar sources of the rapid solar wind during the descendant and minimum phases of solar cycles

G. Maris[1], O. Maris[2]

[1]*Institute of Geodynamics, Bucharest, Romania*
(gmaris@geodin.ro)
[2]*Institute for Space Sciences, Bucharest, Romania*

Abstract – **During each solar cycle, just after its maximum, the polar magnetic reversal takes place; this process might take some months or even 1-2 years. After it has been finished, a new magnetic dipol is born under the solar surface, belonging to the next solar cycle. This is why, during the descendant phase of a solar cycle, some complex interactions between the old and new dipols could occur and, consequently, extreme solar events are registered. The paper analyses the dynamics of the High-Speed Streams (HSSs) in solar wind during the descendant and minimum phases of the solar cycles nos. 20-23 taking into account the stream parameters: the duration, maximum velocity, velocity gradient and importance. We use the well-known HSS catalogs (Lindblad and Lundstedt: 1981, 1983, 1989; Mavromichalaki et al.: 1988, 1998) for solar cycles 20-22 (1964-1996) as well as a new catalog for solar cycle 23 (1996-2006, Maris & Maris, 2007). Obvious differences in the HSS dynamics in respect to their solar origin (flares or coronal holes) have been established. A special analysis of the extreme solar events of 2005 and 2006 and their consequences in solar wind dynamics is made. The HSSs registered in 2005 and 2006 are analysed in comparison with the HSS registered during the corresponding phases of the previous solar cycles.**

Observations of high-energy gamma radiation onboard the CORONAS-F satellite as an indicator of proton acceleration during solar flares

S.N. Kuznetsov[1], V.G. Kurt[1], B.Yu. Yushkov[1], K. Kudela[2]

[1]*Skobeltsyn Institute of Nuclear Physics, Moscow State University, Moscow, Russia (clef@srd.sinp.msu.ru)*
[2]*Institute of Experimental Physics, Slovak Academia of Science, Kosice, Slovakia*

Abstract – **Solar flare gamma radiation with energies > 0.5 MeV is the direct indicator of accelerated proton appearance in the corona. Protons with energies 10-30 MeV generate gamma-line radiation of excited nuclei as well as the neutron capture line 2.2 MeV. Protons accelerated up to at least 300 MeV generate the high-energy gamma radiation as a result of neutral pion decay. This radiation is characterized by wide spectral maximum about 70 MeV and is originated in density matter of the flare volume. The SONG instrument onboard the CORONAS-F detected high-energy gamma radiation produced by several major solar flares at 2001-2005. In flares of 28 October 2003 and 20 January 2005 we determined exact moments of the pion decay radiation and hence of high-energy proton appearance at the Sun. Comparison of the proton acceleration time in the flare with the onset time of following GLE permits to make a conclusion that any delay between the proton acceleration and their escaping is absent.**

An Interpretation of Rapid Changes in the Magnetic Field associated with Solar Flares

I. V. Oreshina, B. V. Somov

Sternberg Astronomical Institute, Moscow State University, Russia
(ivo@sai.msu.ru)

Abstract – **A topological model of the magnetic field is used here for interpreting the recently discovered drastic changes in magnetic field associated with solar flares. The following observational results are self-consistently explained: (1) the transverse field strength decreases at outer part of active regions and increases significantly in their centres; (2) the center-of-mass positions of opposite magnetic polarities converge towards the magnetic neutral line just after flares onset; (3) the magnetic flux of active regions decreases steadily during the course of flares. For X-class flares, almost 50% events show such changes.**

A comparison of Solar Energetic Events of 2005 and 2006 and their differing Geoeffectiveness

A. Radharani[1], G. Rajaram[1], J.B.Ankush [1], J. Rathod [1], D.S. Misra[1], C.G.Patil[2], M.Y.S.Prasad[3]

[1]Indian Institute of Technology-Bombay, India
(radha.alyana@gmail.com)
[2] MCF-ISRO, India
[3]SITAA-SAC, ISRO, India

Abstract **– Years 2005 and 2006 lie on the declining phase of solar cycle 23. The next solar cycle will begin somewhere between March and September 2007. As part of our work we have studied the Solar Energetic Events (SEE) and associated Space weather changes at the dayside Lagrangian point (L1), Geostationary orbit (GSO) and at Earth for these two years. In this paper we highlight the differences between solar wind velocity (Vsw), solar wind density (Nsw), solar wind dynamic pressure (Psw), the interplanetary B and its components, 2 MeV electron flux (Ne) at GSO, geomagnetic index Kp, Cosmic ray neutron monitor (CRNM) count monitored at Earth. All Space Weather show a marked difference between 2005 and 2006. The year 2005 is seems to be far more active than 2006, with 8-10 Solar Energetic Proton (SEP). Events having occurred; in contrast there is only 1 major SEP event in 2006. Comparative values of Vsw between 2005 and 2006 are: above 700 km/s in 2005 and with around 600 km/s in 2006. The peak Psw touches 100 nPa in 2005 but does not even crosses 20 nPa in 2006. Similar differences are seen in the IMF (Bavg and its components), the 2Mev Ne flux at GSO, Kp index and the CRNM count at Earth.**

Transformation and transport of sub-photospheric energy into the corona during solar extreme events in December 2006

V.I.Sidorov, M.Yu.Savinkin, S.A.Yazev

Astronomical Observatory of Irkutsk State University, Russia
(uustar@star.isu.ru)

Abstract – **SOHO magnetograms have been used to analyze the evolution of the magnetic field (MF) in a unique complex of activity (CA) that included the long-lived (at least 4 solar rotations) central sunspot and opposite-polarity elements surrounding it. The analysis revealed an annular zone of emergence of a nonpotential MF into the corona which surrounded the sunspot umbra. The "annihilation" effect of opposite-polarity magnetic elements at the photospheric level has been interpreted as a change in the cross-section of emergent helical magnetic loops accelerated at the inner and outer boundary of the annular zone. We reconstructed the topology of the subphotospheric MF consisting of the central quasi-radial "trunk" of like polarity with weak spiral twisting of MF lines of the quasi-cylindrical envelope surrounding the "trunk" and consisting of different-scale loops with complicated structure ("crown"). We examined the mechanism of sequential transformation of energy: energy of kinematic motion of plasma inside the quasi-cylindrical envelope; non potential energy of the MF inside it; emergence of non potential energy into the corona in the annular zone; accumulation of this energy in the corona; release of accumulated energy in a series of extreme solar events. In this scheme, the emergent MF is an "elevator" for the energy trapped during its movement. The MF of such a CA may be thought of as being a natural "probe" for diagnostics of deep-seated regions of the Sun, as deep as the "bottom" of the convection zone.**

The observation of gamma-ray emission during January 20 2005 solar flare

I. V. Arkhangelskaja, A. I. Arkhangelsky, Y.D. Kotov, , P.A. Kalmykov, A.S. Glyanenko

Astrophysics Institute of Moscow Engineering Physics Institute (State University), 115409, Kashirskoe shosse, 31, Moscow,Russia

***Abstract* – The solar flare of 20.01.2005 (class X7.1) was the biggest one in January 2005 series. It was started at 06:36 UT, ended at 07:26 UT and the maximum of X-ray emission was at 07:01 UT by GOES data. AVS-F apparatus onboard CORONAS-F registered gamma-emission during rising phase of this flare in two energy bands: 0.1-20 MeV and 2-140 MeV. The highest gamma-ray energy was registered during this flare was ~140 MeV. Nuclear lines, positron line, neutrons capture line and spectral feature caused by neutral pions decay were observed in this flare energy spectrum. Also some spectral peculiarities were first observed in the region of 15-21 MeV in time interval of 06:44:52-06:51:16 UT. The possibilities of this feature treatment are discussed.**

***Key Words*— solar flares high energy spectra, solar flares high energy gamma-emission.**

I. Introduction

The observation of the gamma-emission from solar flares gives information about accelerated particles processes and spectrum, ambient media abundance of elements, density, temperature and other properties of surrounding media and so on. Solar flares X-ray and gamma-emission were investigated by various instruments such as GOES, RHESSI, TRACE and other. But only AVS-F apparatus allows obtaining energy spectra in the hard gamma-band with channel width $\Delta N \sim 1$MeV at E_γ up to 30 MeV and $\Delta N \sim 10$ MeV at E_γ~200 MeV and study so high energy spectra in details.

II. Discrimination of n/γ events in AVS-F apparatus

AVS-F (amplitude-time Sun spectrometry) apparatus [1, 2] was installed onboard CORONAS-F satellite (NORAD catalog number 26873, ID 2001-032A). It operated from July 31 2001 to December 6 2005. The orbit of satellite was approximately circular oriented towards the Sun with inclination 82.5° and altitude ~500 km. Gamma-rays were registered by AVS-F in two energy bands by CsI(Tl)-based SONG-D detector ∅20cm and height of 10 cm [3]. The energy bands limits (energy deposition ranges of 0.1-11.0 MeV and 4.0-94.0 MeV by first time calibration data) are shifted during apparatus operation: the energy

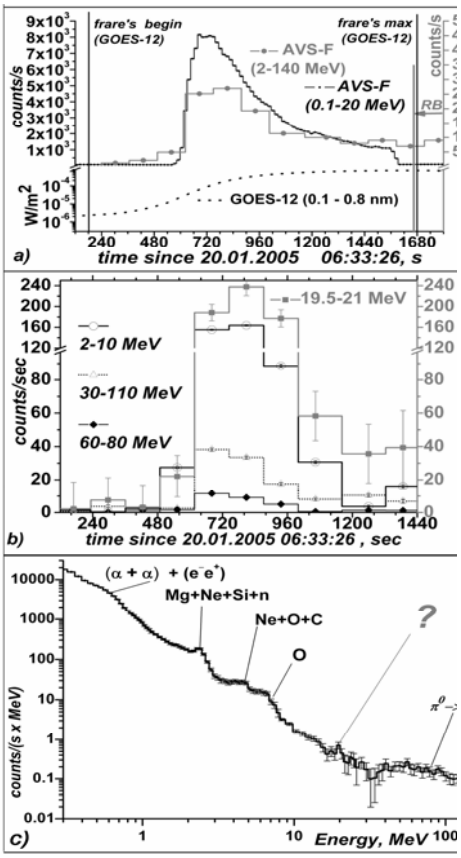

Fig. 1. Solar flares January 20 2005 temporal profiles in by GOES data and in low and high energy γ-bands by AVS-F data (a), ones in different regions of AVS-F high-energy γ-band (b) and two-bands energy spectrum in time interval 06:44:52-06:51:16 UT by AVS-F data (c).

threshold and amplification coefficient of low-energy band changed on 1% and 1.8% per month correspondingly and on January 2005 the low-energy band boundaries were 0.1-20 MeV and high-energy ones were approximately 2-260 MeV [2].

The γ-ray and neutron events discrimination was performed using the selection of events by the scintillation detector light pulse shape based on the dependence of the ratio of intensities of light-output components with different fluorescence decay times to the average ionization density produced by charged particles in the detector material [4]. A scintillation flash in CsI(Tl) consists of two main fluorescence components with decay times $\tau_{fast}\approx$0.5-0.7 μs and $\tau_{slow}\approx$7 μs, and the ratio of the slow component intensity Q_{slow} to the fast component intensity Q_{fast} depends on the interacting particles specific ionization. The method employed in AVS-F instrument is based on the integration of the signal from the SONG-D photomultiplier's preamplifier in two time intervals in which the total charge $Q_{tot}= Q_{slow}+ Q_{fast}$ and slow fluorescence component Q_{slow} were collected. Values of Q_{tot} and Q_{slow}/Q_{tot} for each recorded event were digitized by two 8-bit analog-to-digital converters and transferred as two-dimensional matrix to the system microprocessor controller for subsequent processing. The system energy resolution was 13.0% for γ-quanta from ^{137}Cs (Eγ=0.662 MeV) by ground testing data. The integration time is 16 s in low energy γ-band and 128 s in high energy one for all presented temporal profiles on AVS-F data [1, 2].

III. The Characteristics of January 20 2005 Solar Flare by AVS-F Apparatus

January 20 solar flare was started at 06:36 UT by GOES data and ended at 07:26 UT. Its maximum in energy band 0.1-8 nm was registered at 07:01 UT. It was the most powerful during January 2005 solar flares series – see, for example [5]. Particle event and related this flare GLE#69 were the most intensive ones for period of the last 29 years and since 1956 correspondingly [6]. Also January 20 flare was accompanied by the coronal mass ejection. Active region NOAA 10720 (N14W61) was the source of this flare. Gamma-emission of January 20 flare in energy bands of 0.1-20 MeV and 2-260 MeV was observed by AVS-F apparatus during X-ray emission rise by GOES data. The highest γ-ray energy was registered during this flare was 137±4 MeV. It was not observed statistical significance excess above background level in energy band 141-260 MeV. The count rate in low- and high-energy γ-bands droops to background level before maximum of X-ray emission by GOES data. January 20 flare's temporal profiles shape in wide γ-energy bands is very simple with one maximum and one in X-ray band by GOES data has one maximum too – see Figure 1a. Two bands energy spectrum of January 20 solar flare in time interval 06:44:52-06:51:16 UT by AVS-F data is shown at Figure 1c. Six spectral features were separated at this spectrum and 5 of them are typical for solar flares: nuclear, annihilation, neutron capture at ^{1}H lines and spectral feature caused by neutral pions decay. Spectral feature in the region of 15-21 MeV was

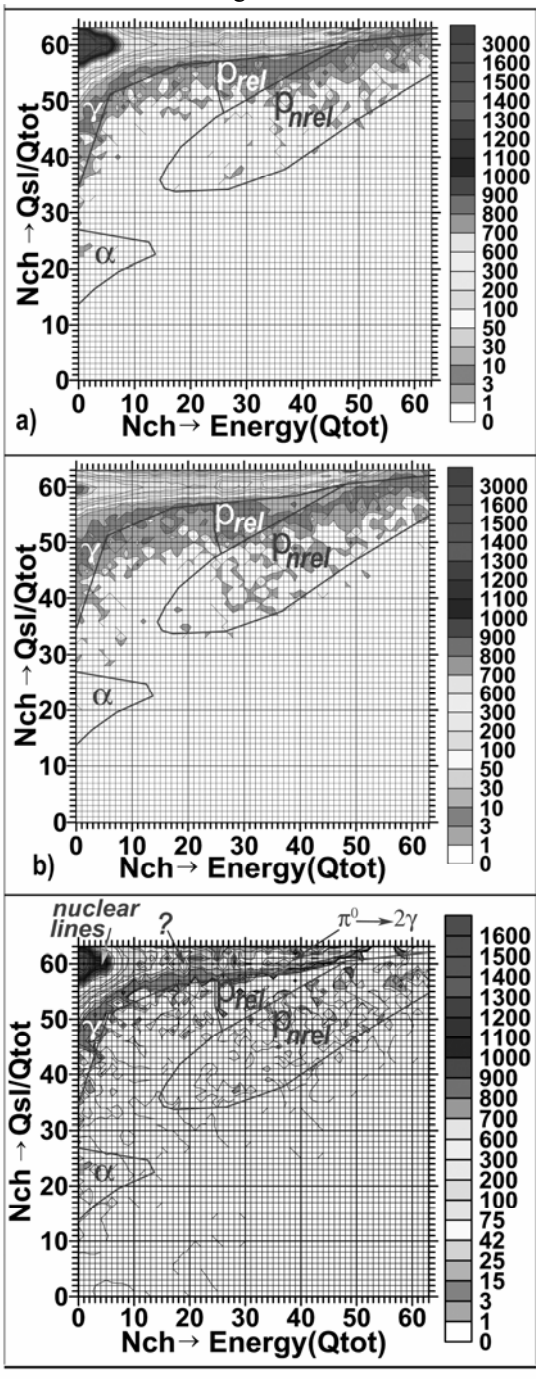

Fig. 2. The ratio Q_{slow}/Q_{tot} in dependence of energy for January 20 solar flare in time interval 06:44:52-06:51:16 UT without (a) and with (c) background subtraction and for background (b).

first registered in solar flare spectrum. Observed spectral features characteristics are presented in Table 1. All spectral features were observed during whole duration of γ-emission registered by AVS-F from this flare. Energy spectra in AVS-F high-energy band obtained from convolution of two-dimensional distribution of ratio Q_{slow}/Q_{tot} in dependence of energy at axis Q_{slow}/Q_{tot}. Analysis of two-dimensional distribution of ratio Q_{slow}/Q_{tot} in dependence of energy shows that in the time interval 06:44:52-06:51:16 UT only γ-emission observed from January 20 solar flare. Areas at two-dimensional distribution which correspond to registration of protons and α-particles contain very small quantity of counts – see Figure 2. So, all spectral features at January 20 energy spectra by AVS-F data was caused only by γ-emission.

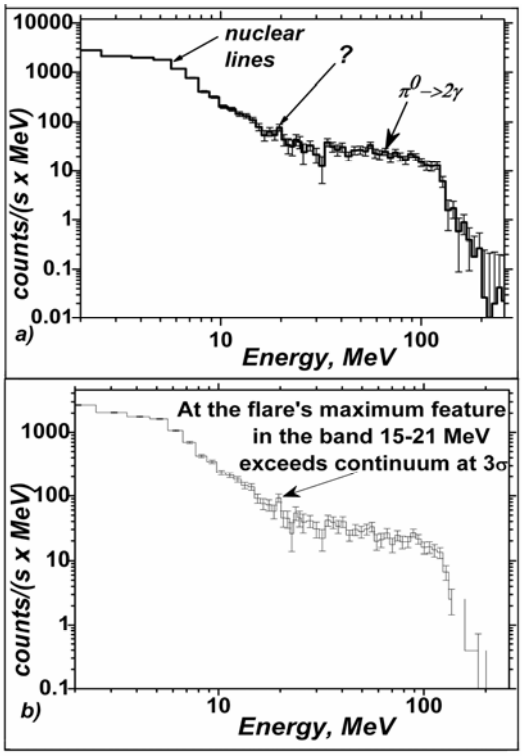

Fig. 3. January 20 solar flare energy spectra in high-energy γ-band: a) obtained from convolution of matrix at Figure 2c (06:44:52-06:51:16 UT), b) corresponding maximum of high-energy γ-emission (in time interval 06:47:00-06:49:08 UT).

Table 1. Spectral features observed during January 20 solar flare in time interval 06:44:52–06:51:16 UT.

Spectral feature	Energy band (MeV)
$\alpha\alpha + e^+e^-$	0.4-0.6
$^{24}Mg + {}^{20}Ne + {}^{28}Si$ + neutron capture	1.7–2.3
$^{20}Ne + {}^{16}O + {}^{12}C$	3.2–5.0
^{16}O	5.3–6.9
?	15–21
$\pi^0 \rightarrow 2\gamma$ (67.5 MeV)	25–110

The temporal profiles of this flare in AVS-F high energy γ-band in regions corresponding to nuclear lines (2-10 MeV), new observed spectral feature (15-21 MeV), pion spectral feature (60–80 MeV and 30–110 MeV) are shown at Figure 1b. It is seen that behavior of temporal profile in the band 15-21 MeV corresponds to nuclear lines one. Maxima in the regions 60–80 MeV and 30–110 MeV are shifted at some tens seconds (acquisition interval in AVS-F high energy γ-band is 128 s). So, spectral feature in 15-21 MeV band looks like nuclear line. The confidence level of this feature separation in summarized spectrum is 2.4 σ, but in the flare hard gamma-emission maximum it separated at 3 σ one – see Figure 3. The preliminary values of intensity ratio between this line and other spectral features observed by AVS-F apparatus are presented in Table 2.

Table 2. Intensity ratios of spectral feature in 15–21 MeV band to other ones.

Spectral feature, MeV	Intensity ratio
1.7-2.3	1500±100
3.2-5.0	200±20
5.3-6.9	120±20

IV. Conclusions

During January 20 solar flare (class X7.1) which was the biggest one in January 2005 series γ-emission during its rising phase in two energy bands: 0.1-20 MeV and 2-140 MeV observed by AVS-F apparatus onboard CORONAS-F satellite. The highest γ-ray energy was registered during this flare was 137 ± 4 MeV. In energy band 140-260 MeV statistical significance excess above background level was not observed. Nuclear, annihilation, neutrons capture at ^1H lines and spectral feature corresponding decay of neutral pions were observed in this flare energy spectrum during whole time of this flare γ-emission registration by AVS-F.

Some spectral peculiarity was observed in the region of 15-21 MeV on 2.5 and 3 standard deviation levels in time intervals 06:44:52-06:51:16 UT and 06:47:00-06:49:08 UT correspondingly.

References

[1] A. S. Glyanenko, Yu. D. Kotov, A.V. Pavlov et al. "The AVS-F experiment on recording rapidly changing fluxes of cosmic and gamma radiation prepared under the CORONAS-F project." *Instrum. Exp. Tech.*, 42, #5, 596-603, 1999

[2] I. V. Arkhangelskaja, A.I. Arkhangelsky, Yu.D. Kotov et al "The solar flare catalog in the low-energy gamma-ray range based on the AVS-F instrument data onboard the CORONAS-F satellite in 2001 2005". *Solar System Research*, 40, 133-141, 2006.

[3] S.N. Kuznetsov; K. Kudela; S. P. Ryumin et al

"CORONAS-F satellite: Tasks for study of particle acceleration." *Adv. Space Res.*, 30, 7, 1857-1863, 2002.

[4] Storey, R.S., Jack, W., Ward, A. The Fluorescent Decay of CsI(Tl) for Particles of different ionization density. Proc. Phys. Soc., 72,1, 1-6, 1958.

[5] Share, G., Murphy, R.J., Smith, D. et al. RHESSI observations of the 2005 January 20 solar flare, talk on SHINE 2006 Special Session on the 2005 January 20 Event,https://creme96.nrl.navy.mil/20jan05/ShareSHINE2006InvitedTalk.pdf, 2006.

[6] J. W. Bieber, J. Clem, P. Evenson, et al "Largest

[7] GLE in half a century: Neutron monitor observations of the January 20, 2005 event." *Proceedings of the 29th International Cosmic Ray Conference. August 3-10, 2005,Pune, India.* Eds by Acharya, B. S., Gupta, S, Jagadeesan,

[8] P. et al. Mumbai: Tata Institute of Fundamental research, v. 1, pp.237-240, 2005.

The role of new gamma-ray observations in investigation of powerful solar flares

I. V. Arkhangelskaja[1], A. I. Arkhangelsky[1], E.V. Troitskaya[2], L.I. Miroshnichenko[2,3,4]

[1]*Astrophysics Institute of Moscow Engineering Physics Institute (State University), 115409, Kashirskoe shosse, 31, Moscow,Russia*
[2]*Skobeltsyn Institute of Nuclear Physics of Moscow State University, 1(2), Leninskie gory, GSP-1, Moscow, 119991, Russia*
[3]*Institute of Terrestrial Magnetism, Ionosphere and Radio Wave Propagation, RAS, IZMIRAN, 142190, Troitsk, Moscow region, Russia*
[4]*Instituto de Geofísica, UNAM, C.U., Coyoacán, 04510, México, D.F., México*
(Mailing address Kashirskoe shosse, 31, 115409, Moscow, Russia)

Abstract **– Gamma-ray emission from solar flares gives information about the nature of the accelerated particles and the physical conditions in the area in which flare occurs and surrounding media. Nuclear lines present the abundance of elements, density and temperature of the ambient solar atmosphere and data concerned with the parameters of the accelerated ions. The possible interpretation of spectra and spectral peculiarities observed during January 20 2005 solar flare is discussed.**

Key Words**— neutron capture at ^{3}He, γ-lines produced by excited stages of ^{12}C, solar flares high energy gamma-emission.**

I. INTRODUCTION

Gamma-ray emission from solar flares gives information about the nature of the accelerated particles and the physical conditions in the area in which flare occurs and surrounding media. In solar flares, γ-emission in the region $E_\gamma \geq 0.1$ MeV produced via:

1) bremsstrahlung emission of electrons (directly accelerated in a flare [1] and generated in decays of π^- produced in interactions of accelerated protons with surrounding solar media [2] – in both cases spectra are continuum, mostly observed at $E_\gamma \geq 10$ MeV in second case [3];

2) annihilation of positrons (produced in decays of radioactive nuclei formed in reactions of interactions of flare-accelerated protons, α-particles, and heavier ions with the solar atmosphere and in decays of π^+ created in flares with accelerated protons [4] – line at 511 keV with some keV FWHM from both direct annihilation and 2γ-annihilation from the positronium singlet state [5] and spectrum continuum from 3γ-annihilation from the positronium triplet state mostly observed at $E_\gamma \geq 10$ MeV [3];

3) secondary processes by radioactive nuclei produced in:

a) interactions of flare-accelerated protons and α-particles with ambient nuclei heavier than He [6, 7, 3, 8] [6, 7, 3, 8]– narrow γ-lines with fractional FWHM ~2% (because recoil velocity of the heavier nucleus is relatively low);

b) interactions of accelerated α-particles and heavier ions with ambient H and He [6, 7, 3, 8] – broad γ-lines with fractional FWHM ~20% (because recoil velocity of nucleus is relatively high);

c) heavy-heavy interactions – relatively narrow γ-lines (for example, 1.634 MeV ^{20}Ne, 1.369 MeV ^{24}Mg and 0.937 MeV ^{18}F [3, 9, 10] – broad γ-lines with fractional FWHM ~20% (because recoil velocity of nucleus is relatively high);

4) neutron capture at ^{1}H and ^{3}He (lines at 2.223 MeV and probably at 20.58 MeV [11, 12, 13, 14, 20, 21] and spectrum continuum

5) decays of neutral pions produced in solar flares mostly in collisions between protons and nuclei of hydrogen and helium ((pp) and (pα)) – broad spectral feature in energy band 35-140 MeV with centrum at $E_\gamma \sim m(\pi^0)/2$ which can be shifted in dependence of proton flux directionality [15, 17].

Nuclear lines present the abundance of elements, density and temperature of the ambient solar atmosphere and data concerned with the parameters of the accelerated ions (Murphy et al, 2007). The shape of annihilation line is a function of transition-region temperatures during the flare and hydrogen concentration [5, 16]. The spectrum of γ-rays from decay of neutral pions is sensitive to the energy distribution of accelerated protons and α-particles with E>100 MeV [17]. Continuum spectral indices, at first, are depended on electron spectral index and directionality [1, 18] and proton spectral index due to decay of negative charged pions [29]. Some other spectral parameters also give us information about the dynamics of accelerated particles and flare region characteristics.

II. 15.11 MeV and 20.58 MeV lines in solar flares

In this work we would like to pay your attention on some spectral features, which allow improve proton spectra parameters and abundance of ^{3}He in flare region if they will be observed during solar flares. One spectral feature is 15.11 MeV line produced by excited stages of ^{12}C [17, 26], other is 20.58 MeV line from neutron capture at ^{3}He [11].

Line 15.11 MeV is produced in direct interactions between protons and nuclei ^{12}C and ^{16}O:

$$p + {}^{12}C \rightarrow {}^{12}C + p' + \gamma; \quad (1)$$

$$p + {}^{16}O \rightarrow {}^{12}C + p' + \alpha + \gamma. \quad (2)$$

In complex with the 4.44 MeV line produced in these reactions too this line allows to obtain parameters of the accelerated protons, because they are pairs of γ-lines from the same nuclei but from de-excitation of levels with widely separated thresholds. The flux ratio $f_{15.11}/f_{4.44}$ depends not only on cross-sections but on spectrum of excited particles and relative isotopic abundance of ^{12}C and ^{16}O. The relation of cross-sections of these reactions is $\sigma_C/\sigma_O \sim 10$ [26,34]. Energy threshold at ^{16}O higher than at ^{12}C – see Figure 1ab. The ratio $f_{15.11}/f_{4.44}$ was studied in [17, 26] and it was obtained that more probable value of it is 0.006 taking into account proton spectra calculation for some real solar flares [35]. The dependence of this ratio from proton spectrum parameters is shown at Figure 1c.

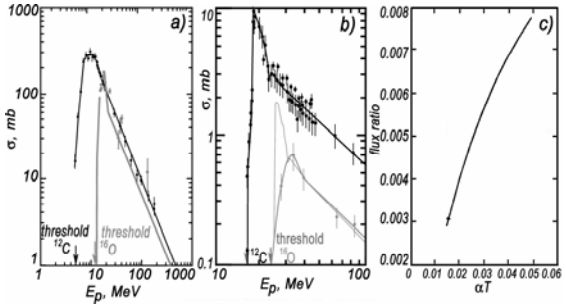

Fig. 1. The cross-sections of γ-ray production at ^{12}C and ^{16}O: a) for 4.44 MeV line in reactions (1, 2); b) for 15.11 MeV line in reactions (1) – black and (2) – gray and c) the dependence of $f_{15.11}/f_{4.44}$ from proton spectrum parameter αT (proton spectra were parameterized by Bessel function $K_2(\alpha T)$). Adopted from [26].

In the interactions of accelerated during solar flare protons and ambient solar material neutrons are produced. Approximately 48% of produced neutrons with energy $E_n \geq 1$ MeV will escape from the solar atmosphere (see, for example, 15). Neutrons, which do not escape from the Sun, can be captured at nuclei of hydrogen and ^{3}He to form deuterons with emissions of γ-quanta with energy 2.223 MeV and ^{4}He with emissions of γ-quantum with energy 20.58 MeV or two γ-quanta in reactions:

$$n + {}^1H \rightarrow {}^2H + \gamma; \quad (3)$$

$$n + {}^3He \rightarrow {}^4He + \gamma; \quad (4)$$

$$n + {}^3He \rightarrow {}^4He + 2\gamma. \quad (5)$$

Reaction (5) gives additional component of spectrum continuum. Also neutrons can be decayed or non-radiative captured at ^{3}He.

The cross-section of reaction (5) is much smaller than one of process (4) for all neutron energies [14]. The possibility of observable contribution of reaction (4) in solar flare spectrum was first suggested and discussed in [11]. Cross-section of reaction (4) was first measured in [13]. Up to now some experiments on studying process of radiative neutron capture by ^{3}He nuclei were carried out and the cross-section of this reaction was studied up to $E_n \sim 20$ MeV (see for example [12, 14, 19, 20 21]. Even if the ratio between neutron capture cross section at ^{1}H and ^{3}He is $\sim 10^4$ at low energy, in region E_n >100 eV this reaction has resonance behavior and in energy band E_n>500 keV the cross-section of this reaction exceeds the cross-section of the reaction (3) of radiative neutron capture by ^{1}H nuclei.

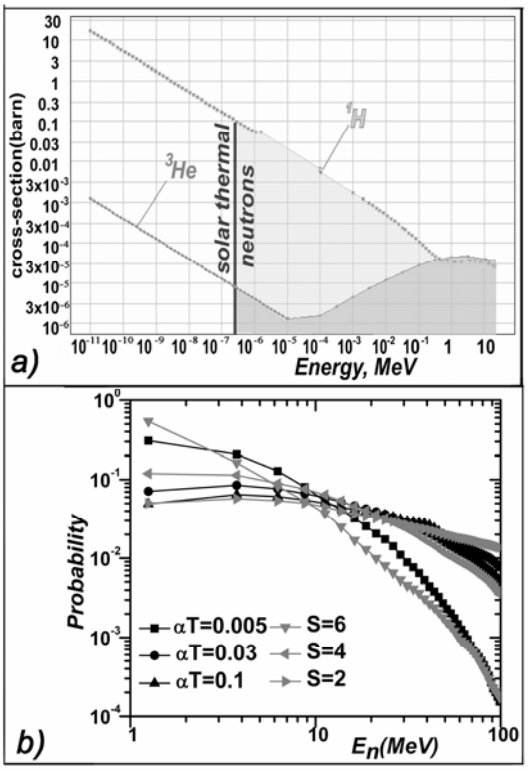

Fig. 2. Neutron interactions: a) neutron radiative capture cross-sections at ^{1}H and ^{3}He (adopted from [20]), b) normalized by unity energy spectra of neutrons produced by incident ions with Bessel function spectra characterized by different αT and power-law spectra characterized by different S values.

There are some arguments for this tendency prolong for neutrons of higher energies. The comparison between cross-sections of these two reactions is shown at Figure. 2a.

Table 1. Preliminary results of calculated ratio between lines of neutron capture at ^{1}H and ^{3}He.

αT or S	^{3}He to ^{1}H lines ratio
αT=0.005	$1.21\cdot10^{-4}$
αT=0.03	$1.17\cdot10^{-4}$
αT=0.1	$1.16\cdot10^{-4}$
S=2	$1.15\cdot10^{-4}$
S=4	$1.18\cdot10^{-4}$
S=6	$1.22\cdot10^{-4}$

We made attempt to preliminary calculate observable ratio between lines of neutron capture at ^{1}H and ^{3}He. In our calculation we use models of neutron spectra based on [23] with initial power-law proton spectra with indexes -6,-4, -2 and parameterized by Bessel function $K_2(\alpha T)$ with αT=0.005, 0.03 and 0.1 and suppose that most part of nonthermal neutrons interacts with surrounding medium. The normalized by unity spectra of neutrons are shown at Figure 2b. Preliminary results of calculated ratio between lines of neutron capture at ^{1}H and ^{3}He are presented in Table 1 for $n(^3He)/n(^1H)=10^{-4}$. In our calculation we used different values of relatively abundance ^{4}He, ^{3}He and ^{1}H following to real solar flares models and observations [17, 10, 22, 23, 25].

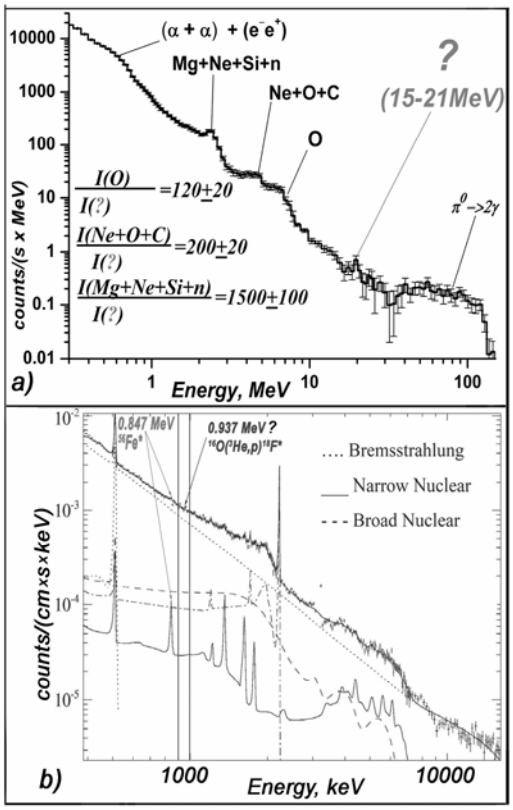

Fig. 3. Energy spectra of January 20 2005 solar flare by AVS-F (adopted from [27]) (a) and RESSI data (adopted from [28]) (b).

III. Solar gamma-rays in energy band 15-21 MeV during January 20 2005 flare

Unfortunately at present there are processed data with sufficient spectral resolution and statistically ensured count rates in energy band E_γ >10 MeV only for January 20 2005 solar flare [27] by AVS-F apparatus [28] onboard CORONAS-F satellite. January 20 solar flare (class X7.1) was the biggest in January 2005 series. This flare was accompanied by SEP and GLE which were most intensive ones for period of the last 29 and 52 years [30, 31] and coronal mass ejection.

During flare rising phase (by GOES data) γ-emission in two energy bands: 0.1-20 MeV and 2-140 MeV was observed by AVS-F apparatus onboard CORONAS-F satellite. The temporal profiles of this flare by GOES, AVS-F, RHESSI and ground neutron monitors data are shown at Figure 4. The wide range energy spectrum of January 20 2005 solar flare by AVS-F data is presented at Figure 3a. Nuclear, positron, neutrons capture at ^{1}H lines and spectral feature

corresponding decay of neutral pions were observed in this flare energy spectrum during whole time of this flare γ-emission registration by AVS-F.

Some spectral peculiarity was observed in the region of 15-21 MeV on 2.5 and 3 standard deviation level in time intervals 06:44:52-06:51:16 UT and 06:47:00-06:49:08 UT correspondingly [27]. The ratio between this feature and lines 2.223 MeV and 4.44 MeV is $\sim 7\times10^{-4}$ and $\sim 5\times10^{-3}$ correspondingly, which is comparable with estimations for 15.11 MeV and 20.58 MeV lines.

The relatively abundance of $n(^3He)/n(^4He)$ for concrete event can be estimated by flux ratio between αα-line and deexcitation lines (0.937 MeV, 1.04 MeV and 1.08 MeV) produced in direct reaction by ^3He, for example [10, 32]:

$$^3He + ^{16}O \rightarrow p + ^{18}F^* \qquad (6)$$

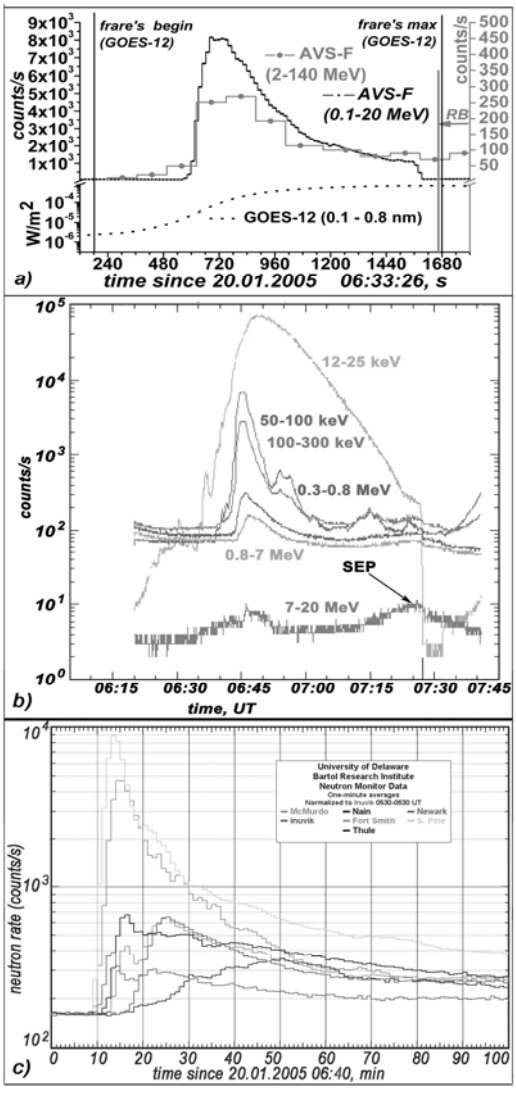

Fig. 4. Solar flare January 20 2005 temporal profiles by GOES data and in low and high energy γ-bands by AVS-F data (adopted from [27]) (a), RHESSI data (adopted from [19]) (b) and ground neutron monitors data (c) (adopted from [31])).

These lines were registered in some solar flares [24, 25] and observations of them can directly measure the ^3He abundance in solar atmosphere. In energy spectrum of January 20 2005 solar flare by RHESSI data (see Figure 3b) some weak peculiarity is presented in the band of 0.9-1.0 MeV slightly less intensive then 0.84 MeV line from ^{56}Fe that can be interpreted as 0.937 MeV ^{18}F line. But it is clear that investigation of such weak spectrum features takes very accurately and complex data analysis. Moreover, some adjacent lines produced in interactions of accelerated α-particles with ambient ^{56}Fe (for example 0.931 MeV, 1.0 MeV and so on) should be taken into account because their presence distorting shape of analyzed deexcitation spectral features [32]. The estimated on SEP data analysis ratio $n(^4He)/n(^1H)\sim0.2$ [30] and upper limit for $n(^3He)/n(^4He)\sim 8\times10^{-4}$ [33], which gives $n(^3He)/n(^1H)\sim 2\times10^{-4}$. This value is comparable with estimations for 15.11 MeV and 20.58 MeV lines.

IV. Conclusions

Last time many interesting results were obtained in solar gamma- and X-ray spectroscopy and elements abundance investigations in solar atmosphere. But only a few of them used data in energy region higher then about 10 MeV. Spectral feature, observed in spectrum of January 20 2005 solar flare in 15-21 MeV energy band [27] possible can be interpreted as 15.11 MeV (excited stages of ^{12}C) or 20.58 MeV (neutron capture at ^3He) gamma lines or may be their combination. Direct observation of this spectral feature can gives very important information about physics of the solar flares.

This work is supported by RFBR grant №05-02-39011

References

[1] J. A. Miller, R. Ramaty, Relativistic electron transport and bremsstrahlung production in solar flares. Astrophys. J., 1, 344, 973-990, 1989.

[2] R. J. Murphy , C. D. Dermer, R. Ramaty, On the origin of pion-decay radiation in the 1982 June 3 solar flare, Astrophys. J. Suppl., 63, 721-748, 1987.

[3] R. J. Murphy, G.H. Share, X.M Hua, Using gamma-ray and neutron emission to determine solar flare accelerated particle spectra and composition and the conditions within the flare magnetic loop. The Astrophys. J. Suppl, v. 168, I 1, pp.167-194, 2007.

[4] C. J. Crannell, R .Ramaty, H.W. Werntz. Positron annihilation in solar flares. 14th, Munich, West Germany, August 15-29, 1975, Conference Papers. Volume 5. (A76-26851 11-93) Munich, Max-Planck-Institut fuer extraterrestrische Physik, p. 1656., 1975.

[5] G. H. Share, R. J. Murphy, H.W. Skibo. High-resolution observation of the solar positron-electron annihilation line. Astrophys. J., 595, 2, 85-88, 2003.

[6] R. E. Lingenfelter, R. Ramaty, High Energy Nuclear Reactions in Solar Flares. In High-Energy Nuclear Reactions in Astrophysics, ed. Shen, B. S. P. (New York: Benjamin), p. 99, 1967

[7] R. Ramaty, B. Kozlovsky, R. E. Lingenfelter. Nuclear gamma-rays from energetic particle interactions. Astrophys. J. Suppl, 40, pp. 487-526, 1979.

[8] E. L. Chupp, D.J. Forrest, P.R. Higbie, Solar gamma rays lines observed during the solar activity of august 2 to august 11, 1972. Nature, v. 241, p. 333-334, 1973.

[9] B. M. Kuzhevskij, W. Q. Gan, L. I. Miroshnichenko, The role of nuclei-nuclei interactions in the productions of gamma-ray lines in solar flares. Chinese J. Astron. Astrophys., v. 5, issue 3, p. 295-301, 2005.

[10] B. Kozlovsky, R. J. Murphy, G. H. Share Positron-emitter production in solar flares from ^{3}He reactions. Astrophys. J., 604, 2, 892-899, 2004.

[11] B.M. Kuzhevskii, Gamma astronomy of the sun and study of solar cosmic rays, Sov. Phys. Usp., 25, 392-415, 1982.

[12] V. P. Alfimenkov, S. B. Borzakov, Ya. Vezhbitski et al. Radiative capture of He^3 neutrons in the energy interval 1-70 keV. JETP Lett. v. 29, p. 100-108, 1979.

[13] R. W. Zurmühle, W. E. Stephens, H. H. Staub, Gamma-rays from neutron capture in helium-3 and deuteron capture in deuterium. Phys. Rev. 132, 2, 751-154, 1963.

[14] V. M. Bystritsky, Vit.M. Bystritskii, T. L. Enik, et al. Experimental Research of the Radiative Capture of Thermal Neutrons in ^{3}He. Communication of the Joint Institute for Nuclear Research, #D15-2006-23. Dubna, v. 565, issue 2, pp.864-875, 2006.

[15] C. C. Cheng, Theoretical Studies of the Flux and Energy Spectrum of Gamma Radiation from the Sun, Space Science Rev, 13, 3-123, 1972.

[16] R. W. Bussard, R. Ramaty, R. J. Drachman, The annihilation of galactic positrons, Astrophys. J., v. 228, 928-934, 1979.

[17] C. J. Crannell, R. Ramaty, H Crannell. Solar gamma-rays above 8 MeV. Astrophys. J., 229, 762-771, 1979.

[18] W. T. Vestrand, D.J. Forrest, E.L. Chupp. The directivity of high-energy emission from solar flares – solar max mission observations. Astrophys. J., 322, 1010-1022, 1987.

[19] G. Share, R. J. Murphy, D. Smith, et al. RHESSI observations of the 2005 January 20 solar flare, talk on SHINE 2006 Special Session on the 2005 January 20 Event, Available: https://creme96.nrl.navy.mil/20jan05/ShareSHINE2006InvitedTalk.pdf , 2006.

[20] M. S. McKinley, B. Beck, and D. P. McNabb, Nuclear and Atomic Data System http://nuclear.llnl.gov/CNP/nads/NADSApplet.html, Lawrence Livermore National Laboratory Report No. UCRL-WEB-152626-REV-1, 2004.

[21] R. J. Komar, H.B. Mak, J.R. Leslie, ^{3}He(n,γ)^{4}He cross section and the photodisintegration of ^{4}He, Phys. Rev. C, 48, 5, 2375-2384, 1993.

[22] F. L. H. Wolfs, S.J. Freedman, J.E. Nelson Measurement of the He-3(n,gamma) He-4 cross section at thermal neutron energies. Phys. Rev. Lett, 63, 25, 2721-2724, 1989.

[23] X. M. Hua and R. E. Lingenfelter Astrophys. J. , Solar flare neutron and accelerated ion angular distributions, v. 323, 779-794, 1987.

[24] G. H. Share, R.J. Murphy Accelerated and Ambient He Abundances from Gamma-Ray Line Measurements of Flares. Astrophys. J., 508 876-884, 1998.

[25] N. Manzhavidze, R. Ramaty and B. Kozlovsky Solar Atmospheric and Solar Flare Accelerated Helium Abundances from Gamma-Ray Spectroscopy. Astrophys. J. Lett., 489, L99-L102, 1997.

[26] C. J. Crannell, F. L. Lang Nuclear gamma-line ratios as spectral diagnostics for protons accelerated in solar flares. Proceedings of a conference "Nuclear Spectroscopy of Astrophysical Sources", held in Washington, D.C., New York: American Institute of Physics (AIP), 1988. Eds. Gehrels, N and Share, G.H.. AIP Conf. Proc., v.170, pp.240-246, 1987.

[27] I. V. Arkhangelskaja, A. I. Arkhangelsky, Yu.D. Kotov et al. "The observation of gamma-ray emission during January 20 2005 solar flare". *Proceedings of the International Symposium SEE 2007: Fundamental Science and Applied Aspects*, in press, 2007

[28] A. S. Glyanenko, Yu. D. Kotov, A.V. Pavlov et al. "The AVS-F experiment on recording rapidly changing fluxes of cosmic and gamma radiation prepared under the CORONAS-F project." *Instrum. Exp. Tech.*, 42, #5, 596-603, 1999

[29] G. H. Share, R.J. Murphy Gamma radiation from flare-accelerated particles impacting the sun. AGU Monograph Series, 165, 177-188, 2006.

[30] R. A. Mewaldt, M. D. Looper, Cohen, C.M.S. et al Solar-Particle Energy Spectra during the Large Events of October-November 2003 and January 2005. Proceedings of the 29th International Cosmic Ray Conference. Pune, India, August 3-10, 2005, eds. Acharya, B. S., Gupta, S, Jagadeesan, P. et al. Mumbai: Tata Institute of Fundamental Research, v. 1, pp.111-114, 2005.

[31] J. W. Bieber, J. Clem, P. Evenson, et al "Largest GLE in half a century: Neutron monitor observations of the January 20, 2005 event." *Proceedings of the 29th International Cosmic Ray Conference. August 3-10, 2005, Pune, India.* Eds by Acharya, B. S., Gupta, S, Jagadeesan, P. et al. Mumbai: Tata Institute of Fundamental research, v. 1, pp.237-240, 2005.

[32] W. Q. Gan, Solar gamma-ray spectroscopy and abundance of elements. Chinese Aston. Astroph, 26, 255-266, 2002

[33] M. I. Desai, G. M. Mason, H. W. Gold, Heavy-Ion Elemental Abundances in Large Solar Energetic Particle Events and Their Implications for the Seed Population. Astrophys. J., 649, 1, 470-489, 2006.

[34] F. L. Lang, C. W. Werntz, C. J. Crannell, et al., Cross sections for production of the 15.10-MeV and other astrophysically significant gamma-ray lines through excitation and spallation of ^{12}C and ^{16}O with protons, Phys. Rev. C, 35 1214-1227, 1987.

[35] R. J. Murphy, R. Ramaty, Solar-flare neutrons and gamma-rays, Advances in Space Research, 4, 7, 127-136, 1984.

Storm measurements of the July 2005 solar extreme events from the low corona to the Earth

C.Caroubalos (a), P. Preka-Papadema (b), H. Mavromichalaki (c),
X Moussas (b), A. Papaioannou (c), E. Mitsakou (b) and A. Hillaris (b)

[a]*Department of Informatics, University of Athens, GR-15783 Athens, Greece*
[b]*Section of Astrophysics, Astronomy and Mechanics, Department of Physics, University of Athens, GR-15784 , Panepistimiopolis Zografos, Athens, Greece*
[c]*Section of Nuclear and Particle Physics, Department of Physics, University of Athens, GR-15784 , Panepistimiopolis Zografos, Athens, Greece*

***Abstract* – A study of the abnormal features observed during solar extreme events of July 2005 is being presented. Recordings from a number of earthbound receivers (such as the ARTEMIS IV radioheliograph, the Athens Neutron Monitors Data Processing (ANMODAP)Center), space experiments (WIND/WAVES mission)as well as data archives provided new insight, as all solar events and their resulting cosmic ray variation were traced from their sources to the Earth. Time sequence of the events indicated that the initiation of coronal mass ejections (CMEs) were accompanied by type IV radio bursts and intense solar flares (SFs), their effects extended from the low corona to the face of the Earth. As a result, the Athens Neutron Monitor Data Processing (ANMODAP) Center recorded an unusual Forbush decrease with a sharp enhancement of cosmic ray intensity appearing right after the main phase of the Forbush decrease on 16 July 2005, only to be followed by a second decrease within less than 12 hours. This peculiar event is neither a ground level enhancement nor a geomagnetic effect in cosmic rays. It rather, appears as the effect of a special structure of interplanetary disturbances originating from a group of CMEs in the 13-14 July 2005 period.**

***Key Words*—Sun: Coronal Mass Ejections, Sun: Flares, Sun: Activity, Sun: X-Rays Cosmic Rays Forbush decreases**

I. INTRODUCTION

Space weather drivers, such as MHD shocks, CMEs and energetic particles are mostly of Solar origin; these modulate the isotropic flux of galactic cosmic rays in the form of Forbush decreases. In the study of the magnetospheric response to energetic phenomena on the Sun, solar radio bursts offer an extremely efficient diagnostic of the drivers onset in the corona. The type II bursts are the coronal counterparts of the interplanetary MHD shocks; a certain subset of them, the CME driven, manifests the coronal origin of an interplanetary shock. The type IV continua on the other hand originate from energetic electrons trapped within plasmoids, magnetic structures or substructures of CMEs (Bastian et al (2001)); those often indicate mass ejection and propagation in the low corona. Lastly, the type III bursts manifest the propagation of energetic electrons through the corona and, often, mark the onset of energy release processes.

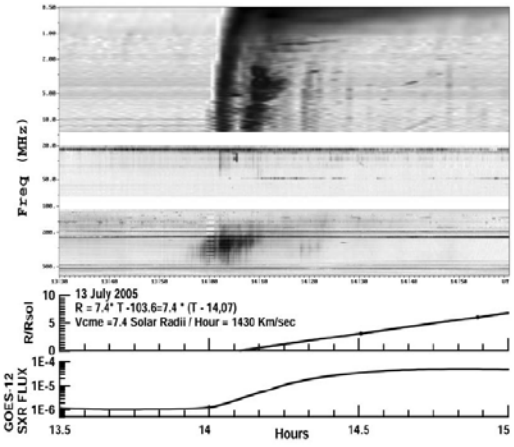

Fig. 1. Top: Composite ARTEMIS–IV/WIND Dynamic Spectrum of the 13 July 2005 Event: A type IV continuum appears from 14:01–14:30 UT while a number of type III electron beams originating in the low corona extends to theWIND/WAVES spectrum. Second Panel: Height Time plot of the CME (The least squares line underlines the CME takeoff at 14:04 UT (14.07) and the plane of the sky speed of 1440Km/sec (7.4 *Rsol*/hour)). Bottom: The corresponding GOES SXR light curve.

In this report, we study, the energetic solar phenomena observed at the Sun in active region 786 (N10*o* W90*o*) on 13-14 July 2005. Their effects are traced at Earths orbit on 16-18 July through neutron monitor measurements. The associated magnetospheric response affected cosmic ray measurements and space weather, marking this activity as the extreme events of July 2005.

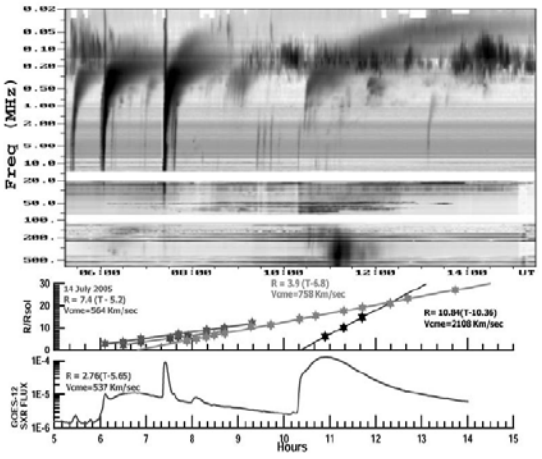

Fig. 2. Top: Composite ARTEMIS–IV/WIND Dynamic Spectrum of the 14 July 2005 Event: Groups of type III bursts extending into the WAVES range; a faint continuum at 06:00–06:30 and a type IV burst at 10:20–12:20 UT (Linear least square fit as in figure 1). Middle: Height Time plot of the fast CME overtaking the slow ones. Bottom: The corresponding GOES SXR light curve.

II. OBSERVATIONAL RESULTS & ANALYSIS

2.1 Data

The data sourses used in our analysis were taken from:

• The Artemis–IV [1] (Caroubalos et al. (2001) also Kontogeorgos et al. (2006)) solar radio–spectrograph at Thermopylae (http://www.cc.uoa.gr/ artemis/); it covers the frequency range from 650 to 20 MHz with time resolution of
0.1 s.
• TheWIND/WAVES receivers (Bougeret et al. (1995)) in the range 14 MHz–20 kHz, complement the 650–20 MHz spectral range of ARTEMIS–IV; the combined observations are used in the study of the continuation of solar bursts in the interplanetary space bridging thus the gap between space borne and ground-based radio observations.

• CME data from the LASCO lists on line (http://cdaw.gsfc.nasa.gov/CME list) (Yashiro et al. (2004))
• The Nan̓Ecay Radio heliograph (Kerdraon and Delouis (1997)) for positional information of radio emission.
• SXR (GOES) light curves and on line records (http//www.sel.noaa.gov/ftpmenu/indices).
• The Neutron Monitor Station of Athens University (Mavromichalaki et al. (2001)) and the corresponding data analysis Center (http://cosray.phys.uoa.gr) (Mavromichalaki et al. (2005))
• Solar wind parameters from the OMNI (http://omniweb.gsfc.nasa.gov/) online database.

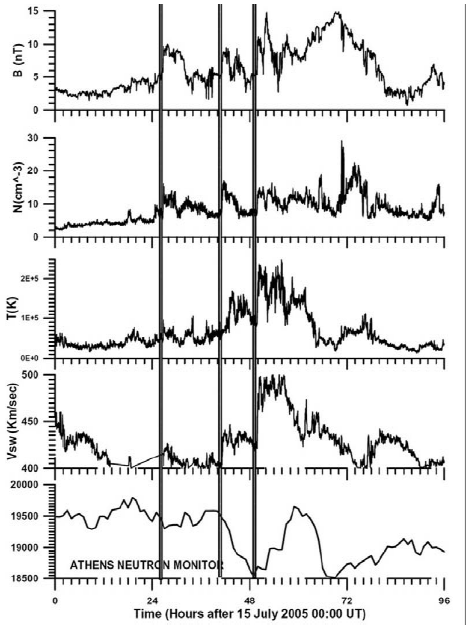

Fig. 3. Solar wind parameters from the OMNI data base; From Top to Bottom: Total magnetic field strength, proton density, proton temperature and Solar Wind Speed. Three weak shocks are marked, where the magnetic field increases (5.8 to 8.0 nT, 5.2 to 8.0 nT and 5.6 to 9.3 respectively); proton density and temperature increase also but the solar wind speed shows rather small changes. Bottom Panel: The Athens Neutron Monitor Recordings of an irregular Forbush decrease, interrupted by a sudden enhancement.

2.2 Solar Activity Observations

Solar activity on the 13 July 2005 starts at 14:01 UT with an M5.0 long duration SXR flare in AR 786 on the west limb (N10*o* W90*o*) which ends at 15:38 UT. A fast halo CME, with speed 1430 km/sec takes off at 14:12 UT. From the ARTEMIS/WIND recordings we establish that a type IV burst (14:01-14:30 UT) overlaps in time with the flare onset and the estimated CME lift–off; from the Nan̓Ecay Radio heliograph images the position of the continuum appears over AR 786. In figure 1 we present a composite ARTEMIS–IV/WIND Dynamic Spectrum combined with the

height – time plot of the CME and the associated SXR flare light curve. The active phenomena of the 14 July 2005 originate in AR 786; they commence with an M9.1 (05:57–07:43 UT) flare followed by an X1.2 (10:16-11:29 UT). The former is associated with type III groups and the lift–off of three slow CMEs, with estimated take off at 05:32 UT, 06:01 UT and 07:02 UT and corresponding speeds 514, 573 & 758 Km/sec; a sharp SXR peak associated with a group of type III and an SF Hα flare (Lear) appears at about 7:59–8:12 UT although is not included in the GOES SXR flare lists. All CMEs start with almost the same position angle (252*o*–282*o*) and with increasing width (14*o*, 60*o*, 103*o*); those appear as successive ejections from AR 786 which eventually merge as the faster overtake the slower. This activity is accompanied by a faint continuum 06:00–06:30 UT in the 500–100 MHz range. The latter flare is associated with a fast CME (2108 Km/sec) which takes off at 10:27 UT overtaking the three slow CMEs at about 12:20 UT. It is also accompanied by type III bursts and a type IV continuum (10:20–12:20 UT). In figure 2 we present a composite ARTEMIS–IV/WIND Dynamic Spectrum combined with the height – time plot of the CME and the associated SXR flare light curve.

2.3 Solar Wind Parameters Analysis - Effects on Cosmic Ray Modulation

A large Forbush decrease (8% - at polar stations) and sharp changes of the anisotropy occurred on 16–17 July 2005; these more or less coincide with medium level disturbances in the interplanetary space (cf. Figure 3). The disturbances correspond to weak interplanetary shocks without coronal counterparts; these shocks were recorded in the OMNI data base (July 16, 02:35 UT, 17:06 & July 17 01:41 UT) and appeared at the near–Earth space 2–2.5 days after the fast CME onsets of the 13–14 July, therefore they are expected to be driven by them; we note that their time difference is about 23 hours while the interval between successive fast CMEs was about 20. The passage of the interplanetary shock was marked by an increase in magnetic field strength (5.8 to 8.0 nT, 5.2 to 8.0 nT and 5.6 to 9.3 respectively), an increase in proton density (6.7 to 11.10 cm−3, 6.7 to 13.7 cm−3 & 6.7 to 11.10 cm−3) and temperature (47800 K to 63100K and subsequently to 165300 K). The variation in the solar wind speed shows rather small changes (cf. Figure 3), implying that only a small part of the mass ejection interacted with the Earth's magnetosphere as the CME was launched from the limb. The shock speeds were computed at the Earth's orbit from v:=(n2v2-n1v1)/(n2-n2), where n1, v1 and n2, v2 the upstream and downstream plasma density and velocity respectively and v the shock velocity, (cf. for example Burlaga (1995)). The calculated speeds were found to be 509, 434 and 557 Km/sec exceeding the solar wind speed values reported in OMNI data base which were 420, 411, 483 Km/sec respectively. The direction of B as reported in the OMNI data base is found to be south (Bz<0) for the first and in part the third IP shock; this is consistent with a small variation of the geomagnetic field (Kp index) and a double sub storm of -60 and -76 nT (Dst index) which were also recorded in the same data set. An intensive Forbush decrease of cosmic rays, recorded on the 16th of July, was observed by the majority of the neutron monitors worldwide (cf. Figure 4).

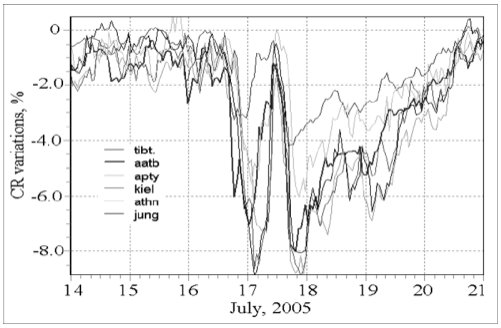

Fig. 4. Cosmic ray variations from 14-18 July 2005 from various stations at diffeent cut-off rigidities: Aatb- Alma-Ata, Apty- Apatity, Athn- Athens, Jung- Jungfraujoch, Kiel- Kiel, Tibt- Tibet.

Right after the main phase of the FD at the 17th of July, a sharp enhancement of cosmic ray intensity occurred and was followed by a second decrease, within 8 hours (cf. Figure3, bottom panel). The peculiarity of this event is due to the fact that it does neither comprise a ground level enhancement of solar cosmic rays nor a geomagnetic effect in galactic cosmic rays due to the fact that this was the result of solar modulation of galactic cosmic rays, which were recorded under quiet geomagnetic conditions. In order to concider such event as a strong geomagnetic one the Dst index should be lower then - 100 nT (Loewe and Prolss (1997)), which would resulted into a strong geomagnetic storm (http://www.swpc.noaa.gov/NOAAscales/). The recorded data on Kp and Dst showed that this was not the case for the event under consideration. Nevertheless, the event was also characterized by unusually high anisotropy of cosmic rays (7-8 %) especially of the equatorial component, with a direction to the western source (Mavromichalaki et al. (2007)). It seems that the sequence of the CMEs and the corresponding interplanetary shocks have produced the above cosmic ray decrease with the two distinct deep minima; the time between them is approximately 20 hours, as is the time interval

between successive interplanetary shocks, and between the fast CME lift–of on the 13 & 14 July respectively. Moreover, this cosmic ray enhancement can not be considered as a Rogue event (Kallenrode and Cliver (2001)) due to the fact that this was the result of galactic cosmic ray modulation and not solar cosmic ray manifestesion.

III. DISCUSSION & CONCLUSIONS

In this report the Solar Extreme Events on the 13 and 14 July 2005 and the associated Forbush decrease has been studied. The observed time sequence of events of this time period indicates that the initiation of CMEs is closely related to the appearance of type IV radio bursts and strong solar flares. Their effects were traced from the base of the solar corona to the near Earth vicinity; they included complex radio bursts and variations in cosmic ray fluxes and space weather. Three interplanetary shocks were observed about 48 hours from the CMEs take off; their time intervals in both cases were similar (about 20 hours) yet they were not accompanied by significant change of the solar wind parameters, the solar wind speed in particular, probably due to the origin of the CMEs on the west limb. A sub storm (Dst double minima of -60 and -76 nT) and a Forbush decrease (double minima with a time interval of 20 hours between then) were recorded; minima is almost the same with the time distance between the IP shocks. It is not unprobable to propose that a closed magnetic structure, of which the Earth felt only a minor part, travelled through interplanetary medium and resulted into this abnormal cosmic ray events that were recorded at this time. It seems that the Earth was influenced by the first shock which resulted to the FD on the 16th-17th of July. Right after the minimum of the decrease, the Earth got outside the closed magnetic structure and thus galactic cosmic rays could register by ground based detectors. On the same day (17th of July), the third shock resulted in the second part of this irregular FD.

ACKNOWLEDGMENT

The authors would like to thank referees for their comments which improved the quality of the paper. This work was financially supported by the Research Committee of the University of Athens and by PYTHAGORAS II which is funded by European Social Funds and National Resourses

REFERENCES

[1] Bastian, T. S., Pick, M., Kedraon, A., Maia, D., & Vourlidas, A., The Coronal Mass Ejection of 1998 April 20: Direct Imaging at Radio Wavelengths, The Astrophysical Journal, 558, L65-L69, 2001.

[2] Burlaga, L. F., Interplanetary Magneto hydrodynamics, (Oxford University Press, 1995).

[3] Bougeret, J.-L., Kaiser, M. L., Kellogg, P. J., Manning, R., Goetz, K., Monson, S. J., Monge, N., Friel, L., Meetre, C. A., Perche, C., Sitruk, L., & Hoang, S., Waves: The Radio and Plasma Wave Investigation on the Wind Spacecraft, Space Science Reviews, 71, 231-263, 1995.

[4] Caroubalos, C., Maroulis, D., Patavalis, N., Bougeret, J.-L., Dumas, G., Perche, C., Alissandrakis, C., Hillaris, A., Moussas, X., Preka-Papadema, P., Kontogeorgos, A., Tsitsipis, P., & Kanelakis, G., The New Multichannel Radiospectrograph ARTEMIS-IV/HECATE, of the University of Athens, Experimental Astronomy, 11, 23-32, 2001.

[5] Kallenrode M. and Cliver E., Rogue SEP events: Observational aspects, Proc. 27th Int. Cosmic Ray Conf., Hamburg, Germany, 8, 3314-3317, 2001

[6] Kerdraon, A., & Delouis, J.-M., The Nancay Radioheliograph, Coronal Physics from Radio and Space Observations; Proceedings of the CESRA Workshop held in Nouan le Fuzelier, France 3-7 June 1996, (Gerard Trottet, ed., Springer, 1997), 192.

[7] Kontogeorgos, A.; Tsitsipis, P.; Caroubalos, C.; Moussas, X.; Preka- Papadema, P.; Hilaris, A.; Petoussis, V.; Bouratzis, C.; Bougeret, J.-L.; Alissandrakis, C. E. & Dumas, G., The improved ARTEMIS IV multichannel solar radio spectrograph of the University of Athens, Experimental Astronomy, 21, 41, 2006.

[8] Loewe C. and Prolss G., Classification and mean behaviour of magnetic storms, J. Geophys. Res., A 102, 14209-14213, 1997

[9] Mavromichalaki, H., Sarlanis, C., Souvatzoglou, G., Tatsis, S., Belov, A., Eroshenko, E., Yanke, V., & Pchelkin, A., Athens Neutron Monitor and its aspects in the cosmic-ray variations studies., Proceedings of the 27th International Cosmic Ray Conference. 07-15 August, 2001. Hamburg, Germany, (IUPAP, 2001), 4099.

[10] Mavromichalaki, H., Souvatzoglou, G., Sarlanis, C., Mariatos, G., Gerontidou, M., Papaioannou, A., Plainaki, C., Tatsis, S., Belov, A., Eroshenko, E., & Yanke, V., The new Athens Center on data processing from the Neutron Monitor Network in real time, First European Space Weather Week 2004, ESA/ESTEC, The Netherlands Annales Geophysicae, 23, 1-8, 2005.

[11] Mavromichalaki, H., Papaioannou, A., Mariatos, G., Papahliou, M., Belov, A., Eroshenko, E., Yanke, V., & Stassinopoulos, E. G. Cosmic ray radiation effects on space environment associated to intense solar and geomagnetic activity. IEEE Transactions on Nuclear Science, 54, 1089-1096, 2007.

[12] Yashiro, S., Gopalswamy, N., Michalek, G., St. Cyr, O. C., Plunkett, S. P., Rich, N. B., & Howard, R. A., A catalog of white light coronal mass ejections observed by the SOHO spacecraft, Journal of Geophysical Research, 109, 7105-7115, 2004.

The biggest Forbush effect in 2003 according to observations on Mt. Hermon in neutron total component and in different multiplicities

L.I. Dorman[1, 2], L.A. Pustil'nik[1], A. Sternlieb[1], I.G. Zukerman[1]

[1]*Israel Cosmic Ray Space Weather Center and Emilio Segre' Observatory affiliated to Tel Aviv University, Technion and Israel Space Agency, Israel*
(lid@physics.technion.ac.i; llid1@post.tau.ac.il)
[2]*Cosmic Ray Department of IZMIRAN Russian Academy of Science, Russia*

Abstract – **We investigate the biggest in 2003 Forbush effect observed by NM of Emilio Segre' Observatory on Mt. Hermon in neutron total component (more than 15%) and in different multiplicities. On the basis of these data we determine rigidity spectrum of cosmic ray intensity decrease, effect of pre-increase, and estimate properties of interplanetary shock wave and moving magnetic trap caused observed giant Forbush effect in cosmic rays. We compare obtained data with results of observations on other sites on the Earth and on satellites.**

Evolution and flare productivity of SEE active regions in the last solar physical cycle (solar cycles 22 & 23)

V.N. Ishkov

Institute of Terrestrial Magnetism, Ionosphere and Radio Wave Propagation by Pushkov, Russian Academy of Sciences (IZMIRAN), Russia (ishkov@izmiran.ru)

Abstract – **Last "physical" cycle of solar activity uniting solar cycles 22 and 23, has brought a lot of new in our understanding of solar active events, especially extreme. It is enough to notice, that practically all the most powerful events 22 solar cycles were carried out in a phase of a maximum, and in a solar cycle 23 extreme solar events were carried out at the latest stage of a phase of a minimum. In cycle 22 similar flare event occurred on March, 1989 (~ max.), June 1991 (~2.5 y). For 10 years of development of 23 solar cycle it is registered only five flares with a x-ray importance (X >=10) (for example, for interval 1 - 15 June, 1991 only, its was 5 too, and there are more solar extreme events, than for all 21 solar cycle) and three of them were the main one during the concerned of flare activity period 19.10 - 04.11.2003 (~ 3.5 y.) Research of active regions with extreme flare events has allowed to reveal general characteristics of these areas and conditions of generation of such events. Attention is drawn to necessity to distinguish actually solar extreme events and extreme displays of disturbances of a Earth's environment space. The last depend on geometrical factors of occurrence and propagation of disturbances from greater flare events more. The last are frequent not extreme. The opportunity of forecasting extreme flare events as result of interaction of new emerging magnetic fluxes and with already existing magnetic structures is considered.**

MHD-Turbulence simulations for solar corona

Z. Romeou[1], M.Velli [2], and G. Einaudi [3]

[1] *Directory of Metrology, Ministry of Development, Athens, Greece ,*
[2] *Department of Astronomy and Space Sciences, University of Florence, Italy, ,*
[3] *Department of Physics, University of Pisa, Pisa, Italy*

Abstract— **The way the energy is disposed in the solar corona has always been an issue of great interest. It remains yet unclear how the low temperature photosphere supports the existence of solar extreme phenomena. In this work a turbulent heating mechanism for the solar corona through the framework of Reduced Magnetohydrodynamics (RMHD) is proposed. Two-dimensional incompressible long time simulations of the average energy disposition have been carried out with the aim to reveal the characteristics of the long time statistical behavior of a two-dimensional cross section of a coronal loop. It was found that a slow photospheric magnetic field driving self-organizes at large scales via an inverse MHD cascade. Scaling laws are being proposed in order to quantify the nonlinearity of the system response. Finally the importance of the photospheric time scales forthe coronal heating problem is analyzed and discussed.**

***Key Words*—Magnetohydrodynamics (MHD), Turbulence, Sun:Activity, Sun:Corona, Sun:Magnetic field .**

I. INTRODUCTION

MECHANISMS of magnetic turbulence have played over the latest years a funtamendal role in the understanding of a number of extreme events related with the solar magnetic field and also in providing some answers to the so far unresolved problem of coronal heating. Different MHD turbulent scenarios effective in the development of the fine scales in the solar corona have been discussed by many authors ([5], [15], [12],[21],[2],[25]).

Numerical modelling in two and three dimensions ([6],[7],[16],[17]) has been developed to validate or disprove the ideas of topological dissipation by Parker,[20], further developed into the so-called nanoflare heating theory.

[9] and [11] were the first to show how the dissipation time-series of the two dimensional magnetically forced simulations of MHD turbulence displayed intermittent behaviour with events following a power-low behaviour. [8], [13],[14] also showed how this model of turbulence of a coronal loop could be relevant to the coronal heating problem. See also related work in [1], [10],[18].

Here we are making a step forward by studying how the dissipation end evolution of the 2D system depends on the time-scales associated with the photospheric forcing.

To begin, we will study the case of a constant forcing, resembling a photospheric shearing motion.

We then carry out simulations with various random generated but spatially large scale-forcing profiles and variable in time over a range of time-scales compared with the internal dynamical time-scale of the turbulence.

The paper is constructed as follows. In Section II we present the assumptions and the details of the model we have used, and in Section III we present and discuss the numerical results. We summarise the results and conclude in Section IV.

II. THE NUMERICAL MODEL

We consider a cross section of a coronal loop threaded by a strong axial magnetic field B_0 with footpoints rooted in the photosphere. Boundary disturbances propagate along the axial direction z with the associated Alfvénic velocity giving rise to perpedicular magnetic and velocity fields $b_\perp$ and $u_\perp$. In the limit of a large loop aspect ratio, one may follow the evolution by using the reduced MHD equations (1) and (2), see[22], [24]:

$$\rho\left(\frac{\partial \vec{u}_\perp}{\partial t} + \vec{u}_\perp \cdot \vec{\nabla}\vec{u}_\perp\right) = -\vec{\nabla}_\perp\left(p + \tfrac{1}{2}b_\perp^2\right) + \\ + \vec{b}_\perp \cdot \vec{\nabla}\vec{b}_\perp + B_0\frac{\partial \vec{b}_\perp}{\partial z} + \nu\nabla^2\vec{u}_\perp \quad (1)$$

$$\frac{\partial \vec{b}_\perp}{\partial t} = \vec{b}_\perp \cdot \vec{\nabla}\vec{u}_\perp - \vec{u}_\perp\vec{\nabla}\vec{b}_\perp + B_0\frac{\partial \vec{u}_\perp}{\partial z} + \eta\nabla^2\vec{b}_\perp \quad (2)$$

where ρ is the mass density, p is the plasma pressure and ν and η are the collisional dissipation coefficients, the kinematic viscosity and the resistivity respectively. For a detailed discussion on the assumptions under which these equations are valid and the final form in which they are used in this model see [23], [9] and [11].

III. NUMERICAL RESULTS

First we investigate the effect of a time constant forcing.

We have calculated time-series of the spatial average of the current dissipation ηj^2 with varying resolutions of 64 x 64, 128x128 and 256x256.
We have shown (see [23]) that passing from 128x128 to 256x 256 does not cause a considerable change. In the following runs we kept a resolution of 128 x 128 grid points with uniform spacing in both directions.
We next investigated how the evolution at long times depends on the initial noise. For that reason we plotted timeseries of the mean dissipation of each η keeping the

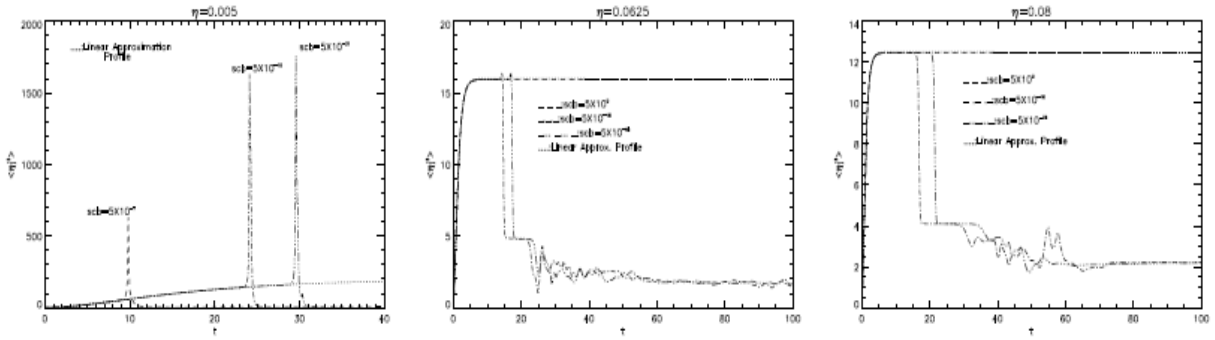

Fig. 1. Dependence of dissipation $< \eta j^2 >$ on scb, scv, namely the amplitudes of the initial profiles given for α and ψ, for a range of η's from 0.005 to 0.08. In each graph, timeseries of averaged current dissipation of a fixed η are plotted for successively smaller values of scb, scv (scb of a dashed line >scb of a dashed-dot line > scb of a dashed-tripple dot line). In the first graph, it is shown that for η = 0.005, in the range of η < 0.0625 and for successively smaller values of scb, scv, the peak is reached later in time and the dissipation peak gets bigger, while for η = 0:0625 (centre graph) and η > 0.0625 (right graph) it reaches an asymptotic value for all values of scb, scv. For comparison, the linear approximation solution is overplotted, dotted line in all graphs. It can be easily shown that the later is given by $< \eta j^2 > \sim (1/\eta)(1 - \exp(-\eta k^2 t))^2$.

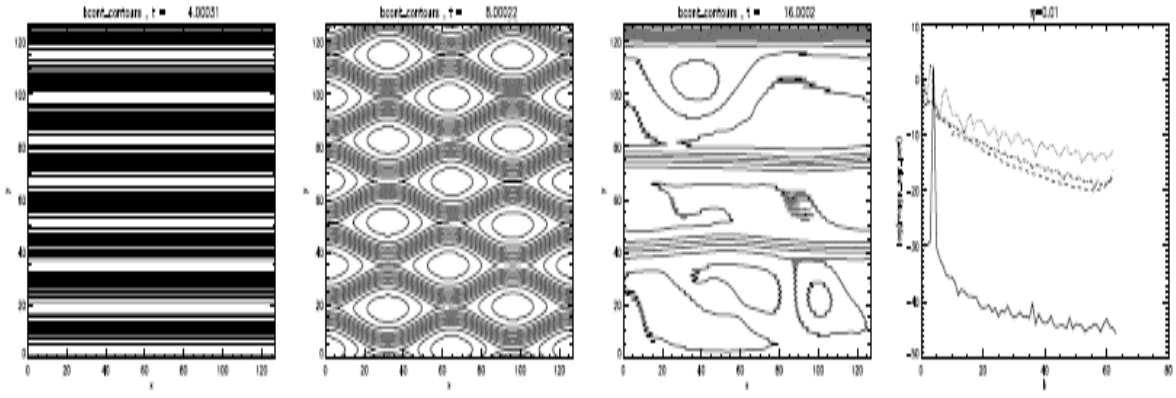

Fig. 2. Graphs 1-3: α -fieldlines contours for η = 0.01. Three dinstinct phases are demonstrated clearly: An initial linear phase followed by the formation of a compact islands structure which at later times disentagles giving way to a more diffused magnetic fieldlines structure. Graph 4: Spectra of the square of the magnetic potential at a time before the peak (solid line), at a time right after the peak (dotted line), and for times long after the peak (dashed and dashed-dotted lines). It is shown the redistribution of the magnetic energy before, during, after, and long after the peak in modes smaller than the k = 4 initially imposed by the forcing, demonstrating the expected appearance of a secondary inverse cascade at longer times where the system seems to relax to larger scales.

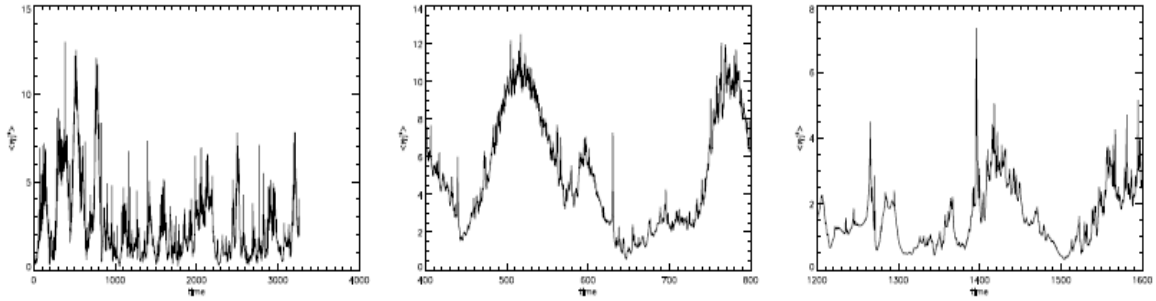

Fig. 3. Typical long time timeseries of $< \eta j^2 >$ with random forcing, for η = 0.004, 128 X 128 resolution, and tkink = 64. The full run is shown on the left, two intervals of which are zoomed in the centre and on the right. The relationship between tkink and the intervals of appearance of dissipation events would be important to understand the role of the time scaling and it is a work under study.

amplitudes of the initial profiles of the fields, namely scb, scv as parameters, and succesively reducing them.

Fig. (1) shows clearly a strong dependence on these two parameters which can be regarded as the seeds of the noise necessary for reconnection to start up.

Decreasing η seems to suppress the contribution of the linear terms and strengthen nonlinearities.

These conclusions only regard the initial phase of the evolution. The long time evolution is not very much affected as long as scb and scv are not too small to allow instabilities to develop.

What changes significantly though with resistivity is the value of the peak and the time it is reached. The time at which dissipation leaves off the linear approximation solution is indicative of the time it takes for the nonlinearities to evolve and for the energy to redistribute and be released via resistive modes.

The appearance of a strong sharp peak therefore reveals the tendency of the system to respond rapidly and intensively to what in the absence of resistivity would have been an ideal MHD energy release.

We then plotted this asymptotic value of the maximum of the mean dissipation against η.

We used these values to plot the dissipation peak against resistivity, the difference of this peak from the linear approximation asymptotic value again as a function of η and finally the time it takes to reach this peak after it leaves off the linear approximation solution.

From the best fit for the lines in the corresponding log-log graphs we obtained the following scaling laws:

for the dissipation peak : $dis_{max} = 0.23\ \eta^{-1.56}$,

for the difference of this peak from the linear approximation asymptotic value as a function of η : $d(dis_{max}) = 0.04\ \eta^{-2.4}$,

and finally for the time it takes to reach this peak after it leaves off the linear approximation solution : $dt_{peak} = 0.64\ \eta^{-0.1}$.

It is evident from these results that with lower resistivity the dissipation peak increases rapidly from the point of view of the order of the magnitude. Nonlinear effects become more effective while dt_{peak} also increases with decreasing resistivity.

We further investigated the structure of the fields and the currents. In all cases there were three distinct phases developing.

This response is typical for the whole range of η's we tried, see Fig. (2).

Another interesting point comes from the study of the spectra. Initially, before the peak is reached the dominant mode for the emission of magnetic energy is the one imposed by the forcing profile, namely k = 4.

Right after, energy is allowed to redistribute in other modes as well. In the long run, the system seems to develop a secondary inverse cascade activity as it is expected for 2D MHD magnetic invariants.

To compare this results with a random time dependent forcing profile, we followed [11],[9],[10] and assumed for the forcing profile a form where the eddy turnover time t_{kinck} is introduced.

We first investigated the dependence with resolution and concluded that seems not to be important when resolution is high enough, for a discussion [23].

We confirmed that initial conditions are soon forgotten and the profiles of the time series resemble the later (after the dissipation peak) stages of the constant forcing case.

Finally we calculated long time timeseries for different t_{kinck} from which we can clearly see how the relationship between photospheric and internal time scale makes a difference, see Fig.[3].

A systematical study for quantifying this dependence is ongoing work.

IV.CONCLUSIONS

Under the assumptions of the Reduced MHD approximation, we have investigated the spatial and temporal response of a coronal loop system in two

different cases. Firstly by assuming constant time forcing and secondly by applying random time dependent forcing.
Using a numerical pseudospectral method for the calculation of timeseries of ηj^2 we have showed:
the dependence with η the effects of resolution, the effects of the initial conditions, and the role of the time scaling in the mechanisms involved.
We have shown that there are three phases appearing, indicated by the development of a strong and fast dissipation peak which falls off rapidly.
The fields are organised into a compact magnetic island structure, which gradually disentagle before a secondary
inverse cascade takes over. Study of the spectral response corroborates this behaviour.
The strength and the duration of the dissipation peak have been scaled with η in order to quantify the non linear response of the system.
Simulations of long time timeseries for the second case where we set the system subject to random forcing for a range of different t_{kinck} and η's revealed the appearance of dissipation events within intervals of the order of the corresponding t_{kinck} demonstrating the significance of the scaling between the photospheric and the internal times of the system.

ACKNOWLEDGMENT

This work was supported by EU grant Contract No. HPRN-CT-200100310. Z.R thanks the Physics Department, University of Patras for their hospitality. We thank R.Betta, M. Ghiglione and E. Buchlin for numerical help and useful discussions.
G. Vekstein & Y.Katsukawa, “Scaling Laws for a Nanoflare-Heated Solar Corona”, The Astrophysical Journal, 541,pp. 1096-1103, 2000.

REFERENCES

[1] V. Aletti, M. Velli & K. Bocchialini, “Microscale Structures on the Quiet Sun and Coronal Heating”, *The Astrophysical Journal*, 544, pp. 550-557, 2000.
[2] A.A .van Ballegooijen,,“Cascade of magnetic energy as a mechanism of coronal heating”, The Astrophysical Journal, 311,pp. 1001 1014, 1986.
[3] D.Biscamp,,in Nonlinear Magnetohydrodynamics,ed. Cambridge,
[4] Energy Release via ideal three-dimensional instability”, Advances in Space Research, 32, 6, pp 1029-1034, 2003.
[5] P. Dmitruk, D.O. Gomez & E.E.DeLuca, “Magnetohydrodynamic Turbulence of Coronal Active Regions and the Distribution of Nanoflares”, The Astrophysical Journal, 505, pp. 974-983, 1998.
[6] G.Einaudi, M.Velli, H.Politano & A. Pouquet, “Energy Release in a Turbulent Corona”, The Astrophysical Journal, 457, pp.L 113-116, 1996.
[7] G.Einaudi, & M.Velli, “The distribution of flares, statistics of magnetohydrodynamic turbulence and coronal heating ”, Physics of Plasmas, 6, 11, pp. 4146-4153, 1999.
[8] M. Georgoulis, M. Velli & G. Einaudi,, “Statistical Properties of Magnetic Activity in the Solar Corona”, The Astrophysical Journal,497, pp. 957-966, 1996.
[9] V. Glukhov,“Tearing Instability of a Neutral Current Sheet of the Solar Corona”, The Astrophysical Journal,469, pp. 936-943, 1996.
[10] T. Gomez, H. Politano & A. Pouquet, “On the validity of a nonlocal approach for MHD Turbulence”, Physics of Fluids,11, 8, pp. 2298-2306, 1999.
[11] D.O. Gomez, P.A. Dmitruk, & L.J. Milano, “Recent Theoretical Results on Coronal Heating”,Solar Physics,195, pp. 299-318, 2000.
[12] A.B. Hassam, “Tearing modes in solar coronal loops”, The Astrophysical Journal, 348, pp. 778-780, 1990.
[13] D.L. Hendrix, & G.van Hooven, “Magnetohydrodynamic Turbulence and Implications for Solar Coronal Heating”, The Astrophysical Journal,467,pp. 887-893, 1996.
[14] Z Mikic, D.D. Schnack, & G .van Hooven, “Creation of current filaments in the solar corona”, The Astrophysical Journal, 338,pp. 1148-1157, 1989.
[15] L.J Milano & D.O. Gomez, “Solar Coronal Heating: AC versus DC”, The Astrophysical Journal, 490, pp.442-451, 1997.
[16] S.A. Orszag & C.M. Tang, “Small-scale structure of two-dimensional magnetohydrodynamic turbulence”, Journal of Fluid Mechanics, 90, pp.129-143, 1979.
[17] E.N. Parker, “Nanoflares and the solar X-ray corona”, The Astrophysical Journal,330, pp. 474-479, 1988.
[18] E. R. Priest, C. R Foley, J. Heyvaerts et al., “A Method to Determine the Heating Mechanisms of the Solar Corona”, The Astrophysical Journal, 539, pp. 1002-1022, 2000.
[19] Z. Romeou, M. Velli & G.Einaudi, “Long Time incompressible 2D MHD Simulations of Coronal Loop Heating: The role of photospheric time-scales”, Proceedings of the SOHO 15 Workshop-Coronal Heating, ESA SP-575, 539, pp. 1002-1022, 2004.
[20] Z. Romeou, M. Velli & G. Einaudi, “Forced MHD Turbulence Simulations for Coronal Loop Heating”, Recent Advances in Astronomy and Astrophysics, 848, pp. 105-114, 2006.
[21] H. Strauss, “Non-linear, three-dimensional magnetohydrodynamics of non-circular tokamacs”, Physics of Fluids, 19,pp. 134-140, 1976. 1993.
[22] G.Boffetta, A.Celani & R. Prandl., “Large Scales instabilities in two dimensional magnetohydrodynamics, ”Physical Review E, 61,4,pp. 4329-4335, 2000.
[23] P.J. Cargill, “Some implications of the nanoflare concept, ” The
Astrophysical Journal, 422, pp.381-393, 1994.
[24] R.B.Dahlburg & G. Einaudi, “MHD unstable modes in the 3D evolution of 2D MHD Structures and the diminished role of coalescence instabiities ”, Physical Letters A, 294, pp.101-107, 2002.
[25] R.B. Dahlburg, J.A. Climchuk, & S.K.Antiochos, “Coronal

Extreme Solar Cycle Elements Prediction for the Running 22-year Cycle (No. 24 – 25 years 2005-2027)

V. Tritakis[*], H. Mavromichalaki[†], G. Giouvanellis [†]

[*]*Research center of Astronomy and Applied Mathematics, Academy of Athens,*
[†]*Nuclear and Particle Physics Section, Physics Department, University of Athens*
vas@academyofathens.gr; emavromi@phys.uoa.gr; giogiouvas@yahoo.gr

Abstract – **Fundamental parameters of a solar cycle could be predicted if we take in mind an existed interdependence between successive 11-year and 22-year cycles. Elements which could be predicted are, the time of rise, the total duration, the yearly extreme values of the activity on the maximum and minimum epochs of the cycles as well as the time of maximum and the second minimum. Predicted values of these parameters for the cycles No. 24 (2005-2016) and No. 25 (2016-2027) are tabulated in this contribution. The small value of standard error (high coincidence between observed and calculated values) which have been succeeded during the application of the present method in the past solar cycles implies success of the proposed method of prediction for the forthcoming cycles.**

I. INTRODUCTION

The impressive progress in the solar physics research during the last decades has not succeeded to describe the exact mechanism of the solar activity development, yet. This is a very serious difficulty to define a confident solar cycle prediction based on pure physics. However, the rapid evolution of new and dynamic branches of solar and space physics like, Space Weather, Solar Variability, Global Change have made the necessity of accurate short-term and medium – term solar activity predictions very urgent.

Since the prediction of the solar activity by physical methods is still impossible but the demand for predictions is very intense, it is reasonable to turn to the only way left which is the development and the improvement of empirical methods which can approach an approximated profile of a forthcoming solar cycle.

This is a very long and old way along which many methods of this category have been developed and a large number of papers have been published on this subject.

The common point of these methods is the use of statistical characteristics of solar cycles or various optical, geomagnetic and interplanetary precursors. All these methods are separated in three major categories concerning to the range of the prediction they can possibly succeed. The short–range category comprises methods they attempt to predict solar activity for the next few days or weeks, the middle-range methods offer forecasting for the next 11-year solar cycle, while the long range methods risk predictions for several solar cycles. Methods of the last category are rather hopeless

or they contain only philological interest because the relatively short duration of systematic observations of the

Sun (120 years or 10-12 solar cycles) does not allow the formulation of a significant prediction way.

On the other hand, short-term methods are mainly based on the continues recording of the solar disk and the near interplanetary medium seeking for some indication of solar activity change. The medium –range methods are based on empirico-statistical characteristics of the previous solar cycles which can be extrapolated to the forthcoming cycles. There are tenths of methods which can be classified in the last category the oldest of which were introduced by legends of the solar activity subject like [1], [2], [3], [4]. In the present study we attempt to forecast the main parameters of the next couple of 11-year solar cycles using some very close relations they exist between two successive solar cycles especially a

couple of an even-odd cycles they form a 22-year magnetic cycle[5].

II. DATA ANALYSIS

A substantial point of the following method is that uses alternative data from the typical Wolf's numbers. These data come from the relation,

$$I_\alpha = 1/2\,(\sqrt{A} + \sqrt{f}) \qquad (1)$$

where I_α is the area index, A and f the areas of sunspots and faculae, measured by the Greenwich Observatory, respectively [6], [7]. The reason we prefer to use this index instead to the well and wide accepted Wolf Numbers (W.N) is the presence of faculae which add physical meaning in the final formula. It is widely known that the faculae are good indicators of the small scale solar magnetic fields they surround active centers and make solar activity more effective. In addition, this index varies smoothly within a rather narrow range of values that makes it very predictable, in contrast to the Wolf's numbers they vary abruptly within a wide range of values. The variations of both the Wolf's numbers (upper panel) and the area index (bottom panel) for the time span 1884-2004 are depicted in Fig. 1. It is obvious that sunspot number values are ranged between 0 and 200 and Area index varies in the range from 7 and 55.

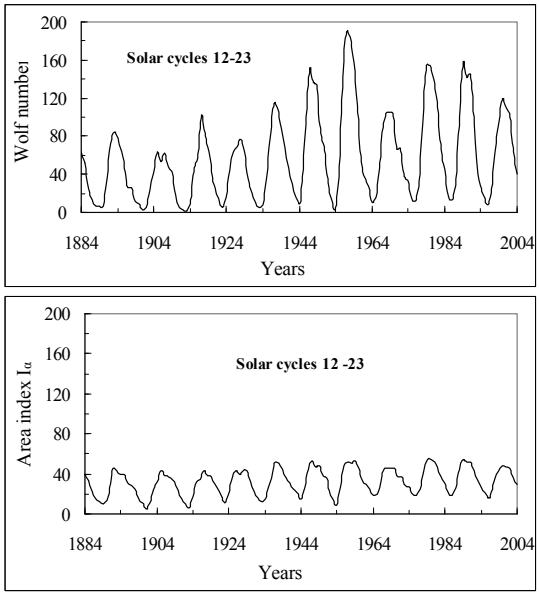

Fig. 1. Time distribution of the Wolf's numbers (upper panel) and the area index (lower panel) for the solar cycles 12-23 (1884-2004).

Fundamental data of both indexes can be easily found and downloaded by the sites: http://www.ngdc.noaa.gov/stp/SOLAR/ftpwhiteligh tfaculae.html and http://www.ngdc.noaa.gov/stp/SOLAR/ftpsunspotn umber.html.

A serious problem we faced during processing was the limited record of faculae which exceeded until the year 1969. After that year, the Greenwich Observatory which compiled this record abolished the areas and faculae observations patrol. Fortunately, the correlation between the I_α and the $\sqrt{R}$ is extremely high, almost 98% (Figure 2), so we were able to complete our faculae time series until nowadays, in a high confidence level 97%, by extrapolating the relation,

$$I_\alpha = 3.98\sqrt{R} + 4.43 \qquad (2)$$

III. THE METHOD

According to our way of prediction, the most important point of a solar cycle is the quasi-triangle area which is limited by the ascending branch of a solar cycle and the vertical from the maximum to the time axis, called "ascending triangle" (Figure 3).

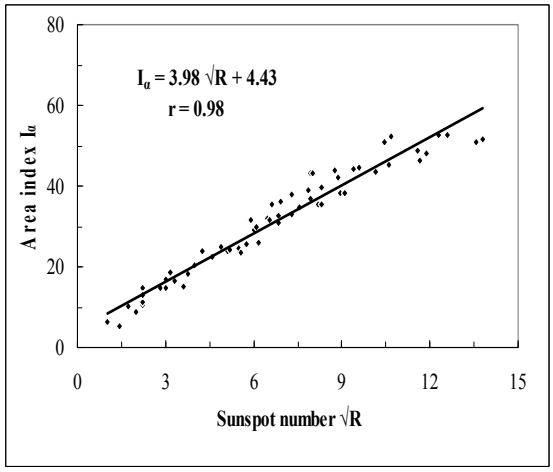

Fig. 2. The regression line between the area index Iα and sunspots number $\sqrt{R}$.

Two very important parameters of this triangle is the slope of the ascending branch m_α which could be calculated by the least square method and the time of rise T_R that is, the time interval from the appearance of the preliminary indications of a new solar cycle to the maximum of it.

It is known that there are differences in solar activity from cycle to cycle. There are series of cycles with very high activity level (odd cycles) as well as series of cycles with quite low activity

(even cycles). A different behavior between even and odd solar cycles is presented in solar activity, where even sunspot cycles are characterized by two well defined 'still stands' in the level of activity during the declining phases of such cycles. If we consider a couple of an even and an odd cycle according the Waldmeier's numbering system of solar cycles (the cycle that starts in the year 1610 is cycle No.1) we verify that there are strong correlations among basic parameters of the cycles they belong to the same couple. At first, there is a strong correlation between the time of rise and the slope of the ascending branch of the even cycle. In addition, the inverse slope of the ascending branch of the all studied here even cycles correlate very well with the rising time of the corresponding next odd cycles given a correlation coefficient 90%. The regression line of the inverse slope of the ascending branch of an even cycle with the time of rise of the next odd cycle as well as the inverse slope of the descending branch of an odd cycle with the rising time of the next even cycle are given in the figure 4, left and right panel, respectively. From this figure it is clear that the rising time of the odd cycles is smaller than the even cycles in general, a result which was expected due to a previous work [9]. The regression in both panels of the figure 4 gives a very good formula for predicting the time of rise of a forthcoming cycle by the slope of the previous cycle which has competed the ascending branch.

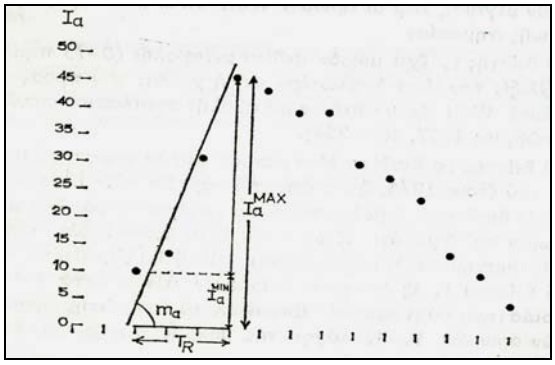

Fig. 3. The ascending triangle of a typical solar cycle. Parameters T_R , m_α , I_α^{max} and I_α^{min} are defined.

The relations which could help in the prediction of T_R are defined ,

$$1/m_\alpha = 0.1T_{R(n+1)} - 0.30 \quad (\text{for even cycles}) \quad (3)$$

$$1/m_\kappa = 0.1T_{R(n+1)} - 0.32 \quad (\text{for odd cycles})$$

where m_α is the slope of a certain cycle and $T_{R(n+1)}$ is the rising time of the next cycle.

The application of the above relations to past solar cycles gave accuracy, that is, a coincidence between real and predicted values of the slope, 91% which is a very high criterion of confidence.

The accuracy for odd cycles is about 91% and for even cycles is also high and about 92%. The choice of two relations and not only one had been guided by the differences of odd and even cycles, that are described by many researchers [10], [11], [8]. Generally, the odd cycles are characterized by one maximum, hard rising time, "saddle-like" shape and "mesa-type" maximum, whereas even cycles are characterized by two maxima, soft rising time, "peak-like" shape and "point-type" maximum [12].

When we succeed to predict the time of rise of a forthcoming cycle we can proceed to the next step which is to predict the total time of a forthcoming solar cycle that is, the time span between the first and the second minimum of the cycle. It could be done by dividing all the solar cycles in two groups. Group1 contains the cycles ({1, 2}, {5, 6}, {9, 10}, {13, 14}, {17,18}, {21, 22}, {25, 26}…) and Group 2 contains ({3,4}, {7, 8}, {11,12}, {15,16}, {19,20}, {23, 24}…). The way we divide solar cycles in the above two groups implies a quasi periodicity of 22 years which coincides to the solar magnetic field inversion [8]. In the figure 5, the correlation between the total time and the time of rise of each cycle for the groups 1 and 2 is depicted, while the equations (5) and (6) below express the relevant relations. If T_R, for each group are the predicted from the relations (3) and (4) values, we can predict the total time with accuracy 95% and 92% for the groups 1 and 2 respectively (Fig. 5)

$$T_{tot} = 0.85\ T_R + 7.63 \quad \text{(group 1)} \quad (5)$$
$$T_{tot} = 0.55\ T_R + 7.62 \quad \text{(group 2)} \quad (6)$$

The maximum area index during a certain cycle could be predicted by the following relations (7) and (8), where T_R is the rising time predicted by the relations (3) with accuracy 96% for group 1 and 95% for group 2 presented in Fig. 6.

$$I_\alpha^{max} = -5.30\ T_R + 70.22 \quad \text{(group 1)} \quad (7)$$
$$I_\alpha^{max} = -6.20\ T_R + 72.16 \quad \text{(group 2)} \quad (8)$$

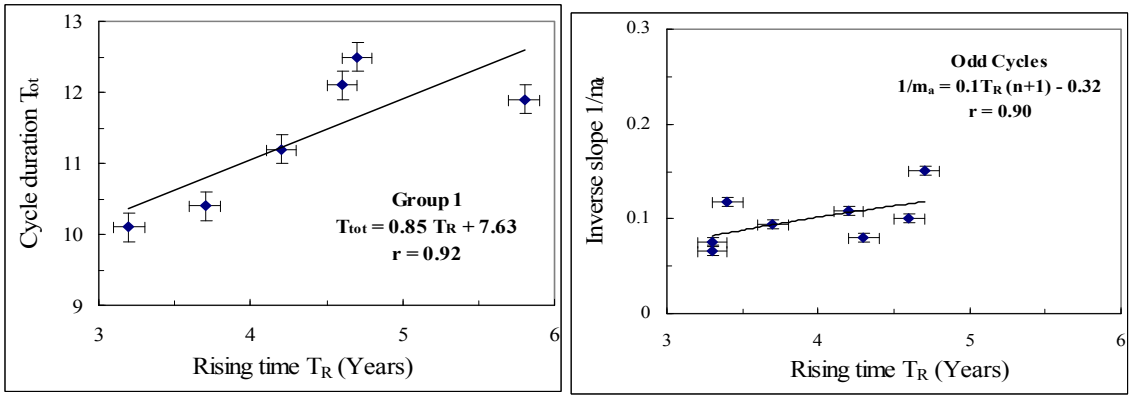

Fig. 4. The regression lines between the inverse slope of an even cycle to the time of rise of the next odd cycle (left panel) and between the same parameters of a couple odd -even cycle (right panel)

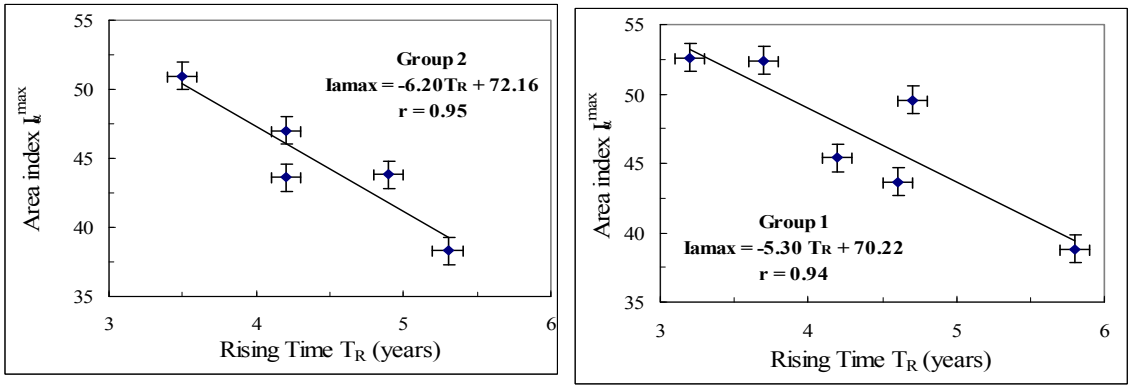

Fig. 5. Regression lines between the total time and the rising time for both group 1 and group 2 cycles.

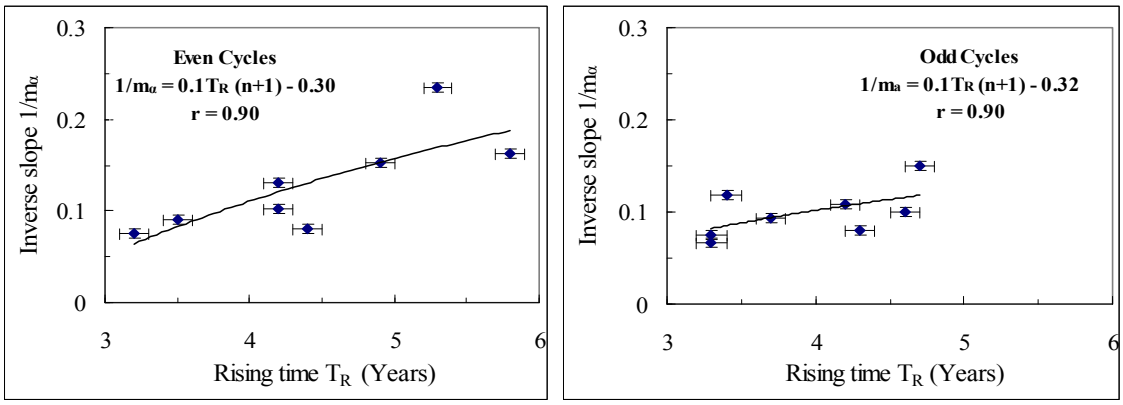

Fig. 6. The regression lines between the area index and the rising time for both group 1 and group 2 cycles

Parameters	Used data cycle 19	Predicted data cycle 21	Observed data cycle 21	Residuals Obs-Cal
m_α	15.02	-	-	-
T_R		3.8 years	4.3 years	**0.5** years
T_{tot}	-	11 years	10.6 years	**0.4** years
I_α^{max}	-	47.43	50.52	**3.09** units
I_α^{max} epoch	-	Jun 1979	Oct 1979	**4** months

TABLE I(a). Results of the application of the proposed model to the cycle 21

Parameters	Used data cycle 20	Predicted data cycle 22	Observed data cycle 22	Residuals Obs-Cal
m_α	7.63	-	-	-
T_R		4.4 years	4 years	**0.4** years
T_{tot}	-	10.7 years	11.2 years	**0.5** years
I_α^{max}	-	47.6	46.9	**0.7** units
I_α^{max} epoch	-	Jul 1989	Mar 1989	**4** months

TABLE I(b). Results of the application of the proposed model to the cycle 22

Parameters	Used data cycle 22	Predicted data cycle 24	Accuracy
m_α	12.51	-	-
T_R		3.7 years	91%
T_{tot}	-	10.7 years	92%
I_α^{max}	-	50.26	92%
Rmax	-	132.59	92%
I_α^{max} epoch	-	Jun 2009?!!	90%

Parameters	Used data cycle23	Predicted data cycle 25	Accuracy
m_α	8,46	-	-
T_R		4.4 years	90%
T_{tot}	-	11.3 years	95%
I_α^{max}	-	46.9	95%
Rmax	-	113.86	92%
I_α^{max} epoch	-	Dec 2020?!!	90%

TABLE II. Predicted values of basic elements of the forthcoming cycles No. 24 and 25 (2005-2027).

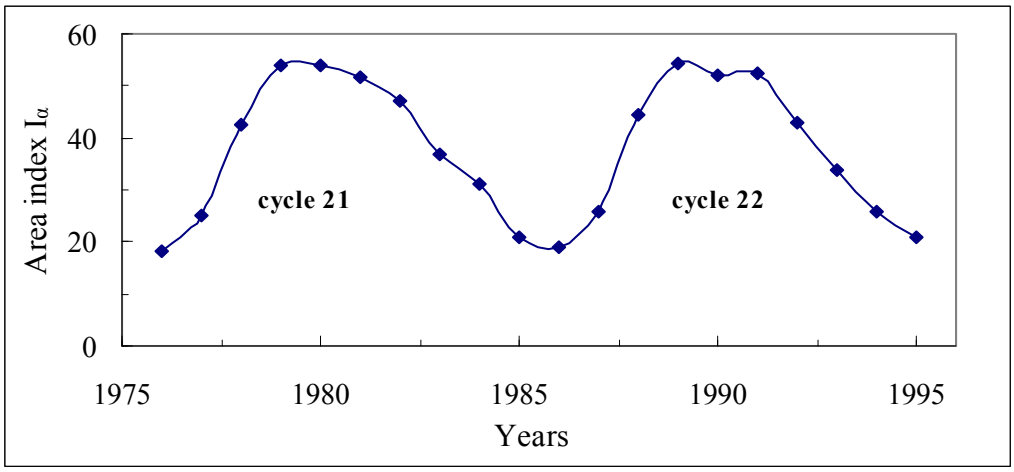

Fig. 7. Time evolution of the solar cycles 21 and 22 (1975-1995).

IV. RESULTS

Application to Past Cycles: As an example we present an application of the proposed method to the past cycles 21 and 22. The time evolution of these solar cycles (1975-1995) expressed by the area index I_α are depicted in Figure 7, while a comparison between observed and predicted by this method values of some important elements of the above cycles are tabulated in the Tables I(a) and I(b). It is obvious that the coincidence between observed and predicted values is very high, something which makes us very optimists concerning the prediction of the same elements for the forthcoming cycles No. 24-25 (2005-2027). It is important to be noticed that the predicted values of the basic elements of cycle 21 are very close to the observed ones. It is noteworthy that the epoch I_α^{max} deviates only four months from the observed value.

Application to Forthcoming Cycles: In the Table II purely predicted values of basic elements of the forthcoming solar cycles No. 24 and 25 (2005-2027) are tabulated. In the last column the accuracies between observed and predicted values of these elements for the past solar cycles No. 12-23 are bolded. The high values of coincidence between observed and calculated elements imply optimistic results for our prediction.

V. CONCLUSIONS

The application of the above prediction method to all the confident past solar cycles supports the aspect that there is a great interdependence between two successive 11-year cycles they form a couple of even-odd cycle, according to the Waldmeier's numbering system. It is obvious that the evolution of an odd cycle depends very much on the evolutionary behaviour of the preceding even cycle. A reasonable exploitation of this interdependence can lead to a high accuracy prediction of the same basic parameters of a forthcoming 11-year cycle. The important point of this method is that the use of the area index values instead of the widely known Wolf's numbers or relative sunspot numbers as solar activity indicator. The reason for this change is the high predictability of the area index in contrast to the Wolf's numbers. The predicted values tabulated above in the Table I(a) give high grade of coincidence between observed and predicted values which in all cases exceed 90%. Concerning to the special characteristics of the predicted cycles we could underline that the prediction for the forthcoming solar cycle No. 24 gives a high solar activity cycle with maximum on June 2009 (fast rising and high maximum). On the other hand, the prediction for solar cycle 25 forms the profile of a moderate solar activity cycle with maximum on December 2020 (slow rising and medium maximum).

ACKNOWLEDGMENTS

Thanks are due to the Hellenic Astronomical Society supporting the student G. Giouvanellis to participate the Hellaset Conference 2005.

REFERENCES

[1] M. Waldmeier, *Astron. Mitt. Zurich*, **14**, 439 (1939)

[2] W, Gleissberg, *Solar Phys*., **21**, 240 (1971)
[3] A. I. Ohl, Solnechnaya Dannyye 9 73 (1976),
[4] A. McNish and J.V. Lincoln, *Trans. Amer. Geoph. Union*, **30**, 5 (1949)
V. Tritakis, Astrophys. Space Sci. 82, 463
[5] (1982)
[6] J. Xanthakis, Nature, 210, 1942 (1966)
[7] C. Poulakos and V. Tritakis, *Solar Phys.*, 229 (1973)
[8] H. Mavromichalaki, A. Belehaki and X. Rafios, *Astron. and Astrophys.* **330**, 764 (1998)
[9] H. Mavromichalaki, E. Marmatsouri and A. Vassilaki, *Earth, Moon and Planets*, **42**, 233, 1988
[10] H. W.Dodson and E. R. Hedeman, Solar Phys. 42, 121 (1975)
[11] M. Storini, *Adv. Space Res.* **16**, 53 (1995) H. Mavromichalaki, A. Belehaki, X. Rafios and I. Tsagouri, *Astrophysics and Space Science* **246**, 7 (1997)

Session C

The chain of physical processes in the solar- terrestrial system
(Sun-Heliosphere-Magnetosphere Ionosphere-Upper Atmosphere - Ground)

Chair: E. Flueckiger, M. Gehmeyr
R. Hippler, L. Miroshnichenko, I. Dandouras, I. Veselovsky

Solar **E**xtreme **E**vents **2007**

Magnetosphere response to the 2005 and 2006 extreme solar events as observed by the Cluster and Double Star spacecraft

Iannis S. Dandouras[1], Henri Rème[1], Jinbin Cao[2], and Philippe Escoubet[3]

[1] *Centre d'étude Spatiale des Rayonnements, CNRS/Université de Toulouse, Toulouse, France,*
[2]*Key Laboratory of Space Weather, CSSAR /CAS, Beijing, China,*
[3]*ESA/ESTEC RSSD, Noordwijk, The Netherlands*

Abstract – **The four identical Cluster spacecraft, launched in 2000, orbit the Earth in a tetrahedral configuration and on a highly eccentric polar orbit (4 - 19.6 R_E). This allows the crossing of critical layers that develop as a result of the interaction between the solar wind and the Earth's magnetosphere. Since 2004 the Chinese Double Star TC-1 and TC-2 spacecraft, whose payload comprise also backup models of instruments developed by European scientists for Cluster, provided two additional points of measurement, on a larger scale: the Cluster and Double Star orbits are such that the spacecraft are almost in the same meridian, allowing conjugate studies. The Cluster and Double Star observations during the 2005 and 2006 extreme solar events are presented, showing uncommon plasma parameters values in the near-Earth solar wind and in the magnetosheath. These include solar wind velocities up to ~900 km s^{-1} during an ICME shock arrival, accompanied by a sudden increase in the density by a factor of ~5 and followed by an enrichment in He^{++} in the secondary front of the ICME. In the magnetosheath ion density values as high as 130 cm^{-3} were observed, and the plasma flow velocity there reached values even higher than the typical solar wind velocity. These resulted in unusual dayside magnetosphere compression, detection of penetrating high-energy particles in the magnetotail, and ring current development following several successive injections of energetic particles in the inner magnetosphere, which "washed out" the previously formed nose-like ion structures.**

***Key Words*— magnetosphere compression, energetic particles, ring current.**

I. INTRODUCTION

The Cluster mission, prepared by the European Space Agency in collaboration with NASA, is based on four identical spacecraft launched in 2000. The spacecraft are on similar elliptical polar orbits with a perigee at about 4 R_E and an apogee at 19.6 R_E, flying in a tetrahedral configuration [1]. This configuration allows the separation between spatial and temporal variations in the plasma populations, encountered along the spacecraft orbit, and the calculation of 3D parameters. During the northern hemisphere winter the apogees of the orbits are in the near-Earth solar wind, allowing to study the magnetopause and the bow shock structure and response to solar wind conditions, whereas due to the annual orbit precession during the other half of the year the spacecraft perform measurements in the magnetotail. There they can analyze the plasma sheet dynamics during magnetospheric stors and substorms. During perigee passes the Cluster spacecraft cross the ring current region, the radiation belts and the outer plasmasphere, from south to north.

On board each spacecraft 11 experiments permit a wide variety of measurements of the plasma parameters (particles and fields). Among them, the CIS (Cluster Ion Spectrometry) experiment is a comprehensive ionic plasma spectrometry package, capable of obtaining full three-dimensional ion distributions with good time resolution (one spacecraft spin) and with mass-per-charge composition determination [2]. The CIS package consists of two different instruments, a Hot Ion Analyser (HIA) and a time-of-flight ion Composition and Distribution Function analyzer (CODIF). A fluxgate magnetometer (FGM) provides high-resolution magnetic field measurements on
board the four spacecraft [3].

The data from the 11 experiments onboard Cluster are in the process of being archived at the Cluster Active Archive (CAA: http://caa.estec.esa.int/). The CAA is a depository

of processed and validated high-resolution data, and is publicly accessible. Its purpose is to maximize

the scientific return from the mission, and to ensure that the unique data set returned by the Cluster mission is preserved in a stable, long-term archive for scientific analysis even beyond the end of the mission.

Since 2004 the Chinese Double Star TC-1 and TC-2 spacecraft have provided two additional points of measurement, on a larger scale: the Cluster and Double Star orbits are such that the spacecraft are almost in the same meridian, allowing conjugate studies. The equatorial spacecraft (TC-1) was launched into an elliptical orbit of 1.09 x 13.4 R_E, inclined at 28.5° to the equator. This enabled it to investigate the Earth's magnetic tail, or the dayside outer magnetosphere during the other half of each year, and then to cut through the inner magnetosphere and get even below the inner radiation belt at perigee (Fig. 1). TC-2 was launched into a polar orbit (1.1 x 6.8 R_E, ~90° inclination).

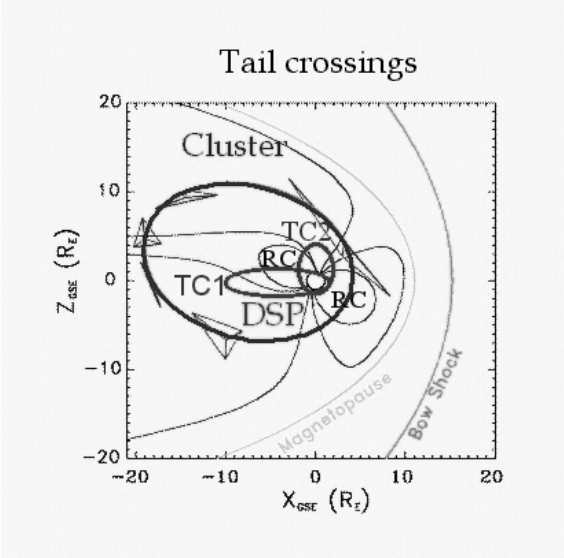

Fig. 1. Orbits of Double Star and Cluster during the magnetotail crossings. The Cluster orbit is given in red and the orbits of the two Double Star (DSP) satellites, i.e. the equatorial TC-1 and the polar TC-2, are in purple. RC is the ring current region.

The Double Star payload comprises a combination of Chinese experiments and backup models of instruments developed by European scientists for Cluster. Among them, the HIA (Hot Ion Analyzer) instrument on board the Double Star TC-1 spacecraft is an ion spectrometer nearly identical to the HIA sensor of the CIS instrument on board the four Cluster spacecraft. This instrument has been specially adapted for TC-1. It measures the 3D distribution functions of the ions between 5 eV/q and 32 keV/q without mass discrimination [4]. The Double Star magnetic field data used come from the FGM (Fluxgate Magnetometer) experiment on board TC-1 [5].

One of the major objectives of Cluster and Double Star is to understand the physical processes by which solar wind particles enter into the magnetosphere. During some of the 2005 and 2006 extreme solar events, presented here, the Cluster and Double Star spacecraft were favorably located to observe the solar wind parameters sudden changes, taking very uncommon values, and/or the response of the magnetosphere to these sudden changes.

21 JANUARY 2005 EVENT

On January 20, 2005, an outstanding solar flare occurred and stimulated one of the largest GLE (Ground Level Enhancement) events produced at the Earth in 50 years [6]. Subsequent to this flare, an ICME (Interplanetary Coronal Mass Ejection) was detected in the near-Earth space on January 21, which showed evidence of current sheet substructure near the periphery of a strongly expanding, fast magnetic cloud [7].

During the ICME arrival (17:10 UT), the Cluster spacecraft were in the solar wind, at MLT≈14.5 hours and at a geocentric distance of 19.4 R_E, whereas the Double Star TC-1 spacecraft was initially in the dayside magnetosphere and then in the in the magnetosheath, at MLT≈17 hours and at a geocentric distance of 10.5 R_E (Fig. 2). As shown in the Cluster data (spacecraft 4 example, Fig. 3), the arrival of the leading edge of the ICME shock resulted in a sudden strong increase of the magnetic field and strong magnetic field fluctuations, in a hardening in the spectrum of the solar wind H^+ and He^{++} ions, in an increase of the solar wind velocity up to ~900 km s^{-1}, and in a jump by a factor of ~5 in the H^+ and He^{++} ion densities. The spacecraft entered then in the ICME sheath, and a secondary front arrival can be identified at 18:44 UT. This is characterized by a sudden increase in the He^{++} density. This He^{++} enrichment is probably indicating the arrival of the flare driver gas [7].

The Double Star TC-1 data are shown in Fig. 4. As a result of the magnetospheric compression provoked by the ICME arrival at Earth the spacecraft, initially in the dayside magnetosphere, entered in the in the magnetosheath at ~17:11 UT, and even a short excursion in the solar wind was observed at 17:37 UT. The magnetosheath is revealed, in the energy-time ion spectrograms, by the heated plasma (broad energy range) presenting a highly anisotropic flow. A second excursion in the solar wind was observed at 18:53 UT, and then the spacecraft re-entered in the magnetosheath at

19:07 UT, traversing the bow shock at a geocentric distance of 8.5 R_E and revealing thus a highly compressed dayside magnetosphere. In the magnetosheath ion density values as high as 130 cm^{-3} were observed, which contrast strongly with the ~30 - 40 cm^{-3} values typically observed there. The plasma flow velocity values measured in this extreme magnetosheath regime reached 630 km s^{-1}, which is even higher than the typical solar wind velocity.

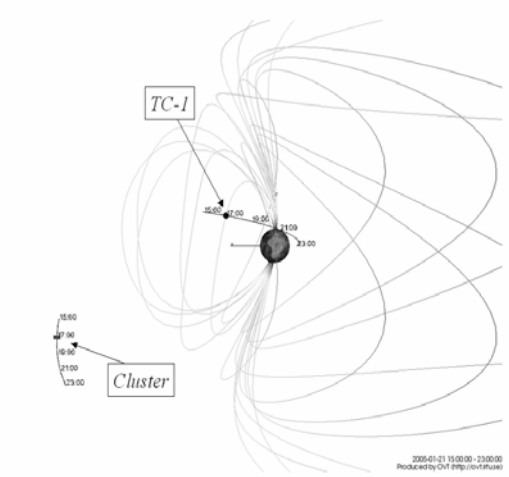

Fig. 2. Cluster spacecraft 4 orbit (in black) and Double Star TC-1 orbit (in red) for the January 21, 2005 event, projected on the Tsyganenko 1989 magnetic field model. The model is plotted for reference, to show the typical magnetospheric configuration under quite conditions. Orbit Visualization Tool plot, courtesy of the OVT team.

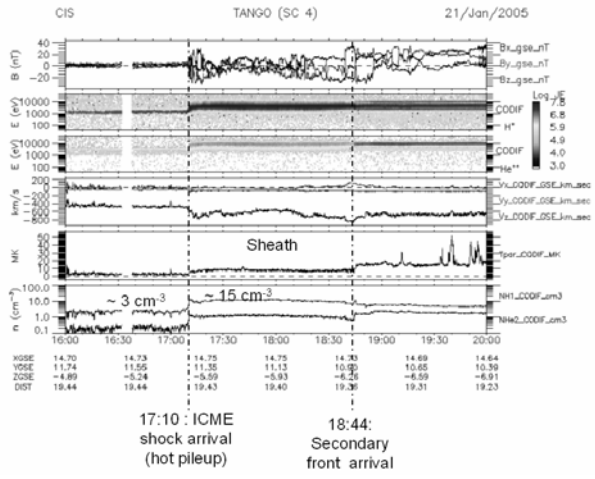

Fig. 3. Cluster spacecraft 4 magnetic field and ion data for the January 21, 2005 event. From top to bottom: magnetic field, CIS-CODIF energy-time spectrograms separately for H^+ and He^{++} (data in energy flux units: keV cm^{-2} s^{-1} sr^{-1} keV^{-1}); H^+ ion bulk velocity; H^+ parallel temperature, H^+ and He^{++} densities, spacecraft coordinates (GSE system) and geocentric distance in R_E..

The spacecraft went then through a highly compressed magnetosphere, and finally entered into the ring current region where a series of injected ion populations were observed, presenting energy dispersion effects.

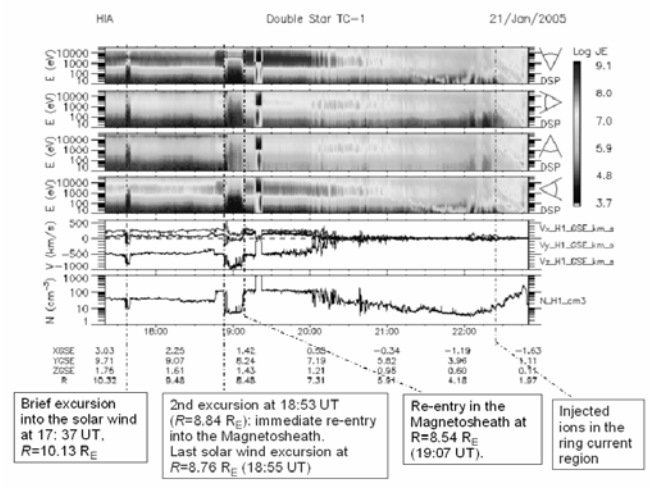

Fig. 4. Double Star TC-1 ion data for the January 21, 2005 event. From top to bottom: HIA energy-time spectrograms (4) for ions arriving in the 90° x 180° sector with a field-of-view pointing in the sun, dusk, tail, and dawn direction respectively, in energy flux units (keV cm^{-2} s^{-1} sr^{-1} keV^{-1}); ion bulk velocity; ion density, spacecraft coordinates (GSE system) and geocentric distance in R_E..

During the January 21, 2005 event the ring current development was also monitored by the Double Star TC-2 and the IMAGE spacecraft. These spacecraft are equipped with the NUADU energetic neutral atom imager [8] and the HENA energetic neutral atom imager [9] respectively, and were both favorably placed to monitor by remote sensing the ring current development. These observations and their analysis are presented in detail in reference [10].

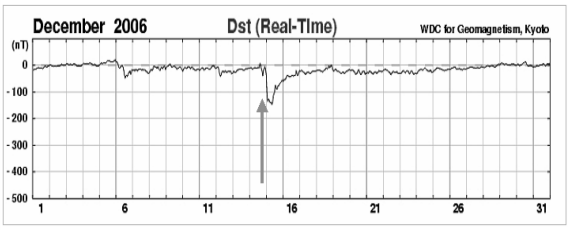

Fig. 5. *Dst* index values for December 2006. On December 14, 2006, the onset of an intense magnetic storm was recorded while the Cluster spacecraft were going through perigee.

14 DECEMBER 2006 EVENT

On December 13, 2006, during the descending phase of the 23rd solar cycle and almost into its minimum, a significant X3 solar flare occurred, followed by a strong Earthward oriented CME [11]. The impact of the ejecta on the Earth's

magnetosphere occurred at ~14:30 UT on December 14, 2006, and a solar wind velocity of 930 km s^{-1} was recorded by ACE (data not shown), associated with a jump of the solar wind density to

~10 cm^{-3} and a southward turning of the IMF.

The inner magnetosphere conditions on December 14 were initially quiet, with the exception of a short negative *Dst* index excursion to -40 nT at 18 UT. But, at 0 UT on December 15, the *Dst* index intensified rapidly to -110 nT, and at 7 UT it reached a value of -147 nT (Fig. 5). The recovery phase of this intense storm started at ~12 UT on December 15, 2006, and the ring current activity returned to quiet conditions on December 17, 2006.

The Cluster and Double Star TC-1 orbits during this event were inside the magnetosphere, and are shown in Figure 6. As deduced from the H^+ spectrogram in the upper panel of Fig. 7, Cluster entered into the ring current region (RC), in the morning sector at ~13:50 UT, while the exit, at the outbound leg of its orbit, was recorded at 16:24 UT. Strong background due to penetrating particles from the radiation belts was recorded in both the inbound and the outbound leg of its orbit, at L-shell values between ~5.5 and 6.5 ("red haze" in the spectrograms around 15 UT and around 16 UT). In the CODIF energy range a "banded" ion structure was observed, with its energy evolving during this pass from 4-12 keV initially to 5-18 keV. This kind of banded structures, also called "nose-like" structures due to the shape they can sometimes take in the energy-time ion spectrograms, are characterized by a deeper inward penetration of particles coming from the tail at a given energy (typically a few keV), and then spreading to both higher and lower energies at larger L-shell values [12, 13]. A similar strong inbound/outbound asymmetry is also observed in the profile of the radiation belts penetrating particles, and it is apparently related to the highly tilted magnetic dipole (Figure 6). It should be noted that the Cluster perigee pass occurred just when the ejecta cloud hit the magnetosphere, but before the ring current intensification as registered by the *Dst* index.

The Double Star TC-1 spacecraft went through perigee at 11:40 UT (Fig. 7). At its inbound leg the HIA instrument recorded an entry into in the ring current at 03:30 UT, in the 23 MLT sector, i.e. in the opposite MLT sector with respect to Cluster. The high-energy resolution of the instrument allows the analysis in two energy bands of the observed, during the inbound leg, nose-like structure, one band at 10-14 keV and one above 20 keV, its upper limit being beyond the instrument energy domain. At its outbound leg, and after the exit from the heavy radiation belts background zone, i.e. after 14 UT, the HIA instrument recorded a much more active ring current ion population, with several successive injections, the bulk of the energy being apparently above the instrument energy domain (E > 32 keV) and HIA detecting only the lower part of their energy spectrum. Starting from 19:39 UT, and when the TC-1 spacecraft was at a geocentric distance of 8.7 R_E in the pre-midnight magnetotail, the instrument recorded a background due to penetrating SEPs (Solar Energetic Particles), which appears as a "green haze" in the energy-time ion spectrogram.

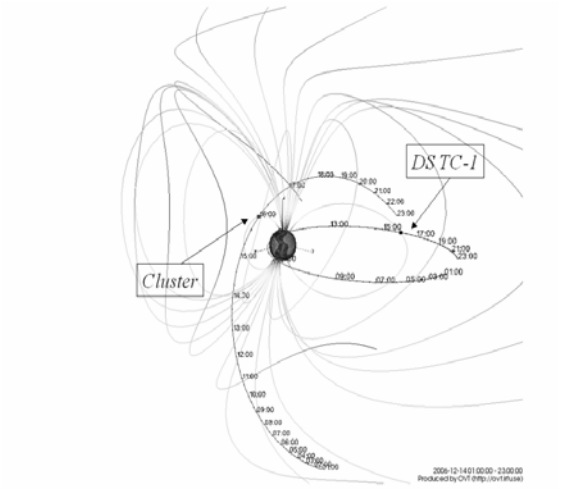

Fig. 6. Cluster spacecraft 4 and Double Star TC-1 orbits for the December 14, 2006 event, projected on the Tsyganenko 1989 magnetic field model.

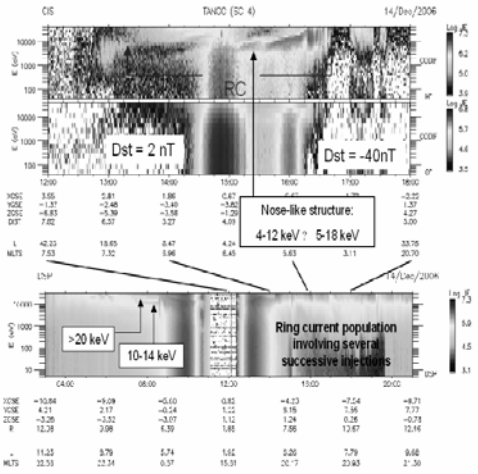

Fig. 7. Combined Cluster sc 4 (CODIF H^+ and O^+ data) and Double Star TC-1 (HIA ion data) for the December 14, 2006 perigee pass.

CONCLUSION

During some of the 2005 and 2006 extreme solar events, the Cluster and Double Star spacecraft were favorably positioned to provide coordinated measurements and monitor the solar wind parameters sudden changes, taking very uncommon values, and/or the response of the magnetosphere to these changes. In particular:

- Solar wind velocities up to ~900 km s^{-1} were measured during an ICME shock arrival, accompanied by a sudden increase in the density by a factor of ~5 (21 January 2005 event).
- During the secondary front of this ICME an enrichment in He^{++} was observed, probably indicating the arrival of the flare driver gas.
- The ICME resulted in a very strong magnetospheric compression. In the magnetosheath ion density values as high as 130 cm^{-3} were observed, and the plasma flow velocity values measured in this extreme magnetosheath regime reached 630 km s^{-1}, which is even higher than the typical solar wind velocity.
- Ring current development was monitored (14 December 2006 event). A "nose-like" ion structure, previously formed in the ring current region and simultaneously detected by the Cluster and Double Star spacecraft in opposite MLT sectors, was "washed out" by several successive injections of energetic particles. These injections resulted in a much harder ring current energy spectrum.
- During this event the arrival of penetrating SEPs (Solar Energetic Particles) was recorded inside the pre-midnight magnetotail, about 5 hours after the impact of the CME ejecta on the Earth's magnetosphere.

ACKNOWLEDGMENT

The author acknowledges the use of ACE data in this study. The *Dst* index was provided by the World Data Center for Geomagnetism, Kyoto.

REFERENCES

[1] C. P. Escoubet, M. Fehringer, and M. Goldstein, "The Cluster mission", *Ann. Geophys.,* 19, 1197-1200, 2001.

[2] H. Rème, et al., "First multispacecraft ion measurements in and near the Earth's magnetosphere with the identical Cluster ion spectrometry (CIS) experiment", *Ann. Geophys*., 19, 1303, 2001.

[3] A. Balogh, et al., "The Cluster Magnetic Field Investigation: Overview of in-flight performance and initial results", *Ann. Geophys*.; 19, 1207, 2001.

[4] H. Rème, et al., "The HIA instrument onboard the Tan Ce 1 Double Star near-Equatorial Spacecraft and its first results", *Ann. Geophys.,* 23, 1432-0576/ag/2005-23-2757, 2005.

[5] C. Carr, et al., "The Double Star magnetic field investigation: instrument design, performance and highlights of the first year's observations", *Ann. Geophys.,* 23, 2713-2732, 2005.

[6] A. V Belov, E. A. Eroshenko, H. Mavromichalaki, C. Plainaki, and V. G. Yanke, "Ground level enhancement of the solar cosmic rays on January 20, 2005", *Proc. 29th Internat. Cosmic Ray Conf*., (Pune), 1, 189-192, 2005.

[7] C. Foullon, C. J. Owen, S. Dasso, L. M. Green, I. Dandouras, H. A. Elliott, A. N. Fazakerley, Y. V. Bogdanova, N. U. Crooker, "Multi-spacecraft study of the January 21st 2005 ICME: Evidence of current sheet substructure near the periphery of a strongly expanding, fast, magnetic cloud", *Solar Phys.,* 244, Issue 1-2, 139-165, 2007.

[8] S. McKenna-Lawlor, L. Li, S. Barabash, K. Kudela, J. Balaz, I. Strharsky, K. Brinkfeldt, C. Shen, J. Shi, C. Jin-Bin, S.-Y. Fu, E.C. Roelof, P. C:son Brandt**,** and I. Dandouras**, "**The NUADU experiment on TC-2 and the first Energetic Neutral Atom (ENA) images recorded by this instrument", *Ann. Geophys.*, 1432-0576/ag/2005-23-2825, 2005.

[9] D. G. Mitchell, S. E. Jaskulek, C. H. Schlemm, E. P. Keath, R. B. Thompson, B. E. Tossman, J. D. Boldt, J. R. Hayes, G. B. Andrews, N. Paschalidis, D. C. Hamilton, R. A. Lundgren, E. O. Tums, P. L. Wilson. H. D. Voss, D. Prentice, K. C. Hsieh, C. C. Curtis, and F. R. Powell, "High energy neutral atom HENA imager for the IMAGE mission", *Space Sci. Rev*., 91, 67-112, 2000.

[10] S. McKenna-Lawlor, L. Li, I. Dandouras, P. C. Brandt, Y. Zheng, S. Barabash, R. Bucik, K. Kudela, J. Balaz, I. Strharsky, C. Shen, J. Cao, and Q. Zong, "Observations in energetic neutral atoms of the development and decay of a ring current event on 21-22 January, 2005", *J. Geophys. Res. (submitted)*, 2008.

[11] C. Plainaki, H. Mavromichalaki, A. Belov, E. Eroshenko, and V. Yanke, "Application of the NM-BANGLE model to GLE70", *Proc. 30th Intern. Cosmic Ray Conf*., Merida, Mexico, 2007.

[12] C. Vallat, N. Ganushkina, I. Dandouras, C .P. Escoubet, M. Taylor, H. Laakso, A. Masson, J-A.Sauvaud, H. Rème, and P. Daly, "Ion multi-nose structures observed by Cluster in the inner Magnetosphere", *Ann. Geophys.,* 25, 171-190, 2007.

[13] I. Dandouras, J. Cao, and C. Vallat, "Energetic ion dynamics of the inner magnetosphere revealed in coordinated Cluster- Double Star observations", *J. Geophys. Res. (submitted)*, 2008.

Balloon measurements of cosmic ray fluxes in the atmosphere and role of these particles in the atmospheric processes

Y. Stozhkov[1], V. Ermakov[2], N. Svirzhevsky[1]

[1]*Lebedev Physical Institute of the Russian Academy of Sciences, Russia*
(stozhkov@fian.fiandns.mipt.ru)
[2]*Central Aerological Observatory of Rosgidromet*

Abstract – **The experimental data on cosmic ray fluxes in the atmosphere obtained in the balloon experiments from 1957 till present time are analyzed. The following questions are discussed: long-term modulation of cosmic rays and negative trend of cosmic ray flux; ion production in the atmosphere; cosmic rays, electric characteristics of the atmosphere and global electric circuit; thundercloud formation and lightning production; global changes of climate in the nearest future.**

Dynamics of the plasma sheet in the magnetotail: Interrelation of turbulent flows and thin current sheet structures

A. P. Kropotkin

Skobeltsyn Institute of Nuclear Physics, Moscow State University, Moscow, Russia
(apkrop@dec1.sinp.msu.ru)

Abstract - **Dynamics of the magnetotail features two different time scales. A short time scale T1 is associated with disturbances propagating in the tail lobes, with their relatively strong magnetic field and low plasma density. A longer time scale T2 is associated with plasma motions in the plasma sheet, with its small normal component of the magnetic field and a greater density. A disturbance appearing in the magnetotail on the time scale T1 produces a weak loss of equilibrium on medium spatial scales (a few RE) in the plasma sheet. It is shown by means of theoretical argument and numerical simulation that the relaxation process which follows on the time scale T2, produces extremely thin embedded current sheets, along with generation of fast plasma flows. The process provides an effective mechanism for transformation of magnetic energy accumulated in the magnetotail, into energy of plasma flows. The fast flows may drive turbulence on shorter spatial scales. In their turn, these motions may serve as an origin for neutral line generation, and reconnection. The latter generates signals in MHD modes, propagating in the magnetotail lobes, and thus new fast disturbances on the time scale T1 are produced. Application to substorm phenomenology is discussed.**

Some peculiarities of the decay of extreme solar energetic particle events

E.I. Daibog, K. Kecskemety, Yu.I. Logachev

Skobeltsyn Institute of Nuclear Physics, Moscow State University,Moscow, Russia
(daibog@srd.sinp.msu.ru)

Abstract – **The majority of few-MeV solar energetic particle (SEP) events exhibit exponential-law decays. The comparison of experimental values of characteristic decay times, tobs, with those obtained in theoretical models considering convection transport and adiabatic deceleration shows that theoretically expected t values, Ttheor = 3r/4V (1 + ν ή γ), V is the solar speed, ν ή γ spectral exponent, r distance from the Sun, depending on environmental plasma parameters, are reasonably close (within about 25 %) to the fitted slopes in nearly 50% of all cases where solar wind speed stays approximately constant. These results were obtained for 1-25 MeV protons on the basis of large statistics of IMP 8 data. On the basis of SOHO COSTEP and ACE EPAM data on proton and electron intensities correlations between their shapes and characteristic decay times in the framework of the above theoretical model are considered. It is shown that in extreme events this correlation deviates from the predicted one. The decay of the event of 23 Sep.1978 is discussed which can be considered as extreme from the point of view of theoretical interpretations. The same peculiarities may be considered as confirmations of CME-associated shock acceleration, particle reservoir and convection transport and adiabatic deceleration models.**

Forecasting the Solar Wind in the Inner Heliosphere

M. Gehmeyr, N. Arge, L. Mayer, D. Odstrcil

University of Colorado, United States of America
(gehmeyr@lasp.colorado.edu)

Abstract – **One main effort of the Center for integrated Space Weather Modeling (CISM) is to develop space weather models for the Sun-Earth chain. Among them is the Solar Wind model that gives a 3 dimensional description of the solar wind structures in the inner heliosphere. It is driven by daily NSO/SOLIS synoptic maps. We employ the Wang-Sheeley-Arge (WSA) algorithm to compute potential field solutions of the solar corona and derive inner boundary conditions for the ideal MHD code ENLIL. It in turn propagates the solar wind structures out to Earth and beyond. With this model we can describe the ambient solar wind at the three locations of the ACE and STEREO space crafts. We predict the plasma parameters for lead times of 1 to 5 days in 8 hour cadences and describe the space environment in the inner heliosphere. This model is implemented at the NOAA Space Environment Center in Boulder, Colorado. We report on validation efforts and prediction performances, and demonstrate how our model supports the activities at the forecast center.**

Topology of the high latitude magnetosphere during large magnetic storms and the main mechanisms of relativistic electron acceleration

E.E.Antonova[a, b], I.P. Kirpichev [b, a], M.V. Stepanova[c], K.G. Orlova[a], I.L. Ovchinnikov[a]

[a]*Skobeltsyn Institute of Nuclear Physics Moscow State University, Moscow, 119991, Russia*
[b]*Space Research Institute RAS, Moscow, Russia*
[c]*Physics Department, Universidad de Santiago de Chile, Casilla 347, Correo 2, Santiago, Chile*

Abstract – **One of the main endeavors of the "Space Weather" program is the prediction of the appearance of very large fluxes of relativistic electrons with energies larger than 1 MeV, because they represent a serious potential hazard for satellite missions. Large fluxes of relativistic electrons are formed in the outer radiation belt during the recovery phase of some storms. The formation of large fluxes is connected to a balance between the acceleration and loss processes. A two-step acceleration process is ordinarily analyzed. A "Seed" population with energies ~hundreds of keV appeared during expansion phase of magnetospheric substorm. A "Seed" population is additionally accelerated obtaining relativistic energies by some other process. Several acceleration mechanisms have been proposed for the explanation of the electron acceleration, including radial diffusion and internal acceleration by wave-particle interactions. Nevertheless, none of them takes into account great changes of magnetospheric topology during a magnetic storm. Such changes are mainly connected with asymmetric and symmetric ring current development. We analyze the changes of magnetospheric topology during magnetic storms. We show that a change of the magnetospheric magnetic field can be the important factor determining the acceleration of relativistic electrons.**

Keywords: **magnetic storms, magnetospheric currents, magnetospheric pressure balance**

I. INTRODUCTION

The problem of acceleration of relativistic electrons continues to be one of the main endeavors of Space Weather programs. Relativistic electrons are called "satellite killers" due to the effects leading to satellite anomalies and even loss of spacecrafts (see, for example, [1]). They appear**,** as a rule**,** during the recovery phase of geomagnetic storms (see the review of [2]). Wave-particle acceleration is usually considered (see, for example, [3], [4], [5], [6]) as the main factor responsible for the acceleration of relativistic electrons. However, it is well known, that the characteristic feature of a magnetic storm is the formation of the ring current. The ring current is greatly asymmetric during the storm main phase and becomes symmetric during the storm recovery phase. The ring current development leads to a depression of the magnetic field inside the magnetosphere. The restoration of the magnetic field produces the regular betatron acceleration of particles injected into the region of the depressed field (seed population of electrons). Therefore, the clarification of the role of turbulent mechanisms of electron acceleration requires the investigation of the action of such a regular mechanism of electron acceleration and therefore the configuration of a storm time magnetic field.

Existing models of magnetic field including the latest version of Tsyganenko model ([7], [8]) suggest that the main sources of the magnetospheric magnetic field are magnetopause currents, tail current, ring current and partial ring current, field-aligned currents. The proper selection of magnetospheric current system is very important as neglecting the contribution of some comparatively powerful systems can lead to real uncertainties during the analysis of the experimental data. For example, [9] had difficulties in the comparison between the measured and predicted **(**by theory**)** positions of the geomagnetic cutoffs because of the uncertainties in the geomagnetic field provided by

Tsyganenko-89 ([10]) and Tsyganenko-04 ([8]) models.

At the beginning of storm research, it was found that depression in the storm time magnetic field is related to the development of the ring current. Nevertheless, later it was suggested (see, for example, [11] and references therein) that tail current closed by magnetopause currents can produce a great**,** sometimes dominant contribution to magnetic field depression inside the magnetosphere, therefore it can strongly affect the value of Dst variation. However, such a suggestion meets with difficulties connected to magnetopause pressure balance on the geomagnetic flanks (see [12]). It was also impossible to explain relationship between the lowest position of the westward electrojet center $L_{\max}$ and the maximal value of Dst -variation $|D_{st}|_{\max}$ (see [13]). It is necessary to point out that this position coincides with the region of the first appearance of relativistic electrons during the storm. In the dipole mapping, according to [13]:

$$\left|D_{st}\right|_{\max} = 2.75 \cdot 10^4 L_{\max}^{-4} \text{ nT} . \qquad (1)$$

In [14], [12], [15] and [16] it was shown that the magnetosphere has an additional current system, named cut ring current (CRC), which was not previously included in the existing models of magnetospheric currents. It is a high latitude continuation of ordinary ring current, mapped into the main part of the auroral oval. The existence of such a current system is connected to the extension of the plasma sheet to the daytime longitudes and to the earthward direction of magnetospheric plasma pressure gradients. However, the value of transverse current in the CRC current system had not been determined till now.

In this paper, we evaluate the value of transverse current in CRC current system during quiet and disturbed conditions and show that the inclusion of CRC into the existing magnetic field models can be very important for the adequate description of the magnetospheric magnetic field and for the solution of the problem of acceleration of relativistic electrons.

II. TOPOLOGY OF MAGNETOSHPERIC PLASMA DOMAINS

Even during the first observations of the auroral oval, it was shown that the oval has a closed quasi-ring structure. [17] obtained a daytime picture of auroral particle precipitations in which plasma sheet particle precipitations come from a region situated at the equator from the low latitude boundary layer (LLBL). [18] improved this picture and showed that the daytime precipitation region identified by [17] as a "void" is the region of plasma sheet like precipitations. The latest results of [19] also show the closed loop structure of plasma sheet precipitations under all geomagnetic conditions. Results of AMPTEE/CCE observations give the possibility to obtain the distribution of plasma pressure at the equatorial plane (see [20], and [21]). The global picture of magnetospheric plasma pressure distribution at L<9 demonstrates the presence of nearly azimuthally symmetric plasma distribution at L~7-9 and plasma pressure isotropy ([21]). Such distribution corresponds to plasma domain surrounding the Earth. The plasma pressure gradient in this domain has an earthward direction, which implies the existence of a westward transverse current. The region from 7 till $9R_E$ is ordinarily recognized as the region of quasitrapping for particles with energies ~100 keV (see, for example, [22]). It is possible to continue this region at larger distances (till the magnetopause near noon) as events of drift echo were observed on the satellite Geotail by [23]) till 12-13R_E near midnight. Drift trajectories of most particles in the region of quasitrapping are closed inside the magnetosphere. It is natural to suggest that westward transverse currents in this region are also closed inside the magnetosphere and form the high latitude continuation of the ordinary ring current (RC). The discussion of the main features of magnetospheric high latitude topology is to be found in the [15].

III. CRC AND ITS MAGNETIC FIELD

[21] reproduced current density in the equatorial plane using the values of plasma pressure gradients derived from AMPTE/CCE satellite and the Tsyganenko-87 ([24]) magnetic field model. The nighttime part of the picture corresponds to comparatively large current densities ~3-5 nA/m^2 and was attributed to the partial ring current. Daytime current densities were smaller ~1 nA/ m^2. However, dayside field lines are very compressed. Minima of magnetic field on these field lines are deposited far from the equatorial plane. Therefore, the values of the daytime current densities obtained by [21] are smaller than the largest current densities at the same field lines.

The position of magnetic field minima can be evaluated using any existing magnetic field models. Fig. 1 shows the configuration of a magnetic field line at Y=0 in GSM coordinate system calculated using Tsyganenko-01 model ([24], [25]) for solar wind magnetic field parameters Bz=-5 nT, By=0, solar wind dynamic pressure equal to 1.6 nPa and Dst=-5 nT.

It is possible to see the decrease of the value of minimal magnetic field with the growth of geocentric distance and the increase of Z coordinate of such minima.

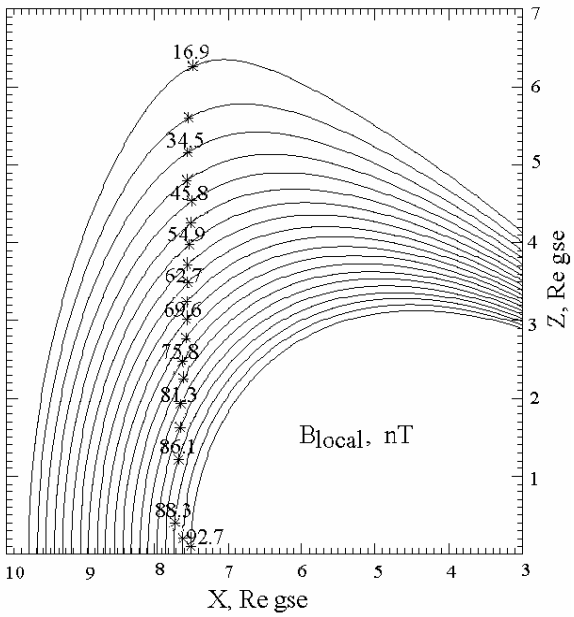

Fig. 1. The position of magnetic field minima on the daytime field lines and values of magnetic field in accordance with Tsyganenko-01 magnetic field model.

The value of plasma pressure constitutes ~0.5 nPa at L~9. Magnetic field pressure $B^2/2\mu_0$ (where μ_0 is the magnetic permeability of vacuum) constitutes ~0.04 nPa if the magnetic field is equal to 10 nT. These denote comparatively high values of a plasma parameter at such field lines in the region of B minimum.

It is possible to evaluate the density of transverse current $\mathbf{j}_\perp$ at the dayside field lines taking into account weak anisotropy of plasma pressure at L>7. In such a case

$$\mathbf{j}_\perp = \mathbf{B} \times \nabla p / B^2 \quad (2)$$

where ∇p is the plasma pressure gradient. Fig. 2 shows the results of such calculations. The values of plasma pressure measured by [20] were used for geocentric distances till 9 Re. The radial dependence of plasma pressure from 9 till 10 Re was approximated used exponential dependence.

It is possible to see by analyzing Fig. 2 that daytime current densities are smaller, but comparable with nighttime current densities calculated by [21] at the same geocentric distances. It is also necessary to take into account that daytime currents are spread at larger areas than nighttime currents. The calculation of the integral current between 7.5 and 9.7Re gives integral current ~$2 \cdot 10^5$ A in each hemisphere or the integral transverse current $4 \cdot 10^5$ A in both hemispheres. This transverse current is supported by plasma pressure gradients inside the magnetosphere and probably is closed by currents inside the magnetosphere. Simple estimations show that the same current value exists at the same geocentric distances in the region, which is ordinarily considered the near Earth tail. Therefore, the suggestion made by [14] about the existence of a transverse current system named cut ring current system (CRC) which is the high latitude continuation of the ordinary ring current seems highly probable. Fig. 3 schematically shows such a current configuration. It was shown by [15] and [16] that most parts of auroral oval are mapped into the CRC region. The plasma sheet like ions with energies ~10 keV produce the main contribution into the plasma pressure in CRC region.

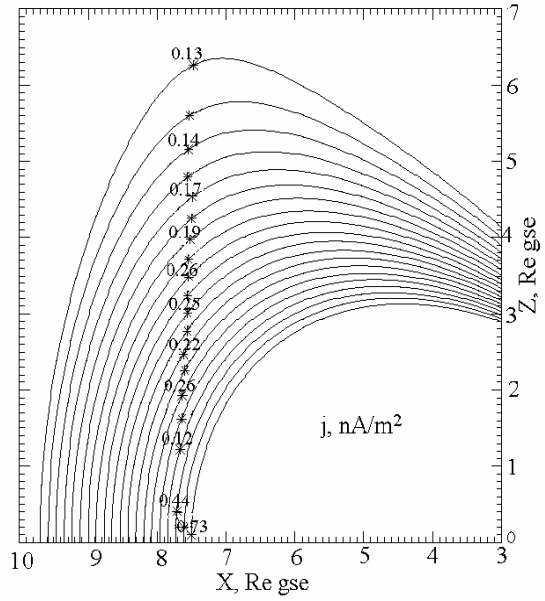

Fig. 2. Transverse current densities in the regions of daytime field lines.

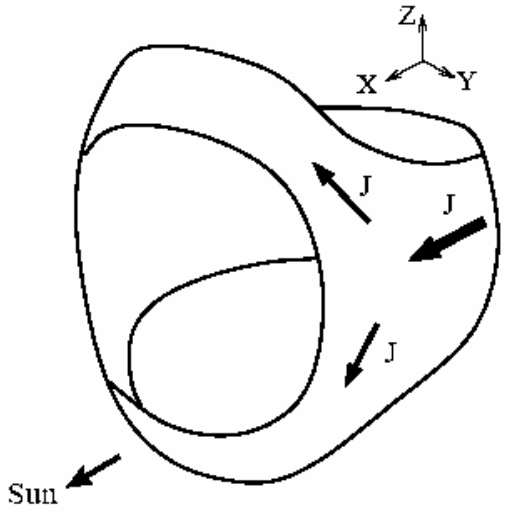

Fig. 3. Sketch illustrating the configuration of currents in CRC.

It is possible to estimate the contribution introduced by the present current system in the distortion of magnetic field near the Earth using the simple model shown on Fig. 4. The center of expected transverse currents situated at the dayside field-lines is deposited at X_{eff}=7.3Re, Z_{eff}=2.7Re. Two oblique to the equator rings shown in Fig. 4 produce $(B_z)_E$=4.96 nT and $(B_x)_E$=0.92 nT at the center of the Earth.

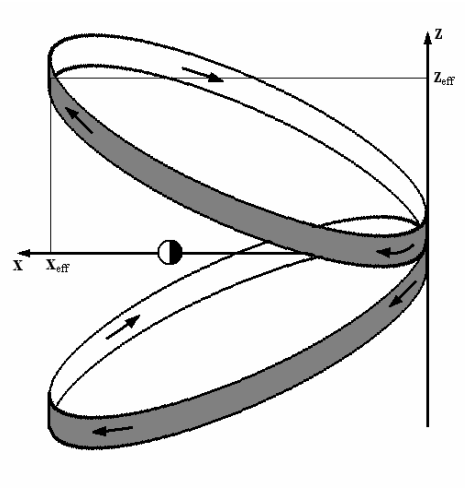

Fig. 4. Model used for the evaluation of magnetic field distortion near the Earth by CRC.

The calculated values are comparatively small. The contribution of such a current in Dst value is possible to evaluate taking into account that $|\mathrm{Dst}| \cong 3(B_z)_E/2$ due to skin effect ([27], [28]). It is equal in our case 7.44 nT. This value is larger than parameter used in Tsyganenko-01 model. However, it has the same order of magnitude. Therefore, CRC can be one of the sources of Dst variation in quiet geomagnetic conditions.

Values of plasma pressure and its gradients are greatly increased during the magnetic storm. The value of the B_z component of the magnetic field near equator is decreased due to the diamagnetic effect of plasma. The auroral oval becomes thicker and moves to the equator. It also becomes much more symmetrical in comparison to a quiet oval. The produced analysis shows that such an effect (which is ordinarily explained as plasma sheet motion to the Earth) is possible to explain as the result of CRC development.

Using the results of our analysis, it is possible to suggest that CRC can be considered as a probable candidate for the present formation of the part of Dst variation during a magnetic storm. To support such a suggestion it is necessary to have the global picture of storm time plasma pressure distribution and results of magnetic field measurements. Unfortunately such a program is far from realization in spite of the existence of comprehensive IMAGE data giving the position and the intensity of ring current. Here we only produce order of magnitude estimations using data presented by [29]. Data of auroral Aureol-3 satellite observations gave the possibility to determine the radial plasma pressure profile for the great magnetic storm March 1-8, 1982 with $|\mathrm{Dst}|_{max}$=211 nT. The auroral oval during this event moved up to 3-4R_E. The increase of plasma pressure of ions with energies till 22 keV constitutes ~1.5 nPa. [30] obtained relation making it possible to evaluate the magnetic field of symmetric plasma ring near the Earth in the near dipole magnetic trap having the form

$$B_z = \frac{2\pi}{R_E}\int \frac{W(p)}{L(p)}dp \qquad (3)$$

where W is the flux tube volume ($W=\int dl/\mathrm{B}$, dl is the element of field line length, B is the value of the magnetic field), p is plasma pressure. $W=32R_EL^4/35B_{eq}=W_0L^4$ in the case of dipole configuration, where $B_{eq}=3.2\cdot10^4$ nT. Estimation using Eq. (2) gives

$$B_z = \frac{2\pi}{B_{eq}}\frac{32}{35}\left(L_{AO}\right)^3\Delta p, \quad (4)$$

where L_{AO} is the averaged position of the auroral oval, Δp is the change of plasma pressure across the oval. Estimations using Eq. (4) show that for L_{AO}=4 and Δp=1.5 nPa, the distortion of the magnetic field in the center of the surrounding Earth plasma ring constituted at least 43 nT. Ring current contribution produced $|\mathrm{Dst}|$=211 nT constituted 141 nT. Therefore ~30% of the value of Dst variation can be connected to the quasi-ring current of ions with energies ~10 keV, i.e. with low energy particles which are ordinarily not included in the analysis of the nature of Dst variation. Traditional ring current of particles with energies ~100 keV ([31]) in such a case produce another 2/3 Dst. Such a result is in agreement with the analysis of magnetospheric energy content during the magnetic storm February 6, 1986 with $|\mathrm{Dst}|_{max}$= 312 nT produced by [32].

Calculated values of magnetic field distortion especially during great geomagnetic storms are much smaller than the value of the magnetic field inside the inner edge of the ring current during great magnetic storms. A very different situation appears when we analyze the asymmetric ring current. For example, [33] observe Bz~0 near the geostationary orbit during the magnetic storm 31 March 2001 with $|\mathrm{Dst}|_{max}$ = 350 nT when **a** great asymmetric ring current was observed by MENA and HENA instruments on IMAGE spacecraft. A symmetric ring current is formed as the stage of

asymmetric ring current development (see, for example, the results of [34]). Local increases of plasma pressure of a partial ring current are "smoothed" around the Earth during the process of symmetric ring current formation. The plasma parameter in the region of the asymmetric ring current is larger than unity and becomes much smaller than unity on the stage of the symmetric ring current. Such effects**,** as were stressed earlier**,** can be very important for the explanation of the acceleration of seed population of relativistic electrons. Such electrons are accelerated during substorms which take place during a storm in the region mapped onto the auroral oval latitudes. Therefore, they can be accelerated by a simple betatron mechanism during the storm recovery phase. Such an effect can help to explain the dependence Eq. (1) taking into account the formation of critically stable plasma pressure distribution (see [35] and references therein).

IV. CONCLUSIONS-DISCUSSION

The present analysis shows that many features of magnetospheric dynamics during a magnetic storm including the appearance of relativistic electrons can be explained taking into account the existence of high latitude continuation of the ring current – cut ring current (CRC). The possible contribution of a tail current in Dst variation in such a case becomes much smaller and it may be neglected in the first approximation. The obtained quantitative results demonstrate the importance of Earth orbiting particles with energies ~10 keV in the formation of Dst variation.

The works of Tsyganenko and Sitnov (2005, 2007) were based mainly on the analysis of magnetic data at the equatorial plane. As analyzed in our paper**,** the daytime part of CRC is situated comparatively close to the magnetopause and is localized far from the equatorial plane. This could be the reason it was not included in existing versions of Tsyganenko models. At the same time, the introduction of CRC in the magnetic field models can help to improve such models during both quiet and disturbed periods.

We try to demonstrate that storm time magnetic field distortion can be the important factor of the acceleration of the seed population of relativistic electrons. This does not imply the absence of another mechanism of acceleration due to wave-particle interaction. However, the role of turbulent mechanisms can be clarified only after the exclusion of the effect of betatron acceleration.

ACKNOWLEDGMENT

The present work was supported by RFBR grant and FONDECYT grant 1070131.

REFERENCES

[1] Baker, D.N., The occurrence of operational anomalies in spacecraft and their relationship to space weather. IEEE Trans. Plasma Sci. 28, 2007-2016, 2000.

[2] Friedel, R.H.W.,. Reeves, G.D., Obara, T. Relativistic electron dynamics in the inner magnetosphere-A review. J. Atmos. Sol. Terr. Phys. 64(2), 265-282, 2002.

[3] Summers, D., Ni, B., and Meredith N. P. Timescales for radiation belt electron acceleration and loss due to resonant wave particle interactions:2. Evaluation for VLF chorus, ELF hiss, and EMIC waves, J. Geophys. Res., 112, A04207, doi:10.1029/2006JA011993, 2007.

[4] Degeling, A.W., Ozeke, L.G., Rankin, R., Mann, I.R. and Kabin K. Drift resonant generation of peaked relativistic electron distributions by Pc 5 ULF waves, J. Geophys. Res., 113, A02208, doi:10.1029/2007JA012411, 2008.

[5] Ozeke, L.G., and Mann I.R. Energization of radiation belt electrons by ring current ion driven ULF waves, J. Geophys. Res., 113, A02201, doi:10.1029/2007JA012468, 2008.

[6] Fok, M.-C., Horne, R.B., Meredith, N.P. and Glauert S. A. Radiation Belt Environment model: Application to space weather nowcasting, J. Geophys. Res., 113, A03S08, doi:10.1029/2007JA012558, 2008.

[7] Tsyganenko, N.A., Sitnov, M.I. Modeling the dynamics of the inner magnetosphere during strong geomagnetic storms. J. Geophys. Res. 110(A3), doi: 10.1029/2004JA010798, 2005.

[8] Tsyganenko, N.A., Sitnov, M.I. Magnetospheric configurations from a high-resolution data-based magnetic field model. J. Geophys. Res., 112(A6), doi: 10.1029/2007JA012260, 2007.

[9] Kudela, K., Bucik, R. Low energy cosmic rays and disturbed magnetosphere. Proceedings of the second international symposium Solar Extreme Events, Fundamental Science and Applied Aspects, Nor-Amberd, Armenia, 26-30 September 2005, pp.57-62, 2006.

[10] Tsyganenko, N.A. On the redistribution of the magnetic field and plasma in the near nightside magnetosphere during a substorm growth phase. Planet. Space Sci. 37(2), 183-192, 1989.

[11] Panasyik, M.I., Kuznetsov, S.N., Lazutin, L.L. et al., Magnetic Storms in October 2003, Kosmicheskie issledovaniya 42(5), 489-535, 2004. (In Russian)

[12] Antonova, E.E. Radial pressure gradients in the magnetosphere of the Earth and the value of Dst –variation. Geomagnetism and Aeronomy 41(2), 148-156, 2001. (In Russian)

[13] Tverskaya, L.V., Pavlov, N.N., Blake, J.B., Selesnick, R.S., Fennell, J.F. Predicting the L-position of the storm-injected relativistic electron belt**.** Adv. Space Res. 31(4), 1039-1044. 2003.

[14] Antonova, E.E., Ganushkina, N.Yu. Inner magnetospheric currents and their role in the magnetosphere dynamics. Phys. Chem. Earth(C), 25(1-2), 23-26, 2000.

[15] Antonova, E.E. Investigation of the hot plasma pressure gradients and the configuration of magnetospheric currents from INTERBALL. Adv. Space Res. 31(5), 1157-1166, 2003.

[16] Antonova, E.E. Magnetostatic equilibrium and current systems in the Earth's magnetosphere. Adv. Space Res. 33, 752-760, 2004.

[17] Newell, P.T., Meng, C.-I. Mapping the dayside ionosphere to the magnetosphere according to particle precipitation characteristics. Geophys. Res. Lett, 19(6), 609-612, 1992.

[18] Starkov G.V., Rejenov, V.G., Vorobjev, V.G., Feldstein, Ya.I., Gromova, L.I. Structure of auroral precipitations in

the daytime sector, Geomagnetism i Aeronomia 42(1), 186-194, 2002. (In Russian)
[19] Yagodkina O.I., Vorobjev, V.G. Dayside auroral precipitation during substorms, Proc. of the 7th International Conference on Substorms. Levi, Lapland, Finland, 21-27 March, 2004, Finnish Meteorological Institute, Helsinki 2004, pp. 95-98, 2004.
[20] Lui, A.T.Y., Hamilton, D.C. Radial profile of quite time magnetospheric parameters, J. Geophys. Res., 97(A12), 19325-19332, 1992.
[21] DeMichelis, P., Daglis, I.A.., Consolini, G. An average image of proton plasma pressure and of current systems in the equatorial plane derived from AMPTE/CCE-CHEM measurements. J. Geophys. Res. 104(A12), 28615-28624, 1999.
[22] Lazutin, L.L., Auroral magnetosphere, Models of Space, V. I, ed. M.I. Panasyik, Moscow, pp. 547-578, 2007. (In Russian)
[23] Hori, T., Ohtani, S., Lui, A.T.Y.,. McEntire, R.W.,. Maezawa, K., Sato, Y., Mukai, T. A substorm associated drift echo of energetic protons observed by Geotail: Radial density gradient structure. Geophys. Res. Lett., 30(6), doi:10.1029/20002GL016137, 2003.
[24] Tsyganenko, N.A. Global quantitative models of the geomagnetic field in the cislunar magnetosphere for different disturbance levels. Planet. Space Sci. 35(11), 1347-1358, 1987.
[25] Tsyganenko, N. A. A model of the near magnetosphere with a dawn-dusk asymmetry: 1. Mathematical structure. J. Geophys. Res., 107(A8), doi: 10.1029/2001JA000219, 2002a.
[26] Tsyganenko, N. A. A model of the near magnetosphere with a dawn-dusk asymmetry: 2. Parameterization and fitting to observations. J. Geophys. Res., 107(A8), doi: 10.1029/2001JA000220, 2002b.
[27] Dessler, A. J., Parker E. N., Hydromagnetic theory of geomagnetic storms, J. Geophys. Res., 64(12), 2239-1152, 1959.
[28] Sckopke, N., A general relation between energy of trapped particles and the disturbance field over the Earth, J. Geophys. Res., 71(13), 3125-3130, 1966.
[29] Stepanova, M., Antonova, E.E., Bosqued, J.M. Radial distribution of the inner magnetosphere plasma pressure using low-altitude satellite data during geomagnetic storm: the March 1-8, 1982 Event. Adv. Space Res., 41, 1658-1665, 2008.
[30] Tverskoy, B.A., Formation mechanism for the structure of the magnetic storm ring current, Geomagnetism i Aeronomia, 37(5), 555-559, 1997. (In Russian)
[31] Lyons, R.L., Williams, D.J. Quantitative aspects of magnetospheric physics. D Reidel Publ. Co., Dordrecht, Boston, Lancaster, 1982, 231 p.
[32] Hamilton, D., Gloeckler, G., Ipavich, F., Studeman, W., Wilken, B., Kremser, G. Ring current development during the great geomagnetic storm of Febryary 1986. J. Geophys. Res. 93(A12), 14343-14355, 1988.
[33] Mitchell, D.G.,.Hsieh, K.C., Curtis, C.C., Hamilton, D.C., Voss, H.D., Roelof, E.C., C:son-Brandt, P. Imaging two geomagnetic storms in energetic neutral atoms. Geophys. Res. Lett., 28(6), 1151-1154, 2001.
[34] Skoug, R.M., Thomsen, M.F., Henderson, M.G., Funsten, H.O. et al., Tail-dominated storm main phase: 31 March 2001, J. Geophys. Res., 108(A6), doi: 10.1029/2002JA009705, 2003.
[35] Antonova, E.E. Magnetospheric substorms and the sources of inner magnetosphere particle acceleration. The Inner Magnetosphere: Physics and Modeling, Geophysical Monograph Series 155, Copyright 2005 by AGU, doi:10.1029/155GM12, pp. 105-111, 2005.

Statistical Properties of the Most Powerful Solar and Heliospheric Disturbances

O.S. Yakovchouk[1], I.S. Veselovsky[1,2], K. Mursula[3]

[1]*Skobeltsyn Institute of Nuclear Physics, Moscow State University, Moscow, Russia,*
[2]*Space Research Institute (IKI), Russian Academy of Sciences, Moscow, Russia,*
[3]*Department of Physical Sciences, University of Oulu, Finland*
olesya@dec1.sinp.msu.ru

Abstract – **We present and discuss here the first version of a data base of extreme solar and heliospheric events. The data base contains now 87 extreme events mostly since 1940. An event is classified as extreme if one of the three critical parameters passed a lower limit. The critical parameters were the X-ray flux (parameter R), solar proton flux (parameter S) and geomagnetic disturbance level (parameter G). We find that the five strongest extreme events based on four variables (X-rays SEP, Dst, Ap) are completely separate except for the October 2003 event which is one the five most extreme events according to SEP, Dst and Ap. This underlines the special character of the October 2003 event, making it unique within 35 years. We also find that the events based on R and G are rather separate, indicating that the location of even extreme flares on the solar disk is important for geomagnetic effects. We also find that S=3 events are not extreme in the same sense as R>3 and G>3 events, while S=5 events are missing so far. This suggests that it might be useful to rescale the classification of SEP fluxes.**

Key Words— **Sun; Heliosphere; Extreme solar events; X-ray flares; Solar proton events; Magnetic storms.**

I. INTRODUCTION

The study of space weather and solar-terrestrial relations remains topical and important both from scientific and practical point of view [1-2]. While the basic concepts of solar-terrestrial physics are well established, many detailed questions and, e.g., the possibility of forecasting needs further investigation [3-6]. Moreover, the unexpected and extreme solar events during solar cycle 23 have raised questions about their causes and properties [7-10].

Geomagnetic storm development can be predicted fairly well based on the solar wind and interplanetary magnetic field measurements upstream from the Earth. Measurements in the L1 libration point allow to do this rather reliably about 10 – 40 minutes in advance, depending on the solar wind velocity. Also, less certain predictions for much longer lead times exist, based on solar observations [11].

Many properties of extreme solar and heliospheric events are still poorly known [12-13]. Their study is difficult because they are rare and sometimes out of the range of measurement capability. Also, reliable theoretical models are still lacking. Nevertheless, one can note on a few interesting properties. Extreme solar flares and active regions demonstrate a complicated multi-scale structure and time behavior characterized by dimensionless scaling parameters [14-15]. Strongest solar and heliospheric events, e.g., major flares and coronal mass ejections have a nonlinear and non-local character from smallest to largest scales. The coupling between the scales, which is still not well understood, often leads to a non-uniform time behavior with multiple energy releases which may be concentrated around one or several active regions, prominences or coronal holes, and have an asymmetric hemispheric or longitudinal distribution [16-17].

II. COMPILATION OF EXTREME EVENT DATA BASE

We are using the 5-scale NOAA classification of space weather disturbances: minor (1), moderate (2), strong (3), severe (4), and extreme (5) [www.sec.noaa.gov/NOAAscales; 12]. Table 1 shows the five X-ray flare classes (R1-R5) ordered by the maximum intensity of soft X-rays in the energy range 1-12.5 keV (0.1-0.8 nm) observed at

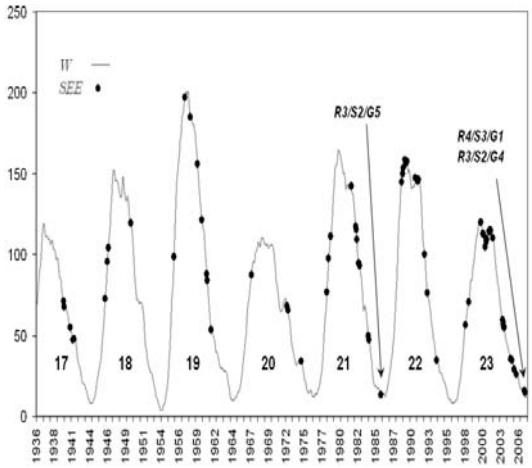

Fig. 1. The temporal distribution of extreme events (dots) during solar cycles 17-23. Extreme events can occur even at solar minima (arrows).

the Earth's orbit. It is worth to mention that X-ray flares can lead to sudden ionospheric disturbances and cause radio communication problems also called radio blackouts (which is why X-ray classification is indicated by R). We have considered extreme and, thereby, included in our data base all those events in the NOAA database that have been classified as R4 or R5 (http://www.ngdc.noaa.gov/stp/SOLAR/ftpsolarflares.html).

Solar proton events (SEP classes S1-S5) are given in units of pfu (proton flux unit), which is the number of protons at the Earth's orbit per cm^2 per steradian per second with energy higher than 10 MeV. Solar proton events appear as a result of particle acceleration in solar flares and in heliospheric shocks. Events with SEP classes S3-S4 are included as extreme events in our data base. Note that no S5 class event has been observed yet [18-19, http://www.swpc.noaa.gov/ftpdir/indices/SPE.txt].

NOAA scale	R Radio Blackouts (X-ray flux)	S SEP (Flux of E>10MeV particles)	G Geomagnetic Storm (Kp value)
5 - Extreme	>X20 ($2x10^{-3}Wm^{-2}$)	>100 000 pfu	9
4 - Severe	>X10 ($10^{-3}Wm^{-2}$)	>10 000 pfu	8 and 9-
3 - Strong	>X1 (10^{-4} Wm^{-2})	>1000 pfu	7
2 - Moderate	>M5 ($5x10^{-5}Wm^{-2}$)	>100 pfu	6
1 - Minor	>M1 ($10^{-5}Wm^{-2}$)	>10 pfu	5

Table 1. NOAA classification of space weather perturbations [www.sec.noaa.gov/NOAAscales; 12].

N	Year	Date	UT	Coordinates	AR	Flare class	CME	SEP	Date (Δt)	Ap	R	S	G
1	1859	01.09.1859									5		5
2	1940	23.03.1940	11:30	N27E37		3			23-27.03 (78)	277			5
3		27.03.1940	17:10	N12W17		3			28.03-2.4(87)	226			4
4	1941	03.07.1941	15:09	N12E03		3+			04.-08.7(69)	222			5
5		17.09.1941	7:35	N08W08		3+			17-20.09 (60)	312			4
6	1946	27.03.1946	4:10	N19E05		3			27-29.03(39)	215			4
7		25.07.1946	16:10	N21E16		3+			25-28.07(36)	212			5
8		19.09.1946	3:15	N21E08		3			21-24.09(63)	214			5
9	1949	19.11.1949		S02W70		3+		41(>435)		80		3	2
10	1956	23.02.1956		N23W80		3		250(>435)		236		4	4
11	1957	31.08.1957	13:21	N25W02		3			01-6.09(105)	221			5
12	1958	07.07.1958	0:20	N28W07		3+			07-10.07(48)	216			5
13	1959	14.07.1959	3:42	N17E07		3+		240(>88)	15-17.07 (42)	252		4	5
14	1960	29.03.1960	6:50	N12E31		2+			30.03-4.4(93)	251			4
15		10.11.1960	10:09	N29E20		3+			11-15.11 (54)	293			4
16		12.11.1960		N26W05		3+		21000				4	5
17		15.11.1960		N26W33		3+		21000				4	4
18	1961	12.07.1961		S07E22		3+		25000				4	4
19	1967	23.05.1967	18:35	N28E25		3B			24-27.05 (45)	241			5
20	1969	10.04.1969	3:59	N11E90		3		1375	------	32		3	1
21		02.11.1969	11:22	N14W90		3+		1317	8-10.11(9)	45		3	2
22	1971	24.01.1971	23:31	N18W49		3B		1171	27-28.01(6)	41		3	2
23	1972	04.08.1972	6:17	N14E08	331	X>5/3B		86000	03-07.08(81)	223	5	4	5
24		07.08.1972			331	X>5.4(>30)		3500	8-10.08(27)	111	5	3	5
25	1974	04.07.1974		S14L156	433			329	4-07.07(57)	142	4	2	4
26	1978	28.04.1978	13:06	N22E41	1092	X5/4B		1000	29.04-5.05(111)	130	4	3	4
27		11.07.1978		N18E45L170	1203	X>12.5? (X15)		20	13-15.07(15)	51	4	1	2
28		23.09.1978	10:23	N35W50	1294	X1/3B		2200	25-27.09(6)	43	3	3	2
29	1981	07.10.1981	23:08	S19E88	3390	X3/1B		2000	10-11.10(15)	51	3	3	2
30	1982	06.06.1982	16:37	S11E26L086	3763	X12.0/3B		30	9-11.06(21)	51	4	1	2
31		09.07.1982	7:20	N18E76	3804	X9/3B		2900	11-15.07(78)	229	4	3	5
32		13.07.1982		N11E36	3804	X7.1/3B		2900	11-15.07(78)	229	3	3	5
33		07.12.1982	23:54	S14W81	3390	X2/0B		1000	9-11.12(15)	50	3	3	2
34		15.12.1982	2:02	S09E24L077	4026	X>12.5?(X12.9/2B)		130	19-12.12(21)	62	4	3	3
35		17.12.1982		S08W20L089	4025	X10.1		85	19-21.12(21)	46	4	1	3
36	1984	24.04.1984		S11E45L334	4474	X>12.5? (X13/4B)		2500	25-27.04(42)	102	4	3	4
37		20.05.1984		S07E63L357	4492	X10.1		31	20-22.05(21)	80	4	1	2
38	1986	06.02.1986	6:06	S08W02	4711	X1/3B		130	6-10.02(63)	228	3	2	5

N	Year	Date	UT	Coordinates	AR	Flare class	CME	SEP	Date (Δt)	Ap	R	S	G
39	1989	06.03.1989	14:05	N33E71L	5395	(X15/3B)		3500	-----	56	4	3	1
40		08.03.1989		N33E71	5395	X>12/3B		3500	12-16.03 (69)	56	4	3	1
41		10.03.1989	18:37	N32E22	5395	X4		3500	12-16.03 (69)	285	3	3	5
42		17.03.1989	17:44	N33W60	5395	X6/2B		2000	20-22.03(36)	70	3	3	3
43		12.08.1989	14:27	S16W38	5629	X2.6/2B		9200	13-16.08 (54)	77	3	4	3
44		16.08.1989	0:54	S15W85L076	5629	X>12.5? (X20)		1000	17.08(3)	44	5	3	2
45		29.09.1989	11:39	S32W90	5698	X9.8/2N		4500	-----	27	4	3	1
46		19.10.1989	12:58	S25E10L211	5747	X>12.5/3B(X13/4B)		39000	19-23.10(69)	236	4	4	4
47		30.11.1989	12:27	N25W52	5800	X2.6/2N(X2/3B)		4340	7300 (20)	80	3	3	2
48	1991	25.01.1991		S12E90L	6471	X10.7			-----	39	4	1	1
49		22.03.1991	22:47	S26E28	6555	X9.4/3B		50000	24-27.03(84)	181	4	4	4
50		01.06.1991	14:56	N25E90L248	6659	X>12.5/1F(26m)			3-7.06(54)	196	5	1	3
51		04.06.1991	3:37	N30E70L248	6659	X>12.5/3B(19m)		3000	3-7.06(54)	196	5	3	4
52		06.06.1991	0:58	N33E44L248	6659	X>12.5/4B(26m)		3000	8-14.06(132)	111	5	3	3
53		09.06.1991		N32E13L248	6659	X10.0		3000	8-14.06(132)	271	4	3	4
54		11.06.1991	1:56	N32W15L248	6659	X>12.5/2B(17m)		3000	16-18.06(24)	179	5	3	4
55		15.06.1991	8:10	N33W66L248	6659	X>12.5/3B(22m)		1400	16-18.06(24)	154	5	3	3
56		07.07.1991	2:23	N26E03	6703	X1/2B		2000	7-10/07(48)	128	3	3	4
57	1992	08.05.1992	15:46	S25E07	7154	M7.4/2N		4550	9-12.05(54)	193	2	3	4
58		30.10.1992	18:16	S22W61	7321	X1/2B2700		2700	-----		3	3	1
59		02.11.1992	2:31	S23W107	7321	X9		2000	4-5.11(18)	44	4	3	2
60	1994	20.02.1994	1:41	No9W02	7671	M4/3B(21-22)		10000	20-23.02(39)	139	2	4	4
61	1997	06.11.1997	11:55	S18W632B	8100	X 9.4/2B	1300	490	06.08.11(21)	49	4	3	3
62	1998	20.04.1998	10:21	S43W90	8194	M1/Epl	1007	1700	23-24.04(6)	40	1	3	2
63		30.09.1998	13:50	N23W82	8340	M2/2N	NA	1200	-----		1	3	2
64	2000	14.07.2000	10:54	N22W07	9077	X5/3B	1674	24000	13-17.07(54)	192	3	4	5
65		08.11.2000	23:06	N10W77	9213	M.7.4/3F	1738	14800	9-11.11(12)	84	2	4	2
66	2001	29.03.2001	10:26	N20W19	9393	X1/1N	942	35	30.03-1.04(42)	192	3	1	4
67		02.04.2001	22:06	N19W90L152	9393	X>17.5(<5m) X20	2505	1100	------	48	5	3	1
68		10.04.2001	5:30	S23W09	9415	X2/3B	2411	335	10-13.04(30)	236	3	2	4
69		15.04.2001	14:06	S20W85L001	9415	X14.4/2B	1199	951	17-19.04(21)	111	4	3	3
70		24.09.2001	10:30	S16E23	9632	X2/2B	2402	12900	25-26.09(21)	154	3	4	3
71		01.10.2001	5:15	S22W91	9628	M9	530	2360	1-4.10(42)	82	2	3	3
72		04.11.2001	16:35	N06W18	9684	X1/3B	1810	31700	05-7.11(39)	142	3	4	4
73		22.11.2001	23:30	S15W34	9704	M9/2N	1437	18900	23-25.11.(30)	104	2	4	4
74	2002	21.04.2002	1:27	S14W84	9906	X1/F1	2409	2520	-----	80	3	3	2
75	2003	28.10.2003	11:30	S16E08L286	10486	X17.2/4B	2459	29500	29.10.-1(78)	252	5	4	5
76		29.10.2003	20:54	S15W02L286	10486	X10/2B	2029	29500	29.10.-1(78)	200	4	4	5
77		02.11.2003	17:30	S14W56	10486	X8.3/2B	2598	1570	04.11.2003	132	3	3	3
78		04.11.2003	19:54	S19W83L286	10486	X>17.5/3B(12m)X28	2657	353	------		5	2	2
79		18.11.2003	8:50	N00E18		2N/M3.2/M39	1660	13	19-22.11(36)	170	2	1	4
80	2004	25.07.2004	15:14	N08W33	10652	M1/1F	1530	2086	26-27.07	300	1	3	4
81		06.11.2004	0:11	N10E08	10696	2N/M9.3/M 5.9/M 3.6	1960	495	7-11.11(90)	206	1	2	4
82		07.11.2004	15:42	N03W17	10696	X2.0/2B	1800	460	7-11.11(90)	161	3	2	4
83	2005	15.01.2005	22:25	N14W08L179	10720	X2.6	2596	5040	16-17/01(66)	91	3	3	4
84		13.05.2005	16:13	N11E11	10759	M8/2B	1689	3140	14-17.05(45)	236	2	3	4
85		07.09.2005	17:17	S06E89L229	10808	X17.1/3B	NA	1880	10-14.09(72)	101	5	3	3
86	2006	06.12.2006	10:45	S06E59	10930	X9.0		1980	-------	20	4	3	1
87		13.12.2006	2:14	S07W22	10930	X3.4		698	14-16.12(33)	120	3	2	4

Table 2. The compiled database of the most powerful perturbations on the Sun and in the heliosphere.

Geomagnetic storms (classes G1-G5) result from the impact of the disturbed solar wind and interplanetary magnetic field upon the magnetosphere of the Earth. The key controlling factor of the intensity and duration of the storm is the southward component of the interplanetary magnetic field. Index G is based on the planetary geomagnetic 3-hour Kp index, which is produced from measurements at 12 ground-based magnetic observatories at mid-latitudes. Geomagnetic storms of index G4-G5 are included as extreme events in the data base (ftp://ftp.ngdc.noaa.gov/STP/GEOMAGNETIC_DATA/, http://swdcwww.kugi.kyoto-

u.ac.jp/kp/index.html).

Table 2 presents our data base of extreme events based on the three parameters (R, S, G) so that if either the R value or the G value of the event was 4 or 5, the event was considered extreme and included in the data base. Also, if the S value was 3 or 4, the event was included in the data base.

The columns in Table 2 indicate the event number, the year, date and UT time of the event in the Sun, the coordinates and NOAA classification.

number of the solar active region, the X-ray and/or optical flare classes, the speed (in km/s) of the possibly related coronal mass ejection according to the SOHO LASCO CME catalogue (http://cdaw.gsfc.nasa.gov/CME_list/), the solar energetic proton flux (in pfu), the date and duration (in hours) of the geomagnetic storm, the maximum Ap-index, and the related five-scale NOAA classes for R, S, and G.

X>10	01.06.1991	X> 12.5/1F (26m)	Dst	14.03.1989	-589
	06.06.1991	X> 12.5/4, (26m)		18.11.2003	-472
	04.11.2003	X> 17.5/3, (11m) X28		29.10.2003	-401
	15.06.1991	X> 12.5/1F (22m)		14.07.1959	-429
	07.09.2005	X> 17.1		29.03.2001	-387
SEP	04.08.1972	86000	Ap	17.09.1941	312
	19.10.1989	39000		10.11.1960	293
	22.03.1991	50000		10.03.1989	285
	14.07.2000	24000		23.03.1940	277
	28.10.2003	33600		28.10.2003	252

Table 4. The five strongest events according to X-ray flux, SEP flux, Dst and Ap indices.

From early 1970s onward, the data base is more or less complete and homogeneous with all three selection parameters (R, S, G) having measured values. In earlier times, since 1932, the event selection was only based on the G value or, from 1942 onwards, partially on both G and S (Miroshnichenko and Perez-Peraza, 2007). As additional information on flare activity, we have also included the flare classes based on white-light (optical) observations. From about 1940 to 1966, the flares observed in white light were classified in three classes (1-3), with 3+ indicating the largest flares. Thereafter they were classified in four main classes (1-4), with subdivisions indicated by letters [see, e.g., 20].

Note that the data base can be extended even further back in time using the long-term geomagnetic indices like the Aa* index (ftp://ftp.ngdc.noaa.gov/STP/GEOMAGNETIC_DATA/). In the future we will extend the data base by using the relation between the Ap/Kp indices known since 1932 with the aa index [21], the recent Ah index [22] and with the extended and corrected Dst/Dcx index [23].

III. Analysis of Extreme Events

Fig. 1 shows the distribution of the extreme events of Table 2 during the solar cycles 17-23. It is seen that extreme events can occur even during solar minima, but quite rarely (e.g., in February 1986 and December 2006).

Table 3 shows the number of extreme X-ray flares (X>10) and the maximum values of the three critical parameters, SEP flux, Ap index, and Dst index for each solar cycle. (Dst index is not depicted in Table 2 because of page limitation). The strongest proton event (highest SEP flux) was observed during solar cycle 20, the largest Ap index was found during solar cycle 19, and the strongest storm (minimum Dst value) was detected during solar cycle 22.

Table 4 presents the five strongest events of Table 2 according to the solar X-ray flux, the SEP flux, the Dst index and the Ap index. It is interesting to note that the five strongest extreme events selected based on each of the four variables are completely separate except for one event in October 2003 which is in three of the four lists based on SEP, Dst and Ap. This underlines the special character of the October 2003 event, making it unique within 35 years. We also note that the fact that the strongest events are separate even in the Ap and Dst index lists underlines their mutual difference.

Fig. 2 shows the histogram distributions of the three critical parameters (R, S, G) for all events in Table 2. One can see that the maxima take place for R=3, S=3 and G=4. So, the maxima for S and G occur for values classified as extreme, while for R it is slightly below it. In all cases, there are several events which have a non-extreme value.

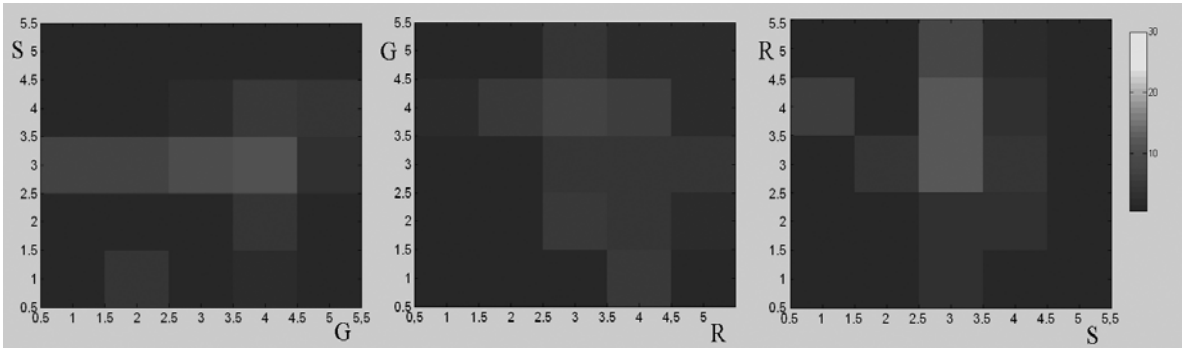

Fig. 3. The occurrence frequency distribution of extreme events in the generalized (R, G, S) space of parameters.

In order to have a homogeneous statistics, we have next selected only those of Table 2 for which all the three critical parameters (R, S, G) are known, and projected them in the three projections of the R,S,G index space in Figure 3. Out of these 65 events, 32 events (roughly 50%) are classified as extreme according to R, 50 (roughly

77%) according to S and 30 (roughly 46%) according to G. This indicates that the selection criterium was less strict for S than the other two variables, in accordance with including even S=3 events as extreme. When studying the statistics of R-based extreme events in more detail, one finds that 78% are extreme also according to S, but only 38% according to G. Similarly, out of the 30 G-based extreme events 40% were extreme also in R and 77% in S. However, out of the 50 extreme S-events, 50% were also extreme according to R and 46 % according to G.

This statistics shows that the extreme events based on R do not typically lead to an extreme event in G and vice versa. Only in about 40% of events, both parameters attain the extreme classification.

SC	Period	Number of flares with X>10	SEPmax	Ap max	Dst min
18	02.1944-04.1954	4		215	
19	04.1954-10.1964	8	25000	293	-429
20	10.1964-06.1976	3	86000	241	-387
21	06.1976-09.1986	6	2900	229	-325
22	09.1986-05.1996	10	50000	285	-589
23	05.1996-11.2006	6	24000	252	-472

Table 3. Largest values for each solar cycle.

This is physically quite understandable since large flares do not have to lead to CMEs that are sufficiently directed towards the Earth to cause an intense storm. Rather, this depends very much on the location of the flare event on the solar disk. The statistics found is very well in accordance with this view. The same argument also applies to correlation of events based on R and S because the direction of protons produced during a flare depends on the flare location and the momentary direction of the interplanetary magnetic field.

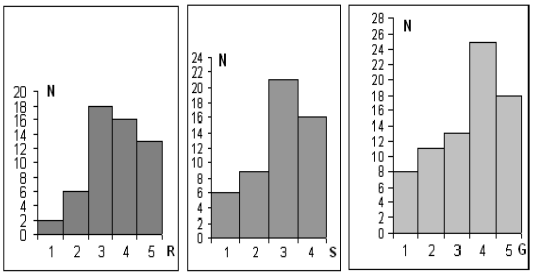

Fig. 2. Distributions of the number of extreme events from Table 2 according to parameters R,S,G

On the other hand, both for R and G based extreme events, a clearly larger percentage (almost 80%) were also extreme according to S. So, fluences of class S=3 could be found in a very large fraction of R-based or G-based extreme events. In reverse, out of S=3 or S=4 events, roughly 50% were extreme in both other parameters. This further indicates that the classification of S=3 is indeed too low to be considered as “extreme” in the same sense as R=4,5 or G=4,5. Remember that our selection of S=3 as extreme was based on the fact that no S=5 events have been observed by now. It might be useful if the classification of proton events was based a denser than a decadal classification.

IV. Conclusion

We have created and presented here the first version of a data base of extreme solar and heliospheric events. The data base contains now the Carrington storm in 1859 and 86 extreme events since 1932. An event was classified as extreme if one of the three critical parameters passed a lower limit. The critical parameters were those used by NOAA: X-ray flux (parameter R), solar proton flux
(parameter S) and geomagnetic disturbance level (parameter G). Extreme events can occur at any phase of the solar cycle, although maximum times are more probable than minima.

Some 40% of R based extreme events are seen as extreme in G and vice versa. This suggests that the location of even extreme flares on the solar disk is important for their geomagnetic effects. We also found that S=3 events are not extreme in the same sense as R>3 and G>3 events, while S=5 events are missing so far. This suggests that it might be useful to rescale the classification of SEP fluxes.

We found that the five strongest extreme events based on four variables (X-rays SEP, Dst, Ap) are completely separate except for the October 2003 event which is one the five most extreme events according to SEP, Dst and Ap. This underlines the special character of the October 2003 event, making it unique within 35 years.

ACKNOWLEDGMENT

This study was supported by the RFBR grants 07-02-00147, 06-05-64500, INTAS 03-51-6202 and MSU Interdisciplinary Scientific Project. It is also a part of the Programs of the Russian Academy of Sciences: "Origin and evolution of stars and galaxies" (P-04), "Solar activity and physical processes in the Sun-Earth system" (P-16, Part 3) and "Plasma processes in the Solar system (OFN-16). O. Ya. is grateful to V.N. Ishkov and N.G. Makarenko for useful discussions.

REFERENCES

[1] D.G. Cole, Space weather: its effects and predictability, *Space Sci. Rev.,* 107(1-2), 295-302, 2003.

[2] R. Schwenn, Space weather: the solar perspective, *Liveng. Rev. Solar Phys.*, 3, http://liwingreviews.org/lrsp-2006-2, 2006.

[3] N.U. Crooker, Solar and heliospheric geoeffective disturbances*, J. Atm. and Solar-Terr. Phys.*, 62(12), 1071, 2000.

[4] N. Gopalswamy, A. Lara, S. Yashiro, M.L. Kaiser, R.A. Howard, Predicting the 1-AU arrival times of coronal mass ejection, *J. Geophys. Res.*, 106(29), 207–218, 2001.

[5] I.A. Daglis, J.U. Kozyra, Y. Kamide, D. Vassiliadis, A.S. Sharma, M.W. Liemohn, W.D. Gonzalez, B.T. Tsurutani, G. Lu, Intense space storms: Critical issues and open disputes, *J. Geophys. Res.* doi:10.1029/2002JA009722, 108(A5), 1208, 2003.

[6] W.D. Gonzalez, A. Dal Lago, A.L. Clúa de Gonzalez, L.E.A. Vieira, B.T. Tsurutani, Prediction of peak-Dst from halo CME/magnetic cloud-speed observations, *J. Atm. Solar-Terr. Phys.,* 66(2), 161-165, 2004.

[7] I.S. Veselovsky, M.I. Panasyuk, S.I. Avdyushin, et al., Solar and heliospheric phenomena in October-November 2003: causes and effects*, Cosmic Res.,* 42(5), 435-488, 2004.

[8] M.I. Panasyuk, S.N. Kuznetsov, L.L. Lazutin, et al. Magnetic storms in October 2003, *Cosmic Research,* 42(5), 489–534, 2004.

[9] Yu.I Yermolaev, L.M. Zelenyi, G.N. Zastenker, et al., A year later: solar, heliospheric, and magnetospheric disturbances in november 2004, *Geomagnetism and Aeronomy,* 45(6), 681–719, 2005.

[10] N. Gopalswamy, S. Yashiro, Y. Liu, G. Michalek, A. Vourlidas, M.L. Kaiser, R.A. Howard, Coronal mass ejections and other extreme characteristics of the 2003 October-November solar eruptions, *J. Geophys. Res.,* 110, A09S15, 2005.

[11] R. Schwenn, A. Dal Lago, E. Huttunen, W.D. Gonzalez, The association of coronal mass ejections with their effects near the Earth, *Annales Geophysicae,* 23, 1033–1059, 2005.

[12] V.N. Ishkov, Solar extreme events: history, realization, prediction, *Solnechno-zemnaya fizika,* 8, 19-23, 2005 (in Russian).

[13] Yu.I. Yermolaev, M.Yu. Yermolaev, I.G. Lodkina, and N.S. Nikolaeva, Statistical investigation of heliospheric conditions resulting in magnetic storms, *Cosmic Research*, 45(1), 1-8, 2007.

[14] P. A. Conlon, P. T. Gallagher, R. T. J. McAteer, J. Ireland, C. A.Young, P. Kestener, R. J. Hewett, K. Maguire, Multifractal Properties of Evolving Active Regions,Solar Phys., in print, 2007.

[15] A. K. Sen, Multifractality as a Measure of Complexity in Solar Flare Activity, *Solar Phys.,* 241, 67-76, 2007.

[16] I.S. Veselovsky, A.V. Dmitriev, I.A. Zhitnik, A.N. Zhukov, M.A. Zel'dovich, S.V. Kuzin, A.A. Naumkin, I.G. Persiantsev, A.Yu. Ryazanov, Yu.S. Shugai, O.S. Yakovchouk, S.V. Bogachev, S.V. Shestov, Global variations and asymmetry of the Sun during extremely high activity in october November 2003, *Solar System Research*, 39(3), 169-175, 2005.

[17] K. Mursula, Bashful ballerina: The asymmetric Sun viewed from the heliosphere, *Adv. Space Res.,* 40, 1034–1041, doi:10.1016/j.asr.2007.05.087, 2007.

[18] M.A. Shea and D.F. Smart, A summary of major solar proton events, *Solar Physics,* 127, 297-320, 1990.

[19] L.I. Miroshnichenko and J. Perez-Peraza, Astrophysical Aspects in the Studies of Solar Cosmic Rays, *submitted to Space Sci. Rev., 2007.*

[20] H.W. Dodson, E.R. Dodson, *WDC-A Report UAG-52*, 1975.

[21] P.-N. Mayaud, Derivation, meaning, and use of geomagnetic indices, *Geophys. Monogr. Ser.,* vol 22, AGU, Washington, D.C., 1980.

[22] Mursula, K. and D. Martini, A new verifiable measure of centennial geomagnetic activity: Modifying the K index method for hourly data, *Geophys. Res. Lett.,* 34, L22107, doi:10.1029/2007GL031123, 2007.

[23] K. Mursula, and A. Karinen, An extended and corrected Dst index: Monitoring magnetic storms for over 70 years, *Proc. 11th European Solar Physics Meeting, Leuven, Belgium,* 11-16.9, 255, 2005.

Possible Influence of Solar Extreme Events and Related Geomagnetic Disturbances on Human Cardio-Vascular Health State: Results of Collaborative Bulgarian-Azerbaijani Studies

S. Dimitrova[1], F. R. Mustafa[2], I. Stoilova[1], E. S. Babayev[2,3], and E. A. Kazimov[4]

[1]Solar-Terrestrial Influences Laboratory, Bulgarian Academy of Sciences, [2]Shamakhy Astrophysical Observatory (ShAO) named after N. Tusi and Laboratory of Heliobiology, Azerbaijan National Academy of Sciences, [3]Institute of Physics, Azerbaijan National Academy of Sciences, [4]Medical Center INAM and Laboratory of Heliobiology,

Abstract – **Arterial blood pressure and heart rate of 86 healthy volunteers were measured on working days during a period of comparatively high solar and geomagnetic activity (autumn 2001 and spring 2002) in Sofia. Altogether 2799 measurements for each of the physiological parameters were gathered and analyzed. Electrocardiograms (ECGs) were registered in 7 healthy volunteers on working days, at a Medical Center in Baku, from 15.07.2006 till 21.04.2007. Obtained 1038 digital recordings were subjected to analyses. ANOVA was applied to check the significance of the influence of geomagnetic activity, estimated by the average daily value of Dst-index on the physiological parameters under consideration. Results revealed statistically significant increment for the mean systolic and diastolic blood pressure values of the group with geomagnetic activity increase. Arterial blood pressure values started increasing two days prior to geomagnetic storms and kept higher values up to two days after them. Heart rate did not react significantly for both groups under geomagnetic changes. Probably the dynamic of arterial blood pressure reveals a compensatory reaction of human organism as adequate reaction to environmental changes. It seems that the heart rate is more stable physiological parameter for healthy persons under these conditions.**

***Key Words*— Solar extreme events; Geomagnetic storms; Heart rate and blood pressure.**

I. INTRODUCTION

All living organisms including human being are continuously exposed to geomagnetic field (GMF) variations. Biological systems have accommodated to these fluctuations in the course of evolution but they have never stopped reacting to any sharp environmental changes. Results presented on that subject in the literature suggest that changes in normal functioning of the central nervous system, vegetative nervous system, cardiovascular system and cognitive performance may be enhanced by significant changes in GMF determined by solar-terrestrial interactions [1]-[4]. Although the interest in revealing the correlation between GMF variations and human functional system has increased [5]-[6], the possible mechanisms through which these variations affect different processes in human organism have not been clearly established yet.

Bulgarian-Azerbaijani collaboration has been established recently. Both our teams in Sofia and Baku have studied possible influence of changes in geomagnetic activity (GMA) by using different indices (Ap-, Kp-, Dst-indices and amplitude of H-component of local GMF) on human physiological and psycho-physiological parameters as well as on some cardio-vascular diseases and mortality in middle latitudes. Results obtained encouraged us to joint our efforts for performing similar investigations at different longitudes and latitudes. These studies could be useful in clarifying phychological and biophysical mechanisms of these relations.

II. EXPERIMENTAL MATERIAL, GEOMAGNETIC DATA AND METHODS OF STUDY

Arterial blood pressure (ABP) and heart rate (HR) data were obtained in experiments with

participation of 86 healthy volunteers carried out in Sofia, Bulgaria (latitude: 42°43' North; longitude: 23°20' East). The average age of the group was 47.8 years. Recording of cardio-vascular parameters was performed every day at the same time for each person on the working days for periods from 01.10.2001 to 09.11.2001 and from 08.04.2002 to 28.05.2002. These periods were chosen because of the high probability of geo-effective solar events and related strong geomagnetic disturbances to occur during the autumn and spring in years of post-maximal solar activity (SA) of the solar cycle 23. Altogether 2799 registrations for each of the physiological parameters examined were gathered (hereinafter: Sofia data).

Digitized electrocardiograms (ECGs) were registered in another group consisting of 7 healthy persons on working days and Saturdays in Baku, Azerbaijan (latitude: 40°23' North; longitude: 49°51' East), in the Laboratory of Heliobiology located at the Medical Center "INAM" from 15.07.2006 till 13.11.2007. The average age of the group was 31.6 years. RR intervals (time series of beat-to-beat heart rate intervals or heart rate period in msec) (minimal RRmin, maximal RRmax and average RRavg) and HR values were derived from digital ECGs (hereinafter: Baku data). Obtained 1532 digital recordings were subjected to analysis. The experiments were conducted in special rooms.

In order to avoid possible psychological effects prior to experiments, the test subjects were not familiarized with space weather conditions before and during experiments. Personality and individual physiological characteristics as well as daily problems of examined persons were taken into account.

Data about GMA (average daily value of Dst-index) were handled from the World Data Center for Geomagnetism, Kyoto (http://swdcwww.kugi.kyoto-u.ac.jp/index.html).

GMA was divided into five levels as shown in Table 1. This table also presents the number of measurements for each of the cardio-vascular parameters and number of days for the corresponding GMA levels during relevant examinations in Sofia and Baku. There were a number of days with relatively high GMA (with several moderate as well as a few major storms and one severe storm on 6 November 2001) during examination periods in Sofia. There was only one major storm (15 December 2006) and 58 weak storms during Baku experiments.

The statistical method of the *ANalysis Of VAriance* (ANOVA), statistical package STATISTICA, ver.6, StatSoft Inc., 2001) was applied to establish statistical significance of the influence of GMA levels on ABP, HR, RRmin, RRmax and RRavg. In general, the purpose of ANOVA is to test for statistical significance between means through comparing variances.

TABLE 1
DST-INDEX LEVELS AND THE NUMBER OF DAYS AND MEASUREMENTS IN SOFIA / BAKU (WHERE "–"DENOTES "NO DATA")

Dst and GMA levels	I quiet GMA	II weak storm	III moderate storm	IV major storm	V severe storm
Dst, nT	Dst>- 20	-50<Dst≤-20	-100<Dst≤-50	-150<Dst ≤-100	Dst≤-150
Days	45 / 428	37 / 58	14 / –	5 / 1	2 / –
N Meas.	1209 / 1328	1053 / 199	321 / –	148 / 5	68 / –

TABLE 2
SIGNIFICANCE LEVELS (*P*-VALUES) OF GMA EFFECT (ESTIMATED BY DAILY DST-INDEX) ON THE CARDIO-VASCULAR PARAMETERS FOR THE DAYS BEFORE (+), DURING (0) AND AFTER (-) GEOMAGNETIC STORMS (SOFIA DATA, WHERE <*> DENOTES STATISTICALLY SIGNIFICANT RESULT)

DAY	*P-VALUES*		
	SBP	DBP	HR
-3	0.227	0.106	0.851
-2	0.000*	0.000*	0.924
-1	0.000*	0.000*	0.637
0	0.000*	0.000*	0.351
+1	0.000*	0.000*	0.015*
+2	0.000*	0.000*	0.099
+3	0.000*	0.000*	0.139

TABLE 3
SIGNIFICANCE LEVELS (*P*-VALUES) OF GMA EFFECT (ESTIMATED BY DAILY DST-INDEX) ON THE CARDIO-VASCULAR PARAMETERS FOR THE DAYS BEFORE (+), DURING (0) AND AFTER (-) GEOMAGNETIC STORMS (BAKU DATA)

DAY	*P-VALUES*			
	HR	RRMIN	RRMAX	RRAVG
-2	0.397	0.592	0.630	0.612
-1	0.565	0.529	0.354	0.595
0	0.683	0.498	0.851	0.596
+1	0.801	0.92	0.65	0.76
+2	0.891	0.892	0.524	0.881

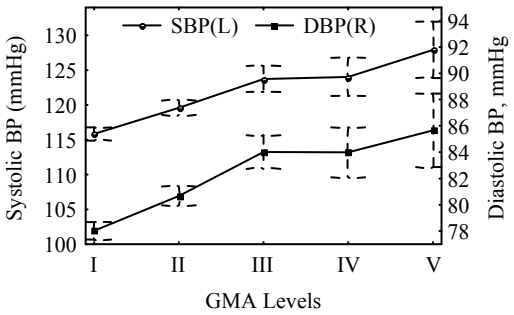

Fig.1. Effect of different GMA levels (I-V) on the dynamics of SBP(L) and DBP (R) (±95% CI); (L) denotes Left axis while (R) – Right axis; Sofia data.

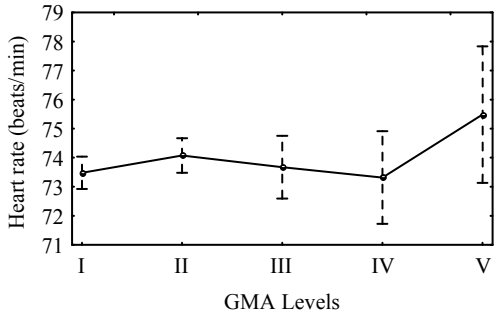

Fig.2. Effect of different GMA levels (I-V) on HR (±95% CI); Sofia data.

The effect of geomagnetic storms on the studied cardio-vascular parameters before and after storm development was also investigated by the help of ANOVA. GMA impact up to 3 days before and 3 days after sharp geomagnetic changes was studied.

Post-hoc analysis (*Newman-Keuls test*), based on the range statistic, was used to determine statistical significance of the differences between the average values of the measured cardio-vascular parameters in the separate factors levels.

The chosen level for statistical significance in our analyses was $p<0.05$.

III. RESULTS

A. Results of ANOVA for the cardio-vascular parameters measured in Sofia

Table 2 presents significance levels p obtained from ANOVA applied for the study of influence of GMA (estimated by the daily Dst-index) on the cardio-vascular parameters recorded in Sofia (systolic blood pressure (SBP, mmHg), diastolic blood pressure (DBP) and HR) for the days before (-3^{rd}, -2^{nd} and -1^{st} day), during (0 day) and after ($+1^{st}$, $+2^{nd}$ and $+3^{rd}$ day) geomagnetic storm's development. One can see that SBP and DBP were statistically significantly affected by GMA (through Dst index) from -2^{nd} up to $+3^{rd}$ day of GMF variations.

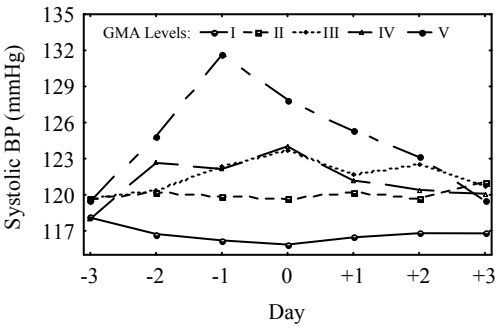

Fig.3. GMA effects on SBP before (-), during (0) and after (+) geomagnetic storms and at quiet level; Sofia data.

Fig. 1 shows the mean values of SBP and DBP for the group during geomagnetic storms with different intensities (I-V GMA levels). Vertical bars in the figure denote 95% confidence intervals (CI). Statistically significant increase of ABP average values of the group was related to Dst-index values decrease. The range of changes for SBP and DBP were respectively 10.4% and 9.7%. *Post-hoc analyses* revealed that all of the SBP mean values were different from each other except the difference of values for III GMA level from the values for IV GMA level. It means that SBP increased statistically significantly still at II GMA level in comparison to I GMA level. It was displayed for DBP as well.

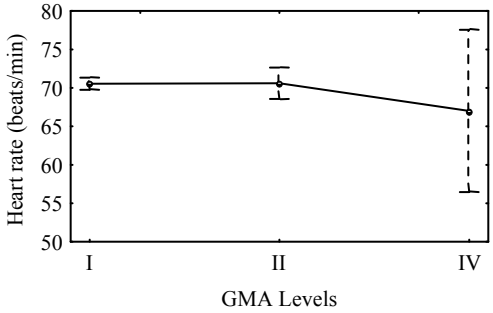

Fig.4. Effect of different GMA levels (I, II and IV) on HR (±95% CI); Baku data.

Variations of HR (beats/min) for different levels of GMA are presented in Fig. 2. This cardio-vascular parameter was not statistically significantly influenced by geomagnetic disturbances estimated by Dst-index (see: Table 2). There were observed a slight decrease of HR during major storms and an increase during severe storms but the maximal range of changes was only 2.9%.

Results show that SBP and DBP were statistically significantly influenced by GMA starting two days prior to geomagnetic storms up to three days after their development (see: Table 2). Fig. 3 shows the dynamics of SBP for the different GMA levels (before (-), during (0) and after (+) sharp changes in GMF). ABP values started increasing on -2^{nd} and -1^{st} days prior to moderate, major and severe geomagnetic storms and kept the high values up to $+2^{nd}$ and even $+3^{rd}$ day after storms' development. The dynamic of DBP was similar.

There was an increase of HR on -1^{st} day of major storms, 0 day of severe storms and $+1^{st}$ day of weak storms, but the range of changes was not so big and the maximal increase was about 5%.

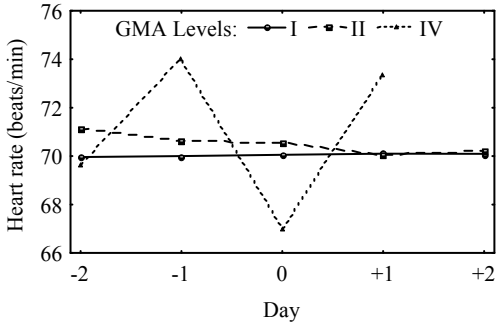

Fig. 5. GMA effects on HR before (-), during (0) and after (+) geomagnetic storms and at quiet level; Baku data.

B. Results of ANOVA for the cardio-vascular parameters measured in Baku

Table 3 shows significance levels *p* obtained from application of ANOVA for studying the potential influence of GMA changes (estimated by daily variations of Dst-index) on the cardio-vascular parameters (HR, RRmin, RRmax and RRavg) recorded during experiments in Baku before (-), during (0) and after (+) geomagnetic storms. ANOVA did not reveal statistically significant influence of GMA on afore mentioned cardiological parameters for considered period of experiments when only one major storm took place. It should be mentioned that these results based on Baku data are quite close to those ones obtained for the changes in HR for healthy persons in Sofia. Continuing Baku experiments on a daily basis (except Sundays) will enable us to get more reliably established results.

There was a slight decrease in HR dynamics (4.6%) during the major geomagnetic storm in comparison with quiet level of geomagnetic conditions (Fig. 4). As there were no moderate and severe geomagnetic storms (according to the gradation of Table 1) during those 16 considered months in Baku data we were not able to compare the results obtained for possible variations of cardio-vascular parameters under different geomagnetic disturbance conditions.

Fig. 5 shows dynamics of HR on the days before (-), during (0) and after (+) different GMF variations. It was revealed an increase of HR at IV GMA level on -1st and +1st days and a decrease on the 0 day. RRavg decreased on -1st and +1st days and increased on the 0 day (Fig. 6). Variations of RRmin were similar to RRavg changes while RRmax increased on -1st day (Fig. 7), which probably was related to disturbances in cardiac rhythm. Results were not statistically significant (Table 3) but the dataset analyzed was comparatively small.

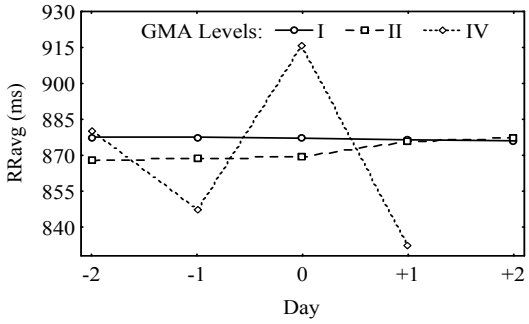

Fig. 6. GMA effects on RRavg before (-), during (0) and after (+) geomagnetic storms and at quiet level; Baku data.

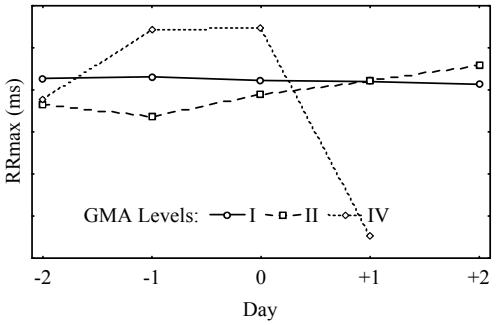

Fig. 7. GMA effects on RRmax before (-), during (0) and after (+) geomagnetic storms and at quiet level; Baku data.

IV. DISCUSSION AND CONCLUSIONS

Conducted investigations have revealed an increase (statistically significant) of SBP and DBP with GMA increment. ABP values began increasing on -2nd day before moderate, major and severe geomagnetic storms and kept the high values up to +2nd and even +3rd day after storms.

The changes established in ABP 1-2 days prior to GMA changes can be explained by advance effect of precursors of geomagnetic storms that provoke adequate physiological reactions. Investigations show that after geoeffective solar events in the days prior to geomagnetic storms extremely low frequency (ELF) fluctuations of electromagnetic field (EMF) occur. These frequencies are close to the frequencies of certain human organs (i.e., human brain's bioelectric waves) and system's functioning. Probably there is a resonance effect of these ELF fluctuations on the human physiological state [7]-[8].

HR did not react statistically significantly for both examined groups in Sofia and Baku under changes of geomagnetic situation. It should be reminded that persons participating in experiments were functionally healthy. It seems that HR is more stable cardio-vascular parameter for healthy

persons under GMF variations than the other considered ones. Probably the dynamics of ABP reveals an adequate compensatory reaction of human organism to environmental changes.

Recent investigations carried out on examination of cardiologic patients revealed that in the case of disturbances in cardio-vascular system functioning (hypertension, cardiac ischemia, infarct) HR can be a quite sensitive parameter, reacting even at low level variations in GMF [9]. It is quite probable that in a case of cardio-vascular pathology misbalance between sympathetic and parasympathetic systems determines these physiological reactions [10].

Fluctuations in HR changes before, during and after geomagnetic changes regarding RRmin, RRmax, RRavg are interesting result which should be subject of further studies and discussion. The possibility that these fluctuations are related with some rhythm disturbances should not be excluded.

Results of these studies could be summarized as:

-experimental studies and their analyses enabled to conclude that human cardio-vascular state could be affected by GMA disturbances;

-there is revealed a statistically significant increment for systolic blood pressure (SBP) and diastolic blood pressure (DBP) of persons examined with GMA increase in the considered period;

-arterial blood pressure (ABP) values started to increase significantly on -2nd day before moderate, major and severe geomagnetic storms; high values of ABP was observed up to +2nd and even +3rd day after storms;

-heart rate (HR) reaction was ambiguous and not significant for healthy persons for both examined groups in Bulgaria and Azerbaijan under different geomagnetic conditions (at quiet level and geomagnetic storms of various intensities);

-for healthy persons under GMF variations heart rate (HR) seems to be more stable cardio-physiological parameter than other considered parameters;

-the dynamics of arterial blood pressure (ABP) probably reveals an adequate compensatory reaction of human organism to environmental changes;

-it is of great importance to conduct complex and synchronic investigation of geomagnetic storms' effects on human beings in different latitudinal and longitudinal areas and to get more and better knowledge about solar and geomagnetic storms and their possible effects on human health state in order to decrease adverse effects of these disturbance factors.

ACKNOWLEDGMENTS

This work was partially supported by the INTAS Grant Nr-06-1000015-6408 of the 2006 YSF Collaborative Call INTAS-Azerbaijan and by the National Science Fund of Bulgaria under contract NIP L-1530/05.

REFERENCES

[1] Brand, W., Denis, S. Geophysical variables and behavior. LVIII Autonomic activity, hemolysis and biological psychokinesis. Possible relationship with geomagnetic field activity. Perceptual and Motor Skills 68, 1243-1254, 1989.

[2] Maynard, N.C. Space weather prediction. Reviews of Geophysics 33(S1), 547-558, 1995.

[3] Pikin, D.A., Gurfinkel', I., Oraevskii, V.N. Effect of geomagnetic disturbances on the blood coagulation system in patients with ischemic heart disease and prospects for correction with medication. Biofizika (Journal of Biophysics) 43(4), 617-622, 1998.

[4] Stoupel, E., Zhemaityte, D., Drungiliene, D., Martinkenas, A., Abramson, E., Sulkes, Klaipeda J. Cardiovascular emergency aid services correlate with 10 cosmophysical parameters by time of occurence. Journal of Clinical and Basic Cardiology 5, 225-227, 2002.

[5] Persinger, M.A., Richards, P.M. Vestibular experiences of humans during brief periods of partial sensory deprivation are enhanced when daily geomagnetic activity exceeds 15-20 nT. Neuroscience Letters 194(1-2), 69-72, 1995.

[6] Zhadin, M.N. Review of Russian literature on biological action of DC and low-frequency AC magnetic fields. Bioelectromagnetics 22(1), 27-45, 2001.

[7] Hainsworth, L. B. The effect of geophysical phenomena on human health. Speculations in Science and Technology 6(5), 439-444, 1983.

[8] Babayev, E.S., Allahverdiyeva, A.A. Effects of geomagnetic activity variations on the physiological and psychological state of functionally healthy humans: some results of Azerbaijani studies. Advances in Space Research 40, 1941-1951, 2007.

[9] Dimitrova, S., Stoilova, I., Breus, T.K., Zenchenko, T. Investigation of human sensitivity towards geomagnetic changes. Proceedings of 3rd Conference "Space, Ecology, Nanotechnology, Safety", 27-29 June 2007, Varna, Bulgaria, (in press).

[10] Stoilova, I., Zdravev, T. Influence of geomagnetic activity on the human functional systems. Journal of the Balkan Geophysical Society 3(1-4), 73-77, 2000.

Thermal neutrons' response to the GLEs

Ekaterina A. Sigaeva[1], Oleg Yu. Nechaev[1], Mikhail I. Panasyuk[1], Andrey V. Bruns[2], and Oleg A. Troshichev[3]

[1] *Skobeltsyn Institute of Nuclear Physics, Moscow State University,*
[2] *Crimean Astrophysical Observatory*
[3] *Arctic and Antarctic Research Institute*

Abstract – **Long-term observations near the Earth's crust have shown that thermal neutrons are very sensitive regarding different processes and phenomena both in the near-Earth space and in the Earth's crust itself by reason of the dual nature of the thermal neutron flux. Its first source is associated with high-energy particles of cosmic rays penetrating into the Earth's atmosphere and interacting with its elements. The second source originates from the radioactive gases contained in the Earth's crust. While the contribution of the second source strongly depends on the Earth's crust conditions and reflects its movements, the contribution of the space-originated source must respond to any variations of high-energy particles flux near the Earth.**
The time period of 2005-2006 was marked with several extraordinary solar flares nevertheless it was close to the minimum of the 23d solar cycle. In particular ground level enhancement (GLE) recorded on January 20, 2005 after one of such flares is comparable to the greatest GLEs over the whole period of observations.
The paper presents the observations of the thermal neutrons monitors during the latest GLEs recorded on January 20, 2005 and December 13, 2006.

***Key Words*—ground level enhancement, thermal neutrons, ground obervations.**

I. Introduction

OBSERVATIONS near the Earth's crust have shown that thermal neutrons are very sensitive regarding different processes and phenomena both in the near-Earth space and in the Earth's crust itself. Experimentally it was found out that thermal neutrons flux variations accompany the New and Full Moons, changes of the polarity of the Interplanetary Magnetic Field and are possessed of seasonal dependence [1].The reason of it is the dual nature of the thermal neutron flux observed near the Earth's surface [2]. Thermal neutrons in the Earth's atmosphere are produced by the reactions between the elements of the atmosphere and cosmic rays' elements on the one hand, and α-particles originated from the decay of the radioactive gases of the Earth's crust, on the other.

The contribution of the second source strongly depends on the specific characteristics of the geographical location of the observation point, on the characteristics of the underlying surface and on the geodynamical conditions. The contribution of the first space-originated source must respond to any variations of high-energy particles flux near the Earth. At the same time changes of the conditions in the near-Earth space can also result in the geodynamical processes and deformations of the Earth's crust, which in its turn will cause variations of thermal neutrons' flux.

II. Experimental equipment

The experimental unit for thermal neutrons registration – so-called thermal neutrons' monitor (TNM) consists of standard neutron counters SI-19N filled with helium-3 at the pressure of 405.3 kPa. Registration of neutrons is a result of the following exothermic reaction: $^3He+n \rightarrow ^3H+p+746\ keV$. The cross-section of this reaction is 5200 b. The counters are intended for registration of neutrons within the wide energy ranges, but detection efficiency is maximum (0.8) for thermal neutrons.

The standard experimental unit consists of several counters (6, 10 or 20), high-voltage power pack, output unit. Information is summarized during different time intervals (from 1 s up to 1 min) and stored in the computer.

Currently there are several experimental units operated in different geographical points (see Table 1). It's necessary to mark that two Moscow stations are fully independent units, situated at a distance of about 1 km from each other. The Moscow-1 unit is located inside the brick building at the altitude of about 20 m from the Earth's surface, the Moscow-2

unit is placed in a building with so-called "thin roof", used for space-physics experiments, at about 10 m from the Earth's surface.

Since the experimental equipment and its operation are quite simple it's possible to modify the standard unit depending on the particular conditions and specific purposes of the experiment. For instance using two planes of the counters interlaid with a cadmium plate of 1 mm thickness provides a possibility for separately registration of the neutron flux from the lower and the upper hemispheres. Such configuration is used at Moscow-1 unit: four groups of counters are put by pairs one above the other and one pair is split by cadmium sheet.

III. GROUND LEVEL ENHANCEMENTS

a. January 20, 2005 event

Ground level enhancement (GLE 69) recorded on January 20, 2005 by the world-wide network of Neutron Monitors is comparable to the greatest GLEs over the whole period of observations in spite of that it occurred at the time period close to the minimum of the 23d solar cycle. The GLE was associated with the solar flare X7.1 on 20 January in AR720 (N12 W58) started at 6:36 UT [3].

Table 1. Thermal neutrons' experimental equipment operated in 2005-2006.

Location	Latitude	Longitude
Antarctic	66.33S	93.01E
Moscow-1,2	55.7N	37.57E
Kamchatka	52.83N	158.13E
Crimea (Ukraine)	44.4N	33.98E

Table 2. Neutron Monitors summary for January 20, 2005 event (maximum increase for 1-minute data is presented).

Neutron Monitor	Latitude	Longitude	Maximum increase inc.%	UT of maximum
South Pole	90S		>5400%	6:50
McMurdo	77.9S	166.6E	>2800%	6:55
Fort Smith	60N	112W	167%, 307%	6:56, 7:05
Oulu	65.05N	25.47E	283%	7:00
Inuvik	68.4N	133.7W	305%	7:05
Moscow	55.47N	37.32E	102%	7:05
Kiel	54.30N	10.10E	103%	7:05
Thule	76.5N	68.7W	123%	7:30

Table 3. Neutron Monitors summary for December 13, 2006 event (maximum increase for 1-minute data is presented).

Neutron Monitor	Latitude	Longitude	Maximum increase inc.%	UT of maximum
Mawson	67.36S	62.52E	68%, 54%	2:56, 3:11
Moscow	55.47N	37.32E	25%	3:01
Oulu	65.05N	25.47E	92%	3:05
Apatity	67.57N	33.4E	86%	3:05
Fort Smith	60N	112W	24%	3:32
McMurdo	77.9S	166.6E	27%	3:34

The largest GLE for the whole period of observation was recorded in 1956 [4], during which in some regions the level of radiation increased by a factor of 47. As it is seen from Table 2 and Fig.1 during the event on January 20, 2005 the neutron rate at the Antarctic stations of South Pole (altitude of 2820 m) and McMurdo (sea level) increased by factors of 56 and 30 respectively. At the same time the recorded effect for the majority of high-latitude stations was "only" 100-300% and for the mid-latitude stations - very small or absent at all. Particularly, at the Moscow IZMIRAN Neutron Monitor the neutron rate increased up to ~100%.

Experimental data obtained by thermal neutrons' units during this event compared with the neighbor Neutron Monitors' data is presented in Fig.2 (Moscow) and Fig.3 (Antarctic). Thermal neutrons' rates increase up to 100% and 130% for two Moscow units and their responses are in good time correspondence with GLEs observed by IZMIRAN Neutron Monitor.

For the Antarctic thermal neutrons unit the observed event became the only one with such a specific shape and amplitude for the over year observation period. It's good time agreement proves its link with GLE, although it started approximately 10 minutes before the beginning of the latter. As distinct from the South Pole Neutron Monitor the counting rate of thermal neutrons in Antarctic increased only three times.

b. December 13, 2006 event

Ground level enhancement recorded on December 13, 2006 and also known as GLE 70 occurred almost at the minimum of the 23d solar cycle. It was associated with the solar flare X3.4 produced on December 13 in AR930 (S6 W23) with maximum at 2:40 UT [6].

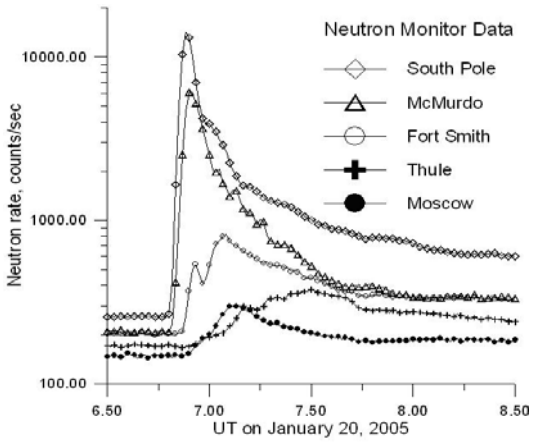

Fig. 1. Cosmic rays data from the world network of Neutron Monitors for January 20, 2005.

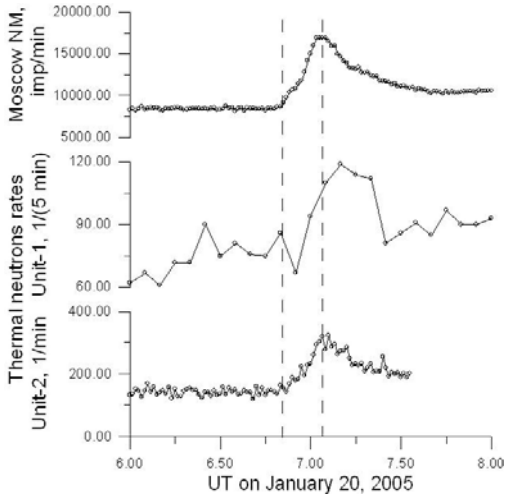

Fig. 2. Thermal neutrons data from Moscow experimental units compared with IZMIRAN Neutron Monitor for January 20, 2005. Dashed lines point the time of beginning and maximum of GLE according to Neutron Monitor.

As compared with the previous GLE this event was not so significant (see Table 3 and Fig.4). Nevertheless at some stations increases of the cosmic ray intensity reached 100% and it aligns this event with the greatest GLEs of the 23d solar cycle. For Moscow Neutron Monitor the neutron rate increased up to ~25% above the background level.

Though only two Moscow units on thermal neutrons registration were under operation during this period, one of them (which is more adjusted to registration of space experiments) registered a 30% increase for this event which is in good time and amplitude agreement with GLE observed by Neutron Monitors.

IV. DISCUSSION

Two last GLEs on January 20, 2005 and December 13, 2006 were accompanied with clear response in thermal neutrons near the Earth's crust. Their conformity with the observed GLE parameters, first of all time of the beginning, allows us to claim that they were produced by high-energy particles of cosmic rays penetrated into the Earth's atmosphere. During these events thermal neutrons units played a part of Neutron Monitors, using the atmosphere as a lead coverage.

Numerous studies of January event [3-5, 7, 8] have proved very hard spectrum and high anisotropy of the initial particles flux. The analysis of the experimental data from about 40 Neutron Monitors using anisotropic and compound models of the solar cosmic rays variations has shown very narrow beam and very hard spectrum of the first particles, came to the Earth, high anisotropy of the flux and much less amount of high energy particles (>3 GeV) comparing with previous giant GLEs (1956 and 1989) [5].

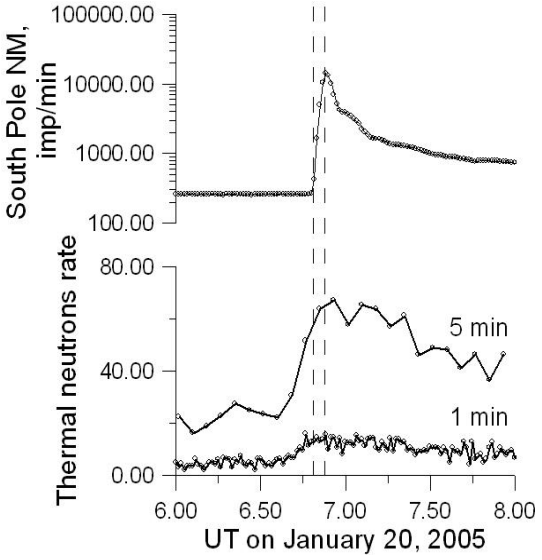

Fig. 3. Thermal neutrons data from Antarctic experimental unit compared with South Pole Neutron Monitor for January 20, 2005. Dashed lines point the time of beginning and maximum of GLE according to Neutron Monitor.

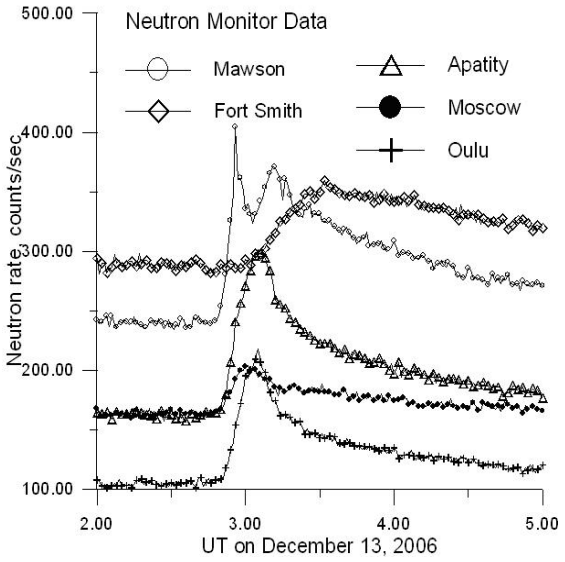

Fig. 4. Cosmic rays data from the world network of Neutron Monitors for December 13, 2006.

These characteristics of the event may be a reason for the fact that in January 2005 thermal neutrons response was detected only in two geographical points. A qualitative agreement between the differences of thermal neutrons' and Neutron Monitors' data for these points (i.e. response in Antarctic was bigger than in Moscow for both instrumentation) also proves it.

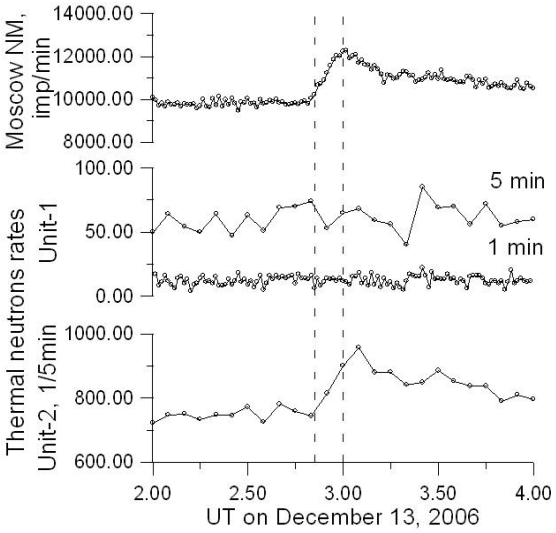

Fig. 5. Thermal neutrons data from Moscow experimental units compared with IZMIRAN Neutron Monitor for December 13, 2006. Dashed lines point the time of beginning and maximum of GLE according to Neutron Monitor.

The fact that in Antarctic thermal neutrons response started approximately 10 minutes before beginning of GLE according to the South Pole Neutron Monitor might have been associated with relativistic solar neutrons event. At the same time absence of any expected time profile for early thermal neutrons increase and very fast arrival of GLE high-energy particles which result in time overlapping do not give us an opportunity to state confidently about the registration of solar neutrons during this event. The same point of view is also expressed by other scientists [9, 10] with references to solar telescopes data and RHESSI observations.

Most likely such time discordance as well as more wide shape for thermal neutrons' increase are explained by the different transport processes for neutrons and charged particles.

December 2006 event was less powerful in comparison with January 2005. Nevertheless one Moscow unit registered quite clear response to this GLE. As for the previous event time and amplitude coincidence prove the fact that registered neutrons were produced by high-energy particles of cosmic rays.

V. CONCLUSION

A. GLE of January 20, 2005 was registered at three ground-based thermal neutrons' units. It was the first clear response to GLE in thermal neutrons' data during the whole period of observations (from 1994). It's quite clear taking into consideration the unique character of this event: great amplitude, high anisotropy and extra-hard spectrum of initial particles flux. The biggest response was observed at Antarctic experimental unit, which is in good time correspondence with the NMs response. The fact that the thermal neutrons' increase (~3 times against the background) was essentially lower than at Antarctic Neutron Monitors (over 50 and 30 times against the background) can be explained by different energy ranges of the registered particles.

B. GLE on December 13, 2006 was registered only by one Moscow thermal neutrons unit, but it corresponds to Neutron Monitor data both in the amplitude and the time of the observed effect. The absence of the response at another Moscow unit must be linked to energy spectra of this event different from GLE 69. At the same time we can't disregard the different operation conditions of Moscow units.

ACKNOWLEDGMENT

The neutron monitors data was taken from the Network of Cosmic Rays Stations, GOES data – from the National Geophysical Data Center.

The work is partly supported by RFBR grant 05-05-65267

REFERENCES

[1] Kuzhevskij, B.M., Nechaev, O.Yu., Panasyuk, M.I., et.al., "The analysis of the neutron splashes near the Earth crust in order to predict the strong earthquakes", in *2004 Proceedings of Int. Conf. "Problems of Geocosmos"*, pp.226-229

[2] Kuzhevskij, B.M., Nechaev, O.Yu., Panasyuk, M.I., et.al. "Neutron field of the Earth, Origin and Dynamics", *The Journal of the Korean Association for Radiation Protection*, Vol.26, №3, pp.315-319, 2001.

[3] Vashenyuk, E.V., Balabin, Yu.V., Gvozdevsky, B.B., et.al., "Relativistic solar cosmic rays in January 20, 2005 on the ground based observations", in *2005 Proceedings of the 29th ICRC*, pp. 209-212.

[4] Beiber, J.W., Clem, J., Evenson, P., et.al. "Largest GLE in half a century: neutron monitor observations of the January 20, 2005 event", *in 2005 Proceedings of the 29th ICRC*, pp. 237-240.

[5] Belov, A.V., Eroshenko, E.A., Mavromichalaki, H., et.al. Ground level enhancement of the solar cosmic rays on January 20, 2005, *in the Proceedings of the 29th ICRC*, pp. 189-192.

[6] Butikofer, R., Fluckiger, E.O., Neutron monitor data for Jungfraujoch and Bern during the ground-level solar cosmic ray event on 13 December 2006, Available http://cosray.unibe.ch/

[7] Vashenyuk, E.V., Balabin, Yu.V., Bazilevskaya, G.A., et.al., "Solar particle event 20 January, 2005 on stratosphere and ground-level observations", *in the Proceedings of the 29th ICRC*, pp. 213-216.

[8] Moraal, H., McCracken, K.G., Schoeman, C.C., et.al., "The Ground Level Enhancements of 20 January 2005 and 28 October 2003", *in the Proceedings of the 29th ICRC*, pp. 221-224.

[9] Miyasaka, H., Makishima, K., Takahashi, E., et.al., "The solar event on 20 January 2005 observed with the Tibet YBJ Neutron monitor observatory", *in the Proceedings of the 29th ICRC*, pp. 101-104.

[10] Fluckiger, E.O., Butikofer, R., Moser, M.R., et.al., "The cosmic ray Ground Level Enhancement during the Forbush decrease in January 2005", *in the Proceedings of the 29th ICRC*, pp. 225-228.

Creation of model of quasi-trapped proton fluxes below Earth's radiation belt

A. N. Petrov, O. R. Grigoryan, S. N. Kuznetsov

Scobeltsin Institute of Nuclear Physics, Moscow State University, Russia
(gluk@srd.sinp.msu.ru)

Abstract- **The object of investigation is the phenomenon of proton (ten's keV, several MeV) flux enhancement in near-equatorial region (L<1.15) at altitude up to ~1000 km (the storm-time equatorial belt). These fluxes are quite small but the problem of their origin is more interesting than the possible damage they can produce. The well known sources of these protons are radiation belt and ring current. The mechanism of transport is first charge-exchange on neutral hydrogen of exosphere and second charge-exchange on oxygen of upper atmosphere. Therefore this belt is something like the ring current projection to low altitudes. Using ACTIVE (Intercosmos-24), MIR station (SPRUT-VI experiment), NOAA POES series, SAMPEX and other satellites data we obtain the average energy spectrum, the approximation of spectrum using kappa-function, the flux dependence on L, B geomagnetic parameters. On the basis of more than 30 years of experimental observations we made the empiric model that extends model of proton fluxes AP8 below 100 keV and to the small L-values (L<1.15). The model was realized as the package of programs integrated into COSRAD system available via Internet (http://cosrad.sinp.msu.ru). The model can be used for revision of estimation of dose that obtains low-orbital space devices.**

CORONAS - F measurements of high - energy solar proton spectra

S.N. Kuznetsov[1], B.Yu. Yushkov[1], K. Kudela[2], R. Bucek[2]

[1]*Skobeltsyn Institute of Nuclear Physics, Moscow State University, Moscow, Russia (clef@srd.sinp.msu.ru)*
[2] *Institute of Experimental Physics, Slovak Academia of Science, Kosice, Slovakia*

Abstract – **Fluxes of protons at the energy range of 0.8 - 4 GeV accelerated during solar flares of October-November 2003 were detected onboard the CORONAS-F satellite having polar circular orbit with an altitude ~450 km. The SONG instrument consisted of a CsI(Tl) crystal of size Ø20 cm ×10 cm and had sufficient geometric factor (~1500 $cm^2 \cdot sr$) to detect directly solar protons as a count rate exceeding above a background level in a wide range of geomagnetic cut-off rigidities calculated in the geomagnetic field described by IGRF and Tsyganenko models. Using the geomagnetic cut-off effect we determined solar proton spectra on 28 October (GLE65) and 29 October (GLE66). Measured spectra are in a good agreement with combined spectra obtained with GOES data and calculated from neutron monitor network data.**

Radiation Environment of the inner magnetosphere: Quiet and storm Periods

M. Panasyuk

[1]*Skobeltsyn Institute of Nuclear Physics, Moscow State University, Moscow, Russia*
(clef@srd.sinp.msu.ru)
[2] *Institute of Experimental Physics, Slovak Academia of Science, Kosice, Slovakia*

Abstract – **The radiation environment near the Earth is characterized by the permanent presence of particles of radiation belts, ring current, galactic cosmic rays,secondary and albedo radiation produced as a result of the interaction between the atmosphere and the particles that precipitated from the belts and penetrated deep into the magnetic field generated by cosmic rays. Solar storms are accompanied by ejections of plasma and energetic particles into the interplanetary medium. Part of the solar material penetrates into the geomagnetic field and changes the spatial and energy distributions of charged particles, which are stationary during quiet periods, but dependent on colar cycle.Solar energetic particles (SEPs) can reach low altitudes and fill both polar caps and outer region of trapping zone during solar and geomagnetic storms, thus resulting in additional radiation effects in the near-Earth environment. On the other hand, geomagnetic disturbances—substorms and storms—arising during solar storms result in an intense transport and acceleration of particles in Earth's environment both inside and outside the region of trapped radiation. In total, these processes lead to complex variations of fluxes of charged particles named radiation storms.The effects of "near -Earth" radiation storms are discussing in this talk.**

Coronal Mass Ejections of Solar Cycle 23

N. Gopalswamy

NASA Goddard Space Flight Center
(gopals@ssedmail.gsfc.nasa.gov)

Abstract – **Coronal mass ejections (CMEs) were first observed in white light in the early 1970s, but their key role in space weather has been established only after the advent of the Solar and Heliospheric Observatory (SOHO) mission. CMEs have been observed over the entire solar cycle by a single coronagraph for the first time, thus yielding a uniform and extended data set. SOHO also observed two CMEs of historical significance with their shocks arriving at Earth in less than 20 hours. Halo CMEs, although known before, have become the most important subset of CMEs for space weather purposes. In addition, SOHO observed the CMEs corresponding to all but one of the ground level enhancement events (GLEs) showing that they belonged to a group of CMEs with highest average energy. I discuss the properties of various subsets of CMEs associated with geomagnetic storms, solar energetic particles (SEPs), magnetic clouds, and interplanetary radio-bursts. I will show that only 10% of all CMEs have significant consequences in the heliosphere.**

The effect of intense geomagnetic storms from the 23rd solar cycle on the radiation belt electrons: satellite data analysis and physical simulations

A. Varotsou

Space Science and Applications Group, Los Alamos National Laboratory,
Los Alamos, USA
(athina@lanl.gov)

Abstract – **The close relationship between the Earth's radiation belt dynamics and solar activity has been well established. At Los Alamos National Laboratory (LANL) a very large database of satellite measurements in the Earth's radiation environment exists. Particle and plasma detectors on board the LANL geosynchronous satellites at around 6.6 Earth radii provide continuous measurements of the trapped electron population's outer boundary, while particle detectors on board the Global Positioning System (GPS) satellites at 4 Earth radii measure the heart of the electron outer radiation belt, a highly dynamic place. During the 23rd solar cycle, data was collected from 7 detectors in operation on geosynchronous satellites and 8 detectors in operation on GPS satellites creating a database which offers a great opportunity to study the Earth's radiation belt dynamics on different timescales. The dynamics are studied on the solar cycle scale as well as on the scale of a single geomagnetic storm and results are presented here. For a better understanding of the radiation belt dynamics and the physical processes involved one has to combine satellite observations with physical simulations. The Salammbo 3D physical model has been extensively used for theoretical physical studies. Here it is used to simulate a real geomagnetic storm from the 23rd solar cycle. The conclusions obtained from the comparison of the simulation results with satellite data are a measure of how good our current understanding of the radiation belt dynamics is.**

Influence of magnetic clouds on the cosmic rays and the near-Earth space environment

Dr. Badruddin

Department of Physics, Aligarh Muslim University, India
(badr_phys@yahoo.co.in)

Abstract – **We discuss the effects of magnetic clouds on cosmic rays as observed by neutron monitors. We also discuss their impact on the geo-magnetosphere by utilizing the indices of geomagnetic activity. Other structure/features associated with magnetic clouds e.g. shock/sheath, interaction region and high speed stream are also considered and their effectiveness in modulating the cosmic ray intensity and geomagnetic activity are synthesized. The use and importance of interplanetary plasma and field parameters during the passage of structures of distinct properties, and physical mechanisms playing important role are also discussed.**

Ozon destruction by solar electrons in relation to Solar Variability and the terrestrial latitude

V. Tritakis[1], G. Korbakis[1], P. Nastos[1], A. Paliatsos[1], Yu. Pisanko[2]

[1]*Research Center of Astronomy and Applied Mathematics, Academy of Athens, Athens Greece (vas@academyofathens.gr)*
[2]*Institute of Applied Geophysics, Moscow, Russia*

***Abstract* – Precipitating electrons from the radiation belts with energies greater than 150 keV to 5 MeV have been correlated with ozone data of a large number of stations located within 40^o - 70^o N. Energetic electrons have been collected by the low altitude polar Russian satellite METEOR while ozone data have been compiled from almost ninety (90) stations located all over the world within the latitude zone 40^o - 70^o N. In more than 60% of the stations examined, we detect a clear decrease of the ozone variation during and after the occurrence of an electron flux excess, which recovers within 3 – 5 days. The more northern is a station located the deeper is the ozone decrease. Moreover, clear evidence that the solar cycle affects ozone destruction through energetic electron events is presented. The preliminary results of the present work stimulate a future attempt for a simple ozone destruction mechanism formulation, which could describe atomic nitrogen ionization by energetic electrons, which in the following merge to atomic oxygen and produce nitrogen oxides. Finally, nitrogen oxides destruct ozone creating characteristic decreases on the normal ozone variation.**

I. INTRODUCTION

One of the most crucial points in the stratospheric physics, especially ozone depletion and climate change, is the balance of the odd oxygen which is highly affected by odd nitrogen. The incidence of the electromagnetic radiation on the atmospheric constituents has been extensively studied in contrast to the energetic particles influence which has been studied much less.
However, some very important studies on the particles reaction with the middle atmosphere elements, especially their contribution to the ozone depletion, have been reported since 1990.

Magnetospheric electrons coupling with stratospheric odd nitrogen and ozone has been explicitly studied by Solomon et al. (1982), Callis et al. (1991), Callis and Lambeth (1998), Randal et al. (1998) while Thorne (1980) and Jackman (1991, 1993) have reviewed the consequences of the particles incidence on the chemical composition of the middle atmosphere.
Reactions involving NO_x, play a dominant role in the stratospheric odd oxygen loss in the ozone layer, mainly through the cycle:

$$NO+O_3 \rightarrow NO_2+O_2$$
$$NO_2+O \rightarrow NO+O_2$$
$$\text{----------}$$
$$\text{net: } O_3+O \rightarrow 2O_2$$

The aim of the present study is to illustrate the relation between strong fluxes of precipitating electrons and ozone depletion detected by ground based observations. We expect in the near future to proceed to a detailed description of the whole procedure by a numerical model which finally could predict place, time and magnitude of ozone depletion on the globe after a strong incidence of precipitating electrons.

II. DATA DESCRIPTION

Daily total ozone measurements covering the time span 1991-1997 of almost 90 ground based stations located between 40^o N and 70^o N and distributed mainly within two wide longitude zones, covering Europe and North America, have been used.
From Figure 1 it is clear that most of the stations under consideration are located within two longitudinal zones, each ~100 degrees wide.

The space origin data we use in this study are relativistic electron precipitation (REP) events collected by two Geiger counters (power law differential spectrum assumed), onboard the satellites N18, N19, N20, N21 of the 'Meteor-2' and the satellites N4, N5, N7 of the 'Meteor-3'

series (both series were placed on circular orbit at 81^o inclination and approximately 1000 km altitude) during the years 1992-1997. The data in use were compiled when the satellite flew between 4 and 6 McIlwain shells in the northern hemisphere because the outer radiation belt contains mainly electrons that provide precipitation events. A REP event is defined as an enhancement in the counting rate by at least two times the yearly standard deviation (σ) of the counting rate observations for the total period. Finally, we examine events that belong to the ascending and descending branch of the orbit separately; the depicted events must be separated with a calm time period (with no precipitation) for at least nine hours. The quiet period between successive REP events is necessary to ensure photochemical equilibrium of the upper stratospheric ozone before a precipitation event. In addition, we ignore events that occur very close to the local sunrise and sunset to eliminate rapid changes of mesospheric properties.

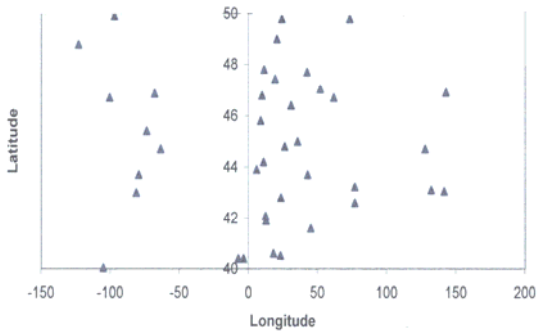

Fig. 1. Longitudinal distribution of the stations under consideration.

III. RESULTS AND DISCUSSION

Daily ozone data collected by a number of ground-based stations located within 40°-70° N have been organized in superposed epoch analysis illustrations (Panofsky and Brier, 1968).

In Figure 2, data from the Churchill and Hradec Kralove stations for the period 1991-1997 have been depicted. The zero day represents the average ozone concentration during days when intense electrons precipitation has been detected by the METEOR satellite at a height of 1000 km. An intense electron event is highlighted when its count-rate exceeds by two times the standard deviation of the average count-rate of the total period. Average ozone measurements for five days before and after the zero day for the period 1991-1997 appear in the Figure 2. A clear decrease of the ozone density after the zero day, is obvious in both stations. The decrease has a magnitude of the order of about 10% in comparison to the ozone average magnitude five days before the zero day.

In the Figure 3, we tabulate all the stations located within the latitude zone 40°-50° N, together with the dates (top line) when electron events (flux > 2σ) occur in the year 1991 (solar maximum). Black cells represent ozone destruction during an electron event (>2σ) occurrence, and gray cells no response on ozone totals. White cells mean lack of data. The same tabulation has been followed in the Figures 4, 5 and 6 but Figure 4 deals with data collected in the latitude zones 50°-60° N and 60°-70° N during the year 1991 while the Figures 5 and 6 deal with data collected in the zones 40°-50° N and 50°-60° N, 60°-70° N respectively, during the year 1997 (solar minimum).

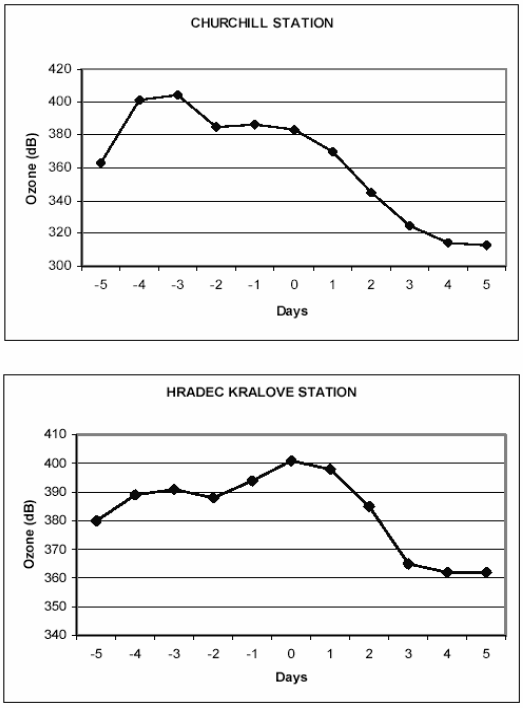

Fig. 2. Ozone data from Churchill and Hradec Kralove stations five days before and after the zero-day where an electron event (>2σ) occurs.

If we compare data collected during the year 1991 (Figs 3, 4) with data collected during the year 1997 (Figs 5, 6), that is Figure 3 with Figure 5 and Figure 4 with Figure 6, very interesting results are derived. At first, it is clear that in the year 1997, which is in the solar minimum epoch there are significantly more gray cells than in the year 1991 of the solar maximum. Since there is a gradual increase of the gray cells number and a decrease of the black ones, from the year 1991 to the 1997, we could come to the conclusion that in the epoch of the solar maximum there is a better relation of the energetic

electrons to the ozone destruction in compare to that of the solar minimum epoch. In addition, in both cases it is clear that the contribution of the electrons to the ozone destruction is larger in the northern latitude zones 50°-60° N and 60°-70° N, than in the middle latitude of 40°-50° N.

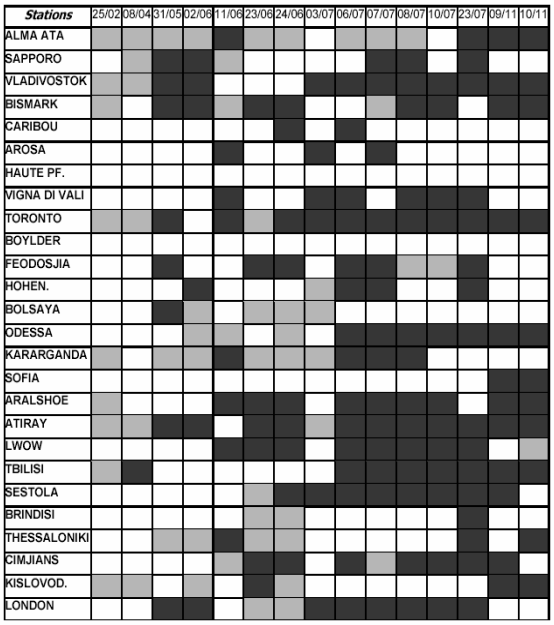

Fig. 3. Ground based stations within the 40°-50° N latitude zone during the year 1991 and the dates when electron events (>2σ) detected. Black cells represent ozone destruction while gray cells express no ozone response. White cells mean luck of data.

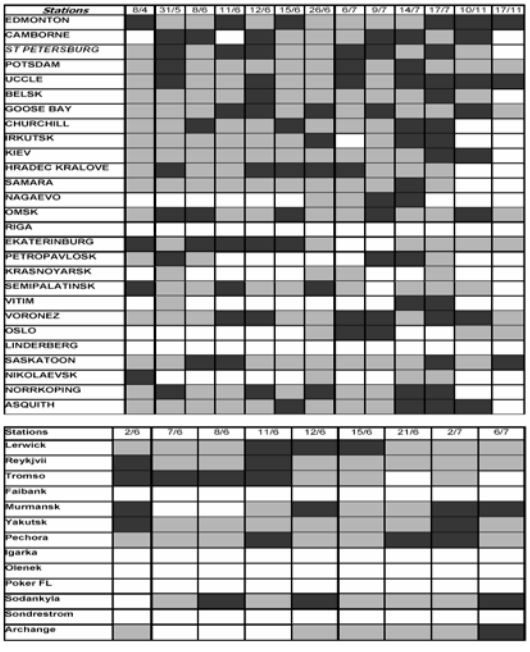

'Fig. 4. Similar to the Figure 3 for stations and events included in the zones 50°-60° N (upper panel) and 60°-70° N (lower panel).

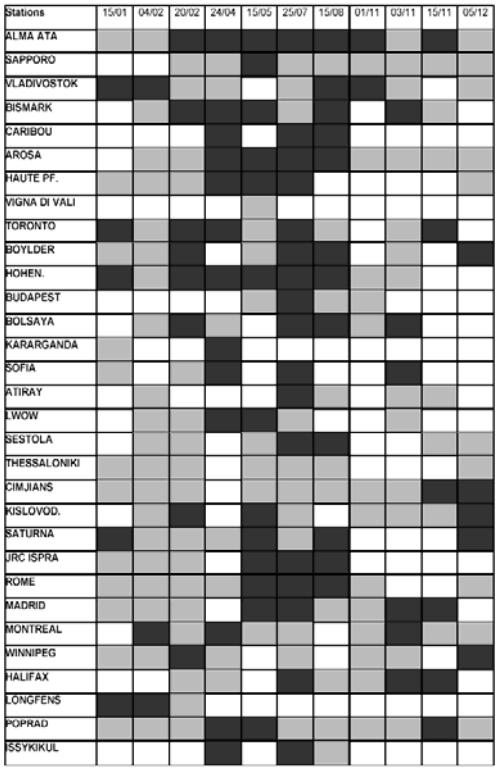

Fig. 5. Similar to the Figure 3, but for the year 1997.

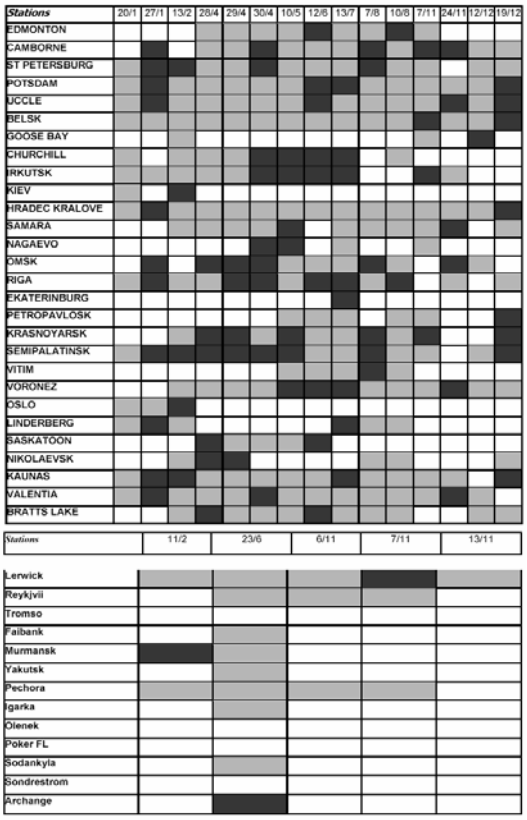

Fig. 6. Similar to the Figure 4, but for the year 1997.

IV. CONCLUSIONS

From the above-mentioned results we can summarize that the energetic electrons response to the ozone destruction is more obvious in ground-based stations situated to the North, higher than 50 degrees. There is also evidence that the phase of the solar cycle plays some role in the ozone destruction. In the epoch of maximum 1991 the relation of the energetic electrons to the ozone destruction seems to be stronger than the year 1997 of the minimum solar activity.

Finally, some ground-based stations show an excellent response of the ozone destruction to the precipitating electrons in contrast to other stations, where the response is very weak or null. In other words, it looks that some stations “feel” the approaching of precipitating electrons while others do not “feel” it. In a future paper, we propose to explain this effect.

REFERENCES

[1] Callis, L.B., Baker, D.N. Blake, J.B. Lambeth, J.D. Boughner, R.E. Natarajan, M. Klebesadel, R.W. Gorney, D.J. Precipitating relativistic electrons: their long-term effects on stratospheric odd nitrogen levels. J. Geophys. Res. 96, ND2, 2939-2976, 1991.

[2] Callis, L.B., Lambeth J.D. NO_y formed by precipitating electron events in 1991 and 1992. Descent into the stratosphere as observed by ISAMS. Geophys. Res. Lett. 25, 11, 1875-1878, 1998.

[3] Jackman, C.H. Energetic particle influences on NO_y and ozone in the middle atmosphere. Geophysical Monograph 75, IUGG Volume 15, pp. 131-139, 1991.

[4] Jackman, C.H. The effects of the October 1989 solar proton events on the stratosphere as computed using a three-dimensional model. Geophys. Res. Lett. 20, 459-462, 1993.

[5] Panofsky, H.A., Brier, G.W. Some Applications of Statistics to Meteorology. University Park, Pennsylvania, 1968.

[6] Randall, C.E., Bevilacqua, R.M., Rusch, D.W., Lumpe, J.D. Polar ozone and aerosol measurement (POAM) II stratospheric NO_2. J. Geophys. Res. 103, 28361-28371, 1998.

[7] Solomon, S., Crutzen, P.J., Robbe, R.G. Photochemical coupling between the thermosphere and the lower atmosphere. 1. Odd nitrogen from 50 to 120 km. J. Geophys. Res. 87, C9, 7206-7220, 1982.

[8] Thorne, R.M., The importance of energetic particle precipitation on the chemical composition of the middle atmosphere. Pure App. Geophys. 118, 128-151, 1980.

Responses of Venus induced magnetosphere under extreme solar conditions

K. Kudela, T.L. Zhang

[1]*Space Research Institute, Austrian Academy of Sciences, Graz, Austria*
[2] *Institute of Experimental Physics, Slovak Academia of Science, Kosice, Slovakia*

Abstract – **The aim of a planetary mission is usually to study the planet itself. It often emphasizes on the surface geological mapping, atmospheric remote sensing and space plasma environment of the planet. However, when properly equipped, an inner planets (Mercury and Venus) mission can be easily used by the space weather community as a sentinel upstream of Earth in the solar wind. Venus Express, the first European planetary mission to Venus, was launched on November 9, 2005 and placed into orbit about Venus on April 11, 2006. Onboard VEX, there are magnetometer and plasma analyzer. Since VEX will spend most of its 24 hour orbit period in solar wind, it will provide us useful data for space weather study. In this paper, we examine the responses of Venus induced magnetosphere under extreme solar conditions in 2006 at solar minimum. The induced magnetosphere behaves much different under these extreme solar conditions: the ionopause increases its altitude to a level seen only at solar maximum; we can identify all the ICME events by magnetic field data although Venus was separated by a great longitudinal angle with Earth; we observed distant bow shock located at a distance about 10 Re which is equivalent to find Earth bow shock at 100 Re by a simple scaling. In all, Venus Express provides us a good opportunity to study the solar extreme events.**

Ionospheric monitoring and short term forecasting at middle latitudes during solar extreme events consequences of violent solar storms

A. Belehaki

National Observatory of Athens, Greece
(belehaki@space.noa.gr)

Abstract – **Ionospheric storms represent an extreme form of space weather with important effects on ground- and space-based technological systems, including radio wave communications, navigation and surveillance systems. At middle latitudes the ionospheric response lead to either positive or negative storm effects. Daytime positive storms are attributed to travelling atmospheric-ionospheric disturbances and subsequent changes in the global wind circulation. Negative storm effects are attributed to neutral gas composition changes which are propagated toward middle latitudes during night and which subsequently rotate into the day sector. These phenomena are driven by highly variable solar and magnetospheric energy inputs to the Earth's upper atmosphere, which continue to provide a major difficulty for attempts now being made to simulate the detailed storm response of the coupled neutral and ionized upper atmospheric constituents. The requirement for quasi-real-time products based upon current ionospheric specification has led to an increased importance of so-called real-time ionospheric models. Ionospheric specification tools comprise terrestrial sounding systems, including real-time networks of ionospheric sounders. The European Digital Upper Atmosphere Server (DIAS) is an advanced real-time network of European digisondes. DIAS delivers products and services for near real-time specification of ionospheric parameters and short term ionospheric forecast up to 24 hours ahead based on empirical and data driven autoregression modelling techniques. The paper reports on the success of near real-time ionospheric specification over large geographic areas, given the advanced capabilities of modern ionosondes, and on the performance of ionospheric prediction models especially during solar extreme events.**

Poster Session C

The chain of physical processes in the solar- terrestrial system
(Sun-Heliosphere-Magnetosphere Ionosphere-Upper Atmosphere - Ground)

Chair: P. Preka-Papadema

Solar **E**xtreme **E**vents **2007**

Solar Cosmic Rays and Solar-Terrestrial Relations: Observational Evidence and Mechanisms

L.I. Miroshnichenko

[1] *N.V. Pushkov Institute IZMIRAN, Russian Academy of Sciences, Troitsk, Moscow Region, Russia*
[2] *Instituto de Geofisica, Universidad Nacional Autonoma de Mexico, Mexico (leonty@geofisica.unam.mx; leonty@izmiran.ru)*

Abstract – **A number of geophysical effects of solar energetic particles (SEPs), or solar cosmic rays (SCR), are reviewed. We concentrate mainly on the observational evidence and mechanisms of some expected effects and/or poor-studied phenomena discovered within 2-3 last decades: depletion of the ozone layer; perturbations in the global electric current; change of the atmospheric transparency; and production of nitrates. Some "archaeological" data on SCR fluxes in the past and upper limit of total energy induced by solar flare protons are also discussed. Due attention is paid to the periodicities in the solar particle fluxes. Actually, many solar, heliospheric and terrestrial parameters changing generally in phase with the solar activity are subjected to a temporary depression close to the solar maximum (Gnevyshev Gap). Similar gap has been found recently in the yearly numbers of the >10 MeV proton events. All above mentioned findings are evidently of great importance in the studies of general proton emissions of the Sun and long-term trends in the behavior of solar magnetic fields. In addition, those data can be very helpful for elaboration the methods for prediction the radiation conditions in space and estimation of the SEPs contribution into solar effects on the geosphere, their relative role in the formation of terrestrial weather and climate.**

Solar protons effect on middle atmosphere during SEEs 28.10.2003 and 13.12.2006

A.S. Kirillov, E.V.Vashenyuk, B.B. Gvozdevsky, Kh. Fadel

Polar Geophysical Institute, Murmansk region, Russia
(vashenyuk@pgi.kolasc.net.ru)

Abstract – **The effect of energetic solar protons on the middle atmosphere (20-80 km) chemical composition during the SEEs October 28-29, 2003 and December 13, 2006 has been studied. The solar proton spectra were obtained from the neutron monitors, balloons and spacecraft data. One-dimensional time-dependent model (Fadel et al., 2006, Adv. Space Res.) has been used to calculate the production and loss of minor atmospheric components during the GLE. For SEE 13.12.2006 the derived depletions of ozone content is in good agreement with experimental data obtained by the Microwave Limb Sounder (MLS) instrument on the AURA spacecraft.**

Interplanetary manifestation of solar extreme events occurred during the past solar maximum of cycle 23

S. Dasso[1, 2], M.S. Nakwacki[1], P. Demoulin[3], C.H. Mandrini[1]

[1] *Instituto de Astronomia y Fisica del Espacio (IAFE), Buenos Aires, Argentina (dasso@df.uba.ar)*
[2] *Departamento de Fisica, FCEyN, UBA, Buenos Aires, Argentina*
[3] *Observatoire de Paris, LESIA, Meudon, France*

Abstract – **We study the fast and huge magnetic clouds associated with the strongest solar eruptions, occurred during the post solar maximum of the solar cycle 23. Magnetic clouds are believed to be closed twisted flux tubes traveling from the Sun to the outer heliosphere. However, their evolution in spatial scales of the order of the Sun-Earth distance is still not fully known. Even the identification of their boundaries is an open question in some cases. We applied a new method to analyze magnetic clouds, which is based on the conservation of the azimuthal flux between the in- and out-bound branches of the cloud, and it is valid for finite distances between the spacecraft trajectory and the cloud axis. The direct method is useful to improve the determination of boundaries and/or orientation when one of these two is known. From this analysis we find that the flux ropes are followed by a large coherent region and we interpret it as the existence of a previous larger flux rope, which partially reconnected with the surrounding environment in its front. Thus, the original flux rope is progressively peeled by reconnection and transformed to the observed interplanetary mass ejection. Our results are put within the frame of the solar measurements obtained from the probably source regions.**

The solar wind charge exchange process as seen in X-rays and plans for a space based telescope

J. A. Carter, S. Sembay

University of Leicester, United Kingdom
(jac48@star.le.ac.uk)

Abstract – **The solar wind charge exchange (SWCX) process has proved to be a significant source of background for space based X-ray telescopes such as XMM-Newton and Suzaku, dependent on specific alignment and observing conditions. SWCX produces emission lines within the soft X-ray band from the interaction of solar ions, including oxygen VII, oxygen VIII, carbon V and magnesium, with neutrals such as geocoronals in the Earth's magnetosheath. It can be used as an indicator of the conditions in the solar wind and the dynamical interaction between the solar wind and the Earth's magnetic field. We present the observational evidence of this effect and discuss the importance for future space missions. We also discuss plans for a lunar based telescope dedicated to observing this phenomenon.**

Solar Energetic Particles Variations and Their Penetration in the Earth's Magnetosphere during Extreme Geomagnetic Storms (2001-2005 years)

S.N. Kuznetsov[1], L.L. Lazutin[1], I.N. Myagkova[1],M.I. Panasyuk[1], A.N. Podorolsky[1], K. Kudela[2]

[1]Skobeltsyn Institute of Nuclear Physics, Moscow State University, Moscow, Russia (irina@srd.sinp.msu.ru)
[2]Institute of Experimental Physics, Slovak Academia of Science, Kosice, Slovakia

Abstract – **More then 50 solar particle events affecting the near-Earth?s environment were observed from August, 2001 till June, 2005 in the experiments on board CORONAS-F. Set of instruments developed by SINP MSU on board this satellite permited to measure charged solar particles fluxes - protons with the energies 1-90 MeV and electrons 0.03-12 MeV, nuclei 2-20 MeV/n and from C to Si 4-40 MeV/n. Penetration of solar energetic particles in the polar caps during the main phase of magnetic storms is one of the important sources of radiation danger in the near-Earth space, especially for low-altitude satellites. The size of the energetic particle penetration area depends both on proton rigidity and on geomagnetic conditions. The most intensive SEP were measured during several solar extreme events periods from 2001 till 2005 years. Some of these SEP event were accompanied by the powerful geomagnetic storms (e.g. November 6, 2001 (Dst=-257 nT), November 24, 2001 (Dst=-221 nT), October 29-30, 2003 (Dst=-400 nT), November 2004, 2004 (Dst=-374 nT)). During the main phase on these storms energetic solar particles have penetrate extremely deep in the Earth?s magnetosphere ? lower than 50 degrees of invariant latitude. It should be noted that even moderate magnetic storms with Dst about 150-250 nT observed during September 2001, April 2002, July 2004, May 2005 caused the SEP penetration rather deep in the Earth?s magnetosphere ? up to invariant latitudes about 55-57 degrees. Obtained results show that the dependence of the SEP boundary on Dst variation value could not be approximated by the simple linear function and one should take into account the influence of even moderate geomagnetic storms on the process of SEP penetration inside the magnetosphere.**

Solar cosmic rays as a factor of Space Weather and their effect on the atmosphere processes in auroral and subauroral zones

V.E. Timofeev, N.G. Skryabin

Yu. G. Shafer Institute of Cosmophysical Research and Aeronomy, Russia
(vetimofeev@ikfia.ysn.ru)

Abstract – **Solar cosmic rays as one of the main factors of influence space weather of on processes in the atmosphere are investigated. The data of high-energy solar cosmic rays (SCRs) are used and the processes initiated by them in the atmosphere at auroral and subauroral latitudes are studied. The formation of SCK intensity distribution in latitude and longitude and its dynamics during proton events are considered using data of neutron monitors at two meridional station networks separated in longitude: Tixie Bay, Yakutsk, Irkutsk in the Eastern Siberia and Barentsburg, Apatity, Oulu, Moscow in Europe. The association between changes of dynamic characteristics of solar wind and their manifestations in SCRs and in some atmospheric parameters is also investigated. The differences in geocosmophysical effects depending on the difference of geomagnetic and geographical latitudes along the auroral zone have been obtained.**

The role of cyclic solar magnetic field variations in the long-term cosmic ray modulation

R.T. Gushchina, A.V. Belov, V.N Obridko, B.D Shelting

Pushkov Institute of Terrestrial Magnetism, Ionosphere and Radio Wave Propagation, Russian Academy of Sciences

Abstract – **Updating the semi-empirical model of cosmic rays (CR) modulation proposed in our previous work has been discussed. In order to provide a description of long-term variations, in which the CR modulation would adequately reflect the complex interaction of global and local solar magnetic fields, we have supplemented the model with the following characteristics: the solar magnetic field polarity, the integral index, the partial indices, the tilt of the current sheet, and the index characterizing the x-ray flares. The role of each index in the CR modulation has been determined. In the multi-parameter description of long-term CR variations using the integral index or one of four partial indexes, the best fit for the period 1977-1999 has been obtained for the integral index and the sector-odd index characterizing the inclined dipole. The discrepancy between the model and observations increases from the beginning of 2000. Therefore, the problematic features in the behavior and modeling of CR during cycle 23 have been discussed. It is suggested that the cycle-to-cycle decrease of the CR density in the minimum epochs of the past solar activity (SA) cycles could be explained by the decrease of the zone-odd index.**

Key Words— long-term cosmic rays variations, solar magnetic field, model of CR modulation, indices of the global magnetic field

I. INTRODUCTION

The solar wind modulates CR in the heliosphere, thus providing a relation between the CR density and solar magnetic fields. The CR density reflects various solar cyclic variations. In order to understand these processes the CR modulation by electromagnetic fields in the heliosphere is modeled. It has been supposed by [1] that the CR modulation during the solar activity (SA) cycle is determined by changing of solar non-axisymmetric (longitudinally averaged) component of open magnetic flux (Φ_{max}), which is created in active regions. This conclusion is based on studies of the empirical connection between CR and the solar open magnetic flux as well as correlations with sunspot numbers, tilt of the heliospheric current sheet, CME rate and value of the equatorial dipole. [1] considered a set of simple models with single modulating index without accounting of CR delay relatively to manifestations of the solar activity. In this work the long-term modulation for 21-23 cycles and separately for the 23rd cycle additionally accounting a CME rate has been studied, since the correlation between Φ_{nax} and CR falls for the last cycle.

The present study of galactic CR modulation in the heliosphere through the 19-23 cycles continues our previous works ([2], [3], [4], [5], [6]) and is based on the long-term distribution of CR obtained by the neutron monitor network. We discuss improving of our semi-empirical model of CR modulation proposed previously. This model shows that the long-term CR modulation depends on cyclic changes of the total energetic characteristic B_{ss}, which provides the information on the total magnetic flux passing across the solar wind source surface, a 'gofferness' of the current sheet in the interplanetary space (i.e. from the tilt η of the heliospheric current sheet) and changes of the polar magnetic field H_{pol}.

For more complete account of complex interaction between global and local solar magnetic fields for the CR modulation during solar cycle development it has been proposed to introduce into the model a new index of x-ray flares and characteristics of the solar magnetic field. A role of each index in the CR modulation is determined with detailed justification of such a choice and accounting the delay time. Our modeling shows that a discrepancy between the model and observations increases beginning from the year of 2000. Therefore we discuss possible problems of CR behavior and its modeling during the 23rd cycle.

II. LONG-TERM BEHAVIOR OF THE CR AND PARAMETERS OF THE MODULATION

Initial data for modeling of CR variations are results of long-term CR observations, characteristics of the solar global magnetic field and solar x-ray

flares (importance ≥ M1). The rigidity spectrum of CR variations for each month was obtained using data of the neutron monitor global network and data of the stratospheric sounding for 1976–2006 (by the method described in [7]). We study amplitude variations of CR with 10 GV rigidity, excluding variations associated with ground level enhancements of solar CR ([6]). Note that for some events a value of the last effect is greater than 3% even for values of monthly averaged amplitude and some particular CR stations used in our analysis. Thus, eliminating the effect of solar CR, amplitude of long term CR variations with 10 GV rigidity obtained by using the method of global survey becomes a value of pure galactic cosmic ray (GCR) origin. Calculations of CR modulation have shown that using amplitude of GCR origin the proposed modulation model is improved.

The structural and quantitative characteristics of the solar global magnetic field as: a heliospheric current sheet tilt η, the solar polar field H_{pol} and the average magnetic field intensity B_{ss} are calculated on the surface of solar wind source. Along with using of the average B_{ss} index of solar magnetic field, the partial indexes have been determined from data of the Wilcox solar observatory (WSO) for 5.1976 – 12.2006. (zone-even ZE, zone-odd ZO, sector-even SE and sector-odd SO). Here we used data of measurements of the large-scale photosphere magnetic field with magnetometer resolution of (3′) performed in WSO [http://quake.stanford.edu/~wso] and processed by the original method described in [8]. There is a problem of the magnetometer sensitivity in results of solar field observations in 2000-2002 and, possibly, after recalibration the data set is not uniform.

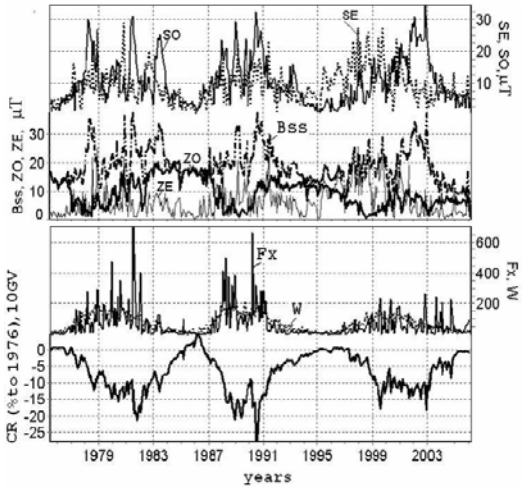

Fig. 1. Temporal changes of CR intensity (% to 1976), flare index Fx, sunspot numbers W, average values of solar magnetic field strength –index B_{ss} and partial indexes ZO, ZE, SO, SE (μT).

The question do various observations of large-scale magnetic fields fit each other in a various degree of conformity year from a year occasionally or they are governed by some real physical mechanism (solar or instrumental) is still unresolved yet ([9]).

In order to understand a modulating influence of local solar activity on CR it is proposed to use F_x, a specially calculated index of solar flares F_x, empirically determined by [6]. The flare index depends on maximum x-ray intensity (events of ≥ *M*1 have been selected) during the flare and its longitudinal location relatively to the Earth

$$Fx = \left[1 + \alpha \ln\left(\frac{I_x}{I_C}\right)\right] \exp\left(-\left(\frac{\varphi - \varphi_0}{\sigma_\varphi}\right)^2\right),$$

where $F_x = 0$, if $I_X < I_C$ (I_X – the maximum flux of x-ray event, $I_C = 10^{-5}$ W/m^2), $\sigma_\varphi = \sigma_E$ for $\varphi < \varphi_0$; $\sigma_\varphi = \sigma_W$ for $\varphi > \varphi_0$. It is supposed $\sigma_W = \sigma_E / 2$. The evaluation of F_x is performed accounting the previous results ([6]), but for other parameters, in particular, for longitudes φ_0 = -18°, -14°, -10°, -6°, -2° and σ_φ = 55°, 60°, 65°, 70°, 75°. In this work given values of the α parameter are α = 65; 70; 75; 80; 85; 90.

Figure 1 shows a behavior of the modulating characteristics in 1976-2006. In the phase of SA minimum all indices of the global field fluctuate nearly zero excepting the quasi-dipole ZO, which has a maximum value. [6] examined features of the F_x variations during the whole interval under investigation and the decay phase of the 23rd solar cycle. The magnetic field indexes were introduced [10] for the potential magnetic field model with the source surface.

Further we use an expansion of the observed magnetic field into the spherical functions (Legendre polynomials) with the coefficients for the expansion of the photosphere magnetic field g_{lm} and h_{lm} with indexes l and m. The coefficients g_{lm} and h_{lm} were calculated according to the WSO data. The partial index ZO (m=0, l=2k+1) partially accounts a magnetic field with odd zone symmetry (analogue of the vertical dipole). The zonal-even index ZE (m=0, l=2k) is small as a result of the Hale law, being by a special case an action of the polarities generalized rule of solar magnetic fields ([11]). The sector-odd index SO (m=l=2k+1) characterizes the tilted structure similar to dipole and reflects an influence of the SA at low and middle latitudes. The sector-even index SE (m=l=2k) is usually manifested in the 4-sector field structure.

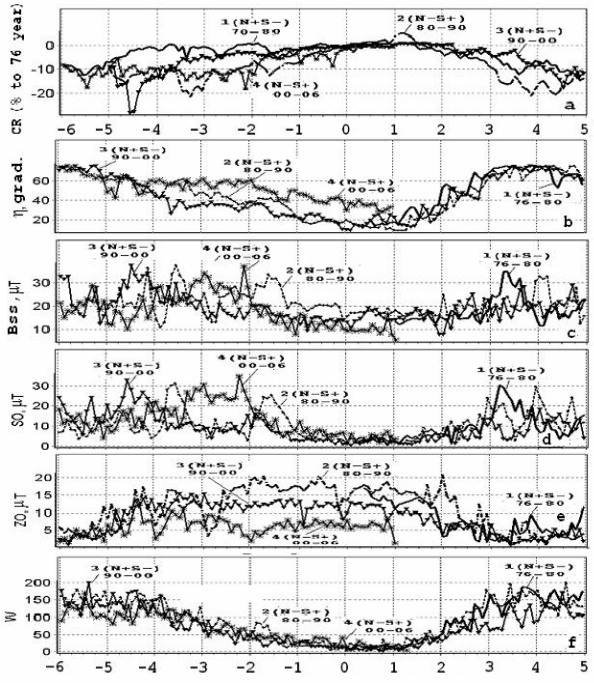

Fig. 2. (a-f). 11-years variations received by the superposition epoch method relative to minimum SA: a – CR % to 1976, rigidity R= 10 GV; b - current sheet tilt η (grad.); c - e - indexes Bss, SO, ZO (μT), f – sunspot numbers W.

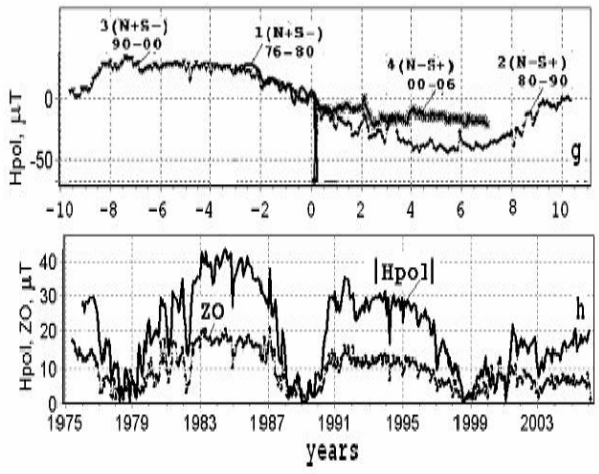

Fig. 2. (g, h). 22 years variations H_{pol} obtained by the superposition epoch method relative to maximum SA – g; temporal changes of $|H_{pol}|$ and index ZO (μT) – h..

In order to obtain a clear picture of time changes of SA and CR during different epoch of the solar cycle variations of the CR (10 GV) intensity and chosen indexes of SA with directions of the global solar magnetic field are shown in fig.2. The CR variations (% to 1976) and solar characteristics are obtained using the method of epoch superposition (the years of SA minimum 1976, 1986, 1996 are accepted as zero years) are presented in fig. 2 (a-f). The 22 year variations of H_{pol} are calculated by the method of superposition epoch relative to the SA maximum (when the field changes a sign) are shown in fig.2 (g); temporal changes of the polar magnetic field module $|H_{pol}|$ and the index ZO are presented in fig.2 (h). Let us underline now some crucial results:

- variations of indexes and CR from cycle to cycle are small and similar to each other during the SA increasing phase;
- time profiles of all indexes are essentially different for periods of decreasing SA in cycles with different direction of the global Sun field. This is especially important for the current sheet tilt η, the zone-odd index ZO and the solar polar field Hpol. The current sheet tilt remains abnormally large during the decay phase of 23rd solar cycle in comparison with other cycles. The η parameter has varied from 60º to 50º during 5,5 years till the middle of 2004. Even in the deep SA minimum of 2007 the tilt η remains large (~30º) and this certainly should be reflected in the CR modulation. The tendency of zone-odd index ZO and polar field $|H_{pol}|$ to decrease from cycle to cycle is clear, especially during the 23rd cycle. The sector-odd index SO significantly increases both during the decay and rise phases of SA, behaviour of the average solar magnetic field B_{ss} shows the same tendency.

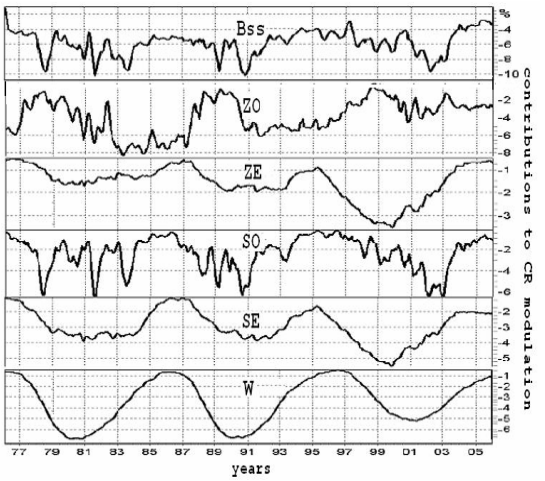

Fig. 3. A contribution (%) of B_{SS}, ZO, ZE, SO, SE, W indexes to simulated CR variations.

Basing on observations of large-scale magnetic fields it is shown, that the largest scale of a magnetic field is connected with dipole component - the global dipole. The full magnetic moment of the dipole and its vertical and horizontal components cyclically

vary and never vanish completely ([12]). The calculations performed on the basis of solar supervisions for last three cycles (1976-2005) shows that the magnetic dipole is strictly vertical at the cycle minimum, so the horizontal dipole vanishes during this epoch and the latitude of the dipole axis becomes close to 90º. Approaching the cycle maximum, the total magnetic moment strongly decreases at some time moments but never vanish. From figures presenting in the paper ([12]) it is clear that the vertical components of a magnetic dipole reduces in SA minima from a cycle to a cycle, the same tendency is appreciable for behaviour of the total magnetic moment. This temporal behaviour is similar to changes of the indexes ZO and Bss, which we use for modeling of the CR modulation. The horizontal component appears in each cycle during periods of the high solar activity, but its values are large sometimes in comparison with vertical component and are characterized by a fairly large scatter close to the epochs of polarity reversals. Temporal behaviour of variations of the sector-odd index SO has a similar tendency. During epoch of the cycle minimum namely the polar region govern the interplanetary magnetic field parameters down to the ecliptic plane. Undoubtedly this circumstance will effect on the integral heliospheric index such as the CR intensity (observed near Earth and at the Earth) by contribution of the H_{pol} and ZO characteristics in the proposed modulation model.

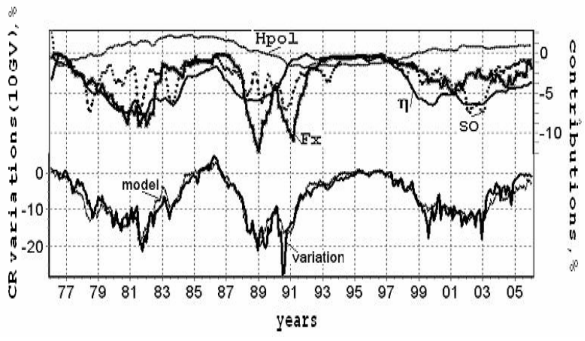

Fig. 4. Monthly CR variations (%) observed and simulated by the multiparameter model for F_x, H_{pol}, SO, η indexes.

Values of all solar indexes and CR intensity differ larger between cycles than do the sunspot number of different solar cycles. These differences have a specific character for each index. So, some features of the 23rd cycle are precisely visible in cyclic changes of η; ZO changes show its reduction from cycle to cycle and the short-term increases of B_{ss} and SO are reflected in their cyclic variations during the increased periods of SA. We may say that the sunspot number is a rather "rough" characteristic of SA and other solar indexes should be added for better accuracy.

III. Discussion results of CR modulation

The model is further improved for reliable representation in CR modulation of short-period variations by introducing the index of x-ray flares. The modified model of CR modulation with account of the partial indexes of solar magnetic field listed above was used to answer the question about influence of various modes of the global Sun field on the long-term CR variations. A joint consideration of following modulating parameters: above-mentioned η, B_{ss}, (or one of the partial indexes) H_{pol} as well the F_x index of x-ray flares is necessary for model description of CR according to the multi-parametric regression analysis**.** Including an influence of solar flares for description of CR variations provides a better representation of observed CR variations for effective range of longitudinal distribution σ_φ=55°-75° for all parameters φ_0 and α>65. Introducing of F_x allows improving representation of observed CR variations. For the period of 1.1977-12.1999 the correlation coefficient increases up to $\rho = 0.96$ in a case of the 4-parameteric model. The performed modeling allows estimating a relative impact of temporal changes of each parameter with its own time delay to the total modulation. The time delay of CR modulation relative to the flare activity obtained in our model of long - term modulation shows that the flare influence is rather prolonged in the heliosphere. It is shown that for the long-term CR modulation of the longitudinal dependence of the flare index is not so important, but there is a strong dependence on flare intensity. However description of short-term CR phenomena (like Forbush-decreases (FD)) includes the longitudinal dependence. Amplitude and other characteristics of FD's strongly depend on flare intensity and longitude of the solar source of interplanetary disturbance.

The multiparameter model of CR modulation, which additionally accounts the index F_x improves the description of observed variations, but once again only up to the year of 2000 only. After the year of 2000 a discrepancy between expected and observed variations increases. It is very difficult to describe the period of 12.1999-12.2006 (and accordingly investigated period 5.1976-12.2006) within the proposed model with a high accuracy.

The description of long-term variations CR was performed with consecutive inclusion into the CR modulation model of the integral index B_{ss} and above-mentioned partial indexes in various combinations with other SA parameters for finding a reason of the specified discrepancy. Calculations

show that such a picture of modulation (with worsening of CR description from the beginning of 2000) is observed for all partial indices under their use in turns as the forth modulation parameter. For the whole period of 1976-2006 the model description of CR variations is presented, which accounts all parameters listed. During this period we have ρ=0.93 and σ = 2.05 %. Figure 3 shows an impact of different index changes to the CR modulation. The behavior of the parameters ZE and SE in cycle 23 is anomalous. A contribution of cyclical variations of these indexes may increase by two reasons. They are either strongly depend on sector structure or there is an error in the WSO data. A contribution of the ZO index decreases from cycle to cycle during last three SA cycles considered.

One of the model results is presented on Figure 4. It is the variant of the description of long-term CR modulation with account of the most effective combination for modulation: current sheet tilt η, the solar polar field H_{pol}, index F_x considering x-ray flares together with sector-odd index SO. For the multiparameter description of long-term CR variations by using the average of solar magnetic field or one of four partial indexes during the period of 1.1977-12.1999 the best fit is obtained for the average of solar magnetic field B_{ss} and the sector-odd index SO, the correlation coefficient ρ=0.96, the minimum value of the rms deviation is σ = 1.73 % (σ = 1.80-1.86% for others indexes)**.** The cyclic variations of SO index are well reflected in the CR modulation, especially clearly in the maximum of cycles and during the active periods on the Sun. So the contribution to modulation from changes SO in 2003 ($\approx$ -6.5 %) exceeds the contribution from changes η, then a sharp drop of SO followed and consequently a decrease of contribution to the CR modulation. Cyclical variations of ZO index are in the phase with CR variations. It is noteworthy that contribution to the modulation from this parameter goes down from cycle to cycle and reduction of the contribution after the maximum of cycle 23 is clearly visible. This impact is much less as compared with the other cycles.

We propose that a negative trend of the CR intensity, which is widely discussed now by space physics community (for example, [13]), could be related with significant decrease of the zone-odd ZO index maximum values and similar decrease of the vertical component of the dipole magnetic moment recently found ([12]). As a result it is possible to tell, that average of solar magnetic field B_{ss} and index ZO play the main role in creation of the long-term CR modulation observed in the heliosphere. The cyclical variation of the total solar magnetic field is defined by variations of the local fields, which provide a large contribution into the average of solar magnetic field B_{ss} (also in index SO) and by the global field, which appreciably defines itself ZO**,** especially on the source surface. We shall note, that a model description of modulation by means of the indices ZO and SO together with Fx and η gives not worse result than modeling with the average of solar magnetic field B_{ss} index and the value of polar magnetic field H_{pol}.

It is necessary to tell, that further improvements of the considered model are possible. In particular, not all possible modulating parameters are considered yet by the model, for example, some additional characteristics of coronal holes and coronal mass ejections might be introduced (in the present model they are described by the F_x index). The specified solar phenomena undoubtedly participate in formation of solar wind irregularities and creation of the observed CR modulation.

IV. CONCLUSIONS

1. The multiparameter model of CR modulation with the additionally included index F_x characterizing x-ray flares allows an inproved description of the observed variations. The longitudinal dependence of the F_x index is not important to the long-term CR modulation, however, there is a strong dependence on the flare intensity, which is characteristic of this type of variations.

2. It is possible to use the partial indices in the CR modulation model along with the mean solar magnetic field.

3. The behavior of the proposed indices of the solar magnetic field and their contribution to the CR modulation are described and analyzed. During the period of 1977-1999, the best fit is obtained for the mean solar magnetic field or (with a very small difference as to the quality of the description) the sector-odd index together with the current sheet tilt, F_x index and polar field.

4. The model for all indices under examination shows a large discrepancy with observations at the beginning of 2000. This is, probably, connected with the anomalous behaviour of the parameters ZE and SE and a significant decrease of ZO in cycle 23. On the basis of the model description of long-term CR variations, it is suggested that the cycle-to-cycle decrease of CR at the minima of the SA cycles be described by the corresponding decrease of the zone-odd ZO index.

ACKNOWLEDGMENT

The authors are grateful to the Russian Foundation for Basic Research (grants 05-02-17251, 06-02-17346, 06-02-39028) and the Presidium of RAS (the program “Neutrino physics”) for supporting this theme.

REFERENCES

[1] Wang Y.-M., Sheeley N. R., Hulburt Jr. E. O. Role of the sun's nonaxisymmetric open flux in cosmic-ray modulation. The Astrophys. J. v. 644. p. 638–645. 2006

[2] Belov A.V., Gushchina R.T., Kharshiladze A.F et al. Global magnetic field of the sun and long-term variations of galactic cosmic rays, J. Atmos. Terr. Phys. v. 63, N18. p. 1923 – 1929. 2001.

[3] Belov A.V., Gushchina R.T., Obridko V.N., et al. Relation of the long-term modulation of cosmic rays to the characteristics of the global solar magnetic field, Geomagnetism and Aeronomiya, 42. N 6. 693 – 700. 2002.

[4] Belov A.V., Gushchina R.T., Obridko V.N. et al. The relation of the global magnetic solar field indices and the solar wind characteristics with the long-term variations of galactic cosmic rays, Proc. 29th ICRC. Pune. v.2. p. 239 – 243. 2005.

[5] Belov A.V., Gushchina R.T., Obridko V.N. et al. Long term variations of galactic cosmic rays in the past and future from observations of various solar activity characteristics, J. Atmos. Terr. Phys, v. 68. N 11. p.1161 – 1166. 2006.

[6] Belov A.V., Gushchina R.T., Obridko V.N. et al. Simulation of the modulation of galactic cosmic rays during solar activity cycles 21—23, Bulletin of the Russian Academy of Sciences: Physics, v. 71, No. 7, p. 974–976. 2007.

[7] Belov A.V., Gushchina R.T and Yanke V.G. Long-term cosmic ray variations: rigidity spectrum, Geomagnetism and aeronomiya. v.38. N4. p.131 – 134. 1998.

[8] Obridko V.N., Shelting B. D. Structure of the heliospheric current sheet as considered over a long time interval (1915-1996) Solar Phys. v.184. p.187-200. 1999.

[9] A.Demidov M.L., Golubeva E. A. Time changes research of difference parameters of large-scale solar magnetic fields on various series of supervision, Proc. of Conf.: "Sun: active and variable" (Crimean Astrophysical Observatory). 2007.

[10] Obridko V.N., Shelting B. D. Cyclic variation of the global magnetic field indices. Solar Phys. v. 137. p.167-177. 1992.

[11] Obridko V.N., Shel'ting B. D. A Generalized polarity rule for solar magnetic fields. The Astronomical J. v. 51. N4. p. 339-343. 2007.

[12] A. Livshits I.M., Obridko V.N. Variations of the dipole magnetic moment of the Sun during the solar activity cycle. Astronomy Reports. v.50. N11. p 926-935. 2006.

[13] Stozhkov Y.I, Svirzhevsky N.S. Cosmic ray fluxes from stratospheric measurements. Proc. 20th ECRS. Lisbon .(http://www.lip.pt/events/2006/ecrs/proc/ecrs06-s0-131.pdf). 2006.

Some Remarks to January 17 - 22, 2005 Event In Space Weather

K.Kudela[1], I. Dorotovic[2], M. Lorenc[1], M. Rybansky[1]

[1]*Institute of Experimental Physics SAS, Kosice, The Slovak Republic*
(kkudela@upjs.sk)
[2]*Slovak Central Observatory, 94701 Hurbanovo, The Slovak Republic*

Abstract – **This contribution can be regarded as a continuation of paper Kuznetsov et al. (2006) on GLE from January 20, 2005 whereas we focused mainly on a study of FD from January 17-18 and 21-22, 2005. As an input for investigation are data from the neutron monitor at Lomnick Peak (1 minute counts) and from the Geomagnetic Observatory in Hurbanovo (1 minute data), both in Slovakia. Data on magnetic field and solar wind from satellites GOES 10 and 12, SOHO-CELIAS, ACE and WIND have been used for understanding of global evolution of the event. Magnetic field is transformed to the RTN system whereas only disturbed part of the field is compared. i.e. daily variation and constant part is subtracted. Field reduction method is described in the contribution. Our results are temporal vector diagrams of variation of all parameters at all positions from where we used data. Amplitudes |B| exceed 100 nT and variations during arrival of wavefront of CME take place in the same minute at ground-based station and at GOES satellites. Variations have such character as if in the CME would be regions with dominant electric charge of opposite sign, eventually electric currents with different orientation. Based on values v_{p} a n_{p} and using certain assumptions we determined mass of CME on 17 and 21 January, respectively, of 10^{12} kg. Decrease of cosmic ray level run suddenly (during 10 minutes) but starting at about 2 hours after a sudden change of magnetic field.**

Variations of aerosol optical properties during an extreme solar event of 20.01.2005

I. Mironova[1], L.Desorgher[2]

[1]*Institute of Physics of St.Petersburg State University, Russia*
(mironova@ge.phys.spbu.ru)
[2]*University of Bern, Switzerland*

Abstract – **A detailed investigation of an extreme solar event of 20.01.2005 from atmospheric point of view is presented. Cosmic rays of galactic origin are the main source of ionization in the Earth's stratosphere and troposphere. An additional flux of solar cosmic protons can significantly increase the effect of ionization of the Earth atmosphere. During the solar event of 20.01.2005 the world network of neutron monitors registered a narrow beam of solar cosmic ray particles leading to a severe Ground Level Enhancement (GLE). The effect of ionization of the Earth's atmosphere due to this GLE --- was calculated using models --- of University of Oulu and University of Bern. Here an analysis of daily variations of the aerosol optical depth is presented for January -- 2005. The results of the investigation show a strong increase of the concentration of sulfate aerosol on the second day after the GLE observed in the south magnetic pole region where the maximum penetration of anisotropic solar cosmic rays took place. This suggests that the enhanced flux of solar energetic particles can lead to essential changes in the chemical and physical properties of the polar troposphere.**

Interplanetary medium conditions and state of the magnetosphere associated with the global Pc5 oscillations

A.S. Potapov, T.N. Polyushkina

Institute of Solar-Terrestrial Physics SB RAS, Irkutsk, Russia
(potapov@iszf.irk.ru)

Abstract – **The most intense geomagnetic pulsations in the Pc5 range occurring during the powerful magnetospheric storms are studied by using data from a wide network of the ground-based stations. Distributions of the main parameters characterizing state of the interplanetary plasma during intervals of global Pc5 have been calculated. Examination of conditions in the solar wind and variations of the interplanetary magnetic field show that there are some prerequisites to global Pc5 occurrence in the magnetosphere. The most favorable conditions arise when the super fast streams of the solar wind flow around the magnetosphere. Being generated global Pc5 activity influences the magnetosphere dynamics contributing to the total level of disturbance. This has been shown by comparing AE index variations with those of the interplanetary electric field defined as a product of the IMF vertical component by the solar wind velocity with negative sign. As a whole, the analysis reveals a complicated picture of the ULF waves participation in the processes of energy entry and drain in the magnetosphere. The work was supported by RFBR grants 06-05-64143 and 07-05-00696 and INTAS grant 06-1000013-8823.**

Evidence of radio-quiet hard X ray precursor of the 13 December 2006 solar flare

I. V. Zimovets [1], M. Gros [2], A. B. Struminsky [1, 3]

[1] *Space Research Institute (IKI) , 84/32 Profsoyuznaya Street, Moscow, 117997, Russia*
[2] *DSM/DAPNIA/Service d'Astrophysique, CEA Saclay, Gif-sur-Yvette, 91191, France*
[3]IZMIRAN, Troitsk, Moscow region,142190, Russia

Abstract – **We report multi-wavelength investigation of the pre-impulsive phase of the 13 December 2006 X-class solar flare. We use hard X-ray data from the anticoincidence system of spectrometer onboard INTEGRAL (ACS) jointly with soft X-ray data from the GOES-12 and HINODE satellites. Radio data are from Nobeyama and Learmonth solar observatories and the CALLISTO radio spectrometer in Badary. The main finding of our analysis is a spiky increase of the ACS count rate accompanied by surprisingly gradual and weak growth of microwave emission and without detectable radio emission at meter and decimeter wavelengths about 10 minutes prior to the impulsive phase of the solar flare. At the time of this pre-flare hard X-ray burst the onset of the GOES soft X-ray event has been reported, positive derivative of the GOES soft X-ray flux has become to rise and a bright spot near the magnetic inversion line has appeared in the images of the Hinode X-ray telelescope (XRT) that can be evidences of the solar origin of the observed pre-flare burst. Since the ACS was not specially developed for solar research and could not prove a solar origin of the burst we discuss a possibility of magnetospheric nature of the pre-flare spikes observed by ACS.**

I. INTRODUCTION

One of the first systematic analysis of solar pre-flare activities was done by [1] who also introduced the term "pre-flare". In addition, the term "precursor" is used to denote transient solar events observed in various wavelengths preceding an impulsive phase of the following flare ([2]-[5]). Due to the great variety of pre-flare activities and insufficient sensitivity of observations so far, solar flare trigger mechanism still remains unsolved riddle. It is not even proved what kinds of pre-flare activities are directly associated with the subsequent flares and which of them represent independent small-scale energy releases within the same active region of forthcoming flares.

Soft X-ray light curves often reveal pre-flare smooth or spiky increases indicating pre-flare heating. Origin of this heating is generally unknown. It may be of thermal or non-thermal nature. Strong evidences of presence of non-thermal electron sources in the solar atmosphere prior to impulsive phase of some but far from all solar flares were found using hard X-ray and radio observations (e. g. [6]-[13]). It is generally accepted that non-thermal electrons emit bremsstrahlung in hard X-rays colliding with coronal or denser plasma and the most energetic part of them (mildly relativistic ones) can also generate microwave emission, mainly attributed to the non-coherent gyrosynchrotron process. Since microwave emission was detected even in the smallest flares, e. g. [14] found it in a lot of microflares with an average GOES soft X-ray flux at the B2.0 level, one can expect that all hard X-ray emitting solar flares and apparently pre-flare activities can emit detectable centimeter waves by gyrosynchrotron process.

Coherent radio emission in decimeter and meter range can be generated during transformation of plasma waves due to non-thermal electron ensembles into electromagnetic waves ([15] and references therein). To the best of our knowledge, there were no systematic observations of such processes' manifestations during pre-flare activities. Furthermore, mechanisms of generation of non-thermal particles prior to solar flares and exact relation of non-thermal pre-flare activity with subsequent flare are not defined yet. Finding of any new observational manifestations of non-thermal pre-flare activity may turn out to be useful.

In Section 2 we refer to instrumentations used for our research. In Section 3 we provide

evidences to confirm presence of large solar hard X-ray burst detected by ACS with relatively weak radio emission in microwave range and without detected one in meter and decimeter range during pre-impulsive phase of the 13 December 2006 solar flare. Possibility of magnetospheric origin of the increased pre-flare ACS count rate and radio silence of some solar X-ray bursts are briefly discussed in Section 4. Conclusion is in Section 5.

II. INSTRUMENTATION

We use anticoincidence shield consists of 91 BGO crystals onboard INTEGRAL satellite ([16], [17]) to detect solar hard X-ray emission. Although, this device was not specifically developed for solar flare research, it is very sensitive to photons with energy above 150 keV because of its great effective area. ACS doesn't provide a spectral resolution but gives high statistics with count rate integrated over 50 ms. Unfortunately the INTEGRAL spectrometer SPI itself was switched off for technical reasons, and did not take any data on the 13th of December 2006. Another hard X-ray oriented device RHESSI ([18]) was behind the Earth during pre-impulsive phase of the 13 December 2006 solar flare and began observations only at 02:28:12 UT. So ACS data can not be correlated to RHESSI data at that time. Thus ACS was the only device could observe solar hard X-ray emission during the pre-impulsive flare phase (the CORONAS-F mission was over one year before on December 6, 2005).

One-minute data sets of soft X-ray flux have been obtained from the X-ray sensor (XRS) aboard GOES-12 satellite. The images of X-ray solar corona were taken from X-ray telescope aboard the Hinode satellite ([19]).

Ground-based radio data were obtained from: the Nobeyama radio polarimeters (NoRP) at frequencies 1, 2, 3.75, 9.4, 17, 35 GHz ([20]); the Learmonth radio telescope at frequencies 245, 410, 610, 1414, 2695, 4995, 8800 and 15400 MHz; and the CALLISTO spectrometer in Badary (Siberia) in overlapping frequency range 45 - 870 MHz ([21]). We use the overlapping radio data from different instruments to be sure in data adequacy.

A significant correlation between EUV and hard X-ray emissions was observed during solar flares ([22]-[24]), therefore, examining a solar origin of the increased pre-flare ACS count it would be useful to compare it with solar EUV flux time profile. Unfortunately EUV data from Transition Region and Coronal Explorer (TRACE) were not available for the time interval between 02:05 and 02:47 UT on 13 December 2006. Data from the Extreme ultraviolet Imaging Telescope (EIT) aboard the Solar and Heliospheric Observatory (SOHO) do not fit the purpose of our analysis because of its cadence of only 12 minutes between 02:00 and 03:00 UT.

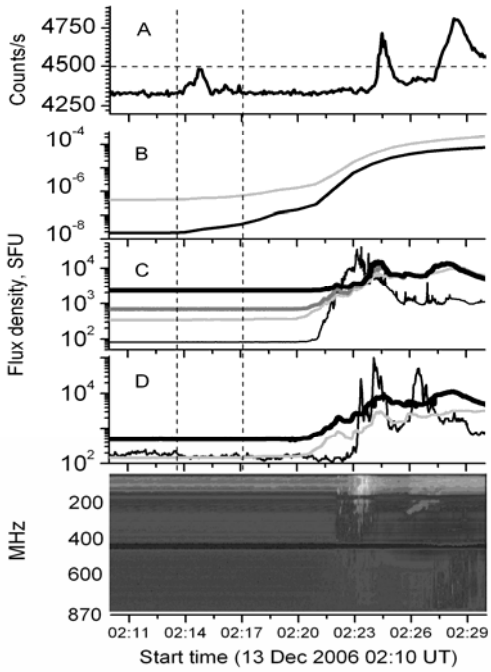

Fig. 1. Pre-flare and onset of the 13 December 2006 solar flare in different wavelengths. (A) The pre-flare ACS (> 150 keV) spiky structure is between two vertical dashed lines (1 s integrated, normalized to 50 ms count rate, background is not subtracted). The left and right vertical dashed lines correspond to the spiky structure start and end respectively; the horizontal dashed line marks peak count rate in the spiky structure. (B) GOES-12 full disc soft X-ray one-minute data (grey: 1-8 A, black: 0.5-4 A). (C) Data of the Nobeyama radio polarimeter at frequencies 2 (thin black), 9.4 (light grey), 17 (dark grey) and 35 GHz (thick black). (D) Data of the Learmonth radio telescope at frequencies 245 (thin black), 4995 (grey) and 15400 (thick black) MHz. (Bottom panel) Radio spectrogram from the CALLISTO in Badary.

III. OBSERVATIONS

3.1 The 13 December 2006 solar flare

This two-ribbon H_α solar flare with heliocentric coordinates S06 W24 started at 02:20 UT inside the NOAA active region 10930 (ftp://ftp.ngdc.noaa.gov/STP/SOLAR_DATA). Its soft X-ray started to rise 6 minutes earlier (02:14 UT, Fig. 1, 2) and had a maximum of X3.4 at 02:40 UT. The flare was accompanied by halo CME first observed at 02:54:04 UT by LASCO/C2 onboard SOHO satellite (http://cdaw.gsfc.nasa.gov/CME_list) and large variety of radio emission (microwave, II, III, IV, V types) with onsets reported not earlier than 02:21 UT. The flare was also accompanied by the ground level enhancement of cosmic ray intensity ([25]). The solar flare hard X-ray emission was

detected by ACS and its impulsive phase started at about 02:24 UT (Fig. 1). The hard X-ray emission was also detected onboard RHESSI but after the end of its night time at 02:28:12 UT.

The flaring active region consisted (at least from 10 December 2006) of two sunspots: a large one with negative magnetic fields and a small one rotating counterclockwise relative to the large one and around itself with positive magnetic fields. The two spots shared common penumbra ([26] Large amount of magnetic flux emerged on the west side of the small sunspot. Because of small sunspot's rotation the core magnetic fields ([26]) became highly sheared. This shear and/or emerged magnetic flux could have lead to the solar flare. It is significant to note the appearance of some ephemeral regions near the magnetic inversion line between the sunspots and their cancellations with surrounding magnetic fields observed during reconfiguration of pre-flare magnetic fields ([27]).

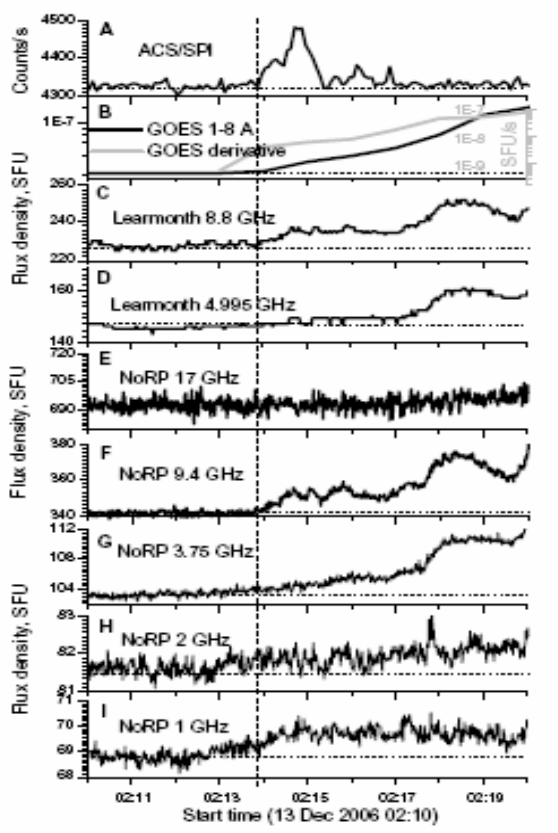

Fig. 2. Thermal and non-thermal emission prior to the 13 December 2006 solar flare. (A) ACS count rate (> 150 keV, 1 s integrated, normalized to 50 ms count rate, background is not subtracted). (B) GOES-12 full disc 1-min 1-8 A soft X-ray data (black line) and its first derivative (grey). (C, D) Radio flux from the Learmonth solar telescope at 8.8 and 4.995 GHz. (E-I) Radio flux from the NoRP at 1, 2, 3.75, 9.4 and 17 GHz. Vertical dashed line marks start of the increased pre-flare ACS count rate. Horizontal dotted lines mark background levels of appropriate emission.

These cancellations were accompanied by TRACE 1600 A line brightening. Precise time of the brightening is not known because of low cadence of observations. Pre-flare activity was also observed in soft X-ray and Ca II H line as well (Section 3.2). Were there any non-thermal manifestations of the pre-flare activity?

3.2 "Precursor" of the 13 December 2006 solar flare

In the paper we discuss the "precursor", which reveals itself as an increase of the ACS count rate during 02:13-02:17 UT (Fig. 1, the upper panel, between two vertical dashed lines, background is not subtracted). We emphasize that we don't refer to the enhanced solar radio emission observed at 02:17-02:24 UT without hard X-rays above background level (Fig. 1 and Fig. 2) before the start of the solar flare impulsive phase. One can see smooth start of radio emission growth observed by the NoRP at frequencies up to 9.4 GHz and by the Learmonth solar observatory at 4.995 and 8.8 GHz at about 02:13-02:14 UT (Fig. 2, vertical dashed line). The NoRP radio emission at 17 and 35 GHz (is not showed in Fig. 2) and the Learmonth ones at 245, 410, 610, 1414, 2695 and 15400 MHz (also is not shown in Fig. 2) do not reveal an increase above its background levels.

The "precursor" is radio-quiet (no radio emission in meter and decimeter range above its background levels were detected by the CALLISTO, see Fig. 1). We also emphasize the great difference in microwave and hard X-ray emission time profiles. For example, peak flux for the NoRP 9.4 GHz channel with subtracted background level in the "precursor" is about two order of magnitude smaller than peak flux in the flare impulsive phase (Fig. 1, 2), whereas ACS peak count rate with subtracted background in the "precursor" is only three times smaller than its count rate in the flare impulsive phase peak (Fig. 1).

Full disc soft X-ray flux observed by XRS and its first time derivative started to grow smoothly at about 02:13-02:14 UT (Fig. 2) indicating some energy release apparently in the active region concerned. Also one can see an appearance of bright spot at 02:14 UT and increase of its brightness at 02:15 UT on XRT images of the flaring active region (Fig. 3). Additional brightening in Ca II H line was observed by Solar Optical Telescope (SOT) aboard Hinode at 02:16 UT ([26]) almost in the same place (near the magnetic inversion line between the sunspots). These facts we may consider as additional evidences of energy release in the active region during the time of the "precursor".

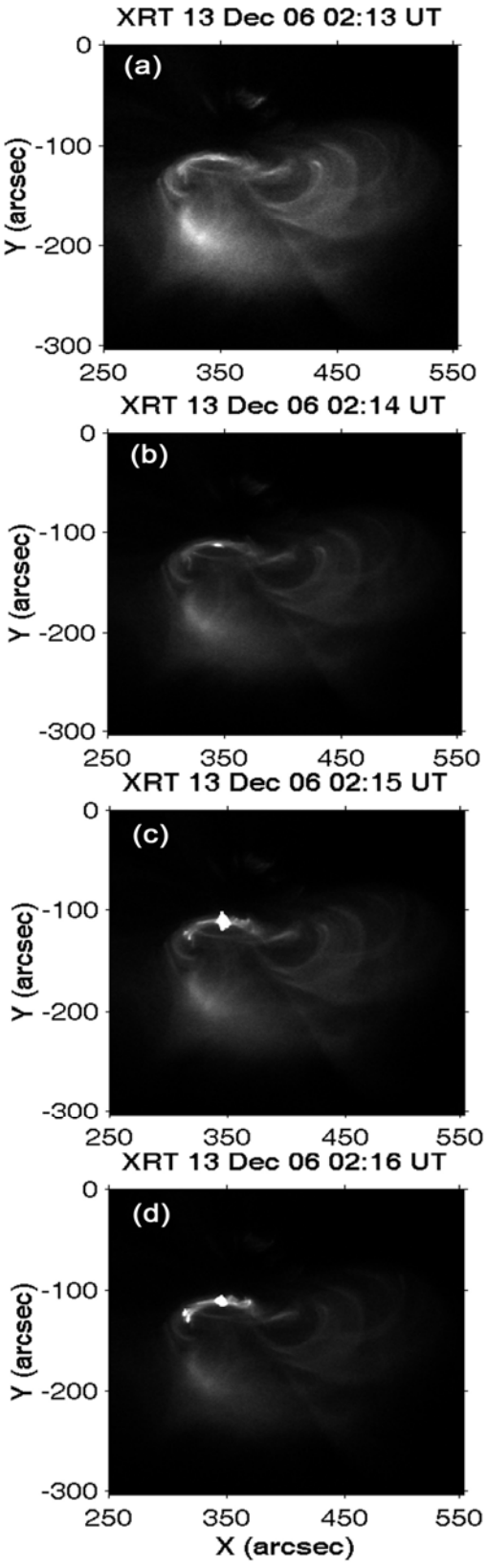

Fig. 3. Absence (a), appearance (b) and evolution (c, d) of the pre-flare soft X-ray bright spots in active region before the 13 December 2006 solar flare observed by XRT aboard Hinode.

IV. DISCUSSION

4.1 Correlations between ACS and other observations during the "precursor"

Time correlations can be found when comparing the ACS pre-flare spiky structure and other available solar observations:

- The "precursor" appeared nearly at the start time of microwave emission observed by the NoRP and the Learmonth telescope.
- The start of the "precursor" corresponds to the start of GOES soft X-ray emission above background level and its positive derivative growth;
- The soft X-ray brightening observed by XRT near the active region magnetic inversion line appeared at the time of the "precursor";
- The brightenings seen in SOT Ca II H line first appeared around the active region magnetic inversion line at the time of the "precursor" maximum ([26]);
- [9] demonstrated that pre-flare activity observed in X-ray emission manifests itself as both thermal and non-thermal discrete and localized brightenings. Before our solar flare near the magnetic inversion line of the active region 10930 there were multiple interactions between fast rotating sunspot and the ephemeral regions ([27]) which could trigger small scale magnetic reconnection and energy release leaded to the "precursor".

These time correlations support strongly that the ACS hard X-ray spiky structure could be related to the solar events occurred in the active region concerned.

4.2 Possibility of non-solar origin of the "precursor"

In spite of the indirect support in favor of solar hard X-ray nature of the ACS count rate increase at 02:13-02:17 UT, a magnetospheric origin can not be completely ruled out. Such ACS spikes can be activated by populations of charged particles in the Earth's radiation belts. However previous observations show that, when INTEGRAL enters in the radiation belts at the end of its 3-day orbit, such ACS spikes usually appear to be merged in large groups with duration of tens minutes or hours. In our case there were not any significant (over three sigma) spikes before the "precursor" (Fig. 4, the upper panel). In Fig. 4 we plot ACS count rate averaged over 1-second intervals and normalized to

real count rate (50 ms integration) from 00:00 till 05:00 UT on 13 and 16 December 2006. Appearance of the first spiky structure in the ACS time profile in immediate proximity to the flare on 13 December 2006 is in favor of its solar origin rather than a magnetospheric one.

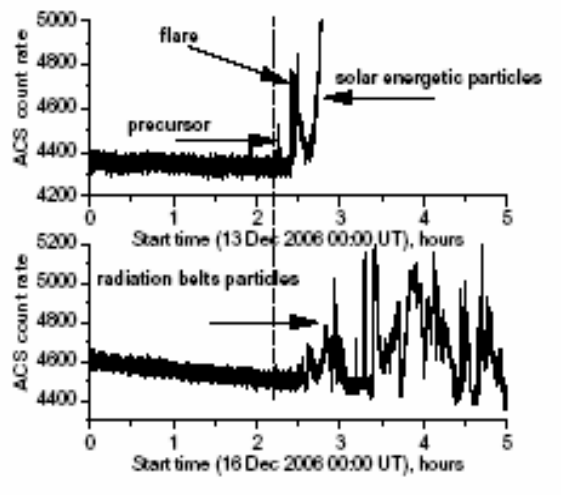

Fig. 4. Five hours of the ACS count rate (1 s integrated, normalized to 50 ms count rate, background is not subtracted) taken from two consecutive 3-days INTEGRAL orbits. INTEGRAL had similar space position during these intervals. One can see that the spacecraft penetrated to the radiation belts a bit later on 16 December. INTEGRAL penetration to the radiation belts on 13 December hidden by arrival solar flare energetic particles.

The ACS count rate during the next INTEGRAL orbit after the flare (Fig. 4, the lower panel) shows a real group of magnetospheric spikes a bit later in the orbital time. Unfortunately it is impossible to verify if such spikes appeared after the 13 December flare because ACS was clogged up by solar energetic particles started to arrive the spacecraft at about 02:37 UT (Fig. 4, the upper panel). This clogging was lasting several hours and during this period INTEGRAL undoubtedly penetrated into the radiation belts. We can not use data from previous INTEGRAL orbit for comparison because of noticeably greater background level during it. Under such background level parasitic spikes become very intensive and visible only some hours after the time is interesting for us. Actually, because of the radiation belts are quite dynamic, magnetospheric spikes can appear with an uncertainty of some hours and we can not predict precisely the first parasitic spike appearance. Also it is impossible to distinguish our spiky structure from the really magnetospheric ones, say, by its shape, because of its short duration.

It would have been useful also to estimate surface distribution of the ACS counts during the "precursor" to determine direction of incident radiation to verify its solar origin, as it was done for intense events as the 2003.10.28 one ([28]). Unfortunately it is impossible for the "precursor" because of its short duration and low intensity.

4.3 Radio silence of non-thermal source

To the best of our knowledge, there were no systematic studies of pre-flare situation in meter and decimeter frequency range. Although, pre-flare pulsations were found at these frequencies in some cases (e. g. [7], [10]). As to solar flares itself, [29] demonstrated cases of hard X-ray solar flares without appreciable metric and decimetric radio emission in the frequency range 100-1000 MHz. This fact was later confirmed by [30] for the frequency range 100 - 4000 MHz. A lack of the radio emission in the frequency range 200-1200 MHz was noticed for the start of gamma-ray flare on 6 March 1989 ([31]). It is important that most of these flares, if not all, were accompanied by centimetric radio emission and radio emission below 100 MHz. [32] have demonstrated that all radio-quite flares in the frequency range of 100-4000 MHz were limb flares and that most of non-limb flares with GOES class larger than C5 were associated with coherent radio emission. A probability to observe the coherent radio emission during solar flares increases with hardening of hard X-ray emission spectrum.

The ACS count rate in the "precursor" does not differ significantly from count rate in the flare impulsive phase peak accompanied by significant radio emission in all available wavelengths. Therefore apparently we can not consider the "precursor" to be a small hard X-ray burst. Lack of microwave emission in the "precursor" in comparison with its amount during the flare impulsive phase can be attributed to lack of high-energy electrons. That is the spectrum of electrons was apparently soft in the "precursor". [32] came to the conclusion that flares with softer hard X-ray spectra more likely tend to have no coherent radio emission above 100 MHz that can be explained in the framework of the theory of velocity space instabilities. Apparently this could take place in the "precursor". The "precursor" is of about B5 GOES class but without distinguishable soft X-ray peak. Low-intensity soft X-ray flares with strong hard X-ray emission were observed ([33]-[35]) and in this sense the "precursor" does not seen strange.

Nevertheless we think it is too early to discuss seriously causes of non-thermal emission peculiarities for this single phenomenon. Moreover, we don not have any hard X-ray spectral and imaging information.

V. CONCLUSIONS

Large spiky structure was observed by the ACS ten minutes prior to the start of the solar flare impulsive phase on December 13, 2006. It was demonstrated that the most probable origin of this structure was the solar hard X-ray burst (>150 keV) from the same active region as the flare. This hard X-ray burst was accompanied by smooth growth of radio emission in centimetric range. No radio emission in meter and decimeter wavelengths was found. To develop a better understanding of such phenomenon we need to obtain more extensive information from other similar events. Today we can not completely exclude the possibility of magnetospheric origin of the considered spiky structure.

ACKNOWLEDGMENT

We thank V. Ishkov, Y. Su, S. Lesovoi and A. Benz for useful discussions and two anonymous referees for critical remarks; K. Shibasaki and N. Meshalkina for the NoRP data assistance; IPS team for the Australian radio data. We also thank P. Burkov for the paper preparation. Hinode is a Japanese mission developed and launched by ISAS/JAXA, with NAOJ as domestic partner and NASA and STFC (UK) as international partners. It is operated by these agencies in co-operation with ESA and NSC (Norway). I. V. Z. was partially supported by the RFBR grants 06-02-17256, 07-02-00319, 07-02-08772 and grant of Scientific school HIII-5359.2006.2.

REFERENCES

[1] Bumba, V. and Krivsky, L. Chromospheric pre-flares. Bull. Astron. Inst. Czech 10, 221-223, 1959.
[2] Gaizauskas, V. Preflare activity. Sol. Phys. 121, 135-152, 1989.
[3] Martin, S. F. Preflare conditions, changes and events. Sol. Phys. 68, 217-236, 1980.
[4] Tappin, S. J. Do all solar flares have X-ray precursor? Astron. Astrophys. Suppl. Ser. 87, 277-302, 1991.
[5] Van Hoven G. and Hurford, G. J. Flare precursors and onset. Adv. Space Res. 4(7), 95-103, 1984.
[6] Asai, A., Nakajima, H., Shimojo, M., et al. Preflare nonthermal emission observed in microwaves and hard X-rays. PASJ 58(1), L1-L5, 2006.
[7] Benz, A. O., Barrow, C. H., Dennis, B. R., et al. X-ray and radio emissions in the early stages of solar flares. Sol. Phys. 83, 267-283, 1983.
[8] Chifor, C., Mason, H. E., Tripathi, D., et al. The early phases of solar prominence eruption and associated flare: a multi-wavelength analysis. Astron. Astrophys. 458, 965-973, 2006.
[9] Chifor, C., Tripathi, D., Mason, H. E., et al. X-ray precursors to flares and filament eruptions. Astron. Astrophys. 472, 967-979, 2007.
[10] Farnik, F., Hudson, H. S., Karlicky, M., et al. X-ray and radio observations of the activation stages of an X-class solar flare. Astron. Astrophys. 399, 1159-1166, 2003.
[11] Kane, S. R. and Pick, M. Non-thermal processes during the "build-up" phase of solar flares and in absence of flares. Sol. Phys. 47, 293-304, 1976.
[12] Kundu, M. R., Velusamy, T., and Becker, R.H. Fine structure of a solar flare region at 3.7 and 11.1 cm wavelengths. Sol. Phys. 34, 217-222, 1974.
[13] Kundu, M. R., Gopalswamy, N., Saba, J. L. R., et. al. A study of solar preflare activity using two-dimensional radio and SMM-XRP observations. Sol. Phys. 114, 273-288, 1987.
[14] Qiu, J., Liu, C., Gary, D. E., et al. Hard X-ray and microwave observations of microflares. Astrophys. J., 612, 530-545, 2004.
[15] Bastian, T. S., Benz, A. O., Gary, D. E. Radio emission from solar flares. Annu. Rev. Astron. Astrophys. 36, 131-188, 1998.
[16] Vedrenne, G., Roques, J.-P., Schonfelder, V., et al. SPI: The spectrometer aboard INTEGRAL. A&A 411, L63-L70, 2003.
[17] von Kienlin, A., Arend, N., Lichti, G. G., et al. Gamma-ray burst detection with INTEGRAL/SPI, in: Truemper, J. E., Tananbaum, H. D. (Eds.), X-ray and gamma-ray telescopes and instruments for astronomy. SPIE conf. proc. 4851, 1336-1346, 2003.
[18] Lin, R. P., Dennis, B. R., Hurford, G. J., et al. The Reuven Ramaty high-energy solar spectroscopic imager (RHESSI). Sol. Phys., 210, 3-32, 2002.
[19] Golub, L., DeLuca, E., Austin, G., et al. The X-ray telescope (XRT) for the Hinode mission. Sol. Phys. 243(1), 63-86, 2007.
[20] Nakajima, H., Sekiguchi H., Sawa, M., et al. The radiometer and polarimeters at 80, 35, and 17 GHz for solar observations at Nobeyama. Publ. Astron. Soc. Japan 37, 163-170, 1985.
[21] Benz, A. O., Monstein, C., Meyer, H., et al. A world-wide net of solar radio spectrometers – e-CALLISTO. Submitted to Earth, Moon and Planets, 2008.
[22] Kane, S. R., Frost, K. J. and Donnelly, R. F. Relationship between hard X-ray and EUV sources in solar flares. Astrophys. J. 234, 669-682, 1979.
[23] Su, Y. N., Golub, L., Van Ballegooijen, A. A., et al. Analysis of magnetic shear in an X17 solar flare on October 28, 2003. Sol. Phys. 236, 325-349, 2006.
[24] Woodgate, B. E., et al. Simultaneous ultraviolet line and hard X-ray bursts in the impulsive phase of solar flares. Astrophys. J. 265, 530-534, 1983.
[25] Vashenyuk, E. V., Bazilevskaya, G. A., Balabin, Y. V., et al. The GLE of December 13, 2006 according to the ground level and balloon observations. "in press, ICRC 30, 2007".
[26] Su, Y. N., Golub, L., Van Ballegooijen, A. A., et al. Evolution of the sheared magnetic fields of two X-class flares observed by Hinode/XRT. In press Publ. Astron. Soc. Japan, 2007.
[27] Zhang, J., Li, L., and Song, Q. Interaction between a fast rotating sunspot and ephemeral regions as the origin of the major solar event on 2006 December 13. Astrophys. J. 662, L35-L38, 2007.
[28] Gros, M., Tatischeff, V., Kiener, J., et al. INTEGRAL/SPI Observation of the 2003 Oct 28 solar flare. Proceeding of the 5th INTEGRAL workshop (ESA SP-552) 16-20 February 2004, Munich, Germany, 669.
[29] Simnett, G. M. and Benz, A. O. The role of metric and decimetric radio emission in the understanding of solar flares. Astron. Astrophys. 165, 227-234, 1986.
[30] Benz, A. O., Grigis, P. C., Csillaghy, A., et al. Survey on solar X-ray flares and associated coherent radio emission. Sol. Phys. 226, 121-142, 2005.
[31] Rieger, E., Treumann, R. A., and Karlicky, M. The radio-silent start of an intense solar gamma-ray flare. Sol. Phys. 187, 59-75, 1999.
[32] Benz, A. O., Brajsa, R., and Magdalenic, J. Are there radio-quiet solar flares? Sol. Phys. 240, 263-270, 2007.

[33] Gburek, S. and Siarkowski, M. Small flares with unusually strong X-ray emission. Adv. Space Res. 30(3), 601-604, 2002.
[34] McDonald L., Harra-Murnion, L.K., and Culhane, J. L. Nonthermal electron energy deposition in the chromosphere and the accompanying soft X-ray flare emission. Sol. Phys. 185, 323-350, 1999.
[35] Siarkowski, M., Falewicz, R., Berlicki, A. Small GOES flares with intense hard X-ray emission. Adv. Space Res. 38(5), 972-978, 2006.

Solar proton enhancements in different energy channels and coronal mass ejections during the last solar cycle

M. Gerontidou[1] , H. Mavromichalaki[1] , A. Belov[2] and V. Kurt[3]

[1]*Nuclear and Particle Physics Section, Physics Department University of Athens, 15571, Athens, Greece (emavromi@phys.uoa.gr; mgeront@phys.uoa.gr)*
[2] *IZMIRAN, Troitsk, Moscow region, 142190, Russia*
[3]*Institute of Nuclear Physics, Moscow State University, 119899, Vorobievy Gory, Moscow, Russia*

***Abstract* – The main properties of 11622 coronal mass ejections (CMEs) observed by the Solar and Heliospheric Observatory (SOHO) mission's Large Angle and Spectrometric Coronagraph (LASCO-C2) from January 1996 through December 2006 are considered. Moreover the extended database of solar proton enhancements (SPEs) with proton flux >0.1 pfu at energy >10 MeV measured at the Earth's orbit is also studied. A comparison of these databases give new results concerning the sources and acceleration mechanisms of solar energetic particles. Specifically, coronal mass ejections with width $>180^0$ (wide) and linear speed >800 km/sec (fast) seem to have the best correlation with solar proton enhancements. The study of some specific solar parameters, such as soft X-ray flares, sunspot numbers, solar flare index etc. has showed that the soft X-ray flares with importance >M5 may provide a reasonable proxy index for SPE production rate. From this work, it is outlined that the good relation of the fast and wide coronal mass ejections to the proton enhancements seems to lead to a similar conclusion. In spite of the fact that in the case of CMEs the statistic covers only the last solar cycle, while the measurements of SXR flares are extended over three solar cycles, it is obvious for the studied period that the coronal mass ejections can also provide a good index for the solar proton production.**

***Key Words*—solar energetic particles, solar flares, coronal mass ejections, proton events**

I. INTRODUCTION

The appearance of solar energetic particles having high fluxes at the Earth's space environment or/and in any point of heliosphere is of great interest and usually these particle storms are called solar extreme events. A component of these events is the solar proton events (SPE) recorded by satellites at 1AU as well as by the ground level neutron monitor network.

During extreme solar events as big flares or/and energetic coronal mass ejections, high energy particles are accelerated by the shocks formed in front of fast interplanetary coronal mass ejections (ICMEs). These CMEs also give rise to large geomagnetic storms which have significant effects on the Earth's environment and human life. Around 15 ground level cosmic ray intensity enhancements (GLEs) events were recorded by neutron monitors during the solar cycle 23 and all but one of them were always followed by a geomagnetic storm with D_{st}<=-50nT within 1-5 days later ([1], [2]). It is notable that during the decay phase of this solar cycle and in particular almost at the very end of this, a number of such events was observed. In the top of them is the ground level enhancement of cosmic ray intensity occurred on 13th of December, 2006 during a magnetically disturbed period manifested by a series of Forbush decreases of the cosmic ray intensity at neutron monitors starting from 6 of December, 2006. In particular the big X-ray flare of 13 December 2006 at 02:14 UT with importance X3.4/4B originated from the active region 10930 and from the west side of the Sun (S06W23) resulted in a big proton flux increase at 1 AU reaching the flux value of 695pfu at energy range >10 MeV and 86 pfu at energy >100 MeV, as it was recorded by GOES-11 satellite. The same day at 02:54 UT a fast hallo CME with linear speed 1774 km/sec was also recorded by SOHO satellite ([3])

The possible connection of these two parameters of solar activity, soft X-Ray flares and CMEs and their results in the interplanetary space and at the Earth as solar proton events is under consideration. Nevertheless, both flares and CMEs are the result of rearrangements of the coronal magnetic field, they are often "associated" one another in some way. However, a major controversy still exists as to whether the particle acceleration occurs in the flare itself or the particles are accelerated by associated CME ([4]).

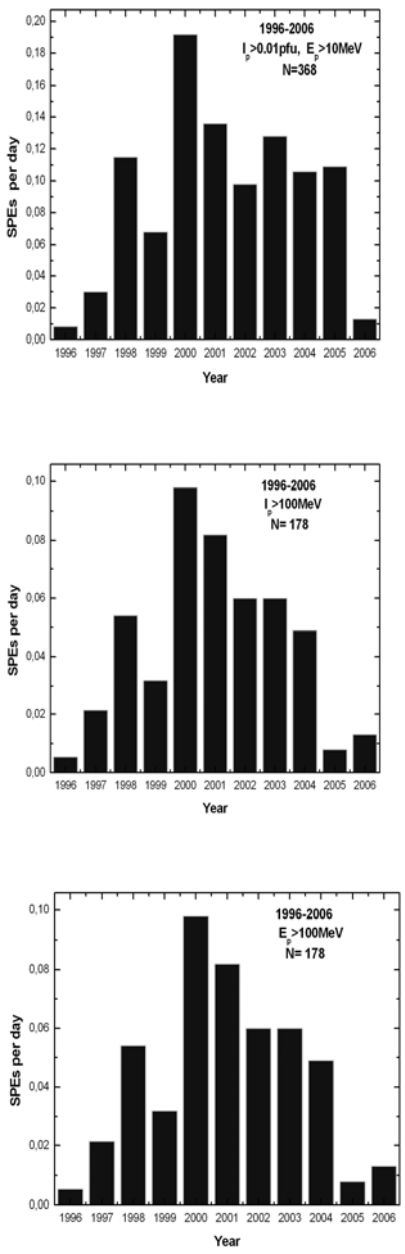

Fig. 1. Time distribution of daily values of SPEs with I_p >0.01pfu and energy >10MeV (top panel), >100 MeV (middle panel) and GLEs >500 MeV (bottom panel).

In order to clarify the role of SXR flares as well as of CMEs to proton events generation and propagation at 1AU, the SPEs are statistically related both to CMEs and SXR flares. From the first studies in this direction was that of Van Hollebeke et al. (1975) in which the flares and the SPEs data from the Goddard cosmic ray experiment on IMP-IV and IMP-V satellites were connected and a procedure for identifying the associated flare with solar proton enhancements in interplanetary space were developed. During the last years, [2], [6] showed that the soft X-ray flares with importance >M5 play an important role in the SPE production rate.

Moreover, [7] and [8] showed that solar energetic particles are also associated with fast CMEs. [9] mentioned that most of large SEP events are associated with wide CMEs having velocities above 400 km/sec. [10] in a detail study of various properties of CMEs during the time period 1996-2002 showed that the fast (average speed >1500 km s^{-1}) and wide (mostly full or partial halo) CMEs are associated with SEPs. In addition, SEP events with ground level enhancements (GLEs) in the ground based detectors are connected with the fastest known population of CMEs (average speed ~ 1798 km s^{-1} (sky-plane)) ([11]). Up to 15% of the CME kinetic energy goes into the accelerated particles suggesting that the CME-driven shocks are efficient particle accelerators ([12]).

Most previous works ([10], [13], [14], [15]) dedicated to the study of energetic proton events and their relationship to CMEs has relied upon the widely used NOAA standard for solar particle events that are defined as events with fluxes >10 pfu at energy >10 MeV. In a recent work by [6], the term solar particle enhancement (SPE) has been applied, including flux intensities well below that of the NOAA standard (>0.1 pfu), in order to emphasize the point that a broad range of near-Earth proton flux intensities is being investigated. A complete database of 1275 solar proton enhancements has been created almost for all the extended period 1976-2006.

In this work, using this extended database of solar proton events for proton enhancements in different energy channels >10 MeV and >100 MeV as well as >500MeV (GLEs) and the complete catalogue of CMEs (http://cdaw.gsfc.nasa.gov/CME_list), we try to study the possible connection of the SPEs and the coronal mass ejections for the entire time period of solar cycle 23 (1996-2006). Specifically the characteristics of CMEs associated with SPEs are considered and compared with previous results.

II. DATA SELECTION

The database of solar proton enhancements updated and expanded from a previous work covering all the solar cycle 23 is used ([6]). In order to obtain this database, we use the integral proton fluxes measured onboard IMP-8 and GO 5-12 satellites. In the earlier period 1975-1986 only data from IMP-8 have been available. At times during the time period 1987-2001 when data from the IMP-8 and GOES satellites were available only one spacecraft's data were used, because of gaps existing in the conjugate set. During the period 2002-2006 only GOES data are available. GOES corrected integral fluxes were extracted for proton energies >10 MeV, >30 MeV, >60 MeV and

>100 MeV (see http://spidr.ngdc.noaa.gov/spidr/) as well as IMP-8 >10 MeV, >30 MeV and >60 MeV data (see http://nssdc.gsfc.nasa.gov/omniweb/ow.html). Additionally, the IMP-8 >106 MeV/n proton and nuclear channel were also incorporated (see http://ulysses.sr.unh.edu/WWW/Simpson/imp8.html)

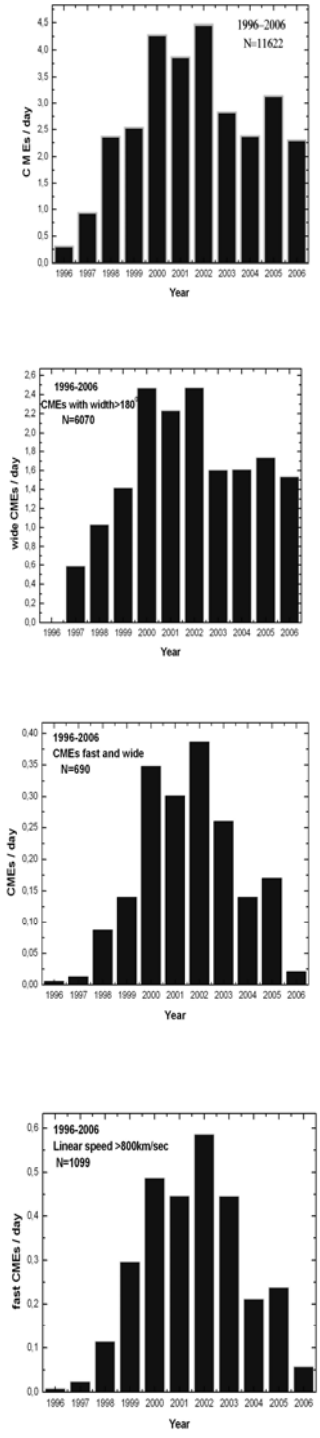

Fig. 2. Time distribution of all detected CMEs (top panel), fast CMEs(bottom panel), wide CMEs (second panel) and fast and wide CMEs (third panel) on a daily basis.

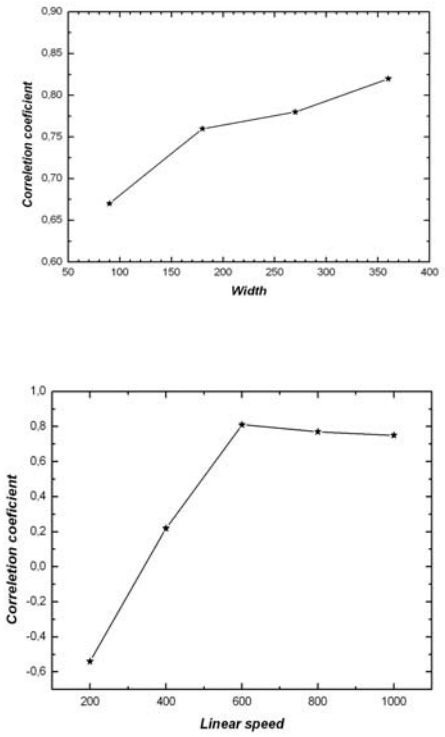

Fig. 3. The calculated correlation coefficient of the CMEs a) in each width range and b) in each linear speed range.

During the years 1996-2006, a number of 368 solar proton enhancements in the energy range of >10 MeV, 178 SPEs having energy >100 MeV and finally only 15 of these events were recorded by Neutron Monitors having cut-off energy ≈500 MeV known as GLEs. The time distributions of SPE rate in these three energy channels during the last solar cycle are presented in Fig. 1. As it can be seen solar proton enhancements in almost all energies follows well the 11-solar cycle variation. The maximum rate in all cases is appeared in the years 2000 and 2001 that is the maximum solar cycle phase. The great number of SPEs during the declining phase of this cycle is also considered.

Coronal mass ejections data were taken from the Large Angle and Spectrometric Coronograph (LASCO) having three telescopes C1, C2 and C3 on board the Solar and Heliospheric Observatory (SOHO) mission (http://cdaw.gsfc.nasa.gov/CME_list). However, in our analysis only C2 and C3 data were used for uniformity, as C1 was disable from June 1998. The existed data gaps were taken into account in our calculations.

A total number of 11622 CMEs were selected and the time distribution on a daily basis for the time span 1996-2006 is given in Fig. 2 (upper left panel).

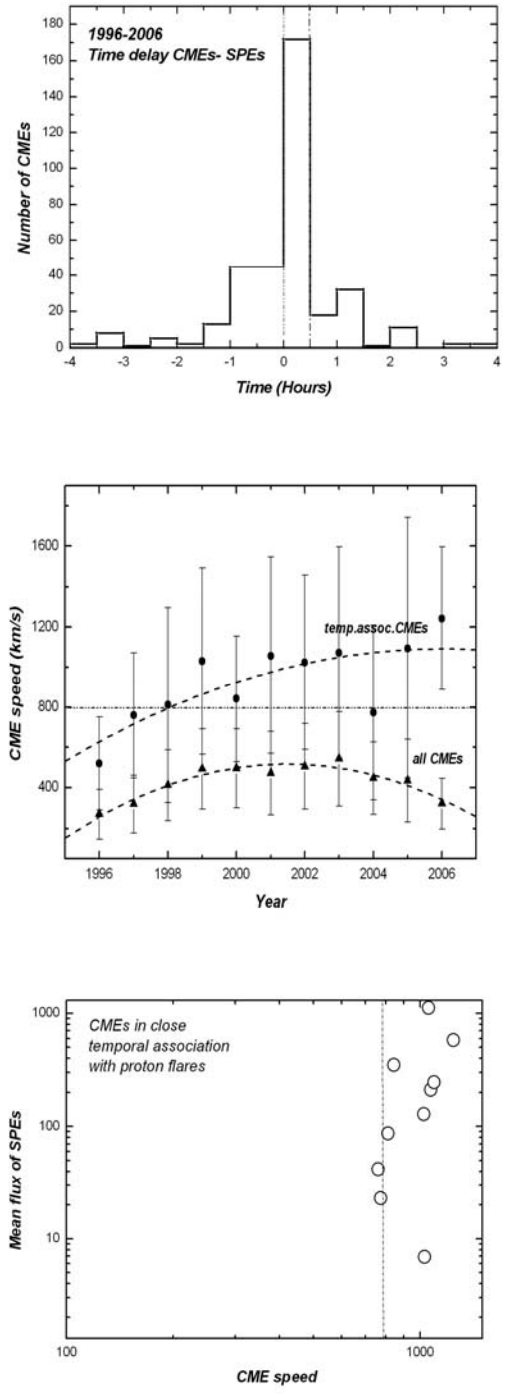

Fig. 4. a) Distribution of the time delay between time detection of CME and SEP (upper panel) b) Yearly average speed of all detected CMEs (triangle data point) in comparison with yearly average speed of CMEs temporal associated with proton flares (filled cycles and) (middle panel) c) Mean flux of SPEs versus linear speed of temporal associated CMEs (lower panel).

Note that CME rate increased from less than 1 per day during solar minimum in 1996 to slightly more than 4.5 in 2002. The mean number of CME rate during the declining phase is more than 2.5 CMEs per day, while in 2005 it was 3 CMEs per day.

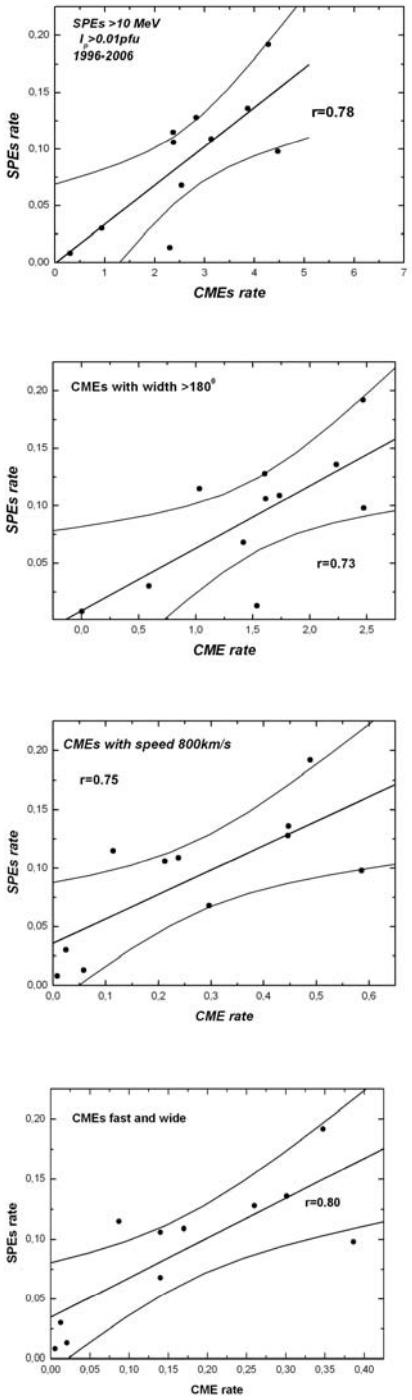

Fig. 5. Scatter plot of yearly SPE rate versus yearly CME rate (from the top to bottom: all detected, wide, fast, fast and wide) during the period 1996-2006.

This year is characterized by many extreme events as those of January 2005, July 2005, August-September 2005 ([16], [17]). According to [18] and [19] the rate during solar maximum is much higher than the

highest corrected rate (3.11 per day) reported in previous cycles.

Separating the number of CMEs that were occurred in every range of width 90^0, the correlation coefficient between them and the rate of SPEs on yearly basis was calculated. Results of the calculated correlation coefficient in each width interval are presented in Fig. 3a (upper panel). As it can be seen the correlation coefficient is growing up with the width of CMEs with a jump for the events with width $>180^0$ called wide CMEs. The same procedure concerning the speed of CMEs is also applied. The results are presented in Fig. 3b (lower panel). It is evident from this figure that slow CMEs with linear speed <200 km/s seem to be not correlated with SPEs and the correlation coefficient becomes positive for CMEs with speed >400km/s. A big value of correlation coefficient (r=0.78) is appeared for the case of CMEs with linear speed >800km/sec. This fact in combination with the result obtained from Fig. 4c, where the speed of CMEs that are in close association with proton flares seems to be greater than 800 km/sec, leads to the conclusion that the fast CMEs are well connected with SPEs. This conclusion is also consistent with previous works where smaller time periods were investigated ([9], [15]).

Since coronal mass ejections bring large-scale changes in the corona, which have fundamental implication for the evolution of magnetic-flux of the Sun, it is interesting to examine the long-term behaviour of the CMEs. Based on the previous results that solar energetic particles seem to be connected with fast and wide CMEs, their solar cycle variation was examined. The time distribution of all detected by SOHO CME rate as well as of the CMEs having linear speed >800 km/s, CMEs with width $>180^0$ as well as CMEs having linear speed >800 km/s and width $>180^0$, called fast and wide during the last solar cycle are presented in Fig. 2. The data are corrected taking into account all the data gaps. This figure shows that all CME rate in all cases follows the 11-year variation of solar cycle. At the end of the cycle, during the years 2005 and 2006 there is an increase at the CME rate that may affect to the unexpected solar extreme events during these years. The time distribution of fast and wide CMEs is more consistent to the solar cycle variation. It is noted that an average value of four CMEs per day is observed near solar maximum ([9]).

III. CORRELATION ANALYSIS

For our correlative analysis in the time period 1996 to 2006, only 317 from 11622 detected CMEs seem to have a close temporal association with the proton enhancements, taking into account the gaps on SOHO data. The term temporal association means that within a window of four hours before or/and after the SPE appearance, one at least CME detection occurs. The distribution of the time delay between CME detection and SPE is presented in Figure 4a. As we can see the great majority of CMEs are detected within the time interval from -1 to +1.5 hours after SPEs detection. As it is obtained from this figure, a great number of SEPs and CMEs appeared in the time interval 0-0.5 hour. It is interest to note that the fraction of these events to the rest event is 1.26. Minor observed sub peaks in the distribution may attribute to different source longitude. However, the general trend of this distribution is a monotonic decrease of this to greater time delays.

	>10 MeV	**>100MeV**
Total CMEs-SPEs	**0.78**	**0.72**
Wide CMEs-SPEs	**0.73**	**0.69**
Fast CMEs-SPEs	**0.75**	**0.76**
Fast and Wide CMEs -SPEs	**0.80**	**0.77**

Table 1. Correlation coefficient of the yearly CME rate and the yearly SPE rate in different energy channels.

A comparison of the yearly average linear speed of all detected CMEs with the yearly average speed of CMEs having close temporal association with proton flares is presented in Fig. 4b. It is noted that the average speed of associated CMEs is much greater than all detected ones. The average speed of CMEs having close temporal association with proton flares is greater than the critical value of 800 km/sec. The time profile of the average speed of all detected CMEs seems to be consistent with the solar cycle variation, while the yearly average speed of temporal associated CMEs deviates at the end of the cycle. This result reflects on the number of solar proton events detected during the years of solar minimum 2005-2006 ([20]). The mean flux of SPEs with the speed of the CMEs associated with the proton flares are given in Fig. 4c.). It is evidence that the fast CMEs seem to be cause of SPEs production.

The total rate of CMEs, the CMEs rate having central position angle $>=180^0$(wide), the CMEs rate having speed >=800km/sec (fast) and the fast and wide CMEs seem to be well connected with the yearly SPEs rate with energy >10 MeV during the last solar cycle (see Fig. 5).

The correlation coefficient of the solar proton enhancements in energy channels >10 MeV and >100 MeV with the different characteristics of the CMEs is presented in Table I. The best correlation coefficient is appeared in the case of fast and wide CMEs. This is consistent with the results of previous works by [10] and [15].

IV. DISCUSSION - CONCLUSIONS

In this work a comparative analysis of 368 solar proton enhancements and 11622 CMEs during the last solar cycle has been performed. It is the first time examined a complete solar cycle in relation to CMEs data. At first we note that all these events follow the 11-year variation. A great number of both these parameters is appeared in the maximum phase of the cycle, while the declining phase seems to be more productive than the ascending one. It was expected if we take into account the differences between even and odd solar cycles ([21]).

In order to clarify the connection between SPEs and CMEs extending our previous studies on SPEs and Soft X-rays flares, studying some special properties of the CMEs as their speed and width, we have concluded that the temporal associated with proton events CMEs, have linear speed much greater than all other detected CMEs. The critical value of CMEs speed that are well connected with solar proton enhancements seems to be >800 km/sec (fast CMEs). CMEs with width $>180^0$ (wide CMEs) are also well associated with solar proton enhancements. The calculated time delay between the detection of CMEs and the onset time of the proton flares reveals a pronounced maximum of this time delay from 0 to 0.5 hours.

Moreover a high correlation coefficient between fast and wide CMEs rate and SPEs examined in different energy channels on an yearly basis has been found for the examined time period. It reaches the value of 0.80 for the case of SPEs with energy >10 MeV and 0.77 in the case of the ones with energy >100 MeV. This correlation one by one does not provide a correct picture for their association as cause and effect, but appears only a statistical connection of them. In order to examine the contribution of CMEs on SPEs production, it may be studied some other properties of them, such as the total energy, the ejected mass of CMEs etc. Nevertheless, studying only some characteristics of CMEs, we can say that CMEs present an important effect on SEP related and non-related events. Extending this work to other properties of CMEs, it will be possible to have a more complete knowledge of this connection for a better understanding of the Solar-Terrestrial phenomena and Space Weather applications.

ACKNOWLEDGMENT

This work is partly supported by the Greek project PYTHAGORAS II funded by European funds and national resources and by RFBR grants 07-02-13525 and 07-02-00915 and Program BR of the Presidium RAS “Neutrino Physics”.

REFERENCES

[1] Whang, R. Large geomagnetic storms of extreme event periods in solar cycle 23, Adv. Space Res. 40, 1835-184, 2007

[2] Belov, A., Kurt V., Mavromichalaki, H., Gerontidou, M. Peak size distributions of proton fluxes and associated soft-X ray flares, Sol. Phys. 246, 457-470, 2007

[3] Plainaki, C, Mavromichalaki, H., Belov, A., Eroshenko, E., Yanke, V. Application of the NM-BANGLE model to GLE70, Proc 30th ICRC, 2007

[4] Cane, H.V., Reames, D.V. and von Rosenvinge, T.T. The role of interplanetary shocks in the longitude distribution of solar energetic particles, J. Geophys. Res., 93, A9, 9555 - 9567. 1988

[5] Van Hollebeke, M.A., MaSung, L.S. and McDonald, F..M. The variation of solar proton energy spectra and size distribution with heliolongitude, Solar Phys., 41, 189-223, 1975

[6] Belov, A., Garcia H., Kurt, V., Mavromichalaki, H., Gerontidou, M. Proton enhancements and their relation to the X-ray flares during the three last solar cycles, Sol. Phys. 135-159 , 2005.

[7] Reames, D.V. Particle acceleration at the Sun and in the heliosphere, Space Science Rev. 90, 413-491, 1999

[8] Kahler, S., Reames, D., Sheeley, N. Jr. A CME associated with an impulsive SEP event, Proc. 27th ICRC 2001, 3443-3448, 2001

[9] Gopalswamy, N., Yashiro, S., Michałek, G. Et al. Interacting Coronal Mass Ejections and Solar Energetic Particles, Astrophys. J., 572, 1, L103-L107, 2002

[10] Gopalswamy N. Coronal mass ejection activity of Solar Cycle 23, J. Astrophys.27, 243-254, 2006

[11] Gopalswamy N., Xie, H. Yashiro, S. and Usoskin I. Coronal Mass Ejections and Ground Level Enhancements, Proc. 29th ICRC 2005. 1, 169, 2005

[12] Emslie, A.G., Kucharek, H.; Dennis, B. R., Gopalswamy, N., Holman, G. D.; Share, G. H.; Vourlidas, A., et al. Energy partition in two solar flare/CME events, J. Geophys.Res.109, A10104, 2004

[13] Reames, D.V. Solar energetic particles: A paradigm shift, U.S. National Report to International Union of Geodesy and Geophysics 1991-1994, 585, 1995

[14] Gopalswamy, N., Yashiro, S., Howard, R. A. Coronal and Interplanetary Environment of Large Solar Energetic Particle Events, Proc. 28th ICRC 3549-3554, 2003

[15] Reinard, A.A and Andrews, M.A. Comparison of CME characteristics for SEP and non-SEP related events, Adv. Space Res. 38, 480-483, 2006

[16] Mavromichalaki, H., Gerontidou, M., Mariatos G. et al. Space weather forecasting at the new Athens center: The recent events of January 2005, IEEE TNS 52, 2307–2312, 2005.

[17] Mavromichalaki, H., Papaioannou, A., Mariatos, G. et al. Cosmic ray radiation effects on space environment associated to intense solar and geomagnetic activity, IEEE TNS 54, 4, 2007

[18] Webb, D. F., Howard, R. A. The solar cycle variation of coronal mass ejections and the solar wind mass flux, J. Geophys. Res. 99, 4201, 1994

[19] Cliver, E. W., St. Cyr, O. C., Howard, R. A., McIntosh, P. S. Rotation-Averaged Rates of Coronal Mass Ejections and Dynamics of Polar Crown Filaments Solar coronal structures. Proc. 144 Colloq. International Astronomical Union, Tatranska, 83, 1994

[20] Hudson H. S. The unpredictability of the most energetic solar events, Astrophysical Journal, 663, L45-L48, 2007

[21] Mavromichalaki H., Marmatsouri, E., Vassilaki, A. Solar-cycle phenomena in Cosmic-ray intensity: Differences between even and odd cycles, Earth, Moon and Planets, 42, 233, 1998

Variations of the trapped proton fluxes measured on board low-orbital satellites

N.V. Kuznetsov, N.I. Nikolaeva

Skobeltsyn Institute of Nuclear Physics, MSU, Leninskie Gory, 1/2, Moscow, 119991, Russia

Abstract – **Trapped proton fluxes measured on board Coronas – F and NPOES-15, -17 satellites from 2001 to 2007 are presented in this work. Variation of trapped protons fluxes depending on solar activity was analyzed. Measured fluxes were compared with the AP8 model predictions for solar maximum and solar minimum. It is found, that The AP8 model underestimates the fluxes of protons with energy less then ~2 MeV, measured by the concerned satellites.**

***Key Words*— AP8 model, trapped proton flux.**

I. INTRODUCTION

FOR over forty years of the investigation of the Earth radiation belts a great amount of the experimental data was collected and the main features of energetic and spatial distributions of trapped particles were well described. These are the underlying data for the empirical models used for predictions of the radiation environment at the orbit of the spacecraft. Nowadays, for the practical purposes the most widely used models are AP8 and AE8 models (NASA) [1],[2] (later appended [3]) and SINP MSU model [4] that determine an averaged trapped proton fluxes for minimum and maximum of the solar activity.

These models were based on the satellite data obtained from 1960 to 1980 (during the anomalous weak 20th cycle of solar activity) and were examined during the last decades [5]-[7]. Reference [5] shows that the trapped proton fluxes measured at low altitudes are underestimated by the model. This fact was taken into account in new models that summarized the data for 22d solar cycle [8],[9]. Solar cycle variation was taken into account in TPM-1 model [10].

We analyze the trapped proton fluxes measured on board Coronas-F (altitude 500km, inclination 83 deg.) and NPOES-15, -17 satellites (altitude 810km, inclination 98 deg.) from 2001 to 2007 (23d solar cycle) using the following data sources: SINP MSU database for Coronas-F (http://smdc.magnetosphere.ru), database for NPOES-15 designed in ONERA (France) and web-site http://poes.ngdc.noaa.gov for NPOES-17.

The following energy channels were considered.

NPOES: 0.8-2.5 MeV (field of view ~10°, Proton Solid State Detector Telescope) and 70-140 MeV (field of view ~180°, Omni-directional (Dome) Solid State Detector).

Coronas-F: 1-5 MeV (field of view ~30°, MKL instrument) and 50-90 MeV (field of view ~140°, MKL instrument).

II. EXPERIMENTAL DATA ANALYSIS

In order to analyze the trapped proton fluxes the following steps were taken. First proton fluxes were divided into groups according to the parameter of the drift shells (from L to L+ΔL, (ΔL=0.01) $F_L(B/B_0)$ depending on the relative magnetic field intensity B/B_0 (where B_0 is the magnetic field intensity at the geomagnetic equator). Then dependences $F_L(B/B_0)$ were reconstructed to pitch-angular α_0 ($\sin\alpha_0 = (B_0/B)^{1/2}$) dependence $F_L(\alpha_0)$, that was used for comparison of the proton fluxes measured by the detectors with narrow field of view (low energies) with the AP8 model.

An example of $F_L(B/B_0)$ and $F_L(\alpha_0)$ dependencies derived from the experimental data is shown at fig.1. It can be seen that wide scattering of the experimental points exists. This scattering is no less then 50% from the averaged values of the trapped proton fluxes. Mean-square errors are also shown at fig.1.

Dependencies $F_L(B/B_0)$ for two energy intervals for several L-shells are shown at fig.2 for the periods of solar maximum (2001) and solar minimum (2007) (NPOES -2007, Coronas-F - 2005). It can be seen from fig.2 that $F_L(B/B_0)$ decrease with the increase of B/B0 values. Equatorial proton flux (B/B_0 = ~ 1) can be

registered only for L<1.3 by NPOES satellites. Coronas-F data are in good agreement with NPOES data.

Equatorial trapped proton fluxes (B/B_0 = 1) measured on board NPOES satellites from 2001 to 2007 for the L-shells less then L=1.2 are presented at fig.3 superposed to the smoothed Wolf numbers. As can be seen from fig. 3 the equatorial proton flux increases with the decrease of the solar activity especially for L=1.14, at L=1.2 only a small increase of the trapped proton flux can be observed. Similar results were obtained by Huston [11] for the previous 22d solar cycle (1985-1996).

III. Comparison with the AP8 model

In order to compare the trapped proton fluxes measured during the 23d solar cycle with the AP8 model data the directional flux of trapped protons with energy 0.8-2.5 MeV (fig.1b) was recalculated to omnidirectional flux $\Phi_L(\alpha_0)$ using formula:

$$\Phi_L(\alpha_0) = 4\pi \int_0^{\pi/2} F_L(\alpha_0)\sin\alpha_0 d\alpha_0$$

Omnidirectional flux for the detectors with wide field of view (70-140 MeV) was calculated by multiplying $F_L(B/B_0)$ by 4π.

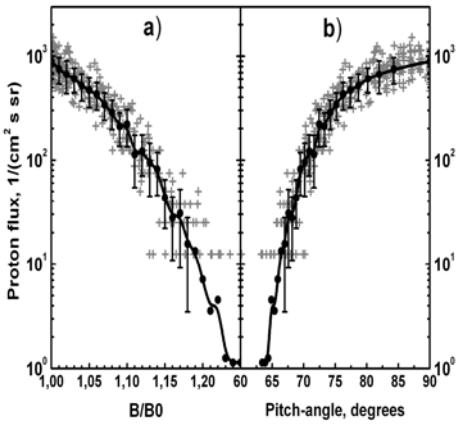

Fig. 1. The 0.8-2.5 MeV proton flux measured by NPOES-15 satellite (crosses) and its average values (dots) depending on B/B_0 (a) and pitch- angle (b).

Omnidirectional fluxes $\Phi_L(B/B_0)$ are shown at fig.4 in comparison with the AP8 model predictions. As it can be seen from this figure in all cases there is a difference between experimental data and the AP8 model predictions. Moreover the AP8 model essentially underestimates the flux of protons with energy 0.8-2.5 MeV (fig.4a) near the geomagnetic equator (B/B_0 < ~1.1).

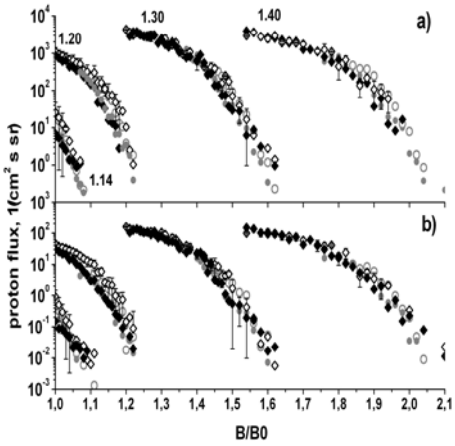

Fig. 2. The 0.8-2.5 MeV (a) and 70-140 MeV (b) proton flux measured by NPOES-15 in 2001 (♦), NPOES-17 in 2007 (◊) and the 1-5 MeV (a) and 50-90 MeV (b) proton flux measured by Coronas –F (grey points) in 2001 (•) and 2005 (o) for several L-shells (in figure field) depending on B/B0.

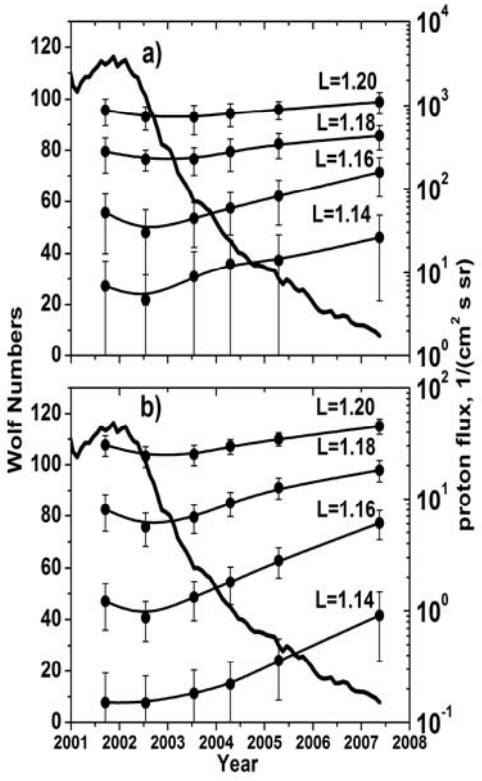

Fig. 3. The 0.8-2.5 MeV (a) and 70-140 MeV (b) equatorial proton flux measured by NPOES satellites from 2001 to 2007 for several L-shells (1.14, 1.16, 1.18, 1.20 Earth radii), superposed to the smoothed Wolf numbers (thick line).

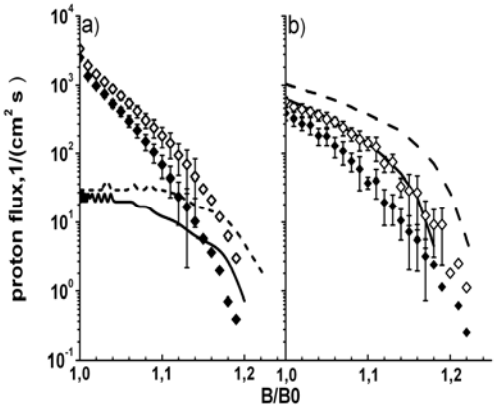

Fig. 4. Omnidirectional proton fluxes with energies 0.8-2.5 (a) and 70-140 (b) MeV measured by NPOES (black) satellites in 2001 (♦) and 2007 (◊) depending on B/B0 in comparison with the AP8 model predictions for solar maximum (solid line) and solar minimum (dashed line).

IV. Conclusions

An analysis of the trapped proton fluxes measured on board NPOES and Coronas-F satellites by the different types of the detectors (with wide and a narrow field of view) in 2001-2007 and comparison of the experimental data with the AP8 model for maximum and minimum of solar activity was done. It was shown that there is an essential difference between trapped proton fluxes with energies 0.8-2.5 MeV measured by NPOES satellites and AP8 model prediction for the L-shell less then L=1.3.

Acknowledgment

Authors appreciate L.I. Starostin for the development of Coronas –F database that was used in this work.

We are grateful to S. Bourdarie and D.Boscher for an arrangement of NPOES-15 database.

References

[1] Sawyer D.M., Vette F.L. The AP-8 trapped proton environment for solar maximum and solar minimum. National Space Science Data Center/World Data Center A For Rockets and Satellites, NSSDC/WDS-A-R&S 76-06, NASA Goddard Space Flight Center, Greenbelt, Maryland, December 1976.

[2] Vette F.L. The AE-8 trapped electron environment for solar maximum and solar minimum. National Space Science Data Center/World Data Center A For Rockets and Satellites, NSSDC/WDS-A-R&S 91-24, NASA Goddard Space Flight Center, Greenbelt, Maryland, November 1991.

[3] Bilitsa D. Models of trapped particle fluxes AE8 (electrons) and AP8 (protons) in inner and outer radiation belts, National Space Science Data Center PT-11B, 1996.

[4] Space model (in Russian), Vol.1. KDU, 2007.

[5] Vampola A.L. Low Energy Inner Zone Protons Revisited, Workshop on the Earth's Trapped Particle Environment: Conf. Proc. 383, AIP Press, American Institute of Physics, Woodbury, N. Y., 1996. P.81.

[6] Armstrong T.W., Colbom B. L. TRAP/SEE Code users manual for predicting trapped radiation environment. NASA , 209879, 2000.

[7] Heynderikcx D. Review on modeling of the radiation belts. International Fournal of modern physics A Vol 17,Nos 12&13, 1675-1684, 2002

[8] Heynderickx D., Kruglanski M., Pierrard V., Lemaire F., Looper M.D. and Blake F.B., A new low altitude trapped proton model for solar minimum conditions based on SAMPEX/PET data, IEEE Trans. Nucl. Sci. V. 46, P. 1475, 1999.

[9] Gussenhoven M. S., Mullen E. G. and Brautigam D. H., “Phillips Laboratory Space Physics Radiation Models”, in Radiation Belts: Models and Standards, Lemaire J. F., Heynderickx D., and Baker D. N. (eds.), Geophysical Monograph 97, American Geophysical Union, p. 93, 1996.

[10] Huston S.L., Space environments and effects: Trapped proton model. Technical report CR- 211784. NASA.2002

[11] Huston S.L., Kuck G.A. and Pfitzer K.A. Solar cycle variation of the low-altitude trapped proton flux, Adv. Space Res.,21(12),1625-1634,1998.

A new statistical index (P_i) for coronal mass ejections

Paouris Evangelos

Astronomy, Astrophysics and Mechanics Section, Physics Department, National and Kapodistrian University of Athens, Panepistimiopolis GR15783, Athens, Greece.
(Astrophysics.Paouris@gmail.com)

Abstract – **In this work we are trying to understand statistically the coronal mass ejections through time and improving the previous P_i–index which is a monthly parameter, defined in this work, from the equation: $P_i = 0.68N_c + 0.32V_p^2$ where Nc is the total number of CMEs per month and Vp^2 is the square of mean plasma velocity of CMEs per month. As we know solar flares or CMEs are events related with magnetospheric events on Earth's atmosphere. The fluctuations of P_i index, for the years 1996-2007, seems to be strongly related with the fluctuations of cosmic rays intensity, especially in periods of violent phenomena. This index is very interesting as can explain the high solar activity even when the sunspot number is almost in the minimum, in the declining phase of the 11 year solar cycle, as it is happens in the very peculiar 23rd solar cycle with a lot of extreme events.**

***Key Words*—Coronal mass ejections (CMEs), Sunspot number, Cosmic rays, Solar activity.**

I. INTRODUCTION

A lot of physical phenomena are related with the solar activity such as solar flares, coronal mass ejections (CMEs) or prominences. For many years there has been debate on whether a solar flare causes a CME or vice versa. After a lot of observations and theoretical models, it is now clearer that neither flares nor CMEs cause the other, but that they are caused by changes driven by the same magnetic activity [1]. Flares also often occur in association with CMEs but they are not necessary and are certainly not the instigator of mass ejection, see [2], as has been sometimes assumed. Flares are believed to be generated by the heating resulting from reconnection of field lines blown open by the CME. Flares and prominence eruptions are different phenomena but often occur simultaneously [3].

High flow speeds and strong magnetic fields, often with strong southward components, are particularly found in interplanetary disturbances driven by fast coronal mass ejections. Thus, the most important link between solar activity and large, non–recurrent geomagnetic storms are CMEs [4]. CMEs are spectacular manifestations of solar activity in which 10^{12} – 10^{13} kg of solar material are suddenly propelled outward into interplanetary space [5], [6] and [3]. A vast magnetic bubble of plasma erupts from the solar corona and travels through the interplanetary space at a speed often well above that of the ambient solar wind [7], with speeds ranging from only a few km/sec to nearly 3000 km/sec. When these energetic solar particles reach the Earth's magnetosphere we have as a result geomagnetic storms, generally CMEs are related to very strong, short-lived Forbush decreases [8] of cosmic-ray intensity at Earth. Reference [9] was among the first to suggest that CMEs might play a role in long-term modulation of cosmic rays [10].

In this work we suppose that CMEs are the most important effect of solar activity and as a result our improved index P_i can gives us more information for the solar activity for the 11-year solar cycle, in opposition with the sunspot number, even when we are in the minimum of the cycle, which is the minimum of sunspot number. As a result for our index we are using only two parameters: the total number of CMEs per month and the square of mean plasma velocity also per month, as a meter for their energy, kinetic energy, as a CME travels from Sun to Earth and sometimes causing catastrophic results.

II. DATA ANALYSIS – THE FORMATION OF THE PI-INDEX

The data for coronal mass ejections are increasing rapidly as now we are using the observing power of three spacecrafts: SOHO, TRACE and Yohkoh. In this work we are using data from Solar and Heliospheric Observatory coronagraphs (SOHO/LASCO) studying the period 1996-2007. So, we can have access in very detailed data for a coronal mass ejection such as the central position angle measured from Solar North in degrees (counter-clockwise), linear speed in km/sec, 2nd-order speed at final height or at 20 R_{SUN} (km/sec), acceleration (km/sec^2) and other measurements. In this work we are using only the number of CMEs per month and their mean linear speed (km/sec), per month, but we should mention that there are no data for CMEs for the months of July, August, and September of 1998 and January of 1999. We introduced the P_i index in a previous work [11] as a relation of two factors, the total number of CMEs (*Nc*) and their mean plasma velocity (*Vp*) per month. It is well known that the rate of CMEs varies and the reason is that it is strongly related with the minimum or maximum of solar activity. The rate of CMEs using pre-SOHO observations has been summarized by [12]. They found a rate of about 0.25 CME/day at solar minimum rising to about 2.5-3 CMEs/day at solar maximum. Furthermore the [13] study obtained a CME rate of 0.7 CMEs/day during three months in early 1997 using LASCO data. It was about a factor of 3 higher than the [12] solar minimum rate. This was because of the increased sensitivity of LASCO compared to previous coronagraphs [3]. The second factor in our relation it was the mean plasma velocity as a meter of their kinetic energy. According to [14] another CME attribute linked with solar activity is the mean speed, which doubled from minimum to maximum. In *Figure 1* we can see the CMEs number per month and the mean linear speed.

The empirical relation of the index was:

$$P_i = 0.65N_c + 0.35V_p \qquad (1)$$

where the Nc is the total number of CMEs and Vp is the mean plasma velocity, per month. The numbers 0.65 and 0.35 are the values as they occur for the best correlation coefficients between the index and the sunspot number and the cosmic-ray intensity [11]. In *Figure 2* we can see the P_i values in relation with the sunspot number, using monthly sunspot numbers from NGDC/NOAA and the normalized cosmic-ray intensity, using data from Oulu Neutron Monitor Station with cut-off rigidity 0.81GV, for the period 1996-2007. The pressure-corrected data for Oulu NM Station were normalized with the intensity taken equal to 1.00 at cosmic-ray intensity maximum at August 1997 and equal to 0.00 at cosmic-ray minimum at October 2003.

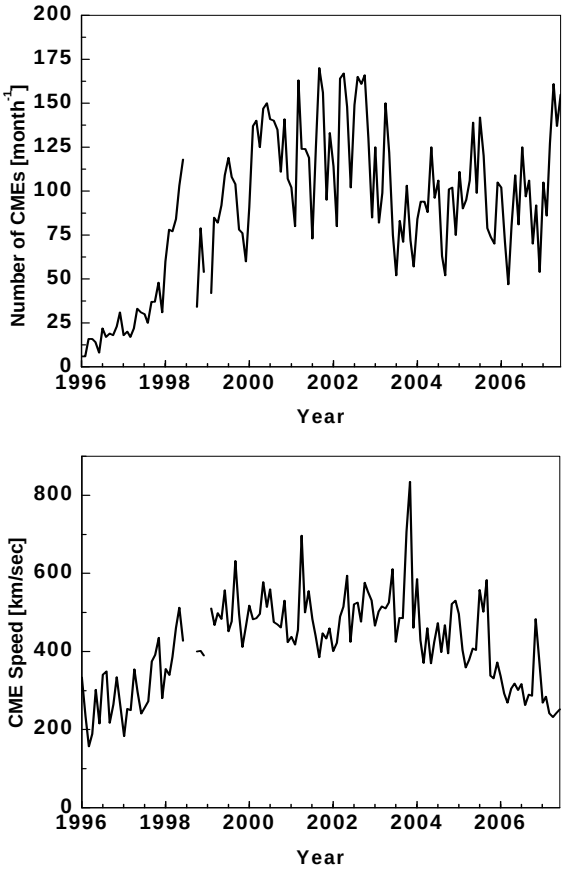

Fig. 1. The number of CMEs per month (up) and the mean linear speed (down). It is characteristic that for the period October-November 2003 we had a CME rate of 2.35-3.35 CMEs per day but in the same time we had extreme events which gave us the maximum for the speed and also for the P_i–index.

It is obvious that P_i shows a same behavior with the sunspot number and the most important result from this figure is that the fluctuations of the P_i–index are corresponding with the fluctuations of the cosmic-ray intensity, which is a strongly proof of the dependence of the cosmic-ray intensity by the solar activity as it is expresses through the P_i–index. Furthermore the study of the P_i–index in relation with the cosmic-ray intensity shows a very high cross correlation coefficient r = –0.82, when in the same time the cross correlation coefficient for the sunspot number in relation with the cosmic-ray intensity is r = –0.87 and for the number of CMEs per month Nc is r = –0.78 [15] which is also another fact for the reliability of the P_i–index.

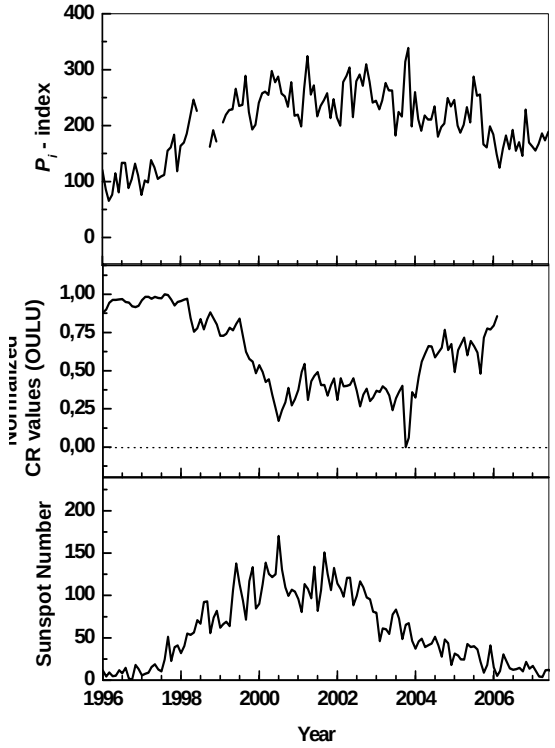

Fig. 2. P_i–index, normalized cosmic-ray values and sunspot number for 1996-2007. The minimum of the cosmic ray intensity –October-November 2003– it is obvious that occurs in the same time with the maximum of the P_i–index, when the sunspot number is in low values and could not justify this very violent period.

III. The Improved CME-index – Results

CMEs are now understood as large-scale magnetized plasma structures originating from closed magnetic field regions on the Sun: active regions, filament regions, active region complexes and trans-equatorial interconnecting regions [14]. As a result, continuing the previous work on this index, we want a relation between the energy of the magnetic fields on the active regions and plasmas in Sun's atmosphere. We suppose that when a CME erupts, the magnetic field energy of the active regions is changing to kinetic energy of the plasma, with a velocity which is the Alfvén speed, by the equation:

$$\frac{B^2}{8\pi} = \frac{1}{2}\rho V^2 \Rightarrow V^2 = V_A^2 = \frac{B^2}{4\pi\rho} \qquad (2)$$

From this equation it is obvious that the most important characteristic of the CME as a meter of their energy is the square of the velocity and not the first power of the linear speed. According to this result we have the new relation:

$$P_i = 0.68N_c + 0.32V_p^{\ 2} \qquad (3)$$

and the results are much more better especially in periods of extra violent phenomena. The factors 0.68 for the number of CMEs per month and 0.32 for the mean plasma velocity are different from the previous factors (Eq. 1). These factors occur from the best cross correlation coefficients of the P_i–index in relation with the sunspot number and cosmic-ray intensity. Especially the cross correlation coefficient for P_i (using Eq. 3) in relation with sunspot number is r = 0.68 and the correlation coefficient factor between P_i and cosmic-ray intensity is r = –0.83, which are the best values. In *Figure 3* we can see the new values of linear speed in square: Vp^2 and P_i–index. To make this plot we divide the Vp^2 by a factor of 10^3 to take results to the same area from 0 to 400 as it was the previous index. As we said before P_i is a statistical index which help us to understand better the solar activity in opposition with the sunspot number which is now in the minimum for the current solar cycle and could not give us details for very violent periods with CMEs which can produce geomagnetic storms.

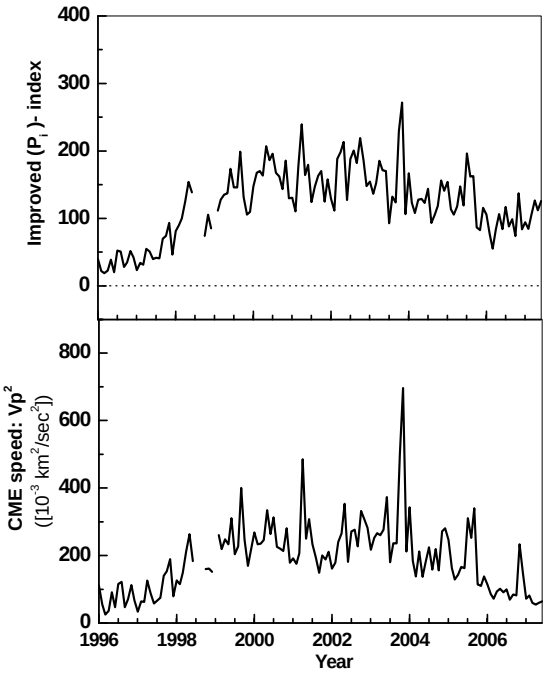

Fig. 3. The improved P_i–index with the square of the CME speed. This graph shows the importance of the CME index. The violent periods like April 2001, October-November 2003, July and September 2005 or November 2006 are easily spotted in opposition with the sunspot number which is in the declining phase (2003-2007).

It is very characteristic the maximum of the P_i–index in the period of October-November of 2003 when the sunspot number is in the declining phase

and as a result we do not have the high values for the sunspot number as it is happens in the period 1999-2001. So, if we take in count only the sunspot number as a meter for the solar activity we haven't any further information for violent phenomena. Some periods which are known for the extra violent activity of the Sun such as April 2001, October-November 2003, July and September 2005 or November 2006 are difficult to explain with the sunspot number curve, but with the CMEs-index these periods are spotted easily because these events are strongly related with the solar activity and especially with the violent activity.

IV. CONCLUSIONS

Previous works [14] showed that CME speed, kinetic energy, seems to be an important parameter characterizing extreme events and if we take in count the fact that the free energy available from the Sun depends on the size of the active region magnetic field we made a very good approach for the improved P_i–index starting our project from the equilibrium of the magnetic field energy with the kinetic energy (Eq. 2). As a result we have the new index using the square of the CME speed and we have better results (Fig. 3) as we can notice now ascending, maximum and descending phases for the index for the years 1996-2007, which is the period of 23rd solar cycle. The 23rd solar cycle is a very peculiar cycle with activity also in the minimum of the cycle. This fact imposes the use of an index with information for the solar activity for the whole cycle and not only for the period of the maximum. The P_i-index could give us information for the whole cycle and especially in periods of extreme activity like October-November 2003.

ACKNOWLEDGMENT

The author acknowledges the local organizing committee of Solar Extreme Events 2007 International Symposium in Athens for participation and support, especially Prof. Helen Mavromichalaki for useful comments on this project.

We also acknowledge:

a) The SOHO/LASCO research team for the CME catalog from: http://cdaw.gsfc.nasa.gov/CME_list. This CME catalog is generated and maintained at the CDAW Data Center by NASA and The Catholic University of America in cooperation with the Naval Research Laboratory. SOHO is a project of international cooperation between ESA and NASA.

b) The Oulu Neutron Monitor research team for easy access in the cosmic ray data from: *http://cosmicrays.oulu.fi*, and

c) The National Geophysical Data Center (of NOAA) for sunspot number data from: ftp://ftp.ngdc.noaa.gov/STP/SOLAR_DATA.

REFERENCES

[1] Harra, L.K., "Changes in the solar magnetic field preceding a coronal mass ejection", *J. of Atm. and Sol.- Ter. Ph*., vol. 64, pp.505–510, 2002.

[2] Gosling, J. T., "The Solar Flare Myth", *J. Geophys. Res.*, vol. 98, pp. 18 937–18 949, 1993.

[3] Cane, H.V., "Coronal mass ejections and Forbush decreases", *Space Sci. Rev.*, vol. 93, pp. 55–77, 2000.

[4] Gosling, J. T., "Coronal mass ejections: The link between solar and geomagnetic activity", *Phys. Fluids B*, vol. 5, pp. 2638–2645, 1993a.

[5] Kahler, S.: "Coronal mass ejections", *Rev. Geophys.*, vol. 25, pp. 663–675, 1987.

[6] Gosling, J. T., D. J. McComas, J. L. Phillips, and S. J. Bame, "Geomagnetic activity associated with Earth passage of interplanetary shock disturbances and coronal mass ejections", *J. Geophys. Res.*, vol. 96, pp. 7831–7839, 1991.

[7] Kudela, K., Storini, M., Hofer, M.Y., et al.: "Cosmic rays in relation to space weather", *Space Sci. Rev.*, vol 93, pp. 153–174, 2000.

[8] Forbush, S. E., "On the Effects in the Cosmic-Ray Intensity Observed During the Recent Magnetic Storm", *Phys. Rev.*, vol. 51, pp. 1108–1109, 1937.

[9] Newkirk, G. Jr, Hundhausen, A. J., Pizzo, V., "Solar cycle modulation of galactic cosmic rays - Speculation on the role of coronal transients", *J. Geophys. Res.*, vol. 86, pp. 5387–5396, 1981.

[10] Cliver, E.W., Ling, A.G., "Coronal mass ejections, open magnetic flux, and cosmic-ray modulation", *Astrophys. J.*, vol. 556, pp. 432–437, 2001.

[11] Mavromichalaki, H., Paouris, E., Karalidi, T., "Long-term Cosmic-ray Modulation during Solar Cycle 23", *7th International Conference of the Hellenic Astronomical Society, AIP Conference Proceedings*, vol. 848, pp. 184–193, 2006.

[12] Webb, D.F., Howard, R.A., "The solar cycle variation of coronal mass ejections and the solar wind mass flux", *J. Geophys. Res.*, vol. 99, pp. 4201–4220, 1994.

[13] St.Cyr, O. C. *et al.*, "White-Light Coronal Mass Ejections: A New Perspective From LASCO: *Correlated Phenomena at the Sun, in the Heliosphere, and in Geospace*", *ESA SP*, vol. 415, pp. 103–110, 1997.

[14] Gopalswamy, N., "Coronal mass ejections of solar cycle 23", *J. Astrophys. Astr.*, vol. 27, pp. 243–254, 2006.

[15] Mavromichalaki, H., Paouris, E., Karalidi, T., "Cosmic-Ray Modulation: An Empirical Relation with Solar and Heliospheric Parameters", *Solar Phys.*, vol. 245, pp. 369–390, 2007.

Upper limit of the total magnetic flux in an Active Region

George Livadiotis[1], Xenophon Moussas[2]

[1] *Department of Astrophysics, Astronomy and Mechanics, Faculty of Physics, National University of Athens, Panepistimiopolis, GR15784, Zografos, Athens, Greece.*
Emails: [1] *glivad@phys.uoa.gr*, [2] *xmousas@phys.uoa.gr*

Abstract – **The Photometric-Magnetic dynamical model handles the evolution of an individual sunspot as an autonomous nonlinear, though integrable, dynamical system. One of its consequences is the prediction of an upper limit of the sunspot areas. This upper limit is analytically expressed by the model parameters, while its calculated value is verified by the observational data. In addition, by considering an upper limit for the magnetic strength inside the sunspot, we obtain the following significant result: The upper limit of the total magnetic flux in an active region is found to be of about 7.23×10^{23}Mx, namely equal to the magnetic flux concentrated in the totality of the granules of the quiet Sun, having a typical maximum magnetic strength of about 12G. Therefore, the magnetic flux concentrated in an active region cannot exceed the magnetic flux concentrated in the photosphere as a whole.**

***Key Words*— active region, magnetic flux, Photometric-Magnetic Dynamical model, sunspots**

I. Introduction

SINCE the sunspots are caused by the presence of a concentrated magnetic field in the photosphere, the fundamental equations concerning their evolution are in principle derived from the magnetohydrodynamics (MHD). Previous models of sunspot decay are all based on suitable simplifications of the primary MHD model. However, the Photometric-Magnetic Dynamical (PhMD) model, introduced in ([1]), handles the sunspot evolution as an autonomous dynamical system, conveniently describing the whole sunspot lifetime, namely both the growth and decay phases.

The PhMD model is formulated by a two-dimensional system of ordinary differential equations (ODE) of the first order with respect to time. The two time-dependent functions are the photospheric sunspot area $A(t)$, and the average magnetic field strength inside the sunspot $B(t)$. The system has the form

$$\begin{aligned}\dot{A} &= -f_1(A) + g_1(B)\\ \dot{B} &= g_{2,in}(A) - g_{2,out}(A) + f_2(B)\end{aligned} \quad (1)$$

where the explanation of the involved terms is as follows: The term $g_1(B) = a_2 \cdot \left(B^2 - {B_0}^2\right)$ describes the creation mechanism of the sunspot (where A_0, B_0 are the initial values). This involves magnetic flux fragments, such as pores or other elementary magnetic microstructures, erupting from below the photosphere due to the magnetic buoyancy (which is proportional to B^2), while their accumulated smaller flux tubes coalesce into a main core of a larger flux tube. The magnetic flux emerging from the solar interior flows in the sunspot through its entire area (i.e. it is proportional to A), but it is also possible to flow locally, originated by a flow-component manifesting itself in regions of sufficiently smaller dimensions compared to those of sunspot (i.e. it is independent of the sunspot dimensions), and thus, the total inflow is described by $g_{2,in}(A) \approx b_{const,in} + b_{area,in} \cdot A$. On the other hand, the outflow is conducted mostly through the boundary of the sunspot (i.e., it is proportional to $\sqrt{A}$), and thus, it is described by $-g_{2,out}(A) \approx -b_{perifery,out} \cdot \sqrt{A}$. The inflow and outflow being combined, form the well known "collar flow", that stabilizes the sunspot ([2]-[5]). Finally, the negative $-f_1(A) = -a_1 \cdot (A - A_0)$ and positive $f_2(B) = b_2 \cdot (B - B_0)$ feedbacks, represent respectively the system's reaction to the increase of the sunspot area because of $g_1(B)$, and to the decrease of the magnetic flux because of $g_{2,out}(A)$.

The main idea of the PhMD model is that a sunspot does not only maintain its existence, but also evolves during its whole lifetime, by interacting

with the simultaneous evolution of its magnetic field. The coalescence of the accumulated smaller flux tubes does not affect only the creation of the sunspot, but it continues during the growth and decay phases ([6], [7]). Hence, the system (1) is written as

$$\begin{aligned}\dot{A} &= -a_1\cdot(A-A_0)+a_2\cdot\left(B^2-{B_0}^2\right)\\ \dot{B} &= b_{11}\cdot A - b_{12}\cdot\sqrt{A}+b_2\cdot B+b_3\end{aligned} \tag{1}$$

where $b_{11}=b_{area,in}$, $b_{12}=b_{perifery,out}$, $b_3=b_{const,in}-b_2B_0$. Further considered conditions are the following: a) Initially there is no increase of the spot area, $\left(A_0,\dot{A}_0=0\right)$. b) a_1=b_2, for the curve $\left(A(t),\dot{A}(t)\right)$ to be closed. c) A proportionality relation between $A(t)$ and A_0. d) Normalization with the dimensionless variables $x(t)\equiv A(t)/A_0$, $y(t)\equiv B(t)/B_0$ and new set of parameters q, p_1, p_2, m. Then, the ODE-system becomes

$$\begin{aligned}\dot{x} &= a_1\cdot\left[-x+q\cdot\left(y^2-1\right)+1\right]\\ \dot{y} &= a_1\cdot\left[p_1\cdot x-p_2\cdot\sqrt{x}+y+m\right],\end{aligned} \tag{2}$$

while, its solution satisfies the Hamiltonian constraint $H(x,y)=h=\text{constant}$, where

$$H(x,y)=\tfrac{1}{3}a_1\left\{q\,y^3+3(1-q-x)y+2\left[-\tfrac{3}{4}p_1(x^2-1)+p_2(x^{3/2}-1)-\tfrac{3}{2}m\,(x-1)+q\right]\right\}=h \tag{3}$$

The fitting of the model predicted curve $\left(A(t)=A_0x(t),\dot{A}(t)=A_0\dot{x}(t)\right)$ to the respective observational data of sufficiently large sunspots ($A_{Max}>35$ MSH), led to the optimal values ([1])

$$q=310\pm10,$$

$$p_1=(1.85\pm0.10)\times10^{-3},$$

$$m=4.90\pm0.03.$$

These model parameters, q, p_1, and m, are considered to have fixed values for all the sunspots. On the other hand, the variation of the sunspots can be caused only by the non-constancy of the values of the parameters p_2, a_1 and the initial value A_0. In particular, for the these parameters, the fitting yielded to

$$p_2=\langle p_2\rangle=0.2760\pm0.0010,$$

$$a_1=\langle a_1\rangle=0.068\pm0.001\ \mathrm{d}^{-1},$$

$$A_0=\langle A_0\rangle\approx0.71\ \text{MSH}.$$

We refer to the values of $p_2=\langle p_2\rangle$, $a_1=\langle a_1\rangle$, $A_0=\langle A_0\rangle$ as "mean values", because they are an outcome of the fitting of the model predicted phase space curve $\left(A(t),\dot{A}(t)\right)$ to 24000 respective observational values, characterizing the totality of sunspots, and statistically modified to 43 pairs $\{(A_i,\bar{\dot{A}}_i)\}_{i=1}^{43}$ by [8]). The initial area A_0, is considered to be of the order of the granule area A_G, i.e. $A_0\approx A_G$, while the mean initial area describes the mean granule area, $\langle A_0\rangle\equiv\langle A_G\rangle$. Indeed, during its evolution, the sunspot does not attain area values smaller than the initial A_0. Thus, A_0 is the smallest value that $A(t)$ may obtain, i.e. $A_0\approx A_{Min}\le A(t)$. Since the smallest sunspot area is limited by the granules area, i.e. $A_G\approx A_{Min}$, then we conclude that $A_0\approx A_G$ ([1], [9]). The mean granule area was deduced, being $\langle A_G\rangle\approx0.71$ MSH. This was achieved by implementing a fitting method (based on the Taxicab norm L^1), between the theoretical and the experimental distribution of the maximum areas ([10], [11]). The area of a circle equal to $A=1$ MSH corresponds to a radius $r\cong984.3$ km (a diameter of $d\cong1968.6$ km), i.e.

$$A=1\ \text{MSH}=10^{-6}\,2\pi(6.96\times10^5)^2\ \text{km}^2\equiv\pi r^2 \quad\Rightarrow\quad r\cong\sqrt{2}\,696\ \text{km}. \tag{5}$$

Hence, the mean granule area $\langle A_G\rangle\approx0.71$ MSH corresponds to a radius $\langle r_G\rangle\approx\sqrt{0.71}\,984.3\ \text{km}\cong830$ km ($\langle d_G\rangle\approx1660$ km), and to a characteristic scale given by the area square root, i.e. $\langle l_G\rangle\approx1470$ km (because of

$$A_G\equiv\pi\,{r_G}^2=\pi\,{d_G}^2/4\equiv{l_G}^2\ \Rightarrow\quad l_G=r_G\sqrt{\pi}). \tag{6}$$

(For l_G≈1400 km, see: [11].)

We stress that the values of a_1 do not affect the curve $y(x)$ (or $B(A)$), and thus, nor the maximum area A_{Max}. Throughout, we handle the sunspot derived from values of $p_2=\langle p_2\rangle$ and $A_0=\langle A_G\rangle$, as an average representative of large sunspots. We also accept that the evolution of sunspots is suitably described by the phase space curves having the initial conditions $(x_0=1,y_0=1)$. (In general, we can define the normalized area and magnetic strength as $x(t)\equiv A(t)/A_G$, $y(t)\equiv B(t)/B_G$, with initial conditions $(x_0=A_0/A_G,y_0=B_0/B_G)$, where B_G can be thought as a characteristic scale of the magnetic strength of the granules surrounding the sunspot. E.g. see: [9]).

We stress that the physical meaning of the

parameters q, p_1, m, and p_2, is directly inherited from the old parameters a_2, b_{11}, b_2 and b_{12}. Namely, q: constant related to the sunspot creation mechanism; p_1, m: fixed parameters related to the magnetic flux inflowing into the sunspot from its entire area A, and from a local originated component, respectively; p_2: variant parameter related to the magnetic flux that outflows through the sunspot from its sideways area, being proportional to $\sqrt{A}$.

In Section II, the phase space portrait is studied. In Section III, we exhibit a model prediction concerning the upper limit for the sunspot maximum area, while in Section IV we proceed in calculating the upper limit for the relevant magnetic flux. Finally, Section V briefly discusses the conclusions.

II. THE PHASE SPACE (X , Y)

The phase space trajectories can be expressed either by $(A(t)=A_0\cdot x(t), B(t)=B_0\cdot y(t))$ or by $\left(A(t)=A_0\cdot x(t),\ \dot{A}(t)=A_0\cdot \dot{x}(t)\right)$. (E.g. in the work of [1] the latter is emphasized, while hereon the former is adopted.) First, we rewrite Eq. (4) in the form of a cubic polynomial in terms of y,

$$y^3-3\beta(x)\cdot y+2\gamma(x;p_2,E)=0 \quad , \tag{7}$$

where

$$\beta(x)=(x+q-1)/q \ ,$$

$$\gamma(x;p_2,E)=\tfrac{1}{2}E+\tfrac{1}{q}\times[-\tfrac{3}{4}p_1(x^2-1)+p_2(x^{3/2}-1)-\tfrac{3}{2}m(x-1)+q] \tag{8}$$

and $E\equiv -3h/a_1q$ is the modified Hamiltonian integral. (We ignore the dependence on the fixed parameters p_1, q, and m.) Depending on the sign of the discriminant $D_3(x;p_2,E)\equiv\gamma(x;p_2,E)^2-\beta(x)^3$ ([12]), the trinomial (7) can exhibit a closed curve solution. In particular, $D_3<0$ corresponds to three real solutions, degenerating for $D_3=0$ to one real solution (multiplicity 1) and one double real solution (multiplicity 2), or only one triple real solution (multiplicity 3), while $D_3>0$ corresponds to only one real solution (multiplicity 1). Obviously, these cases depend on the values of p_2 and E.

The three solutions denoted as $y_i=y_i(x;p_2,E)$, $i=1,2,3$, are given by

$$y_i(x;p_2,E)=2\sqrt{\beta(x)}\times\cos\left[\tfrac{1}{3}\cos^{-1}\left(-\gamma(x;p_2,E)\beta(x)^{-3/2}\right)+\tfrac{2}{3}\pi(i-1)\right], \quad i=1,2,3 \tag{9}$$

In the case of one real solution, e.g. $y_2(x;p_2,E)$, this is one-to-one (univalued function) and thus, it cannot represent a periodic trajectory of the phase space (x,y). On the other hand, in the case of three real solutions, two of them, e.g. $y_1=y_1(x;p_2,E)$ and $y_3=y_3(x;p_2,E)$, can suitably represent one closed curve, i.e. a periodic trajectory, while the remaining third solution $y_2(x;p_2,E)$ is still representing an open curve, i.e. a non periodic trajectory. It is apparent that the sunspot evolution can be described only by a closed curve. This is composed by the two one-to-one functions $y_1=y_1(x;p_2,E)$ and $y_3=y_3(x;p_2,E)$, the former corresponding to the growth phase and the latter to the decay phase of the sunspot evolution.

Furthermore, we deal with the phase space (x,y) mapping, performed, either (i) by the iso-Hamiltonian curves $y_i=y_i(x;E_k;p_2), i=1,2,3$, of various integral values $E=E_k$, $k=1,2,\ldots,n_E$, and of fixed outflow parameter value p_2 (Fig. 1(a)), or (ii) by the iso-outflow curves $y_i=y_i\left(x;p_{2,k};E\right), i=1,2,3$, of various outflow parameter values $p_2=p_{2,k}$, $k=1,2,\ldots,n_p$, and of fixed integral value E (Fig. 1(b)).

In the slightly shaded region of Figs. 1(a),(b), the closed curves surrounding the stable fixed point S_1 are bounded by the separatrix passing through the unstable fixed points U_2, and they are suitable for describing the sunspots evolution. (In particular for Fig. 1(a), the separatrix passes also through the unstable fixed point U_1.) The two stable S_1, S_2, and the two unstable, U_1, U_2, fixed points, are indicated.

In the first representation of the phase space (i), i.e. the Hamiltonian one, starting from an initial point (x_0,y_0) satisfying Eq. (7), each of the closed curves $(x(t),y(t))$ grows, covering the growth phase of the sunspot, and attains the point $[x_{Max}(p_2,E), y(x_{Max}(p_2,E);p_2,E)]$, corresponding to the sunspot maximum area. This maximum area shall be smaller than the corresponding area at the unstable fixed point U_2, i.e. $x_{Max}(p_2,E)\le x_{U_2}(p_2)$. In other words, U_2 implies an upper limit for the sunspot maximum area, i.e. $x_{Max}\big|_{UpLim}\equiv x_{U_2}(p_2)$. Notice that in the iso-Hamiltonian phase space representation, the fixed points are expressed in terms of the outflow parameter p_2. Moreover, as soon as the sunspot reaches its maximum dimensions, formally starts to decay, until the flux tube breaking mechanisms occurs (e.g. magnetic reconnection ([13])).

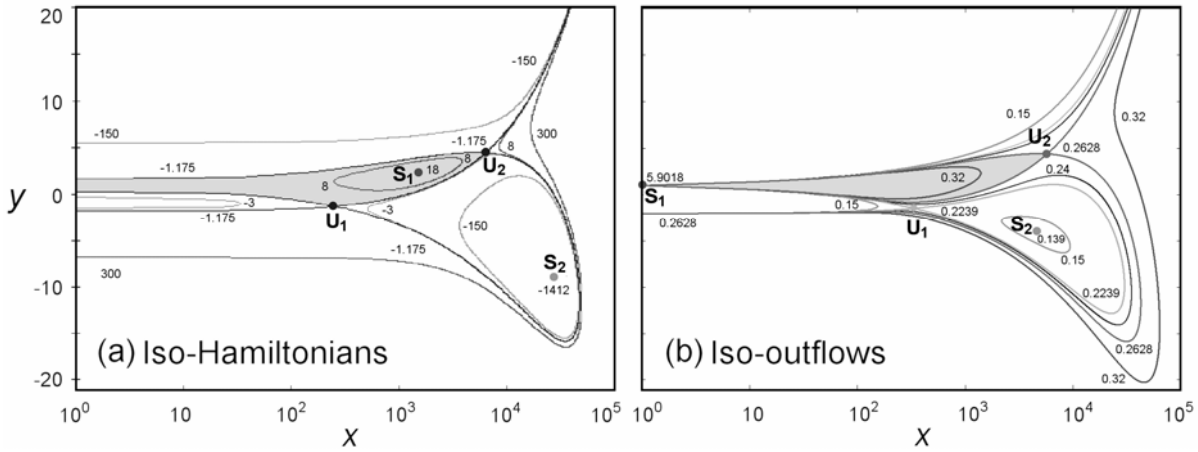

Fig. 1. The phase space portrait represented either (a) by the iso-Hamiltonian curves (with $p_2 = 0.263268$) or (b) by the iso-outflow curves (with E=0).

Figure 1(a) shows the iso-Hamiltonian phase space representation, where the value of the integral E is indicated for each of the depicted iso-Hamiltonian curves. The outflow parameter value, characterizing the whole figure, is $p_2 = 0.263268$. This critical value corresponds to the case where the unstable fixed points U_1, U_2 are joined through the same separatrix, having the Hamiltonian integral value $E = -1.175$.

In the second presentation of the phase space (ii), the contours of iso-outflow curves (constant p_2-valued curves), are depicted, while the value of the Hamiltonian integral E has the role of a fixed parameter. In other words, instead of depicting the iso-Hamiltonians, defined by the Hamiltonian constraint (4), i.e. $H(x,y;p_2) = \varphi_1(x,y) + \varphi_2(x,y)\cdot p_2 = h$, we depict the iso-outflows, defined by the functional

$$P_2(x,y;E) \equiv [h - \varphi_1(x,y)]/\varphi_2(x,y) = p_2 , \quad (10)$$

where

$$\varphi_1(x,y) = \tfrac{1}{3}a_1 \times \left\{ q\,y^3 + 3(1-q-x)\cdot y + 2\left[-\tfrac{3}{4}p_1(x^2-1) - \tfrac{3}{2}m(x-1) + q \right] \right\}, \quad (11)$$

$$\varphi_2(x,y) = \tfrac{2}{3}a_1(x^{3/2}-1) .$$

We stress that the functional $P_2(x,y;E)$ does not constitute the Hamiltonian function of the dynamical system (3). On the contrary, $H(x,y;p_2)$ does. However, it can be easily shown that the explicit expression and the stability type of the equilibrium points is preserved for the phase space portrait, given either by the iso-Hamiltonian curves $H(x,y;p_2)$ or by the iso-outflow curves $P_2(x,y;E) = p_2$.

Indeed, because of the gradients relation $\nabla P_2 = -\nabla H/\varphi_2$, we have that $\partial P_2/\partial x = \partial P_2/\partial y = 0 \Leftrightarrow \partial H/\partial x = \partial H/\partial y = 0$, thus, both of the representations lead to the same equilibrium points, the former being in terms of E, while the latter being in terms of p_2. On the other hand, the Hessian discriminants, D_P of $P_2(x,y;E)$, and D_H of $H(x,y;p_2)$, have the relation $D_P = D_H/\varphi_2^{\,2}$, thus, we have that $D_P < 0 \Leftrightarrow D_H < 0$ or $D_P > 0 \Leftrightarrow D_H > 0$, respectively meaning that a hyperbolic (saddle point) or an elliptic fixed point of $P_2(x,y;E)$, is also a hyperbolic or elliptic fixed point of $H(x,y;p_2) = E$, and vice versa.

The iso-outflowing presentation of phase space can be very useful for studying the sunspots, because they characterized by the specific value of the Hamiltonian integral E=0, while they do not have a specific value of the outflow parameter p_2. On the contrary, the values of p_2 are equidistributed in the interval $p_2 \in (p_{2,Min}, p_{2,Max}]$, with $p_{2,Min}(p_1,q,m) \approx 0.26284686\ldots$ and $p_{2,Max}(p_1,m) = p_1 + 1 + m \approx 5.90185$ (for the values of q, p_1, m given in (5)) ([1]). Notice that, in this representation, the normalized area corresponding to the unstable fixed point U_2 (performing the sunspot area upper limit), is expressed in terms of the Hamiltonian integral E, i.e. $x_{Max}(p_2,E) \le x_{U_2}(E)$. Precisely speaking, for any fixed point, stable or unstable, its phase space coordinates can be expressed either in terms of the outflow p_2 (iso-Hamiltonian representation) or in terms of the integral E (iso-outflow representation).

Figure 1(b) shows the iso-outflow phase space representation, where the value of the outflow parameter p_2 is indicated for each of the depicted curves. The value of the Hamiltonian integral, characterized the whole figure, is E=0. This value corresponds to the initial conditions $(x_0 = 1, y_0 = 1)$, being suitable for the sunspot evolution (see Introduction). Notice that the separatrix, passing through the unstable fixed point U_2, corresponds to p_2=$p_{2,Min}$ ≈0.26284686, implying thus, the outflow parameter value for which the upper limit of the sunspot maximum area is attained.

In the iso-Hamiltonian representation, by setting $\dot{x} = \dot{y} = 0$ on the dynamical system (3), we conclude in the fixed point expression $x_*(p_2)$, given implicitly by

$$p_2 = x_*^{-1/2}[p_1 x_* \pm q^{-1/2}(x_* + q - 1)^{1/2} + m] \quad (12)$$

while in the iso-outflow representation, we consider also the Hamiltonian constraint (7), concluding in the expression $x_*(E)$, given implicitly by

$$\pm q^{-1/2}(x_* + q - 1)^{1/2}\left[(q-1)x_*^{1/2} + 1\right] - \tfrac{1}{4}p_1\left(x_*^{3/2} - 4x_* + 3x_*^{1/2}\right) + \tfrac{1}{2}m\left(x_*^{3/2} - 3x_*^{1/2} + 1\right) - \tfrac{1}{2}q(E+2)x_*^{1/2} = 0 \quad (13)$$

In both the representations, the y-values, i.e. $y_*(p_2)$, $y_*(E)$, can be calculated by

$$y_* = \pm q^{-1/2}(x_* + q - 1)^{1/2}. \quad (14)$$

(Explanation: First, by setting $\dot{x} = 0$ in Eq. (3), we derive Eq. (14), while thereafter, by setting $\dot{y} = 0$, we derive Eq. (12), after substituting $y_* = y_*(x_*)$ given by Eq. (14), and solving in terms of p_2. Moreover, Eq. (13) comes from substituting $y_* = y_*(x_*)$, given by Eq. (14), and $p_2 = p_2(x_*)$, given by Eq. (12), in the Hamiltonian constraint of Eq. (4) or Eq. (8), taking into account that $E \equiv -3h/a_1 q$.)

Thus, for the iso-Hamiltonian representation and for p_2=0.263268 (Fig. 1(a)), we find

U_1: $x_* = 231.772$, $y_* = -1.32077$, E=−1.175;
S_1: $x_* = 1387.22$, $y_* = 2.33916$, E=18.0;
U_2: $x_* = 5760.00$, $y_* = 4.42464$, E=−1.175;
S_2: $x_* = 24414.1$, $y_* = -8.93039$, E=−1412.

For $p_2 = 0.26284686$ (=$p_{2,Min}$, when E=0), we find

U_1: $x_* = 232.574$, $y_* = -1.32175$), E=−1.166;
S_1: $x_* = 1403.21$, $y_* = 2.35016$, E=18.94;
U_2: $x_* = 5693.25$, $y_* = 4.40024$, E=0;
S_2: $x_* = 24334.5$, $y_* = -8.91601$, E=−1402.

On the other hand, for the iso-outflow representation and for E=0 (Fig. 1(b)), we find

U_1: $x_* = 331.46$, $y_* = -1.43736$, $p_2 = 0.22387185$;
S_1: $x_* = 1$, $y_* = 1$, $p_2 = p_1 + 1 + m = 5.90185$;
U_2: $x_* = 5693.25$, $y_* = 4.40024$, p_2=0.26284686;
S_2: $x_* = 4566.9$, $y_* = -3.96595$, p_2=0.13884275.

(For E=0, the stable point S_1 is a singular point in the iso-outflow representation, because $\varphi_1, \varphi_2 \to 0$ for $(x \to 1, y \to 1)$, and the functional $P_2(x, y; E)$ is $p_2 \to p_1 + 1 + m \approx 5.90185$.)

Finally, in Figs. 2(a),(b), x_* is depicted as a function of E and of p_2, respectively.

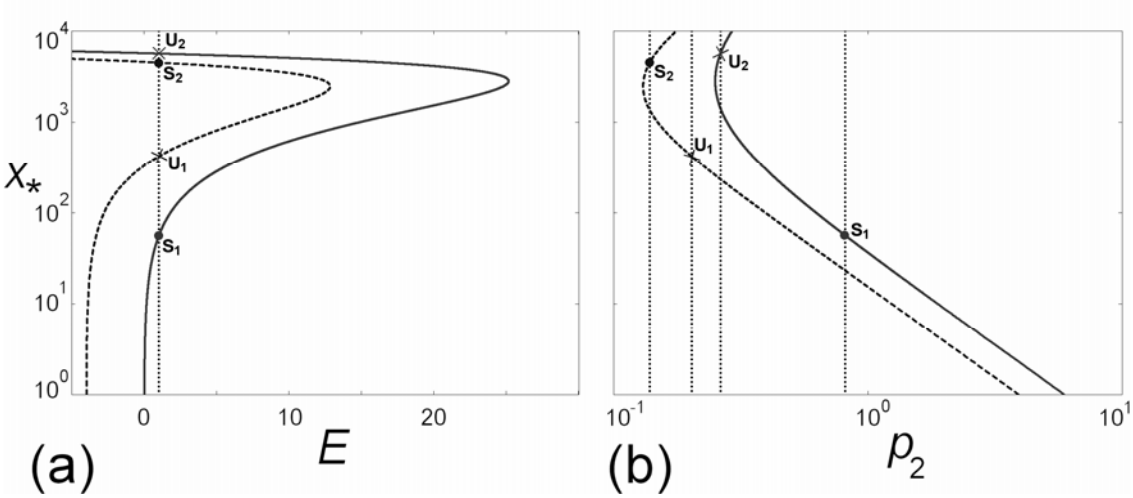

Fig. 2 The normalized area x_* of the stable S_1, S_2 (indicated by small dots), and unstable U_1, U_2 (indicated by small ×'s) fixed points, is depicted with respect to E (a), and to p_2 (b). For a given E value, e.g. E=1 (vertical dot line), we find $x_*(E=1)$ from (a), and then, the respective values of p_2 from (b). Because of the double sign in Eqs.(12,13), there are two curves, the one corresponding to S_1 and U_2 (solid line), and the other corresponding to U_1 and S_2 (dash line).

III. UPPER LIMIT OF THE SUNSPOT AREA

Let us first express the maximum area x_{Max} as a function of the outflow p_2. Setting $\dot{x} = 0$ in Eq. (3) and substituting in the Hamiltonian constraint (7) for E=0, we derive the implicit expression of $x_{Max}(p_2)$, i.e.

$$p_2(x_{Max} \equiv A_{Max}/A_0) = \left(x_{Max}^{3/2} - 1\right)^{-1} \times \left[q^{-1/2}(x_{Max} + q - 1)^{3/2} + \tfrac{3}{4}p_1\left(x_{Max}^{2} - 1\right) + \tfrac{3}{2}m(x_{Max} - 1) - q\right] \quad (15)$$

Figure 3 shows that, the more the outflow decreases, the larger the dimensions of the sunspot becomes. The point of the trajectory corresponding to the maximum area, A_{Max}, attains its largest

theoretical value, when $p_2 = p_{2,Min} \approx 0.26284686...$ This is an upper limit for the value of the sunspot areas, i.e. $x_{Max}|_{UpLim} \approx 5700$.

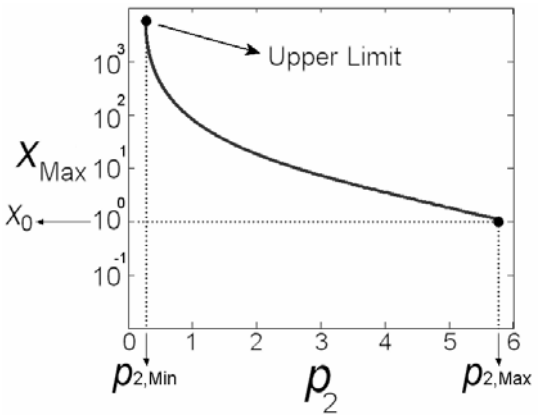

Fig. 3. The maximum normalized area $x_{Max}(p_2)$, depicted for the outflow values $p_2 \in (p_{2,Min}, p_{2,Max}]$ for E=0. The monotonically decreasing dependence from $x_{Max}|_{UpLim} \approx 5700$ to $x_0 = 1$ is shown.

However, the upper limit of the sunspot area depends directly on the value of the initial area, A_0, considered to be of the order of the area of a granule, A_G.

$$A_{Max}|_{UpLim}(A_0) = x_{Max}|_{UpLim} \cdot A_0 \ ,$$

$$A_0 = \langle A_G \rangle \approx 0.71\,\text{MSH} \Rightarrow$$

$$A_{Max}|_{UpLim}(A_0 = \langle A_G \rangle) = 4100 \pm 300\ \text{MSH} \ , \quad (16)$$

$$A_0 = A_{G,Max} \approx 1.1\,\text{MSH} \Rightarrow$$

$$A_{Max}|_{UpLim}(A_0 = A_{G,Max}) = 6300 \pm 400\ \text{MSH} \ , \quad (17)$$

The obtained upper limit values of Eqs. (17), (18) stay in accordance with the observational data. Indeed, the size spectrum of the observed large sunspots has an upper limit to more than 3000MSH ([14]). Precisely speaking, the observations suggest two kinds of the areas upper limit: (i) ≈4000 MSH, and (ii) ≈6000 MSH at least. The former corresponds to the upper limit of Eg. (17) with average initial area, i.e. $A_0 = \langle A_G \rangle$. This can be realized as follows: In Fig. 4, the annual largest area values A_{Max} of individual sunspots are depicted with respect to the year from 1874 to the present. 20 of them attain area values in the range of $A_{Max} > 3000\,\text{MSH}$, having a mean value of about $\langle A_{Max} \rangle \approx 3800\,\text{MSH}$. Moreover, it is clearly shown that the A_{Max} values (except from the case of 1947's peak) are suitably, uniformly bounded by the horizontal dashed line, located approximately at ≈4000 MSH. This can be thought as an upper limit, staying in accordance with the one of Eq. (17). In addition, the exception of 1947's peak defines the second upper limit (ii) at ≈6000MSH, being in accordance with the rare case of sunspots initialized from large scale granules and leading to the large upper limit of Eq. (18).

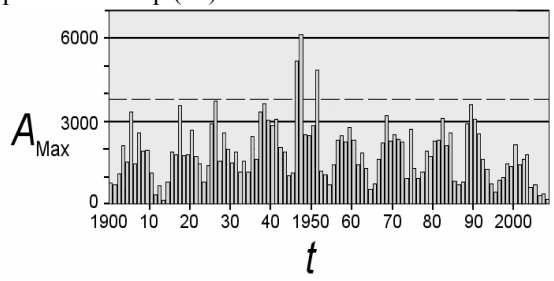

Fig. 4. The annual largest area value A_{Max} of individual sunspots is depicted with respect to the year from 1874 to the present. Only 20 of them are larger than 300MSH. All the A_{Max}-values (except from the 1947's peak) are uniformly bounded from the horizontal dash line, located at ≈4000 MSH.

IV. Upper Limit of the Magnetic Flux

The model predicted evolution of sunspot area (photometric evolution) has been suitably adjusted to the observational data, by considering either individual sunspots or the mean rates of the totality of sunspots ([1]). On the other hand, however, the magnetic evolution has not yet been contributed in any fitting procedure, since the solar magnetic observational data are rather poor and inadequate. Nevertheless, by considering instead of $y(t) = B(t)/B_G$, a generalized linear normalization of (3), i.e. $y(t) = \lambda_1 \cdot B(t)/B_G + \lambda_2$, we adjust the values of λ_1, λ_2, B_G, in order the model to describe satisfactorily the observed characteristics of the magnetic decay.

Indeed, by setting $g_1(B) = a_2 \cdot \left(B^2 - {B_G}^2\right)$, and a common functional type for the feedback components, i.e. $-f_1(A) = a_1 \cdot (A - A_G) + \tilde{a}_1 \cdot (B - B_G)$ and

$$f_2(B) = \tilde{b}_2 \cdot (A - A_G) + b_2 \cdot (B - B_G) \ ,$$

we can reconstruct the dynamical system (3), where the expressions of the normalized magnetic strength y and the parameter q are now given by

$$y \equiv [B/B_G - \tilde{a}_1/(2a_2 B_G)]/[\tilde{a}_1/(2a_2 B_G) - 1] \ ,$$

$$q \equiv a_2 {B_G}^2 [\tilde{a}_1/(2a_2 B_G) - 1]^2 / A_G \ .$$

Then, we have the normalizations

$$x(t) = A(t)/A_G \ , \ y(t) = \lambda_1 \cdot B(t)/B_G + \lambda_2 \ ,$$

where $\lambda_1 = [\tilde{a}_1/(2a_2 B_G) - 1]^{-1}$, $\lambda_2 = -1 - \lambda_1$. Hence,

$$B = B_G \cdot (y + 1 + \lambda_1)/\lambda_1 \ . \quad (18)$$

Thereafter, we calculate the values of λ_1, B_G concerning large sunspots, by utilizing the fact that the magnetic strength of large sunspots has an average maximum value of about $\langle B_{Max} \rangle \approx 3700$ G ([5]), while the followed decay phase has an average

rate of about $\langle \dot{B} \rangle \approx -12\,\mathrm{G\,d^{-1}}$ ([15]). The latter can be written as $\langle \dot{B} \rangle = \frac{1}{T_{MD}} \int_{T_{MD}} \dot{B}(t)\,dt = \Delta B_{MD} / T_{MD}$, where T_{MD} is the decay phase lifetime, wherein the magnetic strength has the total deviation $\Delta B_{MD} = B_{Max} - B_{Min}$. Given Eq. (19), we can write $B_G(y_{Max} + 1 + \lambda_1)/\lambda_1 \approx 3700\,\mathrm{G}$, $B_G \Delta y_{MD} / \lambda_1 T_{MD} \approx -12\,\mathrm{G\,d^{-1}}$, and deriving the values of y_{Max}, Δy_{MD}, and T_{MD} from the model predicted graph of the normalized values (x,y) for E=0 and $p_2 = \langle p_2 \rangle \approx 0.276$, we conclude in $\lambda_1 \approx 25$ and $B_G \approx 3100\,\mathrm{G}$. Then, we calculate the relevant magnetic flux $\psi(t) = A(t) \cdot B(t) = x(t) \langle A_G \rangle [y(t) + 1 + \lambda_1] B_G / \lambda_1$, while in Figs. 5(a-l), we plot $B(A)$, $\psi(A)$, $\psi(B)$, $\dot{A}(A)$, $\dot{B}(A)$, $\dot{\psi}(\mathrm{A})$, $\dot{A}(B)$, $\dot{B}(B)$, $\dot{\psi}(B)$, $\dot{A}(\psi)$, $\dot{B}(\psi)$, and $\dot{\psi}(\psi)$.

The maximum value of the normalized magnetic strength is quite closed to the value at the unstable fixed point U_2, leading thus, to the magnetic upper limit $y_{Max}|_{UpLim} \approx 4.404$, or, from Eq. (19), to $B_{Max}|_{UpLim} \approx 3800\,\mathrm{G}$. Hence, from Eqs. (17) and (18), we respectively conclude in the magnetic flux upper limit, being of about $\psi_{Max}|_{UpLim}(\langle A_G \rangle) \approx 4.4 \times 10^{23}$ Mx for sunspots surrounded by mean dimensions granules, i.e. $A_0 = \langle A_G \rangle \approx 0.71\,\mathrm{MSH}$, while being of about $\psi_{Max}|_{UpLim}(A_{G,Max}) \approx 7.23 \times 10^{23}$ Mx for the rare case of sunspots surrounded by large granules of $A_0 = A_{G,Max} \approx 1.1\,\mathrm{MSH}$.

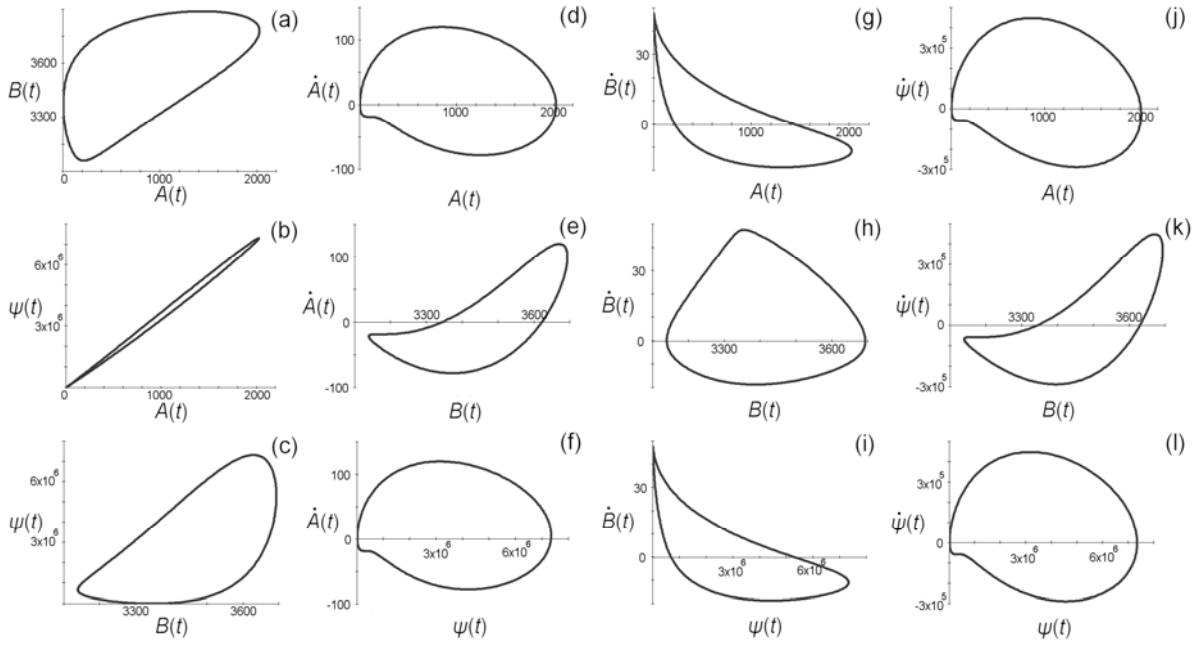

Fig. 5. The graphs of $B(A)$, $\psi(A)$, $\psi(B)$, $\dot{A}(A)$, $\dot{A}(B)$, $\dot{A}(\psi)$, $\dot{B}(A)$, $\dot{B}(B)$, $\dot{B}(\psi)$, $\dot{\psi}(\mathrm{A})$, $\dot{\psi}(B)$, $\dot{\psi}(\psi)$.

V. CONCLUSIONS

The largest active regions reach a maximum magnetic flux of the order of $\psi_{Max} \approx 10^{23}$ Mx ([16], [17]), which is quite closed to the upper limit calculated above, namely $\psi_{Max}|_{UpLim} \approx 7.23 \times 10^{23}$ Mx . It is remarkable that the magnetic flux concentrated in the totality of the granules of the whole area $A_{Sun} \equiv 2 \times 10^6$ MSH of the quiet Sun, having a typical maximum magnetic strength of about $\overline{B}_{Sun} \approx 12$ G , is equal to $\psi_{Sun} = \overline{B}_{Sun} \cdot A_{Sun} \approx 7.2 \times 10^{23}$ Mx ! (For the total magnetic flux of the quiet Sun, see: ([18]-[21]). For the maximum magnetic strength of granules, see: [22], [23] . Therefore, the magnetic flux concentrated in an active region cannot exceed the magnetic flux concentrated in the photosphere as a whole. (It is interesting that the quiet Sun needs to reform weekly a magnetic flux of $\Delta\psi \approx 7.7 \times 10^{23}$ Mx , for preserving its magnetic field ([24]).)

It is evident that the key-point, high-lighting the upper limit in sunspot area and magnetic strength, and thus, in magnetic flux, emerges through the existence of the unstable fixed point U_2. As it is clear from Figs. 1 and 2, the unstable fixed point U_2, yields an upper limit to the extension of the trajectories within the phase space that correspond to sunspots. On the other hand, the existence of the unstable fixed point U_2, is expressed by a lower limit in p_2-values, namely, in the outflow of the magnetic flux. Indeed, Fig. 3 shows the connection between the upper limit of sunspot area and the lower limit of p_2-values. But what is the physical meaning of having a lower limit in the outflow of the magnetic flux? Let us explain this idea, by the following simple hydrostatic analogue.

Consider a closed cylindrical flask of base with area A and height $1/(2\sqrt{\pi})$ (hence, of sideways area $\sqrt{A}$), being filled with water from its upper base with a constant mass-current J, for a fixed time Δt, so that $m(\Delta t) = m_0 + J\,A\,\Delta t = m_{Max}(1+\lambda)$, where $m(\Delta t)$ is the mass of water supplied to the flask after time passage Δt, m_0 is the initially contained mass, m_{Max} is the total capacity of the flask in water, and λ is a positive constant. Apparently, we have overflow and since the time interval Δt is fixed and not variant parameter, the only way for avoiding the overflow of the flask is having an outflow term. Suppose that this outflow is implied by the poriferous material of the flask, so that mass of water can depart homogeneously from the whole flask, independently of the height of the contained water (e.g. consider high vapor pressure), hence the outflow mass rate is given by $-p\sqrt{A}$, where p is a positive parameter. Hence, $m(\Delta t) = m_0 + (J\,A - p\sqrt{A})\Delta t$ $= m_{Max}(1+\lambda) - p\sqrt{A}\,\Delta t$, and in order to avoid the overflow, the flask shall be sufficiently poriferous, namely, there is a minimum value of p, i.e. $p_{Min} = m_{Max}\lambda/(\sqrt{A}\,\Delta t)$, for which $m(\Delta t) = m_{Max}$. In other words, for $p \geq p_{Min} = m_{Max}\lambda/(\sqrt{A}\,\Delta t)$ we have $m(\Delta t) \leq m_{Max}$, and the flask is kept out of either overflowing or break-downing.

We conclude that the sunspot succeeds in avoiding the magnetic overflow, with the help of the outflow of the magnetic flux, expressed by p_2. Moreover, this factor has to be sufficiently large, e.g. $p_2 \geq p_{2,Min}$, for successfully stabilizing the sunspot. Finally, this lower limit in p_2-values leads to an upper limit in sunspot area and magnetic strength, and consequently, in the magnetic flux.

REFERENCES

[1] Livadiotis, G., and Moussas, X., *Physica A* **379** (2007) 436-458.

[2] Duvall, T. L. Jr., D'Silva, S., Jefferies, S. M., Harvey, J. W., and Schou, J., *Nature* **379** (1996) 235-237.

[3] Hurlburt, N. E., and Rucklidge, A. M., *MNRAS* **314** (2000) 793-806.

[4] Kosovichev, A. G., *Astron. Nachr.* **323** (2002) 186-191.

[5] Solanki, S. K., *Astron. & Astrophys. Rev.* **11** (2003) 153-286.

[6] Meyer, F., Schmidt, H. U., Weiss, N. O., and Wilson, P. R., *MNRAS* **169** (1974) 35-57.

[7] Meyer, F., Schmidt, H. U., and Weiss, N. O., *MNRAS* **179** (1977) 741-761.

[8] Hathaway, D. H., and Choudhary, D. P., NTRS (2005) (ID: 20050236988).

[9] Livadiotis, G., and Moussas, X., "The perturbated Photometric-Magnetic dynamical model for describing the evolution of a sunspot", In: "Chaos in Astronomy", Lecture notes in physics, (Springer, Berlin, 2008).

[10] Livadiotis, G., *Physica A* **375** (2007), 518-536.

[11] Foukal, P. V., "Solar Astrophysics", (Wiley-VCH Verlag GmbH & Co. KGaA, Weinheim, 2004), pp. 138–143.

[12] Beyer, W. H., "CRC Standard Mathematical Tables", (28th ed. Boca Raton, FL: CRC Press, 1987), pp. 9-11.

[13] Priest, E.R., "Solar Magnetohydrodynamics" (D. Reidel Publishing Company, 1984), pp. 345-357.

[14] Baumann, I., and Solanki, S. K., *Astron. & Astrophys.* **443** (2005) 1061-1066.

[15] Bumba, V., *Bull. Astron. Inst. Czechoslovakia* **14** (1963) 91.

[16] Vial, J.-C., *Adv. Space Res.* **36** (2005) 1375-1386.

[17] Solanki, S. K., Inhester, B., and Schüssler, M., *Rep. Prog. Phys.* **69** (2006) 563–668.

[18] Wang, Y.-M., Lean, J., and Sheeley, N. R., Jr., *Geophys. Res. Lett.* **27** (2000a) 505-508.

[19] Wang, Y.-M., Sheeley, N. R., Jr., and Lean, J., *Geophys. Res. Lett.* **27** (2000b) 621-624.

[20] Wang, Y.-M., *Solar Phys.* **224** (2004) 21-35.

[21] Fisk, L. A., *Astrophys. J.* **626** (2005) 563-573.

[22] Rabin, D. M., Devore, C. R., Sheeley, N. R., Harvey, K. L., and Hoeksema, J. T., "Solar interior and atmosphere", (Cox, A. N., Livingston, W. C., and Matthews, M. S., Eds., The University of Arizona Press, 1991), pp. 781-843.

[23] Harvey, K. L., "Magnetic Bipoles on the Sun", Ph.D. thesis, Utrecht Univ., 1993.

[24] Worden, J., and Harvey, J., *Solar Phys.* **195** (2000) 247-268.

Regions of a charged particle's equatorial motions in a system of two rotating magnetic dipoles

Tilemahos J. Kalvouridis

National Technical University of Athens

Abstract – **In this contribution we study some aspects of the dynamics of a charged particle in the field produced by two magnetic dipoles that rotate in circular orbits around their common center of mass under their mutual Newtonian attraction. More precisely, we investigate the evolution of the regions of the particle motion on the equatorial plane of each dipole and we explore their parametric variation. The obtained results show that for each particular set of parameters and for certain values of energy these regions are bounded, and therefore the motion of the particle is confined inside them.**

***Key Words*—Charged particle dynamics, moving magnetic dipoles, regions of motions, zero-velocity curves.**

I. INTRODUCTION

The study of the motion of charged particles in the neighbourhood of Earth started with the investigations by Störmer at the beginning of the 20th century. Störmer in his effort to explain phenomena such as the polar aurora that are produced by the continuous bombardment from the Sun with charged particles of different origin, species and energies, Störmer suggested a simple model to simulate the magnetic field of our planet. He then proceeded to a mathematical formulation and, despite the lack of advanced computational tools in his era, he managed to give, in the course of the next 50 years, some first relative results (for a complete list of the scientific works of Störmer see for example [1]). He also achieved to calculate and draw particle periodic orbits opening in this way a new window to the study of this very interesting issue. The work of Störmer was adopted by some contemporary researchers (see for example [2] and [3]). In the decade of the 50's the selected data during the flights of the first artificial satellites led to the discovery of the Van Allen belts ([4]) that surround Earth and the works of Störmer came again on stage. The coming of charged particles in the neighbourhood of Earth and the effects that these drifters produce in many activities of human life led many scientists to resume their research efforts to explain their origin, distribution and paths. The simulation of the mechanisms that generate various phenomena which are associated with the presence of small charged corpuscles was one of the ambitious targets for many scientists with quite different background. Physicists and geophysicists usually work on models that mainly concern the simulation of the real magnetic field of Earth (see for example the works by Tsyganenko ([5]-[7])). High-energy physicists try to find a connection between the streams of charged particles that enter the terrestrial atmosphere with some extreme solar events. The progress on that issue is undoubtedly impressive. The recently obtained results ([8] and [9]) fill us with expectations that very soon an international network of suitably equipped observatories will provide us in time with warning information about a possible attack of highly energetic charged particles. Mathematicians and celestial mechanists have a different approach. They try to approximate the whole problem theoretically by using methods of non-linear dynamics ([10]-[14]). Moving along this latter direction, some years ago a model based on both the original idea of Störmer and the known restricted three-body problem was proposed [15]. This model is referred to either as the magnetic-binary problem ([1], [16]-[18]) or the problem of two rotating magnetic dipoles. Our present contribution concerns some aspects of this problem, the basic configuration of which, as well as its general characteristics will be described in the subsequent.

[1] Description of the model and equations of planar motions of a charged particle

The dynamical system consists of two spherical, homogeneous major bodies P_1 and P_2 that revolve around their common center of mass O under their mutual Newtonian attraction in circular orbits with constant angular velocity ω (Fig.1). Each body possesses a dipole-type magnetic field. It is assumed that this field does not influence the motion of the two bodies. A small charge moves in the electromagnetic field created by these bodies under the action of a Lorentz force which is much stronger than the gravitational attraction exerted on the particle by the two major bodies. Particle motion is usually described in a synodic coordinate system Oxyz, the plane Oxy of which coincides with the plane of motion of the two primaries and the x-axis with the line that joins the centers of the two primaries. Here we shall confine our study on the particle motions that are realized on the equatorial planes of the dipoles,

$$f_i(x,y,z)=a_i(x+(i-1)-\mu)+\beta_i y+\gamma_i z=0,\ \text{i=1,2}\ . \quad (1)$$

The constraint forces which are imposed on the particle are normal on these surfaces. Constraints (1) reduce the problem to one with two degrees of freedom. The condition for the velocity $\underline{v}$ in the equatorial motion is,

$$\underline{v}\square(\alpha_i,\beta_i,\gamma_i)=0\ .$$

For this case we use a Cartesian frame $P_ix_iy_iz_i$, i=1,2 associated to each dipole P_i, i =1,2, the axis Oz_i of which coincides with the axis of the magnetic moment M_i, while axes P_iy_i and P_ix_i, i=1,2 lie on the corresponding equatorial plane. The Lagrangian of the particle is, $L^i=T^i-V^i$, where,

$$T^i=\frac{1}{2}\left(\dot{x}_i^2+\dot{y}_i^2\right)$$

is the kinetic energy of the particle and

$$V^i=-b_1^i\dot{x}_i-b_2^i\dot{y}_i+V_0^i$$

is the velocity-dependent potential function,

$$b_1^i=c_{11}^iA_x+c_{12}^iA_y+c_{13}^iA_z+\omega(c_{12}^ic_{21}^i-c_{11}^ic_{22}^i)y_i+\omega c_{12}^i(i-1-\mu)$$

$$b_2^i=c_{21}^iA_x+c_{22}^iA_y+c_{23}^iA_z+\omega(c_{11}^ic_{22}^i-c_{12}^ic_{21}^i)x_i+\omega c_{22}^i(i-1-\mu)$$

$$V_0^i=-\omega x_i(c_{11}^iA_y-c_{12}^iA_x)-\omega y_i(c_{21}^iA_y-c_{22}^iA_x)+\omega(i-1-\mu)A_y-$$
$$-\omega^2\left\{\frac{1}{2}(x_i^2+y_i^2)-\frac{1}{2}(c_{13}^ix_i+c_{23}^iy_i)^2-(i-1-\mu)(c_{11}^ix_i+c_{21}^iy_i)+\frac{1}{2}(i-1-\mu)^2\right\}$$

$$A_x=\left(c_{13}^ix_i+c_{23}^iy_i\right)p_{1\beta}-\left(c_{12}^ix_i+c_{22}^iy_i\right)p_{1\gamma}$$

$$A_y=\left(c_{11}^ix_i+c_{21}^iy_i\right)p_{1\gamma}-\left(c_{13}^ix_i+c_{23}^iy_i\right)p_{1\alpha}-(i-1-\mu)p_{1\gamma}-q_{1\gamma}$$

$$p_{1u}=\frac{u_1}{r_{1i}^3}+\frac{\lambda u_2}{r_{2i}^3},\ q_{1u}=\frac{u_1\mu}{r_{1i}^3}-\frac{\lambda u_2(1-\mu)}{r_{2i}^3},$$

$$u_i=\alpha_i,\beta_i,\gamma_i$$

$$r_{1i}^2=x_i^2+y_i^2-2(i-1)(c_{11}^ix_i+c_{21}^iy_i)+(i-1)^2$$

$$r_{2i}^2=x_i^2+y_i^2-2(i-2)(c_{11}^ix_i+c_{21}^iy_i)+(i-2)^2\ ,$$

i=1,2,

where c_{kl}^i, i=1,2, k,l=1,2,3 are the directional cosines of the new axes with respect to the original ones of the synodic system. If the axes of the two dipoles lie on the Oxz plane of the synodic system we obtain,

$$c_{13}^i=-c_{31}^i=a_i,\ c_{11}^i=c_{33}^i=\gamma_i,\ c_{22}^i=1,$$

$$c_{12}^i=c_{21}^i=c_{23}^i=c_{32}^i=\beta_i=0\ ,\text{i=1,2.}$$

The system is characterized by 6 parameters: (i) the mass parameter $\mu=m_2/(m_1+m_2)$ which is the reduced mass of primary P_2, (ii) the ratio $\lambda=M_2/M_1$ of the magnetic moments of the two primaries, (iii) two out of three directional cosines α_1, β_1, γ_1 (since the three directional cosines satisfy the orthogonal condition $\cos^2\alpha_1+\cos^2\beta_1+\cos^2\gamma_1=1$) of the axis of the dipole P_1 (iii) two out of three directional cosines α_2, β_2, γ_2 (for the same reason) of the axis of the dipole P_2.

II. REGIONS OF A PARTICLE'S EQUATORIAL MOTION AND PARAMETRIC EVOLUTION

It can be easily proved that there is a Jacobian-type integral of motion,

$$T^i+V_0^i=C,\quad (2)$$

where C is a constant. Integral (2) has a two-fold role. First, it is used to determine the regions where solutions exist. Secondly, it is used to check all numerical integrations, since the problem does not have analytic solutions. The permissible areas of the equatorial motion are bounded by the zero-velocity curves $V_0^i(x_i,y_i)=C$. These curves are also isoenergetic and isotachs. Curves characterized by different values of C don't intersect, but curves drawn for the same C intersect in the equilibrium positions of the particle. As an application we have considered,

$$\alpha_1=\gamma_1=\frac{\sqrt{2}}{2},\ \beta_1=0\ \text{and}\ \alpha_2=0\ ,\gamma_2=1,\ \beta_2=0\ ,$$

which means that the axis of dipole P_2 is perpendicular to the Oxy plane of the synodic system, while that of dipole P_1 forms a 45^0 angle with respect to the x-axis (Fig. 1).

Figs 2 and 3 show the evolution with C of these limiting curves on the equatorial planes of primaries P_1 and P_2 respectively, drawn for various values of parameters λ and μ.

For the given values of direction cosines α_i, β_i, γ_i, i=1,2, only the remaining two parameters of system λ and μ contribute in the formation of the areas of the permissible particle motion on the equatorial planes. In all cases we can see that on both sides of

each dipole two closed kidney-shaped regions are formed.

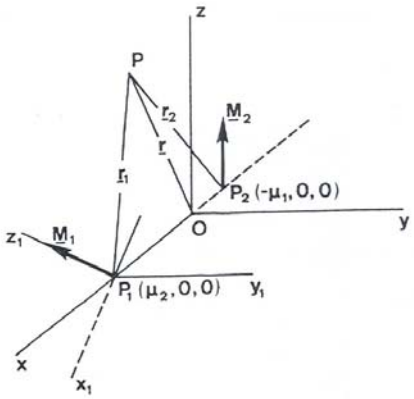

Fig. 1. The magnetic-binary model when the two dipole axes lie on
the xz plane of the synodic coordinate system.

These regions are similar but in general not equal and their size, for a given value of C, depends on the two parameters λ, μ. Since inside these regions the kinetic energy takes positive values, the motion of the particle is bounded there. In other words the particle's motion it is trapped. The size of these regions also changes with the Jacobian constant. The more this constant C increases, the more the size of these regions decreases. For the particle motion on the equatorial plane P_1, only two such regions develop around this dipole. For the particle motion on the equatorial plane P_2, two such pairs of bounded areas are formed. Regarding the effect of the parameters λ and μ on the formation of the networks of the zero-velocity curves, this can be summarized as follows:

- Parameter λ connects the magnitudes of the magnetic moments of the dipoles and consequently its role in the formation of the resultant electromagnetic field is very important. By definition, when λ>1 dipole P_2 possesses stronger magnetic field, the opposite happens when λ<1. As λ increases the closed regions around primary P_1 shrink, while those around primary P_2 extend (compare for example Figs 6b and 8b, 7b and 9b).
- Parameter μ determines the secular motion of the primaries which causes the magnetic fields' variation. However, its effect on the electrodynamical character of the system is weaker than that produced by parameter λ. When μ varies from 0 to 1 the form of the field changes but these changes are more obvious for λ<10 (see for example Figs 2b and 3b, 6b and 7b.

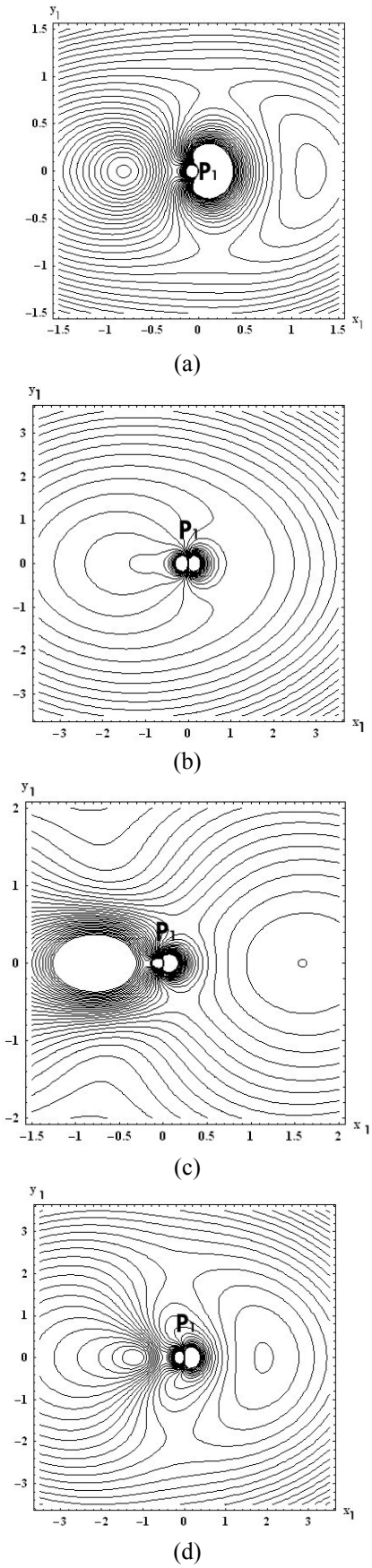

Fig. 2. Networks of zero-velocity curves on the equatorial plane of dipole P_1 for various values of the parameters. (a) λ=1, μ=0.1, (b) λ=1, μ=0.75, (c) λ=10, μ=0.1, (d) λ=10, μ=0.75.

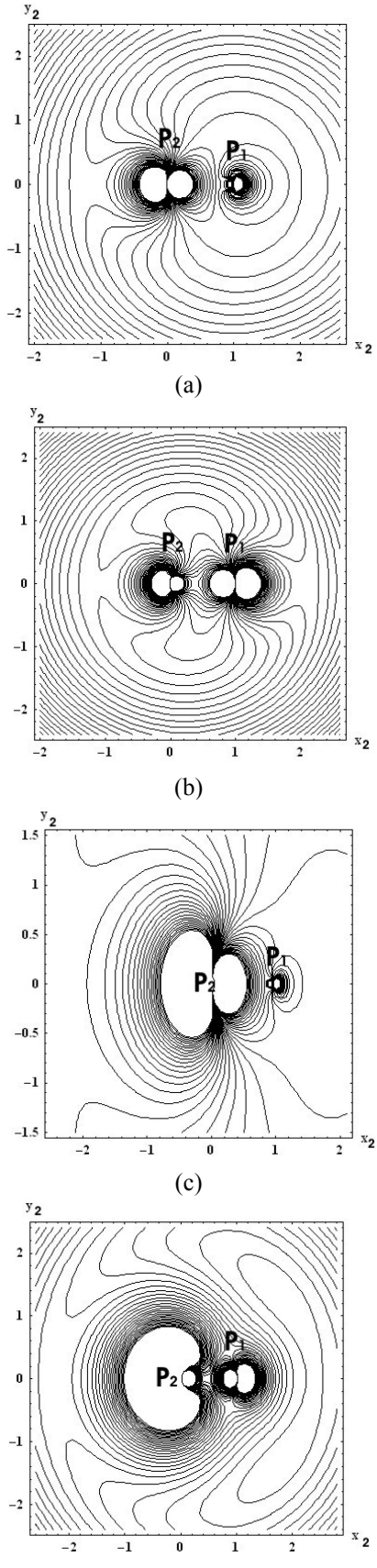

Fig. 3. Networks of zero-velocity curves on the equatorial plane of dipole P_2 for various values of the parameters. (a) λ=1, μ=0.1, (b) λ=1, μ=0.75, (c) λ=10, μ=0.1, (d) λ=10, μ=0.75.

IV. CONCLUSIONS

We described a model consisting of two rotating magnetic dipoles and a small charge moving under the combined action of the produced by the dipoles electromagnetic forces and we investigated the parametric variation of the permissible equatorial motions of the particle and particularly of the areas where this motion is trapped. This model could roughly simulate the Sun-Earth system, if the general magnetic field of the Sun is approximated by a dipole-type field with its axis perpendicular to the ecliptic plane and the magnetic field of the Earth is approximated by another dipole-type magnetic field, the axis of which is inclined to the same plane. The obtained results and the presented plots, show that around primary P_1 (as well as around P_2) closed regions of trapping motion are formed that resemble the ones of the Van Allen belts.

REFERENCES

[1] T.J.Kalvouridis, "Equatorial motions of charged particles in isolated pairs of magnetic bodies", PhD Thesis, National Tech. Univ. of Athens, Athens, 1986.

[2] M.S. Vallarta, "An outline of the theory of the allowed cone of cosmic radiation", University of Toronto series, Appl. Math. Series No3, The University of Toronto Press, Toronto, Canada, 1938.

[3] A. Juarez, "Periods of motion in periodic orbits in the equatorial plane of a magnetic dipole", Phys.Rev. 75, No1, 137-139, 1949.

[4] J. Van Allen, "The geomagnetically trapped corpuscular radiation", J.Geophys.Res. 64, No 11, 1683-1689, 1959.

[5] N.A. Tsyganenko, "Global quantitative models of the geomagnetic field in the cislunar magnetosphere for different disturbance levels", Planetary and Space Sci. 35, No11, 1347-1358, 1987.

[6] N.A. Tsyganenko, "Modeling the Earth's magnetospheric magnetic field confined within a realistic magnetopause", J. Geophys. Res. 100, 5599-5612, 1995.

[7] N.A. Tsyganenko, "A model of the near magnetosphere with a dawn-dusk asymmetry, I. Mathematical structure", J. Geophys. Res. 107, A8, 10.1029/ 2001JAA000219, 2002.

[8] H. Mavromichalaki, C. Plainaki, A. Mariatos, A. Belov, L. Baisultanova, E. Eroshenko, V. Yanke, V.G. Pchelkin, "Magnetospheric effects in cosmic rays during the unique magnetic storm on November 2003", EGU General Assembly, Vienna. Geophys. Res. Abstracts, 7, 07717, 2005.

[9] C. Plainaki., H. Mavromichalaki, A. Belov, E. Eroshenko, V. Yanke, "Modeling of the solar energetic particles recorded at neutron monitors", Proc. 7th Hellenic Astron. Conf., Cephalonia, Sept. 8-11, 2005.

[10] E. Avrett, "Particle motion in the equatorial plane of a dipole magnetic field", J. Geophys.Res. 67, No1, 53-58, 1962.

[11] M. Hones, "Motions of charged particles trapped in the Earth's magnetosphere", J.Geophys. Res. 68, No 5, 1209-1219, 1963.

[12] A. Dragt, "Trapped orbits in a magnetic dipole field", Rev. Geophys. 3, No2, 255-298, 1965.

[2] A.G. Mavraganis, C.L. Goudas, "New types of motion in Störmer's problem", Astrophys.Sp..Sci. 32, 115-138, 1975.

[3] S. Klimopoulos, "Numerical determination and study of periodic solutions of a charged particle in the magnetic field of the Earth", PhD Thesis, Patras, 1976.

[4] V. Markellos, A. Halioulas, "On the totality of periodic orbits in the meridian plane of a magnetic dipole", Astrophys. Sp. Sci. 51, 177-186, 1977.

[5] A.G. Mavraganis, "The magnetic-binary problem: Motion of a charged particle in the region of a magnetic-binary system", Astrophys.Sp.Sci. 54, 305-313, 1978.

[6] T.J. Kalvouridis, A.G. Mavraganis, "The equatorial equilibrium configuration of the magnetic-binary problem", Cel.Mech. 35, 397-408, 1985.

[7] T.J. Kalvouridis, "New families of simple symmetric motions in the equatorial magnetic binary problem", Astrophys.Sp.Sci. 136, 21-41, 1987.

A numerical model approximating extreme energetic electron events involved in the physical and chemical processes if the middle atmosphere

V.P. Tritakis (1), Yu.V. Pisanko (2), A.G. Paliatsos (3), G.K. Korbakis (1), P.Th. Nastos (4)

(1) Academy of Athens, Research Center for Astronomy and Applied Mathematics, Greece
(2) Institute of Applied Geophysics, Moscow, Russia
(3) General Department of Mathematics, Technological Educational Institute of Piraeus, Greece
(4) Laboratory of Climate, Department of Geology, University of Athens, Greece

Abstract – **Relativistic electrons (with energies >150 keV) which originate in the outer radiation belt and detected by the Russian 'Meteor' series of satellites have been correlated with the atmospheric total ozone data compiled by almost 90 stations located around the world within the latitude zone 40^o-70^o N. In more than 60% of the stations examined we have detected a clear decrease of the ozone 3-5 days after the electron flux excess. A numerical model has been applied to approximate this effect based on relativistic electron initiated nitric oxides creation in the upper mesosphere with subsequent atmospheric transport (both vertical and horizontal) towards the upper stratosphere. A first attempt of local and temporal prediction of ozone depletion because of energetic electrons impact in the middle atmosphere, has been illustrated.**

I. INTRODUCTION

Physico-chemical processing in the middle atmosphere triggered by extreme energetic electron events are equally significant for ozone depletion with electromagnetic radiation incidence on atmospheric constituents. The balance of the odd oxygen that is highly affected by odd nitrogen has been extensively studied from the side of the electromagnetic radiation in contrast to the corpuscular radiation influence that has been studied less.

Jackman (1991) reviewed consequences of the particle influence on the ozone layer while the specific role of magnetospheric relativistic electrons was elucidated and emphasized by Thorne (1980) and Callis et al. (1991).

In our study, we have applied a kind of batch processing to the northern hemisphere total ozone and relativistic electron databases for several years to examine possible effects of relativistic electron precipitation (REP) events. A clear decrease of the ozone concentration for 3-5 days after the occurrence of an extreme electron event (excess 2σ in relation to the yearly average electrons flux), is evident. The high frequency of the above phenomenon occurrence has stimulate us to attempt a close approximation of it by a numerical model aiming to a possible prediction of magnitude, place and time of the total ozone variation.

II. DATA DESCRIPTION

Daily total ozone measurements covering the time span 1992-1997 of almost 90 ground based stations located between 40^oN and 70^oN and distributed mainly within two wide longitude zones, covering Europe and North America have been used. From the Figures 1, 2 it is clear that most of the stations under consideration are located within a longitudinal zone
100 degrees wide.

The space data we use in this study are relativistic electron precipitation (REP) events collected by two Geiger counters (power law differential spectrum assumed), onboard the satellites N18, N19, N20, N21 of the 'Meteor-2' and the satellites N4, N5, N7 of the 'Meteor-3' series (both series were placed on circular orbit at 81^o inclination and approximately 1000 km altitude) during the years 1992-1997. The data in use were compiled when the satellite flew between 4 and 6 McIlwain shells in the northern hemisphere

because the outer radiation belt contains mainly electrons that provide precipitation events. A REP event is defined as an enhancement in the counting rate by two times the yearly standard deviation, at least. Finally, we examine events that belong to the ascending and descending branch of the orbit separately; they follow each other with a calm time period (with no precipitation) for nine hours, at least. The quiet period between successive REP events is necessary to ensure photochemical equilibrium of the upper stratospheric ozone before a precipitation event. In addition, we ignore events that occur very close to the local sunrise and sunset to eliminate rapid changes of mesospheric properties.

III. THE MODEL

The mesosphere is the least explored atmospheric region (it is situated too high for regular balloon observations and too low for satellite ones) so the level of mesospheric observational information uncertainty is relatively high. The lack of detailed observational information limits possibilities and leads to the construction of relatively simple models. In this sense, we consider electrons of kinetic energy higher than 150 keV precipitating along geomagnetic field lines from the outer radiation belt to the middle latitude atmosphere. During their passage through the atmosphere they lose part of their kinetic energy to ionisation of the atmosphere which creates excited nitric oxide molecules, that produce 5,3 μm IR emission (Dalgarno, 1963). In turn,, the IR emission causes additional local radiative cooling of the upper mesosphere similar to the thermospheric one (Rees and Fuller-Rowell, 1987). Since downward vertical winds driven by nitric oxide radiative cooling have already been experimentally detected in the thermosphere (Burns et al., 1989), the radiation loss of the upper mesosphere during a REP event could initiate a similar vertical transport, which interacting with horizontal mesospheric winds, could transport nitric oxides to the upper stratosphere.

For the time interval when a REP event is registered onboard a 'Meteor' satellite the projection (along geomagnetic field lines) of the corresponding part of the satellite's orbit on the mesospheric upper boundary is calculated by the satellite orbit data (altitude, latitude, and longitude as functions of time) and the precipitating electron flux at the mesospheric upper boundary is estimated. The latter is done under the assumption of isotropic pitch angle distribution that implies scattering in the regime of strong pitch angle diffusion during a REP event.

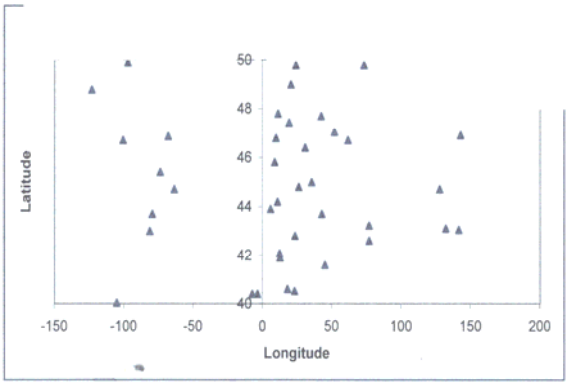

Fig. 1. Geographical distribution of ground-based stations within the latitude zone 40°-50°N.

The average (over the calculated projection) geographic latitude is accepted as the latitude φ_0 of the precipitation area centre, while the average (over the calculated projection) geographic longitude is accepted as the longitude λ_0 of the precipitation area centre. In local Mercator coordinates in the vicinity of the latitude φ_0, we estimate the precipitation area spatial scale as $L=(R_E+z)\cos\varphi_0 \max\{(\lambda-\lambda_0)^2+\ln^2[(1+\sin\varphi)\cos\varphi_0/(1+\sin\varphi_0)\cos\varphi]\}^{1/2}$, where φ,λ - are the current points of the projection, R_E – is the radius of the Earth, z – is the altitude of the mesosphere upper boundary, and the maximum is taken over the projection.

The energy deposition of a relativistic electron in the upper mesosphere is estimated from the Bethe's formula up to the depth that the electron has achieved decreasing its kinetic energy from the initial value to the value of 30 keV. The final part of the ionisation rate is estimated by calculating the ionisation cascade which is based on a known effective cross-section of the air ionisation by electrons (Ivanov-Kholodny and Nikolsky, 1969).

We suppose that the concentration of NO molecules on vibrational level v=1 of the ground state $X^2\Pi$ of nitric oxide $[NO_{v=1}]$ is $C(P/\alpha_{eff})^{1/2}$, where P – is the ionisation rate, α_{eff} – is the effective coefficient of recombination in the ionospheric D-region, C=1,3 (Caledonia and Kennealy, 1982). The vibrationally excited nitric oxide loses energy by both, emitting 5,3 μm IR radiation and colliding with atmospheric constituents.

The concentration of NO molecules deactivated by IR emission is expressed by the equation, $[NO_{v=1}{}^{5,3\mu m}]=[NO_{v=1}]A/\{A+k(N_2)[N_2]+k(O_2)[O_2]+k(O)[O]\}$, where $[N_2],[O_2],[O]$ – are the concentrations of molecular nitrogen, molecular oxygen, and atomic oxygen correspondingly, A – is the Einstein coefficient of spontaneous emission, k(N2), k(O2), k(O) – are the deactivation rate coefficients, so that the cooling rate from IR

emission of additional amount of nitric oxides created by the REP event can be estimated as $L_{NO*}=h\nu A[NO_{v=1}^{5,3\mu m}]$, under the supposition that vibrational band 5,3 μm of NO to be optically thin in the upper mesosphere (Degges, 1970), (Kockarts, 1980) ($h\nu=3{,}726\ 10^{-20}$ J).

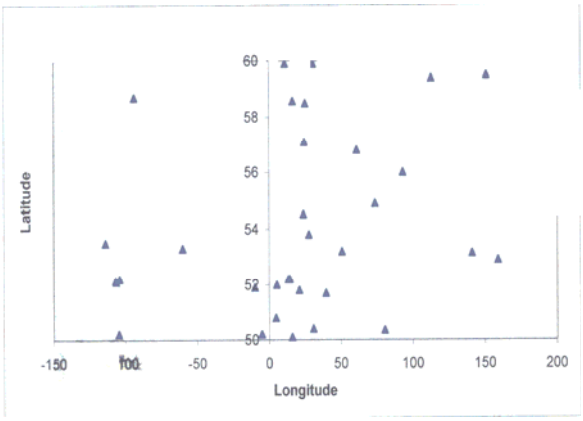

Fig. 2. Geographical distribution of ground-based stations within the latitude zone 50°-60°N.

The air vortex creation due to local cooling of the precipitation area during the REP event could be described by Eulerian formalism, choosing the non-inertial reference frame rotating with the angular velocity of the mesosphere, and considering the equations of dynamic meteorology (three dynamic equations describing four forces: inertia, Coriolis, gravity, and pressure gradient; the continuity equation; the heat transfer equation) in hydrostatic approach (the vertical velocity is put zero everywhere except the continuity equation) and linearized in the relation to horizontal velocity components. We suppose that the vertical mesospheric density variation is much larger than the horizontal one on the spatial scale of the precipitation area.

The heat transfer equation of the linearized system could be expressed by the formula $T=T_0(z)+T_1(x,y,z,t)$, $T_1<<T_0$, while we suppose that the background temperature T_0 decreases linearly with altitude. If the additional nitric oxide amount is injected into the upper mesosphere relatively fast in relation to the diurnal variation, we can conclude that during the injection other heat sources do not evolve significantly so that the linearized heat transfer equation degenerates to the expression $\partial T_1/\partial t \sim -L_{NO*}$. Measurements in rocket flights at Volgograd in October 1971 revealed the middle atmosphere cooling in the time of particle precipitation (Butko et al., 1974). The feature was repeated at Volgograd during a complicated rocket experiment conducted under disturbed geomagnetic conditions in June 1973 (Butko et al., 1976). The observed mesospheric cooling is supposed to be related to changes in minor species composition (Lastovicka, 1996).

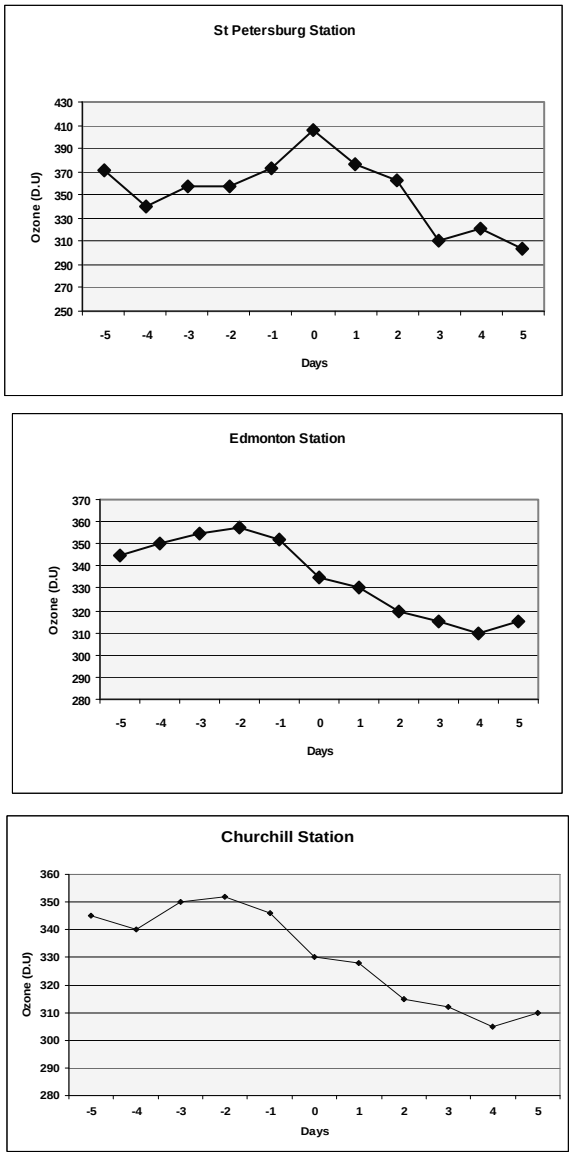

Fig. 3. Ozone variation in three separate stations, located in the zones 40°-50°N, 50°-60°N and 60°-70°N clockwise, five days before and five after the occurrence of a high electrons count rate (day zero). A clear decrease after the day zero is obvious.

If the $\partial T_1/\partial t$ is known, the two linearized dynamic equations for horizontal velocity components of the vortex can be solved analytically in polar coordinates centred in the precipitation area, and the velocity components can be constructed as expansions under the small parameter $L/R_E\cos\varphi_0$.

To ensure the hydrostatic force balance in the vertical direction during precipitation, according to the meteorological practice, we nullify the partial time derivative of the hydrostatic

equation. The equation we obtain, together with the continuity equation under known $\partial T_1/\partial t$ and divergence of horizontal vortex velocity components, allows getting the vertical momentum.

We suppose that horizontal temperature gradients created by local cooling vanish after the end of a REP event. In such a case, the chemically perturbed air flies away from the precipitation area by inertia with velocities it achieved before the end of the REP. The air vortex decay has been described by Lagrangian formalism while the inertial motion it is supposed to continue until the chemically perturbed air reaches the upper stratosphere where it is eventually stopped (Kalkstein, 1962). The transformation to the non-inertial reference frame rotating with the angular velocity of the Earth allows to take into account the motion of the mesosphere itself in the relation to the Earth surface (i.e. the magnitude and the direction of the average mesospheric horizontal wind according to its seasonal variation as well as the possible incline of the rotational axis of the mesosphere to the axis of the Earth' rotation on the day of the REP event).

Chemical bidirectional reactions in the mesosphere convert NO to NO_2 and NO_2 to NO permitting in this way, nitric oxide motions from the mesopause to the stratosphere. The ratio $[NO_2]/[NO]$ decreases when the altitude increases so that $[NO_2]<<[NO]$ in the mesosphere, $[NO]=2[NO_2]$ at 40 km and $[NO]=[NO_2]$ at 35 km (Johnston, 1975).

In order to estimate, except from place and time, the value of the stratospheric ozone depletion caused by chemically perturbed air entering from the mesosphere, we consider the upper stratosphere as oxygen-hydrogen-nitrogen atmosphere (Perov and Khrgian, 1980). In addition, we accept the photochemical equilibrium in a given point of the upper stratosphere before the additional amount of nitric oxide $[NO_2]$ occupies this point and creates the local perturbation of equilibrium in the ozone concentration. We take into account the termination of the nitric oxide catalytic chain of ozone destruction via the chain length parameter (Talrose et al., 1978). As this catalytic chain requires the presence of sunlight, the ozone concentration at a given geographic point is assumed 'frozen' at local night. To calculate total ozone variations, we fix the vertical profile of the ozone concentration above 35 km following Krueger and Minzner (1975), suppose all ozone variations considered in the present study they take place above 35 km, and introduce the parameter $\Delta=\{[X(0)-X(t)]/X(0)\}100\%$ as a measure of the relative ozone depletion at a given geographic point. In this relation,

$X(0)$ – is the mean over the years 1978-1988 total ozone at the geographic point for the month when the particular REP event occurred,

$X(t)$ – is the time dependent total ozone variation calculated by the model at the same geographic point.

The input parameters we use in modelling are, the time of the REP event (year, month, day, hour, 48 second interval), energetic electron fluxes and the satellite trajectory data as functions of the time during the REP event, concentrations of $[N_2],[O_2],[O]$ at 55 km altitude as well as the background temperature T_0 at 55 km altitude and at 85 km altitude in the precipitation area centre at the time just before the beginning of the REP event

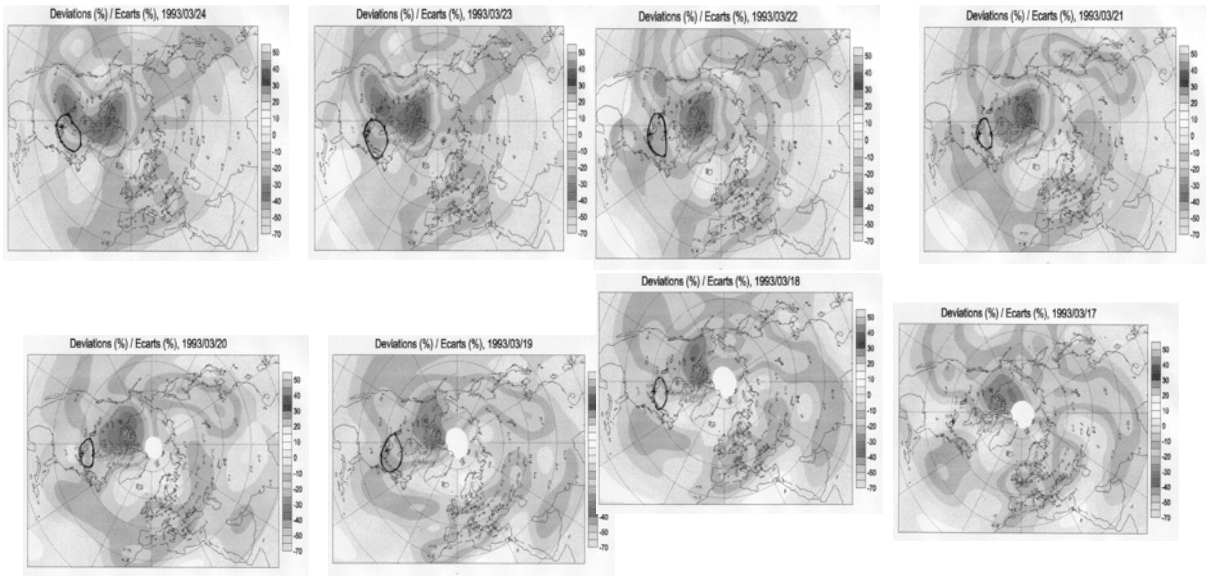

Fig. 4. Results of model application on the March 17, 1993 REP. The electron precipitation area has been marked by a cross (+) (lower right map, arrow). The maps for March 17-24, 1993 represent the evolution of the ozone depletion area caused by the REP event drawn on the basis of ground-level observations. Encircled areas show places where ozone deviation predicted by our model is higher than 4% and 4.5% within the outer and the inner area of the last map, respectively.

(MSIS-E-90 Atmosphere Model), the mean over the years 1978-1988 total ozone geographic map for the month when the REP event occurred (http://es-ee.tor.ec.gc.ca). The model calculates the parameter Δ as a function of the latitude, longitude and time (with the 2 hour time step) for 8 consecutive days after the REP event.

IV. RESULTS AND CONCLUSIONS

The total ozone variations for 10 consecutive days (5 days before and 5 days after the occurrence of a REP event for three ground based stations located within latitude zones 40-50 N, 50-60 N, and 60-70 N) are depicted in Figure 3. The tendency for a total ozone depletion that starts 1-2 days before the occurrence of a REP event (day 0) and lasts for several days after it, is clearly illustrated. The time lag between ozone decrease and REP onset could be attributed to the time, place and height difference of data collection. Similar ozone decreases have been determined in more than 60% of the ground-based stations of our record.

Although statistics is very clear in our case, it is limited to the estimation of the average time delay between the REP events, the total ozone depletion determined at the ground based station and the average magnitude of the effect. However, it is impossible to specify the geographical place where nitric oxide is created by a given REP event, which can be identified as total ozone depletion. The application of a model, the main features of which have been described in the previous paragraph, seems to solve this problem to a great extent. The results of modelling for two REP events that occur on the July 16, 1993 (summer) and March 17, 1993 (spring) are shown in Figures 4 and 5. In these figures, we represent experimentally detected maps of deviations (%) of the total ozone taken from the site of "Environment Canada" (http://es-ee.tor.ec.gc.ca) where the results of our model calculations were incorporated.

The place of the REP event is depicted by "+" (it is situated at the north of the Ural Mountains in the summer event and at the Great Lakes in the spring one). The temporal evolution of the deviations in the centre of the precipitation area is presented on separate graphs in both cases. In the summer event the ozone depletion takes place above Newfoundland (very far from the place of REP event) and later spreads over the south Canada; in the spring event – above the Great Lakes. The difference reflects the seasonal variation of mesosphere horizontal winds. Both occur with time delay of 2-3 days after the REP event.

Encircled areas on the maps represent places where ozone depletion has been predicted by model.

In the "summer" event (fig.4) ozone depletion inside the encircled area of the last map is 4% while the corresponding value in the last map of the "spring" event (fig.5) is 10% . Comparing the two above mention events we could underline that, in the spring event the precipitation area is smaller but the ozone depletion is deeper than in the summer event. The upper limit of about 13% depletion calculated in spring event is the result of the model assumption that all ozone variations occur above 35 km where no more than 15% of the total ozone is contained. The comparison of the observed and calculated total ozone maps indicates that the modelling looks promising in estimating the time evolution both of spatial boundaries and of

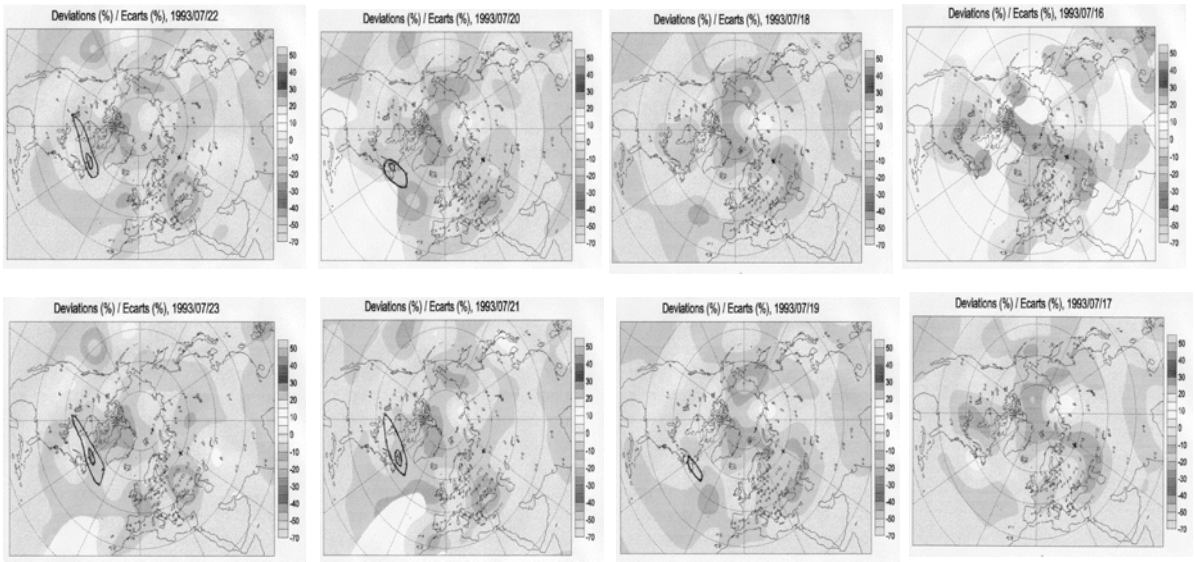

Fig. 5. Similar to Figure 4 but representing the ozone depletion caused by a REP event on the July 16th, 1993 (upper right map). Maximum ozone depletion in the encircled area of the last map has been estimated to 10% (lower left map).

relative values of the local total ozone depletions.

After all, it is clear that intense REP events can cause significant ozone depletion in the middle and high latitudes lasting for several days before recovery. Moreover, it is also clear that a model that could calculate all the forces they navigate a REP event from the upper to the middle atmosphere as well as take under consideration all the chemical reactions they occur in the same area, it could predict place, time and ozone depletion after a high REP detection at a height of 800-1000 km, where low altitude satellites normally fly.

ACKNOWLEDGMENTS

Yu.V. Pisanko is grateful to his colleagues P.M. Svidsky and A.A. Nusinov (Institute of Applied Geophysics both) for helpful discussions of few subjects touched in this paper. The work was supported in the framework of the Bilateral Programme of Cooperation in Science and Technology between Greece and Russia.

REFERENCES

[1] Burns, A.G., Killeen T.L., Crowley G., Emery B.A., Roble R.G. On the mechanisms responsible for high latitude thermospheric composition variations during the recovery phase of a geomagnetic storm, J. Geophys. Res., 94, 16961, 1989

[2] Butko, A.S., Ivanova, I.N., Kokin, G.A., Some peculiarities of thermal and circulation regime of the atmosphere, in 'Solar – atmospheric relationships', Hydrometeoizdat, pp. 125-144, 1974

[3] Butko, A.S., Golubev, E.N., Ivanova, I.N., Kokin, G.A., Mikhnevich, V.V,., Rubin,Yu.N., Speransky, K. E., Daily and semi-daily temperature and wind velocity variation peculiarities over Volgograd station, in Daily and latitude variations of atmospheric parameters and corpuscular emission (results of 1973 complex experiment)', Hydrometeoizdat, Leningrad, pp.86-104 1976 (in Russian)

[4] Caledonia, C.E., Kennealy, J.P. NO infrared radiation in the upper atmosphere, Planet. Space Sci., 30, N10, 1043-1056, 1982

[5] Callis, L.B., Baker, D.N. Blake, J.B. Lambeth, J.D. Boughner, R.E. Natarajan, M. Klebesadel, R.W. Gorney, D.J. Precipitating relativistic electrons: their long-term effects on stratospheric odd nitrogen levels, J.Geophys.Res., 96, ND2, 2939-2976, 1991

[6] Dalgarno, A., Vibrationally excited molecules in atmospheric reactions, Planet. Space Sci., 10, 19-28, 1963

[7] Degges, T.C., Vibrationally excited nitric oxide in the upper atmosphere, Applied Optics, v.10, N8, 1856-1860, 1971

[8] Ivanov-Kholodny, G.S., Nikolsky, G.M. Sun and ionosphere, Nauka, Moscow, 1969 (in Russian)

[9] Jackman, C.H. Energetic Particle Influences on NOy and Ozone in the Middle Atmosphere, Geophysical Monograph 75, IUGG Volume 15, 131-139, 1993.

[10] Johnston, H.S., Global ozone balance, Rev. Geophys. Space Phys., v.13, N5, 593-649, 1975

[11] Kalkstein M., Science, 137, 3531, 645, 1962

[12] Kockarts, G., Nitric oxide cooling in the terrestrial thermosphere, Geophys. Res. Lett., v.7, N2, 137-140, 1980.

[13] Krueger, A.J., Minzner, R.A. A mid-latitude ozone model for the 1976 U.S.standard atmosphere, J. Geophys. Res., v.81, N24, 4471-4481, 1976

[14] Lastovicka, J. Effects of geomagnetic storms in the lower ionosphere, middle atmosphere and troposphere, J. Atm. Terr. Phys., 58, N7, 831-843, 1996

[15] Perov, S.P., Khrgian, A.X. Contemporary problems of atmospheric ozone, Hydrometeoizdar, Leningrad, 1980 (in Russian)

[16] Rees, D., Fuller-Rowell, T.J. Comparison of theoretical models and observations of the thermosphere and ionosphere during extremely disturbed geomagnetic conditions during the last solar cycle. Adv. Space Res., 7(8), 27, 1987

[17] Talrose, V.L., Poroikova, A.I, Larin, I.K. Vinogradov, P.S. Kasimovskaya, E.E. Chemical-kinetic criteria of the effect of natural and anthropogenic substances on ozonosphere, Physics of atmosphere and ocean, 14, N4, 355, 1978 (in Russian)

[18] Thorne R.M., The importance of energetic precipitation on the chemical composition of the middle atmosphere, Pure Appl. Geophys., 118, 128-151, 1980.

[19] http:// es.-ee.tor.ec.gc.ca

Fluxes and Nuclear Abundances of Cosmic Rays inside the Magnetosphere using a Transmission Function Approach

P. Bobik [1], G. Boella [2,3], M.J. Boschini [2,4], M. Gervasi [2,3], D. Grandi [2], K. Kudela [1], S. Pensotti [2] and P. G. Rancoita [2]

[1] *Institute of Experimental Physics, Košice, Slovak Republic*
[2] *INFN -Istituto Nazionale di Fisica Nucleare Milano-Bicocca, Milan, Italy*
[3] *Department of Physics, University of Milano-Bicocca, Milano, Italy*
[4] *CILEA, piazza della Scienza 3, 20126 Milan, Italy*

Abstract – At 1 AU and outside the Earth's magnetosphere, the relative abundances to protons for He (He/p), C (C/p) and Fe (Fe/p) nuclei were calculated using the observation-data of AMS-01 (for p and He) and HEAO-3 (for C and Fe) above 0.8 GeV/nucleon. In addition, the transmission function (TF) for the GCR propagation inside the magnetosphere was evaluated using the IGRF and T96 (introduced by Tsyganenko and Stern) models to obtain permitted and forbidden trajectories inside the magnetosphere. The TF allowed one to derive the primary He-nuclei fluxes in the same geomagnetic regions of AMS-01 observations. These fluxes were found in good agreement with the observation data. Furthermore inside the magnetosphere in addition to the flux of helium, it allowed one to obtain those of the primary p, C, and Fe nuclei and the relative abundances of He, C and Fe nuclei to protons from the same observation-data of AMS-01 and HEAO-3 above ≈ 0.8 GeV/nucleon. Up to a geomagnetic latitude of ≈ 45.84°, the relative isotopic abundances were found to depend on the mass number Iisot and, on average, range from a factor ≈ 2.31 up to ≈ 3.35 larger than those outside the magnetosphere at 1 AU. Thus, the magnetospheric isotopic/nuclear relative-abundances differ from those inside the solar cavity and those in the interstellar space. The usage of the TF approach can allow one to determine the nuclear abundances in the magnetosphere at any geomagnetic latitude and, thus, any orbit, provided that the CR spectra are determined at 1 AU.

I. INTRODUCTION

Galactic Cosmic Rays (GCR's) are the dominant component of the charged particles present in space above few hundreds MeV of kinetic energy. The knowledge of their relative abundances is based on measurements performed by several satellites, most of them operating outside the magnetosphere, and by stratospheric balloons (inside the magnetosphere) during the last 30–40 years. Among GCR's, protons and α-particles are largely the most abundant. In addition, there is a lesser amount of nuclei up to nickel, and an even lesser amount of heavier nuclei. Above several GeV/nucleon, the solar modulation slightly affects their energy spectra and, additionally, these latter exhibit a power law behavior as a function of the kinetic energy per nucleon, Ek, e.g., GCR's intensities are $\sim E_k^{-\gamma}$, where γ is the so-called differential spectral index (e.g., [20], [21], [32]; chapters 5 and 6 of [23]; [25]; chapter 5 of [36]. The spectral index depends on the element, thus the relative abundance may depend on energy. For instance, γ is ≈ 2.74 (2.60– 2.63) for hydrogen (helium) (see Section 5.4.1 [35]). At energies per nucleon large enough to neglect the isotopic rest-mass, the same spectral index can be used to describe the kinetic-energy (and total) dependence. Furthermore, relative abundances are shown in Figure 3 in the paper by [30] at 16.2 GeV/nucleon up to nickel (with atomic number Z = 28) and in Figures 7 and 8 by [20] in the energy range from ≈ 0.8 (0.62 for C) up to 35 GeV/nucleon.

The knowledge of the GCR's abundances can be relevant in determining, for example, the

expected radiation effects on human beings and electronics in a space environment. In fact, to a first approximation, since at these kinetic-energies the energy deposition depends on Z^2 (e.g., see Sects. 2.1.1, 2.1.4 [31]), in such an environment the most abundant nuclei heavier than protons and with masses up to nickel i) largely contribute to the overall energy-deposition process inside matter and, thus, to the absorbed dose, i.e., the total ionizing dose (TID) and the displacement dose due to non ionizing energy-loss (NIEL) processes (e.g., see Sects. 3–3.1.5, 3.3–3.3.3 by [30]), and ii) they have to be taken into account, for instance, in qualification procedures of VLSI components and circuits for space missions (e.g., [13],[14],[15], [16],[17], [18], [29],[30] and references therein).

Moreover, after introducing the radiation weighting factor to account for the biological effectiveness, elements like Fe, Si, Mg and O make even larger contribution to the dose equivalent. Therefore, a realistic evaluation of these effects is needed for long duration space missions, like interplanetary journeys or those for the International Space Station (ISS), particularly for manned missions. Furthermore, for orbital missions with orbits much lower than that geostationary, the local intensities and, thus, relative abundances of GCR's are also expected to be affected by the Earth's magnetosphere, where the propagation of CR's is determined by their rigidities: isotopes with the same kinetic energy per nucleon can have different rigidities, since they are related to the Iisot/Z ratio, where Iisot is the number of nucleons of the nuclide. Thus, these relative abundances are expected to be slightly different among heavy isotopes, but to be largely varied with respect to protons with Iisot/Z ≈ 1. Note that, inside the magnetosphere, the geomagnetic cut-off values for rigidities have been computed since a long time (e.g., see [33]).

Codes, for instance CREME [40] and CHIME [12], can allow one to estimate the fluxes of charged particles inside the magnetosphere at LEO, but i) in CREME, the model Tsyganenko-89 [37] of external magnetic field and only two levels of magnetosphere disturbances are used and ii) in CHIME, the geomagnetic cutoff is estimated for vertical rigidities and a dipole magnetic field, thus it does not properly account for the so-called "penumbra region", in which the incoming CR flux is large.

In the present article using a Transmission Function (TF) approach (e.g.[27], [7],[8],[9]), we have determined the primary fluxes of He-nuclei in the same geomagnetic regions of AMS-01 observations, thus allowing a comparison of the observed spectrum and that obtained using the computed TF and the spectrum at 1 AU. In addition, the local abundances inside the Earth's magnetosphere are determined for p, He, C and Fe (i.e., nuclei among those more abundant in GCR's) exploiting AMS-01 and HEAO-3-C2 data collected with positive solar magnetic-field polarities.

It has to be remarked that the usage of the TF approach can allow one to determine the isotopic/nuclear abundances in the magnetosphere at any geomagnetic latitude and, thus, any orbit,

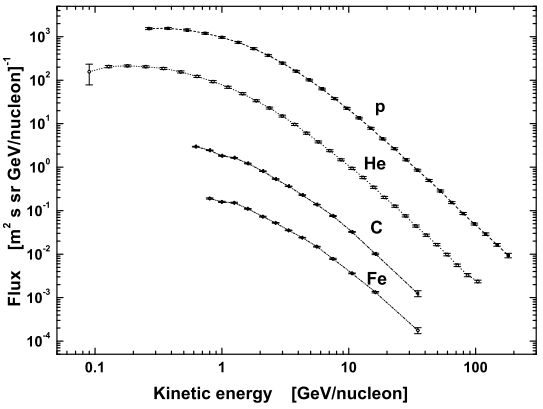

Fig. 1. Differential cosmic fluxes of p, He, C and Fe nuclei. The data for p and He nuclei are from (Alcaraz et al., 2000b; 2000c; Aguliar et al., 2002), for C and Fe from paper by Engelmann et al. (1990). These spectra were recalculated at 1 AU (outside the magnetosphere) by evaluating the effects of the geomagnetic cutoff and detector acceptances on the observation data. The curves are to guide the eye.

provided that the CR spectra are determined at 1 AU. Furthermore, it can be adapted to employ different models of the magnetosphere with the respect to that currently used.

II. OBSERVATIONAL DATA AT 1 AU

In June 1998, AMS-01 collected data on board of the Space Shuttle Discovery (flight STS-91) at an altitude of ~ 380 km and with an inclination of 51.7° from the equatorial plane; the angular acceptance was a cone with an aperture of ~ 32° from the detector axis, which was mostly oriented towards the local zenith during the observation time (a survey of the apparatus and scientific results is available in (AMS Collaboration, 2002; 2000a; 2000b). During the 5–6 days of the data taking, AMS-01 observed ~ 10^7 protons with kinetic energy between $0.22<E_k<199.06$ GeV and ~ 10^6 α-particles with kinetic energy $0.074<E_k<113.61$ GeV/nucl.

The HEAO-3-C2 detector, on board of the HEAO-3 satellite launched in September 1979, measured the isotopic composition of the most abundant components of the CR flux with kinetic energies between 0.8 (0.62 for C) < E_k < 35 GeV/nucl., (relative) atomic masses between $7 \le A \le 56$, atomic numbers between $4 \le Z \le 50$ at an altitude of ~ 500 km and with an orbit inclination from

the equatorial plane of ~ 43.6° [21]. The acceptance cone of the HEAO-3-C2 detector was up to ~ 28° from the axis, which, in turn, was spinning around the direction pointing towards the Sun. The relative atomic mass (A) is the atomic mass in unified atomic mass units (u). It can be shown (e.g., see Sect. 3.1 of [31]) that for nuclides A. I_{isot}, where I_{isot} is the mass number, i.e., the number of nucleons of the nuclide.

For the present publication (Figure 1), we use the proton and helium data from AMS-01 observations during the solar cycle 23; carbon and iron data are from HEAO-3-C2 observations performed from October 1979 up to June 1980, i.e., during the solar cycle 21. In both periods the solar activity was rising from the minimum to the subsequent maximum and the solar magnetic-field polarity was positive. In addition, HEAO-3-2C data periods with Forbush decreases were excluded[21]. These spectra were recalculated at 1 AU (outside the magnetosphere) by evaluating the effects of the geomagnetic cutoff and detector acceptances on the observation data, following the procedures described in detail by [2],[3], [4], for protons and helium nuclides, and by [21] for carbon and iron nuclides.

The angular acceptance of the detectors, the altitude and the inclination of the orbits were such that the observations were obtained under almost similar experimental conditions. For instance, note that by inspecting the proton differential fluxes as function of the kinetic energy, collected with positive solar-polarity in 1998 by AMS-01 (AMS Collaboration, 2000a) and in August 1994 by CAPRICE [10], one can observe slight systematic variations only below ≈ 0.5 GeV (e.g., see Section 4.1.2.3 of [31]) for a further comparison among experimental data). In Figure 1 the differential (cosmic) fluxes of protons and helium nuclei are the primary spectra derived at 1 AU by AMS-01 collaboration (e.g., see AMS Collaboration, 2000b; 2000c; 2002) and those of carbon and iron nuclei reported in Sect. 5 of [21] using HEAO-3-C2 observations. The data of the (cosmic) helium fluxes were published as a function of the helium rigidity (see AMS Collaboration, 2000c; 2002) and recalculated as a function of the kinetic energy of primary ^{4}He nuclei for Figure 1. The slight contamination of ^{3}He in the primary helium nuclei is treated in [3], [4] and affects marginally such a distribution. Moreover, the Transmission Function (discussed in Sect. 3.2) of helium nuclei in the magnetosphere is derived as a function of the helium rigidity and applied to measured fluxes published as a function of the rigidity. The highest lower-limit of the kinetic energy per nucleon is that for Fe observation-data, i.e, ≈ 0.8 GeV/nucleon. Note that the value of 0.8 Gev/nucleon corresponds to the average kinetic-energy of nuclei in a bin energy with a lower limit of ≈ 0.7 GeV/nucleon and an upper limit of ≈ 0.91 Gev/nucleon. For C nuclei, the lowest kinetic-energy bin is from 0.55 up to 0.7 GeV/nucleon with an average value of 0.62 GeV/nucleon.

It has to be remarked that the spectral indexes appear to be different at large energies per nucleon, i.e., where the spectra become steeper (e.g., see Figure 1). Furthermore in the energy region below a few GeV/nucleon, the solar modulation affects the differential energy spectra and, thus, the spectral indexes exhibit some variations (e.g., see Figure 1), which are A-dependent.

II.a ABUNDANCES OUTSIDE THE MAGNETOSPHERE AT 1 AU

In Figure 2, the relative abundances to protons for He (He/p), C (C/p) and Fe (Fe/p) nuclei with the same kinetic energy per nucleon, Ek, are shown as function of Ek: for a kinetic energy of ≈ 0.8 GeV/nucleon, the value of He/p is ≈ 0.084, but ranges between ≈ 0.047–0.054 above ≈ 4.5 GeV/nucleon, while the values of C/p (Fe/p) range from ≈ 0.0021 (0.00017) down (up) to ≈ 0.0016 (0.00021). This lower limit of the kinetic energy per nucleon is that for to the observation data of the Fe nuclei, as discussed in Sect. 2. In addition as shown in Figure 4, this value almost corresponds to the minimal kinetic-energy transferred inside the magnetosphere for He, C and Fe nuclei in the magnetic region 7 (M7). These abundances were calculated using the observation data shown in Figure 1 for the He, C and Fe nuclei and an interpolated curve for the proton differential-flux spectrum. Note that the overall proton flux calculated with the interpolated curve differs from that obtained summing the experimentally observed fluxes in each kinetic-energy interval (Figure 1) by about 0.4% in the overall energy-range between 0.22 and 199.06 GeV. The overall flux above ≈ 0.8 GeV/nucleon is expected to be slightly increased by the non-observable energy component. Since for these spectra the spectral index is almost constant above ≈ 10 GeV/nucleon, it could be estimated that the largest correction, i.e. for the Fe integral flux, is lower than ≈ 0.8%.

The resulting relative abundances from fluxes of particles above . 0.8 GeV/nucl are $Y_{He/p}^{cos}$. $6.66 . 10^{-2}$, $Y_{C/p}^{cos}$. $1.88 . 10^{-3}$ and $Y_{Fe/p}^{cos}$. $1.78 . 10^{-4}$, respectively. These latter may differ from those which are derived using abundances at fixed values of kinetic energy per nucleon, large enough so that the particle is marginally affected by the solar modulation (e.g., see Figure 3 in [30] and Table 24.1 of [41] in particular, the value of He/p results larger since, as discussed above, up to a few GeV/nucleon its relative abundance is larger than that found at high energies. As a consequence, the

overall relative abundances at 1 AU may be affected by the solar modulation and differ from those expected in the interstellar space (e.g., for a discussion see [6] and references therein).

III. PROPAGATION OF GCR's INSIDE THE MAGNETOSPHERE

At 1 AU the so-called magnetosphere, created in the space region surrounding the Earth by the geomagnetic field and that one carried by the solar wind, provides a partial shield against the penetration of GCR's down to the Earth surface. Thus, the GCR's are primary cosmic-rays (PCR) reaching the Earth from the outer space. However the flux of PCR's is only a tiny fraction of the total particle flux observed at the Earth's surface or at Low Orbits around the Earth. A dominant flux of Secondary Cosmic Rays (SCR's) is generated by the interactions of PCR's with the atmosphere (e.g., see chapter 1 in [23] section 2.2.2 in [30] section 4.1.2.5 in [31]) and also references therein).

The transport of cosmic rays through the magnetosphere depends on the rigidity (P) of a charged particle with charge Ze, where e is the electronic charge, and momentum p, corresponding to a kinetic energy per nucleon E_k

$$P = pc/Ze$$

with c the speed of light. As discussed by[7] (see also references therein) and, for instance, [36], [22], [33] and Section 6.2.3.1 in [26], the rigidity of geomagnetic cut-off (Pcut) varies as a function of the observation location and increases with decreasing the geomagnetic latitude. Besides, all nuclei are positively charged, therefore, due to the Earth magnetic field structure, some incoming directions are preferred (this effect is at the origin of the East-West anisotropy). Primary cosmic rays (PCR) with rigidities lower than the local value of Pcut cannot reach that observation region. Furthermore, the rigidity spectrum of secondary protons exhibits a bump close to the local value of Pcut, i.e., inside the so-called penumbra region, where only primary protons are expected [19], [9].

As discussed in Section 2.2.2 of (Leroy and Rancoita, 2007) since the proton (m_p) and nucleon (m_{nucl}) masses are approximately equal (e.g., see Section 3.1 in Leroy and Rancoita, 2008), the rigidity of an isotope heavier than proton with kinetic energy per nucleon E_k is given by

$$P_{isot} = (I_{isot}/Ze).[E_k.(E_k + 2m_{nucl}.c^2)]^{1/2} \approx I_{isot}.P_H/Z \qquad (1)$$

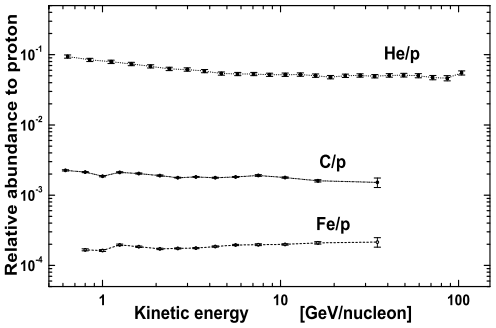

Fig. 2. Relative abundance of He, C and Fe nuclei to proton as a function of the kinetic energy in units of GeV/nucleon, above 0.8 GeV/nucleon. The data for p and He nuclei are from (Alcaraz et al., 2000b; 2000c; Aguilar et al., 2002), for C and Fe from Engelmann et al. (1990). The curves are to guide the eye.

where P_H is the proton rigidity with the same kinetic energy E_k, Z and I_{isot} are the atomic number and the number of nucleons (i.e., the mass number) of the isotope, respectively. In Eq. (1), the ratio Iisot/Z for the most abundant stable isotopes (i.e., up to nickel, see section 2.2 of [30] ranges from 2.0 up to ≈ 2.3 with the exception of ^{3}He for which it is 1.5. As a consequence from an inspection of Eq. (1), less energetic (but heavier than proton) PCRs can penetrate deeply the magnetosphere: in any location, the associated geomagnetic cut-off rigidity, Pcut, requires a kinetic energy of the isotope lower than that of a proton and, thus, the isotopic abundances relative to protons are expected to be larger inside the magnetosphere than those at 1 AU, but outside it, and discussed in Sect. 2.1. [9] described the passage of primary protons through the magnetosphere to the atmosphere by the so-called Transmission Function (TF), which was determined by back-tracking the proton trajectories to determine those allowed to primaries. The TF allowed one to reproduce the observed AMS-01 data on the Shuttle Orbiter Discovery using the AMS-01 primary proton spectrum at 1 AU, i.e., at the Earth location inside the heliosphere but outside the magnetosphere. In this article, a similar approach is followed for calculating the TF's (Sect. 3.2) of He, C and Fe nuclei discussed in Sect. II.

III.a MAGNETOSPHERE AND AMS-01 GEOMAGNETIC REGIONS

To first approximation, the magnetic field close to the Earth surface has a dipole shape, but moving outwards other contributes become

important. Among these we can mention: the

several currents (ring current, Birkeland currents and tail currents) due to charged particles trapped inside the magnetosphere, the effect of the reconnection of the interplanetary magnetic field (few nT) and the geomagnetic field at the magnetopause. Moreover the latitudinal dependence is not geographically symmetric, because the Earth magnetic dipole is tilted with respect to the Earth's rotation axis and shifted from the Earth's center. In addition, the geomagnetic equator is located on a tilted surface, which is slowly moving with time in relation to the locations of the magnetic poles.

The AMS-01 proton data [2] refer to the ten geomagnetic regions (see Table 1), M; the He data [3] to the three super-regions indicated with SM in Table 1. As already mentioned, the observation period was June 1998. These regions (M and SM) are defined by means of the Corrected Geomagnetic Coordinates [11]. CGM coordinates (latitude and longitude) of a point in space are computed by tracing the internal geomagnetic field line through the specified point to the dipole geomagnetic equator, then returning to the same altitude along the dipole field line and assigning the obtained dipole latitude and longitude as the CGM coordinates to the starting point. It is described by the IGRF model, i.e. the DGRF 2000–2005 model, see [5], [24] and references therein; see also Sect. 3.2.

III.b TRANSMISSION FUNCTION AND AMS-01 He-DATA

As discussed in Appendix A by [9], the magnetic field of the Earth's magnetosphere is described using i) the International Geomagnetic Reference Field (IGRF) 2000–2005 [5] for representing the main contribution due to the inner Earth and ii) the external magnetic field model implemented by Tsyganenko and Stern (called T96-model, see [38], [39]) for representing the other current contributions in the magnetosphere.

The International Geomagnetic Reference Field (IGRF) model is the empirical representation of the Earth's magnetic field recommended for scientific use by the International Association of Geomagnetism and Aeronomy (IAGA) (e.g., see[24]). As already mentioned, the IGRF model is employed to evaluate the main (core) field without external sources and consists of a series of mathematical models describing the Earth's main field and its secular variation.

In the region inside the magnetopause, the T96-model calculates the external magnetic field in every point of the space out to 70 Re in magnetosphere tail (where Re is the radius of the Earth). This field component is generated by charged particles circulating outside the solid Earth body. The external field component takes into account the interaction with the solar wind. The more complex morphology of the field and the variability of the solar activity make this one as the critical component. The model includes the following implementations: the position and the shape of the magnetopause, the boundary surface of the magnetosphere, is explicitly defined; the magnetic field of the region around the magnetopause is also considered; the interconnection of the Earth magnetosphere to the solar wind field at the boundary is taken into account too; furthermore the magnetic fields generated by the regions 1 and 2 of Birkeland currents, by the ring current, and by the tail current are added. The Earth's magnetopause is calculated using the Sibeck equation (Sibeck et al. (1991)) modified by Tsyganenko (Tsyganenko (1995)) for the solar wind effect. We have introduced an empirical magnetosphere boundary large 25 Re in the night-side region to avoid long calculations in the far tail.

Table I. Geomagnetic regions covered by AMS-01 (see AMS Collaboration, 2000a; 200b; 2002). The individual magnetic regions (M) and super-regions (SM) are defined according to the corrected geomagnetic latitude (CGM).

Region (M)	Super-Region (SM)	CGM latitude θ_M
1	a	$\lvert\theta_M\rvert \le 0.2$
2	a	$0.2 \le \lvert\theta_M\rvert \le 0.3$
3	a	$0.3 \le \lvert\theta_M\rvert \le 0.4$
4	b	$0.4 \le \lvert\theta_M\rvert \le 0.5$
5	b	$0.5 \le \lvert\theta_M\rvert \le 0.6$
6	b	$0.6 \le \lvert\theta_M\rvert \le 0.7$
7	b	$0.7 \le \lvert\theta_M\rvert \le 0.8$
8	c	$0.8 \le \lvert\theta_M\rvert \le 0.9$
9	c	$0.9 \le \lvert\theta_M\rvert \le 1.0$
10	c	$1.0 \le \lvert\theta_M\rvert$

Access for PCR to some place is supposed to be allowed when the back-traced particle trajectory reaches the magnetopause or the magnetospheric boundary. As internal boundary we have considered a sphere at an altitude of 40 km, corresponding to the surface containing the 99% of the Earth atmosphere. Thus using the time-dependent code discussed in Appendix A of [9], the TF requires the determination of the so-called allowed trajectories of the particles entering the AMS-01 or HEAO-3 spectrometers, following a

back-tracking procedure. The locations (3600) of the particles to be back-tracked are distributed uniformly over a complete sphere surrounding the Earth at an altitude of 400 km, excluding the South-Atlantic anomaly region (i.e. the region with latitude between -55° and 0° and with longitude between -80° and 20°). Charged particles are generated at the position of the space detectors AMS-01. They are back-tracked in time until they reach one of the two boundaries: the magnetopause/magnetosphere boundary or the atmosphere. Some reconstructed trajectories are terminated after a selected number of steps to avoid long calculations for the trajectories of trapped particles. In the first case the particles are considered to be primary CR, otherwise secondary CR. The external field is evaluated taking into account the parameters changing with the solar activity. Those parameters are evaluated at the time of the data taking of the two experiments.

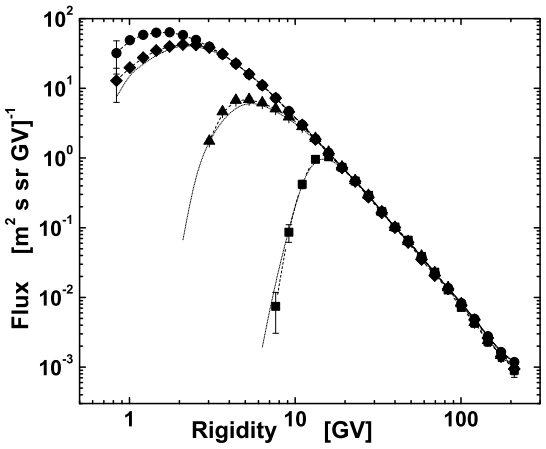

Fig. 3. Fluxes of He nuclei inside the magnetosphere. Values obtained using Eq. (4) (short-dots lines) are compared with AMS-01 data (symbols) for the three Super-Regions: SMa (squares), SMb (triangles) and SMc (diamonds). The full-circles data are those at 1 AU outside the magnetosphere.

Initially, for the He-data of AMS-01 experiment, the particle directions (270) are isotropically distributed within the outward hemisphere and inside the 32° acceptance cone (around the local geocentric Zenith) of the AMS-01 spectrometer. The TF was computed for the same 31 rigidity intervals of the AMS01 data (see Table 1 of paper by AMS Collaboration (2000c)), i.e. the lowest rigidity bin is about 0.76–0.91 GV and the highest about 190.55–229.09 GV. Within the acceptance cone of the AMS-01 spectrometer, about 2.3×10^8 particle trajectories were reconstructed. For the three geomagnetic super-regions, the TFSM has been averaged over all uniformly distributed geographic-locations and weighted to take into account the observation time spent in each region by the flying detector:

$$TF_{SM}(P_{b,He}) = \frac{\sum_{i_{SM}} TF_{SM}(P_{b,He,i_{SM}})}{\sum i_{SM}} \qquad (2)$$

where $P_{b,He}$ is the He rigidity in the b-th rigidity interval of width $\Delta P_{b,He}$, $TF_{SM}(P_{b,He})$ is the transmission function for the position i_{SM} inside the geomagnetic region SM and $\sum i_{SM}$ is the total number of locations for the same region. For the location i_{SM} the $TF_{SM}(P_{b,He})$ is given by:

$$TF_{SM}(P_{b,He,i_{SM}}) = \frac{N_{all}^{i_{SM}}}{N_{total}^{i_{SM}}} \quad (3)$$

Where $N_{all}^{i_{SM}}(P_{b,He,i_{SM}})$ is the number of allowed trajectories and the total (allowed and forbidden) number of computed trajectories is $N_{total}^{i_{SM}}(P_{b,He,i_{SM}}) = N_{all}^{i_{SM}}(P_{b,He,i_{SM}}) + N_{forb}^{i_{SM}}(P_{b,He,i_{SM}})$. The ratio $TF_{SM}(P_{b,He,i_{SM}})$ represents the probability that particles with rigidity $P_{b,He}$ reach the geographic position i_{SM} coming from outside the magnetosphere. Then, for every geomagnetic super-region, SM, the averaged ratio $TF_{SM}(P_{b,He})$ over all the positions i_{SM} expresses the transmission function for a particle with rigidity $P_{b,He}$ to reach that geomagnetic super-region SM, at the altitude of AMS. Each starting position and direction has been chosen in order to have a uniformly distributed sample.

Following the procedure already discussed by Bobik et al. (2006), in each super-region SM the primary flux $\Phi_{SM}^{pri}(P_{b,He,i_{SM}})$ of He-particles with rigidity $P_{b,He}$ can be evaluated using the cosmic ray flux $\Phi^{\cos}(P_{b,He})$ from Table 1 of the paper by Alcaraz et al. (2000c):

$$\Phi_{SM}^{pri}(P_{b,He,i_{SM}}) = \Phi^{\cos}(P_{b,He}).TF_{SM}(P_{b,He,i_{SM}}) \quad (4)$$

The experimental He-fluxes measured by AMS-01 and those calculated using Eq. (4) are in good agreement and are shown in Figure 3.

III.c TRANSMISSION FUNCTIONS AND FLUXES INSIDE THE M-REGIONS

Using the procedure described in Sect. 3.2, the TF's for p, He, C and Fe nuclei were computed for the ten geomagnetic regions M (see Table 1) at

an altitude of 400 km and inside a 28° acceptance cone (around the local geocentric Zenith), i.e., the HEAO-3 acceptance cone which was the smallest of the two spectrometers. For protons (as for helium) the simulated particles were 2.3×10^{8}, for C and Fe nuclei 10^{7}. Note that in paper by Bobik et al. (2006), the TF for protons was computed for the AMS-01 acceptance cone. The TF's are shown in Figure 4 for the three regions M1, M4 and M7 as function of the kinetic energy in GeV for protons and the kinetic energy in GeV/nucleon for He, C and Fe nuclei.

Since the TF's are evaluated using the particle rigidities, the corresponding kinetic energies were computed assuming a negligible ^{3}He contamination in the He-flux of AMS-01 observations (e.g., see Sect. II and footnote 2) and, similarly, C and Fe fluxes consisting mainly of ^{12}C and ^{56}Fe isotopes. The TF becomes 0, when incoming PCR's cannot reach the observation location any more, thus the particle rigidity

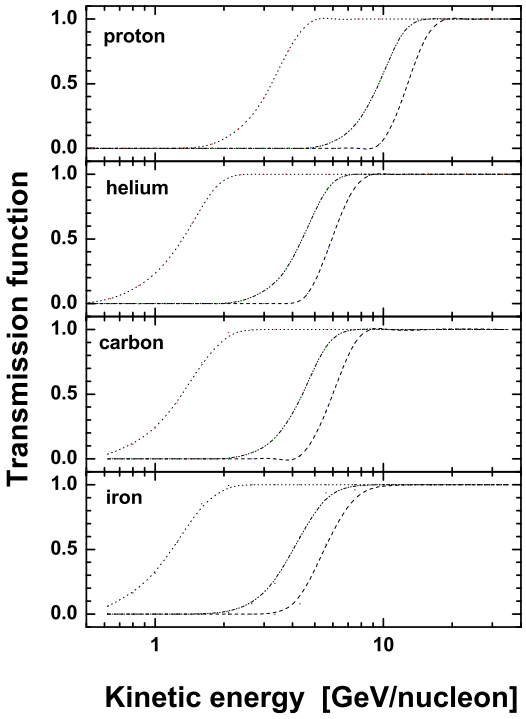

Fig. 4. Transmission Function of p, He, C and Fe for the geomagnetic regions M1 (dot line), M4 (dash-dot-dot line) and M7 (dash line).

is lower than the local rigidity of geomagnetic cut-off (Pcut). It is 1 when the full flux of PCR's can reach that location. The penumbra region corresponds to TF-values larger than 0 and lower than 1. The geomagnetic cut-off rigidity almost similarly affects the propagation of p, He, C and Fe nuclei inside the magnetosphere, but as already discussed, for nuclei the corresponding kinetic energy per nucleon depends on the I_{isot}/Z ratio [Eq. (1)].

In Figure 4, it can be observed the expected shift of the kinetic energies per nucleon, at which the TF becomes 0 or 1 with respect to the kinetic energies for protons. As already mentioned, this effect arises because the ratio I_{isot}/Z . 2 for the most abundant nuclei in GCR's (e.g., see Section 2.2 of [30] and references therein), except for protons for which this ratio is 1. In fact, the transition to a complete propagation inside the magnetosphere (i.e., TFM = 1) occurs at larger energies for protons with respect to those for isotopes with atomic number $Z \geq 2$ (Figure 4). Furthermore, He, C and Fe nuclei with kinetic energies ≈ 0.8 GeV/nucleon can penetrate the Earth's magnetosphere up the region M7. In the geomagnetic region M7, at . 0.8 GeV/nucl the TF is . 0.14, 0.11 and 0.16 for He, C and Fe nuclei (see Figure 4). As a consequence, for observation data with kinetic energies larger than ≈ 0.8 GeV/nucleon (i.e, that corresponding to lower limit for Fe observation data, as discussed in Sect. 2), only the TF's for the magnetic regions M1–M7 can be determined for all nuclei, i.e., including iron.

Using those so calculated TF's, the PCR's fluxes at an altitude of 400 km are obtained from the AMS-01 cosmic flux (i.e., at 1 AU) for p and He and HEAO-3-C2 flux for C and Fe. If $TF_M(E_k)$ is the transmission function for a particle with kinetic-energy (per nucleon) E_k, the primary flux $\Phi_M^{pri}(E_k)$ in the region M is given by

$$\Phi_M^{pri} = \Phi^{\cos}(E_k).TF_M(E_k) \qquad (5)$$

where $\Phi^{\cos}(E_k)$ is the cosmic ray flux of particles with kinetic energy per nucleon Ek.

In Figure 5 the fluxes of p, He, C and Fe nuclei are shown for the regions M1 and M7, as an example.

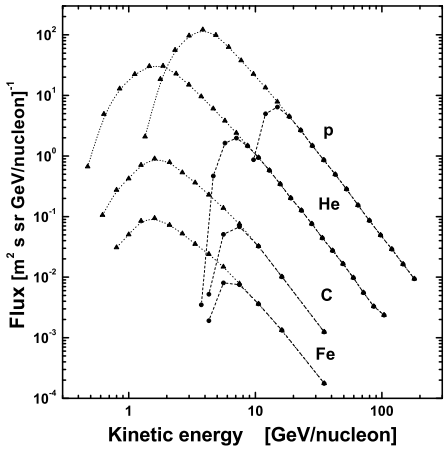

Fig. 5. Flux of primaries p, He, C and Fe, in the geomagnetic regions M1 (circles), and M7 (triangles). The lines are to guide the eye.

The above computed TFs are valid for quiet time conditions. During the strong geomagnetic disturbances their values can be obtained using various geomagnetic field models providing different predictions of transmissivity [28].

III.d RELATIVE ABUDANCES INSIDE THE MAGNETOSPHERE

In the seven magnetic regions (M) for which the TF can be properly calculated, the abundances of PCR's relative to proton are determined using the promary fluxes in Eq. (5) as:

$$\Re_{He/p}(M) = \frac{\int \Phi^{pri}_{M,He}(E'_k)dE'_k}{\int \Phi^{pri}_{M,p}(E'_k)dE'_k} \qquad (6)$$

$$\Re_{C/p}(M) = \frac{\int \Phi^{pri}_{M,C}(E'_k)dE'_k}{\int \Phi^{pri}_{M,p}(E'_k)dE'_k} \qquad (7)$$

$$\Re_{Fe/p}(M) = \frac{\int \Phi^{pri}_{M,Fe}(E'_k)dE'_k}{\int \Phi^{pri}_{M,p}(E'_k)dE'_k} \qquad (8)$$

Note that $\Phi^{pri}_{M}(E'_k) = 0$ below the penumbra region in each geomagnetic region M, i.e. , for $TF_M(E_k) = 0$ as discussed in section 3.3.

As already mentioned in Sect. 2, the high energy component of the isotopic spectra contributes to the integral flux by less than 0.8% in case of iron (i.e., where such a correction is largest). However, the effect of the geomagnetic cut-off rigidity depletes the particle flux with increasing the geomagnetic latitudes. Thus the correction due to the high energy component may become more relevant and, as already mentioned (Sect. 2.1), it can be estimated assuming that for these spectra the spectral indexes are almost constant above ≈ 10 GeV/nucleon. The resulting corrections are ≈ 0.8, 0.8, 3.9 and 7.7% for the proton, He, C and Fe fluxes in the geomagnetic region M1, where they are the largest. These corrections are taken into account in determining the ratios $\Re_{He/p}$, $\Re_{C/p}$, $\Re_{Fe/p}$ shown in Table II.

It has to be remarked that, in particular for the geomagnetic region M7, the TF allows Fe nuclei with kinetic energy per nucleon slightly lower than 0.8 GeV/nucleon to penetrate inside the magnetosphere (e.g., see Figure 4), but HEAO-3-C2 observation data were collected for Fe nuclei with average kinetic-energies per nuclei larger than 0.8 GeV/nucleon for the lowest energy-bin (Sect. 2).

However in the region M7, $\Re_{He/p}$ and $\Re_{C/p}$ are decreased with respect to those reported in Table II by about (0.7–0.8)%, when the fluxes only account for particles with kinetic energies larger than 0.7 GeV/nucleon, which corresponds to the lower limit of that observed for Fe nuclei.

Table II. Relative abundance ratios, $\Re$, and the abundance enhancements, Δ, for the geomagnetic regions M1 to M7.

	$\Re_{He/p}$	$\Delta_{He/p}$
M1	$1.59.10^{-1}$	2.39
M2	$1.60.10^{-1}$	2.40
M3	$1.55.10^{-1}$	2.33
M4	$1.49.10^{-1}$	2.24
M5	$1.61.10^{-1}$	2.42
M6	$1.56.10^{-1}$	2.34
M7	$1.37.10^{-1}$	2.06
	$\Re_{C/p}$	$\Delta_{C/p}$
M1	$5.56.10^{-3}$	2.96
M2	$5.43.10^{-3}$	2.89
M3	$5.39.10^{-3}$	2.87
M4	$5.09.10^{-3}$	2.71
M5	$5.13.10^{-3}$	2.73
M6	$4.88.10^{-3}$	2.60
M7	$4.09.10^{-3}$	2.18
	$\Re_{Fe/p}$	$\Delta_{Fe/p}$
M1	$6.52.10^{-4}$	3.66
M2	$6.58.10^{-4}$	3.70
M3	$6.65.10^{-4}$	3.74
M4	$6.00.10^{-4}$	3.37
M5	$6.26.10^{-4}$	3.52
M6	$5.40.10^{-4}$	3.03
M7	$4.30.10^{-4}$	2.42

Thus, although the fluxes of particles are large for particle with kinetic energies lower than ≈ 1 GeV/nucleon (Figure 1), the resulting lower value of $\Re_{Fe/p}$ in the geomagnetic region M7 with respect to that up to M6 is expected to be marginally affected by the threshold kinetic energy of the observation data.

The ratios $\Re(M)$ and the enhancement factors $\Delta(M) = \frac{\Re(M)}{\Re^{\cos}}$, where the values of $\Re^{\cos}$ were derived in section 2.1, are shown in Table II for geomagnetic regions M1 – M7. The enhancements factors account for the increase of isotopic abundances inside the magnetosphere with respect to the modulated values outside it at 1 AU. From an inspection of Table II, it is possible to note that the ratios $\Delta(M)$ i) depend on the mass number I_{isot}, ii) range from ≈ 2.06 up to ≈ 3.74 in

the seven investigated geomagnetic regions and, finally, iii) exhibit a slight dependence on the geomagnetic latitude of up the geomagnetic region M7: in the first six regions varies from the average by less than ± 4.8, 6.9 and 13.5% for He/p, C/p and Fe/p, respectively. On average in the seven geomagnetic regions, the enhancements factors are ≈ 2.31, ≈ 2.71 and ≈ 3.35 for He/p, C/p and Fe/p, respectively. These factors also account for the variation of the ratio I_{isot}/Z with the mass number and the overall behavior of the spectral indexes with the kinetic energy for the modulated spectra.

IV. CONCLUSIONS

At 1 AU and outside the Earth's magnetosphere, the relative abundances to protons for He (He/p), C (C/p) and Fe (Fe/p) nuclei were calculated using the observation-data of AMS-01 (for p and He) and HEAO-3 (for C and Fe) above 0.8 GeV/nucleon. The relative abundances account for the modulation of GCR's inside the heliosphere and are $\Re^{\cos}_{He/p} \approx 6.66 \cdot 10^{-2}$, $\Re^{\cos}_{C/p} \approx 1.88 \cdot 10^{-3}$ and $\Re^{\cos}_{Fe/p} \approx 1.78 \cdot 10^{-4}$ for He/p, C/p and Fe/p, respectively. These values may differ from those which are derived using abundances at fixed values of kinetic energy per nucleon, large enough so that particles are marginally affected by the solar modulation.

The penetration depth of PCR's inside the magnetosphere depends on their rigidity and observation location, thus on the geomagnetic cut-off rigidity. The rigidity almost similarly affects the propagation of p, He, C and Fe nuclei through the magnetosphere, but for nuclei the corresponding kinetic energy per nucleon depends on the Iisot/Z ratio which differs by a factor almost 2 from that of protons. As a consequence, the relative isotopic abundances with respect to protons are expected to be modified with respect to those at 1 AU but outside the magnetosphere.

An approach using the back-tracking of simulated particles was used to define the probability, i.e. the transmission function, that a primary proton, helium, carbon and iron nucleus can reach the magnetopause from the observation location. Consequently, it has allowed one to describe the transport properties of the PCR's to the geomagnetic regions of the AMS-01 observations (at an altitude of about 400 km) from the upper limit of the geomagnetic field, i.e. the magnetopause.

The fluxes of primary He-nuclei calculated by means of the so derived transmission functions exhibit a good agreement with the spectra observed in three magnetic (super-) regions by AMS-01 experiments. Furthermore, the relative abundances and their ratios with those outside the magnetosphere at 1 AU (called enhancement factors) were also computed for the magnetic regions up to M7. For geomagnetic latitudes ranging from $\approx -45.84^{\circ}$ up to $\approx 45.84^{\circ}$, the enhancement factors, accounting for the variation of the relative isotopic abundances, depend on the mass number Iisot and, on average, range from ≈ 2.31 up to ≈ 3.35. Thus, the magnetospheric isotopic relative-abundances result to be modified because the proton component is more depleted than the other isotopic components of GCR's and differ from those inside the solar cavity and those in the interstellar space.

It has to be remarked that, for any acceptance angle, the usage of the TF approach can allow one to determine the isotopic/nuclear abundances in the magnetosphere at any geomagnetic latitude and, thus, any orbit, provided that the CR spectra are determined at 1 AU.

ACKNOWLEDGEMENTS

KK wishes to acknowledge that this work was supported by the Slovak Grant Agency VEGA, project no. 2/7063/27 and by the Slovak Research and Development Agency under the contract no. APVV-51-053805.

REFERENCES

[1] Alcaraz, J., Alvisi, D., Alpat, B. et al. Protons in Near Earth Orbit. Phys. Lett. B 472, 215-226, 2000a.

[2] Alcaraz, J., Alpat, B. Ambrosi, G. et al. Cosmic Protons. Phys. Lett. B, 490, 27-35, 2000b.

[3] Alcaraz, J., Alpat, B. Ambrosi, G. et al. Helium in Near Earth Orbit. Phys. Lett. B., 494, 193-202, 2000c.

[4] Aguilar, M., Alcaraz, J., Allaby, J. et al. The Alpha Magnetic Spectrometer (AMS) on the International Space Station, Part I, Results from the test flight on the Space Shuttle. Phys. Reports. 366, 331-405, 2002.

[5] Barton, C.E. International Geomagnetic Reference Field: The Seventh Generation, J. Geomag. Geoelectr., 49, 123-148, 1997.

[6] Beliaev, A.A., Nymmik, R.A., Panasyuk, et al. Local interstellar spectra of galactic cosmic rays according to particle flux analysis, J. Rad. Measur., 26 (no. 3), 481-485, 1996

[7] Bobik, P., Boschini, M.J., Gervasi, M., et al. A Back-Tracing Code To Study The Evolution of the Magnetosphere Transmission Function for Primary Cosmic Rays in The Inner Magnetosphere: Physics and Modeling, Proc. of the Chapman Conference (25-29 August 2003, Helsinki, Finland), Editors T.I., Pulkkinen, N.A., Tsyganenko and R.H.W., Friedel, American Geophysical Union (AGU), Washington D.C., Geophysical Monograph Series, Volume 155, ISBN 0-87590420-3, 301-305, 2005a

[8] Bobik, P., Boschini, M.J., Gervasi, M., et al. Magnetospheric transmission function to separate near earth primary and secondary cosmic rays, Int. J. of Modern Phys. A, 20, 6678-6680, doi:10.1142/S0217751X05029782, 2005b

[9] Bobik, P., Boella, G., Boschini, M.J., et al. Magnetospheric transmission function approach to disentangle primary from secondary cosmic ray fluxes in the penumbra region, J. Geophys. Res., 111, A05205, doi:10.1029/2005JA011235, 2006

[10] Boezio, M., Carlson, P., Frabcke, T., et al. The Cosmic-Ray Proton and Helium Spectra between 0.4 and 200 GV, Astrophys. J. 518, 457-472, 1999.
[11] CGM (2005). Web site: http://nssdc.gsfc.nasa.gov/space/cgm/cgm.html
[12] Chenette, D.L., Chen, J., Clayton, E., et al. The CRRES/SPACERAD heavy ion model of the environment (CHIME) for cosmic ray and solar particle effects on electronic and biological systems in space. IEEE Transactions on Nuclear Science 41 6, 2332.
[13] Colder, A., Croitoru, N., D'Angelo, P., et al. Study of Radiation Effects on Bipolar Transistors, Nucl. Instr. and Meth. in Phys. Res. B, 179, 397-402, doi:10.1016/S0168-583X(01)00582-1, 2001.
[14] Colder, A., Croitoru, N., D'Angelo, P., et al. Study of Radiation (neutron, -ray, and carbon-iron) Effects on npn Bipolar Transistors, Proc. of the 7th ICATPP, Como 15-19 October 2001, World Scientific (Singapore), 780-786, 2002a.
[15] Colder, A., Croitoru, N., D'Angelo, P., et al. Effects of ionizing radiation on BiCMOS components for space application, Proc. of the European Space Component Conference, Toulouse 24-27 September 2002, ESA SP-507, p. 377-381, 2002b.
[16] Codegoni, D., Colder, A., Croitoru, N. et al. Radiation Effects on Bipolar and MOS Transistors Made in BiCMOS Technology, Proc. of the 8th ICATPP (6–10 October 2003, Como, Italy), ISBN 981-238-860-5, World Scientific, Singapore, 622, 2004a.
[17] Codegoni, D., Colder, A., Croitoru, N. et al. Investigation of irradiated monolithic transistors for space applications. Nucl. Instr. and Meth. in Phys. Res. B, 217, 65-76, doi:10.1016/j.nimb.2003.08.044, 2004b
[18] Consolandi, C., D'Angelo, P., Fallica, G., et al. Systematic investigation of monolithic bipolar transistors irradiated with neutrons, heavy ions and electrons for space applications, Nucl. Instr. and Meth. in Phys. Res. B, 252, 276-284, doi:10.1016/j.nimb.2006.08.018, 2006
[19] Cooke, D.J., Humble, J.E., Shea, M.A., et al. On Cosmic-Ray Cut-off Terminology, Il Nuovo Cimento, 14C, 213-234, 1991.
[20] Engelmann, J.J., Goret, P., Julinsson, E. et al. Source energy spectra of heavy cosmic ray nuclei as derived from the French-Danish experiment on HEAO-3, Astron. and Astrophys., 148, 12-21, 1985
[21] Engelmann, J.J. Charge composition and energy spectra of cosmic-ray nuclei for elements from Be to NI -Results from HEAO-3-C2, Astron. and Astrophys., 233, 96- 111, 1990.
[22] Fermi, E. Nuclear Physics, Univ. of Chicago Press, Chicago, 1950.
[23] Grieder, P.K.F. Cosmic Rays at Earth, Elsevier, Amsterdam, 2001.
[24] IGRF. Web site: http://nssdc.gsfc.nasa.gov/space/model/magnetos/igrf.html , 2005.
[25] ISO-19390. Space Environment (Natural and Artificial)–Galactic Cosmic Ray Model, Ref. no. ISO 15390, 2004.
[26] Knecht, D.J. and Shuman, B.M. The Geomagneic Field, Chapter 4 of Handbook of Geophysics and the Space Environment, Edited by Jursa, A.S., Air Force Geophysics Lab., Springfield, 1985.
[27] Kudela, K. and I. G. Usoskin. On Magnetospheric Transmissivity of Cosmic Rays, Czech. J. Physics, Volume 54, Number 2, February 2004 , pp. 239-254(16), 2004.
[28] Kudela, K., Bučík, R. and Bobik, P. On transmissivity of low energy cosmic rays in disturbed magnetosphere, Advances in Space Research, 42, 1300-1306, 2008.
[29] Leroy, C. and Rancoita ,P.-G. Physics of cascading shower generation and propagation in matter: principles of high-energy, ultrahigh-energy and compensating calorimetry, Rep. Prog. in Phys., 63, no. 4, 505–606, doi:10.1088/0034-4885/63/4/202, 2000.
[30] Leroy, C. and Rancoita, P.-G. Particle Interaction and Displacement Damage in Silicon Devices operated in Radiation Environments, Rep. Prog. in Phys., 70, no. 4, 403–625, doi:10.1088/00344885/70/4/R01, 2007.
[31] Leroy, C. and Rancoita, P.-G. Principles of Radiation Interaction in Matter and Detection (2nd Edition), World Scientific, Singapore, ISBN 978-981-281-827-0, 2008.
[32] Mewaldt, R.A. Galactic cosmic ray composition and energy spectra, Adv. Space Res. 14, 737-747 , 1994.
[33] Shea, M.A., Smart, D.F. and McCracken, K.G. A study of vertical cutoff rigidities using six degree simulations of the geomagnetic field, J. Geophys. Res., 70 (17), 4117-4130, 1965.
[34] Sibeck, D.G., Lopez, R.E. and Roelof, E.C. Solar wind control of the magnetopause shape, location, and motion, J. Geophys. Res., 96, A4, 5489-5495, 1991.
[35] Stanev, T. High Energy Cosmic Rays, Springer-Praxis, Berlin, 2004.
[36] Stoermer, K. Periodische Elektronenbahnen im Felde eines Elementarmagneten und ihre Anwendung auf Brches Modellversuche und auf Eschenhagens Elementarwellen des Erdmagnetismus. Mit 32 Abbildungen., Z. Astroph., 1, 237-274, 1930.
[37] Tsyganenko, N.A. A Magnetospheric Magnetic Field Model with a Warped Tail Current Sheet, Planet. Space Sci. 37, 5-20, 1989.
[38] Tsyganenko, N.A. Modeling the Earth's magnetospheric magnetic field confined within a realistic magnetopause, J. Geophys. Res., 100, 5599-5612, 1995.
[39] Tsyganenko, N.A. and Stern, D.P. Modeling the global magnetic field of the large-scale Birkeland current systems, J. Geophys. Res., 101, 27187-27198, 1996.
[40] Tylka, A.J., Adams, J.H. Jr., Boberg, P.R. et al. CREME96: A Revision of the Cosmic Ray Effects on Micro-Electronics Code, IEEE Transactions on Nuclear Science, 44, 2150-2160, 1997.
[41] Yao, W.-M., Amsler, C., Asner, D. et al. Review of Particle Physics, J. Phys. G, 33, 1-1232,2006.

Metric Radio Bursts and Fine Structures Observed on 17 January 2005

C. Bouratzis[1], P. Preka-Papadema[1], X. Moussas[1], C. Alissandrakis[2], and A. Hillaris[1]

[1] *Department of Physics, University of Athens, GR-15784 Athens, Greece,*
[2] *Department of Physics, University of Ioannina, 45110 Ioannina, Greece*

***Abstract* — A complex radio event was observed on January 17, 2005 with the radio-spectrograph ARTEMIS-IV, at Thermopylae, Greece; it was associated with an X3.8 SXR flare and two fast Halo CMEs in close succession. We present dynamic spectra of this event; the high time resolution (1/100 sec) of our data in the 450--270 MHz range, makes possible the detection and analysis of the fine structure which this major radio event exhibits. This fine structure, within the metric range, was found to match, almost, the comprehensive Ondrejov Catalogue in the 0.8-2.0 GHz range.**

***Key Words*—Sun: Solar flares, Sun: Radio emission, Sun: Fine Structure**

I. INTRODUCTION

RADIO emissions at metric and longer waves trace disturbances, mainly electron beams and shock waves, formed in the process of energy release and magnetic restructuring of the corona and propagating from the low corona to interplanetary space. The fine structures, on the other hand, including drifting pulsation structures, may be used as powerful diagnostics of the loop evolution of solar flares.

The intense activity from 14 to 20 January 2005 originated in active regions 720 and 718; they produced 5 X-class and 17 M-class flares [1] in the visible hemisphere of the sun.

January the 17th is characterized by an X3.8 SXR flare from 06:59 UT to 10:07 UT (maximum at 09:52 UT) and two fast Halo CMEs within a forty minute interval. The corresponding radio event included an extended broadband continuum with rich fine structure; this fine structure is examined in this report.

II. OBSERVATIONS

A. Instrumentation

The ARTEMIS-IV (**A**ppareil de **R**outine pour le **T**raitement et l' **E**nregistrement **M**agnetique de l' **I**nformation **S**pectral) solar radio-spectrograph operating at Thermopylae since 1996 ([2], [3]) consists of a 7-m parabolic antenna covering the metric range; a dipole antenna was added recently in order to cover the decametric range. Two receivers operate in parallel, a sweep frequency analyzer (ASG) in the 650-20 MHz range at 10samples/sec and a high sensitivity multi-channel acousto-optical analyzer (SAO), in the 270-450 MHz range at 100samples/sec. Events observed with ARTEMIS-IV have been described,

in [1], [4], [5], [6], [7], [8], cf. also [9] for a brief review.

The broad band, medium time resolution recordings of the ASG are used for the detection and analysis of radio emission from the base of the corona to two R_{SUN}, while the narrow band, high time resolution SAO recordings are used in the analysis of the fine temporal and spectral structures.

B. The event of January 17, 2005–Overview

Two groups of type III bursts and a very extensive type IV continuum with rich fine structure characterize the ARTEMIS–IV dynamic spectrum. The high frequency type IV emission starts at 08:53 UT, covers the entire 650-20MHz spectral range (Figure 1, upper & middle panels) and continues well after 15:00; it was associated with an SXR flare and two fast Halo CMEs (CME_1 & CME_2 henceforward) in close succession.

The GOES records (http://www.sel.noaa.gov\ftpmenu) report an X3.8 SXR flare from 06:59 UT to 10:07 UT, with maximum at 09:52 UT; this is well associated with the brightening of sheared S-shaped loops from the EIT

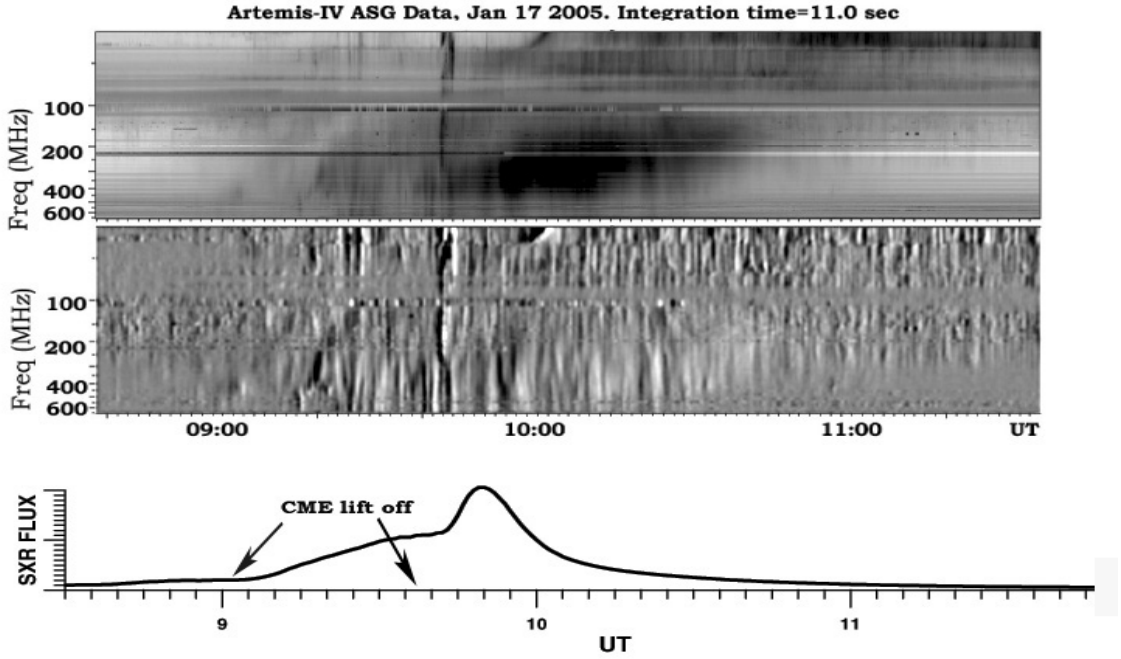

Fig. 1.: ARTEMIS IV Dynamic Spectrum (08:40-11:30 UT). UPPER PANEL: ASG Spectrum, MIDDLE PANEL: ASG Differential Spectrum, LOWER PANEL: GOES SXR flux (arbitrary units); the two CME lift–offs are marked on the time axis.

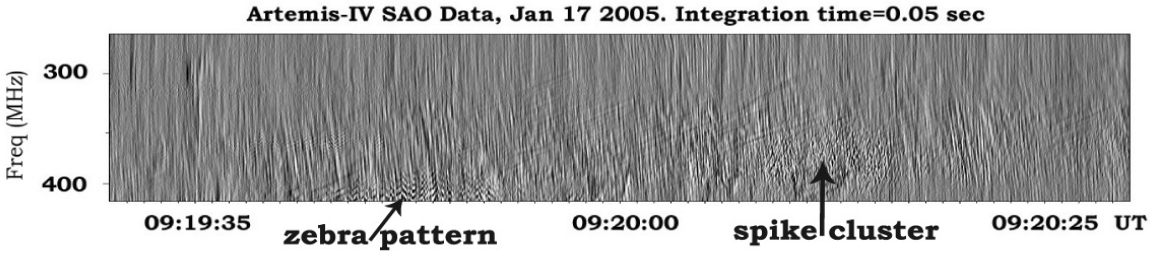

Fig. 2. ARTEMIS IV SAO Differential Spectrum: Zebra pattern (09:19:40-09:19:52 UT) and a spike cluster (09:20:08-09:20:15) on a background of fiber bursts & pulsations (09:19:30-09:20:30 UT); the pulsations with the fibers cover the observation period but they appear more pronounced in the 09:35-09:55 UT interval.

images. The SXR light curve (Figure1, lower panel) exhibits an, initially, slow rising phase which changes into a much faster rising a little before the peak flux is reached; it thus appears on the time–SXR flux diagram as a two stage process.

The CME data from the LASCO lists, [10], (http://cdaw.gsfc.nasa.gov) indicate that each of the stages coincides with the, estimated, lift off time of CME_1 & CME_2 respectively; it is also well associated with the high frequency onset of the two type III groups mentioned above. The halo CME_1 was first recorded by LASCO at 09:30:05 UT. Backward extrapolation indicates that it was launched around 09:00:47 UT. CME_2 was first recorded by LASCO at 09:54 UT; it was launched around 09:38:25 UT and was found to overtake CME_1 at about 12:45 UT at approximately 37 R_{SUN}.

A. Fine Structure

The high sensitivity and time resolution of the SAO facilitated an examination on fine structure embedded in the Type–IV continua within the studied period. In our analysis, the continuum background is removed by the use of high–pass filtering on the dynamic spectra (differential spectra).

As fine structure is characterized by a large variety in period, bandwidth, amplitude, temporal and spatial signatures, a morphological taxonomy scheme based on Ondrejov Radiospectrograph recordings in the 0.8–2.0 GHz range was introduced ([11], [12], [13]); the established classification criteria are used throughout this report.

We present certain examples of fine structures recorded by the ARTEMIS–IV/SAO in the 450-270 MHz frequency range; this range corresponds to ambient plasma densities which are typical of the base of the corona ($\approx 10^9$ cm^{-3}, [14]). The fine structures of our data set are divided according to the Ondrejov classification scheme and described in the following paragraphs (cf. also figures 2, 3, 4 & 5).

B. Broadband pulsations & Fibers

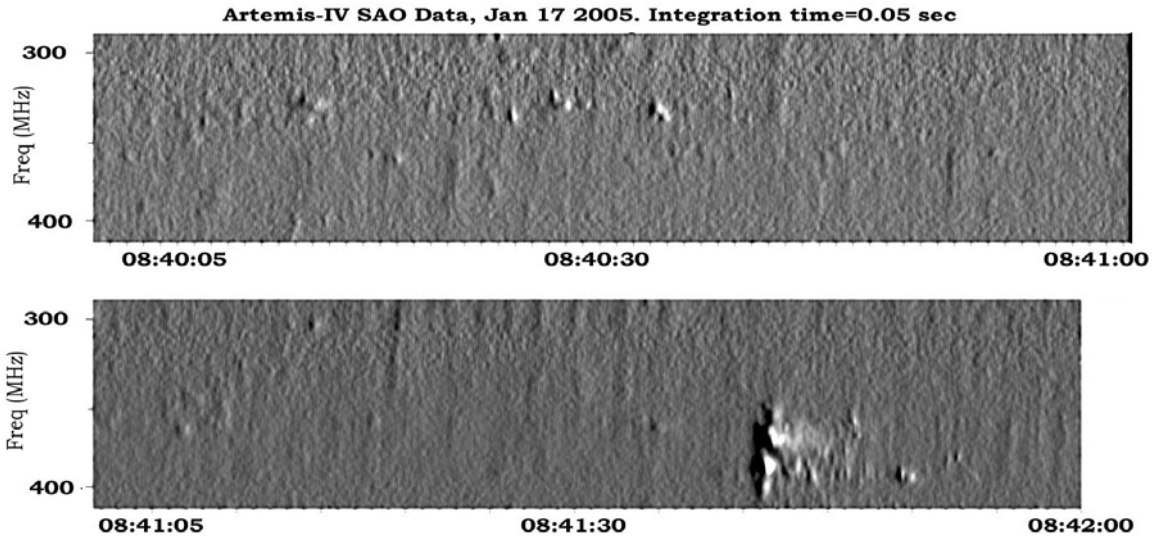

Fig. 3. ARTEMIS IV Differential Spectra of Fine Structures embedded in the Type IV Continuum. UPPER PANEL: Spikes, LOWER PANEL: Narrow Band Type III(U) Bursts.

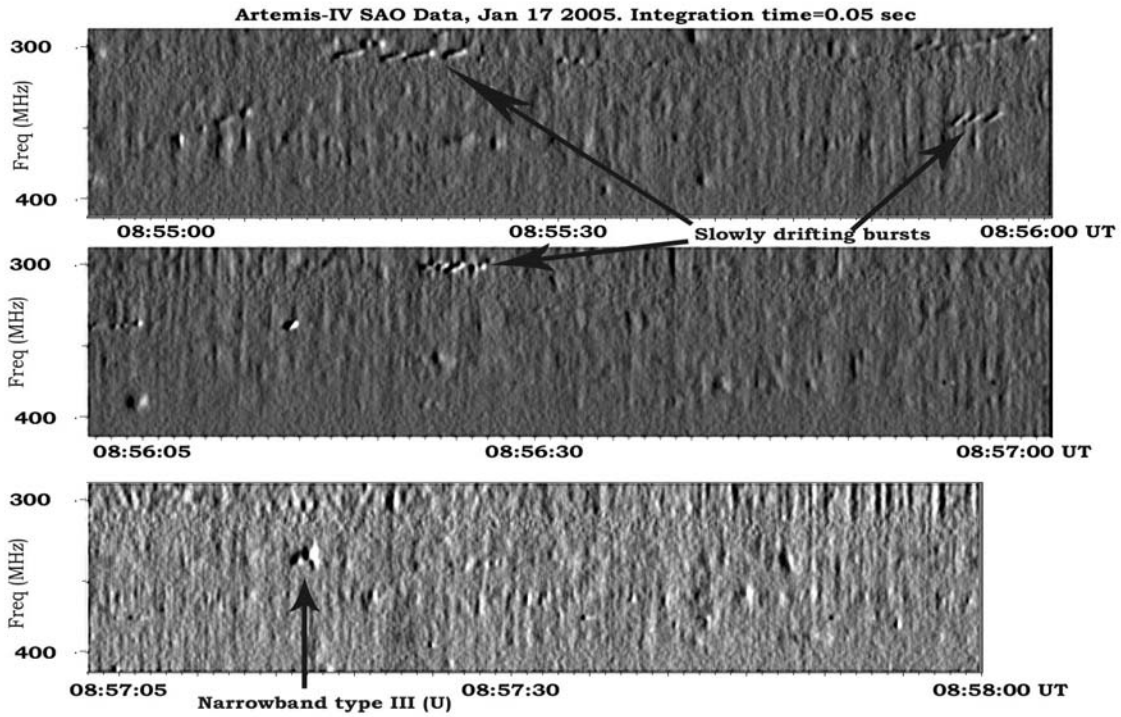

Fig. 4. ARTEMIS IV Differential Spectra of Fine Structures embedded in the Type IV Continuum. FIRST TWO PANELS: Narrow Band Slowly Drifting Bursts LOWER PANEL: Narrow Band Type III(U).

The broadband pulsations appear for the duration of the

type IV continuum; they are, for same period, associated with fibers; these structures intensify within the rise phase of the SXR, which in turn, coincides with the extrapolated liftoff of CME1 & CME2. A closer examination follows:

- **Radio pulsations** are series of pulses with bandwidth > 200MHz and total duration > 10s; they persisted for the duration of the type IV continuum.

Some, with a slow global frequency drift, were of the **Drifting Pulsation Structures** (DPS) subcategory. The pulsations bandwidth exceeded the SAO frequency range, however from the ASG dynamic spectrum we observe a drift of the pulsating continuum towards the lower frequencies, following the rise of CME_2. Three physical mechanisms were proposed as regards the source of this type of structure, [15]:

· Modulation of radio emission by MHD oscillations in a coronal loop

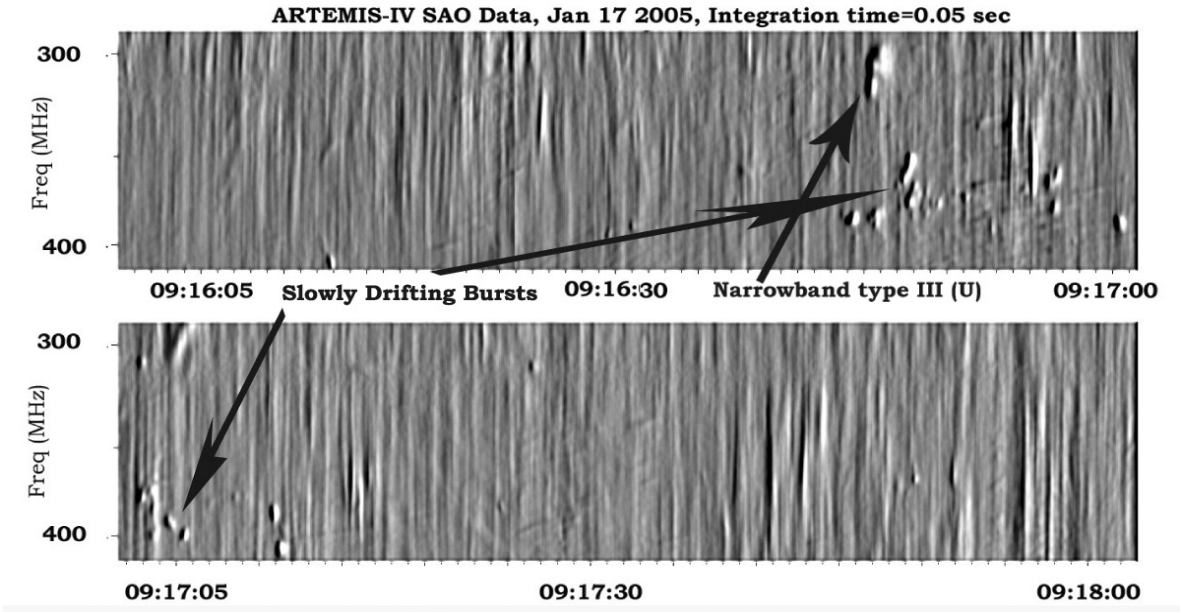

Fig. 5. ARTEMIS IV Differential Spectra of Fine Structures embedded in the Type IV Continuum; narrowband bursts within groups fiber bursts & pulsating structures: UPPER PANEL: Narrowband Type III(U), Narrow Band Slowly Drifting Bursts & spikes; LOWER PANEL: Narrow Band Slowly Drifting Burst & spikes.

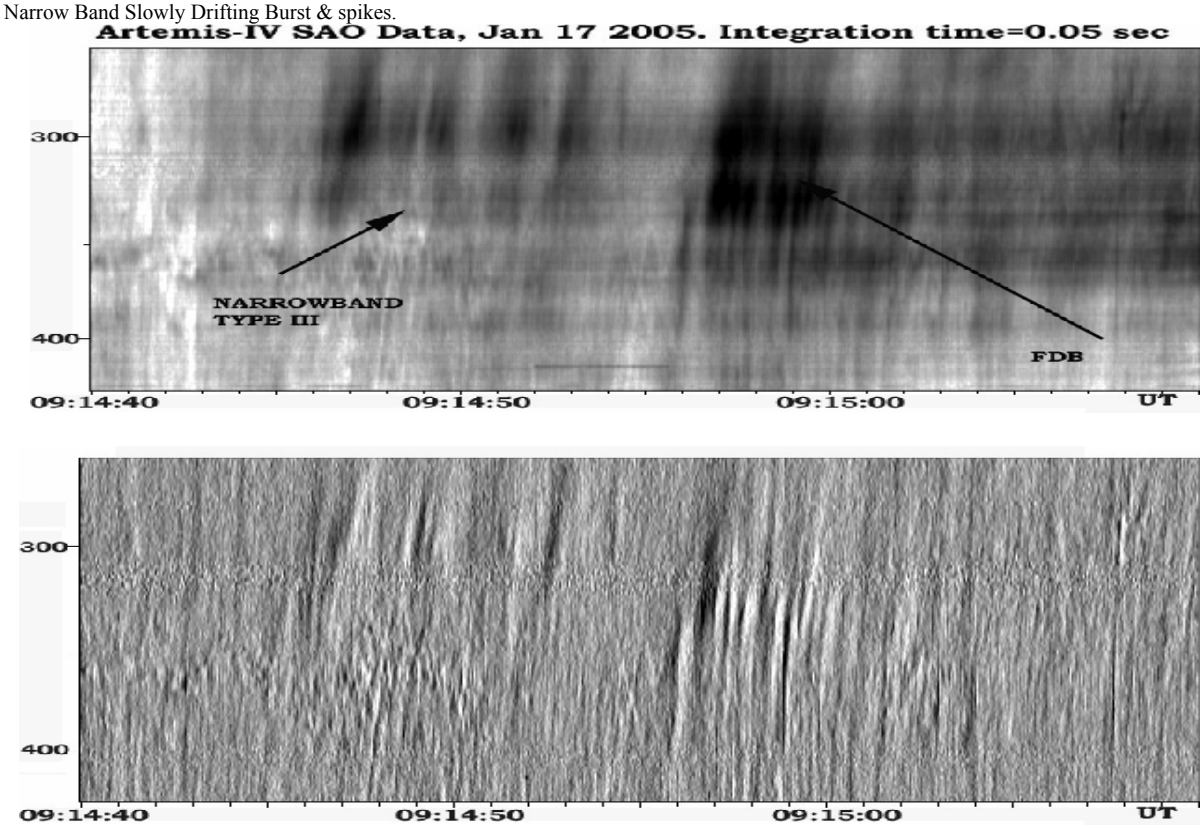

Fig. 6. ARTEMIS IV Spectra of Fast Drift Bursts (FDB), 09:14:55-09:15:00 UT, preceded by narrowband type III bursts. UPPER PANEL: Intensity Spectrum LOWER PANEL: Differential Spectrum.

Non-linear oscillating systems (wave-wave or wave particle interactions) where the pulsating structure corresponds to their limit cycle

· Quasi-periodic injection of electron populations from acceleration episodes within large scale current sheets.

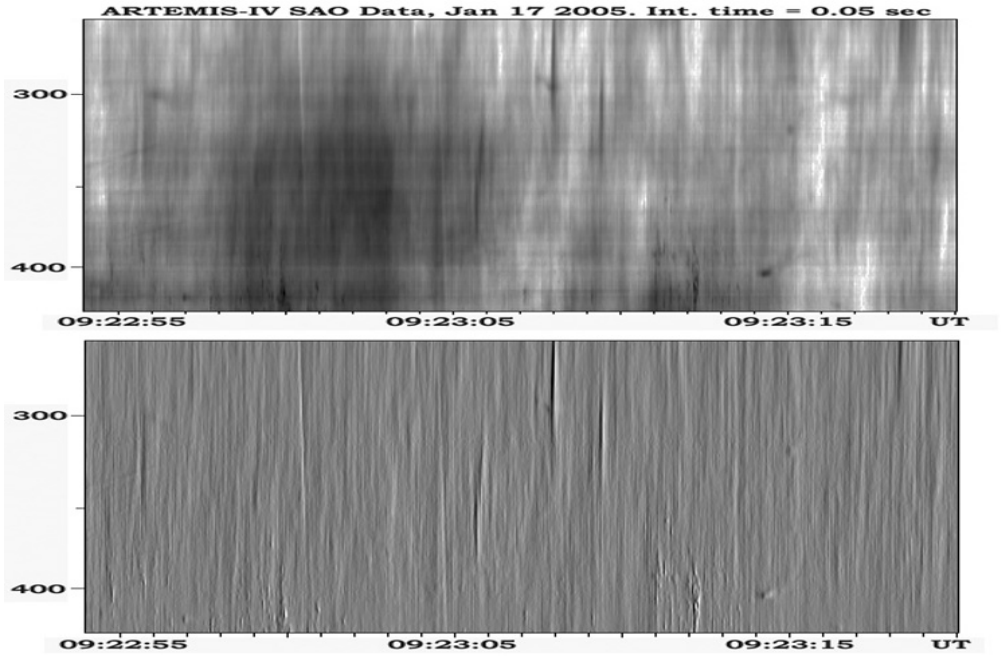

Fig. 7. ARTEMIS IV Spectra of Isolated Pulsating Structures (IPS), 09:22:55-09:23:05 UT. UPPER PANEL: Intensity Spectrum LOWER PANEL: Differential Spectrum

.

Combined Radiospectrograph, radio and SXR imaging and HXR observations ([16], [17], [18]) favor the last mechanism; furthermore they identify the sources of Drifting Pulsation Structures with plasmon ejections.

- **Isolated Broadband Pulses**: Pulsating Structures but with duration ≈ 10 s, (fig. 7).
- **Fast Drifting Bursts**: Short-lasting and fast drifting bursts with frequency drift>100MHz/s; similar to the isolated broadband pulses, except for the frequency drift, (fig. 6).
- **Fibers** or **Intermediate Drift Bursts**: Fine structure bursts with the frequency drift ≈ 100MHz/s; they often exhibit nearly regular repetition.

On our recordings they coincide with broadband pulsations and they also cover the duration of the type IV continuum. They are usually interpreted as the result of whistler coalescence with Langmuir waves in magnetic loops; the exciter is thought to be an unstable distribution of nonthermal electrons, [15].

E. Zebra patterns

The zebra structures are characterized by several emission lines, which maintain nearly regular distance to their neighbors (fig 2).

The zebras from our data set are associated with pulsations and fibers and cover almost the same period with them. They appear, however, more pronounced in the 09:35–09:55 UT interval; this includes the CME_2 estimated launch and the rising of the SXR

flare. Zebra patterns were explained as the result electrostatic upper-hybrid waves at conditions of the double plasma resonance where the local upper hybrid frequency equals a multiple of the local gyrofrequency ($\omega_{UH} = \sqrt{\omega_e^2 + \omega_{Be}^2} = s \cdot \omega_{Be}$), [19], [15]. The upper hybrid waves are excited by electron beam with loss-cone distribution, [20].

F. Narrowband Structures

The narrowband activity (figures 3, 4 & 5), including Spikes, Narrow Band Type III & III(U) bursts as well as Slowly Drifting Structures, is rather intermittent. A large group of spikes appears at about 09:20 UT; this coincides, in time, with the rising of the first stage of the SXR and the start of the first type III group. Three types of Narrowband Structures were recorded:

- **Narrow Band Spikes** are very short (≈ 0.1s) narrowband (≈ 50MHz) bursts which usually appear in dense clusters (fig 2). The models proposed for the spike interpretation are based either on the loss-cone instability of trapped electrons producing electron cyclotron maser emission or on upper-hybrid and Bernstein modes. An open question is whether spikes are signatures of particle accelerations episodes at a highly fragmented energy release flare site.
- **Narrow Band Type III Bursts**: Short (≈ 1 s) narrowband (< 200 MHz) fast drifting (> 100 MHz/s) bursts. A number of this type of bursts, on the SAO high resolution dynamic spectra, exhibit a frequency drift turn over; as they drift towards lower frequencies and after reaching a minimum frequency

(turn over frequency) they reverse direction towards higher frequencies appearing as inverted U on the dynamic spectra. These we have marked as **narrowband type III(U)** on figures 3, 4 & 5. Similar spectra (**III(U)**, **III(N)**) were obtained in the microwave range [21].

- **Narrow Band Slowly Drifting Bursts**: They are similar to Narrow Band Type III Bursts but with a drift rate < 100MHz/s.

III. Summary and Discussion

The ARTEMIS-IV radio-spectrograph, operating in the range of 650-20 MHz, observed a number of complex events during the super-active period of period 14–20 January 2005; the event on January the 17th was characterized by an extended, broadband type IV continuum with rich fine structure.

We have examined the morphological characteristics of fine structure elements embedded in the continuum; it, almost, matches the comprehensive Ondrejov Catalogue ([11], [12]). The latter, although it refers to the spectral range 0.8–2 GHz, seems to produce similar fine structure with the metric range.

The high resolution (100 samples/sec) SAO recordings permitted the spectral study of the fine structures and the recognition and classification of the type III(U) & III(J) subcategory of the Narrow Band Type III Bursts in the metric frequency range; similar structures have been reported in the microwaves, [21].

The pulsating structures and fibers cover the full observation interval but appear enhanced during the SXR rising and the two CME lift off where the major magnetic restructuring takes place. The narrowband structures, on the other hand, are evenly distributed for the duration of our observation interval; this indicates that small electron populations are accelerated even after the flare impulsive phase.

Two types of fine structures from the Ondrejov Catalogue were not detected in our recordings:

- **Continua**: As the long duration pulsations and fibers covered the SAO spectra, any possible appearance of Continua was, probably, suppressed within the pulsating background.

Lace Pattern: It is new type of fine structure, first reported by [11], characterized by rapid frequency variations, both positive and negative. It is very rare with only nine reported in the Ondrejov catalogue out of a total of 989 structures.

Acknowledgements

This work was supported in part by the Greek Secretariat for Research and Technology. The authors would like to thank Prof. C. Caroubalos (University of Athens) for helpful discussions and comments. They also acknowledge many useful suggestions by the two unknown referees; these have significantly improved the quality original draft.

References

[1] Bouratzis, K., Preka-Papadema, P., Hillaris, A. et al, "Radio Bursts in the Active Period January 2005" In: Solomos, N. (Ed.), Recent Advances in Astronomy and Astrophysics., AIP Conference Series. 848, 213-217, 2006.

[2] Caroubalos, C., Maroulis, D., Patavalis, N. Et al.: "The New Multichannel Radiospectrograph ARTEMIS-IV/HECATE, of the University ofAthens". Experimental Astronomy 11, 23–32, 2001b.

[3] Kontogeorgos, A.et al, "The improved ARTEMIS IV multi channel solar radio spectrograph of the University of Athens". Experimental Astronomy 21, 41–55, 2006a.

[4] Caroubalos, C., Alissandrakis, C.E., Hillaris. et al, "ARTEMIS IV Radio Observations of the 14 July 2000 Large Solar Event", Sol. Phys.204, 165–177, 2001a.

[5] Caroubalos, C., Hillaris, A., Bouratzis, C., et al. "Solar type II and type IV radio bursts observed during 1998-2000 with the ARTEMIS-IV radiospectrograph" A&A, 413, 1125–1133, 2004.

[6] Kontogeorgos, A. et al, "Observing the Sun at 20 650 MHz at Thermopylae with Artemis". Space Sci. Rev.122, 169–179, 2006b.

[7] Kontogeorgos, A., et al, "Measuring solar radio bursts in 20650 MHz". Measurement 41, 251-258, 2008.

[8] Petoussis, V., Tsitsipis, P., Kontogeorgos, et al, "Type II and IV radio bursts in the active period October-November 2003". In: Solomos, N. (Ed.), Recent Advances in Astronomy and Astrophysics, AIP Conference Series, 848 199–206, 2006.

[9] Caroubalos, C., Alissandrakis, C.E., Hillaris, A., et al, "Ten Years of the Solar Radiospectrograph ARTEMIS-IV". In: Solomos, N. (Ed.), Recent Advances in Astronomy and Astrophysics. AIP Conference Series. 848 pp. 864–873, 2006.

[10] Yashiro, S., Gopalswamy, N., Michalek, G., et al, "A catalog of white light coronal mass ejections observed by the SOHO spacecraft". J. Geophys. Res.109 (18), 7105, 2004.

[11] Jiřička, K., Karlický, M., Mészárosová, H, "Global statistics of 0.8−2.0 GHz radio bursts and fine structures observed during 1992-2000 by the Ondřejov radiospectrograph". A&A, 375, 243–250, 2001

[12] Jiřička,, K., Karlický, M., Mészárosová, H, "Occurrences of different types of 0.8-2.0 GHz solar radio bursts and fine structures during the solar cycle". In: Sawaya-Lacoste, H. (Ed.), SOLSPA 2001, Proceedings of the Second Solar Cycle and Space Weather Euro conference, ESA SP 477, 351-354, 2002.

[13] Mészárosová, H. et al, "Statistical Analysis of Pulsations and Pulsations with Fibers in the Range 800-2000 MHZ". In: The Dynamic Sun: Challenges for Theory and Observations, ESA Special Publication. 600, pp. 133–136, 2005.

[14] Mann, G., Jansen, F., MacDowall, R.J., Kaiser, M.L., Stone, R.G., "A heliospheric density model and type III radio bursts" A&A, 348, 614–620, 1999.

[15] Nindos, A., Aurass, H, "Pulsating Solar Radio Emission". In: Klein, K.-L., MacKinnon, A. L. (Eds.), Lecture Notes in Physics, Berlin Springer Verlag. Vol. 725, pp. 251–277, 2007.

[16] Karlický, M. et al, "High-frequency slowly drifting structures in solar flares". A&A 395, 677–683, 2002.

[17] Khan, J.I., Vilmer, N., Saint-Hilaire, P., Benz, A.O.: "The solar coronal origin of a slowly drifting decimetric-metric pulsation structure". A&A, 388, 363-372, 2002.

[18] Kliem, B., Karlický, M., Benz, A.O.: "Solar flare radio pulsations as a signature of dynamic magnetic reconnection". A&A, 360, 715–728, 2000.

[19] Chernov, G.P., Sych, R.A., Yan, Y., et al, "Multi Site Spectrographic and Heliographic Observations of Radio Fine Structure on April 10, 2001", Sol. Phys.237, 397–418, 2006.

[20] Kuznetsov, A.A., Tsap, Y., T.: "Double plasma resonance and fine spectral structure of solar radio bursts", Advances in Space Research 39, 1432–1438.

[21] Fu, Q.-J., Yan, Y.-H., Liu, Y.-Y., et al, "A New Catalogue of Fine Structures Superimposed on Solar Microwave Bursts" Chinese Journal of Astronomy and Astrophysics 4, 176–188, 2004

Session D

World-wide particle detector networks for space weather research

Chair: I. Usoskin, G. Basilevskaya

Solar **E**xtreme **E**vents **2007**

Statistical study of the detection of solar protons of highest energies at 20 January 2005

A.Chilingarian

Alikhanyan Physics Institute, Yerevan, Armenia,
Alikhanyan Brothers 2, Yerevan 375036, Armenia

Abstract – **On January 20, 2005, 7:02-7:05 UT the Aragats Multidirectional Muon Monitor (AMMM) registered enhancement of the high energy secondary muon flux (energy threshold ~5 GeV). The enhancement, lasting three minutes, has statistical significance of ~4σ and is related to the X7.1 flare seen by the GOES satellite and the Ground Level Enhancement detected by the world-wide network of neutron monitors and by muon detectors. The most probable proton energy corresponding to the measured 5 GeV muon flux is within 23-30 GeV. Due to upmost importance of the detection of solar particles of highest energies in presented paper we perform detailed statistical analysis of the detected peak. The statistical technique introduced in the paper is also appropriate for the searches of sources of ultra-high energy cosmic rays.**

I. INTRODUCTION

Measurements of the energy spectra of the Solar Cosmic Rays (SCR) up to several tens of GeV will significantly enlarge the basic knowledge on the universal processes of particle acceleration at the Sun and in the Universe and will provide important information for the timely warnings on Space Weather severe conditions. Experimental investigation of the SCR of highest energies is a very difficult problem, requiring large surfaces of the particle detectors located at middle and low latitudes. Solar Cosmic Rays are electrons, protons and stripped nucleus accelerated in vicinity of Sun in flaring processes and by shock waves driven by the Coronal Mass Ejections (CME).

Solar Energetic Particles (SEP) sometimes are energetic enough to generate cascades of particles in terrestrial atmosphere. Cascade particles can reach surface and enlarge count rates of particle monitors normally detecting rather stable flux of cascade particles generated by much more energetic Galactic Cosmic Rays (GCR). Such abrupt count rate changes due to SCR are called Ground Level Enhancements (GLE), encountered not more than 10 times during ~11 years of solar activity cycle.

On 20 January 2005, during the recovery phase of the Forbush decrease a long lasting X-ray burst occurred near the west limb of the Sun (helio-coordinates: 14N, 67 W). The start of X7.1 solar flare was at 06:36 UT and maximum of the X-ray flux at 7:01 UT. The fastest (relative to X-ray start time) SEP/GLE event of 23-cycle (GLE number 69) was detected by space-born and surface particle detectors few minutes after the flare onset. The start of GLE was placed at 6:48; the maximal amplitude of 5000% recorded by Neutron Monitor (NM) at the South Pole is the largest increase ever recorded by NM world-wide network.

Particle detectors of the Aragats Space-Environmental Center (ASEC, see [1], [2]) detected significant excess of count rates at 7:00 – 8:00 UT. From 7:02 to 7:05 UT, the Aragats Multidimensional Muon Monitor (AMMM) detected a peak with significance *~4σ*. It was the first time that we detected a significant enhancement of the >5 GeV muon flux. This short enhancement at 7:02-7:05 exactly coincides in time with peaks from Tibet NM [3], Tibet Solar Neutron Telescope [4] and Baksan surface array [5].

AMMM is located under 14 meters of soil and concrete in the underground hall of former ANI experiment (see details in [2]) and include 42 one m^2 area and 5 cm thick plastic scintillators; the mean count rate of the detector was ~ 126,000 per minute and relative root mean square error of 1-minute time series (RRMSE, usually used measure of particle monitor performance) equals to 0.28%. Therefore, rather large area of detector and corresponding high accuracy allows detection of additional flux due to very weak flux of highest energy SCR. Flux of the muons with energies above 5 GeV detected by the AMMM as we can see from Figure 1 [6], is generated by the primary protons with energies above 15 GeV. The energy distribution of the "parent" protons giving rise to

the energetic muons depends on the power index of the primary proton energy spectra. Energy spectrum of protons, accelerated in Galaxy is very well fitted in wide energy range by power function with index γ = -2.7; the power index of energy spectra of "solar" protons varies from γ = -4 till γ =-7 and less for GeV energies. Our study of energy spectra of GLE N 69 [7] estimates power index between -4 and -5 around 7:00 UT, 20 January 2005, therefore, most probable energy of primary protons, as we can see from Figure 1, is between 23-30 GeV. To gain an insight into distribution of primary energies we calculate also 10 and 90% quartiles (energy regions containing lowest and greatest 10% of distribution) outlining the "improbable" energy regions. Our calculations prove that the most stable distribution parameter is the mode – energy value at biggest histogram bin. This value remains rather stable when we change simulation model.

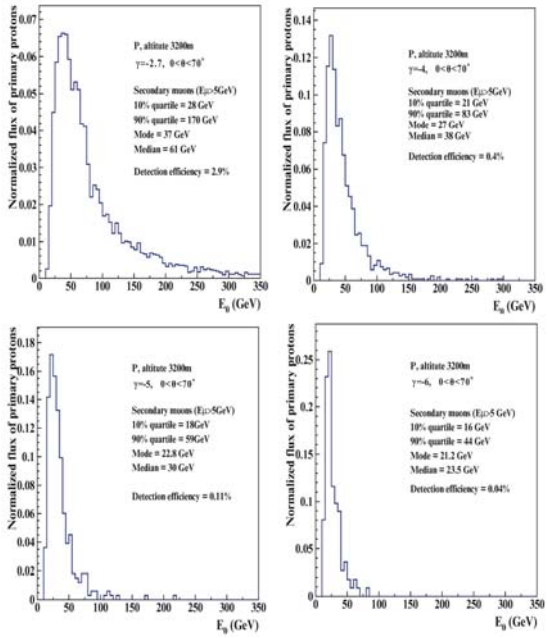

Fig. 1. Energy distribution of the primary protons that generate >5 GeV muons present at 3200 m altitude.

The details of AMMM detection of GLE N 69, are discussed in [8]. In present paper due to upmost importance of the detection of solar particles with highest energies we discuss statistical methods used to reveal peak in the time series of AMMM. In the second section of paper we check the hypothesis that fluctuations of the count rates are well described by the Gaussian model, in the third section we introduce extreme statistical distribution, in forth we describe the computational experiment for checking obtained results.

II. Analysis of the Residuals (Checking the Gaussian Model)

The difficulty of testing hypothesis of Gaussian nature lies in the slow drift of the mean count rate of time series due to systematic changes of several geophysical and interplanetary parameters. Disturbances of the Interplanetary Magnetic Field (IMF) in the end of January 2005 (triggered by passage of several Interplanetary CMEs at 16-20 January) modulate cosmic ray flux, introducing trend in the secondary cosmic ray fluxes.

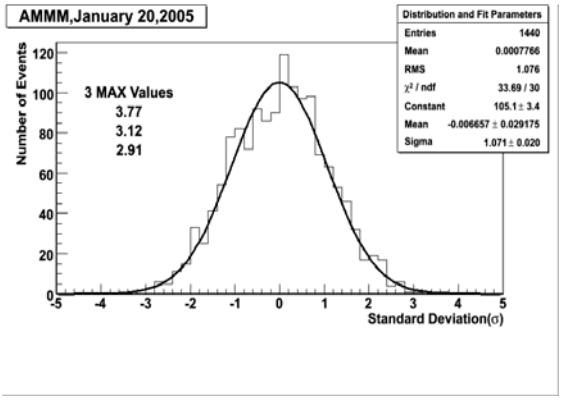

Fig. 2. Normalized residuals calculated by 3-minute AMMM time series at 20 January 2005. In the picture legend are posted the histogram mean and RMS and also fitted curve mean and variance, as well as number of degrees of freedom in the χ^2 test.

To account for the changing mean of the greater than 5 GeV muon flux we calculate the hourly mean count rates and corresponding residuals (fitting errors, differences between observed hourly means and values of 3-minute count rates in this hour; 20 numbers for each hour):

$$X_{i,j} = \frac{C_{i,j} - \overline{C}_j}{S_j}, \quad i = 1,20 \quad j = 1, N_h \qquad (1)$$

where $X_{i,j}$ are normalized residuals, $C_{i,j}$ are 3 minute count rates of the AMMM at j^{th} hour, $\overline{C}_j$ are hourly means of the 3-minute time series and

$$S_j \approx \sqrt{\overline{C}_j}, \; j = 1, N_h \qquad (2)$$

are proxies of root mean square errors and N_h is number of hours.

Statistical distribution (1) represents, so called, multinomial process. Multinomial process consists of sum of j Gaussian random processes; in our case – time series of count rates corresponding to Gaussian process with same variance and different means. In our probabilistic treatment of the problem we normalize time series by the "moving" means $\overline{C}_j$ and variances $S_j{}^2$, estimated each hour. In this way we plan to obtain a

proxy of the standard Gaussian distribution N(0,1) to use later on as a test statistics.

To check our assumptions on Gaussian nature of the distribution (1) we perform calculation of residuals for 20 January 2005 and for whole January 2005. As we describe in [8] we prepare 3-minute time series from the 1 minute ones. Joining 1 minute time series in 3, 5, 10 or 60 minute time series is ordinary operation used by the all groups running the neutron and muon monitors. To account for the arbitrary choice of the start minute we integrate other all 3 possibilities of different starts of the 3-minute time series, therefore number of events in histograms is 3 times more than number of 3-minute count rates.

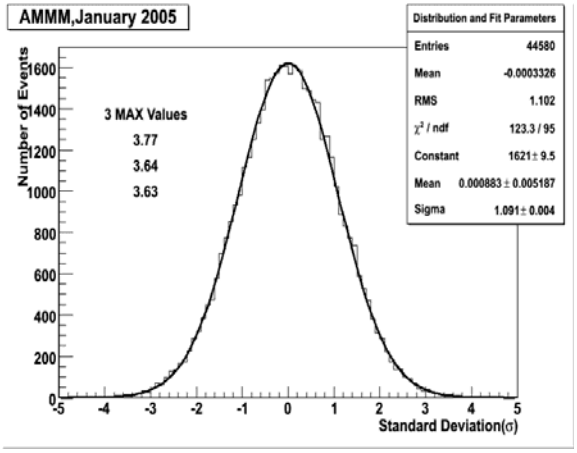

Fig. 3. Normalized residuals calculated by 3-minute AMMM time series at January 2005. In the picture legend are posted the histogram mean and RMS and also fitted curve mean and variance, as well as number of degrees of freedom in the χ^2 test.

The resulting histograms of the normalized residuals are shown in the Figure 2 and 3. We see rather good agreement with standard normal distribution N(0,1); values of the χ^2 test are ~ 1 for degree of freedom. The maximal values of 3.77[1] (see the right tail of histogram in Figure 2) corresponds to GLE at 7:02-7:05 UT. The same maximal value remains maximal also for the one-month histogram (Figure 3). The second maximal value for a month histogram is 3.64.

Proceeding from good agreement of histogram with Gaussian curve and from rather large value of the biggest residual, we can accept the hypothesis that there is additional signal superimposed on the galactic cosmic ray background. Of course, within validity of the Gaussian hypothesis this and larger values can encounter by chance, therefore we'll need additional statistical tests proving that detected peak is caused by the highest energy solar protons.

[1] **We obtain maximal value 3.77 instead of reported in (Bostanjyan et al., 2007) 3.93 due to slightly different procedure of residual calculation.**

III. Calculation of the chance probability

As usually in statistical hypothesis testing, the hypothesis we want to check (named H_0) consists in the opposition to the hypotheses we are interested, i.e. we will check the hypothesis that there is no additional muons in 3-minute time series ("no-signal" hypothesis) and, therefore, that detected peak is random fluctuation only. To prove the existence of signal, we have to reject H_0 with the maximal possible confidence. Detecting large deviations from H_0, i.e. very low probability of H_0 being true, do not imply that the opposite hypothesis is automatically valid. As was mentioned by P.Astone and G.D'Agostini [9] behind logic of standard hypothesis testing is hidden a revised version of the classical proof by contradiction. "In standard dialectics, one assumes a hypothesis to be true, then looks for a logical consequence which is manifestly false, in order to reject the hypothesis. The 'slight' difference introduced in 'classical' statistical tests is that the false consequence is replaced by an improbable one".

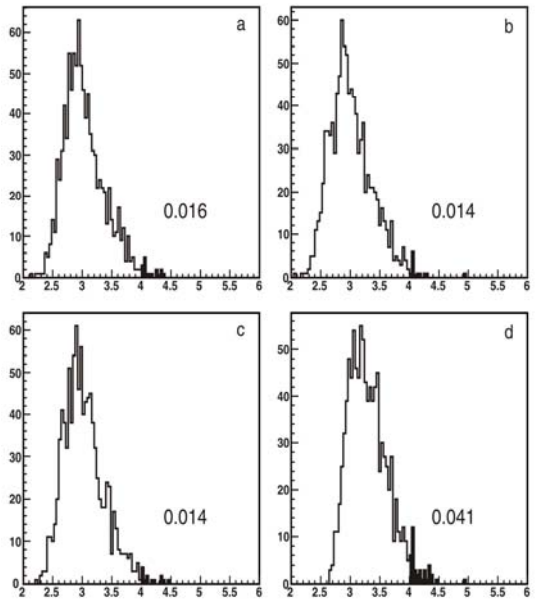

Fig. 4. Histograms of the extreme statistics. a) - c) – selecting extreme statistics for 3 time series (iv);and d) - selecting maximal value among 3 extreme statistics – (v) . Black area in the histograms denote the summation region and number the integral (sum) value from 4 till infinity.

If the experimental data will not differ significantly from test distribution obtained under assumption of "no-signal" hypothesis there will be no reason to reject H_0 and therefore we can't claim that AMMM detected high energy muons of "solar origin". And if we will be able to reject H_0, we can accept with definite level of confidence that there are high energy protons coming from the sun. Usually confidence level is enumerated as "chance probability", the probability of H_0 hypothesis to be true.

The statistical test for accepting or rejecting hypothesis is based on the maximal deviation of most probable value (3.77 in our case) observed in time series. The probability to obtain this or another maximal deviation depends on the number of events considered, i.e. on the time series length. Therefore, the most appropriate test provides the extreme statistics distribution ([10], [11]):

$$c^M(x) = M \cdot g(x)(1 - G_{>x})^{M-1} \quad (3)$$

Where g(x) is standard Gaussian probability density N(0,1).

$$G_{>x} = \int_x^\infty g(t)dt \quad (4)$$

is, so called, standard Gaussian distribution's *p–value*: the probability to obtain the value of test statistics greater than ***x***; M is number of attempts we made to find the biggest deviation from H_0 (number of elements of considered time-series multiplied by number of attempts we made to find greatest deviation).

To obtain the probability to observe extremely deviation equal to ***x*** among M identically distributed random variables (p-value of the distribution $c^M(x)$) we have to integrate $c^M(x)$ in the interval $[x, +\infty)$:

$$C_x^M = \int_x^\infty c^M(t)dt \quad (5)$$

$C_x^M(x)$, *p-value* of the distribution (3), equals to probability that observed test statistics ***x*** maximally deviates from the most probable value under assumption that H_0 is valid. And if this probability is low enough we can reject H_0 and accept alternative hypothesis that observed deviation is not fluctuation, but a mixture of the distribution of different statistical nature, i.e., a signal.

The probability to observe in one from 480 (i.e. during the day) of 3-minute time-series count rate equal to 3.77 equals according to equations (3-5) to: $C_{3.77}^{1440} = 0.1045$

It means that in absence of any signal when examining daily variations of the 3-minute count rates in one case from 10 we can detect the deviation of the mean value equal to 3.77. Equivalent statement: approximately once in 10 days only we will detect 3.77 enhancements in the 3-minute time series of AMMM.

However, we have to correlate the expected signal from protons, accelerated at Sun with time of X-ray flare and CME launch. Of course, we cannot expect the signal from solar protons before X-ray flare and hours after the X-ray flare occurs. The chance probability to detect 3.77 deviation in one hour $C_{3.77}^{60} = 0.0049$, i.e. only in once in 200.

As we can see in the Figure 3 the second maximal monthly deviation equals to 3.64. If we accept hypothesis that 3.77 value was due to solar protons, we have to check if 3.64 is typical monthly maximal deviation. Calculated according (3-5) value of $C_{3.64}^{14340} = 0.2768$ is rather large and we have no reasons to reject H_0; i.e. at January 2005 the residual distribution (Figure 3) was Gaussian with only one outlier attributed to high energy solar protons.

IV. EFFECT OF THE MULTIPLE ATTEMPTS IN SEARCHES OF "BIGGEST" DEVIATION FROM H_0

To check assumption that when calculated significance of signal we should take into account 3 possible starts of time series we perform simulations with simple model of time series.

The model can be described as following:

(i) generate 1440 numbers from the standard normal distribution N(0,1);

(ii) prepare 3 time series summing 3 consequent numbers of the raw, starting from the first, second and the third elements;

(iii) perform according to equation (1) normalization procedure (subtract the mean and divide to root of variance);

(iv) determine and store the maximal element of each of 3 normalized time series;

(v) determine and store the maximal element among 3 time-series maximums;

(vi) repeat i-vi 1000 times and consider 4 histograms of extreme values;

(vii) calculate the frequencies of obtaining values equal or greater than 4 (for simplicity we take 4 instead of 3.77).

Intuitively, when having 3 possibilities physicist will choose one that emphasis the presence of signal (the situation (v)). But as we can see from the Figure 4d, the probability to obtain the fake signal is dramatically enhanced (approximately by 3 times). From the same picture we can see that obtained in d) chance probability 0.041 is in good agreement with value calculated according to equations (3-5): $C_4^{1440} = 0.0436$

V. CONCLUSIONS

Proposed in the paper statistical methodology of calculation of signal significance can be recommended for the treatment of GLE events, especially for revealing weak signals of solar cosmic rays of highest energies.

The extreme statistics are useful tool for the enumeration of the significance of detected peaks in time series. When making different attempts to reject H_0 the probability of obtaining "fake" signal during a given time period increases approximately proportional to number of attempts.

ACKNOWLEDGMENT

Author is grateful to N. Bostanjyan, G. Karapetyan, A.Hovhannisyan, A. Reymers and Zazyan Meri for useful discussions and fruitful collaboration. Work was partly supported by the INTAS grant 8777.

REFERENCES

[1] A.Chilingarian, K.Avakyan et. al, Aragats Space-Environmental Center: Status and SEP Forecasting Possibilities. Journal of Physics G:Nucl.Part.Phys., **29**, 939-952, 2003.

[2] A. Chilingarian et al. Correlated measurements of secondary cosmic ray fluxes by the Aragats Space Enviromental Center monitors", NIM**, A543**, 483-492, 2005.

[3] H. Miyasaka, E. Takahashi, et al. Proc. of of 29th ICRC, Pune, India vol. **1,** 245-2248, 2005.

[4] F.R. Zhu, Y.Q. Tang et. al. Proc of 29th ICRC, Pune, India, **1**, 185-188, 2005.

[5] S.N. Karpov, Z.M. Karpova, Yu.V. Balabin and E.V. Vashenyuk. in Proc. 29th ICRC, Pune, India, vol. **1,** 193-196, 2005.

[6] M.Z.Zazyan, 2008, private communication

[7] A. Chilingarian and A. Reymers. Investigations of the response of hybrid particle detectors for the Space Environmental Viewing and Analysis Network (SEVAN), Ann. Geophys., **26**, 249-257, 2008.

[8] N.Kh. Bostanjyan, A.A. Chilingarian, V.S. Eganov, G.G. Karapetyan. On the production of highest energy solar protons on 20 January 2005, Advances in Space Research **39**, 1454–1457, 2007.

[9] Astone P., D'Agostini G., Inferring the intensity of Poison processes at the limit of the detector sensitivity, CERN-EP/99-126, 1999.

[10] S.C. Chapman, G. Rowlands, N.W.Watkins. Extremum statistics – a Framework for Data Analysis, Nonlinear Processes in Geophysics, **9**, 409-418, 2002.

[11] A.Chilingarian, G.Karapetyan et al. Statistical Methods for Signal Estimation of Point Sources of Cosmic Rays, Astroparticle Physics, **25**, 269-276, 2006.

Interactive database of cosmic ray anisotropy (DB-A10)

Asipenka, A.S., Belov, A.V., Eroshenko, E.A., Klepach, E.G., Oleneva, V. A., Yanke, V.G.

IZMIRAN by Pushkov, Russian Academy of Sciences, Troitsk, Moscow region, Russia
(Mailing address: Cosmic Ray Department, IZMIRAN, 142190, Troitsk, Moscow region, Russia)

Abstract – **The worldwide neutron monitor network is a unique tool for obtaining with high accuracy the information on density variations, energy spectrum and anisotropy of comic rays at the Earth, outside its atmosphere and magnetosphere. These hourly averaged parameters were obtained over the whole period of cosmic ray monitoring by the ground level neutron monitor network (from 1957 till present) and are collected within the MySQL database. The Internet-project has developed for free access and supplying of cosmic ray density and anisotropy data in different formats.**

Keywords - ***cosmic ray anisotropy, neutron monitor network, data base***

I. INTRODUCTION

In the energy range of 1 - 100 GeV cosmic ray (CR) intensity is nearly isotropic. A degree of anisotropy, as a rule, is less than 1%. However, no other CR characteristic is capable to give so a lot of information on conditions in the interplanetary space, as CR anisotropy ([1], [2] and references there). The form, direction, size and power spectrum of anisotropy are connected with concrete structures in heliosphere, with intensity, direction and degree of an irregularity of the interplanetary magnetic field (IMF), with a position of the heliospheric current sheet and also with the solar wind speed. Structural features and processes in a solar wind within the wide spatial (10^9 -10^{14} cm) and time (10^3 – 10^8 s) scales, are reflected in the CR anisotropy observable at the Earth and can be studied with its help [3], [4], [5], [6], [7], [8], [9]. Thus, data on the anisotropy from ground level CR observations derived might be considered as reliable tool for interplanetary space diagnostics.

II. TECHNIQUE OF SEPARATION OF ANISOTROPY

Some variants of a technique of detection of CR anisotropy from ground based CR observations have been considered by [10], [3], [11], [12], [13], [5]. In common, it is always a various modification of spherical analysis method.

Being limited to the zero and first harmonics, CR variations expected on the Earth at point i at the time moment t, are possible to be written down as following in Geocentric Coordinate System (GEO):

$$\delta^i(t) = A_0 C_0^i(\gamma\gamma+ \begin{pmatrix} A_x \\ A_y \\ A_z \end{pmatrix} \begin{Bmatrix} Cos(t) & -Sin(t) & 0 \\ Sin(t) & Cos(t) & 0 \\ 0 & 0 & 1 \end{Bmatrix} \begin{pmatrix} C_x^i \\ C_y^i \\ C_z^i \end{pmatrix} + \delta_{err}^i \quad (1)$$

where $\delta^i(t)$ is observable variation of counting rate at each station (point i), A_0 is isotropic part of CR variations (density), A_x, A_y, A_z are three components of CR anisotropy, and the system of these equations for many stations allows to derive these components, density and its spectral index for each hour; δ_{err}^i is discrepancy between the model of CR variation and real CR observations at every station; $C_0^i(\gamma)$ and C_x^i, C_y^i, C_z^i are reception coefficients between variations outside the magnetosphere and variations observed at the ground at point i for different components. These coefficients depend on coordinates and altitude of the observational point and are calculated for each station separately [14](Yasue et al., 1982). Reception coefficients for zero harmonic A_0 ($C_0^i(\gamma)$) may be determined relatively simply [15] (Belov et al., 2005), and we calculate them for each station:

$$C_0^i(\gamma) = \int_{Rc}^{\infty} R^{-\gamma} W^i(Rc,h,R)dR \qquad (2)$$

where $W^i(Rc,h,R)$ is the coupling function between CR variations above and inside the atmosphere at the level *h* (m, or mb) and at a point with geomagnetic cut off rigidity *Rc* [1], $R^{-\gamma}$ is a rigidity part of power spectrum of zero harmonic with a power index - γ which is defined from the relation $A_0 R^{-\gamma}$.

Calculation of reception coefficients of the first harmonic (C_x^i, C_y^i, C_z^i), on the contrary, is very labor-consuming since it is necessary to consider not only an atmosphere of the Earth, involving a coupling function $W^i(Rc,h,R)$, but also interaction of CR with the magnetosphere [15]. Such calculations accounting asymptotic directions of the particles of different energy beyond the magnetosphere were performed for the NM network by Yasue et al. [14] for those stations which were operating by that time (80-th). For all additional stations in the last years arose these coefficients have been interpolated in our calculations from rigidity and latitudinal dependencies of C_x^i, C_y^i, C_z^i obtained by the known values from Yasue Tables. The matrix in Eq. (1) accounts the Earth rotation in geographic coordinate system (GEO) to fix axis X on the Sun direction. The solution of an inverse task, i.e. the solution of the equation (1) system by the RLS method (recursive least square error method having a fast convergence rate and a better minimum mean square error) relative to A_0, γ, A_x, A_y, A_z in approach of the first harmonic defines density A_0, its spectral characteristics γ and vector of anisotropy of CR (A_x, A_y, A_z) near to an orbit of the Earth outside its atmosphere and magnetosphere.

Hourly averaged values of these parameters have been calculated by mentioned above method of global survey (GSM), in version described in [15], by the data from up to 130 neutron monitors throughout the epoch of CR monitoring, since 1957 till present time. The list of all implemented stations is given in Table 1 (see also [16]). We used neutron monitor data from IZMIRAN data base (http://cr0.izmiran.rssi.ru/mosc/main.htm), where they are collected in more complete volume than in any WDC. Of course, we calculated the CR variation parameters only after data correction for drifts, jumps (because of change of electronic or number of counters). But this is not a universal method (it is impossible), it is only data checking and verification by the way of comparison different stations with similar conditions (close coordinates, cut off rigidity and altitude).

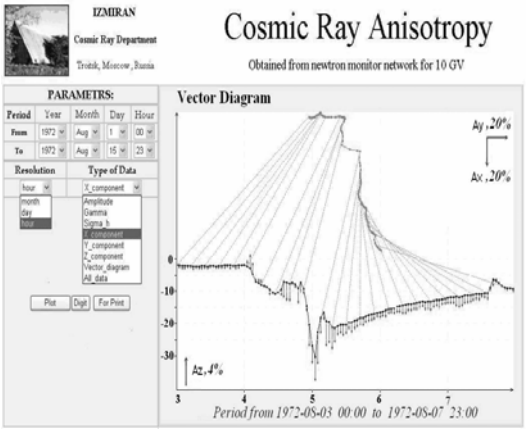

Fig. 1. Page of the site http://cr20.izmiran.rssi.ru/AnisotropyCR/Index.php on the CR anisotropy database DB-A10. On the left side is a table with knocks allowing the selection a kind of presentation (digital or plot), required time interval, resolution of data and sort of results. On the right side there is a graphical presentation of CR parameters for one of the biggest Forbush effect on 4-5 August 1972. Explanation of different designations, please, find in the next figure.

We calculate and publish such parameters for different time periods during at least 15 years. We could process data for 2-3 years during one year because of careful and long procedure of data preparing. That's why the main requirement to every station is its stable and reliable operating which can provide high quality data.

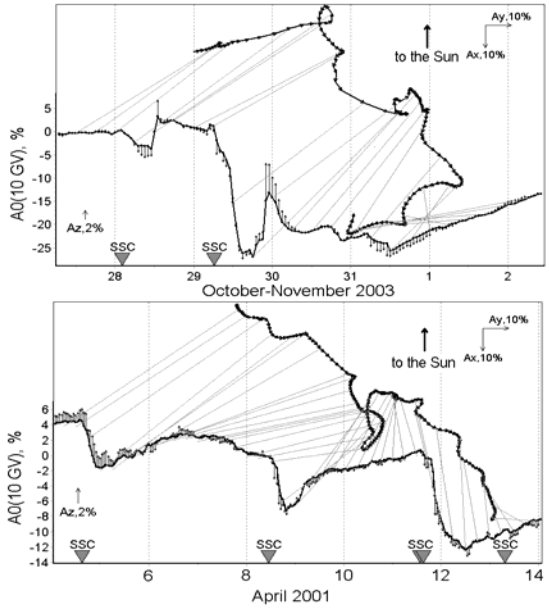

Fig. 2. Examples of the largest FEs in different time periods. Solid line is the CR density behavior (beyond the Earth's atmosphere); couple vector diagram shows equatorial component of CR anisotropy; thin lines connect the equal time points of diagram and curve of density in every 6 hours; vertical lines correspond to the north-south CR anisotropy derived also for each hour during the event.

We should emphasize that not all and not a constant number of stations operated at every moment (due to breaks down, closing of stations, run the new ones and so on) and in various periods there was different number of stations; in the average 33-45, fully suited for calculations. A plenty of used stations has allowed us to provide both a good accuracy of obtained characteristics, and fully continuous data set on CR anisotropies over a whole considered period.

As the given technique is labor-consuming enough, it is important to make these data free accessible for the scientists. At the solving of many problems of solar terrestrial physics it is necessary to have variations of CR outside the magnetosphere instead of data of any individual station, let even reliably working, but containing the contribution of magnetosphere and atmospheric effects (e.g.[5]). Data on variations of CR density and anisotropy near Earth above the magnetosphere for the cosmic rays of 10GV rigidity presented in DB_A10 are the global CR characteristics and they don't depend on the local position of detectors. CR density variations, obtained for this rigidity (10 GV), have high accuracy and reflect all solar wind changes responsible for CR disturbances.

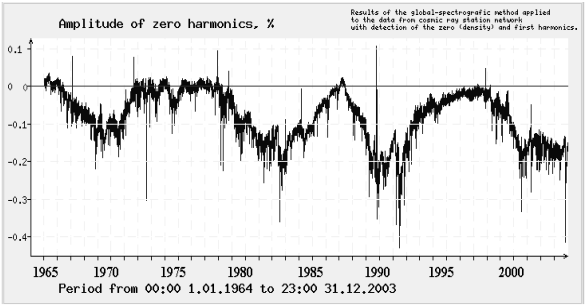

Fig. 3. Hourly means of the amplitude of zero harmonic of CR variations (CR density A_0) over the 1965-2003 period of ground level CR observations, as it is plotted by DB-A10 software.

Among above-mentioned parameters the mean square deviations (*SigmaH* – the residual dispersion in the RLS method which is defined by discrepancy δ^i_{err} in formula (1)) of experimental data from that derived by the accepted model were calculated by the data of high latitude stations. This parameter evidences the adequacy of implemented model: in some periods a large discrepancy between real and model data (increase of *SigmaH*) indicates a possible impact of second and higher order harmonics, or existence of geomagnetic effect in cosmic ray variations.

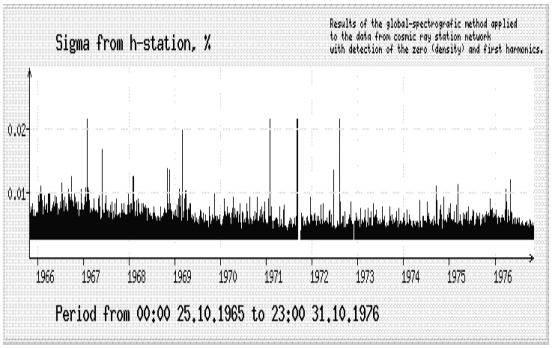

Fig.4. Residual dispersion (SigmaH) between real data and model calculation (hourly values within a time period from 1966 to 1976).

III. GENERAL DESCRIPTION OF THE DATA BASE DB_A10

The results of calculations are collected in the MySQL data base on CR anisotropy. A number of records in the DB-A10 database are about 450000, capacity of 600 MB. As new calculations become available the monthly updating and updating in real time is being possible. Free access is available by the address: http://cr20.izmiran.rssi.ru/AnisotropyCR/Index.php

The data is stored in a MySQL database, and access is provided through php scripts.

Using widely and successfully realized combination of script-language Php and MySQL databases, the Internet-project have been created on supplying of CR anisotropy data in different formats to a final user.

A usage of the Php language and MySQL in pair provides operability and rapidity for access to data even from the Internet, because requests and further operations are performed at the project server.

IV. DIGITAL DATA PRESENTATION:

Every user can get data from DB_A10 for any time period in digital form. It allows the implementation of 10GV CR parameters for different calculations, modeling, correlations and other analysis in fundamental science and for Space Weather applications as well. It should be noted that results for 1957-1964 are not yet in the database, although they are ready to be inserted, and it will be done in the nearest time.

List of parameters presented in Data base (DB_A10) includes:

A_0 Cosmic ray density (zero harmonic)

with rigidity 10 GV in percentages normalized to 1976;

γ Spectral index of zero harmonic of CR variations, which is defined as $A_0 R^{-\gamma}$; index γ is derived for different basis periods and it may be used in the analysis within only short periods. In the next versions it will be normalized to a single basis;

A_x, A_y, A_z Components of the CR anisotropy vector (for 10 GV particles) in the GCS, in percentages; north-south anisotropy A_z is derived with accuracy up to constant (we derive variations of Z component, but its absolute value is unknown).

A_{xy} Magnitude of the equatorial component of CR anisotropy (%);

φ Direction of the equatorial component of CR anisotropy (in equatorial plane); 0 – is direction to the Sun;

SigmaH Residual discrepancy between a model and real measurements for high latitude neutron monitors, which

Sigma characterizes the model adequacy, in particular, indicates an availability of higher order harmonics;

Residual discrepancy between a total model of CR variations and real measurements at the neutron monitors from the whole set of NMs.

3.2 Graphical data presentation

vector diagram Coupled vector diagram – direction and magnitude of equatorial component of CR anisotropy consequently from hour to hour (Fig.1). In the bottom part of picture a vector of north-south anisotropy a_z is shown along the time connected with graphic of CR density variation (A_0);

All Data Plots All parameters are plotted simultaneously: density variation (A_0), north-south anisotropy A_z, magnitude and direction of equatorial component A_{xy} of CR anisotropy. In the upper part of picture a direction 0 (from the Sun) is shown.

By the internet project data of CR density (A_0) and three components (A_x, A_y, A_z) of anisotropy vector are published in graphical and digital formats. Besides, for any chosen period it is possible to generate a diagram of connected vectors of CR anisotropy in the equatorial plane (*Ax, Ay*). Fig. 1 presents an example of web page of DB-A10 for users. On the right side a vector diagram for selected period from 1 to 15 August 1972 during one of the biggest Forbush effect (FE) is plotted. Such a picture may be generated for any requested period of any Forbush effect. For example, Fig. 2 demonstrates the behavior of CR parameters for two other biggest FEs plotted by the data from DB-A10. The amplitude and direction of the equatorial component of CR anisotropy (*Axy*) are plotted as coupled vector diagram of *(Ax, Ay)*, variations of north – south anisotropy (A_z) are presented by vertical vectors along the curve of CR density variation (A_0), thin lines connect corresponding time points on the vector diagram and density curve.

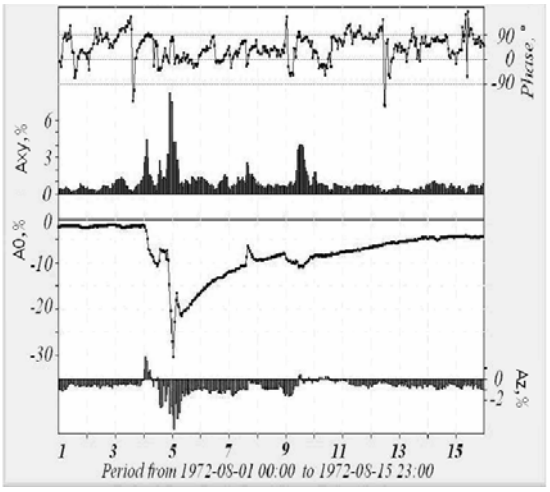

Fig. 5. Presentation of four parameters of CR variations simultaneously: phase and amplitude of CR anisotropy (equatorial component A_{xy}), density of CR variations (A_0) and north south component of CR anisotropy (A_z) during the large (~30%) FE in August 1972.

Another kind of pictures presents long time behavior of some CR parameters. For example, Fig. 3 shows variation of CR density (A_0) by hourly averaged data throughout the period of observation (1965-2003). These variations are displayed relatively base year 1976.

It is possible also to plot hourly values of *SigmaH* (Fig.4) which indicate an adequacy of the used model for CR variations. There is also a possibility to plot for any arbitrary period simultaneous behavior of all characteristics in a graphical form as it illustrates Fig. 5, where temporal variations of amplitude of CR anisotropy vector in the equatorial plane (*Axy*), its phase, density variation A_0 and north-south anisotropy A_z are presented altogether. Data in graphical and digit formats can be obtained upon the request for any time interval with hourly, daily and monthly averaging.

V. USAGE OF DB A10 FOR SCIENTIFIC AND APPLIED PROBLEMS

Database of CR anisotropy can be used in two types of problems. The first one is an investigation of structural characteristics of SW and their dynamics, calculations of CR gradients, searching for correlations between parameters of the interplanetary medium and characteristics of CR variations ([3], [4], [5], [6], [7], [8], [17], [18]). As an example of this DB usage, in Fig. 5 the long term behavior of monthly means of amplitude and phase of the CR daily anisotropy is shown through 1965 - 2005.

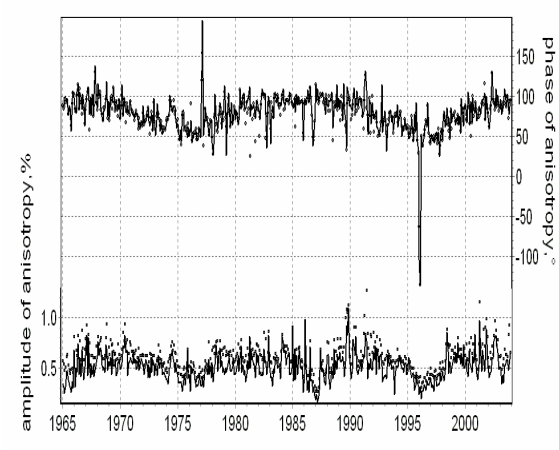

Fig. 6. Monthly values of the amplitude and phase of the CR solar diurnal anisotropy for the quiet (solid lines) and disturbed (points) periods derived by the hourly data through 1965-2003.

One can see the 22-year recurrence of the phase and 11-year recurrence of amplitude of CR anisotropy. On this background the numerous fluctuations and anomalies are seen, certainly not of statistic origin since the statistic errors are very small here. Especially big jumps in the phase behavior revealed in 1976 and 1996- in the minima of the solar cycles. It is pertinent to note that analogous behavior was observed also in 1954 as it was mentioned in ([4] and references there). In Fig.6 long term changes of the anisotropy vector are shown during the whole period of CR monitoring for the quiescent and disturbed days. The method of quiescent and disturbed day selection is described in details in [7]. There are about 340000 monthly vectors for almost 4 cycles of solar activity. These monthly values are obtained by the hourly parameters of CR anisotropy derived from the neutron monitor network data by the GSM method. One can see that anisotropy in disturbed days has bigger amplitude and differs by the phase from that in the quiet days. The mostly noticeable changes of the anisotropy phase have occurred after a reverse of the solar magnetic field in 1970-1972 and 1991-1992. However, well pronounced changes are also seen as before so after the reverse, in the solar activity minimum, when the abrupt decrease of the anisotropy amplitude is also indicated.

The second field of DB_A10 implementation is applied problems, for instance, a forecast of geomagnetic storms by the characteristic behavior of CR anisotropy prior the interplanetary shock arrival at Earth [9], [6], [18], [19]. Besides, in some cases it is necessary to exclude CR variations from observations, for example, during the latitudinal survey or estimation of water equivalent of snow cover thickness [20]. With this goal the Internet project, which would allow getting the expected variations within the model (1) for any period at any point on the globe, based on DB A10 data, is developing in interactive mode. These data will be also important for a more accurate determination of barometric coefficient for all available NMs ([21]).

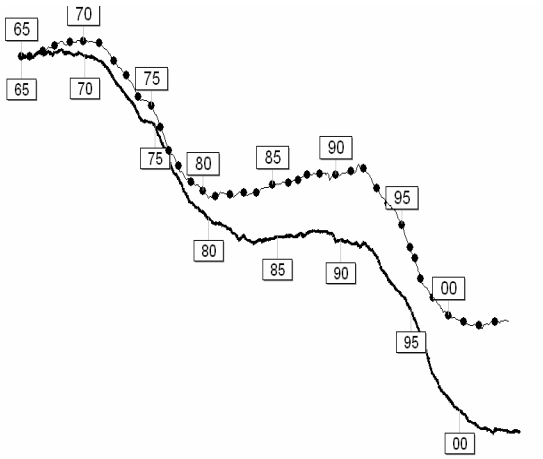

Fig. 7. Vector diagram of solar-diurnal anisotropy for the period 1965-2003: points correspond to the quiescent and tick solid line –to disturbed days.

VI. CONCLUSIONS

Basic parameters of CR variations (density and daily anisotropy for 10 GV particles) have been calculated and permanently used in various studies for a single case and separated periods. To extend these studies and to make the information easy accessible for a wide scientific community it was real necessity of data collection and combination the results for the whole period of CR monitoring into a single Data base.

The interactive database described (DB_A10) might be used for solving as pure

scientific well as applied problems. At present stage the users can take data only by format fixed in our database: they firstly have to select interactively the parameters, to form digital data saving them in some file and after this to process these data on their computer. But there is another way to work with MySQL database when we give an access to database and description of a structure of data storage, and user himself, without our mediate service writes a request to necessary fields which he can specify by a program. User may interactively get specific set of data (of course, within the frame of our DB). We can implement this function if to arrange access only for reading and publish the structure of data storage (name of tables and fields of database + description). In this case it will be possible that the MySQL database will provide data coupling with external systems and databases, using in other projects. This database would be very approval if to use CR parameters in real time mode- it would be real help in Space Weather forecasting. In fact, it is almost ready for such implementation if to add several stable working stations with real time data presentation.

ACKNOWLEDGEMENTS

This work is supported by RFBR grants 07-02-00915, 06-02-39028 and Program BR of the Presidium RAS "Neutrino Physics", and see also http://cr0.izmiran.rssi.ru/ThankYou/main.htm.

REFERENCES

[1] Dorman, L. I. Cosmic Rays, Variations and Space Explorations. North Holland, Amsterdam, 1974

[2] Krymsky G.F., Kusmin A.I., Krivoshapkin P.A., Samsonov I.S., Skripin G.V., Transky I.A., Chirkov N.P. *Cosmic rays and solar wind*, edited by G.V. Shafer, "Nauka", Novosibirsk, 1981 (in Russian).

[3] Nagashima K., *Three Dimensional Anisotropy in Interplanetary Space*, Part I, Rep. of Ionosphere and Space Res., 25, 3, 189, 1971.

[4] Belov A.V., E.A. Eroshenko, V.A. Oleneva, V.G. Yanke, Anomalous behavior of Cosmic Ray Anisotropy in the Last Minimum of the Solar Activity, 26-th ICRC, 7, 268-271, 1999

[5] Belov, A. V., J. W. Bieber, E. A. Eroshenko, P. Evenson, R. Pyle, and V. G. Yanke, CR anisotropy before and during the passage of major solar wind disturbances. Jornal Advances in Spase Res., v.31, N4, pp. 919-924, 2003a.

[6] Belov A. V., Eroshenko E. A., Heber B., Yanke V. G., Raviart A., Muller-Mellin R., Kunov H., Latitudinal and radial variation of >2 GeV/n protons and alpha particles in the southern heliosphere at solar maximum: Ulysses COSPIN KET and neutron monitor network observations, Annales Geophysicae, 21, No 6, 1295, 2003b.

[7] Belov, A.V., E. A. Eroshenko, V. A. Oleneva, V. G. Yanke, H. Mavromichalaki, Long-term behavior of the Cosmic-ray Anisotropy derived from the Worldwide Neutron Monitor Network Data, Proc. 20th ECRS-2006, http://www.lip.pt/events/2006/ecrs/proc/ecrs06-s0-123.pdf), 2006a.

[8] Belov, A.V., E. A. Eroshenko, H. Mavromichalaki, A. Papaioannou, G. Mariatos, V. G. Yanke, Cosmic ray modulation in August-September 2005, Proc 20th ECRS-2006, (http://www.lip.pt/events/2006/ecrs/proc/ecrs06-s0-173.pdf), 2006b.

[9] Leerungnavarat, K., Ruffolo, D., and Bieber, J.W. Loss Cone Precursors to Forbush Decreases and Advance Warning of Space Weather Effects, K. Astrophys. J., **593**, 587-596, 2003.

[10] Krymsky G.F., Kusmin A.I., Chircov N.P., Krivoshapkin P.A., Skripin G.V., Altuchov A.M. Cosmic ray distribution and reception vectors of detectors, G&A, 6, 991-997, 1966.

[11] Alania M.V., Belov, A.V., Blokh,Ya.L., Dorman, L.I., Eroshenko, E.A., Inosemtseva,O.I., Kaminer, N.S., Rodionov, A.V., Shatashvili,L.Kh. Preliminary results of a study of cosmic ray variations in August 1972. Izv. AN USSR, ser. Phys., 37, No 6, 1211-1221, 1973.

[12] Baisultanova L., Belov A., Dorman L., Yanke V., Magnetopheric effects in cosmic rays during Forbush decrease, Proc. 20th ICRC, Moscow, v. 4, 231, 1987.

[13] Dvornikov, V.M., Sdodnov, V.E. Time variations of the cosmic ray distribution function during a solar event of September 29, 1989. J. Geophys. Res. 102, A11, 24209–24219. 1997.

[14] Yasue S., Mori S., Sakakibara S., Nagashima K. "*Coupling Coefficients of Cosmic Ray Daily Variations for Neutron Monitor Stations*", Rep. of Cosmic Ray Research Laboratory, Nagoya University, Japan, No. 7, 1982.

[15] Belov, A., Baisultanova, L., Eroshenko, E., Mavromichalaki, H., Yanke, V., Pchelkin, V., Plainaki, C., Mariatos, G.. Magnetospheric effects in cosmic rays during the unique magnetic storm on November 2003, *JGR*, Vol. 110, A09S20, doi:10.1029/2005JA011067, 2005

[16] Shea, M.A., and Smart, D.F., Fifty years of cosmic radiation data. Space Science Rev., 93, 229-262, 2000.

[17] Belov, A.V., E. A. Eroshenko, V. A. Oleneva, V. G. Yanke. Connection of Forbush effects to the X-ray flares, JASTP, doi:10.1016/j.jastp.2007.08.021, 2007.

[18] Munakata, K., T. Kuwabara, S. Yasue, C. Kato, S. Akahane, M. Koyama, Y. Ohashi, A. Okada, T. Aoki, K. Mitsui, H. Kojima, and J. W. Bieber, A "Loss-Cone" Precursor of an Approaching Shock Observed by a Cosmic-Ray Muon Hodoscope on October 28, 2003,Geophys. Res. Lett., **32**, L03S04, doi:10.1029/2004GL021469, 2005.

[19] Qin, G., J. W. Bieber, and G. P. Zank, Loss-cone precursors to Forbush decreases and Advance Warning of Space Weather Effects, Astrophys. J. (Lett.), **590**, L53-L56, 2003

[20] Paquet E., Laval M., Belov A.V., Eroshenko E.F., Kartyshov V.G, Struminsky A.B., Yanke V.G., Definition of the snow thickness from the absorption of cosmic ray neutron component. Proc. 30 ICRC, SH.3.6, 2007.

[21] Belov, A.V., Dalgatova, Kh.I., Eroshenko, E.A., et al. Long Time Modulation of the Neutron Monitors Barometric Coefficients. Proc. of 23ICRC, V.3, 623, 1993

Appendix 1: FULL LIST OF NEUTRON MONITORS USED FOR THE DATA BASE

Name	Lat	Long	Alt	H0	Rc	C10	A11	Ph11	Type From-to
1 AATA	43.25	76.92	806	938	6.66	0.044	0.606	79.5	6NM64 57-08 ALMA-ATA A
2 AATB	43.14	76.60	3340	675	6.69	0.038	0.660	86.0	18NM64 73-08 ALMA-ATA B
4 AHMD	23.01	72.61	50	1000	15.94	0.066	0.456	69.3	18NM64 57-73 AHMEDABAD
5 ALRT	82.50	-62.33	57	1003	0.10	0.800	0.083	37.0	18NM64 65-88 ALERT
6 APTY	67.55	33.33	177	1000	0.65	0.488	0.592	39.9	18NM64 61-08 APATITY
7 ATHN	37.97	23.72	40	1000	8.72	0.107	0.493	77.1	3NM64 70-78 ATHENS
8 BKSN	43.28	42.69	1700	820	6.91	0.000	0.000	0.0	6NM64 03-08 BAKSAN
9 BERN	46.95	7.98	570	1000	4.49	0.000	0.000	0.0	12IGY 77-08 BERN
10 BJNG	39.08	116.27	48	1000	9.56	0.050	0.435	73.2	18NM64 84-08 BEIJING
11 BRBG	78.12	14.42	0	1013	0.20	0.000	0.000	0.0	6NM64 00-08 BARENTSBURG
12 BRSB	-27.42	153.12	0	1010	7.21	-0.060	0.531	80.4	12IGY 68-73 BRISBANE
13 BUEN	-34.60	-58.48	0	1000	10.63	-0.053	0.471	64.5	18IGY 57-66 BUENOS AIRES
14 CALG	51.08	-114.13	1128	883	1.08	0.135	0.761	25.3	12NM64 64-08 CALGARY
15 CAPS	68.92	-179.47	0	1016	0.45	0.510	0.573	32.9	12NM64 67-08 CAPE SHMIDT
16 CDBA	-31.42	-64.20	434	982	11.45	-0.071	0.524	64.1	12IGY 64-70 CORDOBA
17 CHCL	-16.32	-68.15	5200	552	13.10	-0.045	0.627	69.1	12NM64 61-75 CHACALTAYA
18 CHGO	41.83	-87.67	200	1000	1.72	0.000	0.000	00.0	12IGY 57-71 CHICAGO
19 CHUR	58.75	-94.08	39	1000	0.21	0.459	0.634	19.6	18NM64 57-73 CHURCHILL
20 CLMX	39.37	-106.18	3400	685	3.03	-0.132	0.705	50.1	12IGY 53-08 CLIMAX
21 COLL	64.08	-147.83	91	1013	0.54	0.387	0.666	15.2	12IGY 57-68 COLLEGE
22 DALS	32.98	-96.73	208	1017	4.35	-0.123	0.620	55.8	18NM64 64-73 DALLAS
23 DENV	39.67	-104.97	1600	850	2.91	-0.101	0.705	45.2	12IGY 64-66 DENVER
24 DPRV	46.10	-77.50	145	996	1.02	0.166	0.726	37.4	48NM64 57-95 DEEP RIVER
25 DRBS	50.10	4.60	225	987	3.24	0.142	0.643	60.6	6NM64 69-97 DOURBES
26 DRHM	43.10	-70.83	0	1000	1.41	0.113	0.711	43.5	18NM64 64-91 DURHAM
27 ELSW	-77.72	-41.13	0	1000	0.79	0.000	0.000	0.0	12IGY 59-61 ELLSWORTH
28 ERVN	40.17	44.25	2000	800	7.60	0.040	0.550	80.0	18NM64 88-08 EREVAN
29 ERV3	40.17	44.25	3200	700	7.60	0.040	0.580	86.0	18NM64 99-08 EREVAN3
30 ESOI	33.30	35.79	2055	800	10.00	0.040	0.450	70.0	6NM64 98-08 ESOI mt.Hermon
31 FSMT	60.02	-111.93	0	1000	0.30	0.000	0.000	0.0	18NM64 00-08 Fort SMITH
32 FRBG	48.00	7.80	0	1000	3.41	0.000	0.000	0.0	12IGY 57-59 FREIBURG
33 FUSH	37.75	140.48	66	1000	10.55	0.029	0.438	65.9	6NM64 74-78 FUKUSHIMA
34 GOTT	51.52	9.93	273	1000	3.00	0.000	0.000	0.0	12IGY 57-59 GOTTINGEN
35 GSBY	53.27	-60.40	46	1011	0.52	0.349	0.677	38.8	18NM64 64-08 GOOSE BAY
36 HALL	51.48	11.97	100	1000	3.07	0.160	0.640	59.9	12IGY 60-71 HALLE
37 HBRT	-42.90	147.33	0	1000	1.88	-0.127	0.697	49.6	9NM64 67-73 HOBART
38 HEIS	80.60	58.00	20	1000	0.10	0.715	0.327	38.2	12IGY 58-70 HEISS ISLAND
39 HFLK	47.31	11.38	2290	830	4.37	0.093	0.660	68.8	3NM64 68-95 HAFELEKAR
40 HLE1	20.72	-156.27	3052	724	13.30	-0.091	0.511	62.7	12IGY 63-08 HALEAKALA1
41 HLEA	20.72	-156.27	3052	724	13.30	-0.091	0.511	62.7	6NM64 85-08 HALEAKALA
42 HRMS	-34.42	19.22	26	1013	4.90	0.073	0.554	58.1	12NM64 57-08 HERMANUS
43 HRST	50.87	0.33	23	1000	2.93	0.000	0.000	0.0	12IGY 57-60 HERSTMONCEUX
44 HUAN	-12.03	-75.33	3400	704	13.45	-0.063	0.545	67.1	12IGY 53-96 HUANCAYO
45 INVK	68.35	-133.72	21	1011	0.18	0.542	0.568	8.6	18NM64 64-08 INUVIK
46 INVC	-46.50	168.37	0	1000	1.86	0.000	0.000	0.0	12IGY 58-60 INVERCARGILL
47 IRK2	52.37	100.55	2000	800	3.66	0.090	0.637	59.6	12NM64 81-08 IRKUTSK2
48 IRK3	51.29	100.55	3000	715	3.66	0.090	0.637	59.6	6NM64 81-08 IRKUTSK3
49 IRKT	52.47	104.03	433	965	3.66	0.090	0.637	59.6	18NM64 58-08 IRKUTSK
50 JUN1	46.55	7.98	3550	643	4.48	0.078	0.696	70.6	12IGY 58-08 JUNGFRAUJOCH1
51 JUNG	46.55	7.98	3550	643	4.48	0.078	0.696	70.6	3NM64 61-08 JUNGFRAUJOCH
52 KAMP	0.33	32.55	1196	900	14.98	0.078	0.495	63.8	12IGY 57-69 KAMPALA (MAKERERE)
53 KERG	-49.35	70.25	0	1000	1.19	-0.103	0.733	19.5	18NM64 57-08 KERGUELEN
54 KHAB	48.50	135.20	0	1003	5.54	0.005	0.584	69.0	18NM64 71-77 KHABAROVSK
55 KIEL	54.33	10.13	54	1007	2.29	0.202	0.659	55.2	18NM64 57-08 KIEL
56 KIEV	50.72	30.30	120	1000	3.62	0.136	0.650	59.0	18NM64 70-98 KIEV
57 KLNG	54.12	11.77	70	1000	2.43	0.201	0.674	55.1	12IGY 64-67 KUHLUNGSBORN
58 KODI	10.23	77.48	2343	786	17.47	0.069	0.509	67.9	12IGY 57-64 KODAIKANAL
59 KRNA	67.83	20.43	400	979	0.54	0.510	0.593	41.0	12NM64 70-74 KIRUNA
60 KULA	20.73	-156.33	915	933	13.30	-0.074	0.509	61.1	3NM64 66-72 KULA
61 LAES	-6.73	147.00	0	1000	15.52	0.000	0.000	0.0	12IGY 57-66 LAE STATION
62 LARC	-62.20	-58.96	40	1000	3.00	0.000	0.000	0.0	6NM64 96-08 LARC King George
63 LEED	53.83	-1.58	72	1008	2.20	0.216	0.655	56.4	18NM64 57-83 LEEDS
64 LINC	40.82	-96.68	350	994	2.22	0.000	0.000	0.0	12IGY 57-59 LINCOLN
65 LMKS	49.20	20.22	2634	733	4.00	0.105	0.685	65.9	8NM64 58-08 LOMNICKY STIT
66 LNDH	51.60	10.10	140	1000	3.00	0.174	0.653	59.2	18NM64 59-73 LINDAU
67 LND1	51.60	10.10	140	1000	3.00	0.174	0.653	59.2	12IGY 59-70 LINDAU
68 LNDN	51.53	-0.10	45	1000	2.73	0.174	0.653	59.2	12IGY 57-65 LONDON
69 SNTG	-33.48	-70.71	540	960	11.00	0.000	0.000	0.0	6NM64 01-08 SANTIAGO
70 MCMD	-77.85	166.72	48	992	0.01	-0.798	0.118	106.6	18NM64 60-08 MCMURDO
71 MGDN	60.12	151.02	0	982	2.10	0.148	0.664	45.0	18NM64 71-08 MAGADAN
72 MWSN	-67.60	62.88	30	990	0.22	0.000	0.000	0.0	18NM64 57-08 MOWSON

73 MINA -23.10 -65.70 4000 646 12.51 -0.040 0.562 68.2
12IGY 57-69 MINA AGUILA
74 MKPU 21.30 -157.65 100 1000 13.23 0.000 0.000 0.0
12IGY 57-63 MAKAPUU POINT
75 MUNC 48.20 11.60 500 972 4.14 0.000 0.000 0.0
12IGY 59-69 MUNCHEN
76 MOSC 55.47 37.32 200 1000 2.46 0.202 0.661 51.6
24NM64 58-08 MOSCOW
77 MRCH 80.05 18.25 0 1000 0.06 0.000 0.000 0.0
12IGY 57-59 MURCHISON BAY
78 MRKA 39.70 141.13 135 1000 10.16 0.028 0.454 68.9
20NM64 70-87 MORIOKA
79 MRNY -66.55 93.02 30 1013 0.04 -0.606 0.522 -7.9
12NM64 63-08 MIRNY
80 MTNR 36.11 137.55 2770 720 11.39 0.005 0.497 68.5
12NM64 56-92 Mt. NORIKURA
81 MTWL -42.92 147.23 725 946 1.89 -0.122 0.720 50.0
6NM64 57-95 Mt. WELLINGTON
82 MTWS 44.30 -71.30 1900 822 1.24 0.122 0.758 44.2
12IGY 55-91 Mt. WASHINGTON
83 MURM 67.55 33.33 0 1000 0.65 0.000 0.000 0.0
12IGY 58-61 MURMANSK
84 MWSN -67.60 62.88 0 1010 0.22 -0.484 0.623 -5.5
6NM64 57-71 MAWSON
85 MXCO 19.33 -99.18 2274 794 9.53 -0.077 0.494 71.2
6NM64 69-08 MEXICO CITY
86 NAIN 56.55 -61.68 0 1000 0.40 0.000 0.000 0.0
18NM64 00-08 NAIN
87 NDRH 52.20 5.20 0 1000 2.76 0.000 0.000 0.0
12IGY 58-65 NEDERHORST
88 NRLK 69.26 88.05 0 1005 0.63 0.503 0.579 36.4
18NM64 71-08 NORILSK
89 NTHF 44.47 -93.25 287 1013 1.43 0.000 0.000 0.0
12IGY 58-58 NORTHFIELD
90 NVBK 54.80 83.00 163 1000 2.91 0.165 0.654 53.5
24NM64 71-08 NOVOSIBIRSK
91 NWRK 39.68 -75.75 50 1013 1.97 0.039 0.699 47.5
9NM64 78-08 NEWARK
92 OTWA 45.44 -70.68 101 1008 1.08 0.154 0.720 39.2
12IGY 54-72 OTTAWA
93 OULU 65.02 25.50 0 1000 0.81 0.431 0.619 42.0
9NM64 64-08 OULU
94 PICD 42.93 0.25 2860 734 5.36 0.084 0.652 78.6
9NM64 57-77 PIC-DU-MIDI
95 PTFM -26.68 27.10 1351 869 7.30 0.052 0.477 58.8
12IGY 71-08 POTCHEFSTROM
96 PUTR -18.18 -69.55 3589 665 12.00 0.000 0.000 0.0
3IGY 03-08 PUTRE
97 PWNK 54.98 -85.44 0 1000 0.50 0.000 0.000 0.0
18NM64 00-08 PEAWANUCK
98 PRED 47.70 12.90 1614 900 4.29 0.000 0.000 0.0
3NM64 80-86 PREDIGTSTUHL
99 RIOD -22.95 -43.17 0 1013 11.73 0.000 0.000 0.0
12IGY 57-62 RIO DE JAN.
100 ROME 41.86 12.47 60 1009 6.32 0.100 0.528 77.3
17NM64 57-08 ROME
101 RSLT 74.68 -94.90 17 1000 0.10 0.737 0.298 8.9
6NM64 57-70 RESOLUTE BAY
102 SDNY -33.89 151.19 43 1013 4.69 0.000 0.000 0.0
12IGY 58-59 SYDNEY
103 SEOL 37.53 126.93 45 1005 10.79 0.045 0.454 66.3
6NM64 72-77 SEOUL
104 SLMA 51.20 -115.60 2283 781 1.14 0.113 0.786 26.0
6NM64 57-77 SULPHUR MT.
105 SLM1 51.20 -115.60 2283 781 1.14 0.113 0.786 26.0
12IGY 57-71 SULPHUR MT.
106 SNAE -70.67 -2.85 52 987 1.06 -0.296 0.685 20.4
6NM64 64-08 SANAE
107 SNA8 -70.30 -2.35 52 987 1.06 0.296 0.685 20.4
4NM80 85-93 SANAE8
108 SOPO -90.00 0.00 2820 680 0.11 -0.750 0.435 -8.6
3NM64 64-08 SOUTH POLE
109 SOPB -90.00 0.00 2820 680 0.11 -0.750 0.435 -8.6
3MNM 64-08 SOUTH POLE, without PB
110 SVER 56.73 61.07 300 997 2.30 0.217 0.668 48.1
18NM64 73-88 SVERDLOVSK
111 SWTH 39.90 -75.35 80 1013 1.92 0.043 0.701 47.3
9NM64 64-78 SWARTHMORE
112 SYWA -69.00 39.60 15 1000 0.42 -0.409 0.662 1.0
12IGY 60-68 SYOWA BASE
113 TASH 41.33 69.62 565 963 8.34 0.074 0.531 77.4
18NM64 75-92 TASHKENT
114 TBLS 41.72 44.80 510 950 6.91 0.085 0.551 76.0
18NM64 63-08 TBILISI
115 TERA -66.65 140.01 45 1000 0.01 -0.722 0.361 18.7
9NM64 67-08 TERRE ADELIE
116 TIBT 30.11 90.53 4300 606 14.10 0.000 0.000 0.0
28NM64 98-08 TIBET
117 TKYO 35.75 139.72 40 1014 11.61 0.037 0.468 66.0
18NM64 70-97 TOKYO (ITABASHI)
118 THAI 18.58 98.48 2565 690 17.10 0.000 0.000 0.0
20NM64 07-08 DOI INTHANON
119 TSMB -19.20 17.58 1240 880 9.29 0.040 0.440 59.0
18NM64 76-08 TSUMEB
120 THUL 76.50 -68.70 260 1005 0.10 0.774 0.230 26.5
9NM64 57-08 THULE
121 TXBY 71.60 128.90 0 1000 0.53 0.510 0.573 32.9
18NM64 66-08 TIXIE BAY
122 UPPS 59.85 17.55 0 1013 1.43 0.316 0.663 47.5
12IGY 57-71 UPPSALA
123 USHU -54.80 -68.30 0 1020 5.68 -0.073 0.547 76.5
12IGY 57-72 USHUAIA
124 UTRT 52.10 5.12 0 1013 2.76 0.176 0.652 59.2
18NM64 63-78 UTRECHT
125 VICT 48.42 -123.32 71 1000 1.86 0.031 0.710 30.6
18NM64 64-69 VICTORIA
126 VSTK -78.47 106.87 3488 632 0.10 -0.855 0.284 -55.6
6NM64 63-82 VOSTOK
127 WELL 41.22 174.92 0 1013 3.42 0.000 0.000 0.0
12IGY 57-65 WELLINGTON
128 WLKS -66.42 110.45 0 1010 0.01 -0.673 0.451 -3.2
12IGY 62-69 WILKES
129 YKTK 62.02 129.73 105 1000 1.70 0.243 0.674 44.3
18NM64 57-08 YAKUTSK
130 ZUGS 47.42 10.98 2960 707 4.24 0.088 0.688 69.4
12IGY 57-78 ZUGSPITZE

The designations used: **Name**- name of the station from 4 symbols as it was standardized by M. Shea and L. Gentile for GLE Data base;

Lat, Long, Alt –Latitude, Longitude (in degrees) and Altitude (in meters) of the station;

H0 – Standard atmospheric pressure for the station (in mb);

Rc – geomagnetic cut off rigidity for the epoch of 1965.

C10 –reception coefficient for isotropic part of CR variations for =0, and upper rigidity 100GV;

A11(Cx) and **Ph11(Cy)**-reception coefficients for equatorial component of CR anisotropy (for spectra with index 0 and upper rigidity 100 GV) as it is present in Yasue et al., (1983)

Type means a type of NM used on the station. In this Table the types for the last period of operating are entered. Many stations have changed equipment during the history of observation. This is reflected in more detailed Table by Shea and Smart, 2000.

Column **"From-to"** means the years through station operated. Of course, many stations worked on IGY monitor up to at least 1964 when NM64 has been invented.

The last column gives the full name of station.

Real-time database for high resolution Neutron Monitor measurements

C. T. Steigies, O. M. Rother, R. F. Wimmer-Schweingruber, B. Heber

Institut fuer Experimentelle und Angewandte Physik,
Christian-Albrechts-Universiatat zu Kiel, Kiel, Germany
(steigies@physik.uni_kiel.de)

Abstract – **The worldwide network of standardized neutron monitors is, after 50 years, still the state-of-the-art instrumentation to measure spectral variations of the primary cosmic ray component. These measurements are an ideal complement to space based cosmic ray measurements. Data from the approximately 50 IGY and NM64 neutron monitors is stored locally but also available through data collections sites like the World Data Center (WDC) or the IZMIRAN ftp server. The data from the WDC is in a standard format, but only hourly values are available. IZMIRAN collects the data in the best available time resolution, but the data arrives on the ftp server only hours, sometimes days, after the measurements. Also, the high time-resolution measurements of the different stations do not have a common format, a conversion routine for each station is needed before they can be used for scientific analysis. We propose to setup a real-time database where high resolution cosmic ray measurements can be store and accessed immediately after the measurement. Stations that do not have 1-minute resolution measurements should be upgraded to 1-minute or better resolution with an affordable standard registration system, that will submit the measurements to the database via the internet in real-time. This resolves the problem of different data formats and for the first time allows using real-time cosmic ray measurements for space weather predictions.**

Advanced Date Acquisition System for SEVAN

Suren Chilingaryan[1], Ashot Chilingaryan[2], Varuzhan Danielyan[2], and Wolfgang Eppler[1]

[1] *Institut fuer Prozessdatenverarbeitung und Elektronik, Forschungszentrum Karlsruhe, Hermann-von-Helmholtz-Platz 1, 76344 Eggenstein-Leopoldshafen, Germany,*
[2] *Cosmic Ray Division, Alikhanyan Physics Institute, Alikhamyan Brothers st. 2, Yerevan 36, Armenia*

Abstract – **For a reliable and fast forecast of Space Weather world-wide networks of particle detectors are operated at different latitudes, longitudes, and altitudes. Based on a new type of hybrid particle detector developed in the context of the International Heliophysical Year (IHY 2007) at ASEC (Aragats Space Environmental Center) we start to prepare hardware and software for the first sites of SEVAN (Space Environmental Viewing and Analysis Network). In the paper the architecture of the newly developed data acquisition system for SEVAN is presented. We plan to run SEVAN network under one-and-the same data acquisition system, enabling fast integration of data for on-line analysis of Solar Flair Events. An advanced data acquisition system is designed as a distributed network of uniform components connected by web services. Its main component is URCS (Unified Readout and Control Server) which controls the underlying electronics by means of detector specific drivers and makes a preliminary analysis of the on-line data. The lower level components of URCS are implemented in C and a fast binary representation is used for the data exchange with electronics. However after preprocessing, the data is converted to a self-describing hybrid XML/Binary format. To achieve better reliability all URCS are running on embedded computers without disk and fans to avoid the limited lifetime of moving mechanical parts. The data storage is carried out by means of two high performance servers working in parallel to provide data security. These servers are periodically inquiring the data from all URCS and storing it in MySQL database. The implementation of the control interface is based on high level web standards and, therefore, all properties of the system can be remotely managed and monitored by the operators using internet browsers. The advanced data acquisition system at ASEC in Armenia was started November, 2006. The reliability of the multi-client service was proofed by continuous monitoring neutral and charged cosmic particles. 7 particle monitors are located at 2000 and 3200 meters above sea level at a distance of 40 and 60 km from the main data server.**

***Key Words*— Data Acquisition, IHY, Particle Monitor, Detector Network.**

I. INTRODUCTION

GCR (Galactic Cosmic Rays, mostly protons and heavier nuclei), may be accelerated in our Galaxy by supernova explosions in jets ejected from black holes or by other exotic stellar sources. After traveling millions of light years in our Galaxy they arrive in solar system as highly isotropic and stable flux. On the other side, our Sun is a very variable object changing radiation and particle flux intensities on many orders of magnitude within a few minutes. Because of sun's closeness the effects of changing fluxes have a major influence on the earth, including climate, safety and other issues [1].

Therefore the solar flux of cosmic rays can be described as a modulation of the stable galactic cosmic ray "background". The sun modulates GCR in several ways. The explosive flaring processes on the Sun result in ejection of huge amounts of solar plasma and in acceleration of the copious electrons and ions. These particles constitute, so called, SCR (Solar Cosmic Rays). The SCR reach the earth and initiate secondary elementary particles in the terrestrial atmosphere, increasing the counting rates of particle monitors by several percents. This effect is called ground level enhancement. Other, non-direct solar modulation effects influence also the intensity of GCR. The solar wind "blows out" the lowest energy GCR from the solar system, thus changing the GCR flux intensity inverse proportionally to the sun activity. The very fast solar wind from the coronal holes, huge magnetized plasma clouds and shocks initiated by coronal mass ejections are traveling in the interplanetary space and interact with GCRs. On arrival at the earth the magnetic field of the plasma cloud deplete the GCR, measured as decrease of the secondary cosmic particles (so called Forbush decrease) [2].

Hybrid particle monitors at ASEC (Aragats Space Environmental Center [3, 4]) measure both charged and neutral components of secondary cosmic rays and provide a good coverage of different species of secondary cosmic rays with different energy thresholds. A multivariate correlation analysis of the detected fluxes of charged and neutral particles is used for analysis of geo-effective events, i.e. Ground Level Enhancements, Forbush decreases, Geomagnetic Storms and for reconstruction of the energy spectra of SCR [4].

The particle monitors are located in the two research stations on the slopes of Aragats Mountain at altitudes 2000 and 3200 meters above sea level and are connected with the data analysis center in Yerevan by means of a wide-range radio network. Additionally, there is an ongoing process of establishing a world-wide network of detectors operating at different latitudes, longitudes and altitudes.

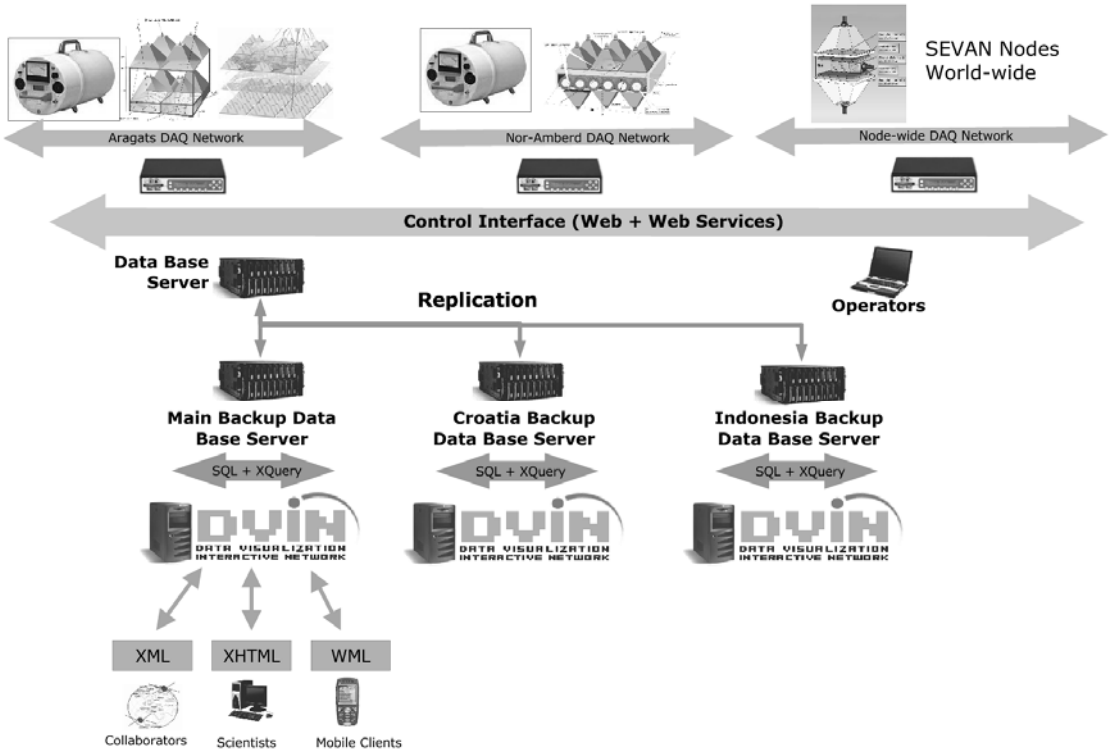

Fig. 1. The figure represents a layout of the new ASEC data acquisition system. Several detector arrays are operating at Nor-Amberd and Aragats research stations. The detectors are controlled by URCS which are installed on each station. The data dissemination and detector control is facilitated by web services. The DVIN is used to distribute the data to end users.

I. Aragats Data Acquisition System

The ADAS (Aragats Data Acquisition System [5]) is developed having in mind the distributed nature of GCR detection networks often consisting of multiple detectors located in hardly accessible places world-wide. To simplify cooperation of research groups and open a way for integration with other particle detection networks the inter-component communication is released on top of high level standards. The new extensible XML based data format is used for the data storage and exchange.

ADAS is constructed from uniform autonomous components, named URCS (Unified Readout and Control Server). The URCS server takes care for the readout of experimental data from SEVAN particle detectors provides detector control, preliminary analysis and distribution of the data to other system components. The important point on URCS architecture is independence from external information. The collected data is in local data storage and distributed to the clients upon a request using web services. Therefore, the server can operate without connection to the rest of the data acquisition network for a long time.

The dissemination of the data is established by means of the Web Services. Along with treating the experimental measurements the URCS server provides a set of control interfaces for both detector electronics and URCS software behavior. On the basis of these control interfaces the web frontend provides the operator with a full set of remote management

capabilities.

In addition to the URCS servers the ADAS incorporates alarm services, data storage subsystems running on local file servers. The alarm service is used to issue e-mail notifications about severe conditions of Space Weather or/and electronic failures. The data storage servers are periodically inquiring the data from all URCS servers and storing it in a database on reliable servers in each of the SEVAN sites. Further, the stored data is analyzed by off-line software and made available for the physical analysis by means of DVIN (Data Visualization Interactive Network [6]) interface. The **Fig. 1**presents the overall system design.

A. Frontend Computers

In order to improve the system stability we are using the same Minibox M100 (VIA C3 533MHZ, 512 MB RAM) computers based on VIA Eden platform at all research stations. The computers are equipped with Gentoo Linux based operating system which is used in conjunction with the 2.6 family Linux kernel optimized for the real-time applications. The major advantage of the platform is the complete absence of moving mechanical parts. The system has passive (fan-less) cooling. Instead of a hard drive, the CF (Compact Flash) memory card is used. A small LCD keypad embedded into the computers is used to represent current system status, notify operators about critical failures and provides a way for basic system management.

The usage of CF (Compact Flash) cards drastically simplifies the software installation and upgrade. The installation can be performed on any computer equipped with CF card reader facility. The installation software asks several questions on the URCS configuration (Name, IP address, Type of Hardware etc.) and, then, installs all required system files, URCS software and configuration files on a provided CF disk.

To upgrade URCS software on the running system it is only needed to replace current CF card with a newer one. This operation is very simple and can be performed by the technical staff.

B. Unified Control and Readout Server

The URCS server is complex software consisting of multiple interacting components. In the first place it is a URCS daemon - readout software which takes care of communication with underlying electronics. The communication is performed by means of dedicated drivers while most of the software is the same for all supported detectors. The daemon reads the data from underlying detectors, makes preliminary analysis if necessary, and stores it in the files on the local file system.

The communications with remote components are carried out by means of web services running on a Apache web server. These web services hide the details of the URCS daemon providing a very simple interface for both the data dissemination and control capabilities to the external world. The data access is well structured. Each underlying particle monitor has its own address space and may provide to end client one or more independent data sets. The data channels in all data sets are described by metadata properties. These properties may include information on SEVAN sites (names of destination, geographical co-ordinates, altitudes, cut-off rigidities, etc). The set of properties describing all data sets belonging to a certain SEVAN site are collected in the site description and are available to the clients upon a request as well.

The client applications are able to request the latest data from the desired data set or the data for certain historical periods.

C. URCS Operator Frontend

The operator web frontend is a URCS component providing a uniform way for the remote control of URCS servers and underlying electronics. By means of the interface the operator is able to perform a full range of monitoring and control operations. It is possible to view various aspects of the current URCS operation, modify actual configurations, start and stop readout daemons or access the URCS log files for the desired period.

The operator is able to browse the data stored on the remote URCS servers. The current data is presented in a fully annotated fashion using associated detector descriptions. The historical data is available in XML, HTML and/or CSV (Comma-Separated Values) forms.

The continuous data quality monitoring is feasible by the provided AJAX (Asynchronous JavaScript and XML) interface which is depicting various aspects of the most recent data by means of SVG (Scalar Vector Graphics) charts. Additionally, metadata properties specify special conditions demanding the operator intervention. If such condition is met the interface will signal an alarm to the operator.

D. Error Handling

The URCS server allows auto-recovery from system failures. In the case of a hardware failure the problem is logged and the controlling driver performs the hardware re-initialization. Most of possible software problems are handled internally. If a non-recoverable error is encountered the daemon leave an emergency message in the log. In the last case it would be automatically restarted by a special system daemon which is monitoring status of all URCS components and restarting them in the case of a detected problem.

E. Data Storage

The data is stored by means of two powerful servers working in parallel at the main lab. The dual-core AMD Athlon X2 4800+ systems equipped with 4GB of memory and two Serial-ATA 500GB hard drives are used. The hard drives are as a mirroring raid configured. These servers periodically inquire the data from all URCS servers and store it in a MySQL database.

Additionally, in order to enhance data safety and optimize data access for local clients each of the SEVAN sites is equipped with mirror database server. The database synchronization is achieved using replication mechanism of the database engine.

II. Data Format

To simplify cooperation of SEVAN research groups, to enable data processing automation and to open a way for integration of all SEVAN sites new extensible XML based data format is developed for the data storage and exchange.

The ADASS data is consisting of two components:

(i) Collected data along with several properties characterizing the data, including the data timestamp, data quality, etc.

(ii) SEVAN site description providing detailed information on the detector location and orientation.

The detector description consists of three main components: Global Detector Description, Detector Geometry and Logical Data Layout. The Global Detector Description provides standard metadata describing the whole detector. It contains detector name, country, institution, group, principal investigators contact information, geographical location, etc.

The Detector Geometry describes the detector component parts as well as their positions and dimensions.

The multiple Data Layout sections indicate the physical meaning and acceptable value ranges of the data values. The first two components are preliminary filled during the detector setup and the data layout is automatically generated by the URCS software. Still additional properties may be specified manually on the setup stage.

The data collected by each of the detectors are divided into one or more independent data sets. Each data set is represented as a sequence of data vectors associated with the acquisition time (time series) and one or more Data Layout records in the detector description. The multiple layout records are considered to handle cases when the data set structure is changing during the detector operation. In a way similar to one used by the old data acquisition system at Aragats the data is represented by “space”-delimited ASCII strings. These ASCII strings are enclosed in the XML structure providing basic information about the enclosed data and referencing appropriate Data Layout sections of the detector description with the information on the values meaning. Example:

```
<Data installation="installationid" layout="layoutid">
  <Time>2006-02-25T16:50:00.0000000+04:00</Time>
  <Duration>PT30.0000000S</Duration>
  <Quality>100.00</Quality>
  <Value>1846 2760 1956 1848 1763 </Value>
</Data>
```

This example illustrates the representation of a single data element by the ADASS format. The installation and layout attributes are referencing the appropriate layout in the detector description. The Time and Duration elements are indicating the end and duration of the data integration time slice (both the timestamp and duration are represented following the encoding rules defined by the ISO-8601 specification). Special conditions encountered during the data acquisition are described using Quality element. Usually, this element indicates hardware failures resulting in partly or completely inaccurate data. The Value element holds a data vector in the space delimited ASCII representation.

The data storage subsystem at file servers downloads the data from the URCS server and stores it in the MySQL database. For each data set a separate table is created and for each attribute and element (installation, layout, Time, Duration, Quality) an individual column is used. All values will be represented by individual columns as well. Such mapping allows easy and fast access to the data, while the original XML form could be easily recovered. The description is not transported together with the collected data but available upon request from the URCS servers. However, the collected data and detector description can be reconciled in a single document for data exchange with collaborating groups.

Using the described approach the legacy application can easily extract ASCII strings from the data set and use them in the old fashion. The new applications are considering the XML description in order to extract the appropriate data subset from the data set.

III. Conclusion

In this paper a new data acquisition and control system for SEVAN network is proposed. The system has a modular layered architecture and is designed to work in the distributed environments. The most attention is devoted to the possibility of autonomous operation, error recovery and remote management capabilities.

To simplify cooperation of research groups and open a way for integration with other particle

detection networks the inter-component communication is released on top of the web services. New extensible self-describing data format is invented for the data storage and exchange.

To achieve better reliability the control software is running on embedded computers without disk and fans to avoid the limited lifetime of moving mechanical parts. The optimal performance is achieved by a multi-level abstraction model of the readout software. The tiny time critical hardware drivers are executed with a real-time priority and used to facilitate the communication with hardware. The main part of the software is executed with lower priority.

The control and monitoring subsystem is implemented using AJAX based dynamic web interfaces and is available to the operators by use of Internet browsers.

Since November 2006 ADAS is implemented at ASEC on the two research stations on the slopes of Aragats Mountain. After 10 months of operation the architecture of the system is ready for implementation in SEVAN world-wide particle detector network. In the next step the SEVAN network will be installed at Croatia, India and Indonesia.

REFERENCES

[1] K. S. Carslaw, R. G. Harrison, and J. Kirkby, "Cosmic Rays, Clouds, and Climate," *Science*, vol. 289, pp. 1732-1737, 2002.

[2] K. Munakata and et. al, "Precursors of geomagnetic storms observed by the muon detector network," *Journal of Geophysical Research*, vol. 105, pp. 27,457-27,468, 2000.

[3] A. Chilingarian and et. al, "Aragats Space-Environmental Center: Status and SEP Forecasting Possibilities," in *Journal of Physics G*, vol. 29, 2003, pp. 939-952.

[4] A. Chilingarian and et. al, "Correlated measurements of secondary cosmic ray fluxes by the Aragats Space-Environmental Center monitors," *Nuclear Instruments & Methods in Physics Research*, vol. A543, pp. 483-496, 2005.

[5] S. Chilingaryan, "Universal Data Exchange Solution for Modern Distributed Data Acquisition Systems and Its Implementation for Cosmic Ray Monitor Networks," vol. Ph.D. Yerevan, 2006.

[6] A. Chilingarian and A. Yeghikyan, "Data Visualisation Interactive Network for Aragats Space Environmental Center," presented at Inernational Symposium "Solar Extreme Events", Nor Amberd, Armenia, 2005.

Poster Session D

World-wide particle detector networks for space weather research

Chair: O. Kryakunova

Solar **E**xtreme **E**vents **2007**

Thorough phenomenological study of major Forbush decreases: Does the recovery depend on energy?

I.G. Usoskin, G.A. Kovaltsov, O.G. Gladysheva, T. Jamsen

Sodankyla Geophysical Observatory (Oulu unit), University of Oulu, Finland
(Ilya.Usoskin@oulu.fi)

Abstract **– We present a thorough statistical study of major Forbush decreases during the last decades, using cosmic ray data from ground based detectors – neutron monitors and muon telescopes. We show that many events depict features that are unexpected from the standard theory and earlier considerations, based on poorer statistical studies: (1) the recovery time of a Forbush decrease strongly depends on the mean response energy of the detector; (2) an over-recovery is observed in the most energetic cosmic ray data (muon detector). Such a behavior is not expected from the standard theory of a Forbush decrease and implies a need for a more detailed model. Here we suggest a simple qualitative scenario for the observed phenomenon.**

Multiplicity and Coupling Function of the neutron αnd muon components

E.V. Pletnikov[1], V. G. Kartyshov[1], V. G. Yanke[1], Ch. Sarlanis[2], G. Souvatzoglou[2]

[1] Institute of Terrestrial Magnetism, Ionosphere and Radio Wave Propagation by Pushkov, Russian Academy of Sciences (IZMIRAN), Russia (yanke@izmiran.ru)
[2]Nuclear and Particle Physics Section, Physics Department, Athens University, Athens, Greece

Abstract **– At present universally recognized software packages appeared on the calculation of cascade processes in different medium and energy ranges. The most fitted for our tasks version is the package of ATMOCOSMOS. Using this software the integral multiplicities for neutron, muon and electron-photon components of cosmic ray were obtained for different depths in the atmosphere and for 1-100 GeV energy range for the primary particles. Taking into account the sensitivity function the response functions have been calculated for some detectors and their approximation for a practical usage. Special attention was paid to a region of small.**

On the possibility to modernize existent network of Neutron Monitors

A.Chilingarian, G.Hovsepyan, K.Arakelyan, A.Avetisyan, S.Chilingarian,
V.Danielyan, K.Avakyan, A.Reymers, S.Tserunyan

Alikhanyan Physics Institute, Cosmic Ray Division, Armenia
(hgg@crdlx5.yerphi.am)

Abstract – **Despite decades of tradition, neutron monitors remain the state-of-the-art instrumentation for measuring spectral variations in the energy range from about 500 MeV to 20 GeV of the primary cosmic ray component (above the Earth's atmosphere). The worldwide network presently consists of about 50 standardized IGY and NM64 neutron monitors. We propose an update of this network by introducing new detectors and new electronics to be added to existing detectors, significantly enlarging its performance for solar physics and space weather research. We propose to locate scintillation detectors above and below (if construction of AM allows) the standard sections of NM. New scintillator detectors of size 1 x 1 x 0.01 m3 produced by the Institute of High Energy Physics, Protvino, Russia are compact and provide uniformity light collection. Measuring both neutral and charged flux of the secondary cosmic rays will allow to:**

- **Significantly enlarge the count rate of detector; note that flux of low energy charged particles is ~10 times higher than neutron flux;**
- **Explore more energetic population of the primary cosmic rays, giving possibility to estimate spectra of the solar cosmic rays;**
- **Distinguish Ground level Enhancements originated by solar neutrons;**
- **Estimate the incident direction of the additional flux of solar cosmic rays.**

New Data Acquisition (DAQ) electronics will provide also possibility to count total number of the evaporated neutrons originated in lead by hadrons entering NM. Number of neutrons is good proxy of the incident hadron energy

A 3NM-64_3He added to LARC for Solar Extreme Event studies

M. Storini, F. Signoretti, P. Diego, F. Re, M. Laurenza

INAF/IFSI-Roma, Via del Fosso del Cavaliere, 100 – 00133 Roma, Italy
(E-mail: storini@ifsi-roma.inaf.it)

***Abstract* – The Antarctic Laboratory for Cosmic Rays (LARC, acronym for *Laboratorio Antartico per I Raggi Cosmici* or *Laboratorio Antártico para Rayos Cósmicos*) operates on King George Island (South Shetlands). Since January 1991 a standard 6NM-64 detector has been recording continuous cosmic ray measurements and several Ground-Level Enhancements have been registered. Here we describe the different phases performed in Italy for the realization of a 3NM-64_3He detector, which started its measurements during the Italian XXII Antarctic Summer Campaign. Data recorded during solar activity cycle 24 will furnish an useful research tool for the next Solar Extreme Events.**

I. INTRODUCTION

The Antarctic Laboratory for Cosmic Rays (LARC) is presently the result of the joint collaboration between the Department of Physics of Chile University (UChile/FCFM) and the Institute of Interplanetary Space Physics of the National Institute for Astrophysics (IFSIRoma/INAF). The project is also supported by the National Antarctic Institute of Chile (INACH) and the National Program for the Antarctic Research (PNRA) of Italy. Since January 1991 a 6NM-64 has been operating at LARC, on a South Shetlands Island (King George, Fildes Bay, Ardley Cove; geographic coordinates determined by the Air Force of Chile: 62.20° S – 301.04° E; height: about 40 m). This neutron monitor was equipped with standard BP-28 (10BF3) counters, as well as most of the IQSY detectors of the world-wide network for cosmic ray measurements. Several aspects related to the standard 6NM-64_10BF3 and LARC characteristics were described in the past (e.g. Storini and Cordaro, 1997; Storini et al., 1998; Storini et al., 2000b). Also a careful evaluation of the attenuation coefficient for LARC data was performed (see, for instance, Cordaro and Storini, 1995; Massetti et al., 1998a, b). Moreover, the particle rigidity cut-off at LARC location was estimated by taking into account the secular variation of the geomagnetic field and considering not only the internal (Storini et al., 1995; Storini et al., 1999; Shea and Smart, 2001; Storini et al., 2002a) but also the external geomagnetic field (Kudela et al., 1998; Storini et al., 2000a; Bobik et al., 2003). Longterm cut-off variations by using the McIlwain (1961) L-parameter were also faced (Kudela and Storini, 2001; Storini et al., 2008). For Solar Extreme Events like Ground-Level Enhancements (GLEs) a careful analysis of the LARC data reliability was performed, and files (required by the scientific community) were prepared in the international format (see Cordaro et al., 2000; Storini, 2001 and Storini et al., 2002b; Damiani et al., 2008).

During the years 2002-2003 several tests were performed at Rome SVIRCO (acronym for ***S**tudio **V**ariazioni **I**ntensità **R**aggi **CO**smici*) Observatory & TPL (acronym for ***T**errestrial **P**hysics **L**aboratory*), to evaluate the possible use of 3He proportional counters (LND 25373 type) inside the standard neutron monitors. The results of such preliminary tests suggested the compatibility of the 3He counters with the 10BF3 ones. For this reason, during 2004-2006 more tests were performed; the counter response to the cosmic ray particle incoming was accurately checked and a new monitor was fully realized (a 3NM-64_3He). In January 2007, during the last Italian Antarctic summer campaign, the new detector was added to LARC instrumentation, in order to improve the data statistics and the short time resolution, especially required for the registration of solar particle events. The aim of this paper is to share with the cosmic ray scientific community the experimental results obtained by our work.

II. APTEC BP-28 VERSUS LND 25373 PROPORTIONAL COUNTERS

The proportional counter is the sensitive element of a neutron monitor. Table 1 illustrates the main characteristic parameters of each type of counter: APTEC BP-28 and LND 25373 (Figure 1 shows a picture of them); some relevant differences as for the

effective diameter, the gas pressure and the operating voltage can be identified at glance.

Fig. 1. Picture of the two proportional counters in use by the SVIRCO Observatory & TPL (Rome – Italy).

The distribution curves of the output pulses of the amplifiers, connected to the counters, give us more information about the counters themselves. The amplitude spectrum is double peaked for the 10BF3 counter (due to the two allowed channels of neutron capture: 2.30 MeV and 2.78 MeV), whereas the 3He one is single peaked (764 KeV). Using a pulse height analyzer (multichannel analyzer) both the anti-coincidence and the coincidence spectra can be taken. The first spectrum shows the height distribution of all the amplifier output pulses, while the second one takes into account only the pulses which overcome the threshold of a discriminating circuit. Plotting both the distributions on the same graph (see Figure 2) it is possible to determine the best value of the bias. Experimental tests show that this setting is very critical for the helium counter, because of the narrow gap between the curve of γ plus background pulses and the neutron pulses. The coincidence pulse height distributions of a 3He counter, taken at different operating voltages, show up that strayed pulses are counted, when the spectrum shifts according with voltage increasing (see Figure 3); the opposite when the voltage decreases: the counting rate is cut. In order to obtain a suitable spectrum stability we designed and provided each counter with a variable gain amplifier, achieving that the higher is the operating voltage the lower is the gain and the other way round. The coincidence distributions of a counter equipped with the "spectrum stabilizer" prove its immunity against operating voltage variations in a wide range (from 1350 to 1450 Volts; see Figure 3, lower panel). Figure 4 illustrates the test equipment used during the experimental work at the SVIRCO Observatory & TPL. Figure 5 exemplifies the data recorded in Rome during July 3 – September 28, 2004 with a 17NM-64_10BF3 and a 3NM-64_3He.

A good correspondence in the acquired data trend is found, despite the statistical errors due to the low counting rate of the helium detector. Figure 6 shows the regression plot of hourly data recorded in January-March/July-September, 2004 (winter/summer time) with both the detectors. The correlation coefficient (R) resulted to be about 0.95. Finally, Figure 7 reports the distribution of the hourly ratios obtained from the 3NM-64_3He and the 3NM-64_10BF3 rates for the same investigated period. A ratio of 107 % ± 1 % was derived, implying that the helium detector has in Rome (geographic coordinates: 41.86° N – 12.47° E; height: about s.l.) a rate of about 7% higher than the boron one.

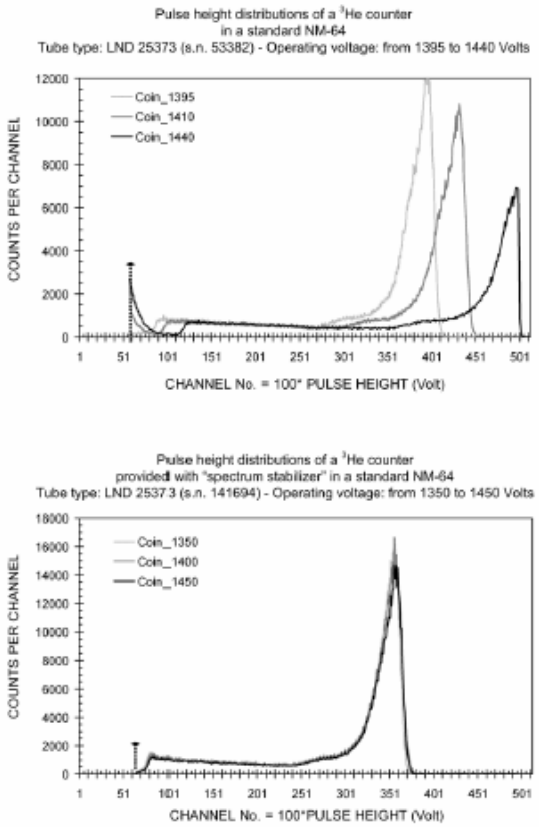

Fig. 2. Pulse height distributions (Anti-Coin: anti-coincidence; Coin: coincidence) as obtained from boron and helium counters inside the NM-64 or with the bare helium counter (see legend inside and outside the panels).

III. Assembling the 3He neutron monitor for LARC

The geometry of the new detector (3NM-64_3He) is just the same of the standard 3NM-64 one, with regard to the polyethylene reflector, moderator and the lead producer.

Table 1 – Main characteristic parameters for the two proportional counters in use at the SVIRCO Observatory & TPL (Rome – Italy).

Counter Type	APTEC BP-28	LND 25373
Effective diameter (cm)	14.85	4.97
Effective length (cm)	190.80	190.80
Cathode material	Stainless steel	Stainless steel
Operating voltage (V)	2700-3000 DC -	1200-1450 DC +
Gas filling	BF_3 (96% ^{10}B)	97% ^3He + 3% CO_2
Gas pressure (mm Hg)	200	3040

Also the round supports, we used to align the counters inside their cylindrical slots, are shaped alike the shields equipping the BP-28 counters at their both ends (see Figure 8). Lead free neutron monitors (i.e. only with neutron moderator) were proposed in the last years to study the environmental radiation. They are called *neutron flux meters* and are very appropriate for their use in high mountain observational sites (normally with low anthropogenic impact; see, for instance Mishev et al., 2007). For this reason we have tested helium bare counters during different cosmic ray modulation processes.

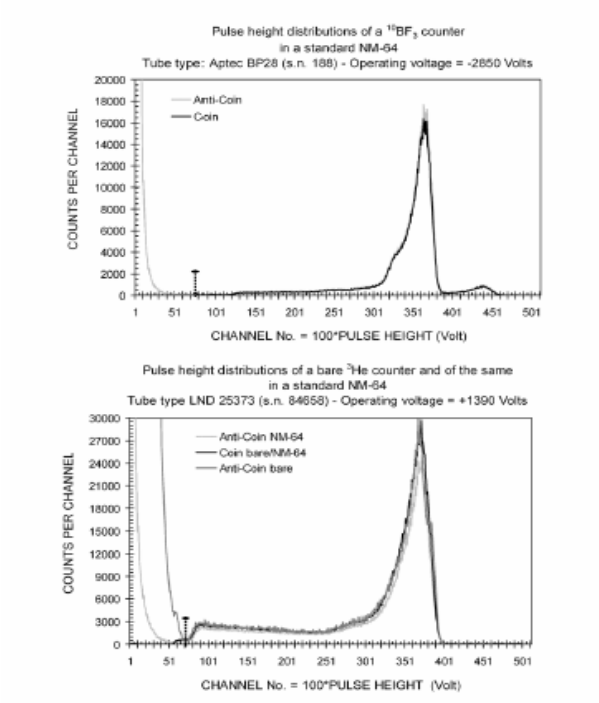

Fig. 3. Pulse height distributions for helium counters inside the NM-64 for different operating voltages without the spectrum stabilizer (upper panel) or with the stabilizer (lower panel).

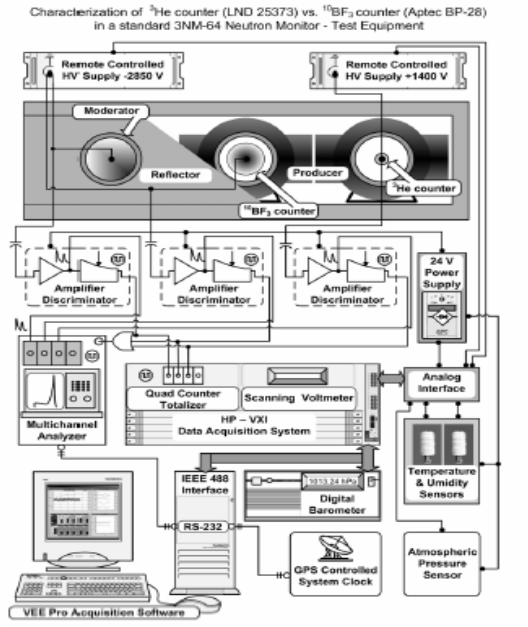

Fig. 4. Elemental test equipment of the SVIRCO Observatory & TPL for the determination of the 10BF3 and 3He counter performances inside a 3NM-64 unit.

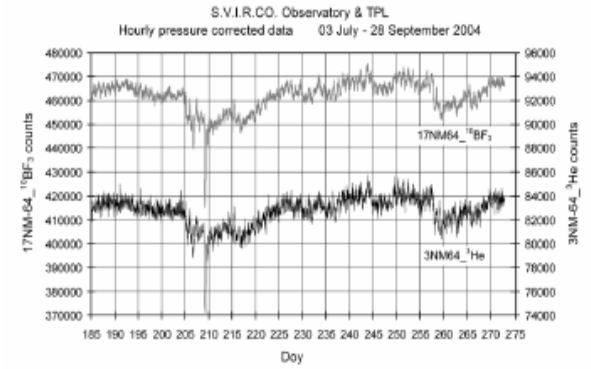

Fig. 5. Time history of the nucleonic intensity, as registered by the SVIRCO Observatory & TPL, with a 17NM-64_10BF3 (left scale) and the 3NM-64_3He (right scale) during 3 July – 28 September, 2004.

Figure 9 illustrates, as an example, the intensity recorded by the Rome 20NM-64_10BF3 and by 3-3He bare counters during July 12-22, 2005. The period includes the unusually extreme cosmic ray event occurring between 16 July and 20 July, described by Papaioannou et al. (2006). The intensity peak (17 July 2005) inside the Forbush decrease is well reproduced by the bare 3- 3He counters. Being the intensity peak not related to the arrival of solar relativistic particles (GLE) nor to an intense geomagnetic perturbation able to cause the lowering of the rigidity threshold at the measurement site, we should conclude that it is caused by an intense anisotropic cosmic ray flux in the equatorial plane (see the detailed description furnished by Papaioannou et al., 2006). In fact, a similar time history for the event was recorded by other equatorial-looking detectors around the world (e.g. Kiel, Jungfraujoch, Athens). Nevertheless, while the peak intensity reached the pre-Forbush decrease level in most of such measurement sites, in polarlooking cosmic ray stations the intensity peak is strongly reduced and practically null at Thule (see Figure 10, where data from three neutron monitors operated by the Bartol Research Institute/University of Delaware are reported).

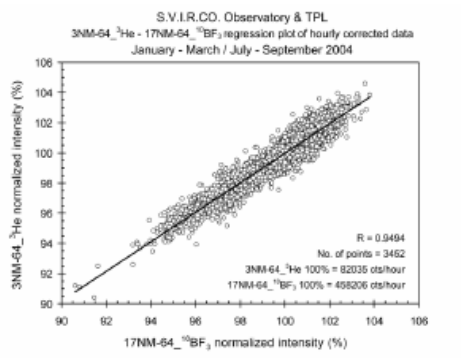

Fig. 6. Regression plot of 3452 hourly nucleonic intensities contemporary registered by the 17NM-64_10BF3 and the 3NM-64_3He during winter/summer time of 2004.

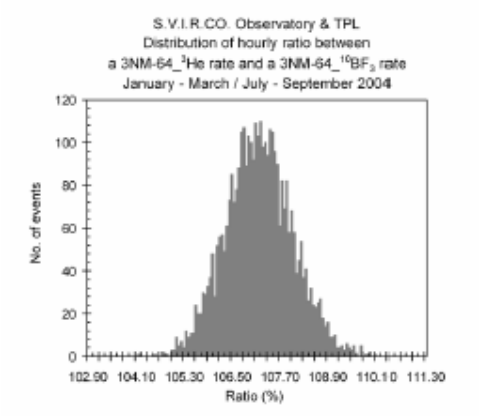

Fig. 7. Hourly ratio distribution of the 3452 data reported in Fig. 6 (see the text for details).

We also compared the helium counter performance by recording simultaneous data (see Figure 11) from a bare counter (F3 in Figure 11), a counter inside the polyethylene tube (counter slot with a wall thickness of 2 cm and an outside diameter of 24.5 cm; see F2 in Figure 11) and a
counter inside a lead free NM-64 configuration (F1 in Figure 11). Figure 12 reports the data acquired at the SVIRCO Observatory & TPL for another interesting period (January 16-25, 2005). The lower panel illustrates the nucleonic intensity registered by the standard 20NM-64 (the small peak of January 20 refers to GLE69) running in Rome, while the upper panel shows the time history of data recorded by F1, F2 and F3 counters. From such trends it is easy to see that:

- the bare counter has the maximum counting rate among the three helium counter
configurations;
- the counter with its moderator tube looses about 2% of the bare counter rate;
- the counting rate reduces its level to about 50% in the free lead detector;
- in all the data trends no traces of the GLE69 occurrence can be identified if the statistical errors are considered.

We believe that our experimental results can be useful for planning new neutron monitors (or environmental cosmic ray detectors) based on proportional counters. Finally, the 3NM-64_3He was assembled in Rome and a training week for younger researchers was performed before the detector moving to Antarctica. The Italian PNRA took care of the detector transport to Punta Arenas (Chile) during the Southern springtime of 2006 and then it was moved to King George Island during the summer time. The helium detector started to operate continuously in the new site on January 27, 2007 (see, for more details, Storini et al., 2008).

Fig. 8. The 3NM-64 configuration prepared for LARC with three helium bare counters on the top and related counter elements.

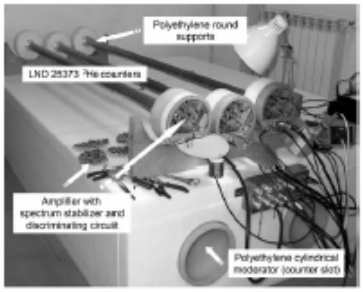

Fig. 9. Time history of the nucleonic intensity, as obtained with the standard 20NM-64 (left scale) and three helium bare counters (right scale) during July 11-22, 2005 at the Rome Observatory.

Fig. 10. As in Fig. 9 for three neutron monitors of the Bartol Research Institute (Mac Murdo: upper data trend; South Pole: middle data trend; Thule: lower data trend).

I. CONCLUSIONS

In this paper we shortly described experimental work performed at SVIRCO Observatory & TPL (Rome) during 2004-2006, in order to compare APTEC BP-28 versus LND 2537 counter performances during different solar activity levels. Figure 5 shows the response of the IQSY detectors with both the counters (the top trend for the boron one and the bottom trend for the helium one) to a series of cosmic ray modulation phenomena. Moreover, during two solar extreme event periods (January and July 2005) we reported the acquired LND 2537 data for different experimental configurations (see Figures 9 and 11).

We conclude that the 3NM-64_3He at work on King George Island (LARC) since January 2007 is going to become useful for studies related to the Solar Extreme Events that will be identified during solar activity cycle 24.

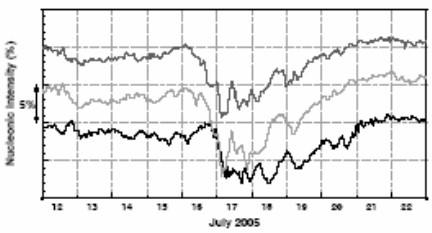

Fig. 11. Helium counter configurations used for experimental tests: F1: inside the 3NM-64 without lead; F2: only with the counter slot; F3: bare configuration.

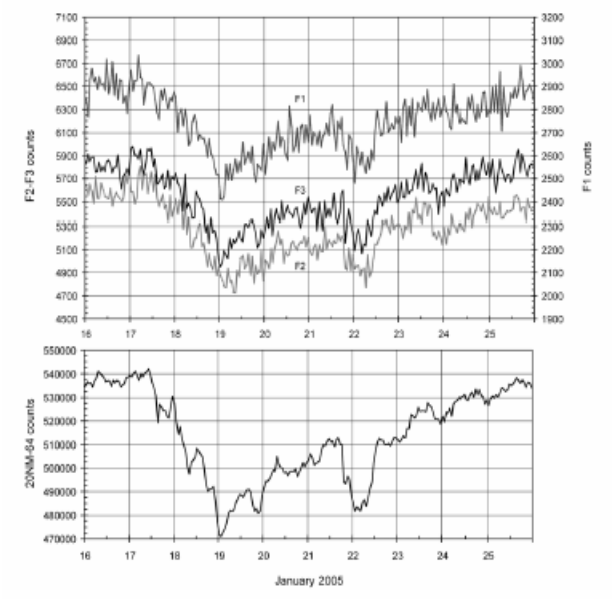

Fig. 12. January 16-25, 2005 time history of the recorded data by the standard 20NM-64 (lower panel) and by the three counters illustrated in Fig. 11 (see the text for details).

ACKNOWLEDGMENT

Work partly supported by the PNRA of Italy in the frame of Science for Solar-Terrestrial Relations and by IFSI-Roma/INAF. The SVIRCO Observatory is presently supported by the Department of Physics of the Roma Tre University and the Institute of Interplanetary Space Physics (IFSI-Roma) of the Italian National Institute for Astrophysics. The Bartol Research Institute NM Program is supported by the US/NSF under grant ATM-0527878.

REFERENCES

[1] Storini, M., Cordaro, E.G. Italia/Chile collaboration for LARC. Nuovo Cimento 20C, 1027-1032, 1997.

[2] Storini, M., Signoretti, F., Massetti, S., Re, F., et al. LARC towards the new century, in: Colacino, M., Giovanelli, G. and Stefanutti L. (Eds.), 7th Workshop Italian Research on Antarctic Atmosphere, SIF Conference Proceedings, vol. 62, Bologna, pp. 335–344, 1998.

[3] Storini, M., Signoretti, F., Re, F., Cordaro, et al. Antarctic Laboratory for Cosmic Rays: Instrument check after five years of work, in: Colacino, M., Giovanelli, G. (Eds.), 8th Workshop Italian Research on Antarctic Atmosphere, SIF Conference Proceedings, vol. 69, Bologna, pp. 221–228, 2000b.

[4] Cordaro, E.G., Storini, M. LARC/6-NM-64: Atmospheric pressure effects. Ser. Cien. INACH 45, 57-66,1995

[5] Massetti, S., Storini, M., Cordaro, E.G. Attenuation coefficient during solar cycle n. 22, in: Medina J. (Ed.), Rayos Cósmicos, Universidad de Alcalá, pp. 87-90, 1998a.

[6] Massetti, S., Storini, M., Cordaro, E.G. Barometric effects on LARC data, in: Colacino, M., Giovanelli, G.and Stefanutti L. (Eds.), 7th Workshop Italian Research on Antarctic Atmosphere, SIF Conference Proceedings, vol. 62, Bologna, pp. 345–355, 1998b.

[7] Storini, M., Smart, D.F., Shea, M.A., Cordaro, E.G. Cosmic ray asymptotic directions for Chilean neutron monitors, in:

Proceedings of the 24th ICRC Rome, vol. 4, pp. 1074–1077, 1995.

[8] Storini, M., Shea, M.A., Smart, D.F., Cordaro, E.G. Cutoff variability for the Antarctic Laboratory for Cosmic Rays (LARC: 1955–1995), in: Proceedings of the 26th ICRC Salt Lake City, vol. 7, pp. 402–405, 1999.

[9] Shea, M.A., Smart, D.F. Vertical cutoff rigidities for cosmic ray stations since 1955, in: Proceedings of the ICRC 2001, vol. 10. Copernicus Gesellschaft, Hamburg, pp. 4063–4066, 2001.

[10] Storini, M., Smart, D.F., Shea, M.A. Summary of LARC particle asymptotic changes from geomagnetic reference field models: 1955 to 1995, in: Colacino, M. (Ed.), 9th Workshop Italian Research on Antarctic Atmosphere, SIF Conference Proceedings, vol. 80, Bologna, pp. 409–421, 2002a.

[11] Kudela, K., Storini, M., Bobik, P., Kaššovicová, J. Access of cosmic rays to Lomnický Štít and Rome stations, in: Medina J. (Ed.), Rayos Cósmicos, Universidad de Alcalá, pp. 71-74, 1998.

[12] Storini, M., Bobik, P., Kudela, K. Problems with charged particle rigidity cutoffs in the Antarctic ground, in: Colacino, M., Giovanelli, G. (Eds.), 8th Workshop Italian Research on Antarctic Atmosphere, SIF Conference Proceedings, vol. 69, Bologna, pp. 229– 239, 2000a.

[13] Bobik, P., Storini, M., Kudela, K., Cordaro, E.G. Cosmic-ray transparency for a medium-latitude observatory. Nuovo Cimento 26C, 177-189, 2003.

[14] McIlwain, C.E. Coordinates for mapping the distribution of magnetically trapped particles. J. Geophys. Res. 66, 3681-3691, 1961.

[15] Kudela, K., Storini, M. Long-term cutoff changes and L parameter at LARC neutron monitor location, in: Proceedings of the ICRC 2001, vol. 10. Copernicus Gessellschaft, Hamburg, pp. 4103–4105, 2001.

[16] Storini, M., Metteo, P., Moreno, G. Effects of geomagnetic secular variations on cosmic ray access to the terrestrial environment. Adv. Space Res. 41, 70-75, 2008.

[17] Cordaro, E.G., Storini, M., Massetti, S., Hofer, M.Y. LARC: Ground level enhancements during the current heliomagnetic cycle, in: Aiello A., and Blanco A. (Eds.), 9th GIFCO Conf. on What are the Prospects for Cosmic Physics in Italy?, SIF Conference Proceedings, vol. 68, Bologna, pp. 33–37, 2000

[18] Storini, M. GLE Metadata file using CEN/TC 287. Report CNR/IFSI-2001-7, 2001.

[19] Storini, M., Massetti, S., Signoretti, F., Re, F., et al. LARC database for ground-level enhancements, in:

[20] Colacino, M. (Ed.), 9th Workshop Italian Research on Antarctic Atmosphere, SIF Conference Proceedings, vol. 80, Bologna, pp. 423–432, 2002b.

[21] Damiani, A., Benedetti, E., Storini, M., Rafanelli, C. Italian polar data center for capacity building associated with the IHY. Adv. Space Res. 41, 223-226, 2008.

[22] Mishev, A., Boukliysi, A., Visca, L., Borla, O., et al. Neutron flux meter at Basic Environmental Observatory Moussala, in: Proceedings of the ICRC 2007 – Pre-Conference Edition, Merida, 4 pages, 2007.

[23] Papaioannou, A., Gerontidou, M., Mariatos, G., Mavromichalaki, H. et al. Unusually extreme cosmic ray event in July 2005, in: http://esa spaceweather.net/spweather/workshops/eswwII/proc/Session1/SESWWPapaioannou-Poster-pdf.pdf

[24] Storini, M., Signoretti, F., Diego, P., Laurenza, M., et al. A new detector added to the Antarctic Laboratory for Cosmic Rays, in: Proc. SEE 2007: Fundamental Science and Applied Aspects, Athens, 2008 (in press).

Data Visualisation Interactive Network for the Aragats Space-environmental Center

A.Yeghikyan

Cosmic Ray Division, Yerevan Institute,
Alikanyan Brothers str. 2, Yerevan 36, Armenia,

Abstract - **The Aragats Space Environmental Center(ASEC) facilities provide real time monitoring of cosmic particle fluxes with a number of particle detectors located at high-altitude research stations at Mt. Aragats, Armenia. For the issuing of warnings and alerts on sudden changing of the near-earth radiation environments and for the detailed collaborative analysis of the most important solar modulation events we developed distributed data analysis interface with automatic data storage and processing. For the physical inference based on the changing particle fluxes the DVIN (Data Visualization Interactive Network) software is use). Data from ASEC monitors is accessible on-line from http://crdlx5.yerphi.am/DVIN3 and currently is widely used in research of the solar physics and Space Weather. In the paper we illustrate the how DVIN should be operated taking as example famous Halloween events (28October -2 November 2003).**

I. INTRODUCTION

Networks of particle detectors are continuously monitoring changing fluxes of particles reaching earth surface. Charged and neutral particles are born in cascade processes initiated by protons and nuclei incident on the terrestrial atmosphere. Fast majority of these primaries are from numerous galactic sites traveling tens of millions years in Galaxy and arriving to solar system as rather stable and isotropic population. Balloon and satellite spectrometers enumerate the Galactic Cosmic Ray (GCR) fluxes with rather high accuracy. Our nearest star, the sun, by disturbing interplanetary magnetic field and by accelerating protons and ions (producing so called Solar Cosmic Rays – SCR) is modulating the GCR flux, and as a result – the particle fluxes measured by surface detectors. Among numerous sun modulation effects Ground Level Enhancements (GLE) is one of the most essentials, both from point of view of fundamental physics processes and Space Weather effects.

The universal processes of particle acceleration in the Universe can be studied although on the much smaller scale, but much more detailed by measuring fluxes of protons and ions from solar accelerators. The satellite spectrometers due to tiny sizes can measure only huge fluxes of low energy particles; surface detectors are much larger and they use atmosphere for the particle multiplication. Therefore, rather small highest energy fluxes of solar particles can be studied by measured secondary particle flux on earth surface.

The problem of revealing signal (SCR) against overwhelming background (GCR) is one of the most complicated in high energy astrophysics. We implement several data analysis procedures in DVIN to solve this problem. Measuring highest energy particles it will be possible to determine the spectra of the major solar event in progress. Hard spectra at highest energies will manifest abundant SCR flux at low and medium energies and consequently radiation hazard to crew of space stations, to space-born and surface industries. There is not much time for issuing warnings and alerts (15-45 minutes), therefore physical inference have to be made very fast. Physical analysis should invoke also data from space spectrometers and particle detectors from world-wide networks.

It is why DVIN is strategically important as a scientific application to help develop space science and to foster global collaboration in solar physics and in space weather research. The system is highly interactive and exceptional information is easily accessible online. Data can be monitored and analyzed for desired time spans in a fast and reliable manner by the remote users world-wide.

II. ASEC EXPERIMENTAL SET-UP

The ASEC consists of two high altitude stations on Mt. Aragats in Armenia (Geographic coordinates: 40°30'N, 44°10'E. Cut-off rigidity: ~7.1 GV, altitude 3200m and 2000m) (Chillingarian et al., 2005; 2007). At these stations several monitors continuously measure the intensity of the cosmic ray

fluxes and send data to the Internet in real time. The two *18NM-64 neutron monitors* (in operation at Nor-Amberd (2000m elevation), and at Aragats, (3200m elevation) research stations are called the Nor -Amberd Neutron Monitor, and the Aragats Neutron Monitor, respectively. The monitors are equipped with interface cards, providing time integration of counts from 1 sec up to 1 minute. *The Solar Neutron Telescope*, is in operation at 3200m above sea level at the Aragats research station. The main detecting volume consists of four 1 m^2 surface, 60 cm thick scintillation blocks overviewed by photomultipliers type FEU-49 with 12 cm large photocathode.

The *Nor-Amberd Muon Multidirectional Monitor*, consists of two layers of plastic scintillators above and below one of the three sections of the Nor Amberd NM. The lead filter of the NM absorbs electrons and low energy muons. The threshold energy of the detected muons is estimated to be 250 MeV. The NAMMM consists of 6 up and 6 down scintillatores, data acquisition system of the NAMMM can register all coincidences of detector signals from the upper and lower layers, thus, enabling measurements of the arrival of the muons from different directions.

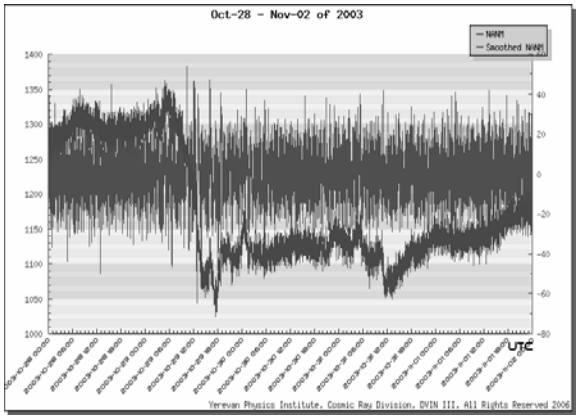

Fig. 1. The residuals time series (in red) of Nor Amberd NM time series (black).

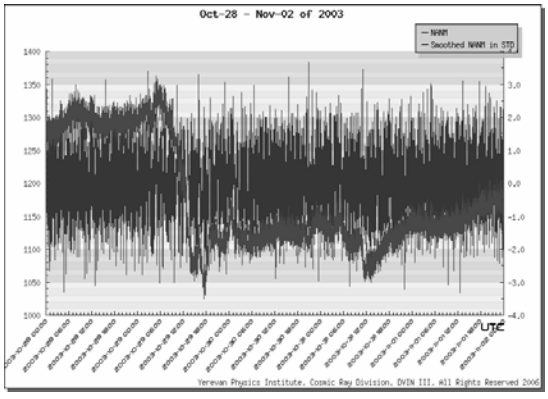

Fig. 2. Standard Deviation of residuals, of Nor-Amberd Neutron Monitor.

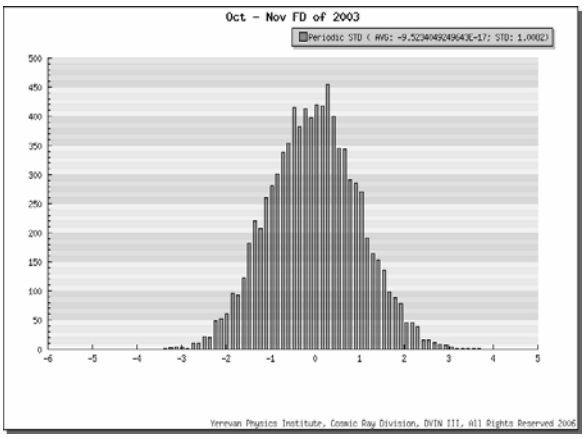

Fig. 3. Histogram of the normalized residuals of Nor-Amberd Neutron Monitor.

In the underground hall, originally constructed for the ANI Cosmic Ray experiment 150 plastic scintillators with area of 1 m^2 each of are located to measure the muon content of the EAS. The 6 m thick concrete blocks plus the 7 m soil filter the electrons and the low energy muons. Thus, only muons with energies > 5GeV reach the detectors. The *Aragats Multidirectional Muon Monitor* consists of 15 m^2 scintillation detectors, located on top of the ANI concrete calorimeter and 72 m^2 array of same type of detectors 24 m below.

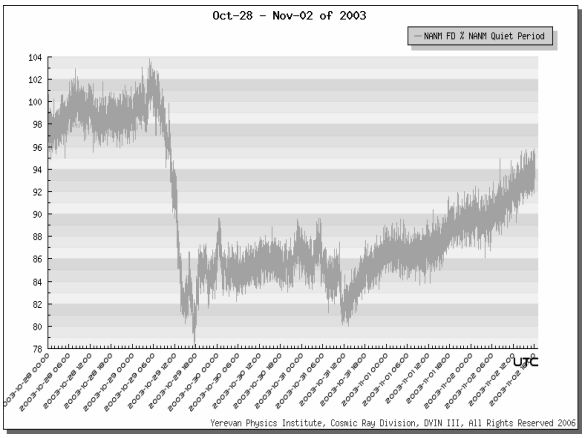

Fig. 4. Nor-Amberd Neutron Monitor, FD of Oct-Nov of 2003. FD: 22 Percent in comparison.

The *MAKET-ANI* surface array, consists of 92 particle density detectors formed from plastic scintillators with thickness of 5 cm. 16 of the 1 m^2 are continuously measuring the count rates of low energy charged component of the secondary cosmic rays (energy threshold ~7 MeV).

Data from this variety of particle detectors is automatically downloaded and stored in DVIN for joint analysis with ASEC monitors. DVIN provides

wide possibilities for sharing data and sending warnings and alerts to scientists world-wide, which have fundamental and practical interest in knowing the space weather conditions.

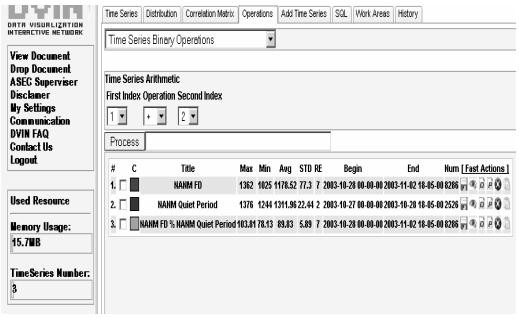

Fig. 5. The "Operations menu.

DVIN gives opportunity to remote groups to share the process of analyzing, exchange data analysis methods, prepare joint publications and maintain networks of particle detectors. DVIN gives users the set of online methods enabling physical interface from the time series of changing secondary particle fluxes.

III. OVERVIEW OF THE MAIN OPERATIONS

There are two main types of Operations so called moving and periodic operations.

The periodic and moving operations are calculated by 3 given values: the length of period, function type and offset. The difference between the moving and periodic operations is in defining of the next portion of time series. In periodic operations the next portions are selected with step given by the "Period" option and in the moving operations the step is always 1.

Periodic functions are as following:

- Average;
- Standard Deviation;
- Median;
- Linear Regression;
- Periodic rebinding (adding successive time series in larger time unit) of the initial time series

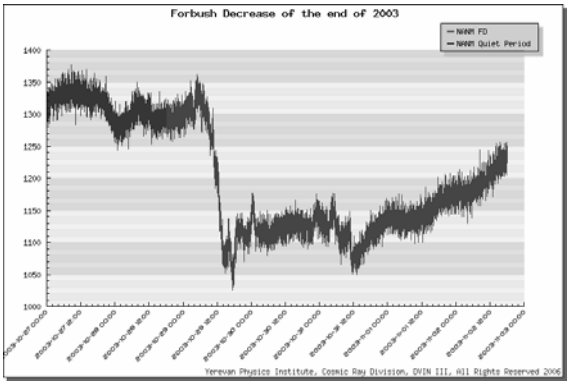

Fig. 6. Red part is the normal period, and Blue part is the observed one. The transformation to percents are produced relatively the "Red" one.

Periodic and moving operations provide very flexible and powerful tool for examining of time series. User controls the time period, offset of period (start point of rebinding operation) and interpolation mode (within chosen time period) of time series. Using these options user can rebin (add) successive monitor counts for examining long time periods and reveal non-trivial structures in time series. For example, adding initial (parent) 1-minute time series in 3 minute by the "periodic sum operation" helps to discover the Ground Level Enhancement (GLE) detection on 20 January 2005 by the AMMM monitor, obscured by the large fluctuations of 1-minute time series. "Offset" option defines the particular grouping of initial time series. There are 3 possible ways to group 1 minute time series in 3 minute ones; each outlining slightly different structures. "Periodic Average Operation" and "Linear Regression Operation" are interpolating time series by the piecewise continuous functions (see Figure 1). All the periodic operations have "compatibility" option, leaving the number of elements in time series unchangeable. For example, if we interpolate the 1- minute time series by hourly average, in each of the 60 hourly minutes of the transformed time series the same average value will be.

Then, by subtracting a time series from another user we can obtain the residuals time series (see Figure 1). By dividing obtained residuals to the variance we obtain the, so called, normalized residuals obeying the standard Gaussian law (see Figure 2). By the time series of normalized residuals we can select the outliers for a further analysis. The histograms of the residuals (see Figure 3) can be compared with standard Gaussian probability density function by χ^2 test. Large values of $\chi 2$ point on failures in detector channel operation. Therefore, the described operations modes of DVIN can be used for the check of detector channels.

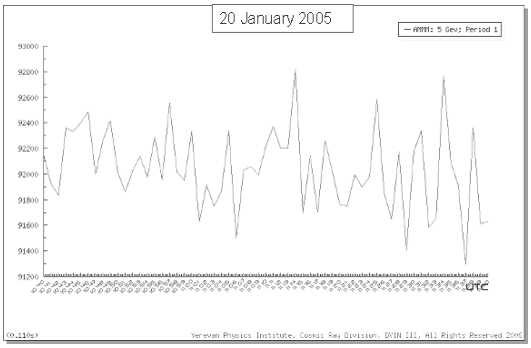

Fig. 7. Minutely data of AMMM.

After proving the "Gaussian" nature of the residuals positive outliers are examined as candidates for the Ground Level Enhancement (GLE) or "Geomagnetic storm" events. Large positive deviations (greater than 4σ) pointed on the possible non-random character of the deviation from mean count rate, i.e. on the solar modulation effects.

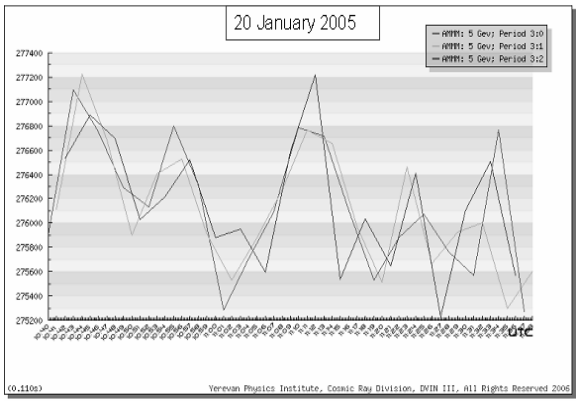

Fig. 8. 3 Minutely data with all the offsets.

The same Forbush decrease (Fd) as in Figure 1, is also presented in Figure 4 with the counting rate expressed in percents. To calculate the decrease in percents we get the average count rate at the no disturbed period of October 28 and using this value as a 100 percent recalculating the values into percents.

The transformation of the time series into percents of observed period relatively to the "quiet" period is widely used for getting quantitative description of the "deepness" of Forbush decrease.

Transformation of the Time Series into percents relatively to

the other time series are made by following steps

1. Selection examined time periods;
2. Selection of reference time period;
3. Using the "%" operation in "Binary Mode".

In the Figure 6 are presented the non disturbed (in red) and Forbush Decrease (in blue) periods of October-November of 2003 which was translated to percents.

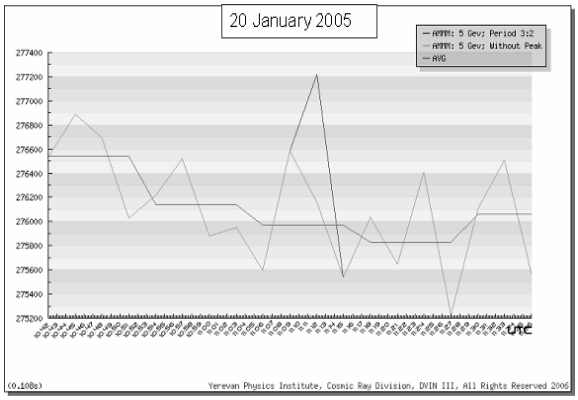

FFig. 9. AMMM: 5 GeV; Period 4:3 with and without peak and periodic AVG of i.e. Time Series without Peak.

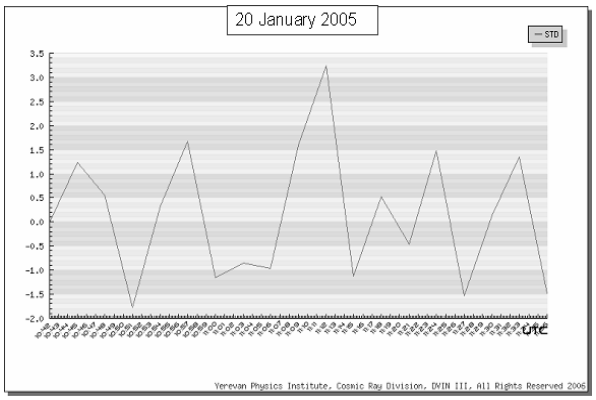

Fig. 10. Normalized residuals of AMMM 3 minute counts.

Table I: Characteristics of the AMMM detection of GLE candidate

	Max	Min	$\overline{C}$	STD	RMSD	S
1 min counts	92821	91296	92040	315.45	0.34	0.33

Time Series | Distribution | Correlation Matrix | Operations | Add Time Series | SQL | Wc

	1	2	3	4	5
1 NANM	100	98	97	96	97
2 ArNM	98	100	96	95	96
3 SNT: Threshold 120 Mev	97	96	100	96	99
4 SNT: Threshold 290 Mev	96	95	96	100	96
5 SNT: Charged particle monitor 5cm scintillators	97	96	99	96	100

Fig. 11. Screenshot of correlation matrix of 29-10-2003 in percents.

IV. ANALYZES OF THE GLE CANDIDATE WITH AMMM DETECTOR

Variety of the ASEC monitors is "selecting" different populations of the primary energy spectra, because of different energy thresholds. Among ASEC monitors the Aragats Multidirectional Muon Monitor (AMMM) selects highest primary energies, because detector is located in the underground hall and 14 m. of soil and concrete filter low energy muons and electrons. Only muons with energy greater than 5 GeV can reach detector location. The energy of "parent" proton should be greater than 15 GeV to give birth to 5 GeV muon. These energies are extremely rare in SCR and if encounter lasting several minutes only. Therefore, in AMMM time series we are looking to very narrow peaks in coincidence with solar flares and GLEs detected by surface particle detectors sensitive to lower primary energies.

Time Series | Distribution | Correlation Matrix | Operations | Add Time Series | SC

	1	2	3	4	5
1 SNT: Threshold 120 Mev	100	31	29	13	16
2 SNT: Threshold 290 Mev	31	100	8	0	7
3 SNT: Charges Particles 5 cm Scintillators	29	8	100	17	19
4 NANM	13	0	17	100	13
5 ArNM	16	7	19	13	100

Fig. 12 Screenshot of correlation matrix of 08-04-2006 in percents.

The 1- minute time series of the AMMM are presented in Figure 7. Enhancement of the count rate is seen at 10:12 -10:14 UT. Unfortunately 14 from 45 channels of the AMMM detector were not operational at the time, therefore only 31 m^2 of muon detectors were in use to measure the high energy muon flux. The estimated mean count rate of the Galactic Cosmic Rays (GCR) as measured by the 31 m^2 of the AMMM detector during the 10:40 – 11:40 UT time span, excluding the enhanced interval from 10:12 to 11:14 UT, is 92040 particles per minute.

The statistical parameters of one minute time series are given in Table I. In order to check the significance of the GLE candidate we calculate the significance according to the Poisson distribution and standard Relative Mean Square Deviation (RMSD):

$$RMSD = \sqrt{\left(\frac{\sum_{i=1}^{i=N}(C_i - \bar{C})^2}{N-1}\right)} \Big/ \bar{C},$$

Where normalized residuals, C_i, are 1 minute count rates of the AMMM, $\bar{C}$ is hourly mean of the 1-minute time series and $\sqrt{\bar{C}}$ - is the hourly Poisson deviation of the count rates.

Maximal value at 10:14 – 92821, enhancement (possible signal) is Δ =Max-Min =781. The relative enhancement $\Delta_r = \Delta / \bar{C} = 0.85\%$, corresponds to significance of Δ_r / RMSD = 2.5σ.

To emphasize the peak in the AMMM time series we group the 1-minute time series in 3-minute time-intervals. Three different possibilities of regrouping the 1- minute time series in 3 ones are presented in Figure 8. All these three demonstrate slightly different temporal pattern of time series. The particular time series started from the second element (10:41) provide the biggest peak. In Figure 8 the 3-minute time series emphasized the peak

and offset 2 provides maximal. However, the size of peak is not large enough to claim that AMMM detects the SCR and not only GCR fluctuation. In the next steps of processing the offset 2 is used as a Time Series with a maximum Peak.

For further calculation we remove the Peak using "Up-Down Limit Cut" which replaces the points located in the given range with Periodic Median. Two Time Series with and without Peak are presented in Figure 9. In the following Table II the statistical parameters of these time series with peak and without peak are presented.

Table II. Statistical parameters of the time series with the peak and without peak

Name	**Max**	**Min**	**Avg**	**STD**	**R.E.(100*STD/AVG)**
AMMM: 5 GeV; Period 3:2	277219	275225	276165	497	0.178
AMMM: 5 GeV; Period 3:2 without peak	276892	275225	276109	434	0.159

From the Figure 10 we can see that the significance of the peak did not exceed 3.3; such enhancements can be detected several times during the day. Therefore we cannot reject the hypothesis that the detected peak is only background fluctuation.

V. CORRELATION ANALYSIS

Correlation Analysis is a new tool for the physical inference on multiple time series. Different ASEC monitors are sensitive to different populations of the primary protons and ions. If Neutron Monitors are detecting neutrons generated by primary protons with energies just after the cut-off rigidity, the 5 GeV muons are generated by >15 GeV protons. Also different channels of the Solar Neutron Telescope (SNT) are selected slightly different energy populations of primaries. Therefore, measuring correlations between changing count rates of ASEC monitors we can get information about energy spectra of the solar cosmic rays (SCR), or about the nature of geomagnetic disturbance changing the actual value of the cut-off rigidity.

In Figures 11 and 12 the correlation matrices of two periods are depicted, 2003-10-29 which corresponds to the enormous Forbush decrease (correlations are very large, approaching ~1) and 2004-03-05 which corresponds to the calm phase of the Space Weather (no geomagnetic disturbances) there are detected no significant correlations.

VI. DATA EXCHANGE BETWEEN USERS

Users of DVIN can interchange processed data and establish virtual collaboration. They interchange work areas using communication section. When user gets data from another user he can continue analyzing in the received work area or concatenate own work area with new one. One selects another users from the list of DVIN users and selecting the list of available work areas send him the processed data.

VII. CONCLUSION

DVIN is the first online system used in Cosmic Ray Division allowing users to perform online collaborations not only at the level of information interchange but also at the level of physical analysis, using general interconnected platform. It allows scientists from different countries to exchange data, analysis methods and physical inferences.

ACKNOWLEDGMENTS

The author is grateful to Ashot Chilingaryan, Surren Chilingarian and Tigran Hovhannisyan for technical assistance and idea generation and to the ASEC members for stimulating interest and support. Also thanks are due to Arthur Reymers and CRD students for reporting bugs in DVIN.

REFERENCES

[1] Chilingarian, A., Arakelya, K,. Avakyan, K., et al. Correlated measurements of secondary cosmic ray fluxes by the Aragats Space – Environmental Center monitors, Nucl. Instrum. Methods Phys. Res., Sect. A, 483-496, 2005.

[2] Chilingarian,A. A., Reymers,A.: Particle detectors in solar physics and space weather research, Astropart. Phys., Astropart. Phys., 27, 465-472, 2007.

[3] MySQL Reference Manual

[4] (URL:http://dev.mysql.com/doc/)

[5] PHP Manual (URL: http://www.php.net/docs.php)

[6] MathWorld (URL: http://mathworld.wolfram.com/)

Characteristics of the Space Environmental Viewing and Analysis Network (SEVAN)

A.Chilingarian, G.Hovsepyan, K.Arakelyan, A.Avetisyan, S.Chilingarian,
V.Danielyan, K.Avakyan, A.Reymers, S.Tserunyan

Alikhanyan Physics Institute, Armenia
(arthur@crdlx5.yerphi.am)

Abstract **– One of the major advantages of multi-particle detectors is probing of the different populations of the primary cosmic rays, initiated particle cascades in terrestrial atmosphere. With basic detector of SEVAN network we are measuring fluxes of neutrons and gammas, of low energy charged component and high energy muons. This diversity of information obtained from SEVAN network located mostly at low and middle latitudes will give possibility to estimate the energy spectra of the highest energy Solar Cosmic Rays (SCR). SEVAN network will be sensitive to very weak fluxes of SCR above 10 GeV, very poorly explored till now. To understand sensitivity of new type of particle detectors to highest energy solar ions we investigate the response of SEVAN basic units to galactic and solar particles. New physical inference methods are proposed and tested for:**

- **estimation of the index of power spectra of solar cosmic rays incident on the terrestrial atmosphere**
- **distinguishing of the ground level enhancements initiated by solar neutrons.**

New electronics for the Aragats Space Environmental Center (ASEC) particle detectors

K.Arakelyan [1], S.Abovyan[1], A.Avetisyan, A.Chilingarian[1], S.Chilingarya,[1,2], V.Danielyan[1], G. Hovsepyan[1], A.Oganissyan, D.Pokhsraryan[1]

[1] *Cosmic Ray Division, Alikhanyan Physics Institute, Alikhanyan Brother 2, Yerevan 36,Armenia*
[2]*Institut fuer Prozessdatenverarbeitung und Elektronik, Forschungszentrum Karlsruhe, Hermann-von-Helmholtz-Platz 1, 76344 Eggenstein-Leopoldshafen,Germany*

Abstract – **The functionality of the Data Acquisition (DAQ) system for the particle detectors operated at Aragats Space Environmental Center (ASEC) monitors is very flexible and can be tuned by the software. Devices having from 8 to 64 analog inputs, receive pulses from the scintillator detectors buffer amplifiers and from proportional counters. A newly designed readout is based on the concept of full software control of the detector parameters and maximum utilization of all detector data. Modern fast microcontrollers are used as the base element of the detector control system and physical information storage, analysis and retrieval. The Integrated Silicon Pressure Sensor and ATMEL 8-bit microcontroller is placed in a special pressure-tight box with a possibility of periodic calibration using a Hg standard barometer. The rate of pulses of ground-based particle monitors (not exceeding 10 KHz) allows for a new concept of the DAQ systems heavily using on-line analysis software to select all interesting physical events. The multi-channel DAQ unit consists of input discriminator-shapers with the programmable threshold, Digital-to-Analog Converters (DAC) for the threshold settings, simple logic, microcontroller and serial interface for connecting to the host computer.**

Key Words—**Cosmic rays, Space weather, DAQ, FPGA, neutron monitors**

I. INTRODUCTION

The design and fabrication of modern electronic devices for readout and storage of physical information (for so called, Data Acquisition – DAQ) from the particle detectors were performed by the electronics group of the Cosmic Ray Division of Yerevan Physics Institute for the particle detectors of the Aragats Space Environmental Center (ASEC, [1], [2], [3]). The standard requirements for the DAQ system are reliable and consistent registration of all electronic signals from the particle detectors. During multiyear measurements the parameters of DAQ system should be continuously monitored to keep them stable. Electronics should not introduce a significant loss of particle detection efficiency due to "dead times" and miscounts. Additional complexity of DAQ design was introduced by the following requirements:

1. Counting not only the number of registered particle in the definite time span, i.e., time series, but also the amplitude of the Photomultiplier (PM) signals. This amplitude is proportional to the amount of light reaching PM cathode.
2. Particle identification by registering all logical combinations of the signal occurrence in the multilayered particle detector systems; particle detectors of operating world-wide networks monitoring solar activity have very limited possibility of particle identification and energy estimation. New electronics combined with multilayered detectors interlayer by the lead filters gives much wider options for the identification of particles, various solar activity events and different physical phenomena. It became possible:

3. to identify charged and neutral particles hitting detector;

- to identify primary solar particles hitting terrestrial atmosphere;
- to estimate direction of incident muons, which is good proxy of the incidence of the primary particle on the terrestrial atmosphere;
- to investigate very rare events of muon capture by lead nuclei;
- to measure burst spectra of cosmic rays;
- to measure spectra of horizontal muons, and so on.

4. Correlating information from different particle detectors; Secondary cosmic rays are products of interactions of the primary high energy particles with terrestrial atmosphere, therefore fluxes of charged and neutral particles are correlated.

The ASEC detector network currently consists of 6 detectors located at two research stations on the slopes of Mount Aragats. The possibility of the network extension to several near-equator countries is also being considered by the data acquisition system design [4].

The two 18NM-64 neutron monitors are in operation at Nor-Amberd and Aragats research stations, at altitude 200 and 3250 m accordingly. Other ASEC detectors consisted of plastic scintillators overviewed by the Photomultipliers (PM). The scintillation is used to detect charged particles passing through the detector. The PM is attached to an electronic amplifier and other electronic equipment to count and possibly quantify the amplitude of the signals produced by the photomultiplier. The following subsections present a brief description of the DAQ systems used by detectors operating at ASEC.

I. 24 Channel Neutron Monitor (NM) Readout Module

The main function of the 24 Channel Readout Module is receiving and counting signals from each of the 18-channels of the ANM and NANM. It also has 6 auxiliary universal counter channels, to be used in future for attaching other neutron detectors. The module (see Figure 1) functionally can be divided into 4 units.

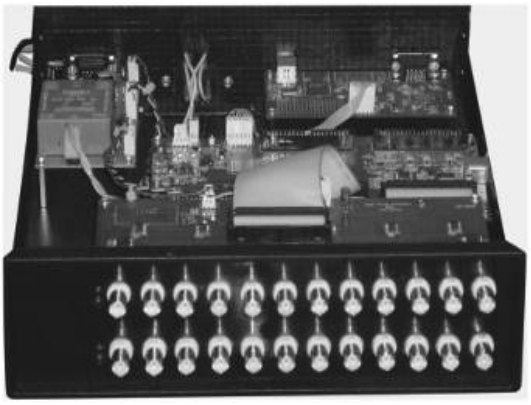

Fig. 1. 24 Channel readout module

1. Two Programmable Threshold 12-channell Discriminator/Counter boards.
2. Universal Multichannel Event Counter (UMEC) board.
3. Universal Microcontroller Interface module (MultiIFC) board.
4. RS-485 and Local Power supply module.

The pulses from the detector preamplifier are discriminated and shaped in the unit 1. The discrimination threshold can be programmed in the 4mV-1000mV range with a 4mV step. The duration of the output TTL pulses is 400ns. The shaped pulse enters the input of Xilinx Spartan 3E FPGA (Field Programmable Gate) in the unit 2. Inside module, the FPGA pulse is applied to three counters: to the first – directly, and to the other two through programmable dead time circuits. The dead time values are 350us (#2) and 1500us (#3), see Figure 3. The last value coincides with the one used for both Neutron Monitors at Aragats and Nor-Amberd during the 23rd solar activity cycle (1996-2007).

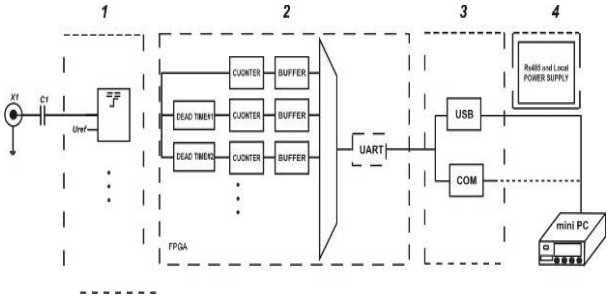

Fig. 2. Functional diagram of the 24 readout module

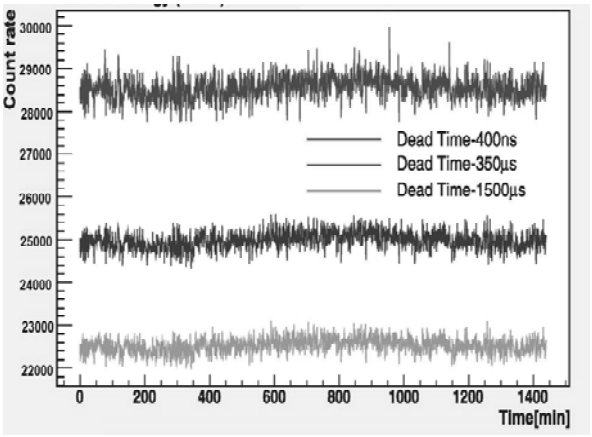

Fig. 1. Time series of the Nor-Amberd Neutron Monitor corresponding to 3 dead times.

The contents of all 60 (3*18 + 6) counters are downloaded each second in plane ASCII code to the PC through USB (or COM) interface Along with the main output connection, the unit has a RS-485 interface for connecting to the Detector Control Local Network for the on-line programming of the thresholds.

Each energetic hadron (mostly a neutron or proton) generates a number of evaporated neutrons in lead. Only small fraction of these neutrons (~5.7% for NM64) is registered by the counter. One of the most important parameters of NM is the so called, multiplication coefficient" – the mean number of the termalized neutrons registered by the NM section as response to one incident high energy hadron. The first value of the dead time is very small and allows us to calculate all thermilized neutrons entering the same proportional counter. The last biggest value of the dead time counts primary particles only, because the "decay" time of the termalized neutrons in NM section is ~350 us. Therefore, by dividing the count rates correspondent to the shortest and the biggest dead times, we can estimate the multiplication coefficient in one proportional chamber. Due to the tight connections of the lead filters of each of 8 chambers of a NM section there is a probability that termilized neutrons will be also registered by the neighboring counter. Therefore, we should correct the obtained multiplicity coefficient to effect of the "correlated counts" in the neighboring counters. Our measurements and simulation studies of NM cross-channel correlations give preliminary value of 1.45 for the multiplication coefficients of a section of Nor Amberd NM (2000 m. above sea level).

SEVAN DAQ Electronics

A network of middle to low latitude particle detectors called SEVAN (Space Environmental Viewing and Analysis Network) [6] is planned in the framework of the International Heliophysical Year (IHY), to improve fundamental research of solar accelerators and space weather conditions. Besides the main DAQ function, the unit also acts as a master for the detector control Local Area Network (LAN) which is used for programming and monitoring high voltage values and for programming the ADC thresholds.

Data Acquisition electronics implementing registration of the charged and neutral fluxes of secondary cosmic rays consists of 8-Channel Discriminator/Counter Unit (8DCU) and 3 High Voltage supplies with presetting and automatic control, which are located in the corresponding PMT cases.

8DCU parts are:

The 8-channel Programmable Threshold Comparator and Counter board (8CNT)

Universal RS232/RS485 interface/power supply module - IFCC,

Power transformer - 220V50Hz to 2x8V 0.5A + 2x15V 1.25A

The main features used in 8DCU are:

8 programmable threshold analog input,

Threshold programming range 4mV-1000mV with 4mV step,

Powered by AC 50-60Hz 220V, 30W

Maximal counting frequency – 60kHz,

LEDs to indicate the input pulses in each of 8channels, module power and programmable trigger condition,

8 input BNC connectors,

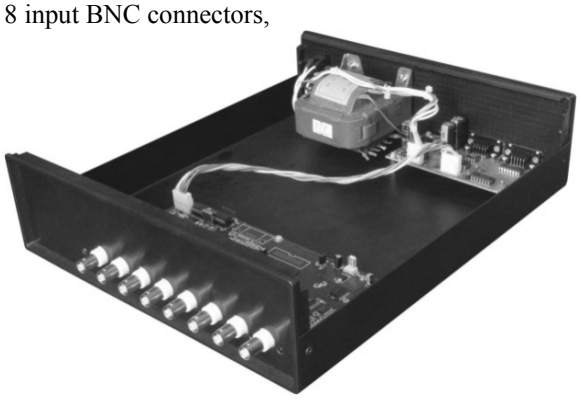

Fig. 4. 8 Channel DAQ electronics for SEVAN detector

8CNT board is used as a standalone 8-channel counter (scalar) with a programmable threshold. For the threshold programming and the output data readout, it can communicate with the host PC (local network) through the IFCC module by any of RS-232 or RS-485 interface ports. The module counter and interface logic is based on the Atmel AVR Atmega88 8-bit microcontroller.

DAQ software consists of the host PC program and the microcontroller program (firmware). The firmware for the DAQ and control is written in C language and stored in the microcontroller reprogrammable flash memory. Below is presented the functionality, implemented for the SEVAN detector setup. In this case the microcontroller

operates both for the thresholds presetting and control and as a main DAQ controller, with listed below functions:

1. Counting of signals in each of 8 channels,
2. Counting of all types of coincidences of signals in channels 1-3.

The data collection time is set by the microcontroller firmware, so any other value can be chosen. The IFCC interface module has three connections: to the microcontroller, to the RS232 connector (DSUB9F) and RS485 connector (DSUB9M). The signals propagate from each of the mentioned connections to both of others. The power for the PMT High Voltage supplies (15V unregulated, 1.2Amax) is supplied from the 8DCU through the RS485 interface connector.

II. Programmable Regulated High Voltage DC Power Supply (PRHVPS)

The Programmable Regulated High Voltage DC Power Supply is designed to supply high voltage to different electrodes on photomultipliers and various elementary particle detectors, it consists of:

- Current-driven, low-noise sine wave DC/DC converter, with up to 2 stage RC output ripple
- Pulse Width Modulated programmable DC regulator
- Local +5V linear voltage regulator
- Atmel microcontroller
- RS485 interface chip
- Optional temperature sensor

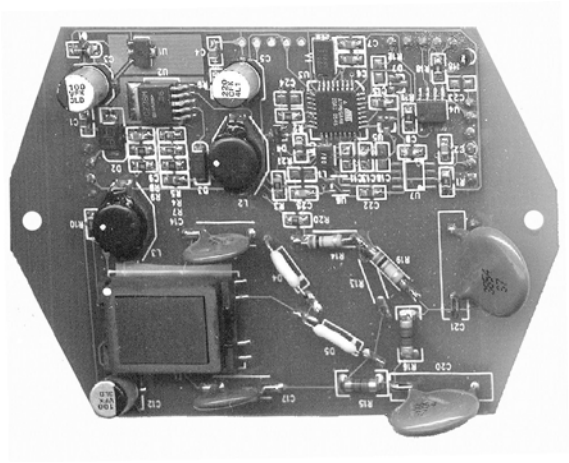

Fig. 5. Programmable regulated high voltage DC power supply.

The Printed Circuit Board (PCB) can be assembled with various options for different output polarity, programmable voltage range, and so on.

Specific Features:

- Voltage programming in two hardware selectable ranges ± 900V to 2100V and ±1500 to 3000V in 2V steps
- Output voltage ripple less than 1mV
- Max. output current 1.2 mA for ± 900V to 2100V range; 0.8 mA for ±1500 to 3000V range
- Input voltage from +12V to +15V
- Absolute output voltage regulated to accuracy ±1V
- Optional temperature sensor
- RS-485 half-duplex 2-wire 9600 baud interface for programming and monitoring the output voltage

III. The Pressure, Humidity, Temperature - PHT SENSOR

PHT SENSOR is a general purpose microcontroller unit, designed for environmental measurements: pressure, temperature and humidity. It can be equipped with two types of temperature sensors: the precise combined Humidity Temperature digital sensor SHT11 and/or the low precision low cost analog temperature sensor LM61C.

In addition to the main sensors mounted on the board, it has two auxiliary connectors with pinned out microcontroller input/output port pins, which can be used for other measurement and control purposes.

- It has two alternative interfaces to integrate it into a system: RS232 and half-duplex RS485.
- It has Frequency Modulated (FM) output TTL for compatibility with the existing Cosmic Ray Detector equipment. The frequency is proportional to the measured pressure.

The microcontroller software (firmware) supports all the mentioned sensors and interfaces and can be easily upgraded for additional measurements and control options.

Specific Features:

- Pressure sensor Motorola MPXA6115 [9] has 15 to 115 kPa measurement range with 1.5% maximum error in the 0 to 85°C temperature range. Using an external calibrating procedure, the error can be significantly decreased. The sensor is connected to a 16-bit resolution ADC. The measured data is averaged in software to minimize the noise. The real pressure resolution depends on the averaging time and can be as good as 15-bit (~1/32000 of full scale).

- The SHT11 has a humidity measurement range from 0 to 100% RH with 3% accuracy at 25°C and -40°C to 123.8°C temperature measurement range with 0.4°C accuracy at 25°C.
- The LM61C sensor has -30°C to 100°C temperature measurement range with 3% accuracy.
- Both RS232 and RS485 interfaces can run with any standard baud rate up to 115200 bit/sec.
- The ATMEL Atmega8-16AI microcontroller can be easily reprogrammed using the ATMEL standard serial programming protocol.
- The board has built-in +5V regulator, thus it can be powered by any regulated or unregulated power supply with 100mA current.

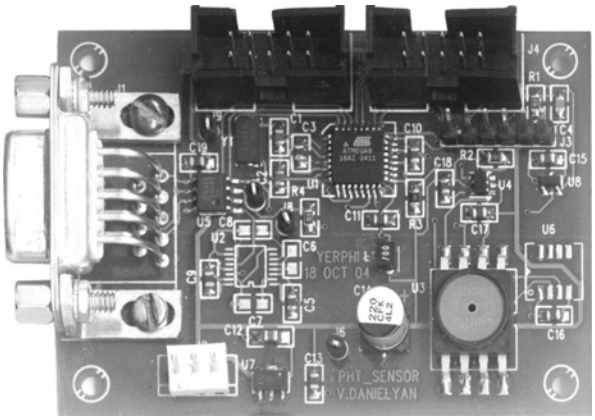

Fig. 2. PHT sensor

To calibrate the pressure sensitivity of the device, we place the PHT sensor in a barochamber in which we can vary and measure the pressure with very high accuracy (0.5mbar) using a mercury barometer. We calibrate our sensor output against the mercury barometer of the barochamber.

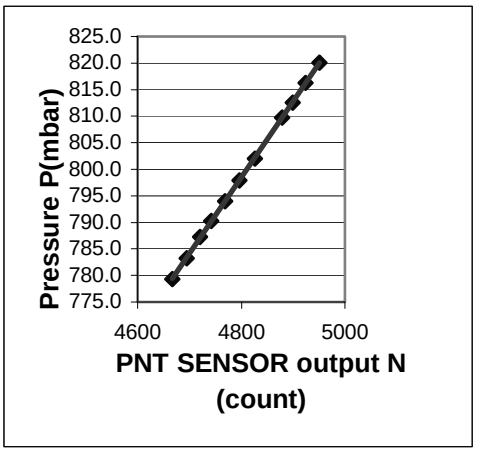

Fig. 7. Pressure sensor calibration curve

In the Fig.7 one can see the calibration curve for our PHT sensor. The sensor output is linear with respect to the pressure in the range of 780 to 820 mb. The correlation line equation is P(mbar) = 0.1429 N + 112.46 with a χ 2 fit of 0.9999.

REFERENCES

[1] Chilingarian, A., Avakyan, K., Babayan, V., et al.: Aragats Space – Environmental Center: status and SEP forecasting possibilities, J. Phys. G: Nucl. Part. Phys., Vol. 29, 939 – 952, 2003.

[2] Chilingarian, A., Arakelya, K. Avakyan, K., et al.: Correlated measurements of secondary cosmic ray fluxes by the Aragats Space – Environmental Center monitors, Nucl. Instrum. Methods Phys. Res., Sect. A, 483-496, 2005.

[3] Chilingarian, A.A., Reymers, A.E.,: Particle detectors in solar physics and space weather research,Astropart. Phys., Astropart. Phys., 27, 465-472, 2007.

[4] W.-K. Chen, *Linear Networks and Systems* (Book style). Belmont, CA: Wadsworth, 1993, pp. 123–135.

Cosmic ray research at Spitsbergen

E.V.Vashenuyk, B.B. Gvozdevsky, Yu.V.Balabin

Polar Geophysical Institute, Murmansk region, Russia
(gvozdevsky@pgi.kolasc.net.ru)

Abstract **– By spring of 2003 the neutron monitor in Barentsburg (78.06N, 14.22E) at Spitsbergen archipelago has been installed and put into operation. It became the northernmost instrument of such kind among more than 40 neutron monitors of the worldwide network. The installation of the neutron monitor at Spitsbergen allowed filling in a gap in observations of cosmic rays coming from the northern areas of heliosphere and magnetosphere. With the help of the neutron monitor in Barentsburg 5 events with relativistic solar cosmic rays have been already registered: October 28 and 29, November 2, 2003, January 20, 2005 and December 13, 2006. In first 4 of these events the steady South-North anisotropy of solar cosmic rays was observed. The solar cosmic ray flux from the South considerably exceeded a flux from the North that can testify to global asymmetry in the heliomagnetosphere in a current phase of the solar heliomagnetic cycle. The asymmetry disappeared by the end of 2006 as it was not observed during the GLE on 13.12.2006. The possible role of the neutron monitor at Spitsbergen in revealing connections of cosmic rays with local weather and climate changes is discussed also.**

Session E

Integrated systems of forecasting and alerting on the dangerous consequences of violent solar storms

Chair: M. Parisi, A. Belehaki

Solar **E**xtreme **E**vents **2007**

Cosmic rays and space weather effects: methods of forecasting

L. I. Dorman[1, 2]

[1]*Israel Cosmic Ray & Space Weather Center and Emilio Segre' Observatory, affiliated to Tel Aviv University, Technion and Israel Space Agency, Israel*
[2]*Cosmic Ray Department of IZMIRAN, Russian Academy of Science, Moscow Region, Russia*
(lid@physics.technion.ac.il,)

Abstract – **This report based on many original papers of author and his colleagues on the using of cosmic rays (CR) for continue monitoring and forecasting of great natural hazards for people and technologies from space weather effects. It consists from 5 parts.**
Part 1. Cosmic rays and space weather influence on global climate change (determining of the part of global climate change caused by the long-term change of CR intensity through influence on air ionization and planetary clouds formation; examples from the past; method of forecasting of the part of global climate change caused by space weather effects).
Part 2. Global natural disaster from great magnetic storms connected with big CR Forbush-decreases and their assessment by using world-wide network of CR stations (great geomagnetic storms affect adversely global technology systems, high frequency radio communications are disrupted, electric power distribution grids are blacked out when induced currents causes safety devices to trip, and atmospheric warming causes increased drag on satellites and anomalies in their operation, increasing of frequency of infarct myocardial, brain strokes, car and train accidents; examples of electric power and long oil tubes catastrophes in the past in Canada and other countries; we show that by using on-line one hour CR data from world-wide network of stations is possible to made exact assessment of this natural hazard for 15-20 hours before of the storm sudden commencement).
Part 3. Global natural disaster from great intense radiation hazards for astronauts, crew and passengers on regular airline flights (on the standard altitude about 10 km), and some time for people on the ground due to great solar flare CR events (statistical distribution, examples from the past; we show that this advertisement, with high occurrence probability, can be given 30-60 minutes before the arrival of the more dangerous particle flux). This method is based on the well known fact that the main part of radiation hazard in space and in atmosphere is caused by particles with small energy (few hundreds MeV) that reach the Earth 1-2 hours after their acceleration on the Sun; on the contrary the relatively small flux of high-energy (≥ 2 GeV) particles, which can be detected by super neutron monitors and practically are not involved in the radiation hazard, reach the Earth much more quickly. Several minutes of observation of the first-coming solar high-energy particles can give enough information on intensity, energy spectrum, transport parameters, and source function to make it possible to predict the time-space distribution of radiation hazard in interplanetary space (for astronauts and space-probe technology) and in the Earth atmosphere as a function of latitude (geomagnetic cut-off rigidity) and altitude.
Part 4. Prediction of the interaction of a dust-molecular cloud with the solar system by measurements of changes in the galactic CR distribution function. From the past we know that the dust from clouds between the Sun and the Earth leads to decrease of solar irradiation flux with sufficient decreasing of global planetary temperature (on 5-7° in comparison with 0.8° from green effect). The plasma in a moving molecular dust cloud contains a frozen-in magnetic field; this field could modify the stationary galactic CR distribution outside the Heliosphere. The change in the distribution function can be significant, and it should be possible to identify these changes when the distance between the cloud and the Sun becomes comparable with the dimension of the cloud. The continuous observation of a time variation of the CR distribution function for many years should provide the possibility of determining the direction and the speed of the cloud relative to the Sun, as well as its geometry. Therefore one could predict its evolution in space and determine whether it will catch the Sun or not. In the case of high probability of capture, we could predict the time of the capture and how long the solar system will be inside the cloud.
Part 5. Prediction of the radiation hazard produced by CR particles generated in a nearby Supernova explosion (SE). From the energetic balance of CR in the Galaxy it was estimated that the full power for CR production is $W_{CR} \sim 3\times10^{40}$ erg/s. Now it is common accepted that the Supernova explosions are the main source of galactic CR. At each explosion the average energy transferred to CR is $E_{SE} \sim 10^{50} - 10^{51}$ erg. From this we can determine the expected frequency of SE in our Galaxy and in vicinity of the Sun. We estimate the probability of Supernova explosions inside different distances from the Sun and expected radiation hazard, and its variation with time. We show that in some cases the level of radiation may increases about 1000 times in comparison with present level, and it will be very dangerous for the Earth's civilization and biosphere. But we show that by high energy CR measurements by ground and underground muon telescopes and low-latitude neutron monitors on the Earth will be obtain information on the source function and diffusion coefficient for many years before when real radiation hazard will be formatted on the Earth. We show how on the basis of this information we can made exact forecasting on developing in time of the radiation hazard in space and in the atmosphere on different altitudes and cutoff rigidities (different geomagnetic latitudes) by using method of coupling functions, and experts must to decide how to prevent the Earth's civilization (in some cases it will be necessary for people to live underground or in special protected buildings for several hundred years, and go out only for very short time). It is important that on the basis of obtained forecast the Earth's civilization will have time at least several tens years to prepare the life underground and in special protected buildings.

Real-time GLE alert in the ANMODAP Center for December 13, 2006

H. Mavromichalaki[1], G. Souvatzoglou[1], C. Sarlanis[1], G. Mariatos[1], A. Belov[2], E. Eroshenko[2], V. Yanke[2]

[1]*Nuclear and Particle Physics Section, Physics Department, Athens University Pan/polis-Zografos 15771 Athens, Greece (emavromi@phys.uoa.gr)*
[2]*Institute of Terrestrial Magnetism, Ionosphere and Radio Wave Propagation (IZMIRAN), 42092, Troitsk, Moscow Region, Russia (abelov@izmiran.rssi.ru)*

Abstract – **Within the last years, a real-time system to monitor high energy cosmic rays for space weather use has been operated at Athens cosmic ray station. Neutron monitors and satellite high resolution data in real time are used, making it possible to observe cosmic rays in dual energy range observations. In large solar energetic particle (SEP) events, ground level enhancement (GLE) can provide the earliest alert for the onset of the SEP event. This system watches for count rate increases recorded in real time by twenty-three neutron monitors, which triggers an alarm if a ground level enhancement (GLE) of cosmic ray intensity is detected. Our effort is to determine optimal strategies for detecting the GLE event at a very early stage, while still keeping the false alarm rate at a very low level. We have studied past events to optimize appropriate intensity threshold values and a baseline to determine the intensity increase. We define three levels of alarm (watch, warning, and alert) on the basis of the number of stations that record a significant intensity increase. For every station there is a program which every minute calculates in real time the mean value of the last sixty minutely measurements and compares this value with a threshold. If we have 5 pre-alert points in succession, we define a Station Alert. If we see at least three stations in station alert mode, another program provides a General GLE Alert. A statistical analysis on the last ten GLEs recorded from 2001 till 2006 using 1-minute data from our database, produced GLE alarms for nine events in our system. Alarm times for these nine events are compared with satellite data separating if the event is GLE or magnetospheric one. The GLE alert precedes the earliest alert from GOES (100 MeV or 10 MeV protons) by 4-33 min. When the alert is final then an automated e-mail is sent to all the interested users. An Alert signal was established at December 13, 2006 by the ANMODAP Center and for first time an automated e-mail alarm signal was sent out by our system determining the onset of the GLE70 event. A detailed analysis of this alert is discussed.**

***Key Words*—Ground Level Enhancement, Neutron Monitor Network, Space Weather, GLE alert system.**

I. INTRODUCTION

Neutron monitors and muon detectors record secondary cosmic rays created by interactions of >1 GeV primary cosmic rays (predominantly protons and heavier nuclei) with Earth's atmosphere. With suitable analysis, ground-based detectors can yield unique information on conditions in the near-Earth interplanetary medium. Neutron monitors can also detect the most energetic solar energetic particle (SEP) events. SEPs that propagate to Earth can cause damage to satellite electronics, and can pose a radiation hazard to astronauts and air crews. In a typical SEP event, the particle flux increases in the 10 to 100 MeV energy range, but these energies are insufficient to produce an ejecta in ground level detectors. However, in the most extreme SEP events, the particle flux increases at energies >500 MeV, and these can be detected by ground based neutron monitors as a ground level enhancement (GLE). Because the time propagation of SEPs from Sun to Earth depends on the energy, charged particles the Earth reached will be recorded by neutron monitors usually earlier than low energy proton flux on the satellites. Furthermore, at higher energy the time to reach maximum intensity is also shorter. Consequently, GLE observations make it possible to warn of the arrival of SEP event earlier than methods based upon lower energy charged particles [1].

Moreover, ground level observations (neutron monitors, neutron telescope and muon telescope) are the only way to identify the occurrence of SEP event on the ground, and would be valuable even if satellite data were not readily available. The University of Delaware provides real-time displays of the cosmic

Stations	Abbrev	Lat (^{0})	Long(^{0})	Alt (m)	H_0 (mb)	R_C (GV)
FORTSMITH	FTSM	60.00	-112.00	0	996.10	0.30
INUVIK	INVK	68.35	-133.72	21	1019.10	0.14
McMURDO	MCMD	-77.85	166.72	48	985.10	0.00
NAIN	NAIN	56.50	61.70	46	1000.00	0.40
PEAWANUCK	PWNK	54.98	- 85.44	0	1000.00	0.50
THULE	THUL	76.50	- 68.70	260	1005.00	0.10
NEWARK	NWRK	39.68	- 75.75	50	1013.00	1.97

Table I. Stations from ANMODAP database used for real-time alarm.

ray intensity of several ground-based neutron monitors with good statistics and 1-min time resolution (Bartol Research Institute at the University of Delaware, http://neutronm. bartol.udel.edu/spaceweather). This article describes the development of a system that watches for count rate increases recorded in real time at neutron monitors and triggers an alarm if a GLE is detected. We determine optimal strategies for detecting the GLE event at a very early stage on the basis of an approach described in [2], while still keeping the false alarm rate at a very low level. Using the strategies derived in this work, the GLE alarm system is back tested at recent GLEs. Because the onset of SEPs are regularly monitored by the GOES satellites and alerts are issued by e-mail and on the Web by the NOAA Space Environment Center (http://www.sec.noaa.gov), we compare the issue times of NOAA SEC alerts with the GLE alarm times to determine how useful our system is ([3], [4]).

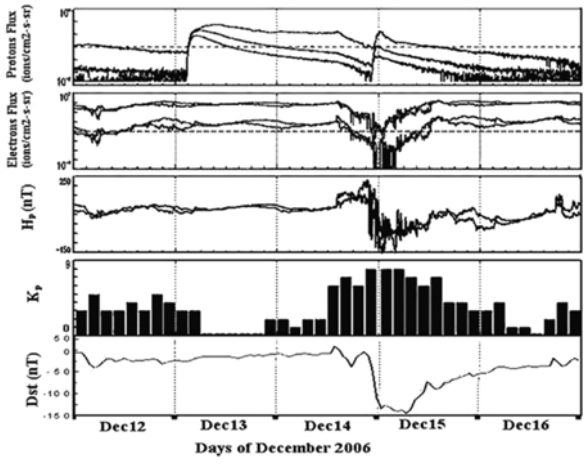

Fig. 1. Interplanetary and geophysical data (NOAA Space Environment Center Web site and Kyoto's on line database).

II. DATA ANALYSIS

On December 13, 2006 the last GLE of the 23rd solar cycle, was occurred. This event, also known as GLE70, started on the neutron monitors at ~ 2:48 UT and reached its maximum at~3:00-3:10 UT [5]. In northern Europe the event was registered with big amplitudes that in some cases reached ~ 70-90%, rendering this recent enhancement in one of the greatest GLEs of the 23rd solar cycle.

For a reliable alert signal all the available space data were collected for use. That is why interplanetary and geophysical data from NOAA Space Environment Center (http://www.sec.noaa.gov) are also recorded in real time at the ANMODAP center. The GOES satellites and the Kyoto Center provide all the available data, a part of which for this event is presented in Fig 1.

Solar activity ranged from very low to high levels through this period. Activity was very low during 11 – 12 December with numerous B-class flares from active region 930 and increased to high level on 13 December by virtue of an X3/4B flare at 13/0240 UTC from the same region.

The time profiles of the cosmic ray intensity during the event GLE70 recorded at the Neutron Monitors used in the alert system in Athens are illustrated in Fig. 2. The characteristics of these stations are given in Table I. All these data are directly extracted from the database nested at the ANMODAP Center. A dedicated program for each station in a variable rate downloads data from all the stations of the network. One of the most important capabilities of this database is the real time availability for immediate analysis. This is crucial in order to have as small as possible delay time between the event and the initiation of the alert. From the main database of the ANMODAP Center, a special 1min database is populated every 1min in order to provide all the data needed for the alert system.

Data with 1-minute resolution and extracted in real time from the online local database are used. The downloaded files construct a simple .txt file with the counting rate and timestamp is used as an input to the system. Because of the variety of problems that appears in real time situations a preliminary scan of the data has been performed in order to put all of them in the same preferred format for the program input. The general alert is initiated if three of them are in the alert phase, in order to prevent data failure in one of them totally seven stations instead of three are monitored.

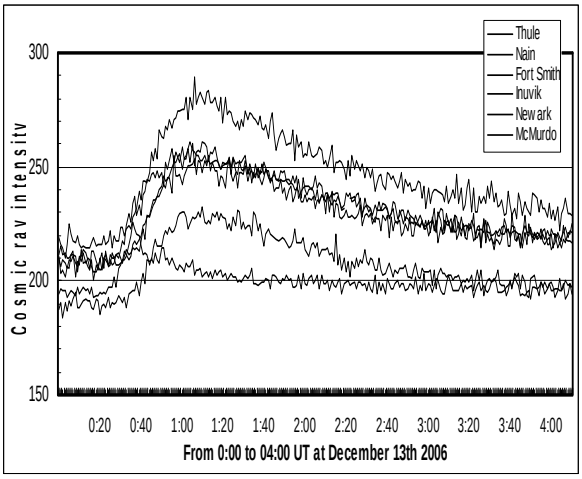

Fig. 2. Time profiles of 1min cosmic ray data from the NM stations used in the study of the GLE70. From top to bottom: McMurdo, Nain, Fort Smith, Thule, Inuvik, Newark.

III. REAL TIME ALGORITHMS

The need for a system that is fast enough for a detection of the GLE without loosing its accuracy guide us to the development of the following algorithm. Firstly the system uses four running states: Quiet, Watch, Warning, and Alert on the basis of the number of stations that record an intensity increase with a defined way. These states visualize in real time the status of the stations which provide their data at the ANMODAP center.

The use of one minute data corrected for pressure from all the available stations is preferred for not to miss an increase at some detectors. The collection of the data is carried out in real time. For every station there is a specific downloader program at the ANMODAP center's database. The program requests the data from the remote station every 1-minute, downloads them at the Center's database, checks their validity and makes a common format for all stations. Then for every station a program named [station]_GLE_alert.exe initiates to analyze. This program every minute calculates in real time the mean value of the last 60 minutely measurements and the value of the standard deviation. Using these parameters the moving threshold of each station is defined every minute by using the formula

$$I_{Threshold} = I_{MEAN} + n*\sigma$$

Where $I_{Threshold}$ is the final value of the threshold for the next minute, I_{MEAN} is the mean value of the counting rate, σ is the standard deviation of the counting rate and n is a value of the threshold multiplier varying from 1 to 3. This number has been defined for every station using data for the past seven years of GLE alerts. The n value fulfils the condition of maximum number of true alerts with the minimum number of false.

Setting the threshold level (n value) for each station, requires a trade off between the generation of the possible earliest station alarm, which favours at lower threshold, avoiding at the same time the false alarms that favour a higher threshold. Stations that record usually lower intensity increases and less sudden rises of intensity, demand smaller threshold multiplier in order to be able to give early alarm signal.

As illustrated in Figure 3, variable threshold level is set for the cosmic ray intensity increase that can be different for every station. If the last measurement exceeds the moving threshold, the program writes down a pre-alert point. If provided with 5 pre-alert points in succession a Station Alert is initiated. A program named 'check_for_alert.exe' is supervising the number of station alerts. A General Alarm is generated when the number of station Alerts exceeds three. The most of the time the system is in normal quiet mode. When the first station alert is occurred then the system is in a watch mode, an expiration timer of 15 minutes is set and the system waits for the next stations to get in station alarm mode. When the second station alert is occurred then the system is in a warning mode. When the third station alert occurs the system produces a general GLE alert. If the timer expires 15 minutes and there is no second or third station alert mode then the system gets into the normal quiet mode again waiting for the next event [6].

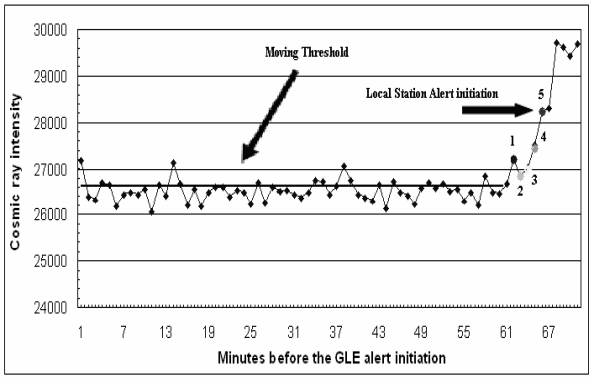

Fig. 3. An example of the visualization of the moving threshold approach in a local station alert for a typical time interval. Numbers show the progress of the Alert.

IV. FIRST REAL TIME GLE ALERT NOTIFICATION IN ATHENS

On 13/12/2006 at 3:05 UT the first real time event was recorded with the use of the ALERT system at the ANMODAP center [7]. The stations appeared with bold letters in Table II are the ones by which data the

December 13, 2006						
Stations		1σ		2σ		3σ
THUL		03:13 UT		03: 13 UT		03: 15 UT
NAIN		03: 02 UT		03: 03 UT		03: 05 UT
FSMT		03:08 UT		03: 08 UT		03:11 UT
INVK		03: 15 UT		03: 30 UT		NO GLE
NWRK		02: 56 UT		03: 01 UT		03: 01 UT
McMD		03: 05 UT		03: 08 UT		03: 09 UT

Table II. The times of the GLE alert signal initiation for each station are given. Stations in bold are the ones that produced the alert on December 2006.

alert signal was produced and a graphical representation of the alert from the ANMODAP centre web page in real time is also available in Fig. 4. During an unexpected failure on the visualization part of the Alert system it was not possible to produce the exact picture of the event at that day. The typical alert file can't be plotted. This is why the present picture is a reconstruction of the event by all the available data.

As mentioned above, the Alert Time was defined at 03:05 UT, the Onset Time was 02:51. Six stations were in local GLE alert at the system that day: Fort Smith, Inuvik, McMurdo, Newark, Thule, Nain and three of them: Nain, McMurdo and Newark- were the first to fulfill the condition for producing the alert signal. These signals were compared with the ones that NOAA produced that day, as NOAA Space Environment Center (NOAA/SEC) provides real-time monitoring of the proton flux observed by the GOES satellites during solar and geophysical events and issues alarms on the Web and via e-mail (NOAA Web site, http://www.sec.noaa.gov).

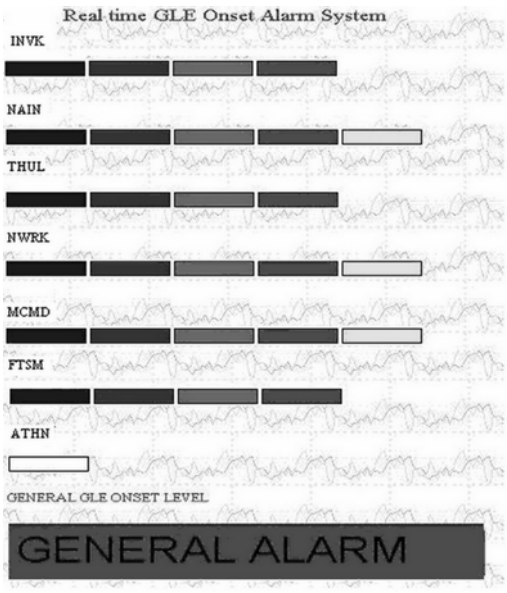

Fig 4. Real -time evolution of the GLE alert situation. Picture extracted from the ANMODAP's server.

The two available energy channels of proton data with energy >10 MeV and >100 MeV and also the two levels of alarm (warning and alert) that are issued during SEP events are evaluated from our system. A warning message is issued when a flux level above 10 particle flux unit (pfu) is predicted at >10 MeV or when greater than 1 pfu is predicted for >100 MeV. It is noted that the SEC's use of the term ''warning'' is rather different from our usage for the GLE alarm, as it is a prediction rather than an actual detection of SEP. Issue times of the alarms can be used as a barometer of how fast an SEP event is detected in low-energy proton data, therefore we compare our alarm time with these issue times. It is obtained from Fig. 5 that a NOAA SEC alert is typically not issued till some minutes after the relevant threshold is crossed, however we consider the issue time of an alert to be the relevant one for this comparison.

V. HISTORICAL GLE RESULTS

In order to examine the accuracy of the algorithm the last eight GLE events starting from 2001 have been tested. The evaluation of the system is performed by the comparison of the time of alert signals established from the application with the announced time of the real events by NOAA (2006). Data from the following stations are used for the offline analysis: CAPESCHMIDT, FORTSMITH, INUVIK, KIEL, LOMNICKY STIT, McMURDO, MOSCOW, NORILSK, NEWARK, OULU, THULE, NAIN and INUVIK. Depending on the kind of the event a selection of a number of them is made in order to have the best results. The results of this analysis of the GLE events and the comparison with NOAA SEC alerts are presented in Fig. 5.

One event that occurred on 17 January 2005 is excluded from this analysis, because the intensity increase was only 2% at South Pole station. We considered these eight events to determine optimal parameters for use in a GLE alarm system, and we also employed these events for back testing the system and determining its performance in relation to presently available SEP alarms.

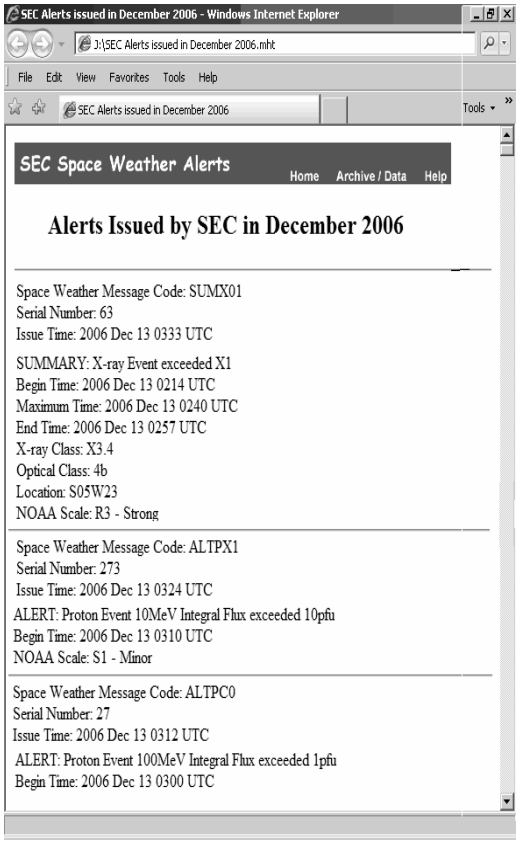

Fig. 5. GOES Alert signal for December 13, 2006.

VI. DISCUSSION AND CONCLUSIONS

One of the main problems in real time operation of the GLE Alarm system is the validity of the collected data. The system uses one minute data updated every minute in real time. In order to have a continuous operation of the system it is necessary to use as many stations as possible from the world wide Neutron Monitor Network provided their data. In this way three stations can be selected in order to provide continuous analysis for the alarm signal. Depending on the way that every station gives out its own one minute data we have the following problematic situations.

1. The stations provide different data formats and different technologies in data sharing. Using different types of downloader programs (ASP, FTP, SSH and http technologies) the data are formatted at the same type.

2. Although data are with 1-min resolution, they are not updated every 1-min but periodically every 5 minutes or every hour. A problem of this type can be overcome only with direct upgrade of the remote station. For these stations our data collection program works with a time window in the past (one hour or 5 minutes) but it runs every minute in order to be ready for 1-minute updating of these stations.

3. Minutely data update stops for some reasons, no data at all, unexpected messages in data files or not valid flags, network of remote station not reachable. In all these situations the downloader program automatically sends the message "Not valid input file" to the higher level programs and the station gets out from the team of stations that participate the alarm system without affecting the running of the others.

4. Data from different stations don't have the same UT timestamp for the same minute. A several minute differences between station clocks have been noticed. GLE system gives at real time collected measurements from the different stations additional timestamp from the local time server. In this way we record the data that all station give in the same minute with common time so we can reproduce the revolution of a historic event based in common time for all stations that give

GLE number	Event Date	Flare Time (UT)	Location	Flare's type	GOES Alert (100MeV, >1pfu)	Stations GLE Alert (UT)	Difference of the two alerts (min)
60	15 April 2001	13:19	S20W85	2B/X14.4	14:21	14:07	14
61	18 April 2001	02:11	S20WLimbb	C2	3:11	2:51	20
64	24 August 2002	00:49	S02W81	1F/X3.1	1:48	1:44	4
65	28 October 2003	09:51	S16E08	4B/X17.2	11:51	11:18	33
66	29 October 2003	20:37	S15W02	2B/X10.0	---------	NO GLE	----------
67	2 November 2003	17:03	S14W56	2B/X8.3	17:56	17:46	10
68	17 January 2005	-------	----------	--------	--------	NO GLE	----------
69	20 January 2005	06:36	N14W61	2B/X7.1	7:04	6:56	8

Table III. Comparison of the GLE alarm times from our system to the alarm times on the basis of satellite proton data.

one minute data updated every minute with one minute good synchronization [8].

The bad synchronization of the stations is a problem when running historic non real time data in the past. The alert time that is produced for the past GLEs is based in the assumption that the stations were well synchronized. In nowadays we can mark several minutes' time differences between stations for the same moment. This means that the results for the runs of the historic events are worse (more delayed GLE alarms) than those that would be produced if the system is running then in real time. And this means that at real time the system will give even earlier GLE alarms than that exacted from the analysis of historical data.

According to the above analysis the designed system proves to be able to produce real time alert signals earlier than those that NOAA system produces. Time difference between the two systems varies depending on the event. The ANMODAP Center, using its experience and tested methods, works on elaborating of more modern methods, in order to carry out a timely and feasible prognosis of the GLEs using all the available data from the worldwide NM network. It is clear that the joint complex analysis of the relevant information from space-borne and ground-based detectors will minimize the number of false alarms and will maximize the reliability and the timely forecasting of the arrival of dangerous fluxes and disturbances from space.

ACKNOWLEDGMENT

The authors thank the collaborators from the following real time CR stations who kindly provide us with the data used in this analysis: CAPE SCHMIDT, FORT SMITH, INUVIK, KIEL, LOMNICKY STIT, McMURDO, MOSCOW, NORILSK, NEWARK, OULU, THULE, NAIN (see also in http://cr0.izmiran.rssi.ru/ThankYou/main.htm).
This work is partly supported by the Greek Project 'PYTHAGORAS II" funded by European funds and National resources and by RFBR grants 07-02-13525 and 07-02-00915, and Program BR of the Presidium RAS "Neutrino Physics".

REFERENCES

[1] Dorman, L., Pustil'nik, L., Sternlieb, A., Zukerman, I.: Using ground-level cosmic ray observations for automatically generating predictions of hazardous energetic particle levels, Adv. Space Res., 31, 847 - 852, 2003.

[2] Dorman, L.I., Pustilnik, A., Sternlieb, A., Zukerman, I. G., Belov, A. Eroshenko, E., Yanke, V., Mavromichalaki, H., Sarlanis, C., Souvatzoglou, G., Iucci, N., Villoresi, G., Fedorov, Yu., Shakhov, B. A. and Murat, M.: Monitoring and Forecasting of great solar proton events using the Neutron Monitor Network in real time, IEEE for Plasma Science 32, 4, 1, 2004

[3] Kuwabara, T., Bieber, J. W., Clem, J., Evenson, P., Pyle, R. Development of a ground level enhancement alarm system based upon neutron monitors, Space Weather, 4, S10001, doi:10.1029/2006SW000223, 2006a.

[4] Kuwabara, T., Bieber, J. W., Clem, J., Evenson, P., Pyle, R., Munakata, K., Yasue, S., Kato, C., Akahane, S., Koyama, M., Fujii, Z., Duldig, M. L., Humble, J. E., Silva, M. R., Trivedi, N. B., Gonzalez, W. D., Schuch, N. J. Real-time cosmic ray monitoring system for space weather, Space Weather, 4, S08001, doi:10.1029/2005SW000204, 2006b.

[5] Plainaki, Ch., Mavromichalaki, H., Belov, A., Eroshenko, E., Yanke, V.: Application of the NM-BANGLE model to GLE70, Proc. 30th ICRC, SH, 2007

[6] Mariatos, G., Souvatzoglou, G., Sarlanis, C., Mavromichalaki, H. 'Alert systems for ground level cosmic ray enhancements prediction at the Athens neutron monitor network in real time', Journal of Modern Physics A, 20, 6711-6714, 2005.

[7] Mavromichalaki, H., Gerontidou, M., Mariatos, G., Plainaki, C., Papaioannou, A., Sarlanis, C., Souvatzoglou, G., Belov, A., Eroshenko, E., Yanke,V., Tsitomeneas, S.: Space Weather forecasting at the New Athens Center: The recent events of January 2005, IEEE NSREC TNS 52, 2307-2312, 2005a.

[8] Mavromichalaki, H., Souvatzoglou, G., Sarlanis, C., Mariatos, G., Gerontidou, M., Papaioannou, A., Plainaki, C., Tatsis, S., Belov, A., Eroshenko, E., Yanke, V.:The new Athens center on data processing from the neutron monitor network in real time. Annales Geophys., 23, 1–8, 2005b.

MuSTAnG --- Muon Space weather Telescope for Anisotropies at Greifswald

R. Hippler[1], A. Mengel[1], F. Jansen[1], G. Bartling[1], W. Guoehler[1], K. Kudela[2]

[1]Institute of Physics, University of Greifswald, Germany
(Hippler@physik.uni-greifswald.de)
[2]Institute of Experimental Physics, Slovak Academia of Science, Kosice, Slovakia

Abstract – **The Muon Spaceweather Telescope for Anisotropies at Greifswald (MuSTAnG) MuSTAnG became operational during November 2007. MuSTAnG is dedicated to space weather forecasting. First space weather observations were made during the 13 December 2007 event. Results in comparison with those of other muon telescopes will be presented at the conference.**

Poster Session E

Integrated systems of forecasting and alerting on the dangerous consequences of violent solar storms

Chair: S. Dimitrova

Solar **E**xtreme **E**vents **2007**

Generation of ALERT signal for solar cosmic ray ground level enhancements (GLEs)

A.V. Belov[1], E. A. Eroshenko[1], E. G. Klepach[1], V. G. Yanke[1], G. Souvatzoglou[2], Ch. Sarlanis[2], H. Mavromichalaki[2], E. Dryn[3], O. Kryakunova[3], N. Nikolaevsky[3]

[1]*Institute of Terrestrial Magnetism, Ionosphere and Radio Wave Propagation by Pushkov, Russian Academy of Sciences (IZMIRAN), Russia (erosh@izmiran.ru; erosh5@rambler.ru)*
[2]*Nuclear and Particle Physics Section, Physics Department, Athens University, Athens, Greece*
[3]*Institute of Ionosphere, Kazakhstan*

Abstract – **The system of elaboration of ALERT signal by real time data on ground level enhancements recorded by neutron monitor network is described and discussed in this work. On the retrospective experimental data (solar X-ray radiation, solar protons of >100 MeV, ground level enhancements) starting from 1986 the strategy was studied for elaborating the earliest signal of the ground enhancement onset. Only in two cases of 30 observed enhancements (GLE 040-069) the system could not generate a true ALERT signal because of very low amplitude of enhancement; in all other cases output ALERT signal is ahead of analogous signal generated by the data of GOES channel (p>100MeV) in average on 20 min. This time is enough to perform the estimation of the solar proton spectra from data of ground level monitoring and make a prognosis of time profile for solar protons >100 MeV practically at the initial phase of enhancement. The basic points of a program solution for output ALERT signal generation are outlined and possibilities to improve the proposed method are considered. A complete description of this system and its developing are presented at http://cr0.izmiran.ru/Alert/AlertGLE.htm.**

The method of forecast of solar proton events

V.M. Dvornikov, M.V. Kravtsova, A.A. Lukovnikova, V.E. Sdobnov

Institute of Solar-Terrestrial Physics SB RAS, Irkutsk, Russia
Russia, 664033, Irkutsk p/o box 291; Lermontov st., 126a, (sdobnov@iszf.irk.ru)

Abstract — **The dynamic processes in the interplanetary space have been investigated on the basis of the time variations in the parameters of the cosmic-ray rigidity spectrum. It is established that the change in the electromagnetic characteristics of the heliosphere begins before the sporadic phenomena on the Sun. In particular, it is shown that the sporadic phenomena are preceded by generation of local polarization electric fields, a decrease in the magnetic field strength in small-scale heliospheric structures, and an increase in the potential difference between the pole and ecliptic plane. The use of these signs makes it possible to predict solar proton events with a lead time from several hours to several tens of hours with a high degree of confirmation.**

I. INTRODUCTION

Carrying out the forecast of solar proton events (SPE) is concerned with sufficient difficulties conditioned by the set of complicated circumstances general of which is the absence of theoretically proved algorithms for the given problem solution. Because of this reason we cannot determine the necessary and sufficient features for the identification of the pre-flare situation on the Sun. But, even in the case if this problem was solved there would appear the difficulties with the forecast of localization fluxes of accelerated particles in the interplanetary space and, consequently – with the forecast of their reaching the Earth. Almost the only possible situation where the problem of SPE forecasting can be solved is the situation when the accumulation of the flare energy takes place as a result of the dynamics of current systems localized not only in solar corona, but spreading up to some distances in heliosphere. In this case it is worth trying to find the SPE precursors on the basis of heliosphere diagnostics according to the effects in cosmic rays (CR). Moreover, such diagnostics is carried out in the field lines of interplanetary magnetic field (IMF) that bind at the present moment the Earth with the corresponding regions on the Sun. Notes for the existence of such situations are taken from the works [1], [2], [3]. The goal of the proposed work is the realization of such an opportunity.

II. DATA AND METHOD

For the analysis we had used the middle-hour observation data of protons intensity of the energetic scales 4–9, 9–15, 15–40, 40–80, 80–165 and 165–500 MeV obtained at the satellite GOES-10 *http://spidr.ngdc.gov/spidr/index.html* [4] and the CR intensity variations data of various rigidities obtained by the method of spectrographic global survey (SGS) [5] according to the ground measurements at the global network of neutron monitors (38 stations).

When analyzing, for describing the CR rigidity spectrum in a wide range of energies, we had used the analytical expression obtained in the supposition that the rigidity spectrum in the Galaxy is described by the degree function from the CR rigidity and their intensity variation in the interplanetary space takes place (because of the energy change in regular electromagnetic fields of heliosphere) in accordance with the Liuville theorem, i.e. on condition of constant density of particles along the traveling trajectories in the phase space [5]. Spectrum parameters $\Delta\varepsilon_1$, $\Delta\varepsilon_2$, α, β, and R_0 reflect the following heliosphere characteristics: parameter $\Delta\varepsilon_1$ characterizes the CR energy variations at the expense of the gradient and the centrifugal drift of particles in the helical IMF against the inducted electric field and it is proportional to the IMF intensity, and $\Delta\varepsilon_2$ – in the fields of coronal mass ejections (CME) and it is proportional to the field intensity in CME and the SW velocity [5]. Parameter $\beta=B/B_0$, B_0 – intensity of the background and B – of the variable in time IMF, reflects the influence on the CR spectrum (by the magnetic rigidity of particles $R \le R_0$) by the non-stationary in time magnetic fields, and the parameter $\alpha=E_{pl}^2/B^2$, – polarization electric fields E_{pl}, appearing at the time of accelerated particles propagation in inhomogeneous fields of heliosphere. Supposition for existence of such fields is based on the Lindberg

laboratory experiments on researching the flux movement of accelerated plasma in the curved magnetic field [7] *and references there*. In particular, it is shown in the given work that in a definite range of the flux parameters when plasma reaches the region of curved field there the charges division takes place as a result of electrons and protons drift in opposite direction. Polarization electric field appears orthogonally to magnetic field depolarizing the longitudinal currents and longitudinal electric fields, under the influence of which the anomalous deflection of the flux takes place, the flux transforms from the cylinder into the flat one and the depolarizing currents distort the initial magnetic field.

It is reasonable to suppose that the energy change takes place through such fields between the accelerated particles and the background particles of solar wind plasma and CR in heliosphere, and as a result there happens the transformation of rigidity spectrum of background CR. This circumstance was taken into account when deriving an analytical expression for rigidity spectrum used in analysis.

Thus, determining the parameters of differential CR rigidity spectrum according to the data of its measurements in a wide range of energies for each observation hour it is possible to monitor the electromagnetic characteristics of heliosphere and their dynamics. While using this method the monitoring of interplanetary environment was carried out for the period October–November, 2003 and 2004–2005.

I. Analysis Results

In the fig. 1 at three upper panels the observations data of proton intensities in energetic intervals 4–9 MeV (0.108 GV), 9–15 MeV (0.223 GV) and 5 GV are represented by blue triangles, and the calculation results with the use of model spectrum and obtained values of its parameters by red curves. At the fourth panel the Dst-index values are represented. At the four lower panels the average hour values of parameters of rigidity spectrum $\Delta\varepsilon_1$, α, β, and R_0 are represented. They are determined for the researched period.

On the basis of the comparing of the temporal variations of CR rigidity spectrum parameters with the temporal profiles of low energy CR intensity (the first two panels in the fig. 1) we can make a conclusion that on the day before the solar proton events the changes of heliosphere electromagnetic characteristics take place. In particular, we can see that for several hours or tens of hours before SPE the generation of local polarization electric fields takes place (parameter α increase), decrease in intensity of magnetic fields in small-scale structures of heliosphere (parameter β decrease), and also the increase of intensity of a large-scale spiral IMF (parameter $\Delta\varepsilon_1$).

This circumstance allows us hope to have an opportunity for the SPE forecast when monitoring the electromagnetic characteristics of heliosphere (in the real time regime) according to the effects in cosmic rays.

Combination of these three features was used for the SPE forecast at the two-month data selection in October–November, 2003. At the upper panel in the fig. 1 realization moments of the shown features are marked by the vertical lines that are predictors for given events. In the fig. 2 the similar information for the 2004–2005 period is represented that demonstrates the high level (about 90 %) of truth for the worked out method of forecast.

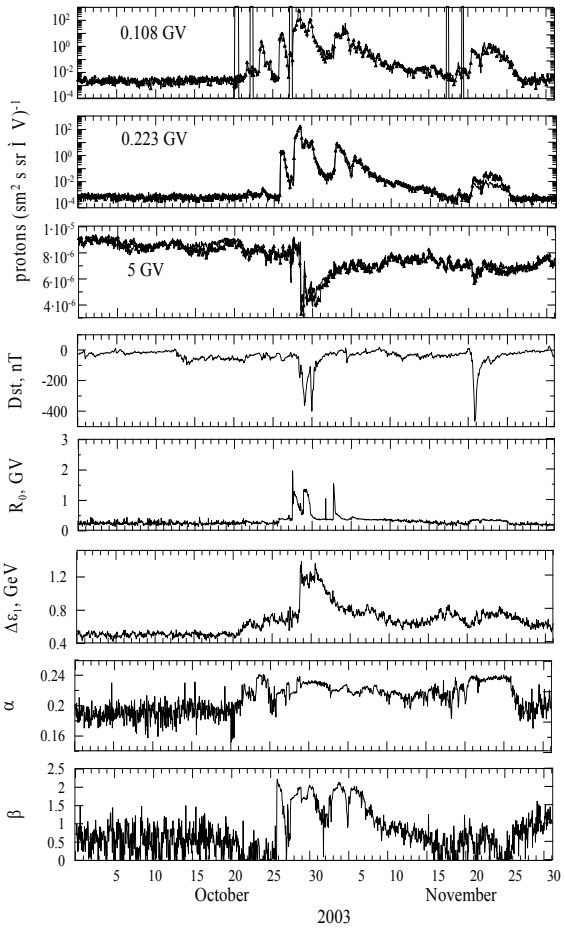

Fig. 1. Temporal profiles of CR intensity with R=0.108, 0.223 and 5 GV (line – calculation, triangles – observations data), Dst-index and parameters of CR rigidity spectrum R_0, $\Delta\varepsilon_1$, α, β for the period October–November, 2003. Moments of SPE predictors' manifestation are marked by the vertical at the upper lines panel.

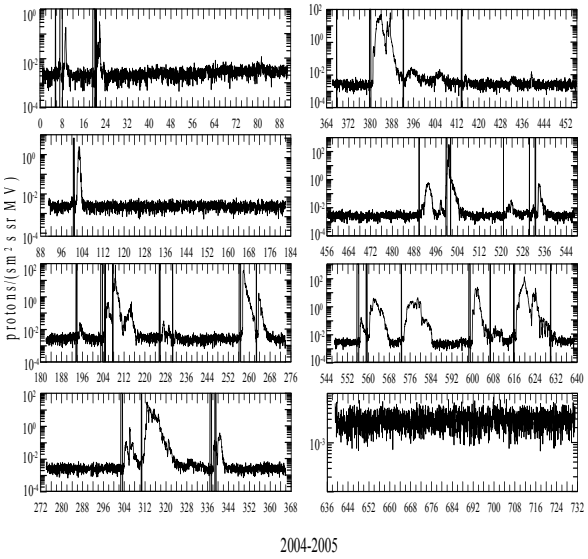

Fig. 2. Time profile of CR intensity in energetic range 4–9 MeV in 2004–2005. Moments of SPE predictors' appearance are shown by red vertical lines.

II. CONCLUSION

Diagnostics of electromagnetic conditions in the interplanetary space according to the effects in CR allows carrying out the forecast of solar proton events in advance time of several hours up to several tens of hours with high level of truth. And that shows us the adequacy of the used modulation model and of the validity of obtained information about dynamic processes in heliosphere.

ACKNOWLEDGMENT

This work is provided by the complex integration project SB RAS-2006 № 3.10 and the program of Presidium RAS «Neutrino physics» in the frames of the project «Research of modulation effects of cosmic rays by the method of ground and stratosphere monitoring».

REFERENCES

[1] Volodichev, N.N., Kuzhevsky, B.M., Nechaev, O.Yu., Savenko, I.A. Zaderzhka vyhoda solnechnyh protonov vysokoj energii v mezhplanetnoe prostranstvo. Kosmicheskie issledovaniya. 23, Ed. 5, 748–753. 1985. (in Russian)

[2] *Dvornikov, V.M., Sdobnov, V.E., Sergeev, A.V.* Rekurrentnye dvojnye vspleski pitch - uglovoj anizotropii kosmicheskih luchej i ih svyaz' s solnechnymi protonnymi sobytiyami. Rep. AN USSR. Ser. Phys. 48, 11. 2140–2142. 1984. (in Russian)

[3] *Dvornikov, V.M., Sdobnov, V.E., Sergeev, A.V.* Anomal'nye variacii kosmicheskih luchej v zhestkostnom diapazone 2–5 GV i ih svyaz' s geomagnitnymi vozmuscheniyami. Rep. AN USSR. Ser. Phys. 52, 12. 2435–2437. 1988. (in Russian)

[4] http://spidr.ngdc.gov/spidr/index.html.

[5] *Dvornikov, V.M., Sdobnov, V.E.* Time variations of the cosmic ray distribution function during a solar event of September 29, 1989. J. Geophys. Res. 102, A11, 24209–24219. 1997.

[6] *Dvornikov, V.M., Kravtsova, M.V., Sdobnov, V.E.* Uskorenie kosmicheskih luchej v geliosfere. Baikal International School on Fundamental Physics. Irkutsk. 167–169. 2005 (in Russian).

[7] *Alfven, H.* Cosmic plasma. Dordrecht, Holland, p. 213. 1981.

Session F

International Heliospheric Year 2007 (IHY 2007)

Chair: K-L. Klein, H. Moraal

Solar **E**xtreme **E**vents **2007**

IHY Science

N. Gopalswamy

NASA Goddard Space Flight Center
(gopals@ssedmail.gsfc.nasa.gov)

Abstract **– One of the key aspects of the International Heliophysical Year (IHY) Program is to address scientific questions that need international collaboration in the form of scientific campaigns. This effort is termed as the Coordinated Investigation Program (CIP). There are more than 60 CIPs proposed so far and each has a unique objective in understanding some aspect of the physical processes taking place in heliospace. This talk provides an overview of the IHY program with a special emphasis on the CIPS. Selected examples will be discussed in more detail especially those CIPs that are relevant to Sun-Earth connection.**

The role of the electronic geophysical year (eGY) in exploiting multi instrument, multi-band data via virtual observatories (VO) for solar extreme events analysis

M. Messerotti[1,2], Bernd Ritschel[3] and the eGY Team

[1] *INAF-Astronomical Observatory of Trieste, Italy*
(messerotti@oats.inaf.it)
[2] *Department of Physics, University of Trieste, Italy*
[3] *GeoForschungsZentrum (GFZ), Potsdam, Germany*

Abstract – **A varied set of ground- and space-based instruments produces, on a routinary and/or on a targeted basis, large volumes of remote and in-situ data relevant to the Sun, to the heliospheric environment and to the geospace. A comprehensive analysis of solar extreme events and their effects on geospace needs the capability to observe the relevant solar phenomena, to track the associated perturbations propagating in the interplanetary space and to identify the response of the terrestrial/planetary magnetosphere, atmosphere and ionosphere. Such an analysis can be carried out by accessing and retrieving non-homogeneous data sets from different providers relevant to multi-instrument, multi-band observations. An effective tool for carrying out this task is the Virtual Observatory (VO), which provides advanced means for data searching, retrival, visualization and analysis from geographically distributed, non-homogeneous data repositories, in a unified operating framework via a common Graphical User Interface (GUI). With reference to that, the electronic Geophysical Year (eGY; http://www.egy.org) is an international initiative aimed at promoting easy and effective data access and standardization in the Geosciences, at the provider side, whenever possible, or via the VO intrinsic features, when unfeasible. Scheduled from July 2007 to July 2008 under the auspices of the International Union of Geodesy and Geophysics (IUGG), eGY has been setting the bases for achieving this goal by various actions in synergy with the other I*Y initiatives like the International Heliophysical Year (IHY), the International Polar Year (IPY), and the International Year of Planet Earth (IYPE). In this framework, we will outline the organization of eGY activities relevant to facilitating the analysis of heliospheric data via VOs and we will stress the synergetic role of eGY-Europe (http://egy-europe.oats.inaf.it), the European section of eGY.**

The heliosphere

X. Moussas

University of Athens, Faculty of Physics,
Department of Astrophysics, Astronomy and Mechanics, Athens, Greece
(xmoussas @ phys.uoa.gr)

Abstract **– The heliosphere is a huge region in the Galaxy dominated by the solar wind, rarefied plasma that is continuously emitted by the Sun and expands till its pressure is balanced by the pressure of the interstellar medium that surrounds all stars. The heliosphere is an important chapter of space physics. It changes continuously from the variations of velocity, density, magnetic field and structure of the solar wind. The heliosphere is the large scale environment of humans, and as such it greatly affects our lives on Earth (even more in space), mainly through the modulation of cosmic rays. A brief presentation of the heliosphere is given, fast and slow streams in the heliosphere are described, the heliospheric current sheet, the termination shock, the heliosheath and the heliopause are presented and its influence to the galactic cosmic rays and energetic particles. A quick reference is also given concerning education and research on the heliosphere and more generally Space Physics in Greece.**

The Antikythera Mechanism, the oldest known astronomical computer

X. Moussas[1], T. Freeth[2,3], Y. Bitsakis[1,5], J.H. Seiradakis[4] , A.Tselikas[5] , E. Magkou[6], M. Zafeiropoulou[6], R. Hadland[7], A. Ramsey[7], M. Allen[7], D. Bate[7], A. Crawley[7], T. Malzbender[8] , M.G. Edmunds[2]

[1] National & Kapodistrian University of Athens, Department of Astrophysics, Astronomy and Mechanics, Panepistimiopolis, GR15783, Zographos, Greece (xmoussas @ phys.uoa.gr)
[2] Cardiff University, School of Physics and Astronomy, Queens Buildings, The Parade, Cardiff CF24 3AA, UK. (Mike.Edmunds @ astro.cf.ac.uk)
[3] Images First Ltd 10 Hereford Road, South Ealing, London W5 4SE, UK. (tony @ images-first.com)
[4] Aristotle University of Thessaloniki, Department of Physics, Section of Astrophysics, Astronomy and Mechanics, GR-54124 Thessaloniki, Greece (jhs @ astro.auth.gr)
[5] Centre for History and Palaeography, National Bank of Greece Cultural Foundation, P. Skouze GR10560 Athens, Greece (bitsakis @ gmail.com)
[6] National Archaeological Museum of Athens, 44 Patission Str, GR 106 82 Athens, Greece.
[7] X-Tek Systems Ltd, Tring Business Centre, Icknield Way, Tring, Herts HP23 4JX, UK.
[8] Hewlett-Packard Laboratories, 1501 Page Mill Road, Palo Alto, CA 94304, USA.

Abstract **– The Antikythera Mechanism is the oldest scientific instrument and the oldest known astronomical computer we have in hands. It dates from the 2nd century BC. This extraordinary mechanism was found by sponge divers in an ancient shipwreck off the island of Antikythera, Greece in 1900. This peculiar device is much more complex than any known astrolabe. It is an exact astronomical instrument which works with gears and has several complicated exact scales, circular and spiral. It is relatively small; the size of a laptop, and it was definitely a portable instrument. This computer comes with an embedded user's manual, written in Greek with fonts of the 2nd CBC. The instrument has been studied by Rediadis, 1902, Theofanidis, 1932, Price, 1959, 1975, Wright, 1995, 2002 and it was known to be a complex astronomical calculator. We have performed a new study of this miraculous Mechanism using modern non-linear high resolution computer tomography of X-tek Systems and Polynomial Texture Map (PTM) 3D surface photography by HP. These techniques enabled us to have very detailed representations of the interior of the Mechanism, to read the computer manual, which has been hidden for over 21 centuries in the rust, to reconstruct and understand better the Antikythera Mechanism. The manual has a mechanical section, an astronomical, some geographical notes (the name ISPANIA in these texts is the oldest reference to this country) several references to the motion of planets. The term "stationary point" of a planet appears several times. There are several dials and scales, two of them spiral, one for the Saros and Exeligmos cycle (18 year plus 8 hours and 54 years and one day for the eclipses of the Sun and the Moon, with inscriptions of the eclipses on the scale, a second spiral scale for the Meton's cycle (19 years) and Callippic cycle (76 years) for an accurate calendar. The Moon mechanism shows the position and phase of the Moon during the month. The velocity of the Moon is variable following the theory of Hipparchus, which is an approximation Kepler's second law for the angular velocity, i.e. the Moon goes faster near the perigee and slower at the apogee. The study continues and we have new results almost continuously.**

Solar **E**xtreme **E**vents **2007**

Workshop on Neutron Monitors
'The present and the future of NMs'

Chair: X. Moussas, A. Belov

Solar **E**xtreme **E**vents **2007**

Neutron Monitor Workshop

Neutron Monitor Station	Principal Investigators
ALMA - ATA	O. N. Kryakunova
ATHENS	H. Mavromichalaki
EREVAN	A. Chilingarian
ESOI	L. Dorman
IRKUTSK	V. M. Dvornikov
IZMIRAN	E. Eroshenko
JUNGFRAUJOCH	E. Flueckiger
KERGUELEN ISLAND/ TERRE ADELIE	K.-L. Klein
KIEL	C. Steigies
LOMNICKY STIT	K. Kudela
NEW MEXICO	J. Valdes-Galicia
OULU	I. Usoskin
PLATEAU DE BURE	J.-L. Autran
POTCHEFSTROOM/SANAE	H. Moraal
ROME	M. Storini

High mountain Alma-Ata cosmic ray station: current state of cosmic ray research by means of Neutron Monitors

O. N. Kryakunova

Institute of Ionosphere, Ministry of Education and Science, Kazakhstan
(krolganik@yandex.ru)

Abstract - **The Alma-Ata high mountain (3340 m above see level) neutron monitor has a counting rate of 1200 c/s and can detect solar flare particles with energy higher than 6.7 GV. The station has been operated since 1973 providing 1-hourly 5-minute and 1-minute data. All data are accessible in the electronic database, and real time data are presented in on-line regime at Web sites: http://tien-shan.org/ionos/index.htm, and http://213.211.74.116/CosRay/index.htm and http://213.211.74.116/CosRay/prod05.htm (data bank). Now the systems of presentation of 1-minute NM data in real time and counting rate of each canal are created.**

The activities in the Athens Neutron Monitor Station

H. Mavromichalaki
Athens Cosmic Ray Team

Nuclear and Particle Physics Section, Physics Department, Athens University
Pan/polis15771 Athens, GR (emavromi@phys.uoa.gr)

Abstract- **Cosmic ray measurements at Athens (37.58˚N, 23.47˚E) initiated in November 2000 with a standard 6NM-64 neutron monitor. Athens station was the sixth one to present both graphical and digital data in real time (http://cosray.phys.uoa.gr). Thanks to its high cut-off rigidity (8.53 GV), the Athens neutron monitor station records secondary cosmic ray data that correspond to the high energy part of the primary spectrum. Within the last years an effort in collaboration with IZMIRAN Cosmic Ray group has been made in order to construct an effective database of both NM and satellite data in real time, regarding the necessities of space weather monitoring (Athens Neutron Monitor Data Processing Center – ANMODAP Center). This Center, using the onset algorithm produces real time alert signals for GLEs and magnetospheric events sending them out by email notices. Apart from the alert signals, GLE treatment is realized with the application of the Neutron Monitor-Basic Anisotropic Ground Level Enhancement (NM-BANGLE) model, using data from many neutron monitor stations widely distributed around the globe and determining the time evolution of several GLE-parameters. Additionally, radiation doses during important radiation effects due to the very energetic particles reaching the vicinity of the Earth, are calculated. A simulation on space radiation using the Space Environment Information System (SPENVIS) tool is also being considered. Also, correlation of the cosmic ray variations with physiological parameters that play important role for human health, is calculated. Therefore, the ANMODAP Center provides the scientific community with an extremely useful tool for space weather monitor or/and prognosis operating in real time.**

Neutron Monitors operated at Aragats Space – Environmental Center (ASEC)

A. Chilingarian

Alikhanyan Physics Institute, Yerevan, Armenia
(chili@aragats.am)

Abstract - **The Aragats Space Environmental Center (ASEC) provides monitoring of different species of secondary cosmic rays and consists of two high altitude research stations on Mt. Aragats in Armenia. Geographic coordinates: 40°30'N, 44°10'E, cutoff rigidity: ~7.1 GV. Among various particle detectors In 1996 we restarted our first detector - the Nor Amberd Neutron Monitor 18NM64 type Neutron Monitors (NM) are operating at Nor Amberd research station (2000m above sea level) and at the Aragats research station (3200m above sea level). Recently modernized electronics of both monitors allows simultaneously registration of 3 time series according to 3 prefixed dead times. New installed "slow control" system allows control and automatic tuning of high voltage for each proportional camber of NM. Advanced Data Analysis system provides data storage on file servers, data transfer to computer center and various possibilities of control and visualization. Very interesting features of ASEC NMs consist in possibility of measuring simultaneously neutral and charged fluxes of cosmic rays. System of scintillator detectors build around NM allows estimation of the arrival direction of the primary cosmic rays. Correlated information on neutral and charged fluxes is very useful for alerting on dangerous conditions of the Space Weather and for fundamental research in Solar Physics.**

Israel Cosmic Ray and Space Weather Center: Past, Present, and Future

L. Dorman

Israel Cosmic Ray and Space Weather Center, Israel Israeli-Italian Emilio Segre Cosmic Ray Observatory TEL AVIV, ISRAEL, POB 2217, QAZRIN 12900, ISRAEL
(lid@physics.technion.ac.i; llid1@post.tau.ac.il)

Sayan mountain spectrographic complex of Neutron Monitors of ISTP SB RAS

V. M. Aleshkov, V. M. Dvornikov, A. A. Lukovnikova, V. E. Sdobnov

Institute of Solar-Terrestrial Physics SB RAS, Irkutsk, Russia

Abstract - **The conception of developing the Sayan mountain spectrographic complex of cosmic rays (CR) as well as its realization history is presented. Characteristics of stations forming the complex and the corresponding results of analysis of variations of rigid spectrum parameters and geomagnetic cutoff rigidities are given. As concluded, there is no possibility for obtaining reliable information of CR intensity variations and geomagnetic cutoff rigidities from only spectrographic complex data. Means for operating the Sayan complex within the world network of stations are discussed, and the results are shown under given approach.**

The world wide neutron monitor network: at present and in future

E. A. Eroshenko

IZMIRAN, 142190, Troitsk, Moscow region, Russia
(erosh@izmiran.ru; erosh5@rambler.ru)

Abstract - **Neutron Monitor, 60 years ago invented, till now remains as one of the main cosmic ray detector. The world wide neutron monitor network entering its second part of century continues its extension and improving. At present the main problems of NMN Network are an operative collection of data and their processing in real time regime.**

The Swiss Neutron Monitors

E. O. Flückiger, R. Bütikofer, B. Pirard, L. Desorgher

Physikalisches Institut, Universität Bern, Bern, Switzerland
(erwin.flueckiger@space.unibe.ch)

Abstract - **The Cosmic Ray Group of the Physikalisches Institut of the University of Bern has been operating an 18 IGY neutron monitor (NM) since 1958 and a 3 NM64 since 1986, both at Jungfraujoch (geographic latitude: 46.55° N; geographic longitude: 7.98° E; effective vertical cutoff rigidity, Epoch 2000.0: Pc = 4.50 GV; altitude: IGY 3570 m asl, NM64 3475m asl). These NMs, together with the NM at Lomnický Štít, fill the latitude gap between the Rome station (Pc = 6.19 GV) and the Kiel station (Pc = 2.20 GV). The 3500 m altitude of Jungfraujoch provides good response to galactic and solar primary cosmic ray protons and ions near the geomagnetic cutoff rigidity of ~4.5 GV, and to solar neutrons with energies as low as ~250 MeV. The mid-latitude location entails an enhanced sensitivity to geomagnetic effects and therefore permits the study of magnetospheric perturbations. The records of a special neutron monitor in Bern (46.95° N, 7.45° E; 570 m asl) allow a rapid qualitative analysis of the spectral variations of the primary nucleonic cosmic radiation, and they complement the measurements of the Jungfraujoch neutron monitors (e.g. attenuation length of solar cosmic ray events). The paper gives an overview of the NM sites, the technical and operational aspects of the detectors, and their observational characteristics. In addition, examples of the most relevant observations in the past are presented to illustrate the significance of the Swiss NMs in the European and global NM network.**

The neutrons at Kerguelen Island and Terre Adelie and related activities at Paris Observatory

K. L. Klein, N. Fuller

Observatoire de Paris, LESIA-CNRS UMR 8109 F-92195 Meudon
(ludwig.klein@obspm.fr)

Abstract - **The two French neutron monitors at Kerguelen Island and at Terre Adelie are operated by the French Polar Institute (IPEV). Paris Observatory is responsible for he scientific use of the data. Simultaneously the Meudon solar physics group is active in research on solar coronal dynamics, using ground-based and spaceborne instruments in the whole electromagnetic spectrum. We'll give a brief description of the neutron monitors and of our related activities: the investigation of the origin of solar energetic particles and provision of input for the monitoring of radiation doses of aircraft crews.**

The Neutron Monitor of Kiel

C. Steigies

Christian-Albrechts Universität zu Kiel , Germany
(steigies@physik.uni_kiel.de)

Cosmic Ray Measurements at Lomnický Štít

K. Kudela, V. Kollár, R. Langer, I. Strhárský

Dept. Space Physics, Institute of Experimental Physics, Slovak Academy of Sciences, Watsonova 47, 04001 Košice, Slovakia (http://space.saske.sk)
(kkudela@kosice.upjs.sk)

Abstract - **During IGY in 1957 the cosmic ray measurement started also in High Tatra mountains. Neutron monitor data from Lomnický Štít (2634 m above sea level, 49.40 N, 20.22 E, vertical geomagnetic cut-off rigidity ~4 GV) are available since 1958. The experimental device was several times reconstructed. Average counting rate was increased and time resolution was improved. From 1982 the neutron monitor with 8 tubes in 4 sections is in operation with 5 min resolution and from 1984 with 1 min resolution. High statistical accuracy (average counting rate ~ 440 s^{-1}) allows to study the details of the variability of primary cosmic ray flux. The detailed description of 8 NM 64 at LS can be found in [1]. Preliminary data in real time are available at http://neutronmonitor.ta3.sk. In addition, neutron multiplicity measurements are running for the past three years. Selected results based on these measurements are described briefly with references in [2].**

This work is supported by Slovak Grant Agency APVV, project no. 51-053805.

1. Kudela, K., Bobík, P., Kollár, V., Langer, R., Strhárský, I. and S. Štefánik, Neutron Monitor at Lomnický Štít: brief decsription and Revised Data for 12/1981-12/1999, preprint IEP SAS Košice, pp. 80, 2000

2. Kudela, K., Kollár, V., R. Langer and I. Strhárský, Cosmic Ray measurements in High Tatra Mountains: 1957-2007, presented at Workshop „50 years from the beginning of continous cosmic ray registration“, convener M. Storini, Mérida, Mexico, July 4-5, 2007, under submission to Adv. Space Res., 2007

Virtual Earth-Sun Observatory (VESO) at Universidad Nacional Autonoma de Mexico

J. F. Valdes-Galicia

Instituto de Geofisica, UNAM, Mexico
(jfvaldes@geofisica.unam.mx)

Abstract - **The study of solar perturbations traveling to Earth, have reached great importance and the term "Space Weather" has been coined to describe the state of perturbation on the interplanetary medium and the magnetic behavior around Earth. As part of these studies running by the international community, the *Instituto de Geofísica* of the *Universidad Nacional Autónoma de México* (UNAM) undertake the endeavor to join four separate observatories to shape a Virtual Observatory to monitor the Earth-Sun environment. These four instruments participate actively, in collaboration with other observatories and spacecrafts with similar objectives; they are:**

1.The Solar Radio Interferometer (SRI) is a Sun observing telescope in the 4 centimeter wavelength recording microwave solar emissions during eight hours every day, this emission is approximately constant except when a Solar flare takes place. Flares are the first indicators of solar activity and usually are followed by a Coronal Mass Ejection.

2. The MEXican Array RadioTelescope (MEXART)of Coeneo (Michoacán) tracks high scale transitory perturbations in its course from the Sun to the Earth using the Interplanetary Scintillation technique. The MEXART is a radiotelescope configured to detect cosmic sources of radio affected by solar activity (interplanetary scintillation). The antenna is composed by a 4096 (64X64) array dipole-kind antennas reaching a total physical area of 9,500 square meters. Length East-West of this array is 140 meters, and North-South is 80meters.

3. The lowest energy cosmic ray flux ($E< 10^{11}$eV) is controlled by the Heliosphere. Cosmic Rays should go through the solar wind pushing them outward of the Solar System. Changes in the solar wind conditions induce variations in cosmic ray intensity, this variability contain important information of solar activity and Heliosphere conditions. The Neutron Monitor at the *Universidad Nacional Autónoma de México* campus in Mexico City tracks cosmic rays with energies from $8.2x10^{9}$eV.

4. The Geomagnetic Observatory in Teoloyucan measures geomagnetic field variations from internal and external sources. The Worldwide Geomagnetic Observatories Network (INTERMAGNET) detects diverse external features, such as solar perturbations that reach Earth producing Geomagnetic Storms after going through interplanetary medium. Solar activity also has influence over the electric currents in Ionosphere and in Earth's magnetic field resulting as a diurnal variation in every single station of the network.

The Teoloyucan Geomagnetic Observatory is part of this international network, it measures on the Earth's surface the last stage of disturbed or steady solar wind conditions (among other related phenomena) closing a physical circuit of VESO's measurements tracked in the first instance, in the Sun. The VESO main objective is to analyze, study and spread information along with the interconnected observatories; this will permit to perform an interdisciplinary research of Heliospheric phenomena.

The OULU neutron monitor: 43-years measurements

I. Usoskin

Sodankyla Geophysical Observatory, Finland
(Ilya.Usoskin@oulu.fi)

The new Plateau de Bure Neutron Monitor and the Altitude Test Single-Event Effects Test European Platform (ASTEP)

J. L. Autran

L2MP-CNRS Bâtiment IRPHE, Marseille, France
(Jean-Luc.Autran@up.univ-mrs.fr)

Abstract - **This talk will present the construction of the Plateau de Bure Neutron Monitor (PdBNM) and the preliminary results obtained during the verification/calibration step performed in Marseille at sea level. This new monitor neutron (type 3NM64 with high pressure He3 detectors) will be definitively installed at the altitude of 2252m on the ASTEP platform, the Altitude Single-Event Effects Test European Platform. The first motivation for the PdBNM is to provide an experimental characterization of the neutron flux on ASTEP, in order to correlate flux variations (an possible GLE) with Single-Event Effects (SEE) electrically detected in the microelectronics components and circuits under test in the same location. Real-time data from PdBNM should be also collected and online published in the framework of national and European initiatives concerning the compilation of neutron monitor databases.**

An intercalibration of the world's neutron monitors

H. Moraal

Northwest University, Potchefstroom 2520 South Africa
(harm.moraal@nwu.ac.za)

Abstract - **The status of a project to intercalibrate the worldwide network of neutron monitors with a mobile neutron monitor will be reported. The purpose of this intercalibration is to derive intensity spectra of secondary cosmic rays, so that continuous spectral information about cosmic-ray modulation, to at least one decade higher in energy than is typically available from spacecraft, can be determined. However, to be useful, this intercalibration must be accurate to within ± 0.2%. Results will be presented of the stability, energy response, temperature sensitivity and environmental effects of the calibration neutron monitor, how successful we are likely to be to achieve this ± 0.2% limit, and our current status with the calibration project.**

The SVIRCO Observatory (INAF/UNIROMA3 Collaboration): Present status

M. Parisi, M. Storini, F. Signoretti

INAF/IFSI-Roma, Roma, Italy
(parisi@fis.uniroma3.it)

Abstract - **The Rome/SVIRCO (Studio Variazioni Intensità Raggi Cosmici) station (now Observatory) performs uninterrupted cosmic ray measurements since July 1957. In May 1997 the neutron monitor was moved from the Physics Department of "La Sapienza" University of Rome (41.90 N, 12.52 E, 60 m a.s.l.) to the Physics Department of Roma Tre University (41.86 N, 12.47 E, sea level). In this short summary we describe the present status of the neutron monitor operation, the data acquisition systems and the recent upgrade of the detector from 17 to 20 NM-64. This enhancement improved the overall counting rate and then the statistical quality of the recorded data. The increased reliability of the short-time data acquisition allows to analyse with more accuracy cosmic ray events.**

Participants List

Name	Institute	email
Agrawal, Rekha	Department of Physics, Government Model Science College, Jabalpur, India	rm_jbp@yahoo.co.in
Fr. Anagnostopoulos, George	University of Thrace, Greece	ganagno@ee.duth.gr
Angelov, Ivo	South west University 'N. Rilski', Bulgaria	i_angeloff@mail.bg
Antonova, Elizaveta	Skobeltsyn Institute of Nuclear Physics Moscow State University, Russia	antonova@orearm.msk.ru
Arakelyan, Karen	Alikhanyan Phisics Institute, Cosmic Ray Division, Armenia	karen@crdlx5.yerphi.am
Arkhangelskaja, Irene	Moscow Engineering Physics Institute (State University), Russia	irene.belousova@usa.net
Arkhangelskij, Andrew	Moscow Engineering Physics Institute (State University), Russia	angel1966@list.ru
Asgarov, Abbas	Shamakhy Astrophysical Observatory named after N.Tusi, Azerbaijan Republic	asgarov@gmail.com
Asipenka, Aliaksandr	IZMIRAN, Russian Academy Of Sciences, Russia	asipenka@gmail.com
Avgouli, Orsoula	National & Kapodistrian University of Athens, Greece	aorsoula@yahoo.gr
Babayev, Elchin Safaraly-oghlu	Azerbaijan National Academy of Sciences, Azerbaijan Republic	ebabayev@yahoo.com
Badruddin,Dr.	Aligarh Muslim University, Aligarh, India	badr_phys@yahoo.co.in
Bampasidis, Georgios	National & Kapodistrian University of Athens, Greece	gbabasid@phys.uoa.gr
Bazilevskaya, Galina	Lebedev Physical Institute, Russia	gbaz@rambler.ru
Belehaki, Anna	National Observatory of Athens, Greece	belehaki@space.noa.gr
Belov, Anatoly	IZMIRAN, Russian Academy of Sciences, Russia	abelov@izmiran.ru
Braun, Isabel	Max-Planck-Institut fuer Kernphysik, Heidelberg, Germany	isabel.braun@mpi-hd.mpg.de
Buetikofer, Rolf	Physikalisches Institut, University of Bern, Switzerland	rolf.buetikofer@space.unibe.ch
Carter, Jennifer	University of Leicester, United Kingdom	jac48@star.le.ac.uk

Chillingarian Ashot	Alikhanyan Phisics Institute, Cosmic Ray Division, Armenia	chili@aragats.am
Crosby, Norma Bock	Belgian Institute for Space Aeronomy, Belgium	norma.crosby@oma.be
Daibog, Elena	Institute of Nuclear Physics of Moscow State University, Russia	daibog@srd.sinp.msu.ru
Dandouras, Iannis	Centre d'Etude Spatiale des Rayonnements, CNRS / UPS, Toulouse, France	Iannis.Dandouras@cesr.fr
Dasso, Sergio	Instituto de Astronomia y Fisica del Espacio (IAFE), Buenos Aires, Argentina	dasso@df.uba.ar
Diego, Piero	INAF/IFSI-Roma, Italy	piero.diego@ifsi-roma.inaf.it; diego@fis.uniroma3.it
Dimitrakoudis, Stavros	National & Kapodistrian University of Athens, Greece	steeve_dim@hotmail.com
Dimitrova, Svetla	Solar Terrestrial Influences Laboratory, Bulgarian Academy of Sciences, Bulgaria	svetla_stil@abv.bg
Dorman, Lev	IZMIRAN, Russia Academy of Sciences, Russia & Tel Aviv University, Israel	lid@physics.technion.ac.i; llid1@post.tau.ac.il
Dvornikov, Valery	Institute of Solar-Terrestial Physics, Irkutsk, Russia	sdobnov@iszf.irk.ru
Eroshenko, Eugenia	IZMIRAN, Russia Academy of Sciences, Russia	erosh@izmiran.ru erosh5@rambler.ru
Fuller, Nicolas	Observatoire de Paris Meudon, France	nicolas.fuller@obspm.fr
Flueckiger, Erwin	Physikalisches Institut, University of Bern, Germany	erwin.flueckiger@space.unibe.ch
Gehmeyr, Michael	University of Colorado, USA	gehmeyr@lasp.colorado.edu
Gerontidou, Maria	National & Kapodistrian University of Athens, Greece	mgeront@phys.uoa.gr
George Giouvanellis	National & Kapodistrian University of Athens, Greece	giogiouvas@yahoo.gr
Gopalswamy, Nat	NASA Goddard Space Flight Center, USA	gopals@ssedmail.gsfc.nasa.gov
Gremos, Ioannis	TEI of Piraeus, Greece	iegremos@otenet.gr
Gushchina, Raisa	IZMIRAN, Russian Academy Of Sciences	rgus@izmiran.ru
Gvozdevsky, Boris	Polar Geophysical Institute, Russia	gvozdevsky@pgi.kolasc.net.ru
Hippler, Rainer	University of Greifswald, Insitute of Physics	Hippler@physik.uni-greifswald.de
Hovsepyan, Gagik	Alikhanyan Physics Institute,Cosmic Ray Division, Yerevan	hgg@crdlx5.yerphi.am
Ishkov, Vitaly	IZMIRAN, Russian Academy Of Sciences, Russia	ishkov@izmiran.ru
Kalegaev, Vladimir	Institute of Nuclear Physics, Moscow State University, Russia	klg@dec1.sinp.msu.ru

Karanikas, Costas	Department of Informatics,Aristotle University of Thessaloniki, Greece	karanika@csd.auth.gr
Kartyshov, Valery	IZMIRAN, Russian Academy Of Sciences, Russia	vl@izmiran.ru
Kefala, Eleni	National and Kapodistrian University of Athens, Greece	ayni171@gmail.com
Klein, Karl-Ludwig	Observatoire de Paris, LESIA, France	ludwig.klein@obspm.fr
Klepach, Eugeny	IZMIRAN, Russian Academy Of Sciences, Russia	yanke@izmiran.ru
Koen, Stegen	Belgian Institute for Space Aeronomy	koen.stegen@oma.be
Kropotkin, Alexey	Skobeltsyn Institute of Nuclear Physics, Moscow State University, Russia	apkrop@dec1.sinp.msu.ru
Kryakunova, Olga	Institute of Ionosphere, Ministry of Education and Science, Kazakhstan	krolganik@yandex.ru
Kourakou, Diamanto	National and Kapodistrian University of Athens, Greece	iamakkaika12@yahoo.com
Kurt, Viktoria	Skobeltzyn Institute of Nuclear Physics Moscow State Univesity, Russia	vgk@srd.sinp.msu.ru
Lazutin, Leonid Lazutin	Scobeltsyn Institute for Nuclear Physics, Moscow, Russia	lll@srd.sinp.msu.ru
Mariatos, George	National & Kapodistrian University of Athens, Greece	gmphysics@yahoo.com
Maris, Georgeta	Institute of Geodynamics 'Sabba S. Stefanesku ', Romania	gmaris@geodin.ro
Mavromichalaki, Helen	National & Kapodistrian University of Athens, Greece	emavromi@phys.uoa.gr
Messerotti, Mauro	INAF-Astronomical Observatory of Trieste, Italy	messerotti@oats.inaf.it
Mironova, Irina	Institute of Physics, St. Petersburg, State University, Russia	mironova@ge.phys.spbu.ru
Miroshnichenko, Leonty	IZMIRAN, Russia; Instituto de Geofisica, UNAM, Mexico	leonty@geofisica.unam.mx, leonty@izmiran.ru
Mitsakou, Eleftheria	National & Kapodistrian University of Athens, Greece	emitsaku@phys.uoa.gr
Moraal, Harm	North-West University, South Africa	harm.moraal@nwu.ac.za
Myagkova, Irina	Skobeltsyn Institute of Nuclear Physics, Russia	irina@srd.sinp.msu.ru
Nikolaeva, Natalia	Skobeltsyn Institute of Nuclear Physics, Russia	nni@srd.sinp.msu.ru
Nymmik, Rikho	Skobeltsyn Institute of Nuclear Physics, Russia	nymmik@sinp.msu.ru
Oleneva, Viktoria	IZMIRAN, Russian Academy Of Sciences, Russia	olene@izmiran.ru
Oreshina, Inna	Sternberg Astronomical Institute, Moscow State University, Russia	ivo@sai.msu.ru
Paouris, Evangelos	National & Kapodistrian University of Athens, Greece	Astrophysics.Paouris@gmail.com

Panasyuk Mikhail	Skobeltsyn Institute of Nuclear Physics, Russia	panasyuk@srd.sinp.msu.ru
Papailiou, Maria - Christina	National & Kapodistrian University of Athens, Greece	mpapahl@phys.uoa.gr
Papaioannou, Athanasios	National & Kapodistrian University of Athens, Greece	atpapaio@phys.uoa.gr
Petrov, Alexey Nikolaevich	Scobeltsyn Institute of Nuclear Physics, Moscow State University, Russia	gluk@srd.sinp.msu.ru
Pizanias, Marios	National and Kapodistrian University of Athens	mpizanias@yahoo.gr
Plainaki, Christina	National & Kapodistrian University of Athens, Greece	cplainak@phys.uoa.gr
Potapov, Alexander	Institute of Solar-Terrestrial Physics SB RAS, Russia	potapov@iszf.irk.ru
Preka – Papadema, Panagiota	National & Kapodistrian University of Athens	ppreka@phys.uoa.gr
Radharani, Alyana	Indian Institute of Technology-Bombay, India	radha.alyana@gmail.com
Raymond, Dioya	Federal University Of Technology Minna, Nigeria	ambassadorty@yahoo.co.uk , dioyaraymond@gmail.com
Reymers, Artur	Yerevan Physics Institute, Cosmic Ray Division, Armenia	arthur@crdlx5.yerphi.am
Romeou, Zaharenia	University of Patras, Greece	zrom@arcetri.astro.it
Rother, Oliver	Christian-Albrechts Universität zu Kiel , Germany	rother@physik.uni-kiel.de
Sarlanis, Christos	National & Kapodistrian University of Athens,Greece	csarl@isnet.gr
Savinkin, Maksim	Astronomical Observatory of Irkutsk State University, Russia	uustar@star.isu.ru
Sdobnov, Valery	Institute of Solar-Terrestial Physics, Irkutsk, Russia	sdobnov@iszf.irk.ru
Sidorov, Vladimir	Institute of Solar-Terrestrial Physics, Siberian Division of Russian Academy of Science, Russia	uustar@star.isu.ru
Sigaeva, Ekaterina	Skobeltsyn Institute of Nuclear Physics, Moscow State University, Russia	belka@srd.sinp.msu.ru
Signoretti, Fabrizio	INAF/IFSI-Roma, Italy	signoretti@fis.uniroma3.it or fabrizio.signoretti@ifsi-roma.inaf.it
Souvatzoglou, George	National & Kapodistrian University of Athens,Greece	gsouv@isnet.gr
Steigies, Christian	Christian-Albrechts Universität zu Kiel , Germany	steigies@physik.uni_kiel.de
Struminsky, Alexey	Space Research Institute, Russia	astrum@iki.rssi.ru
Timofeev, Vladislav	Yu. G. Shafer Institute of Cosmophysical Research and Aeronomy, Russia	vetimofeev@ikfia.ysn.ru
Tokhchukova, Susanna	Special Astrophysical Observatory of Russian Academy of Science, Russia	stokh@mail.ru
Tritakis, Vasilis	Academy of Athens	vas@academyofathens.gr

Troitskaya, Evgenia	D.V. Skobeltsyn Institute of the Nuclear Physics Moscow State Univertity, Russia	troi@srd.sinp.msu.ru; troi@dec1.sinp.msu.ru
Usoskin, Ilya	Sodankyla Geophysical Observatory, Finland	Ilya.Usoskin@oulu.fi
Valdes-Galicia, Jose F.	Instituto de Geofisica, UNAM, Mexico	jfvaldes@geofisica.unam.mx
Varotsou, Athina	Los Alamos National Laboratory, USA	athina@lanl.gov
Vashenyuk, Eduard	Polar Geophysical Institute, Russia	vashenyuk@pgi.kolasc.net.ru
Vassilaki Antonia	National & Kapodistrian University of Athens,Greece	johnant@otenet.gr
Vedenkin, Nikolay	Skobeltsyn Institute of Nuclear Physics, Russia	cool23@pochtamt.ru
Veselovsky, Igor	Institute of Nuclear Physics, Moscow State University, Russia	veselov@dec1.sinp.msu.ru
Yakovchouk, Olesya	Institute of Nuclear Physics, Moscow State University, Russia	olesya@dec1.sinp.msu.ru
Yanke, Viktor	IZMIRAN, Russian Academy Of Sciences, Russia	yanke@izmiran.ru
Yazev, Sergey	Astronomical Observatory of Irkutsk State University, Russia	uustar@star.isu.ru
Yeghikyan, Aram	Alikhanyan Physics Institute, Cosmic Ray Division, Armenia	eghikyan@gmail.com
Yushkov, Boris	Skobeltsyn Insitute of Nuclear Physics, Russia	clef@srd.sinp.msu.ru
Zimovets, Ivan	Space Research Institute Russian Academy of Science, Russia	ivanzim@mail.ru


Solar Extreme Events 2007: Fundamental Science and Applied Aspects
SEE 2007: International Symposium
Athens, Greece
Monday 24 September– Thursday 27 September 2007
COSPAR Colloquia

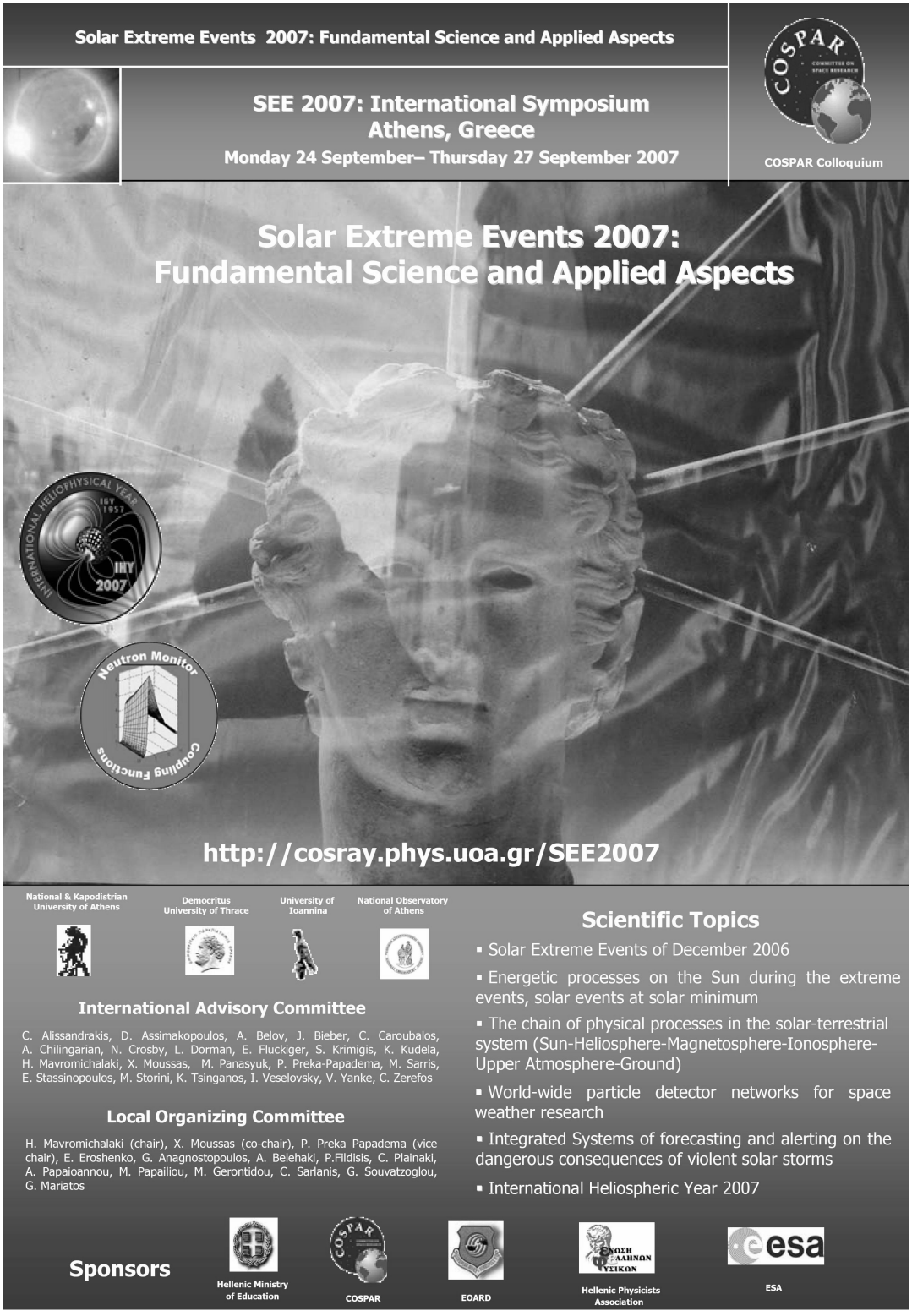
Solar Extreme Events 2007: Fundamental Science and Applied Aspects
SEE 2007: International Symposium
Athens, Greece
Monday 24 September– Thursday 27 September 2007
COSPAR Colloquium
Solar Extreme Events 2007:
Fundamental Science and Applied Aspects
INTERNATIONAL HELIOPHYSICAL YEAR
IGY 1957
IHY 2007
Neutron Monitor
Coupling Functions
http://cosray.phys.uoa.gr/SEE2007
National & Kapodistrian University of Athens
Democritus University of Thrace
University of Ioannina
National Observatory of Athens
International Advisory Committee
C. Alissandrakis, D. Assimakopoulos, A. Belov, J. Bieber, C. Caroubalos, A. Chilingarian, N. Crosby, L. Dorman, E. Fluckiger, S. Krimigis, K. Kudela, H. Mavromichalaki, X. Moussas, M. Panasyuk, P. Preka-Papadema, M. Sarris, E. Stassinopoulos, M. Storini, K. Tsinganos, I. Veselovsky, V. Yanke, C. Zerefos
Local Organizing Committee
H. Mavromichalaki (chair), X. Moussas (co-chair), P. Preka Papadema (vice chair), E. Eroshenko, G. Anagnostopoulos, A. Belehaki, P.Fildisis, C. Plainaki, A. Papaioannou, M. Papailiou, M. Gerontidou, C. Sarlanis, G. Souvatzoglou, G. Mariatos
Scientific Topics
▪ Solar Extreme Events of December 2006
▪ Energetic processes on the Sun during the extreme events, solar events at solar minimum
▪ The chain of physical processes in the solar-terrestrial system (Sun-Heliosphere-Magnetosphere-Ionosphere-Upper Atmosphere-Ground)
▪ World-wide particle detector networks for space weather research
▪ Integrated Systems of forecasting and alerting on the dangerous consequences of violent solar storms
▪ International Heliospheric Year 2007
Sponsors
Hellenic Ministry of Education
COSPAR
EOARD
Hellenic Physicists Association
esa
ESA